Experimental Investigations of Driven Pile Group Behaviour in Belfast Soft Clay

by

Bryan A.M. McCabe BA BAI MIEI

submitted to the
Department of Civil, Structural and Environmental Engineering,
Trinity College Dublin
in partial fulfillment of the requirements for the
Degree of Doctorate in Philosophy

August 2002

Declaration

I declare that this Thesis has not been submitted in whole or in part to any other University as an exercise for a degree. I further declare that, except where reference is given in the text, it is entirely my own work**.**

This Thesis may be lent or copied by the library.

Signed: _____ Date: _____

Bryan A.M. McCabe

Acknowledgements

This Thesis has been shaped by contributions from a considerable number of people over the last four years. The Author would like to offer his thanks to all who offered their time and knowledge along the way.

A considerable debt of gratitude is owed to Prof. Barry Lehane whose insight and geotechnical expertise was crucial to the evolution of this published work. Barry's availability to offer constructive advice at all times was greatly appreciated.

The technical staff at Trinity College Dublin deserves immense praise for surmounting challenging site conditions during the piling programme, while nevertheless contributing to a very memorable experience. Particular thanks are due to George Jones, Dave McAulay, Gerard McGranaghan, Eoin Dunne and others for their technical proficiency, resourcefulness and great camaraderie. The great effort and interest of Martin Carney in field and laboratory testing is duly acknowledged. All will agree that an Ulster Fry in Altona House was an experience that lived with you for quite a while. Thanks also to Chris O'Donovan, Chief Technician, who efficiently managed his squadron and facilitated everything asked of him.

None of the site work would have been possible without the collaboration of Lagan (formerly Lowry and Lowry McKinney) Piling, and their financial and technical contribution is greatly appreciated. In particular, Michael J. Troughton gave unselfishly of his time and resources to enable the piling program to proceed as smoothly as possible. His excellent engineering and project management skills and genuine interest in progress are sincerely acknowledged.

Thanks to my colleagues in geotechnics, particularly Declan Phillips. Tramore Summits I and II proved to be landmark events in recent years, but Tramore III promises to be the best of all. Encouragement from Declan and Kenneth Gavin helped no end at times of difficulty.

Thanks to Adam Pellew, Emilio Saldivar and Prof. Richard Jardine, all of Imperial College London, for their contributions to the static and cyclic test programmes.

The Author could not wish for five better friends whose support was exceptional throughout the course of this Thesis; they are Shane "The Gentleman" Murray, Jan Cronin, Quentin Heaney, Caitríona Gowing and Niall Holmes.

Most of all, thanks to Mum, Dad and Mairéad, for paving my path all these years. Thanks for everything!

TABLE OF CONTENTS

FIGURES

TABLES

SUMMARY

In 1996, a site adjacent to Kinnegar Sewage Treatment Plant, near Belfast, was made available (by the Northern Ireland Department of the Environment) to Trinity College Dublin to perform load tests on driven piles. Since 1997, investigations at Kinnegar have included lateral load tests on single piles (Phillips 2002) and vertical load tests (both static and cyclic) on single piles and small pile groups (reported in this Thesis). Extensive site investigation data has also been assimilated over this period.

Vertical load tests were carried out single reference piles and groups of five piles (centre to corner spacing of s/B=3). Each precast concrete driven pile was 250mm square and with an embedded length of 6m, much of its load was carried in shaft friction. Some of these piles contained internal instruments allowing load distributions and horizontal total stresses to be estimated. Slow static load tests (in tension and compression, for single piles and groups) were of the maintained load type with a final displacement rate of 0.24mm/hour for each load increment. One-way cyclic tension tests (on single piles and groups) were carried out at a rate of 1 cycle/minute for between 180 and 550 cycles.

There are two distinct facets to group action in driven piles: (i) the effect of neighbouring installations and (ii) the effect of loading adjacent piles. Both effects are likely to determine how the load-displacement relationship of a pile within a group differs from that of an isolated single or reference pile. It is commonly assumed that the soil surrounding any group pile is stiffened due to adjacent piling (i.e. its shear modulus increases) leading to improved individual performance under load. However, although the maximum excess pore pressures and total stress associated with group installation are higher than for a single pile, these are transient and return to original values very quickly. In fact, total stresses immediately after the installation of a five-pile group fall *below* those expected for a single pile. Upon full equalization of horizontal effective stresses, the value for the group appears to fall slightly below that expected for a single pile. This suggests that adjacent pile installation may have a small negative effect on subsequent pile performance. Independent data also suggests either a neutral or small negative installation effect.

Group action in Belfast soft clay appears to be governed predominantly by the load transferred between group piles when under load. Tests on tension and compression five-pile groups (s/B=3) are consistent in indicating that on average, the stiffness of the group is typically ≈45% that of a single pile at a typical working load per pile[1] (alternatively, the group has displaced by over twice the amount of a single pile). The relative stiffnesses of the centre and corner piles (corresponding to a working load per pile) are more difficult to determine due to inconsistent pile cap flexibility; nevertheless the centre pile is typically ≈65%-85% as stiff as a corner pile at any *stage*[2] of group loading. While relative pile capacities depend upon the flexibility of the pile-cap, the ultimate load in the centre pile falls 25-30% below that of a single pile for a rigidly capped group.

A load test on one group pile (with settlement measurements on adjacent non-loaded piles) proved instructive. It provided data to show that non-linear superposition (of displacements) is unsuitable for predicting the response of closely spaced piles but may be acceptable when widely spaced. The importance of choosing non-linear soil models is emphasized, as linear elastic 'interaction factors' grossly overestimate the amount of load transferred between piles and may lead to inefficient piling solutions. This data also contributed to the development of a trendline relating the stiffness efficiency to the pile spacing/width ratio (s/B), a useful design guide for small groups of the Belfast configuration. Its use in tandem with a suitable indication of the cost of constructing a capped group indicates that the economy of the solution is relatively insensitive to spacing in the range 4B<s<8B; spacings closer than 4B are not recommended.

Cyclic loading to 'failure' degrades the shaft capacity of driven single piles by 25%; further 'damage' is entailed for the five pile groups (35%). However, cycling to loads below 50% of the pile's dynamic capacity (as would be the case for piles with a factor of safety >2) causes little cyclic degradation. Failure in one-way cyclic tension is governed by the accumulation of mean pile head displacements and is not amplitude-driven.

[1] ≈40% of the capacity of a single pile (at 10% of the pile width)
[2] i.e at a certain average displacement for the pile group.

Chapter 1

Introduction

1.1 The Evolution of Piling

The driving of bearing piles to support structures is one of the earliest instances of the art and science of the civil engineer. Construction of dwellings secure from the hazards of living and the need for safety of passage across watercourses prompted man to drive robust stakes into the ground as early as 4000 years ago. Evidence of piled settlements has been found on lake shores in Switzerland, Italy, Scotland and Ireland, where food, water and easy transport were readily available. It has been estimated that 100,000 timber piles were used in a settlement at Robenhausen, Switzerland dating back at least two millennia. Closer to home, 30,000 ancient timber piles (including primitive sheet piles) were discovered in 1863 at Lough Drumkeery, Co. Cavan.

Greek and Roman engineers constructed many Mediterranean sea ports on timber piles, however severe attack on the submerged timber by the teredo worm leaves little archaeological legacy from this era. Some major European rivers (including the Danube) were traversed by pile-supported bridges. There is evidence to indicate that one of Rome's earliest bridges, the Pons Subilicus was pile supported.

Between the 8th and the 11th century, a number of cities were built upon piled foundations, the most notable of which were Venice and Amsterdam. Refugees were believed to have sought sanctuary on the Lagoon of Venice from Barbarian invaders; this prompted the development of a city in this easily defended location. Piles of length 15-20m support most of Amsterdam. When installed, the piles were sawn off level and capped with thick planks. The Romans, on the other hand, often capped their piles with a mixture of stone rubble and concrete. Although the load carrying capacity of timber piles were limited by the girth of trees and the ability of the material to withstand splitting or splintering due to hammer driving, considerable experience was accumulated with their use for different applications.

No further advances in the art of piling were forthcoming until the beginning of the 19th century. The strength, lightness, durability (when permanently submerged) and ease of cutting and handling contributed to the widespread use of timber piles. Timber was superseded by concrete and steel when the greater capacity of these materials for sustaining compressive, tensile and bending forces (for piles of the same dimensions) was recognized.

Reinforced concrete, developed as a structural medium in the late 19th century, replaced timber for use in high-capacity piling on land. RC may be precast in various forms to suit the imposed loading and ground conditions, and its durability is satisfactory for most soil and immersion conditions. The partial replacement of driven precast piles by a number of cast-in-situ alternatives began in the 1930s in Britain. This reflected the development of highly efficient machines for drilling large diameter holes to a great depth in a wide spectrum of soil and rock profiles rather than any deficiency in the performance of the driven pile. In fact, the bored pile concept may be traced to earlier times. The Taj Mahal (constructed 1632-1650) is an example of a building founded on a 'well' foundation, with stone slabs carried up from the base of each excavation or boring. The advent of RC meant that concrete could be poured in from the surface without need to descend the hole; with the result that small diameter piles of this type were no longer precluded. Today, the majority of bored piles are constructed using rotary augering machines. Machines are available to bore pile diameters ranging from 150mm to 2m, while concrete or grout may be injected to form a pile through a hollow stem of a continuously flighted auger as the laden auger is withdrawn from the soil. Driven piles have developed considerably in tandem; in particular, long piles which were cumbersome to handle with standard piling plant have been substituted with precast jointed piles. In addition, driving techniques have advanced considerably from the steam-driven drop hammers to the diesel hammers (post Second World War) and the more environmentally friendly hydraulic-operated devices of today.

Cast-iron pipe-piles date from the 1830s and were used in projects where durability was an important concern. Steel I- and H-sections followed at the beginning of the 20th century. The shape of the steel H pile offers the advantage of minimal soil displacement and can withstand hard driving more readily than precast concrete piles. The direct load and bending capacity offered by tubular piles often render them most suitable for harbour works or offshore applications such as oil platform foundations. Pile corrosion in marine environments may be overcome by suitable treatment such as cathodic protection. Steel piles may also be preferred if the expected tensile (or cyclic) stresses exceed the serviceable limit offered by concrete piles.

1.2 Modern day Piling Practice

Advances in the field of piling, due to an improvement in understanding and construction techniques alike, have ensured that sites previously deemed unsuitable for construction may now be fully utilized to cater for the ever-increasing development.

Specialist contractors offer skill and experience with various piling techniques to come up with a solution in even the most problematic of ground conditions. Thorough site investigation is an imperative step in any piling project; not only will it enlighten the pile design and choice of the most suitable construction technique, but it will minimize the risk of unforeseen problems which may impose delays and considerable expense should they arise. Increasing pressure to reduce on over-conservatism and optimize pile designs requires them to be sound and durable. Integrity testing has ensured that sub-standard construction may be detected in time, with the result that high standards in construction has virtually become commonplace.

1.3 Advances in Pile Design

Unfortunately, an increase in the worldwide use of piles as a foundation solution has not been matched by a complete understanding of the geotechnical behaviour of the pile-soil system.

Driven piles may be instrumented more readily than bored piles, so recent research has concentrated mainly upon driven pile behaviour. Shear stress, pore pressure and radial total stresses have been measured on the shafts of piles during driving, equalization and loading and correlated with governing soil properties. Unfortunately, findings from this research have been slow to filter into the design codes, which remain strongly empirical. A complete understanding of the soil's response to the pile installation process has remained very elusive, with the result that design methods for displacement piles remain somewhat deficient.

While the soil disturbance associated with the construction of non-displacement piles is likely to be less severe than for displacement piles, the obvious difficulty remains as to how pore pressures and radial total stresses may be reliably measured on a bored pile shaft. Full-scale load testing of contract piles is still the only sure method of determining the single pile settlement corresponding to the design working load.

Over the last thirty years, the exponential growth in computer power has enabled pile design to shift gradually from empiricism towards approaches involving a sounder theoretical but more computationally rigorous basis. However, the booming construction industry has meant that there is a parallel increase in the scale and complexity of pile group configurations and soil conditions which need to be analysed. Packages which analyze large and complex groups of piles and still incorporate representative soil models are rarely available to the design engineer. Although the rigour of an analysis may be diluted in many situations while retaining a piling solution of acceptable accuracy, the relative merits of group design methods remain unknown due to the scarcity of full scale pile group load tests available to appraise them. The purpose of this Thesis is to make some contribution to our understanding of pile group behaviour by carrying out full scale field tests on small groups of driven piles.

1.4 Scope of Thesis

A soft clay test bed near Belfast served as the location of an extensive test programme devised to examine group action in piles. A number of load tests have been conducted on pile groups in tension and compression, under both static and cyclic loading. Single pile tests provide a reference by which group action may be evaluated. Internal instrumentation in selected piles provides valuable data regarding the immediate effect of installation on the soil, soil re-consolidation over a period of time and group loading.

All of the pile test data published in this Thesis was gathered over the period 1997-2001 from a soft clay test bed at Kinnegar, near Holywood, Co. Down in Northern Ireland. Located on the shores of Belfast Lough, the site is about six miles north east of Belfast city centre and may be accessed through the Tillysburn Gates to the Belfast Harbour Industrial Estate, adjacent to Kinnegar Sludge Dewatering Plant. A general area map is shown in Figure 1-1, while Figure 1-2 identifies the half-hectare zone north of a freshwater pond (not shown) where the pile testing was concentrated. The site has been indefinitely leased from the Northern Ireland Department of the Environment for an ongoing programme of geotechnical research. Lagan Piling (formerly Lowry McKinney and Lowry Piling) carried out all of the piling work, with Trinity College Dublin responsible for the planning, load testing and data reduction.

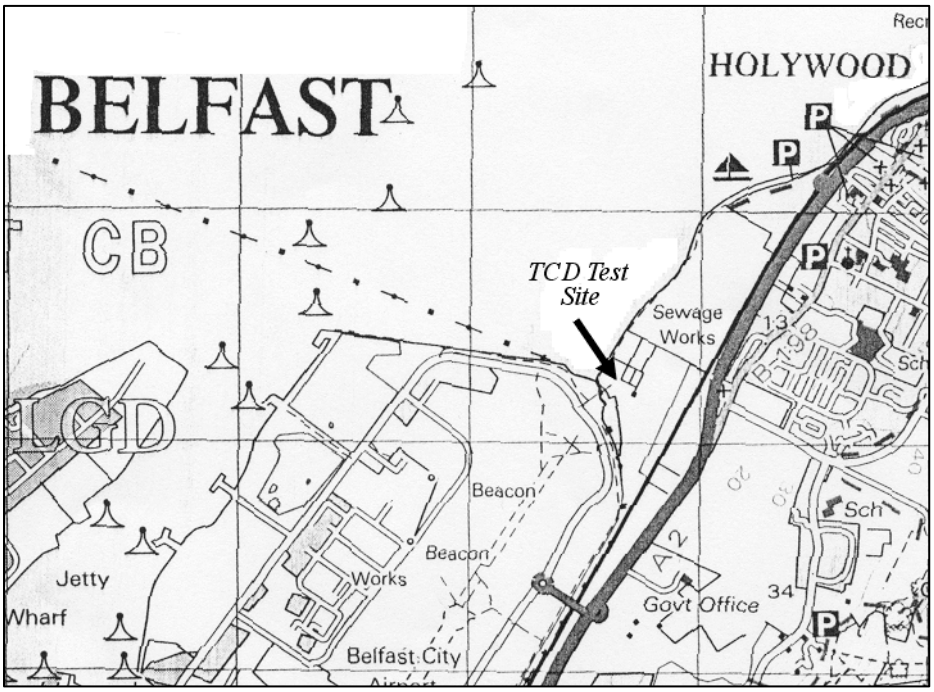

Figure 1-1: Belfast Area Map

There are two main programmes within the body of work carried out at Belfast. The static testing programme, which is the principal focus of this Thesis, was sponsored primarily by the ICE Research and Development Enabling Fund, with further contributions from Imperial College London and John Barnett and Associates, Dublin. A programme of cyclic tests was directed by Imperial College London for the Higher Education Authority (UK).

Chapter 2 provides a summary of the current state of knowledge of pile group behaviour. Some numerical approaches used to determine the stiffness[1] of a single pile are reviewed, as many of these form a partial basis for the pile group analyses which follow. Published pile group analysis methods include both empirical and numerical approaches; these are categorised according to the technique used and the associated degree of thoroughness. Although a large number of algorithms have been identified, most are based upon different combinations of a limited number of mathematical techniques. The relative merits of the more widely used programs are appraised. Some design charts are presented based upon these methods; these identify the effects of the different variables that dictate pile group behaviour.

[1] Applied pile head load per unit displacement of the pile head.

Also in Chapter 2, the diversity of pile group behaviour emerges from observations made from a limited database of case histories, some of which are re-examined in Chapter 8. The emphasis is placed upon pile groups in fine-grained soil.

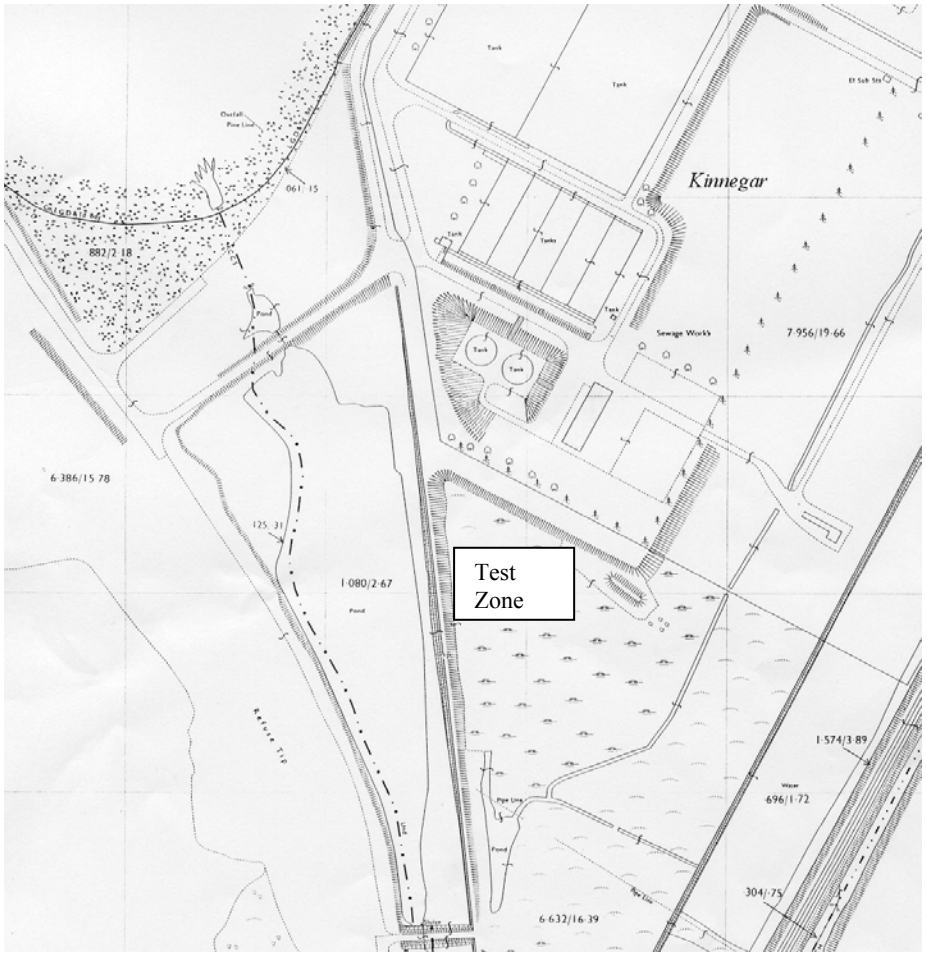

Figure 1-2 Location of Test Site

Interpretation of the pile test data hinges on a good understanding of the properties of the soft clay deposit. Both Crooks and Graham (1976) and Bell (1977) report the results of site investigations at a number of Belfast locations, one of which (Kinnegar) is adjacent to the current test site. An independent site characterization study was carried out as part of this Thesis, encompassing laboratory tests on piston samples and some standard field tests identifying the geotechnical characteristics of the deposit. Some similarities between the properties of the Belfast deposit and those at the well-characterized soft clay site at Bothkennar, Scotland, are identified.

An overview of the entire experimental programme is presented in Chapter 4. A chronological list of all principal site activities is given, which provides a useful reference for later chapters. All site-related activities including pile casting and installation, instrument calibrations and data acquisition, loading mechanisms and procedures are all described in detail. The pile notation system used to distinguish the different single piles and pile groups is introduced at this stage.

The main results of the static pile test programme are presented in Chapter 5, including measurements pertaining to installation, equalization and pile loading. Since the measured *maximum* pile loads over the complete test programme all fall within a 40kN band, a consistent basis is presented by which overall pile and shaft capacities may be deduced. Further corrections (including aging, reloading, loading rate) are applied to the raw data so that subsequent comparison between piles is justified.

The cyclic load test data is presented with minor interpretation in Chapter 6. It should be noted that the cyclic testing has not been the main focus of this Thesis but that the author wishes to pursue further interpretation of the cyclic work at a later date. The development and validation of a (OASYS SAFE/BRICK) non-linear finite element model is described in Chapter 7; this model provides supplementary information which is used to complement the site measurements.

The main findings from this Thesis are discussed in Chapter 8 and fall within a number of distinct categories. These categories are:

- Appraisal of some standard single pile capacity prediction methods.
- Features of the installation and equalization processes for pile groups.
- The effect of load interaction on the *stiffness* and stiffness efficiency of pile groups. The choice of an optimum pile spacing is also discussed.
- Methods of predicting the stiffness of pile groups, with particular emphasis upon the role of non-linearity in predicting the extent to which piles interact.
- Self-contained predictions of group pile behaviour (based solely upon load tests discussed in Chapter 5).

- Features of pile group behaviour observed from a limited database of case histories in clay soils.

Conclusions from the static and cyclic testing programmes are presented in Chapter 9. The Appendices contain data from the pile tests and other work referred to in the text.

Chapter 2

Single Pile and Pile Group Literature Review

Part 1

Single Piles

2.1 Introduction to Single Pile Analysis

Many of the factors which influence the capacity of isolated piles have been uncovered in recent times by data from high quality instrumented pile tests. Institutions such as Imperial College London (ICL), the Norwegian Geotechnical Institute (NGI) and Massachusetts Institute of Technology (MIT) have been to the forefront of informative research programmes. Direct measurements of local shear stresses, radial total stresses and pore pressures at the pile-soil interface at individual sites have highlighted critical features of pile installation, equalization and loading. Moreover, the collation of such measurements from a wide variety of soil types has allowed empirical correlations to be developed between these stresses and some governing soil parameters. These findings have been incorporated by Jardine and Chow (1996) into new design methods for driven piles. Equations recommended for estimating both the shaft and base capacity of both closed and

E	**Shaft capacity of closed-ended piles in clay**	
E1	$Q_s = \pi D \int \tau_f \, dz$	**Shaft capacity** Integral of local shear stresses along the embedded shaft length
E2	$\tau_f = \sigma'_{rf} \tan \delta_f$ $\sigma'_{rf} = 0.8 \, \sigma'_{rc}$	**Local shear stress** Coulomb failure criterion
E3	$\sigma'_{rc} = K_c \sigma'_{v0}$ $K_c = [2 - 0.625 I_{vr}] \, YSR^{0.42} \, (h/R)^{-0.20}$ or $K_c = [2.2 + 0.016YSR - 0.870 \Delta I_{vy}] YSR^{0.42} (h/R)^{-0.20}$ and $\Delta I_{vy} = \log S_t$	**Local radial effective stress** Function of: free-field effective overburden pressure, σ'_{v0}; I_{vr} and ΔI_{vy} (as defined on Figure 15); Yield Stress Ratio (YSR) and h/R (h/R is limited to a minimum of eight).
E4	$\delta_{peak} > \delta_f > \delta_{ultimate}$	Interface angle of friction, should be measured in interface ring shear tests. Operational value depends on degree of progressive failure, pile roughness, clay type and shearing history. Trends for North Sea clays shown on Figure 16.
F	**Shaft capacity of open-ended piles**	
F3	K_c taken from either of the expressions given in Step E3, but with $R^* = (R^2_{outer} - R^2_{inner})^{1/2}$ substituted for R in h/R terms	**Modified radius, R^*** Lower limit: $h/R^* = 8$.

Table 2-1(a) Shaft Capacity of Piles in Clay (Jardine and Chow, 1996)

H	**Base capacity of closed-ended piles**	
H1	Undrained loading $q_b = 0.8\ \overline{q_c}$ Drained loading $q_b = 1.3\ \overline{q_c}$	**Pile base resistance** is controlled by CPT resistance at the founding depth and the drainage conditions during loading. $\overline{q_c}$ is averaged 1.5 pile diameters above and below the tip.
J	**Base capacity of open-ended piles**	
J1	If $[D_{inner}/D_{CPT} + 0.45\ \overline{q_c}/P_A]$ is less than 36, the pile plugs	**Plugging** appears to take place according to the criterion given opposite. Note D_{CPT} = 0.036 m and atmospheric pressure P_A = 0.1 MPa or 100 kPa.
J2	$Q_b = q_b \pi D^2/4$ Undrained loading: $q_b = 0.4\ \overline{q_c}$ Drained loading: $q_b = 0.65\ \overline{q_c}$	**Fully plugged piles** develop half of the end resistance of closed-ended piles given by Equation I1 after a pile head displacement of D/10.
J3	$Q_b = q_{ba} \pi (R^2_{outer} - R^2_{inner})$ Undrained loading $q_{ba} = \overline{q_c}$ Drained loading $q_{ba} = 1.6\ \overline{q_c}$	**Unplugged piles** sustain end bearing on the annular area of steel only. Base resistance is equal to average CPT end resistance at the founding depth. This may be increased by a factor of 1.6 for drained conditions. Contributions from internal shear stresses should be ignored.

Table 2-1(b) Base Capacity of Piles in Clay (Jardine and Chow, 1996)

open ended piles in clay are shown in Table 2-1. The shaft response of piles in clay depends on the relative void index I_{vr} (a term which reflects both the sensitivity of the soil and its level of overconsolidation) and the yield stress ratio ($\sigma'_{vy}/\sigma'_{vo}$ as measured in oedometer tests on undisturbed soil). The magnitudes of the shaft stresses also vary with position relative to the pile tip normalized by the pile radius (h/R). Lehane et al (2000) (see Appendix 2-1) have since devised a method of shaft capacity prediction for driven piles in clay which substitutes OCR with the less subjective and widely measured corrected cone end resistance q_t as the principal soil property. It may also be seen in Table 2.1(b) that the cone penetration end resistance (q_c) is most useful in estimating ultimate pile base resistance.

The research reviewed by Jardine and Chow (1996) has been slow to infiltrate into everyday pile design practice. Despite a grave neglect of some factors which have an important bearing upon pile response, the α- and β- methods remain the most widely used estimates of shaft capacity. The peak shear stresses are assumed to be proportional to the undrained shear strength (typically from UU tests) with the α-method and the free field vertical effective stress with the β-method. Base capacity is calculated using a bearing

capacity factor (typically 9) as a factor on the undrained shear strength (c_u) at pile base level. Lehane (1992) and Chow (1997) offer a thorough critique of these techniques.

While these formulations enable the ultimate capacities of single piles to be determined, they provide no information on the pile load-displacement behaviour at typical working load levels. The remainder of this section concentrates on a number of widely used pile stiffness[1] prediction methods, both linear elastic and non-linear.

2.2 Continuum Methods for determining Single Pile Stiffness

2.2.1 Finite Element Methods

A number of Finite Element analysis packages are commercially available in which either a full 3-D (considering axial, lateral loads and torsion) or an axisymmetric analysis (axial load only) may be conducted on a single pile. Both soil and pile are discretised into a mesh of elements within a boundary sufficiently distant to avoid influencing the analysis output. Soil inhomogeneity/layering, anisotropy and non-linearity (subject to the packages' available suite of soil models) may be treated in a consistent manner at the pile-soil interface and over the entire soil mass. The success of this approach may be improved by facilitating relative movement (slip) at the interface between pile and soil. The axisymmetric single pile analysis of Desai and Holloway (1972) illustrates how 'interface' elements were used for this purpose; their mesh is shown in Figure 2-1.

The use of computer programs is essential and the method is more suited to research, complex problems or validation of less thorough approaches (e.g. load transfer approaches) than to everyday design.

2.2.2 Boundary Element Methods

Widespread use is made of the boundary element (or integral equation) method as a relatively thorough yet computationally efficient method of modelling single piles. Elastic solutions have been developed by Poulos and Davis (1968), Poulos (1968), Mattes and Poulos (1968) (on which the OASYS PILSET program is based) and also by Butterfield and Banerjee (1971). The following steps are common to most boundary element analyses:

[1] Defined for single piles as the pile head load divided by the pile head displacement

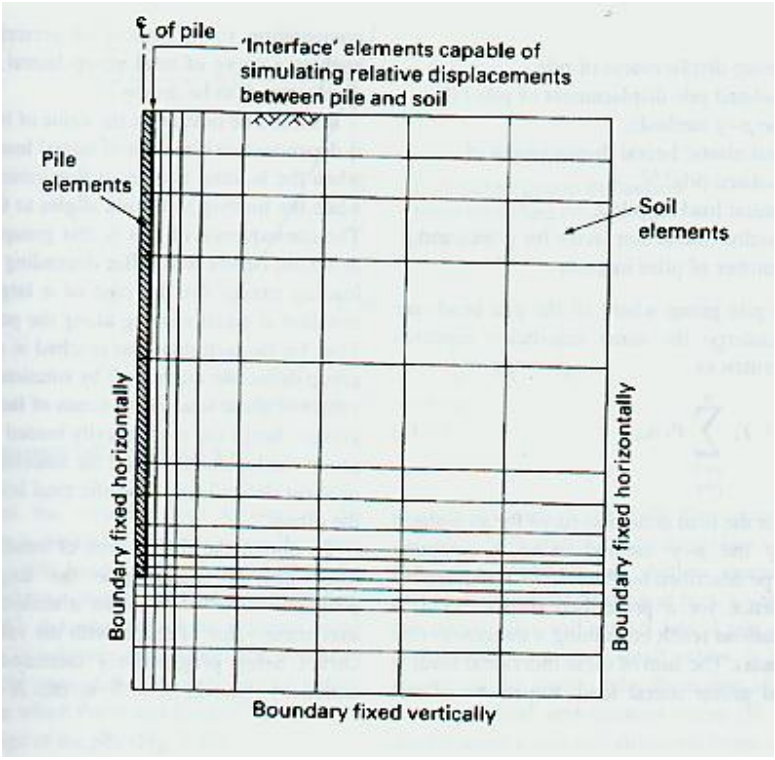

Figure 2-1 Axisymmetric analysis of single pile (after Desai and Holloway 1972)

(i) The interface between soil and pile is subdivided into a sufficient number of elements. An equivalent cylindrical pile is assumed (if the pile is not circular in section) with cylindrical elements along the shaft and a single element disc at the base (see Figure 2-2). The applied load and displacement on each separate element may be associated through an integral equation incorporating an appropriate Green's function. Mindlin's (1936) continuum solutions are generally preferred.

(ii) Either finite element or finite difference methodology may be used to set up corresponding equations for the structural response of each pile.

(iii) The sets of equations in (i) and (ii) may be solved, in the view of global equilibrium criteria, to determine the unknown forces on the pile. Load distributions and pile load-displacement responses may also be computed.

Lehane and McCabe (1999) employed a similar approach to model laterally loaded pile groups.

Alternatively, the same approach may be thought of as the application of a set of fictitious stresses (ϕ) to the boundaries of the pile in the elastic half-space (Butterfield and Banerjee, 1971)[2]. Particular values are chosen to generate displacements which are identical to the specified boundary conditions of a real pile system and also satisfy the stress boundary conditions on the free surface. These ϕ stresses are not necessarily the actual stresses acting on the real pile surfaces (only those applied to the imaginary half space), yet real stresses and deformations anywhere within the half-space may easily be determined. Integral equations incorporating Mindlin's solution for each element may be written in the form:

$$\{\phi\} = [K]^{-1}\{W\}$$

where {W} is a vector comprising vertical and radial displacement terms at the shaft and vertical displacement at the base; the [K] matrix emerges from Mindlin's theory. If desired, pile compressibility may also be included within this framework.

2.3 Load Transfer Methods

The axial deformation of a pile depends both on its compressibility and the shape (departure from linearity) of the load transfer curves. Load transfer curves for the pile shaft may be thought of as an integration (in the radial direction) of the shear strain (γ) in the soil, leading to relationships between the shear stress (τ) applied at the pile shaft and the local pile displacements (w):

$$w = \int \gamma dr = \int \frac{\tau}{G} dr$$

Similar expressions may be assigned to the pile base. The soil continuum is idealised into a number of horizontal layers each having its own load transfer relationship; the problem is mathematically equivalent to modelling a structural member supported by discrete springs (see Figure 2-3). With the exception of very compressible piles, vertical stress changes in the soil will be small in relation to changes in shear stress, which provides justification for the load transfer approach.

[2] The basis for PGROUP described later.

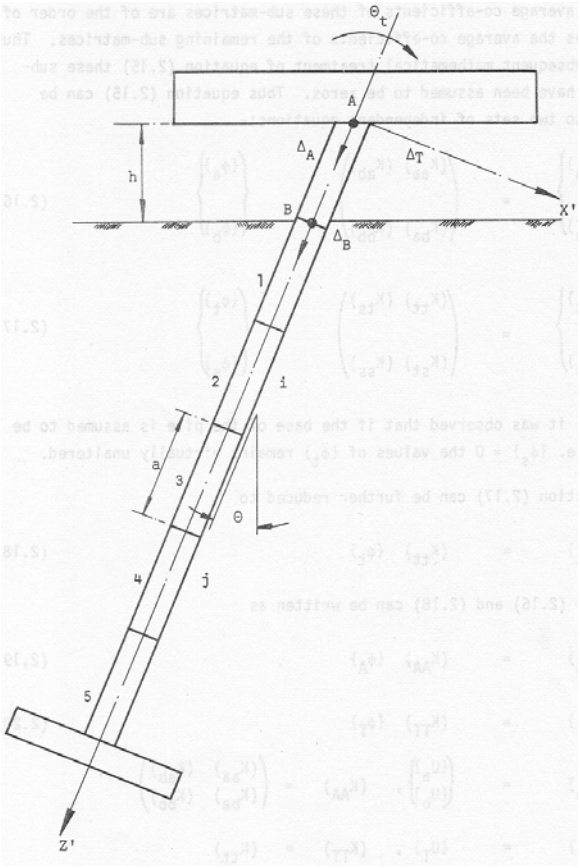

Figure 2-2 Discretization of pile-soil interface (after Banerjee and Driscoll, 1976)

The second order differential equation governing the axial compression of the pile (w), incorporates appropriate load transfer relationships between τ_o and w:

$$\frac{d^2w}{dz^2} = \frac{2\pi r_o}{(EA)_p}\tau_o$$

where z is the depth, E and A are the pile Young's modulus and cross sectional area respectively, τ_o is the shear stress at the pile shaft (where the radius $r=r_o$). Finite difference expressions are often used to approximate the second derivative term at a series of equally spaced nodes along the pile. Non-linear load transfer curves require iteration at each load increment. Alternatively, where pile elements of varying size and properties must be considered, the finite element method is more versatile. Vijayvergia (1977) proposed a general form of load transfer curve applicable to both shaft and base.

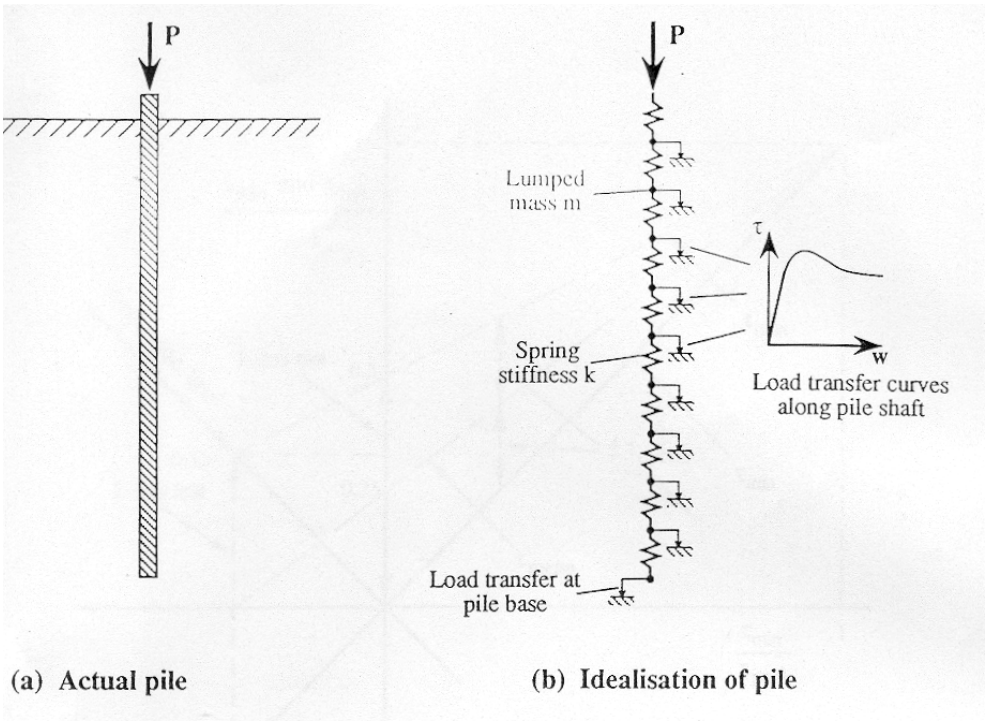

Figure 2-3 Load transfer non-linear springs (after Randolph, 1985)

Load transfer curves for axial and lateral loading are referred to as t-z and p-y curves respectively. They are arguably the most widely used technique for single pile analysis, particularly when non-linearity and varied stratification are important considerations. In most cases, computer resources are needed. The remainder of Section 2.3 is devoted to detailing a number of these approaches. The theoretical work of Randolph and Wroth (1978b) for linear elastic soil is described, in addition to the non-linear applications of Kraft et al (1981), RATZ (Randolph 1986) and CEMSET (Fleming 1992). Experimental load transfer curves compiled from high quality instrumented field tests form the basis of the API RP2A recommendations which are also discussed.

2.3.1 Randolph and Wroth (1978b)

The theoretical load transfer method of Randolph and Wroth (1978b) is arguably the most widely used approach for assessing the stiffness of a single pile; its closed form nature provides an immediate appreciation of how pile stiffness depends upon pile and soil parameters.

Randolph (1977) and Randolph and Wroth (1978a) contributed to the development of an approximate closed form solution for the elastic stiffness P/w (the pile head load per unit pile head displacement) of a friction pile. The soil is assumed to be characterized by linearly varying shear modulus (G) and constant Poisson's ratio (ν) profiles. This solution was extended to cater for end-bearing piles by Randolph and Wroth (1978b) with the facility to model a higher value of G below the pile base.

It is assumed that the transfer of load to both the pile shaft and base may be uncoupled and treated independently. The soil mass is separated into two horizons divided by an imaginary horizontal line at the level of the pile base; the soil above this horizon is deformed by stresses on the pile shaft, while the soil below this line is deformed only by pile base stresses.

Solution for an incompressible pile in homogeneous soil

If the shear stresses distant from the pile shaft are assumed to decay inversely with pile radius, and the shear strains are assumed to be predominantly vertical, the strains may be integrated within the zone of influence bounded by r_m to give the shaft settlement (w_s):

$$w_s = \int \gamma dr = \int_{r_o}^{r_m} \frac{\tau}{G} dr = \int_{r_o}^{r_m} \frac{\tau_o r_o}{rG} dr = \frac{\tau_o r_o}{G} \ln(\frac{r_m}{r_o}) = \zeta \frac{\tau_o r_o}{G}$$

The pile base settlement (w_b) is based on Boussinesq's (1885) expression for a rigid punch:

$$w_b = \frac{P_b (1-\upsilon)}{4 r_o G} \eta$$

where η represents the ratio of the under-reamed pile radius to the radius of the pile shaft. Since the pile is incompressible, the pile head stiffness may be obtained by summing the shaft and base stiffnesses, to give the following closed form solution for a cylindrical pile:

$$\frac{P}{G r_o w} = \frac{P_b}{G r_o w_b} + \frac{P_s}{G r_o w_s} = \frac{4}{\eta(1-\upsilon)} + \frac{2\pi}{\varsigma} \frac{l}{r_o}$$

Incorporation of pile compressibility and soil inhomogeneity

The expression for the settlement of the pile shaft may be changed to take account of pile compressibility by allowing both w_s and τ_o to vary along the pile shaft (i.e. with z):

$$w_s(z) = \zeta \frac{\tau_o(z) r_o}{G_s}$$

The compressive strain in a compressible pile shaft is a function of the load level P(z):

$$\gamma(z) = \frac{\partial w(z)}{\partial z} = \frac{-P(z)}{A_o E_p} = \frac{-P(z)}{\pi r_o^{\,2} \lambda G_s}$$

where $\lambda = E_p/G$. The loads and shear stresses may be related quite simply by the expression:

$$\frac{\partial P(z)}{\partial z} = -2\pi r_o \tau_o(z)$$

Either a homogeneous or a Gibson soil (soil stiffness varying linearly with depth, with slope m) may be modelled, with the distribution of shear stress $\tau_o(z)$ having a similar profile. The degree of inhomogeneity with depth is captured by the ratio ρ, which relates the shear modulus at mid-depth to that at the end of the pile shaft of length l. End bearing piles may be modelled by a stiffness increase at base level defined by ξ:

$$G(z) = G_o + mz \qquad \rho = \frac{G_{l/2}}{G_l} \qquad \xi = \frac{G_l}{G_B}$$

When all of these factors are considered, the result is the following closed form solution for pile head stiffness :

$$\frac{P}{G_l r_o w} = \frac{\dfrac{4\eta}{\xi(1-\upsilon)} + \dfrac{2\pi}{\zeta}\rho\dfrac{\tanh(\mu l)}{\mu l}}{1 + \dfrac{1}{\pi\lambda}\dfrac{4\eta}{\xi(1-\upsilon)}\dfrac{l}{r_o}\dfrac{\tanh(\mu l)}{\mu l}}$$

where:

$$(\mu l)^2 = \frac{2}{\zeta\lambda}\left(\frac{l}{r_o}\right)^2$$

$$r_m = 2.5\frac{l}{r_o}\rho(1-\upsilon)$$

This method enables a quick estimate of the secant pile head stiffness corresponding to a given secant shear stiffness value of the soil. Conversely, initial stages of measured single pile load test data may be used in conjunction with this expression to backfigure the initial 'elastic' stiffness of the soil modified by installation. A feature of all load transfer approaches is that only the split between shaft and base may be determined; it is not possible to compute the load distribution along the pile shaft. The proportion of pile head load carried at the pile base is given by (Randolph 1994 and others):

$$\frac{P_b}{P} = \frac{\dfrac{4\eta}{(1-\upsilon)\xi}\dfrac{1}{\cosh\mu l}}{\dfrac{4\eta}{(1-\upsilon)\xi} + \rho\dfrac{2\pi}{\zeta}\dfrac{\tanh\mu l}{\mu l}\dfrac{l}{r_o}}$$

A rigorous treatment of layered soil deposits is precluded by this approach. However Poulos (1989) illustrates how a suitable average soil stiffness may be chosen, which may vary with depth so as reflect the general trend of stiffness within the individual layers. Randolph and Wroth (1978b) claim that for the low strain levels developing at typical working loads, elastic pile stiffnesses determined by this analytical approach differ by no more than 20% from the results of more rigorous boundary element and finite element analyses.

2.3.2 RATZ (Randolph 1986)

RATZ incorporates two distinct load transfer options for monotonic loading. The first is a *general* curve which is intended to be sufficiently flexible to enable most aspects of soil

response to be captured. The curve is shown in Figure 2-4, with three distinct portions identified. These are:

(a) A linear stage extending from zero shear stress up to some proportion, ξ, of the peak shear stress, τ_p. The shear stress (τ_o) is proportional to the pile displacement normalised by the pile radius (w/r_o). The constant of proportionality may be related to the shear modulus (Randolph and Wroth 1979) according to:

$$k = \frac{G}{\ln\left(\frac{r_m}{r_o}\right)}$$

(b) A parabolic stage with gradient reducing from k at $\tau=\xi\tau_p$ to zero at $\tau=\tau_p$,

(c) A strain softening stage ($\tau>\tau_p$) in which the skin friction is related to the absolute pile displacement according to:

$$\tau_o = \tau_p - 1.1(\tau_p - \tau_r)\left[1 - \exp(-2.4\left(\frac{\Delta w}{\Delta w_{res}}\right)^{\eta})\right]$$

The residual skin friction is given by τ_r at a post peak displacement of Δw_{res}. The shape of the curve is fixed by the parameter η.

The value of ξ determines the proportion of the pre-peak displacement which is linear or parabolic and may be set to either extreme, with values of 1 and 0 respectively. Typical values of the strain softening parameter η are about unity, with larger values causing more gradual and smaller values causing more sudden strain softening.

Alternatively, a true hyperbolic curve may be used in the form reported by Kraft *et al* (1981). The ratio of secant to initial shear modulus (G_{sec}/G_o) varies linearly with stress ratio (τ/τ_f). The shear stiffness at $\tau=\tau_f$ is fixed by the value of R_f.

$$\frac{G_{sec}}{G_o} = 1 - R_f\left(\frac{\tau}{\tau_f}\right)$$

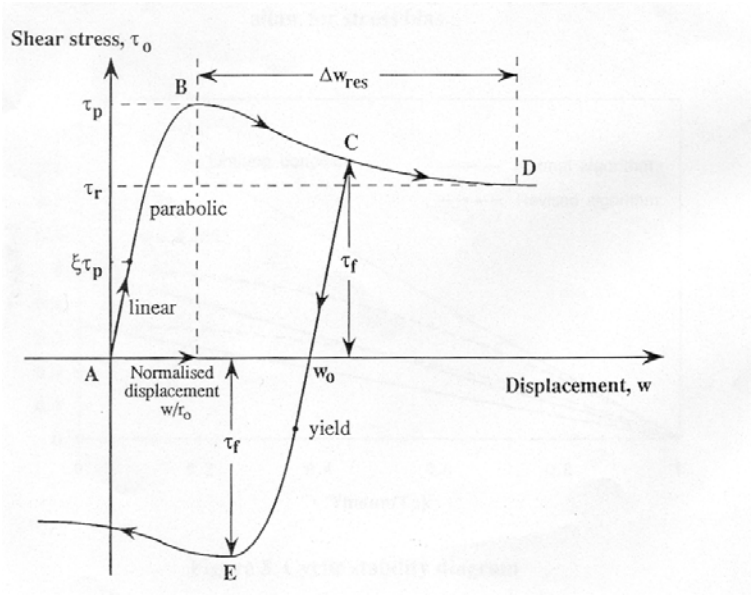

Figure 2-4 General load transfer curve available in RATZ

The load transfer curve, based on this hyperbolic response, effectively replaces the linear load transfer factor ζ (Randolph and Wroth 1978b) with its hyperbolic equivalent ζ*.

$$\zeta^* = \ln\left[\frac{\frac{r_m}{r_o} - \psi}{1 - \psi}\right] \qquad \psi = R_f \frac{\tau_o}{\tau_p}$$

The base response is assumed to be parabolic in form (the vertex positioned at ultimate base load) with unloading and reloading assumed to remain elastic. A hyperbolic base response in which the stiffness of the pile base spring $(k_b)_{sec}$ reduces with increased load level is also available, according to:

$$\left(k_b\right)_{\text{sec}} = 2\frac{q_{bf}}{w_{bf}}\left(1 - \frac{q_b}{q_{bf}}\right)$$

where q_b and w_b denote base stress and displacements and subscript f denotes failure. With either load transfer model, the solution of the differential equation governing pile behaviour is cumbersome using conventional means. This is somewhat alleviated in RATZ where the

pile is discretised into a number of elements and an explicit time stepping integration approach is used. Other features of RATZ's monotonic loading capabilities include creep effects, external pile movements, residual stresses and thermal strains.

Many soils respond with considerable non-linearity and in many cases, a parabolic curve gives a closer fit. The m term in the following expression conveniently represents the ratio of the displacement at full shaft friction to the extrapolated elastic response:

$$\frac{w}{r_o} = m\zeta \frac{\tau_p}{G_o}\left[1-\left(1-\frac{\tau_o}{\tau_p}\right)^{\frac{1}{m}}\right]$$

where τ_p is the limiting shaft friction. Care should be exercised in fitting a hyperbola to the shaft response, where a significant proportion of the shaft displacement occurs far from the pile in soil at low shear stress levels. The ultimate shaft load is reached abruptly (typically of the order of 1% of the pile diameter).

2.3.3 CEMSET (Fleming 1992)

The use of a single amalgamated hyperbolic load transfer curve to represent combined shaft and base responses stems from Chin (1970, 1972). A single hyperbola, however, does not always provide an acceptable fit to measured data. In addition, Chin's extrapolation procedure is only used to define ultimate loads and is not linked with soil parameters.

Fleming (1992) improves upon this approach by assigning separate hyperbolic load-displacement functions to the shaft and base of a pile. Each curve is related to soil parameters obtainable from laboratory tests. The elastic shortening of the pile is computed independently and both elements are combined in the CEMSET algorithm.

Stage 1: Hyperbolic load transfer curves

Chin's hyperbolic extrapolation procedure enables a prediction of the ultimate capacity (at infinite displacement) of a rigid pile as the inverse slope of a plot of w/P versus w, where w and P represent the pile head settlements and loads respectively. Treating the shaft

(subscript s) and base (subscript b) responses separately, Figure 2-5 shows that the ultimate capacity ($P_{s\,ult}$) may be expressed as:

$$P_{s\,ult} = \frac{w_s}{\frac{w_s}{P_s} - K_s} \qquad \Rightarrow w_s = \frac{K_s P_{s\,ult} P_s}{P_{s\,ult} - P_s}$$

where K_s is the (initial elastic tangent) value of w/P at low values of w. Since the shaft settlement (w_s) is proportional to the pile diameter and many studies indicate that K_s varies inversely with P_s, the three terms may be related by a dimensionless influence factor (M_s) which typically lies in the range 0.001-0.004. M_s is equivalent to $\xi\tau_s/2G$ in the notation of Randolph and Wroth (1978).

$$K_s = \frac{M_s D_s}{P_s}$$

This leads to the following hyperbolic load-settlement relationship for the pile shaft:

$$w_s = \frac{M_s D_s P_s}{P_{s\,ult} - P_s}$$

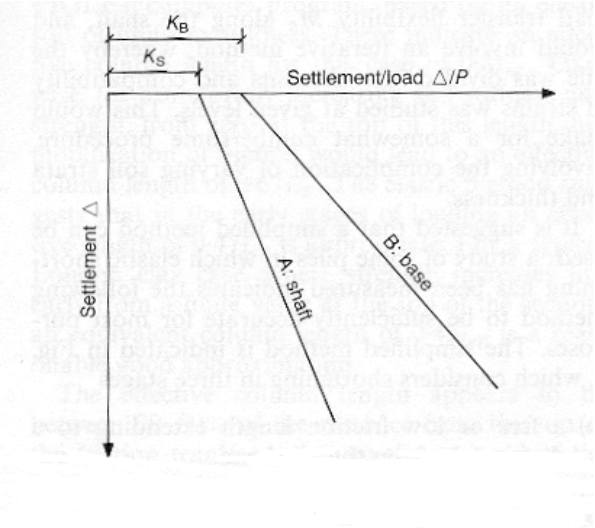

Figure 2-5 Individual shaft and base performances (Fleming 1992) [3]

[3] Δ in the notion of Fleming (1992) is represented in this section by w.

The ultimate base capacity of the pile can be expressed by a corresponding hyperbolic formulation:

$$w_b = \frac{K_b P_{b\,ult} P_b}{P_{b\,ult} - P_b}$$

The initial elastic K_b value is assessed by considering the following linear expression for the settlement of a circular footing (of diameter D_b), where E_b is the modulus of the soil underneath the footing, q is the applied base pressure and f_1 is a settlement reduction factor related to depth:

$$w_b = \frac{\pi}{4}\frac{q}{E_b} D_b \left(1-\upsilon^2\right) f_1$$

The secant value of E_b used is typically that at one quarter of the ultimate stress in non-linear situations ($P_{b\,ult}/4$), which, when υ=0.3 and f_1=0.85 leads to:

$$w_b = \frac{0.6075 q D_b}{E_b}$$

At a load of $P_{b\,ult}/4$, the coefficient K_b can be determined at the point where the hyperbolic function and the linear elastic functions coincide, giving:

$$K_b = \frac{0.6}{D_b E_b}$$

whereupon, the base settlement may be expressed as:

$$w_b = \frac{0.6 P_{b\,ult}\ P_b}{D_b E_b (P_{b\,ult} - P_b)}$$

The total load settlement behaviour of the rigid pile is obtained by rearranging the expression for shaft and base settlement so that shaft and base loads sum to the applied total load; for a rigid pile w_s=w_b=w_t.

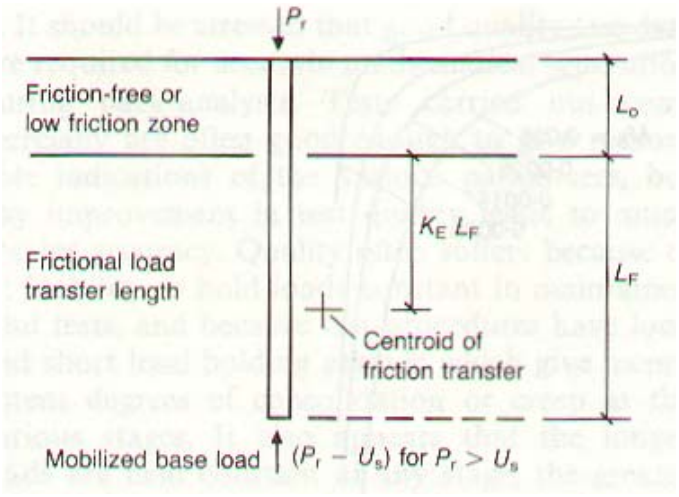

Figure 2-6 Simplified method for calculating elastic shortening

Stage 2: Elastic shortening of the pile

A rigorous determination of pile shortening is computationally cumbersome; an approximation sufficiently accurate for most scenarios is detailed by Fleming (1992). Figure 2-6 clarifies the method of calculating elastic shortening; three stages are considered: (a) a free or low friction zone extending a distance of L_o below the pile head, (b) a length l_f over which friction is transferred and (c) the whole pile shortening as a column once ultimate shaft friction has been reached.

The elastic shortening of the first stage is straightforward and for a circular pile with $E=E_c$, it is given by:

$$w_1 = \frac{4}{\pi} \frac{L_o P_t}{D_s^{\,2} E_c}$$

The second stage represents the elastic shortening up to the point at which the peak friction arises, and will be equivalent to that of a column of effective length $K_e L_f$, with K_e depending upon a number of factors, including the soil stiffness profile.

$$w_2 = \frac{4}{\pi} \frac{K_e L_f P_t}{D_s^{\,2} E_c}$$

When P_t exceeds P_s, additional load causes shortening of the full length L_f so that it may be treated as a column carrying the excess load, with

$$w_3 = \frac{4}{\pi} \frac{L_f \left(P_t - P_s\right)}{D_s{}^2 E_c}$$

The total elastic shortening is w_1+w_2 pre-peak and w_1+w_3 post-peak. Fleming (1992) publishes design charts based on these equations which enable the total settlement to be determined.

Stage 3: *Linking the hyperbolic functions to soil parameters*
The principal design values are M_s for shaft loading and E_b for base loading. These require good quality test data for accurate mathematical separation during back-analysis.

2.3.4 Semi-Empirical Load Transfer Curves

Both model and full-scale tests on instrumented piles in a wide variety of soil conditions have lead to the development of a number of semi-empirical load transfer curves. Coyle and Reese (1966) describe load transfer processes in clay soils; the behaviour of granular material is reported by Coyle and Sulaiman (1967). Vijayvergyia (1977) describes curves for both granular and cohesive soils on which the API RP2A (1993) design recommendations are based.

The API RP2A (1993)-recommended curves for non-carbonate soils are provided in terms of the normalised shaft and base stresses (t/t_{max} and $P_b/P_{b\,max}$) as a function of the local pile deflection normalised by the diameter (z/D), and are shown in Figure 2-7 and 2-8 respectively. The post peak softening data (assumed to lie somewhere within the range 0.7-0.9 t_{max}) is intended only as a guide and are best supplemented with laboratory testing which replicate factors including stress-strain behaviour and stress history, pile installation process and pile load sequence. Responses to lateral load (p-y curves) are also recommended.

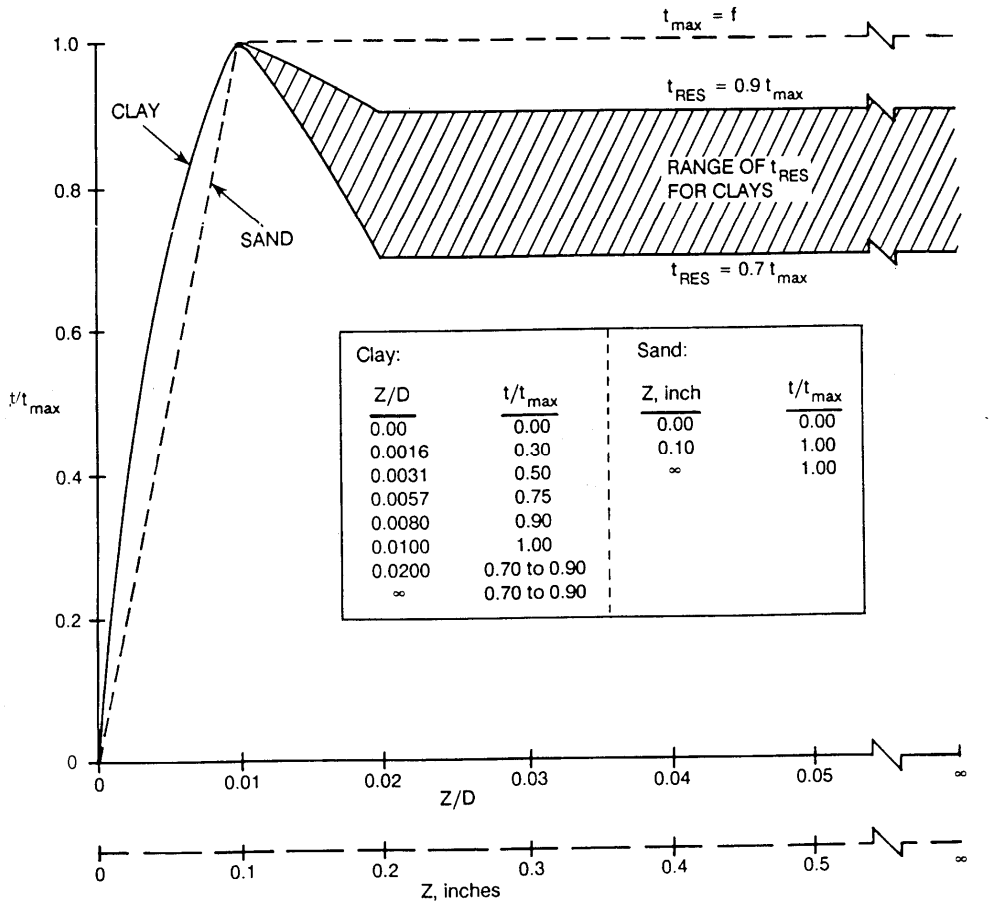

Figure 2-7 Pile shaft load transfer curves API RP2A (1993)

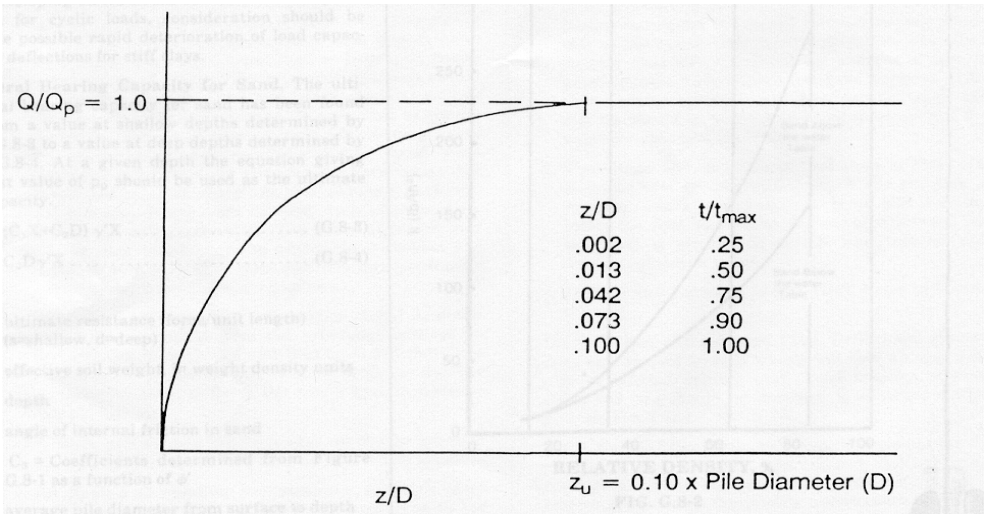

Figure 2-8 Pile base load transfer curves API RP2A (1993)

2.4 Methods of Analysing Piles subjected to Cyclic Loading

Piles, particularly those in offshore environments, may be subjected to regular load cycles. Cycling may either be one-way (compression or tension) or two-way (tension and compression). Some of the methods used to assess the shear stress degradation associated within cyclic loading are described in this section.

2.4.1 RATZ

The RATZ load transfer approach for monotonic loading of single piles (Section 2.3.2) may be extended to cater for load cycling by modelling the degradation in the load transfer capability of a pile. The general load transfer model (Figure 2-4) must be employed for this purpose (the hyperbolic model is precluded). Emphasis is placed upon determining the cyclic yield criteria for which three approaches are available.

The standard yield criterium is based on the assumption that the yield point descends the unloading path at a rate of 0.5(1-ξ) times the current stress displacement point. The yield point (τ_y) is thus defined in terms of minimum (τ_{min}) and peak (τ_p) skin friction values:

$$\tau_y = \tau_{\min} + 0.5(1+\xi)\left(\tau_p - \tau_{\min}\right)$$

constraining the yield stress never to exceed the initial yield point ($\xi\tau_p$). The post-peak plastic displacement is treated in the same manner as for monotonic loading. This results in gradual degradation from peak to residual skin friction. This will occur if τ_{max} exceeds the elastic limit, which is given by the following expressions (for one-way (left) and two-way cycling (right)).

$$\tau_{\max} = 0.5(1+\xi)\tau_p \qquad \tau_{\max} = \left[\frac{1+\xi}{3+\xi}\right]\tau_p$$

For loose or compressible soils with a tendency to contract under cyclic loading, experimental observations show that a more conservative expression is relevant and has been incorporated in RATZ:

$$\tau_y = \tau_{\min} + \left(\xi\right)\left(\tau_p - \tau_{\min}\right)$$

The cyclic loading algorithm is capable of showing the number of cycles to failure for loading of various frequency, amplitude and mean stress. The effect of the pile radius and the various load transfer parameters may be ascertained. This approach may also be modified by including parabolic yield criteria (Poulos 1988).

2.4.2 Interaction Diagram (Karlsrud and Haugen 1986)

Karlsrud and Haugen (1986) carried out a number of one- and two-way cyclic tests on instrumented piles[4] in Haga clay. The results are presented in the form of the interaction diagram in Figure 2-9. The interaction diagram allows the number of cycles to failure to be determined for any combination of the mean cyclic load Q_{ave} and the cyclic load amplitude Q_c. Both of these measures of cyclic load are normalised by the reference static capacity Q_s, carried out in advance of the cyclic test. Peak cyclic loads are corrected for the influence of prior shearing (see Section 2.5.2).

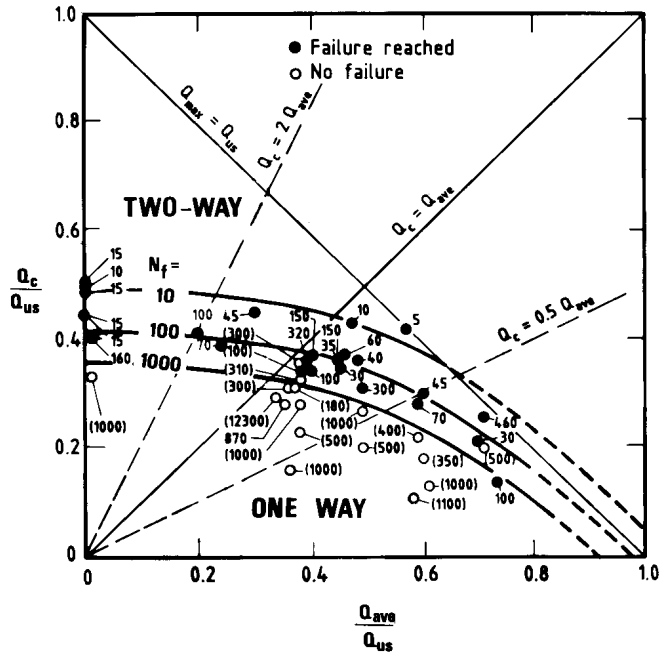

Figure 2-9 Cyclic interaction diagram (Karlsrud and Haugen 1986)

[4] L=5.15m, diameter = 153mm

The interaction diagram shows that the number of cycles to failure depends on cyclic load level. Also evident is the smaller cyclic capacity under two-way loading than one-way loading; the reduction in capacity appears to occur gradually as the average load Q_{ave} decreases and the cyclic load pulse Q_c increases.

2.4.3 Cyclic Stability Diagram (Poulos 1988)

Poulos (1988) is responsible for the cyclic stability diagram concept in which the mean and cyclic axial loads on a pile are plotted and three regions are identified (Figure 2-10):

(i) A stable zone in which cyclic loading has no effect on pile capacity (A)

(ii) A metastable zone in which cyclic loading causes some limited reduction of load capacity (B).

(iii) An unstable zone in which cyclic loading will result in failure of the pile within a specified number of cycles (C).

The stability diagram is a useful means of defining the response of a pile to various combinations of mean load and cyclic load amplitude[5]. The upper boundary to the cyclic stability diagram is the pair of straight lines (FC and TF) that represent the combinations of mean and cyclic loading necessary to cause failure if no degradation of load capacity occurs. These upper boundary lines are defined as follows:

$$Failure\ \ in\ \ Compression\ \ (CF) \qquad \frac{P_o}{Q_c}+\frac{P_c}{Q_c}=1$$

$$Failure\ \ in\ \ Tension\ \ (TF) \qquad \frac{P_o}{Q_c}+\frac{P_c}{Q_c}=-\frac{Q_t}{Q_c}$$

For the cyclic stability diagram shown above, as N increases, the stable and meta-stable zone boundaries will tend to move, with the cyclically unstable zone C increasing in size. Poulos (1988) states that it is possible that some strength increase may occur around the pile due to reconsolidation of the clay following relatively low levels of cyclic loading. However, these effects cannot be easily taken into account in the present analysis.

[5] The pile is subjected to N cycles from a minimum $P_{min}=P_o-P_c$ to a maximum load $P_{max}=P_o+P_c$

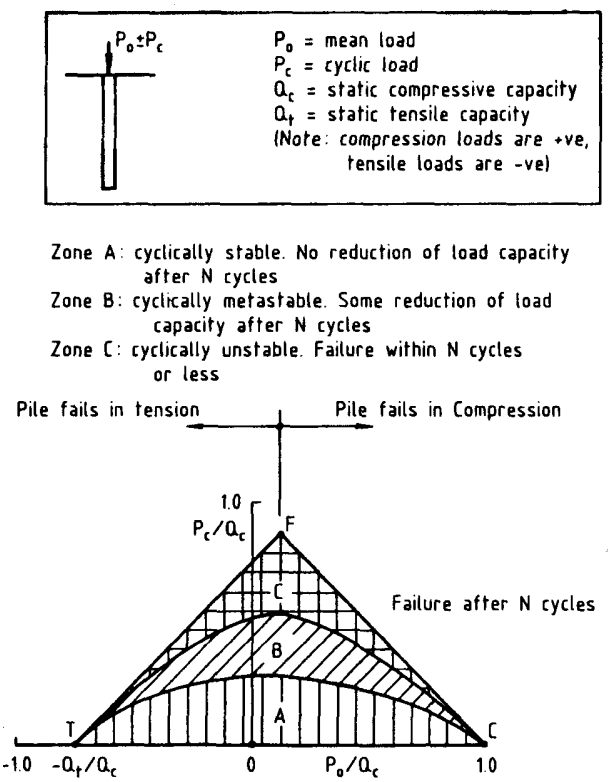

Figure 2-10 Cyclic stability diagram (Poulos 1988)

2.5 Time Related Effects on Pile Capacity

Research has shown that the capacity of piles may be time-related. Two such time-related effects are referred to in this Thesis as 'undisturbed aging' and 'aged (drained) reloading', and have been quantified approximately for single piles in Haga soft clay by Karlsrud and Haugen (1986).

2.5.1 Undisturbed aging

Undisturbed aging describes increases in soil shear strength of a soil over time which are unrelated to changes in effective stress but probably due to chemical changes in the soil/pore water and/or pile material. Once full equalization has been reached, piles in certain soils continue to show a gain in capacity with time. A suite of mainly tension pile tests (in which different periods were observed between installation and loading[6]) showed

[6] but ensuring full equalization was achieved.

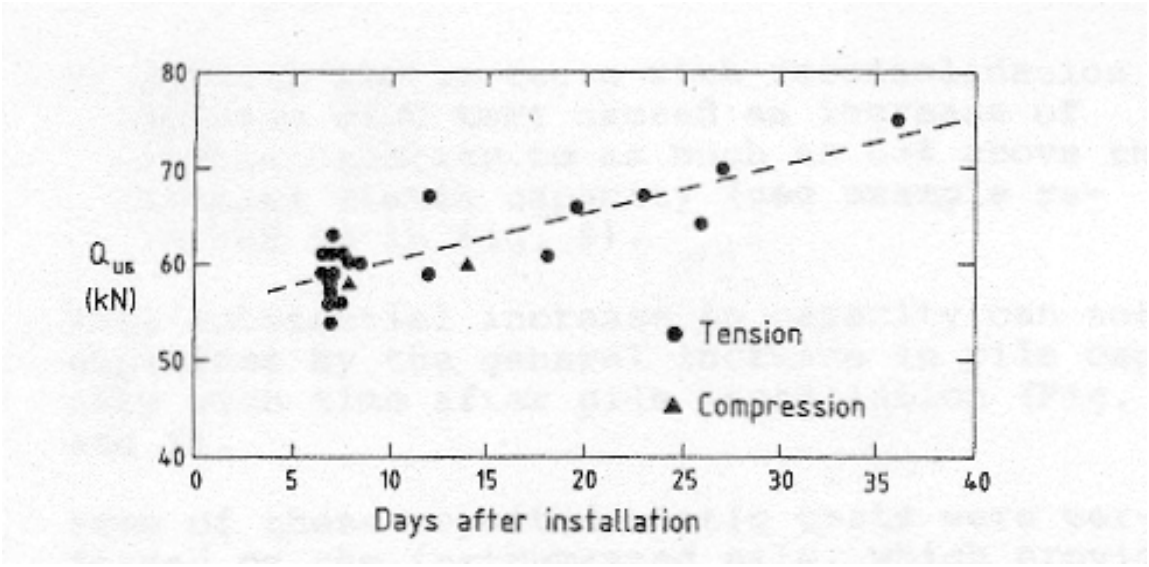

Figure 2-11 Aging effects in Haga clay (Karlsrud and Haugen 1986)

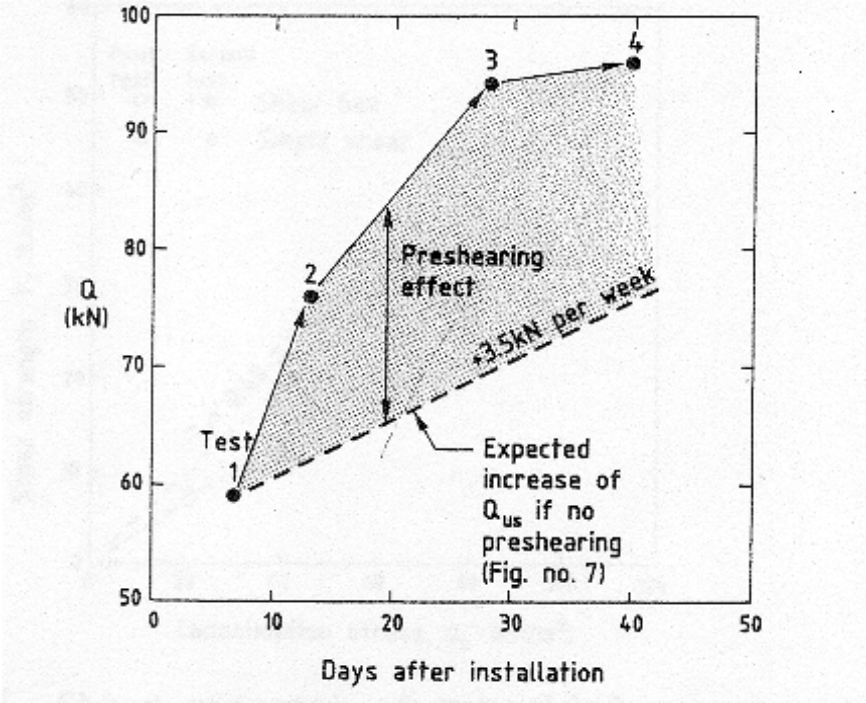

Figure 2-12 Separation of aged reloading and aging effects in Haga clay (Karlsrud and Haugen 1986)

that pile capacity in Haga clay typically gains ≈3.5kN per week due to undisturbed aging (up to a period of 40 days since driving, Figure 2-11).

2.5.2 Aged reloading

Another feature of the Haga tests was the capacity gain that arose when piles were loaded for the second time, with further gains arising from subsequent re-tests. The virgin static capacity of a Haga pile and the 'total' capacity increase with further retesting is presented in Figure 2-12. This 'total' capacity gain incorporates both the effects of aged reloading and undisturbed aging; so the data of Figure 2-11 is superimposed to separate reloading (or pre-shearing) effects.

The capacity gain at Haga for first reloading (due to preshearing alone) is ≈25%. The magnitude of the capacity gain decreases with further load testing. Repeated simple shear tests on remoulded reconsolidated clay specimens produced a similar capacity gain, but the same trend was notably absent from tests on intact samples.

Part 2

Pile Groups

2.6 Introduction to the Analysis of Vertically Loaded Pile Groups

The primary goal of pile group analysis is to determine the overall absolute or differential settlement of the group. An accurate prediction of the response of a single pile is fundamental to the problem. The solution also relies heavily on accurate estimation of any additional settlement a pile will experience when neighbouring piles are loaded. Prediction methods fall into two broad categories: (a) simple empirical methods such as the equivalent raft and equivalent pier methods amenable to hand calculations and (b) numerical approaches which are benefitting from the ongoing development of computer resources. The processing time in approaches of type (b) is a function of factors including the rigour of the analysis technique, the number of piles in the group and the complexity of soil model chosen. In design office situations, a compromise must be reached between the accuracy/reliability of the solution and the time/expense entailed in achieving it. For example, the assumption of a linear elastic soil may liberate computer resources to examine large pile groups, whereas the size of pile groups examinable will be curtailed should a more representative non-linear soil model be employed.

The more rigorous methods involve a complete group analysis, where the pile group is examined as a unit. A less thorough but widely employed approach involves the use of *interaction factors,* which are simple approximations to the interaction between each pair of piles within the group. The overall settlement of any group pile is computed by superimposing all pile-pair interactive displacements upon the displacement due to its own loading.

2.6.1 The Process of Pile Interaction

Analysis packages for pile groups address the calculation of increased settlement due to pile interaction, but assume that the piles are embedded in a soil which remains homogeneous within the group perimeter after installation.

A pile will settle under its own *applied* load; the attenuation of displacement down the pile shaft will depend upon how compressible the pile is in relation to the soil. A settlement field will be generated around this pile due to the horizontal transfer of shear stress. The

zone of influence of the pile extends to some radius r_m, beyond which its influence may be considered negligible. However, if other piles are located within the zone of influence of the first pile (i.e at spacings less than r_m), then they will be loaded themselves (by the shear stresses in the soil) and dragged downwards even though no *external* load has been applied (Figure 2-13). Therefore for a group pile to fully mobilize its shaft capacity, it must settle further than a corresponding single pile.

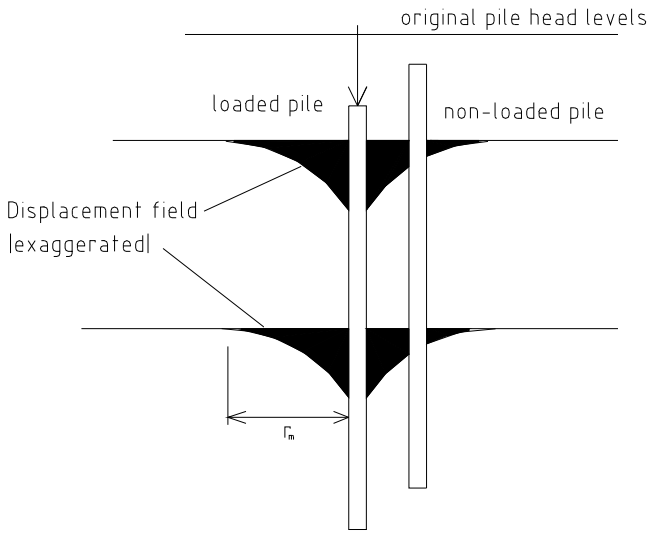

Figure 2-13 Load interaction between a pair of piles

Alternatively, pile interaction may be considered in terms of pile loads. The *absolute* capacities of all group piles are the same and equate to that of an isolated single pile (provided the soil within the group is assumed to be homogeneous). However, the load that must be *applied* to a group pile to bring it to 'ultimate conditions' is less than this absolute capacity, because a group pile is simultaneously carrying some load that is transmitted through the soil from neighbouring loaded piles. In the absence of an 'installation effect', group piles will carry lower loads than single piles due to load interaction.

A group of piles with a flexible pile cap will be constrained to carry equal load. In this instance, those piles subjected to most interaction, i.e. the interior piles will settle furthest, with external piles settling least. In practice, pile caps are closer to being rigid than flexible,

whereupon the whole group settles relatively uniformly. The interior piles now cannot mobilize as much load as the exterior piles as they are restricted to the same displacement as the exterior piles. As a result, the load is biased towards the outside of the group, with interior piles carrying lower proportions of the group load.

2.6.2 Interaction factors

A convenient method of quantifying the displacement interaction between piles is the "interaction factor" (often denoted α) originating from the work of Poulos (1968), This quantifies the displacement of a pile, over and above that due to its own loading, which arises from the loading of an identical neighbouring pile. The total settlement (w_{tot}) of the i-th pile within a group of n piles is given by:

$$w_{tot} = w_i + \sum_{j=1}^{n} w_j \alpha_{ij}$$

where w_i is the settlement of the i-th pile under its own loading.

Poulos (1980) presents interaction charts (for completely flexible and completely rigid pile caps) which show the dependence of interaction factors on soil inhomogeneity, pile soil slip, Poisson's ratio, underreamed bases, finite layer thickness and compressibility of the soil beneath pile base level. Their use for non-identical piles involve further simplifications.

The lateral variation of strain level between two interacting piles prompted the development of a modified interaction factor approach by Poulos (1988). This defines two distinct zones with different stiffnesses, a low stiffness (E_s) adjacent to the pile shaft reflecting higher strains and a higher value (E_{sm}) removed from the piles reflecting lower strains. A weighted average value (E_{sav}) is used in the interactive analysis, as shown in Figure 2-14. The effect of concentrating strains closer to the piles is to reduce the interactive settlements in relation to those predicted by the classical interaction approach. The extent of the reduction depends on υ, pile spacing and geometry and the relative stiffness of the piles.

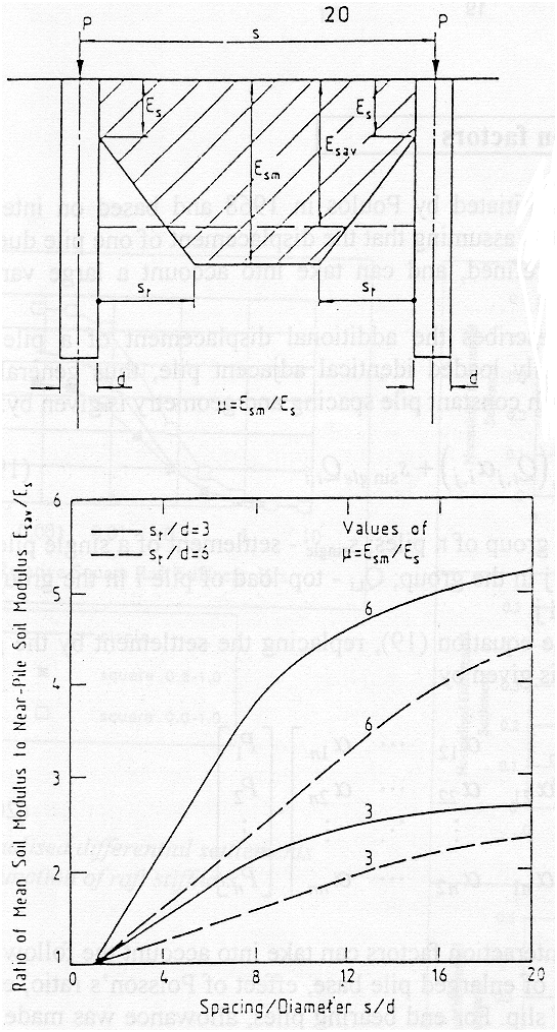

Figure 2-14 Modified interaction factor approach (Poulos 1988)

Interaction factors are typically used in conjunction with the load transfer methods as an alternative to considering full continuity in the soil. However simplified continuum based models have been developed incorporating interaction factors, generally with the aim of cutting down on levels of computation.

2.6.3 Pile Group Analysis Techniques

A number of standard pile group analysis approaches are discussed in Sections 2.7 to 2.10; some are empirical, while others are numerically based.

The equivalent raft approach is widely used to estimate group settlement; a particular pile group may be idealized as an equivalent raft foundation loaded at some depth below the piles heads. The equivalent raft dimensions are dictated by the overall dimensions of the pile group. Alternatively the group may be modelled as a single 'pier' foundation of the same size as the group, whose stiffness is a weighted average of the pile and soil material.

The analytical procedures available for predicting pile group settlement are quite diverse but most fall within the following three categories:

- *Continuum-based methods*: these methods allow a complete and thorough analysis of the pile group acting together as a unit and entail either finite element or boundary element methodologies. Methods exist involving various degrees of rigour.
- *Load transfer methods*: these are based on measured or theoretical relationships between load and settlement for the shaft and base of a single pile. Continuity of the pile and soil mass is ignored (i.e piles are considered as discrete/independent objects), so predictions are generally less accurate than in (a). The effects of group action are catered for through the use of *interaction factors.*
- *Hybrid methods*: single pile responses are determined from (non-linear) load transfer springs, and subsequently coupled with a continuum model used to assess interaction between piles.

2.7 Empirical pile group analysis methods

2.7.1 Equivalent Raft

Numerous equivalent raft approaches have been proposed (e.g. Bowles 1988, Van Impe 1989, Tomlinson 1994) which assume that the piled area behaves as a buried raft foundation, whose rigidity depends on the cap flexibility and the superimposed structure. A load spread of 1 in 4 is assumed (Tomlinson 1994) to allow for load transferred to the soil in skin friction. The position of the base of the equivalent raft depends on the mechanism of load transfer, as shown in Figure 2-15.

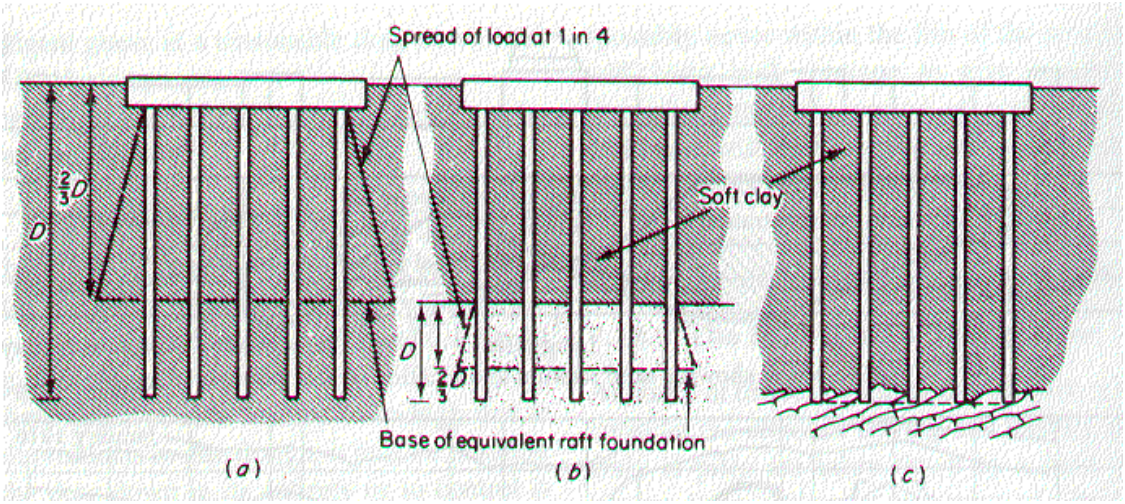

Figure 2-15 Load transfer between piles and soil (after Tomlinson 1994)

Once the raft dimensions are decided, the net immediate (elastic) settlement beneath the flexible loaded area may be calculated from the equation:

$$w_i = qB\frac{1-\upsilon^2}{E_u}I_p$$

where B is the raft width, E_u is Young's modulus for undrained loading, υ is Poisson's ratio, q is the net foundation pressure acting at raft base level and I_p is an influence factor. Replacement of E_u with the drained modulus E' allows total settlement (immediate and consolidation) to be estimated. The influence factor (I_p) is a function of the thickness of the compressible layer (H/B < 4) and the length to width ratio (L/B) and may be determined from the curves of Steinbrenner (Figure 2-16).

The Steinbrenner curves assume that the deformation modulus is constant with depth. Butler (1974) suggests a linear variation of soil modulus with depth of the form:

$$E_d = E_f\left(1+\frac{kz}{B}\right)$$

where E_f is the soil modulus value at raft level.

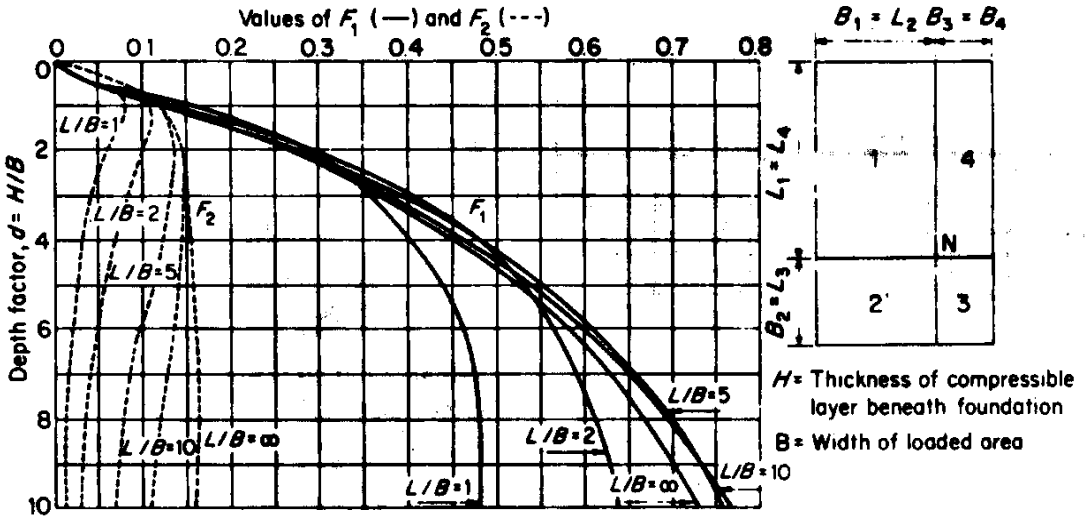

$$\upsilon = 0.5 \qquad I_p = F_1$$

$$\upsilon = 0 \qquad I_p = F_1 + F_2$$

Figure 2-16 Steinbrenner's curves for determining Influence Factor (I_p) beneath corner of loaded area

The influence factor (I_p) may be determined from Butler's curves (Figure 2-17) once a suitable value of k is calculated from measurements of E_d (υ=0.5). Further corrections which may be applied to be immediate settlements are as follows:

(a) A rigidity factor, typically 0.8, is applied to the calculated settlement in the case of a rigid foundation,
(b) A depth factor, recognising the effect of foundation depth on immediate settlement, determined curves attributable to Fox (1948).

Where E_d may be assumed constant with depth, it is more convenient to work with the average immediate settlement ($w_{i\,av}$) of the raft is given by the expression (Christian and Carrier 1978) for a homogeneous soil deposit:

$$w_{iav} = \frac{\mu_0 \mu_1 qB}{E_u}$$

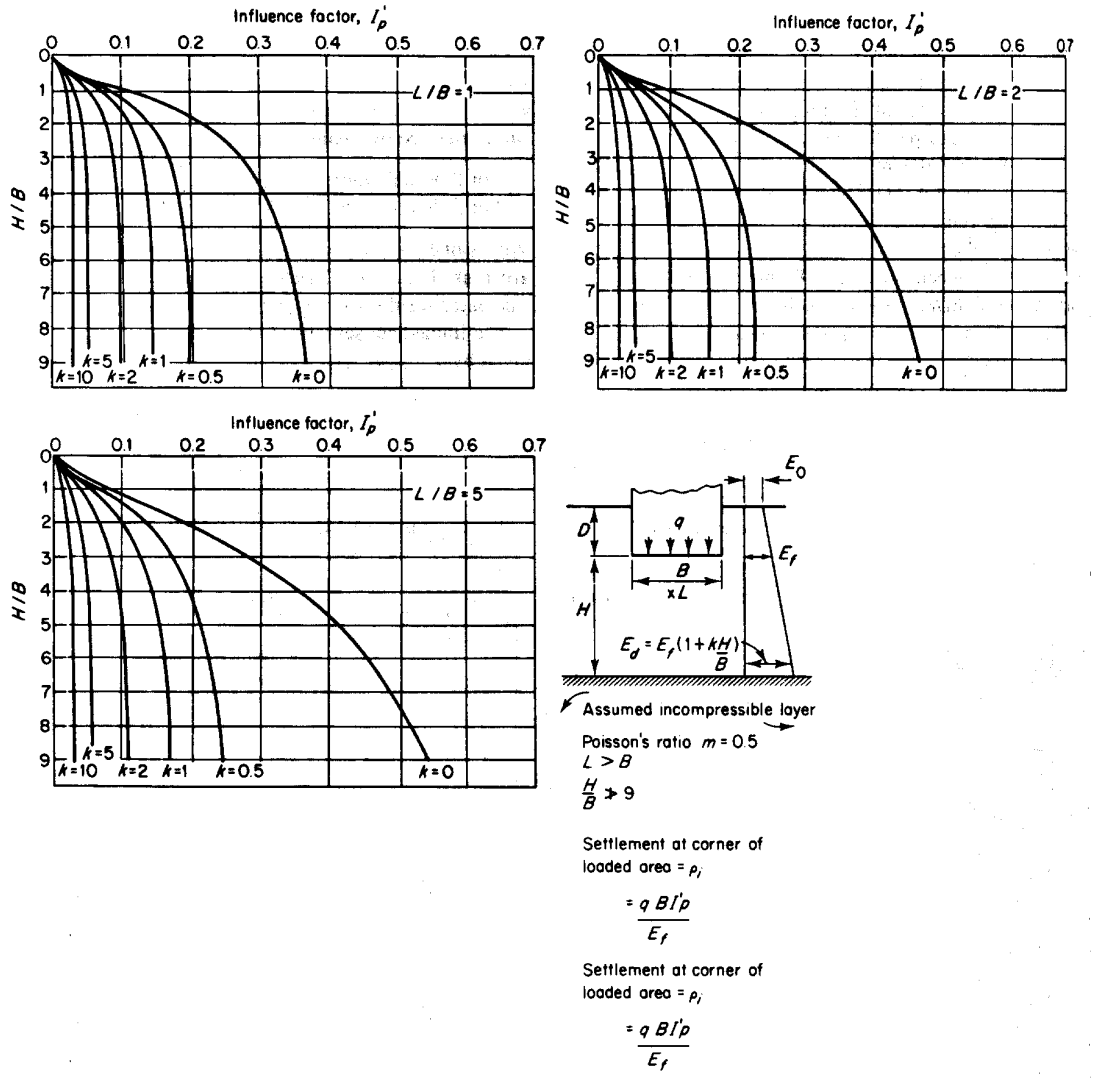

Figure 2-17 Butler's curves for Gibson soil

μ_0 is a function of the depth of the equivalent raft (D/B) and μ_1 depends upon the length to width ratio of the raft (L/B) and the depth of compressible soil underlying the raft (H/B) as shown in Figure 2-18. This expression is subject to neither the rigidity nor depth corrections described.

The validity of the settlement predictions described by Tomlinson (1994) strongly depend upon the selection of a suitable value of E_u, derived from plate bearing tests in boreholes or

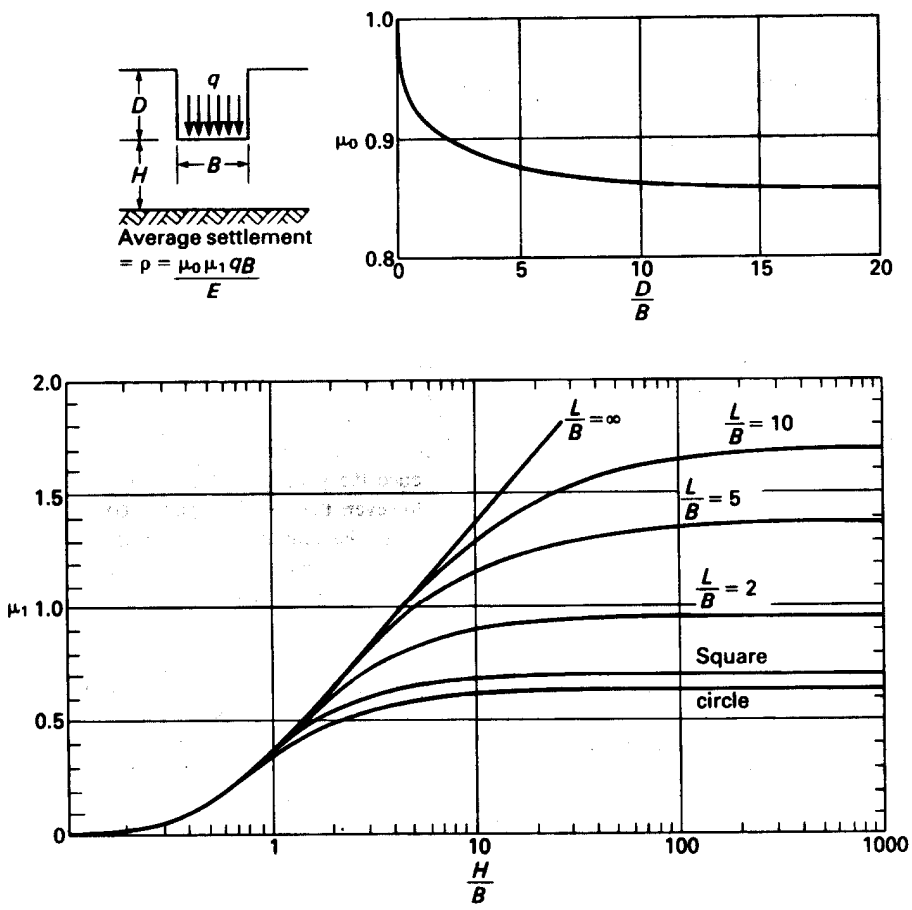

Figure 2-18 Christian and Carrier (1978) μ_0 and μ_1 parameters

trial pits or from in-situ pressuremeter or Camkometer tests. E_u is typically determined as the secant to the stress-strain curve at 1.5 times the compressive stress at the base of the equivalent raft.

Variations in soil stiffness (E_s) beneath the raft are catered for by the approach of Poulos (1993) which is based upon elastic influence factors (I_ε) for the vertical strain distribution below the raft. The embedment depth is not related to the ground surface but to the top of the main bearing stratum. Fox's correction (F_d) for raft embedment below the ground surface is then incorporated. The influence factors in Figure 2-19 pertain to the centreline of the raft and the value of w_{raft} should be reduced by approximately 20% to represent the average raft settlement.

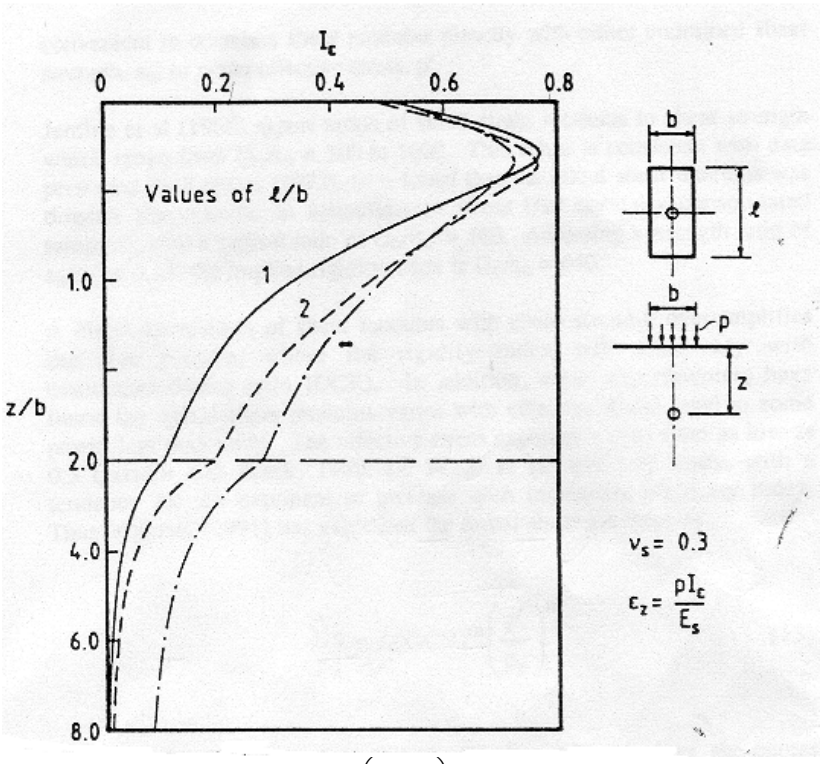

$$w_{raft} = F_d\, q \sum_{i=1}^{n} \left(\frac{I_\varepsilon}{E_s} \right)_i h_i$$

Figure 2-19 Influence factors for vertical strain (Poulos 1993)

A different form of the equivalent raft method was devised by Van Impe (1988), which is most relevant to groups of closely spaced piles and distinguishes between predominantly shaft and end-bearing piles. For a pile group of length L and width B, the settlement of the equivalent raft is assumed to arise over a depth of 1.5B below the raft base. If the pile group is embedded to a depth H, the raft is assumed to be founded at a depth H for end-bearing piles and at 2H/3 (as Tomlinson 1994) for friction piles. A schematic diagram is shown in Figure 2-20. The following (incremental) expressions are used in the settlement calculation:

End bearing :
$$w_{tot} = \sum_{z=H}^{H+1.5B} \sigma_{v,0,z} \frac{\Delta z}{E_s} \ln\left(\frac{\sigma_{v,0,z} + \Delta\sigma_z}{\sigma_{v,0,z}} \right)$$

$$\Delta\sigma_z = i_z \left(\frac{Q - F}{BL} \right)$$

$$F = 2\tau_m (B + L) H$$

Shaft friction :

$$w_{tot} = \sum_{z=\frac{2H}{3}}^{\frac{2H}{3}+1.5B} \sigma_{v,0,z} \frac{\Delta z}{E_s} \ln\left(\frac{\sigma_{v,0,z} + \Delta\sigma_z}{\sigma_{v,0,z}}\right)$$

$$\Delta\sigma_z = i_z\left(\frac{Q-F}{BL}\right)$$

$$F = 2\tau_m (B+L)\frac{2H}{3}$$

where $\Delta\sigma_z$ is the vertical effective stress increment at depth z in the middle of a layer of thickness Δz, i_z is the influence factor of Figure 2-19, Q is the effective building and foundation weight at z=H part of which (F) is discharged as shaft friction on the pile group perimeter, τ_m is the mobilised shaft friction on the outer perimeter of the pile group, $\sigma'_{v,0,z}$ is the initial vertical effective stress at z=H, and E_s is the Young's modulus. Both τ_m and E_s are derived from CPT data for which correlation tables are shown in Figure 2-21.

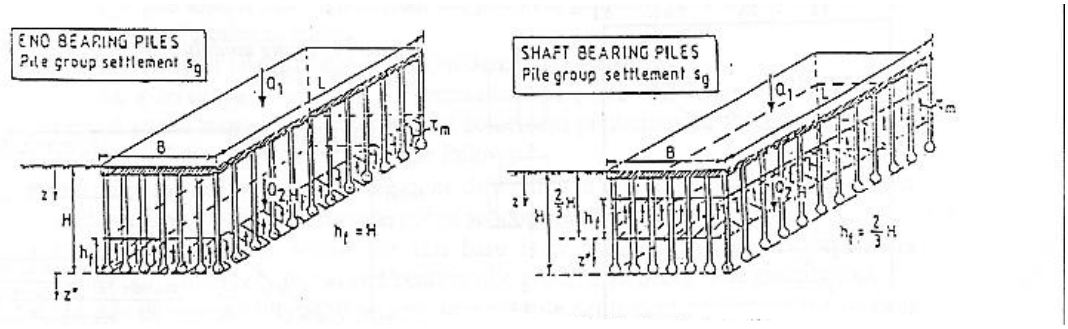

Figure 2-20 Van Impe's (1988) Equivalent Raft Method

TYPE OF PILE \ TYPE OF SOIL ALONG THE PILE SHAFT	CLEAN SAND (q_c > 8 MPa) and PREDOMINANTLY SANDY LAYERS (q_c > 15 MPa)	COMPACT SILT LOAMY OR CLAYEY SAND LAYERS (5 MPa < q_c < 15 MPa)	CONSISTENT CLAY 0.3 < I_f < 0.6 (2 MPa < q_c < 8 MPa)	STIFF CLAY I_f < 0.3 (q_c > 2 MPa)
DISPLACEMENT CONCRETE PILES	$\frac{1}{300}q_c$	$\frac{1}{500}q_c$	$\frac{1}{300}q_c$	$\frac{1}{350}q_c$

q_c = cone resistance from CPT-E1 tests; measured in the pile group after pile installation, at distances of 1.5 Ø pile from pile axis

TYPE OF PILE \ TYPE OF SOIL ALONG THE PILE SHAFT	CLEAN SAND (q_c > 8 MPa) and PREDOMINANTLY SANDY LAYERS (q_c > 15 MPa)	COMPACT SILT LOAMY OR CLAYEY SAND LAYERS (5 MPa < q_c < 15 MPa)	CONSISTENT CLAY 0.3 < I_f < 0.6 (2 MPa < q_c < 8 MPa)	STIFF CLAY I_f > 0.6 (q_c > 2 MPa)
DISPLACEMENT CONCRETE PILES	$\frac{1}{150}q_c$	$\frac{1}{200}q_c$	$\frac{1}{250}q_c$	$\frac{1}{300}q_c$
BORED PILES	$\frac{1}{300}q_c$	$\frac{1}{400}q_c$	—	—

q_c = cone resistance from CPT-E1 tests; measured in the pile group after pile installation, at distances of 1.5 Ø pile from pile axis

Figure 2-21(a) Correlations between τ_m and q_c (Van Impe 1988)

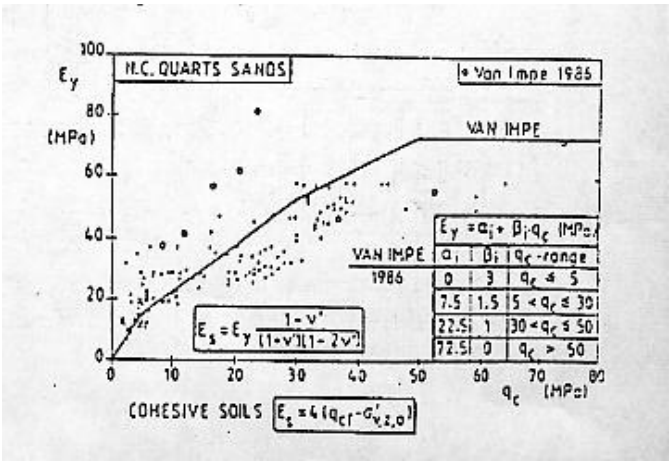

Figure 2-21(b) Correlations between E_s and q_c (Van Impe 1988)

This approach is only applicable if the n piles in the group (each with A_p as cross sectional area) are spaced sufficiently closely spaced to have:

$$\frac{nA_p}{BL} \geq 0.1$$

The value of w_{tot} should be corrected to account for the compressibility of the piles. Jessberger-Thaher (1990, 1991) extended the equivalent raft method by facilitating load transfer to the soil at several levels. This effectively involves the use of a number of component rafts instead of just one.

Experiences with equivalent raft methods in design may be summarized as follows:

(i) There is no unanimous agreement as to the equivalent raft dimensions,

(ii) The load distribution beneath the raft base is restricted only to elastic soil behaviour which may be acceptable for an end bearing group but not for a friction pile group,

(iii) The pile compressibility may be important in settlement prediction but there is insufficient evidence to include the corresponding value in raft settlement.

2.7.2 Equivalent Pier Approach

An alternative to the equivalent raft approach is found by considering the soil within the group perimeter as an equivalent continuum. The pile group is modelled as a pier of equivalent dimensions and stiffness (Poulos and Davis 1980) as shown in Figure 2-22. The equivalent pier is assumed to be of the same length as the piles and of diameter given by:

$$d_{eq} = \sqrt{\frac{4}{\pi} A_g} = 1.13\sqrt{A_g}$$

where A_g is the area of the group. The Young's modulus of the equivalent pier is given by weighting the moduli for pile (E_p) and soil (E_s) by the appropriate areas A_p and A_s respectively.

$$E_{eq} = E_p \frac{A_p}{A_g} + E_s\left(1 - \frac{A_p}{A_g}\right)$$

Equations providing the load-settlement response of a single pile may be applied to determine the *average* settlement of the equivalent pier, such as that by Randolph and Wroth (1978) or alternatively the design charts of Poulos and Davis (1980). Solutions for rock socketed piles (e.g. Carter and Kulhawy 1988) are particularly applicable as the L/D ratio of the equivalent pier will be similarly low.

Insight into whether a pile group behaves as a raft or pier (and thus the appropriateness of using either the equivalent raft or pier approach) is given by the overall aspect ratio (R) of the pile group (Randolph and Clancy 1993). For a group of n piles of diameter d separated by a spacing s, the value of R is:

$$R = \frac{\left(\sqrt{n} - 1\right)s + d}{L} \cong \sqrt{\frac{ns}{L}}$$

The value of R reflects the degree to which the group behaves like a raft or a pier. Pile groups with values of R>4 can be modelled well using the equivalent raft foundation approach. For lower values, in particular for R<2, it is more appropriate to use the

equivalent pier approach. Randolph and Clancy (1993) have also illustrated the role of R in controlling differential settlement in pile groups.

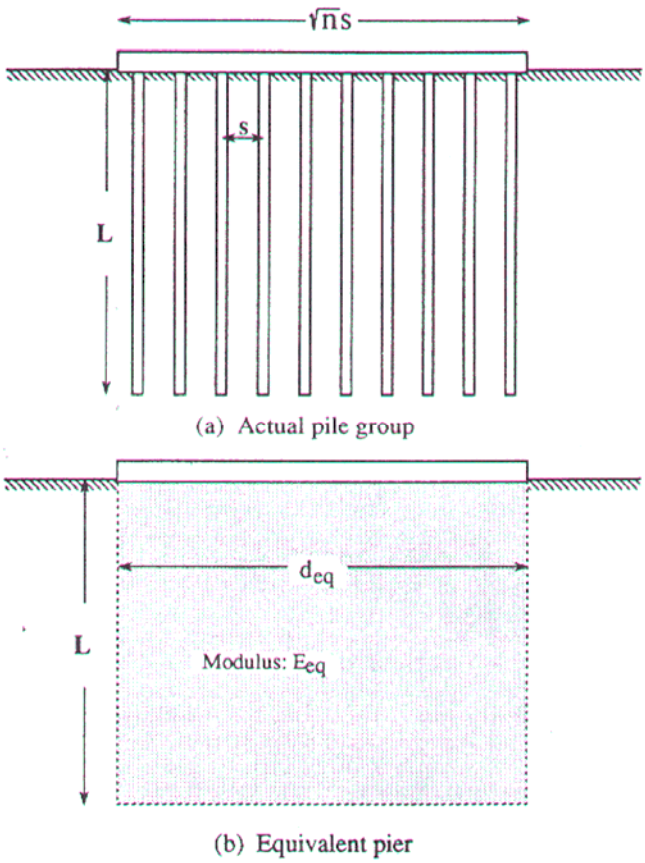

Figure 2-22 Equivalent pier (Randolph 1994)

2.8 Continuum Based Approaches

2.8.1 Finite Element Methods

A 3-D Finite Element approach is the most powerful and rigorous tool available for group analysis. While axisymmetric analyses are generally useful for single piles or extremely small pile rows/clusters, they fail to capture the 3-D nature of most pile groups.

The 3-D finite element approach is sufficiently adaptable to allow individual pile settlements and shear stress distributions to be assessed for a wide variety of imposed loading conditions. However, the major impediment appears to be the lack of 3-D software

which incorporates realistic constitutive models for soil. While its many benefits have been outlined in Section 2.2.1, the FEM is not widely used in the design of groups. The method has severe practical drawbacks due to the large amount of elements that must be generated, with a substantial amount of computations needed for the simplest of pile group configurations. The analysis of pile groups more complex than a regular 8^2 group are thus precluded (Guo and Randolph 1999), with the assumption of linear elastic soil conditions often enforced. Furthermore, an analysis of pile driving is beyond the scope of numerical techniques at present.

Limited FEM applications to pile groups have been published. The work of Ottaviani (1975), although small in scale and linear elastic, nevertheless contributes to an understanding of interaction effects. The intricate mesh detail required for the 3x3 group analysed by Ottaviani (1975) is illustrated in Figure 2-23.

The 3-D FE method has been used more extensively (in conjunction with Mindlin's (1936) equation for a point load in a semi-infinite half space) for the analysis of the raft portion of piled-raft foundations. This has three purposes: to check the structural response of the raft itself, to determine the contact pressures at the underside of the raft and to determine how much load is applied to each of the piles (the starting point of a pile group settlement analysis).

2.8.2 Complete Boundary Element Methods

Boundary Element or Integral Equation analysis represents the next most thorough continuum based approach. The response of all of the group piles is analysed simultaneously. Although the thoroughness of the finite element approach is diluted, considerable computational savings arise when only the pile-soil boundaries (and not the entire soil and pile masses) are discretised. The smaller equation set for any given pile group and soil conditions accounts for its more widespread use.

The early pioneering work of Butterfield and Banerjee (1971) was extended by Banerjee and Driscoll (1976) to create the PGROUP algorithm. Originally modelling soil as a linear

elastic material, PGROUP underwent further refinement by Banerjee and Butterfield (1981) to incorporate non-linearity in an approximate fashion using *volume cells*. The use of the latter soil model has the unfortunate effect of limiting PGROUP to analysing groups having no more than 25 piles.

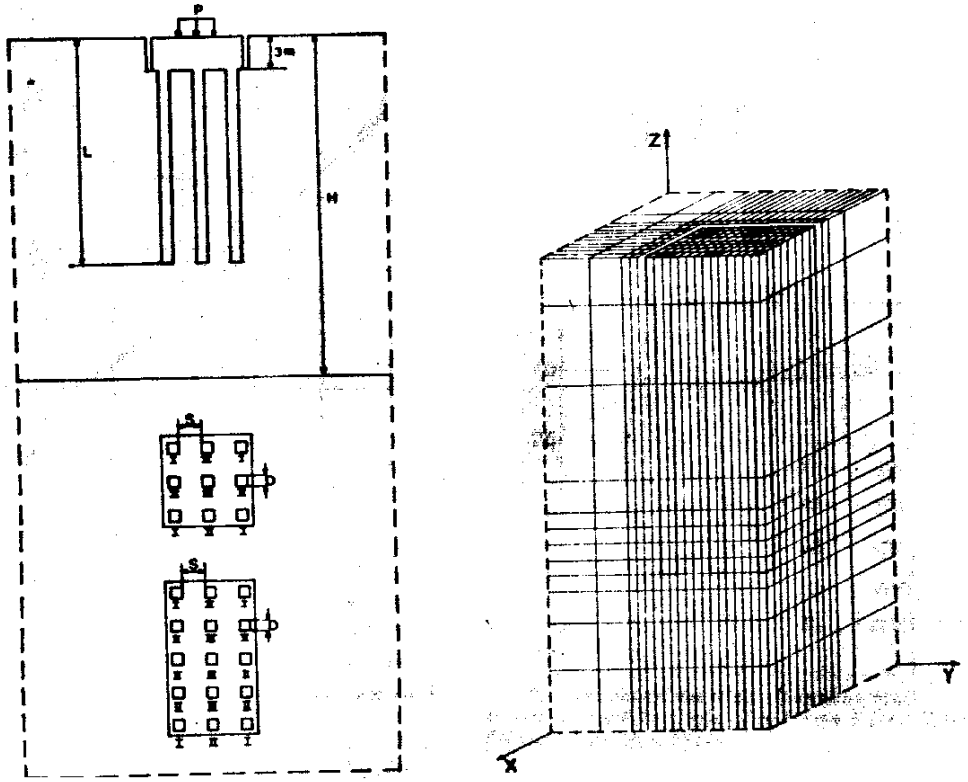

Figure 2-23 3-D FE mesh used by Ottaviani (1975)

Basile (1999) describes a complete boundary element approach called PGROUPN which is based on PGROUP but is more computationally efficient. Symmetry and similarity of terms in the single pile flexibility matrix is exploited, in addition to symmetry of interaction between similarly loaded group piles. Mindlin's (1936) solution, numerically integrated in PGROUP to calculate the singular part of diagonal terms of the global flexibility matrix, is now integrated analytically in PGROUPN. These steps significantly reduce the processing expense associated with PGROUP, releasing resources to allow both soil non-linearity and large pile groups to be examined.

Soil non-linearity is catered for approximately assuming elastic perfectly plastic behaviour. The yield criteria for pile shaft and base are deduced from profiles of undrained shear strength (c_u).[1] The only other soil parameter required is the initial tangent Young's modulus which may vary in proportion with depth. Output from PGROUPN is restricted to pile groups with free-standing rigid caps.

2.8.3 Simplified Boundary Element Methods

Examination of larger pile groups requires more computing time which may be offset by further simplification to the complete boundary element method. The rigour of a continuum based analysis of the overall group response is sacrificed and replaced with an *interaction factor* approach. A thorough boundary element analysis of a single pile is retained and accompanied by a similar complete analysis of a pile pair from which interaction factors representing all of the relevant pile spacings are developed. Two of the more widely recognized SBE methods are DEFPIG (Poulos 1980) and GRUPPALO (Mandolini and Viggiani 1997). The essential features of both simplified boundary element approaches are detailed below:

(i) The axial (and lateral or rotational) behaviour of a single pile is computed from a rigorous boundary element analysis in both cases (or alternatively may be supplied to the DEFPIG program). The ALPHAPALO procedure (Mandolini and Viggiani 1997) for single pile analysis may also be used to backfigure the stiffness values of the soil layers where load test data are available. A limiting stress at the pile soil interface attempts to simulate non-linear response.

(ii) Interaction factors are calculated for a pile pair from further boundary element analyses, and take account of pile geometry, spacing, compressibility and the assumed subsoil modulus distribution. DEFPIG calculates elastic interaction factors according to the approach of Poulos (1971). Alternatively, these may be inputted if sufficient experience is available of pile behaviour in a particular soil. The

[1] $\tau = \alpha\, c_u$ (limiting shear stress on pile shaft), $q = N_c\, c_u$ (limiting compressive resistance at pile base)

interaction factors in GRUPPALO are based upon the work of Caputo and Viggiani (1984) in which non-linearity is assumed to be concentrated at the interface of pile and soil due to the pile's own loading, with pile-pile interaction modelled sufficiently accurately with a linear model. Interaction factors α_{ij} are assumed to be constant with load level while α_{ii} varies according to the hyperbolic load-displacement relationship of Chin (1970, 1972):

$$\alpha_{ii} = \frac{1}{1 - \frac{P_i}{P_{i,\lim}}}$$

where P is the axial load in the pile.

(iii) Interaction factors may be derived in GRUPPALO for non-identical piles whereas DEFPIG interaction factors are based upon identical piles only.

(iv) Non-homogeneous soil conditions may be included in DEFPIG using the assumptions of Poulos (1979), while it is assumed in GRUPPALO that the soil consists of horizontal layers, each of which may be assigned a separate stiffness.

2.9 Load Transfer Approaches

2.9.1 PIGLET

Developed by Randolph (1980) and based heavily upon the work of Randolph and Wroth (1978a&b, 1979), PIGLET is arguably the most widely used pile group analysis package. PIGLET was developed from the approximate but compact closed form solutions for single pile behaviour (described in Section 2.3.1), coupled with interaction factors for each pile pair. The single pile solutions have either been derived theoretically (axial and torsional loading) or fitted to the results of finite element analyses (lateral loading). Interaction factors have been determined by fitting expressions to the results of finite element analyses for a pile pair.

The load transfer functions upon which the single pile response is based are linear elastic and overlapping displacement fields are assumed to be additive in determining interaction effects. Under purely axial loading, the expressions for the shaft and base settlement for a single pile (Section 2.3.1) may be supplemented with the additional interactive settlement due to loading of neighbouring piles. For an interacting pile pair, the expressions assume the following form:

$$w_s = \frac{\tau_o r_o}{G} \ln\left(\frac{r_m}{r_o}\right) + \frac{\tau_o r_o}{G} \ln\left(\frac{r_m}{s}\right)$$

$$w_b = \frac{P_b(1-\upsilon)}{4 r_o G} + \frac{P_b(1-\upsilon)}{4 s G} \frac{2}{\pi}$$

where s is the pile spacing, and r_{mg} is the radial influence term applicable to groups. These may readily be extended for a group consisting of n piles:

$$\left(w_s\right)_j = \sum_{i=1}^{n} \left(w_s\right)_{ij} = \frac{1}{G} \sum_{i=1}^{n} \left(\tau_o\right)_i \left(r_o\right)_i \ln\left(\frac{r_{mg}}{s_{ij}}\right) \qquad \textit{where} \quad s_{ij} = r_o \quad \textit{at} \quad i = j$$

$$\left(w_b\right)_j = \sum_{i=1}^{n} \left(w_b\right)_{ij} = \frac{2}{\pi} \frac{1-\upsilon}{4 G_L} \sum_{i=1}^{n} \frac{\left(P_b\right)_i}{s_{ij}} \qquad \textit{where} \quad s_{ij} = r_o \quad \textit{at} \quad i = j$$

Pile compressibility may be incorporated into the interaction terms by providing an expression for w_t as a function of both w_s and w_b for a particular value of pile head load; this requires knowledge of how load is distributed along a single compressible pile in the same material. Randolph and Wroth (1979) provide these simplified relationships for piles in homogeneous, Gibson and non-homogeneous soil; with the latter requiring an iterative solution process.

The choice of the radial influence term (r_{mg}) applicable to pile groups is complicated. Randolph (1977) explains how r_{mg} depends on the degree of interaction between the soil layers above and below the level of the pile base. If the base of a pile group is assumed to act as a single rigid punch, the lower soil layer deforms more gradually with radius, giving

larger r_m values. Randolph and Wroth (1979) suggest that the value of r_m for a single pile be supplemented by r_g, a term reflecting the pile group size. The recommended value of r_g is the radius of the circle of equivalent area to the group's plan area.

$$r_{mg} = r_m + r_g = 2.5l\rho(1-\upsilon) + r_g$$

2.9.2 Fleming et al (1992)

Fleming et al (1992) recommends the use of the CEMSET single pile analysis (Section 2.3.3) combined with a capacity efficiency approach for establishing overall group capacity. The capacity of component group piles cannot be determined by this method.

Pile group capacity efficiency (η_{cap}) is defined as the inverse of the settlement ratio (R_s):

$$\eta_{cap} = \frac{1}{R_s} = \frac{k_g}{nk_s}$$

k_s is the pile head stiffness of a single pile, whereas k_g is the stiffness of the complete group of n piles. The group capacity efficiency is empirically related by a simple power law to the number of piles in the group:

$$\eta_{cap} \approx n^{-e}$$

giving the group stiffness as:

$$k_g \approx n^{1-e}k_s$$

The value of e is typically 0.3-0.5 for friction piles and 0.6 or greater for end bearing piles. Fleming et al (1992) presents a set of design charts shown in Figure 2-24 which allow four corrections to be applied to a base value of e_1 which is solely dependent upon the pile slenderness ratio (L/D). These corrections are pile compressibility (c_1), group spacing to diameter ratio (c_2), soil homogeneity (c_3) and Poisson's ratio (c_4).

$$e = e_1(l/d)\left\{c_1(E_p/G)c_2(s/D)c_3(\rho)c_4(\nu)\right\}$$

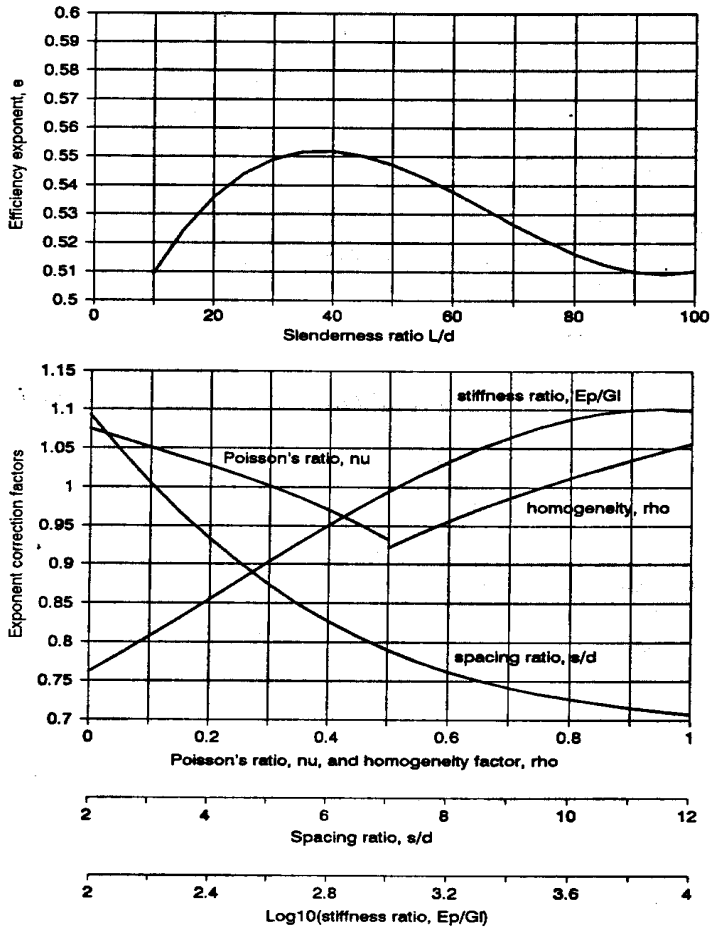

Figure 2-24 Group efficiency design charts (Fleming et al 1992)

2.9.3 RATZ

RATZ may be extended to quantify group action by conducting an analysis on a single pile with an appropriately factored load transfer curve. The factoring is based upon the group settlement ratio R_s which is defined as the ratio of the group to the single pile load transfer multiplier:

$$\zeta^* = \ln\left(\frac{r_m}{r_o}\right) + \sum \ln\left(\frac{r_m}{s_i}\right) \qquad R_s = \frac{\zeta^*}{\zeta}$$

Only the elastic portion of the RATZ single pile load transfer curve (at shear stresses below $\xi\tau_p$) is factored by R_s. Since the plastic component of the curve is assumed to be due to the pile's own loading alone, summation due to interaction is not appropriate and it is simply

added unfactored to the new (factored) elastic component to obtain the overall group response, as shown in Figure 2-25.

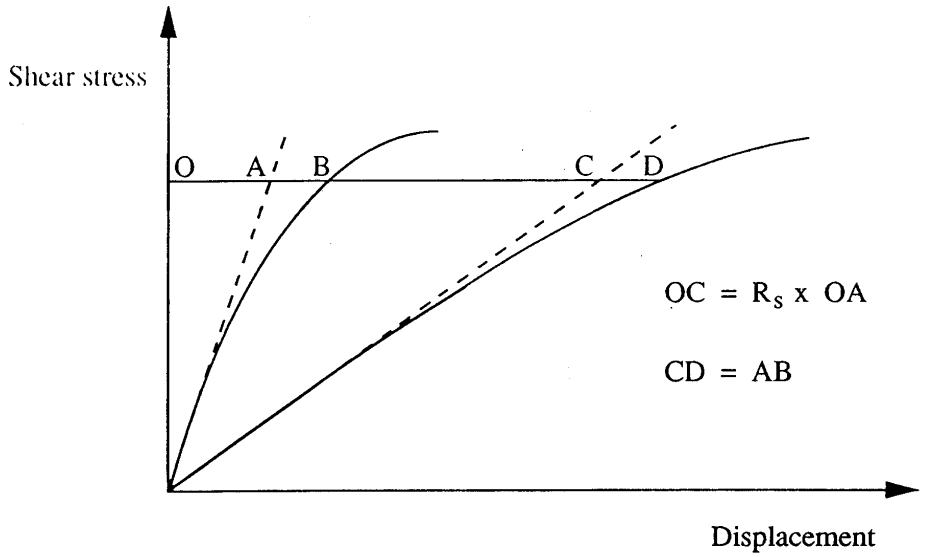

Figure 2-25 Modelling group effects in RATZ by scaling the load transfer curves

2.9.4 GASGROUP (Guo and Randolph 1999)

GASGROUP provides closed form solutions for estimating the settlement of pile groups in linear elastic non-homogeneous soil. Formulations are based upon a load transfer approach derived from elastic theory. While the methodology differs from previous closed form solutions (e.g. Randolph and Wroth 1979), the principal practical improvement is the inclusion of a rigid layer at a certain depth providing a lower bound to a finite layer of compressible soil.

Closed form single pile responses have been published by Guo and Randolph (1997), in which the elastic shear modulus of the soil is assumed to vary according to the power law:

$$G = A_g z^x$$

Load transfer functions along pile shaft and at the pile base correspond to those employed by Randolph and Wroth (1978). However, the value of the radius of influence (r_m) has been

modified, mainly to incorporate the influence of the soil non-homogeneity factor (x), with expressions for A and B derived from numerical FLAC analyses (Guo 1997):

$$r_m = A\frac{1-\upsilon_s}{1+x}L + Br_o$$

The extension of this term to pile groups must also take account of the presence of the rigid layer at depth H below the ground surface. The recommended group value is:

$$r_{mg} = r_m + \left[1 - e^{\left(1-\frac{H}{L}\right)}\right] r_g$$

Suitable values of r_g are suggested by Randolph and Wroth (1979) and Lee (1991).

Extension of this single pile approach to two piles is facilitated by replacing the single pile shaft and load transfer factors with those for a pile pair (PIGLET, Section 2.9.1). The load settlement ratios for piles are defined in terms of Bessel functions, which are considerably more complex than those used in PIGLET. Interaction factors for a pile pair are expressed in terms of normalised pile head stiffnesses, i.e.

$$\alpha_{12} = \frac{P_t/G_L r_o w_t}{\left(P_t/G_L r_o w_t\right)_2} - 1$$

which are also redefined in Bessel format. Extension of two-pile interaction factors to a pile group involves solving the equation below (for a flexible pile cap or its inverse for a rigid pile cap).

$$w_i = w_1 \sum_{j=1}^{n} P_j \alpha_{ij}$$

2.10 Hybrid Analysis Methods

Two main hybrid methods involving a combination of the load transfer and continuum based approaches are attributed to O'Neill *et al* (1977) and Chow (1986b, 1987). Both approaches entail a non-linear load transfer analysis of a single pile coupled with an interactive analysis of the group piles which considers soil continuity. Both approaches deal

differently with the interactive analysis. Shen *et al* (1999) also reports a hybrid method which combines load transfer analysis of a single pile with a variational approach to assessing group effects.

2.10.1 PILGP1 (O'Neill et al, 1977)

O'Neill et al (1977) devised the PILGP1 algorithm with three stages: (a) single pile load transfer analysis, (b) group response without interaction and (c) group response with interaction incorporated.

Single Pile Load transfer analysis

O'Neill et al (1977) developed pile-soil load transfer curves from a database of instrumented pile tests enveloping a wide variety of soil conditions. Soil and pile unit response curves are used in conjunction with finite difference formulae and imposed boundary conditions to develop pile head response curves. Separate curves are developed for axial translation, lateral translation, rotation due to moments and rotation due to torsion. The points on the pile head response curves are fitted by continuous cubic spline functions.

Non-interactive analysis

The responses of the individual group piles are first assessed without considering interaction. Pile head relationships are first approximated by their initial tangents, but subsequently recalculated at each load increment as the tangent to the curve at the appropriate value of accumulated deformation. This procedure continues until the sum of the load increments reaches the total imposed load. The pile head response curves are then used independently to compute soil reactions, displacements and stresses on each pile of the system.

Interactive analysis

Interactive soil displacements are now calculated for a general pile arising from the stresses on every other pile calculated in the non-interactive stage. The individual piles of the group are assumed to be spaced sufficiently distant for these additional displacements to be elastic

(Focht and Koch 1972). Mindlin's solution for point loads in the interior of a semi-infinite half space is used to determine these displacements.

The non-linear single pile load transfer curves are now scaled by an amount recognising the additional settlement computed in the interactive analysis (effectively non-linear superposition). These revised curves are substituted into the non-interactive analysis for recalculation. Further refinement is achieved by repeating this process.

2.10.2 Chow (1986a, 1987)

Elastic load-transfer functions for single piles, such as those of Randolph and Wroth (1978a), are replaced with functions based on hyperbolic stress-strain relationships of Kraft et al (1981). The tangent shear modulus (G_t) is assumed to reduce from its initial value (G_i) according to:

$$\frac{G_t}{G_o} = (1 - \frac{\tau R_f}{\tau_f})^2$$

τ is the shear stress, τ_f is the failure shear stress and R_f is a hyperbolic curve fitting constant. Soil stiffness is 'lumped' at the pile shaft and its tangent value is given by:

$$\frac{P}{w_t} = k_s^t = \frac{2\pi G_i L}{\ln\left(\frac{r_m - \beta}{r_o - \beta}\right) + \frac{\beta(r_m - r_o)}{(r_m - \beta)(r_o - \beta)}}$$

$$\beta = \frac{\tau_o r_o R_f}{\tau_f}$$

The equivalent hyperbolic base response is given by:

$$k_t^{base} = \frac{4Gr_o}{1-\upsilon}\left(1 - \frac{P_b R_f}{P_f}\right)^2$$

Unlike Randolph and Wroth (1979), interaction effects are not based upon interaction factors, but from a continuum analysis based upon Mindlin's solution for a vertical point load in a homogeneous, isotropic elastic half-space. For soil which is non-homogeneous,

interaction effects are approximated by averaging the soil shear modulus at node *i* (where the displacement is evaluated) and node *j* (where the load is applied) in Mindlin's solution.

The non-linear soil behaviour causes slippage to arise at high strains along the pile-soil interfaces of the individual piles. This slippage is concentrated within a narrow soil zone adjacent to the pile shaft, while the bulk of the soil between the piles is assumed to remain elastic. Therefore the non-linear behaviour of the individual piles controls group response, with interactive displacements remaining essentially elastic. Once a node has yielded, it can contribute no further to the interactive process.

2.11 Appraisal of Pile Group Analysis Methods

Some of the relative merits of the analytical pile group methods (described in Sections 2-8, 2-9 and 2-10) are discussed in this section. Further detail regarding the trends/design charts arising from some of these theories is provided in Appendix 2-2, which also includes selected parametric studies of factors on which interaction depends. Poulos (Rankine Lecture 1989) provides an excellent summary of these factors based on broad experience with many analytical techniques.

2.11.1 Interaction Factors and Soil Stiffness Non-linearity

Ignoring continuity of the soil mass is the principal flaw in the interaction factor approach. In real situations, there are likely to be intervening piles along the line of an interacting pile pair and these represent 'pockets' with greater stiffness than the surrounding soil mass. In addition, the stiffness of the soil around any displacement pile may depend on the influence of adjacent pile installations, and so the soil stiffness may not be uniform with the perimeter of a closely spaced group.

Load distributions in piles cannot be determined from interaction factor methods. These are often estimated from single pile solutions (as with PIGLET). Despite proposals by Poulos and Davis (1980) and Mandolini and Viggiani (1997), the use of interaction factors for dissimilar piles remains questionable.

Measurements of ‘true’ interaction factors (i.e. based on field measurements) are rare. Two such cases arise in the literature:

- Pellegrino (1983) performed similar tests with Franki piles driven in a 20m thick volcanic layer. Settlements were measured on a number of load-free piles adjacent to the loaded pile (Figure 2-26). (Caputo and Viggiani (1984) suggests that interaction factors may be considered as elastic on the basis of this and other work.).

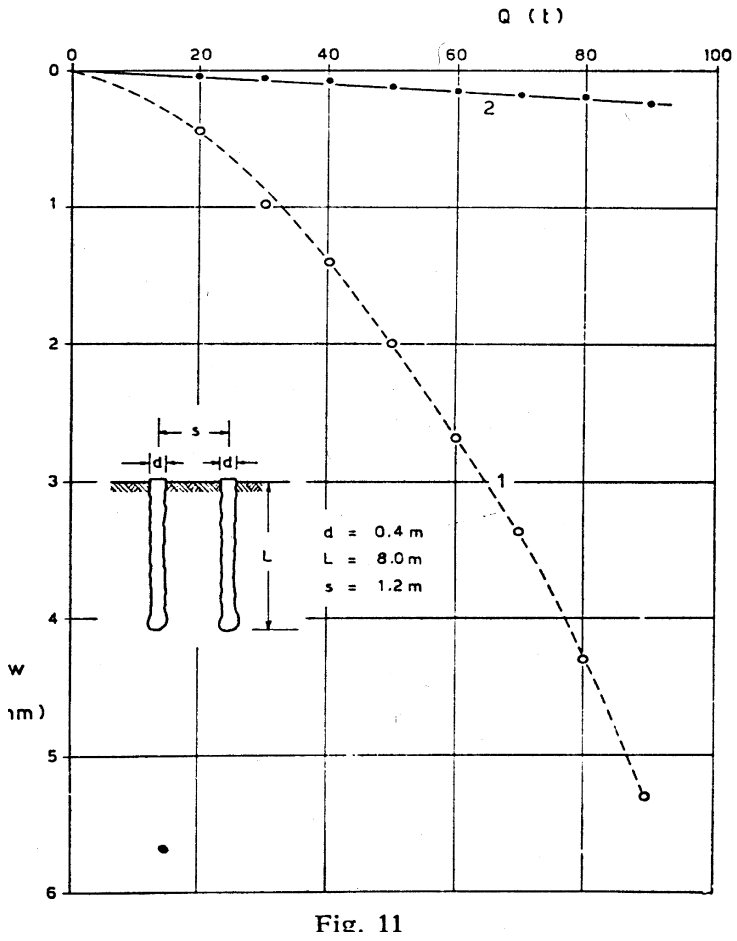

Figure 2-26 Displacements measured on load-free piles (Pellegrino 1983)
(1=loaded pile, 2=load-free pile)

- Cooke et al (1979) present tests on 2- and 3-pile rows in London clay. In addition to testing all piles in the row together, they also loaded one pile alone and measured the displacements on the non-loaded piles. (On the basis of their tests, it was

concluded that superposition of displacements provided a satisfactory means of predicting pile group load-displacement response).

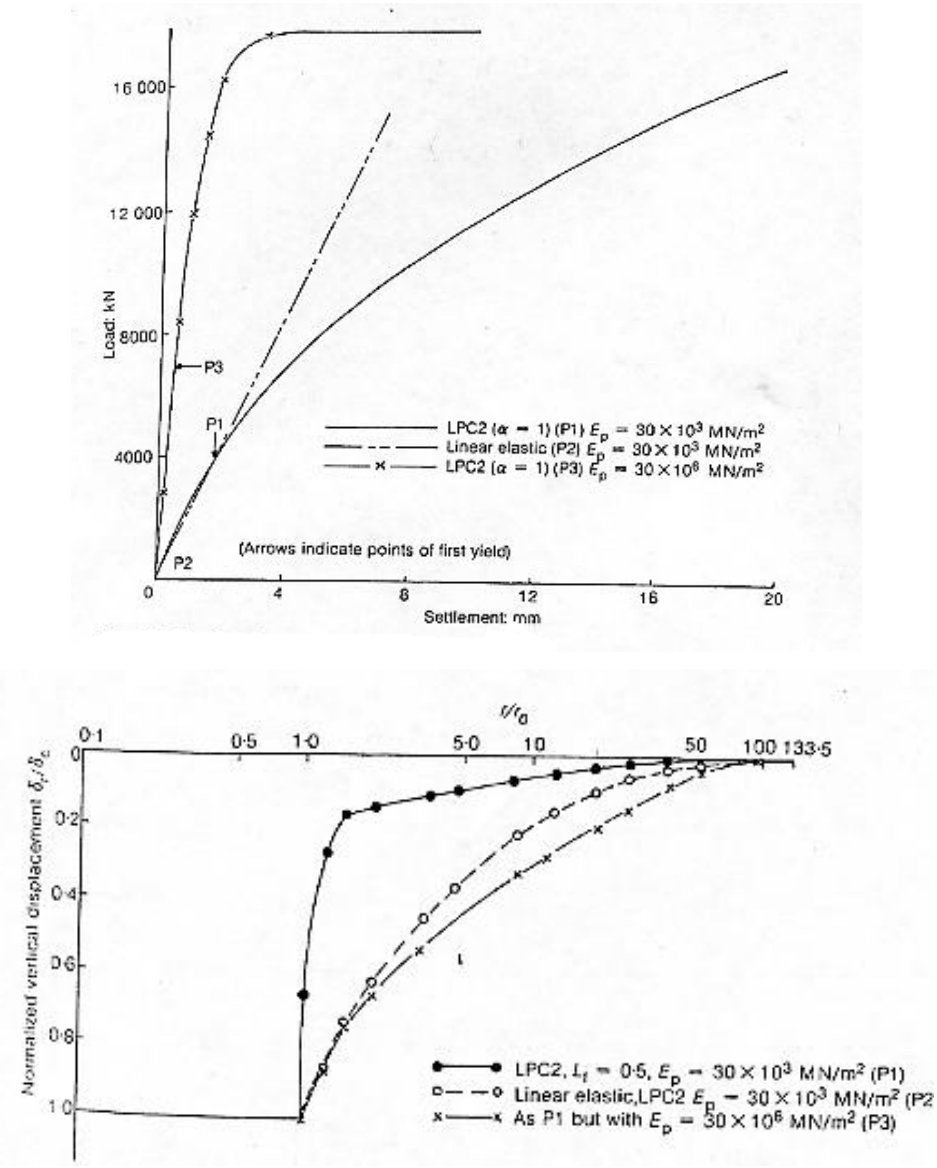

Figure 2-27 Effect of soil non-linearity on pile displacement field (Jardine et al 1986)

Jardine et al (1986) demonstrated the effects on modelling soil non-linearity in a number of geotechnical problems; the settlement trough around a loaded single pile obtained from finite element analysis is shown (Figure 2-27). Use of the (LPC2) non-linear soil model generates greater stress concentration closer to the pile shaft but more rapid horizontal

decay of settlement than the LE model. Therefore, at practical pile spacings, interactive settlements predicted by the non-linear model are much lower than predicted by the LE model. For groups with a flexible cap, the settlement of all piles will be overestimated. This may lead to over-conservative design and some redundancy in the interior piles.

Continuum analyses (PGROUP, PGROUPN)[2] and SBEMs (DEFPIG, GRUPPALO) model soil non-linearity with an elastic-plastic stress-strain relationship. Pile capacity may be estimated by imposing a limit stress to the soil (absent from LE techniques). However, piles are rarely at a state of failure, so elastic-plastic models will also overestimate interaction. Certain methods (Chow (1986a, 1987), GRUPPALO and RATZ) agree on the importance of considering non-linearity for each pile's own loading, but suggest that the use of linear elastic interaction factors is sufficiently accurate.

2.11.2 Load distributions

As already mentioned, load distributions cannot be determined by interaction factor methods. This is also the case with load transfer methods in general, whether interaction factors are used (i.e. PIGLET) or not (i.e. Chow 1986). Such methods conveniently assume an average shaft load acting over the pile length, but do not attempt to predict the variation in the shear stress along the pile shaft. While the increased proportion of load carried by the pile base may be estimated, the redistribution of load towards the lower pile shaft, due to interaction and/or the restraining effect of the pile cap cannot be quantified. A knowledge of the spread of load among the group piles and the load distribution in each pile is also precluded by the method of Fleming et al (1992) where group effects are quantified empirically in terms of average capacity efficiency for the group.

2.11.3 Installation effects on soil stiffness within group

The soil mechanisms in response to single pile installation are not fully understood, and to date, the Strain Path Method[3] (Baligh 1985) used in conjunction with the MIT-E3 soil

[2] Yielded soil elements contribute no further to the interaction process, stress redistributed to elements that have not yet yielded.

[3] The soil is assumed to behave as a fluid and installation is treated as soil flow around a stationary penetrometer.

model has proved to be the most satisfactory approach. Bored piles are arguably more accurately analyzed than driven piles, as there is generally less soil disturbance involved in their placement.

Back-analysis of single pile load test data is often deemed to be a satisfactory method of determining a single value of soil stiffness to model the entire group behaviour. However, if a common value of soil stiffness is assigned to all soil within the group perimeter, differential disturbance due to neighbouring pile installation is not modelled.

2.12 Facets of Group behaviour observed from published case histories

Case histories of instrumented pile groups are relatively scarce. A limited database has been compiled for use in this Thesis; tests in this database reveal some consistent features of group action and other aspects which differ among tests. The differences emphasize the importance of expanding pile group test databases as a basis for appraising/improving design techniques. Previous published work is now discussed under a number of headings:

2.12.1 Capacity Efficiency of group piles in clay

It is a broadly held belief that an average group pile in clay 'fails' at a lower load than an equivalent single pile, whereas an average group pile in sand has a higher capacity than a single pile. Evidence from the case history database suggests that such a definition may be too general.

There should be little or no disturbance caused by forming bored piles in clay soils, in which case the group piles should reveal load interaction effects alone. A number of case histories reveal expected interaction trends as illustrated in Section 2.6.1:

- Cooke et al (1981) report an investigation of 351 bored piles (s/D=3.6) in London Clay. The corner piles were found to carry over twice the load of an internal pile, with edge piles having intermediate values (Figure 2-28).
- In Frankfurt clay (another stiff overconsolidated soil), Franke et al (1994) shows similar load sharing patterns within a 42 pile group (s/D = 3 to 3.5); see Figure 2-

29. Reports on other bored-pile building foundations (Greenfield 1971, Hooper 1973) are consistent.

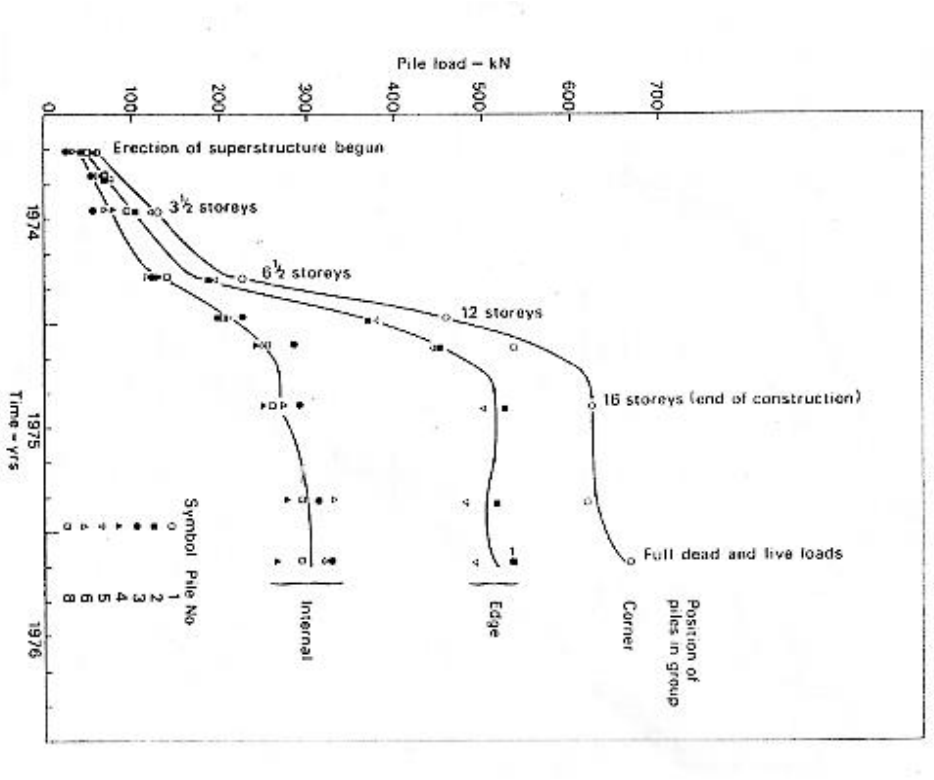

Figure 2-28 Bored pile foundation at Stonebridge park (Cooke et al 1981)

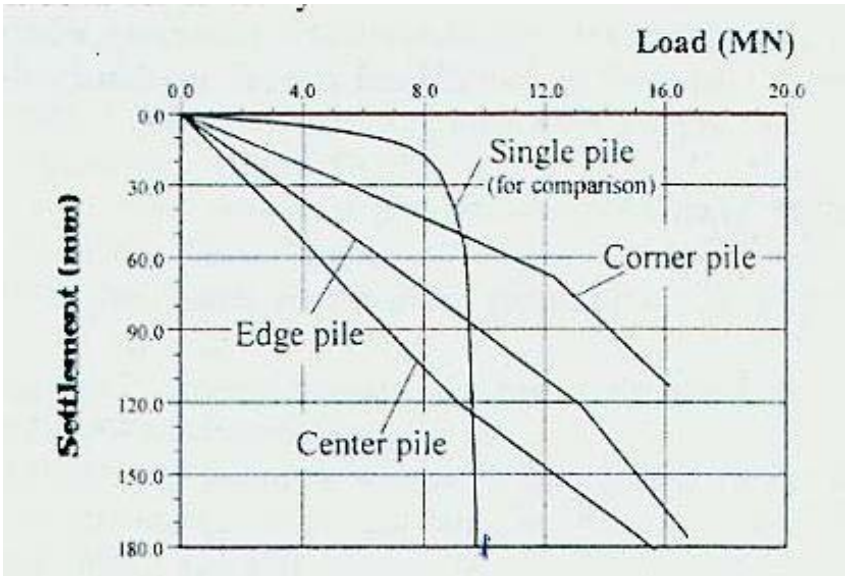

Figure 2-29 Bored pile group in Frankfurt clay (Franke et al 1994)

Most case histories do not offer any insight into the relative effects on group pile capacity of adjacent installations and load interaction. However, limited measurements are available which describe the installation process alone:

- O'Neill et al (1982) conducted load tests on a group of 9 driven piles (s/D=3) in overconsolidated clay. Extensive (installation and equalization) total stress and pore pressure measurements were made on group and single piles to distinguish their pre-loading behaviour. There was no apparent difference between the equalized radial effective stresses for the group and single piles, suggesting that there are no 'differential' installation effects within the group. However, the group capacity was found to equate to that of nine single piles which, surprisingly, implies that the piles did not interact under load.
- With the same group configuration as above, Koizumi and Ito (1967) noted no appreciable difference between the equalized radial effective stresses of the mid-edge and centre pile of the group (Figure 2-30). Unfortunately no single pile reference is reported. The distribution of applied load among the piles in the load test shown in Table 2-2 is consistent with load interaction effects. Tokyo clay is a highly sensitive overconsolidated clay.

Pile position	**Pile load/Average load**
Centre (Pile No. 2)	0.46
Corner	0.89
Mid-edge (Pile No. 1)	1.25

Table 2-2 Load sharing in 9-pile group (Koizumi and Ito 1967)

- Tests on groups of four teak piles in lightly overconsolidated sensitive marine clay (Brand et al 1972) produced group capacity efficiencies of unity and slightly greater, regardless of spacing in the range $2<s/B<5$. This data (Figure 2-31) would suggest that when closely spaced, the piles may be subjected to a 'positive' installation effect.

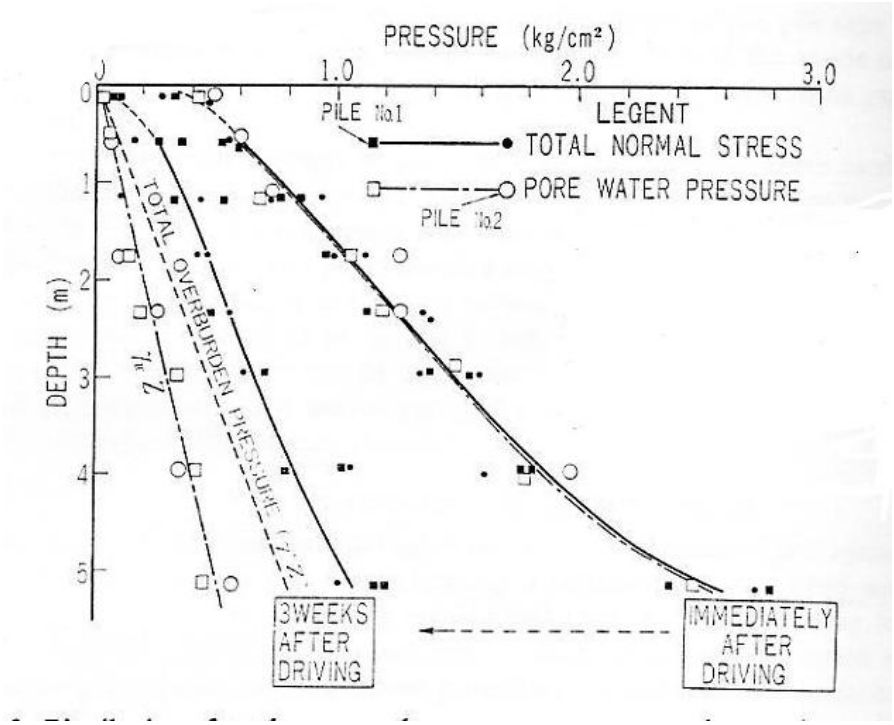

Figure 2-30 Group pile shaft total stresses and pore pressures (Koizumi and Ito 1967)

2.12.2 Capacity Efficiency of Group Piles in Sand

The large range of capacity efficiencies obtainable for pile groups in sand reflects its potential for volume change when sheared. Both Liu et al (1985) and Ekstrom (1989) give evidence that bored piles in sand have greater load carrying capacity than single piles, with piles towards the centre of the group assuming most load. However, the bored pile foundation in sand of Koerner and Partos (1983) carried greater load towards the group periphery, suggesting that load interaction effects may outweigh installation effects.

Chow (1995) measured a capacity efficiency in excess of unity for a driven pile pair (s/D=4.5) in Dunkirk sand. A group of five driven piles (s/D=3) reported on by Briaud et al (1989) were equally as efficient as a single pile.

These case histories serve to show the difficulties associated with predicting the capacity of group piles in either cohesive or granular soils.

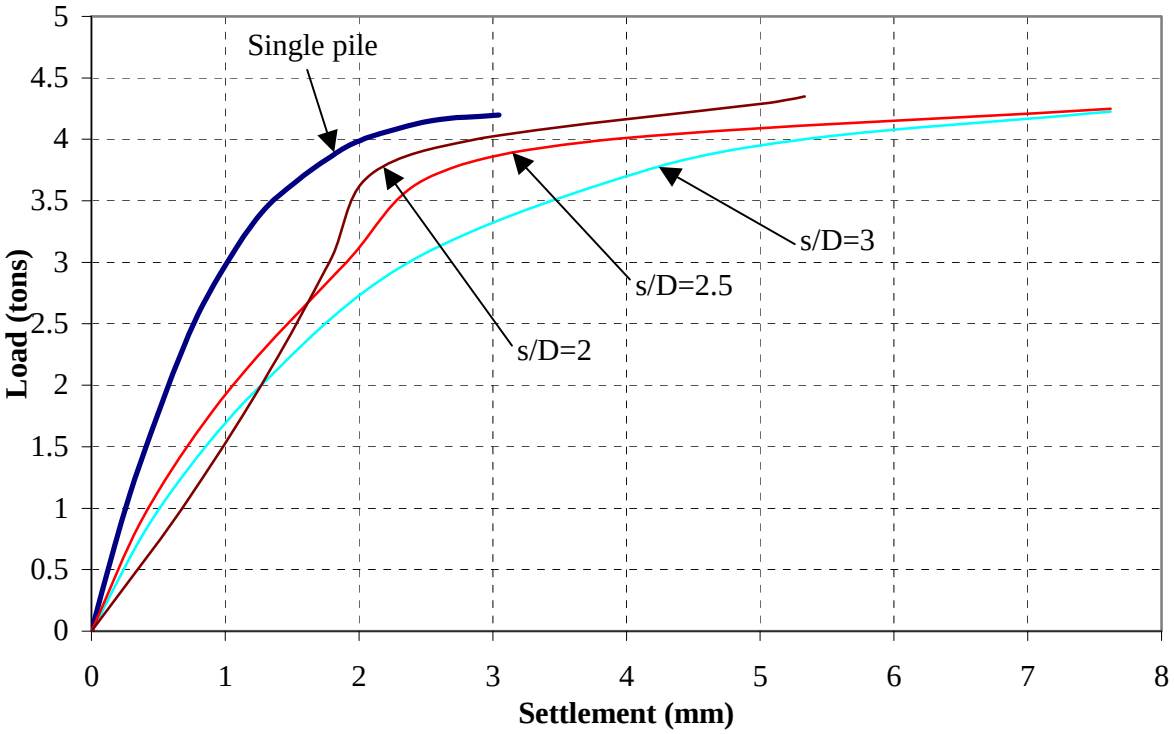

Figure 2-31 Group tests in Bangkok marine clay (Brand et al 1972, *reproduced*)

2.12.3 Effect of group action on shaft/base load split

Available case history data suggests that the capacity efficiencies of the pile shaft and pile base should be considered separately in preference to the use of one global pile capacity efficiency estimate.

Tests on rows of 2 and 3 driven piles (s/D=3) in London clay are used by Cooke et al (1980) to investigate the effect of interaction upon the load split between shaft and base[4]. Negative shear stresses are imposed upon the upper portion of each pile shaft due to the loading of nearby piles. Lower load is mobilized for a given settlement, enforcing an increase in settlement (over that of a single pile) to enable a given load to be carried. This is manifested through an increase in positive shear stress further down the pile shaft and an increase in load at the pile base. Evidence may be seen for the 2-pile row in Figure 2-32.

[4] Load distributions deduced from internal strain measurement.

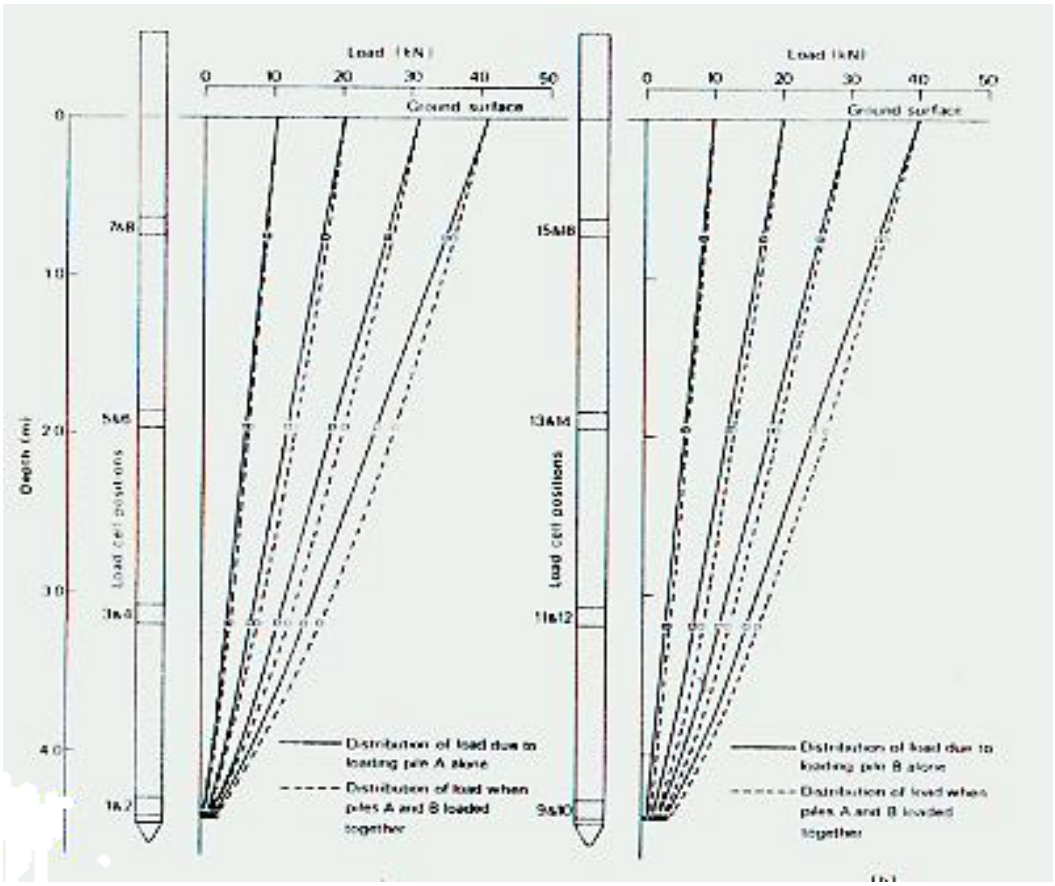

Figure 2-32 Load distributions in 2-pile row (Cooke et al 1980)

Similar evidence is provided by the bored pile group[5] of Cooke et al (1981), also in London clay. The mean base resistance at the interior was twice that of a corner pile, while the shaft friction was little greater than one-third (see Figure 2-33). However, Sommer's (1985) bored pile group in Frankfurt clay indicates degradation in *both* shaft and base capacities as the level of interaction increases.

Chow (1995) and Briaud et al (1989) both show that the findings of Cooke et al (1980, 1981) for clays are reversed for sands. The enhanced shaft capacity (over an equivalent single pile) is due to increases in radial effective stresses at the pile soil interface developed when neighbouring piles are driven. Neighbouring pile driving also loosens the prestressing beneath the pile base (by uplifting the pile), resulting in pile base load efficiencies less than

[5] 351piles

unity. The compensating effects of shaft gain and base losses would possibly be overlooked in a standard uninstrumented pile load test.

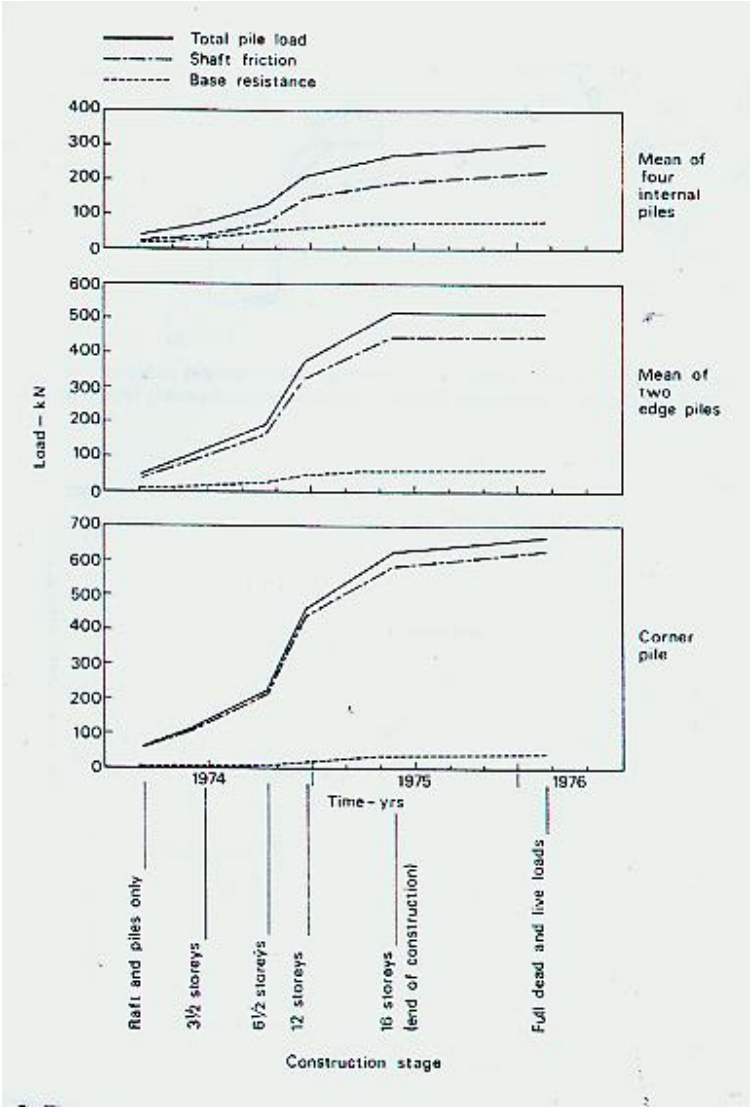

Figure 2-33 Split between shaft and base resistance within pile group (Cooke et al 1981)

It may be concluded that unconservative predictions may result from the use of a single efficiency factor on total pile capacity, especially for end-bearing piles in sand or predominantly friction piles in clay. Separate efficiency factors for shaft and base are therefore advised.

2.12.4 Pile Group Failure Mechanisms

Whitaker's (1957) model pile tests reveal two distinct mechanisms by which ultimate conditions may be reached in a group. Block failure occurs at close spacings; a slip plane forms joining the perimeter piles and the group plunges as a unit. At wider spacings, the failure is associated with local penetration of some or all of the piles. A point exists at some critical spacing which represents the transition between the two mechanisms. This point has important implications for the dependence of group capacity efficiency and group settlement upon pile spacing. For spacings initiating block failure, the efficiency falls rapidly with closer spacing, but it increases only gradually with greater spacing. Higher values of the settlement ratio arise at the transition point (for any load level), decreasing rapidly closer spacing and less rapidly with wider spacing. Brand et al (1972) notes a similar effect in Bangkok clay. The widespread experiments on full-scale groups by Liu et al (1985) refute that block failure arises for bored piles in sand, despite closely spaced piles or the pile cap in contact with the soil. Relative pile-soil movement was measured in the tests that would be absent in the block failure mechanism.

The pile-row tests of Cooke et al (1980) suggest that the presence of a cap in contact with the soil restricts the development of shear stress towards the upper portion of the piles in the group. Therefore, pile caps have effectively the same effect as interacting piles; greater load is transmitted to the soil through lower regions of the pile shaft and through the pile base. Tests on a 3^2 group in silty sand by Liu et al (1985) highlights the effect of settlement hardening, softening and the effect of the pile cap, and illustrates how these effects may either be additive or may compensate each other. Settlement *hardening* and settlement *softening* are terms used to describe how the group pile continues to respond once the peak single pile shear stress is mobilised. The shear stress continues to rise (settlement hardening) if piles exceed 1.5 times the breadth of the pile cap in length. A decay in shear stress (settlement softening) arises for piles shorter than the breadth of the pile cap. The occurrence of either of these phenomena is influenced by pile spacing. The same factors are also identified by Hansbo (1993) as the most influential on group performance.

Liu et al (1985) also shows that the low-set pile cap has a weakened effect on skin friction development and a strengthening effect on base resistance. For piles with $L/B_c>1.5$, the weakening effect of the pile cap is outweighed by the strengthening effect of settlement hardening. For $L/B_c < 1$, both the pile cap and settlement softening combine, entailing a significant drop in shaft resistance.

A low-set cap also improves the base resistance; the effect increases as the pile is shortened or as the spacing is widened (beyond s/D=2). The base resistance is thought to reduce due to the overlying stress fields of neighbouring piles, but increase due to uplift of the soil underneath the base of the other piles. A spacing of 3D is shown to represent the most efficient compromise between these conflicting effects.

Chapter 3

Properties of the Belfast Estuarine Deposits

3.1 Introduction

The piling research described in this Thesis was performed at a soft clay test bed at Kinnegar, on the eastern coast of Belfast Lough. The site was selected for the following reasons:

(i) Site investigations by Fugro McClelland, the Northern Ireland Department of the Environment and others (1974 –1995) have identified a considerable depth (up to 8m) of soft soil at the site.

(ii) Queen's University Belfast and the Department of the Environment have previously assimilated extensive information on the geotechnical characteristics of this deposit.

(iii) The site was remote and deemed to be relatively secure.

Further specific investigations have been conducted or commissioned by Trinity College Dublin. These have been ongoing since 1997 in conjunction with the vertical pile load tests described in this Thesis and lateral pile load tests (Phillips 2002). In-situ and laboratory testing carried out since 1997 are reported in this Chapter. Comparisons are drawn with the clay-silt at Bothkennar, which has been the subject of extensive research (special edition Geotechnique on Bothkennar, 1992).

3.2 Previous published research in Belfast soft clay

The upsurge in construction around Belfast in the early 1970's prompted the need for an enhanced understanding of the geotechnical characteristics of the stratigraphy underlying Belfast and its hinterland. The most notable contributions have been published by Crooks (1973), Crooks and Graham (1976), Bell (1977). Site investigations conducted at a limited number of sites have facilitated detailed laboratory tests on block and piston samples. An understanding of the behaviour of normally consolidated and lightly overconsolidated clay behaviour was aided by the findings of the above publications in conjunction with research in similar soils, most notably in Norway, Sweden and Canada.

One of the sites (Kinnegar) reported in these publications was in close proximity to the current test bed. Their principal observations may be summarized as follows:

(i) The top and base of the soil profile is mainly composed of sand, but 80-90% of the main sedimentary unit is composed of silt and clay sized particles.

(ii) The exchangeable cations sodium, magnesium, potassium and calcium were found in this order of abundance throughout the deposit, although the exact concentrations varied widely.

(iii) The organic content and pH are relatively constant below 2.5m depth, with slightly higher organic contents and slightly lower pH values at shallower depths. The plasticity index depends on the sodium cation content and the percentage of organic matter present.

(iv) The soil has medium to high sensitivity, believed to be due to the reduction in the concentration of the magnesium cation content due to leaching. Particular care was therefore required to preserve the microstructure when sampling[1].

(v) The Kinnegar deposit is lightly overconsolidated. It is believed that the soil has not been subjected to the removal of overburden. The overconsolidation in the bulk of the profile is believed to have resulted from a combination of groundwater level changes and secondary consolidation. The greater overconsolidation in the top few centimetres of the profile is possibly due to desiccation, frost action or chemical weathering.

(vi) Beyond the preconsolidation pressure, the compressibility and rate of secondary consolidation are high in relation to other recent clays and are more in line with those from extrasensitive deposits. The compression index (C_c) is related to the liquid limit and the coefficient of secondary consolidation[2] (C_α) is related to the plasticity index.

(vii) The soil possesses an initially stiffened response to undrained shearing and attains peak resistance at small strains due to overconsolidation.

(viii) Anisotropy (with respect to yield) of undrained strength is confirmed, since extension undrained strengths are lower than comparable compression strengths. Yielding, believed to be associated with important changes in the soil microstructure, occurs under undrained as well as drained conditions.

[1] Hand trimmed block samples and thin walled piston samples were used.
[2] Subsequently referred to as the creep coefficient.

3.3 Scope of Current Site Investigation

The Site Investigation work carried out since 1997 includes:

- Sampling using 100mm diameter piston samples (carried out by the Northern Ireland Department of the Environment) and 'Geonor' 54mm diameter samples (carried out by TCD)
- Trial pits conducted by TCD (in material that could not be sampled)
- Standard electric cone penetration tests, piezocone tests, piezocone dissipation tests and in-situ shear vane tests (TCD)
- Seismic cone, cone pressuremeter and dilatometer tests (Building Research Establishment, UK)
- Classification testing at TCD, including X-Ray Diffraction and Electron Microscope Analyses
- Chemical testing (University of Massachusetts, Amherst, USA)
- Parameter determinations at TCD in oedometer, shear box, ring shear, simple shear and triaxial tests.

The locations of boreholes and in-situ tests are shown in Figure 3-1.

3.4 Geology of the Belfast Area

3.4.1 Overview of geological history

The sleech at the Belfast site is a relatively recent deposit in a geological context. A period of fluctuating sea levels followed the retreat of the glaciers[3] that covered most of North Eastern Ireland. While sea levels rose due to thawing of the glacial ice, the surface level of the land rose by a least an equal amount by a process referred to as *isostatic unwarping*. When depressed under the weight of ice sheets for long periods, land masses tend to uplift in response to the release of this load.

Deposits formed after recession of the ice sheets (i.e. post-glacial) are believed to be approximately 9000 years old. A fragmented peat layer was formed on top of the glacial deposits before the sea level began to rise. The area now occupied by Belfast city and its

[3] Bell (1977) reports four well established phases of glacial retreat.

environs was in turn overlain with clastic materials. These were deposited by the Lagan, Connswater and Blackstaff rivers, all of which confluence into Belfast Lough.

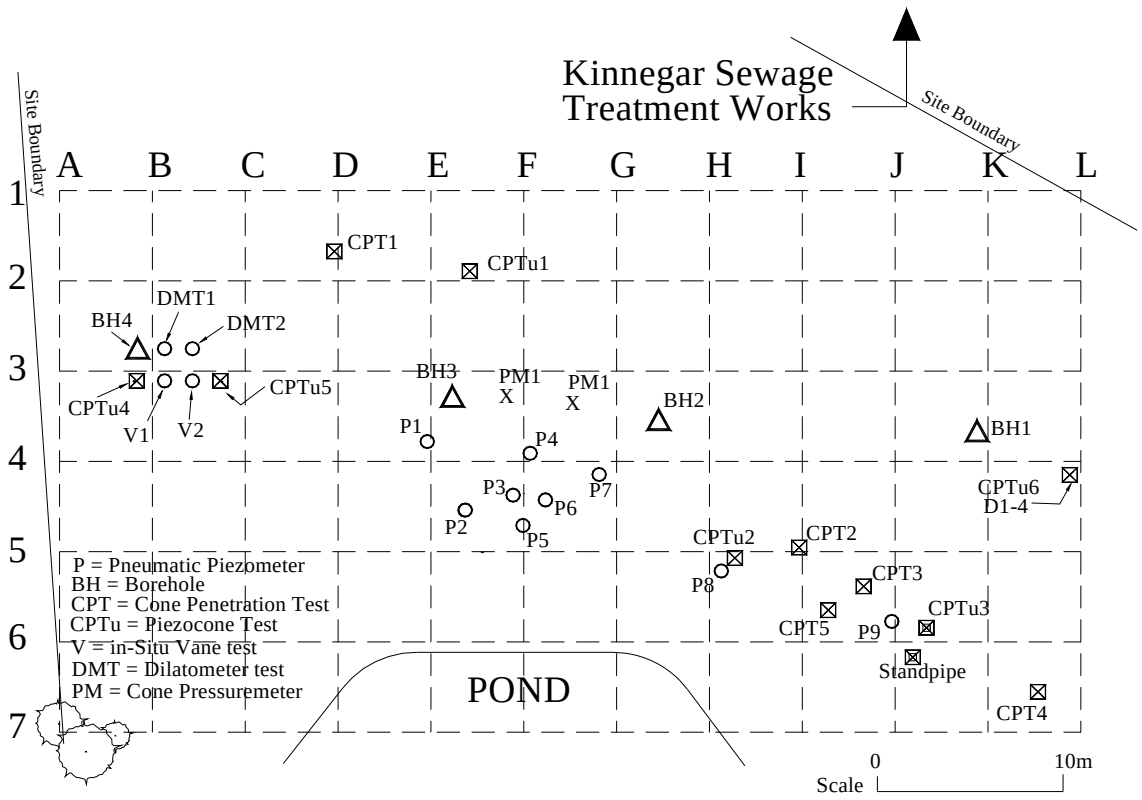

Figure 3-1: Site plan identifying borehole and in-situ test locations

3.4.2 Relevance to site stratigraphy at Kinnegar

Glacial deposits

The main feature of the glacial retreat was deposition rather than erosion. Extensive amounts of boulder clay were formed in much of the Belfast area, with the exception of the central district and some zones in the north and east. This glacial deposit been categorized into three distinct regions: (i) Upper Boulder Clay, (ii) Malone sands and (iii) Lower Boulder Clay. Dark, brown, silty, laminated clays have been found both at the base of the Malone sands and elsewhere in the lower boulder clay. Both the laminated clay and the Malone sands are believed to have been formed in a glacial lake during the retreat of the main glacier. Some red marine clay has also been found, believed to be the result of the (geologically) sudden inundation of a large area of land by the sea.

The intermittent strata of sand and clay identified from DoE boreholes below the base of the soft clay at Kinnegar are broadly consistent with the chronology of glacial deposition described (Section 3-5).

Post-glacial Peat

The intermittent yet extensive deposit of peat immediately formed after glaciation (dated at 8000-9000 years old by radio-carbon testing) appears to be absent at the Kinnegar site.

Estuarine deposits

Based upon data published by Wilson (1972) and Manning et al (1972), Bell (1977) has compiled the sequence of geological events within the era from the end of glacial retreat to the present day (Figure 3-2). It is clear that the net level of the land has risen considerably (relative to sea level) since late glacial times. Movius (1953) suggests that the land today may be as much as 37m above its post-glacial level. Considerable fluctuation has occurred in the intervening spell.

In late Boreal times, a general rise in sea level took place. Geomorphological evidence (Stephens and Synge 1966) suggests that the sea may have risen to 18m above present levels. This covered the peat layer laid down earlier in the Boreal period. From the later Boreal into the Atlantic period, estuarine clays were deposited on top of the peat, primarily by the Lagan, Connswater and Blackstaff rivers.

Manning et al (1972) subdivide the estuarine deposits into three phases. The Lower Estuarine clay was deposited under flat tidal conditions. Warm, low-salinity open water 5.5m deep facilitated the deposition of the Intermediate clay. The upper clays were deposited in cooler conditions and laid down in 9m of salt water. This entire process took place over 3000 years. Crooks and Graham (1973) suggest that the overall thickness of estuarine deposits does not exceed 15m in the Belfast area.

The Lower horizon comprises brownish-blue sandy clay including shells, roots and grass-wrack leaves. The Upper horizon is composed of blue-grey clay with fewer shells. The estuarine deposits were subsequently exposed in certain areas by further isostatic

uplift. Bell (1977) suggests that considerable variations occur. Although the material described shows broad agreement with TCD samples taken from 2.5-8.5m, the samples do not contain the amount of sand that is implied by the sandy clay at the lower end of the estuarine deposit. Crooks (1973) found that although grain-size, structure and organic content are location dependent, the mineralogy is quite consistent throughout.

Post-Depositional Processes

The post depositional processes and their influence on the soil properties are discussed by Bell (1977) and are believed to include bonding, some leaching and fluctuations in ground water levels. Approximately 1m of sandy fill material was placed on the site in the vicinity of the piles tests during construction of the adjacent Kinnegar Sludge Dewatering Plant about 20 years ago.

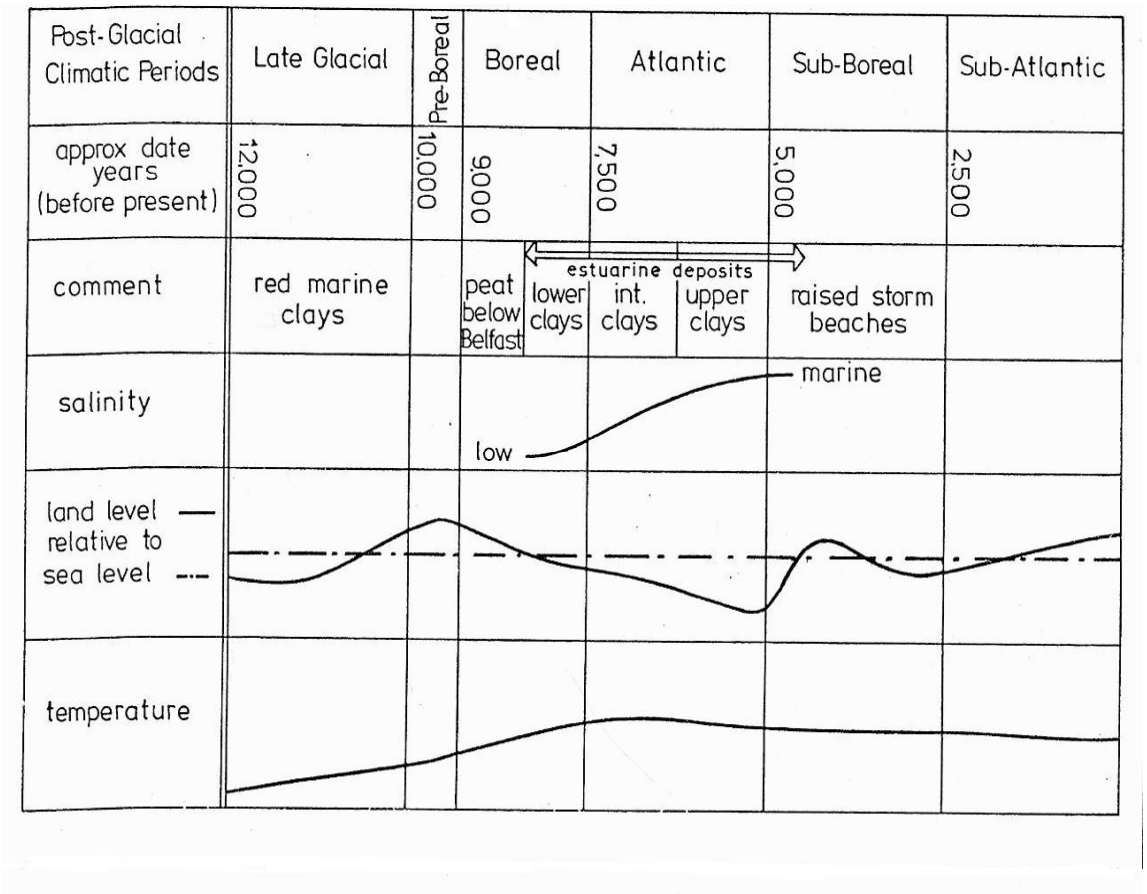

Figure 3-2 Suggested chronology of post-glacial geology of Belfast (Bell 1977)

3.5 Site Stratigraphy and Soil Composition

The boreholes, trial pits and Cone Penetration Tests performed in the general area of the pile tests revealed the stratigraphy summarized in Table 3-1.

Stratum	Approx. Depth (m)	Soil description
1	0 – 1.0 m	Matrix of building rubble with loose to dense silty sand to very silty gravel overlain by 0.1m of topsoil.
2	1.0 – 1.3/2.5 m	Loose dark grey organic very silty SAND with some clayey silt lenses and shell fragments
3	1.3/2.5 - 8.5/9.0 m	Soft dark grey organic clayey SILT with shell fragments
4	8.5/9.0 – 11.0 m	Medium dense brown silty fine to medium SAND

Table 3-1 Summary classification of Kinnegar stratigraphy

Most of the soil classification tests were performed on samples from the estuarine deposits from Strata 2 and 3. These two strata are collectively referred to by the local term *sleech*, although their properties differ somewhat.

The following general classification data is presented:

- Water contents and Atterberg limits, bulk unit weight, particle size distributions, organic content and pH (Figure 3-3)
- Percentages of Calcite and Dolomite; Specific Surface Area (SSA) and Cation Exchange Capacity Values on material smaller than 40μm (Appendix 3-1)
- X-Ray Diffractograms on the clay fraction (Appendix 3-2)
- Selected Electron Microscope Images of the sleech (Figure 3-4, also Appendix 3-3)

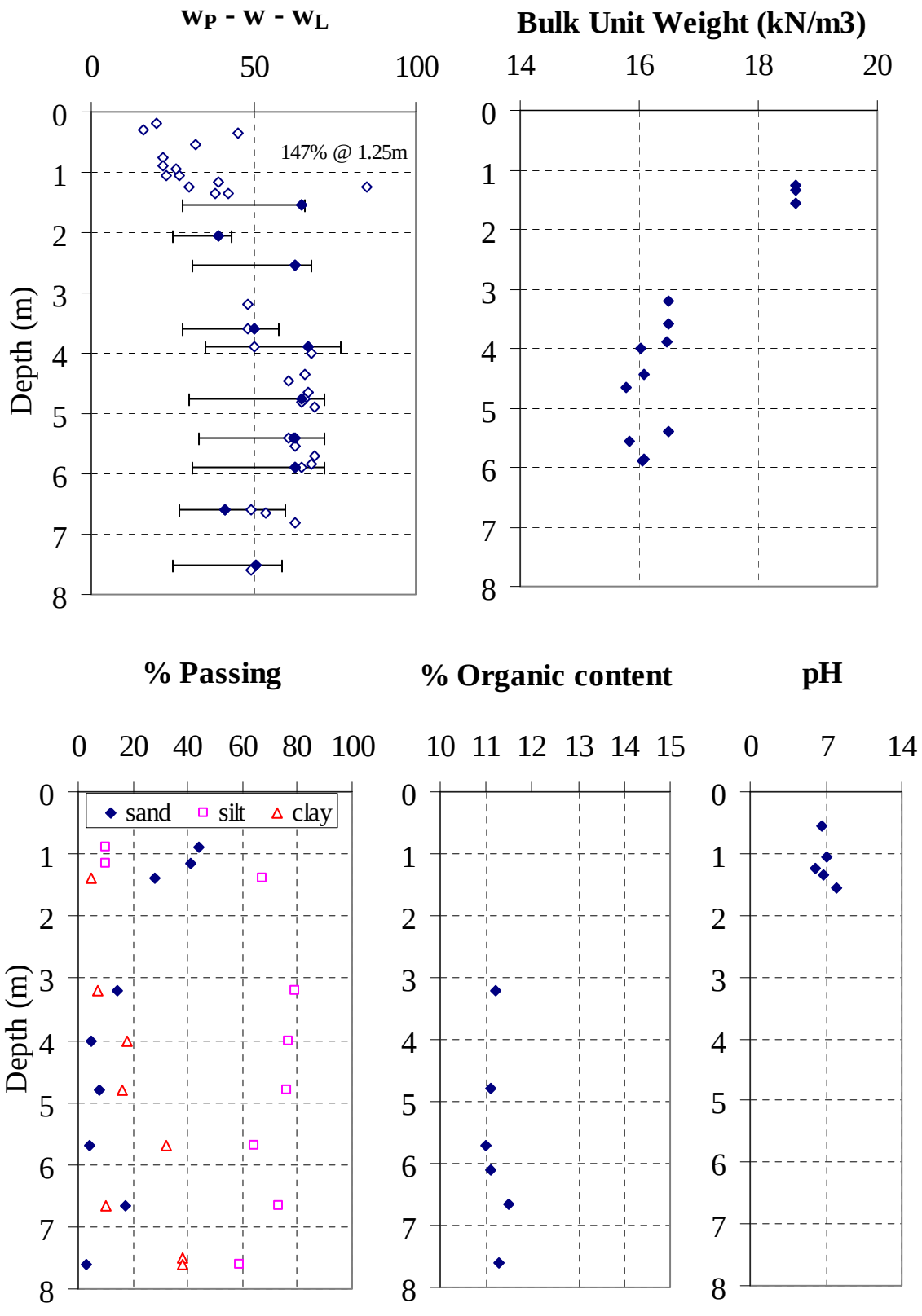

Figure 3-3 General Classification data for Strata 2 and 3

3.5.1 Stratum 1

Stratum 1 is highly variable in composition. It is typically ≈1m thick at the pile test locations, but reduces in thickness towards the pond south of the working area of the site. While it can generally be classified as sandy gravel or gravelly sand, topsoil was observed to extend to a depth of 1m in certain places. Poorly compacted building rubble, including bricks and concrete, was found at most locations. A discontinuous 100mm thick vein of fibrous peat existed at the base of this layer in one trial pit.

3.5.2 Stratum 2

Although being of the same colour and containing similar quantities of organic matter as Stratum 3, this stratum is generally non-plastic and contains a much high percentage of coarse silt and fine sand. The natural water content is typically 20-45%. Observations made in the trial pits and in the CPTs indicate that the stratum is primarily a silty sand but contains layers of sandy silt and occasional clayey silt. The soil contains occasional shell fragments, usually no greater than 5mm, although a large flat shell (60mm across) was found in a bulk sample from a trial pit.

3.5.3. Stratum 3

Stratum 3 comprises the bulk of the deposit, and its properties are summarized below:

Clay composition

- Stratum 3 may be described as a clayey organic silt, although the clay fraction ranges between 8% and 38% showing an increase with depth.
- X-Ray Diffraction analyses show that the clay fraction is principally composed of illite and chlorite. Moreover, illite and chlorite are also the only two clay minerals which are described by *both* the SSA and the CEC measured ranges.[4] Smaller quantities of chlorite and kaolinite were identified, in addition to traces of pyrite, dolomite and plagioclase feldspar. The swelling material smectite was also found in a poorly crystallized form[5].

[4] Interpretation of SSA and CEC based on Mitchell (1976).
[5] The presence of smectite is found by comparing untreated slides with slides treated in ethylene glycol overnight at 600^{o}C.

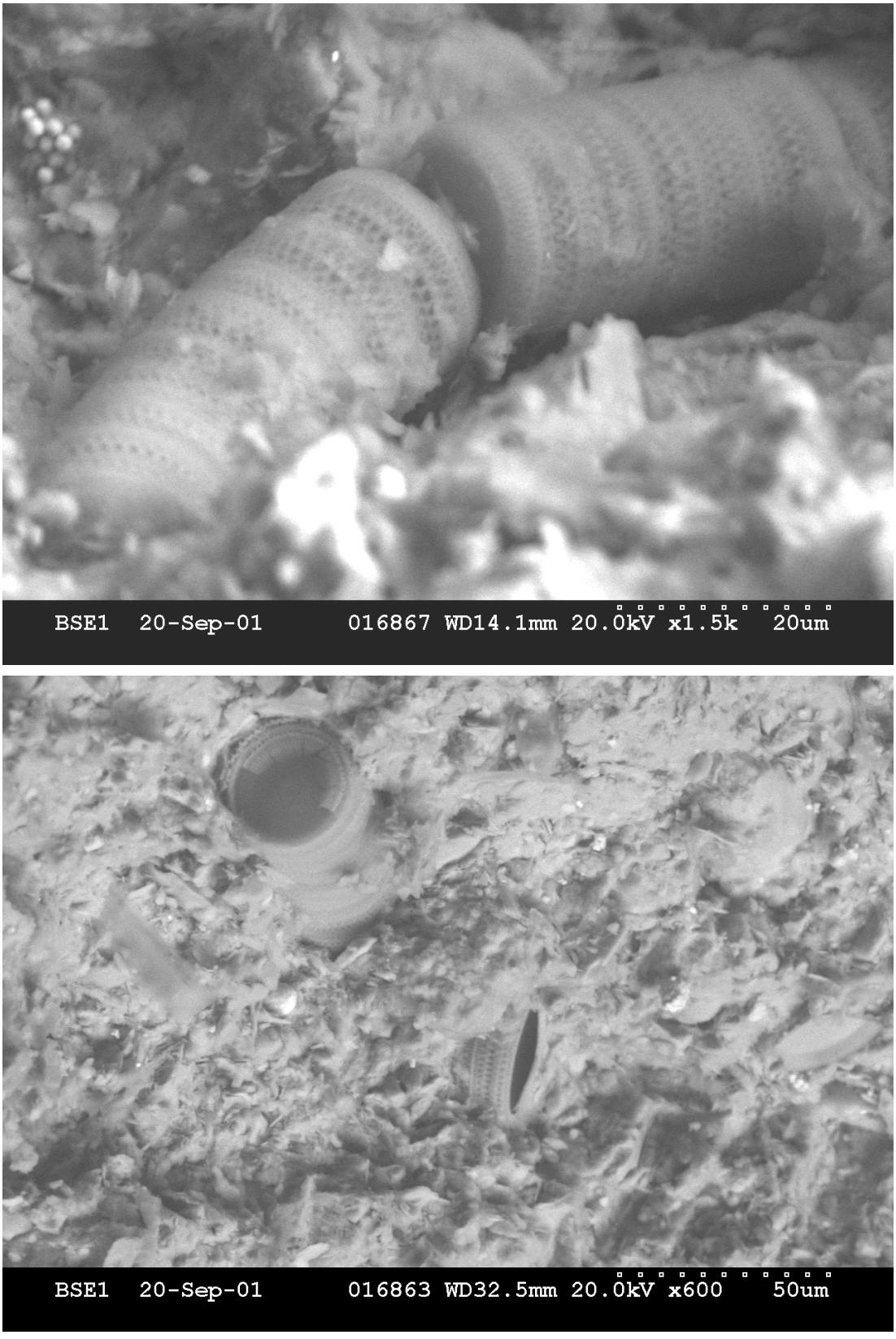

Figure 3-4 Electron microscope images of sleech showing diatoms

- The organic content determined by the loss upon ignition method at 450^{o}C is typically 11.3±0.2%. The 4±1% value quoted by Crooks and Graham (1976) pertains to the higher ignition temperature of 850^{o}C.
- Chemical analyses on material smaller than 40μm indicate a composition comprising about 50% quartz, between 15% and 20% dolomite and between 4 and 8% calcite.
- Electron microscope images such as those shown in Figure 3-4 confirmed the presence of clay minerals and the increase in clay content with depth. The images revealed a significant quantity of (siliceous) diatoms; the implications of which are discussed by O'Loughlin (2001).

Mechanical Properties

- The natural water content of the material of Stratum 3 is typically 60±10% and the average liquidity index of ≈0.8 throughout is consistent with a lightly overconsolidated material.
- The mean liquid limit of 65±10% and plasticity index of 35±5% plot in the high plasticity range of the Casagrande plasticity chart.
- A number of Atterberg limit determinations performed on samples with the organic fraction removed (by loss on ignition at 450^{o}C) indicated that the liquid limit fell by about 20% and the plastic limit remained unchanged. The material with the organic fraction removed falls in the intermediate plasticity range. This plasticity, according to Hight et al (1992), is likely to be more indicative of its mechanical characteristics. Sample inspections revealed that at least part of the organic fraction is composed of coarse fibrous plant material, which does not contribute to an apparent high plasticity. As with the Bothkennar clay-silt, the organic fraction is therefore also likely to comprise the residue of marine organisms which have attached themselves to the clay.

3.5.4 Stratum 4

No laboratory tests have been performed on this Stratum and reliance is placed on visual inspections, which describe it as a 'uniform fine to medium sand'.

Below 11.0m, boreholes taken by the DoE indicate alternate clay and sand layers (of varied thicknesses and consistencies). The maximum depth of exploration recorded in these boreholes was 36m, terminated on either a boulder or basalt dyke. Since rock coring was not performed, this provides the best estimate of rock head.

3.6 In-situ tests

In-situ tests performed during this test programme include:

- Five standard electric cone penetration tests (CPT1-CPT5)
- Six piezocone tests (CPTu1-CPTu6), q_c profiles and Robertson's charts shown in Appendix 3-4
- Three dissipation tests (D1-D3)
- Two shear vane profiles
- Seismic cone tests
- Cone pressuremeter tests.

A summary of in-situ test results is provided in Figure 3-5, including the measured range of CPT end resistance (q_c) values, peak strengths from in-situ vanes (c_u-vane), shear wave velocities from seismic cone tests (v_s) and limit pressures in cone pressuremeter (CPM) tests (p_L). The following observations may be made:

- The q_c values display quite clearly the transition between Strata 1/2 and Stratum 3 in all cases. The significant variability in the soil consistency of the fill (Stratum 1) and the sandy sleech (Stratum 2) is evident. For example, the lower bound q_c profile suggests a virtual total absence of Stratum 2 while the upper bound q_c profile indicates relatively competent soils (q_c as high as 7MPa) to a depth of 2.5m.
- The stronger consistency of Stratum 2, compared to Stratum 3, is confirmed by the higher vane strength and (slightly higher) shear wave velocities measured at 1.9m and the higher CPM p_L value at 2.3m.
- The q_c profiles in Stratum 3 are remarkably uniform, despite the variations in composition indicated by Figure 3-3. Total cone resistances, q_t (i.e. q_c corrected for pore pressures acting on the cone's filter stone) increase linearly with depth

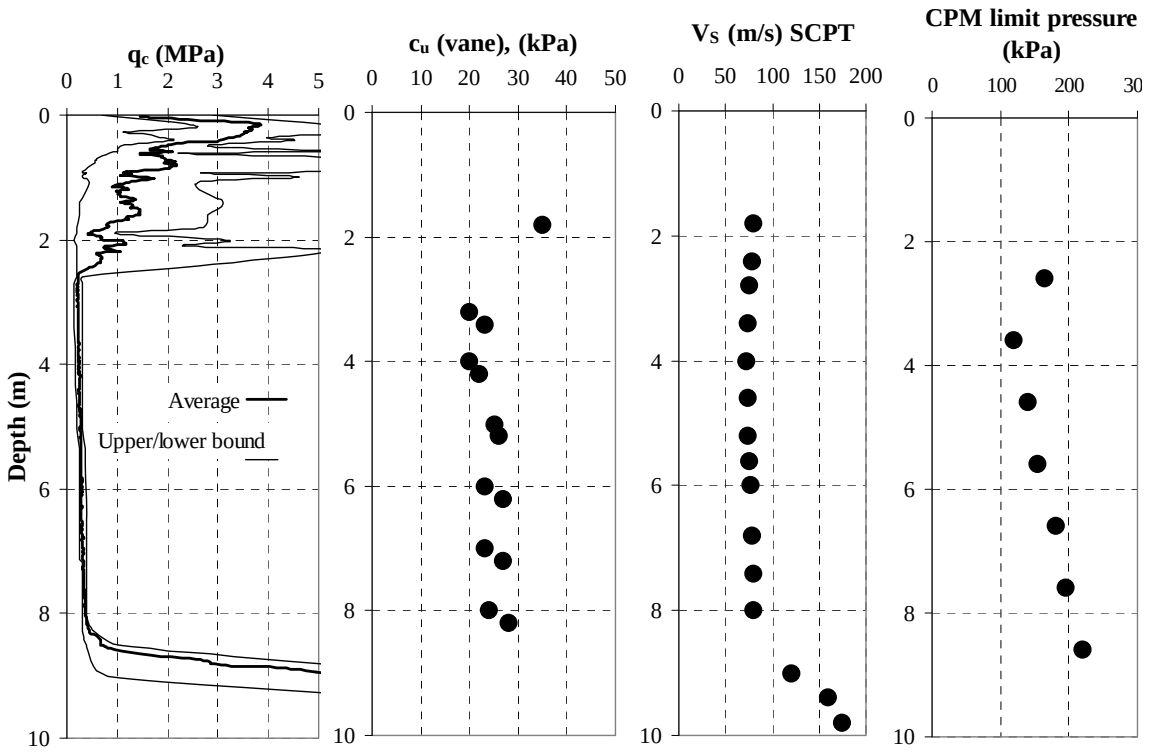

Figure 3-5 Summary of in-situ test results

from ≈200 kPa at 2.5m to 400kPa at 8m. Vane strengths[6] increase marginally over the corresponding depth interval from ≈20 kPa to 25 kPa and shear wave velocities increase from ≈72m/s to 80m/s[7].

- Much of the CPTu data falls within the normally consolidated band in Robertson's charts (see Appendix 3-4).
- Although pore pressure measurements were not *always* reliable, pore pressures at the cone shoulder increased linearly from the groundwater level[8] to 200±50kPa at the base of the *sleech* layer. Piezocone dissipation tests (D1-D3) indicate that the horizontal coefficient of consolidation, c_h (determined using the procedure of Houlsby and Teh 1988) varied between $7m^2$/year and $12m^2$/year.

[6] Vane strengths presented in Figure 3-5 without correction.
[7] $G_{seis}=\rho(V_s)^2$, $\rho\approx1630kg/m^3$, equivalent G_{seis} values are typically [8500-10500] kPa.
[8] Water table level changes with the season and tides, extremes of 1.0m and 1.3m below ground level noted in standpipe.

3.7 Behaviour in 1-D compression

Standard 24-hour 1-D compression tests were carried out on:

- intact specimens (from 100mm diameter samples)
- a specimen reconstituted at a water content of 1.3 times the liquid limit (from 54mm diameter samples)

In general, the 100mm samples were subjected to a greater degree of disturbance, which is reflected in the absence of a sharp yield point, even when the data is plotted within the $\log_e(1+e)$ against $\log_e(\sigma'_v)$ framework. All results are reproduced in Appendix 3-5, with a summary provided in Figure 3-6.

3.7.1 Compressibility Characteristics

The initial classical response of a natural intact soil is shown for a typical specimen in Figure 3-7, (i.e. a compression curve which is well above the intrinsic compression line) followed by general convergence with the ICL at a stress of about 1MPa. Measured compression indices for the reconstituted soil (C_c*) were in close agreement with those deduced from the Burland (1990) correlation between C_c* and the void ratio at the liquid limit[9]. Use of this correlation for all oedometer tests indicated a relatively constant C_c/C_c* ratio of 1.3 ±0.1 (where C_c, which had a average value of 0.6, is the measured normal consolidation compression index of the intact soil up to σ'_v= 1MPa).

The swelling indices (C_s) are typically 4-6 times lower than C_c values but also correlate well with the liquid limit. The sleech showed a tendency to creep in the oedometer tests and the creep coefficient, C_α, was relatively constant at 0.04 ±0.01 in all oedometer tests in the normally consolidated range (Appendix 3-6).

3.7.2 Overconsolidation

Vertical yield stress ratio ($YSR=\sigma'_{vy}/\sigma'_{vo}$)[10] inferred from oedometer tests on Stratum 3 varied from ≈1.6 at a depth of 3.0m to about unity at a depth of 8.0m. The reduction in YSR with depth reflects the relatively constant preconsolidation pressure (σ'_{vy}) of 55±5

[9] C_c*=0.256e_L-0.04; e_L is the void ratio at the liquid limit
[10] Determined by Casagrande construction

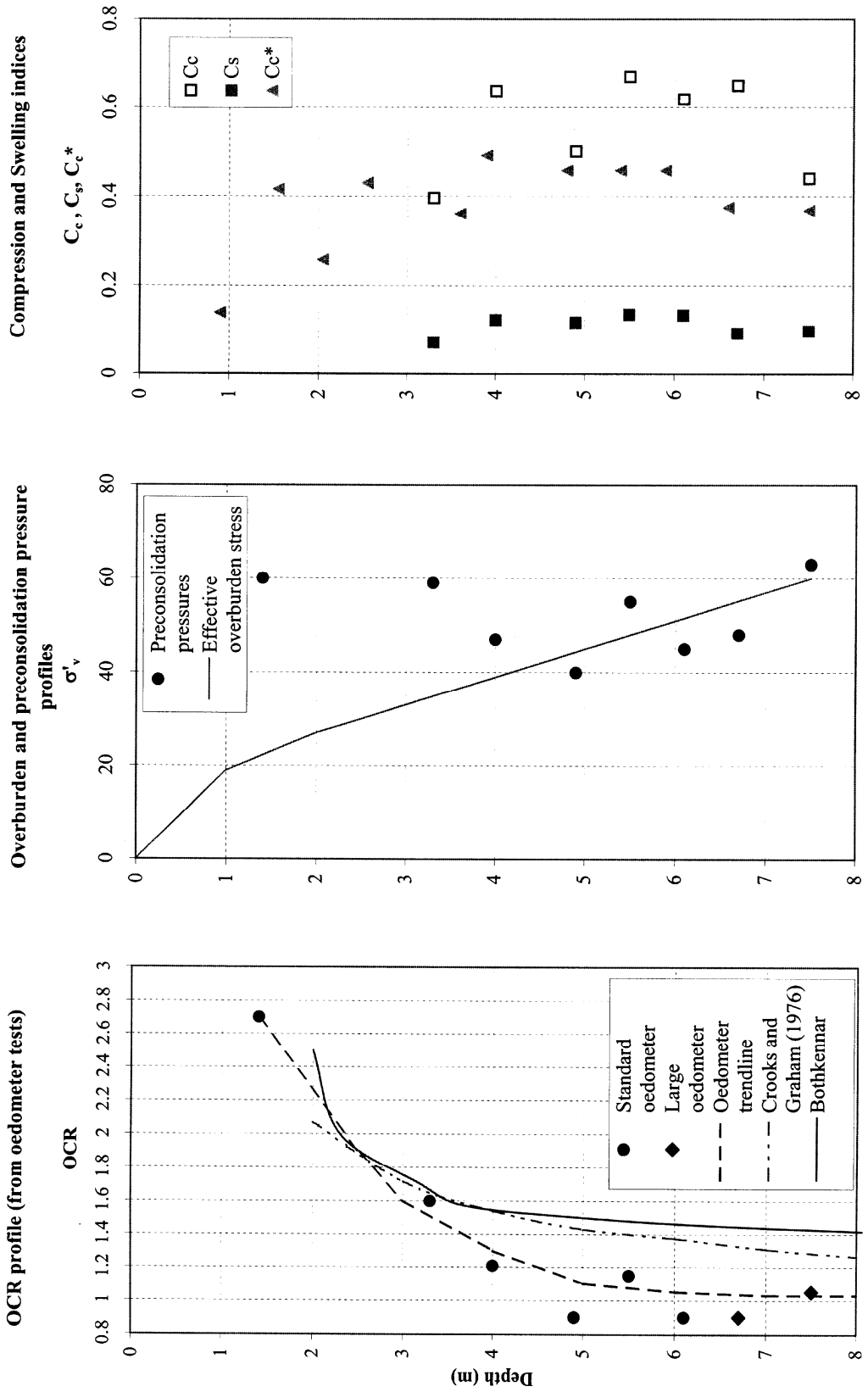

Figure 3-6 1-D Compression parameters deduced from oedometer tests

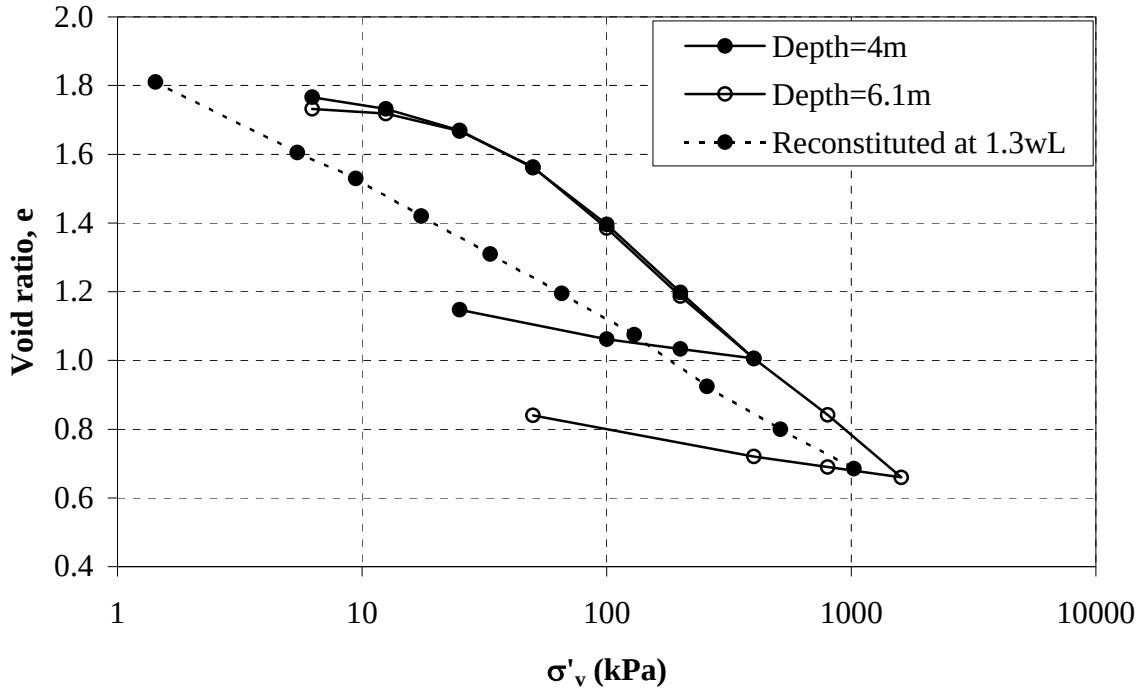

Figure 3-7 e-log σ'_v curves for intact and reconstituted sleech specimens

kPa. YSR values are slightly lower than measured by Crooks and Graham (1976), possibly due to the addition of the fill layer in the meantime. The YSR profile of Crooks and Graham (1976) is virtually coincident with that reported by at Bothkennar by Leroueil (1992).

Crooks and Graham (1976) suggest that watertable fluctuations were the principal cause of the light overconsolidation in the deposit. Constant differences between yield stress and vertical effective stress (σ'_{vy}-σ'_{vo}) when plotted against depth have been proposed by Parry (1972) to illustrate groundwater fluctuations at some stage in geological history. Crooks and Graham (1976) show that this observation is applicable to Belfast *sleech*; the effect of sampling disturbance may in fact conceal this trend from emerging in the most recent tests.

Although the bulk of the material in Stratum 2 is silty sand, one sample of a clayey silt was recovered from 1.4m. The value of σ'_{vy} is similar in Stratum 2, so the higher YSR

(=2.7) reflects the greater consistency of the material at shallower depths. The C_c value of 0.28 is roughly 50% of the average in Stratum 3.

3.7.3 Permeability and Coefficient of Consolidation

The permeability estimated from oedometer tests on Stratum 3 reduced with increasing stress levels but were typically in the range 1.5×10^{-10} to 5×10^{-10} m/s at in-situ stress levels. Vertical coefficients of consolidation (c_v) determined from the same set of tests reduced from about $3m^2$/year in the overconsolidated region to $0.5m^2$/year at a vertical effective stress of 100kPa.

Overall, it appears that, despite the high silt content in Stratum 3, the clay fraction is sufficiently influential for the soil mass to have permeabilities and coefficients of consolidation more typical of a clay than a silt.

3.8 Strength Properties of Sleech

3.8.1 Undrained Strength in Triaxial Compression

A summary of all undrained triaxial tests performed on Stratum 3 specimens is provided in Table 3-2[11]. In each of the CIU and CK_oU tests, the in-situ stress state was recovered approximately by consolidation and swelling[12] to artificially induce the required level of overconsolidation. The 54mm diameter samples were allowed a one-day 'ageing' period, before undrained shearing in all cases at axial strain rates of 4.5% per day.

The quality of sample tested is not consistent throughout T1 to T17 and the effects of disturbance are seen in some of the 100mm DoE-recovered samples[13] as:

(i) A tendency for the 'sleech' to dilate at mobilized friction angles of about 30^o.

(ii) The axial strains required to develop peak deviator stresses (ε_a>5%) are much higher than might be obtained had better sampling techniques been available ($\varepsilon_a \approx$ 0.1-1%).

[11] see also Appendix 3-7.
[12] K_o=0.5 for anisotropic consolidation, K_o=0.6 for anisotropic swelling.
[13] Tested up to one year after sampling.

Reference	Depth (m)	Diameter (mm)	Test	Isotropic OCR
T1	3.6	38	UU	1.0
T2	3.9	38	UU	1.0
T3	5.5	38	UU	1.0
T4	5.8	38	UU	1.0
T5	4.2	100	CK_0UC	1.0
T6	5.45	100	CK_0UC	1.5
T7	5.4	100	CIUE	1.5
T8	4.0	100	CK_0UC	1.5
T9	6.8	100	CIUC	1.5
T10	6.6	100	CIUC	1.5
T11	4.45	38	CIUC	2.0
T12	4.65	38	CIUC	4.9
T13	5.85	38	CIUC	1.5
T14	6.1	38	CIUC	1
T15	3.8	54	CK_oUC	1.2
T16	4.8	54	CK_oUC	1.15
T17	5.0	54	CK_oUE	1.15

Table 3-2 Triaxial tests performed upon Stratum 3

Typical q-p' stress paths for 54mm triaxial compression specimens T15 and T16 are shown in Figure 3-8. The undrained stress paths are typical of lightly overconsolidated soils in CK_oUC tests; the contraction of the sample is reflected in the sharp drop in deviator stress as the mean effective stress falls and the mobilized friction angle increases. Test T16 shows the sharper peak, which was reached at $\varepsilon_a \approx 0.5\%$. A suite of 38mm diameter CIU tests (Figure 3-9) with varying degrees of imposed isotropic overconsolidation ($1<OCR<5$) also highlights post-peak contractant behaviour.

Measured values of the undrained strength ratio (c_u/σ'_{vo}) determined in the triaxial compression tests and direct simple shear tests are compared in Figure 3-10 with the range proposed by Ladd et al (1977):

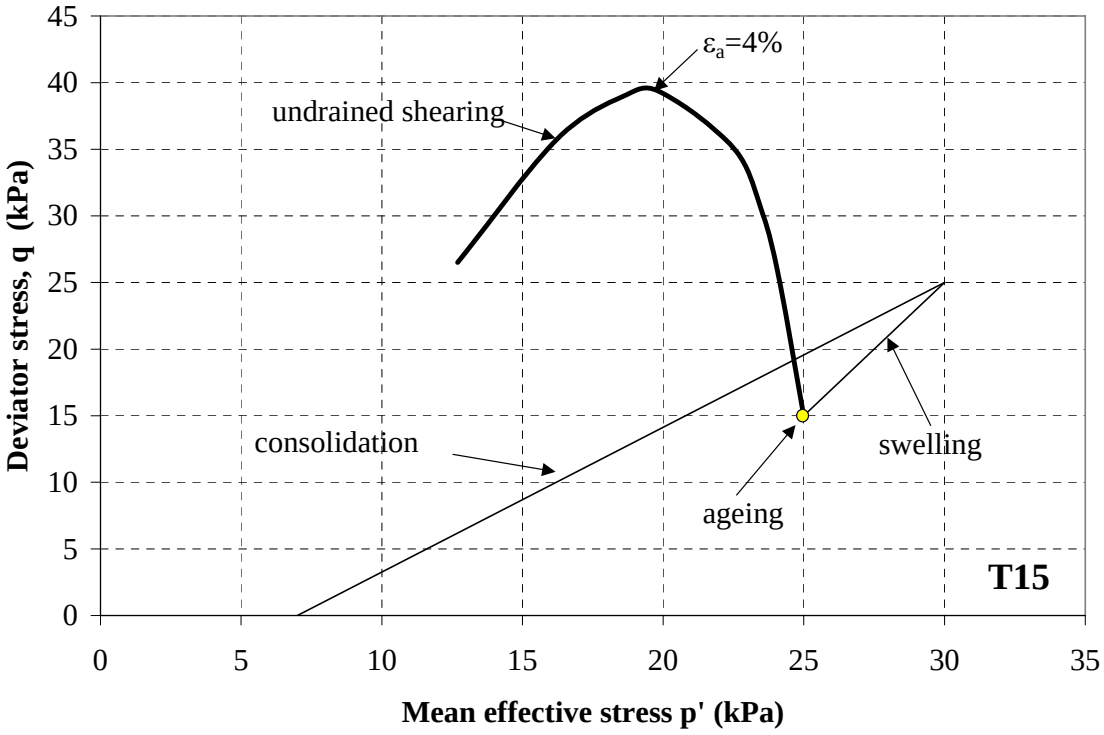

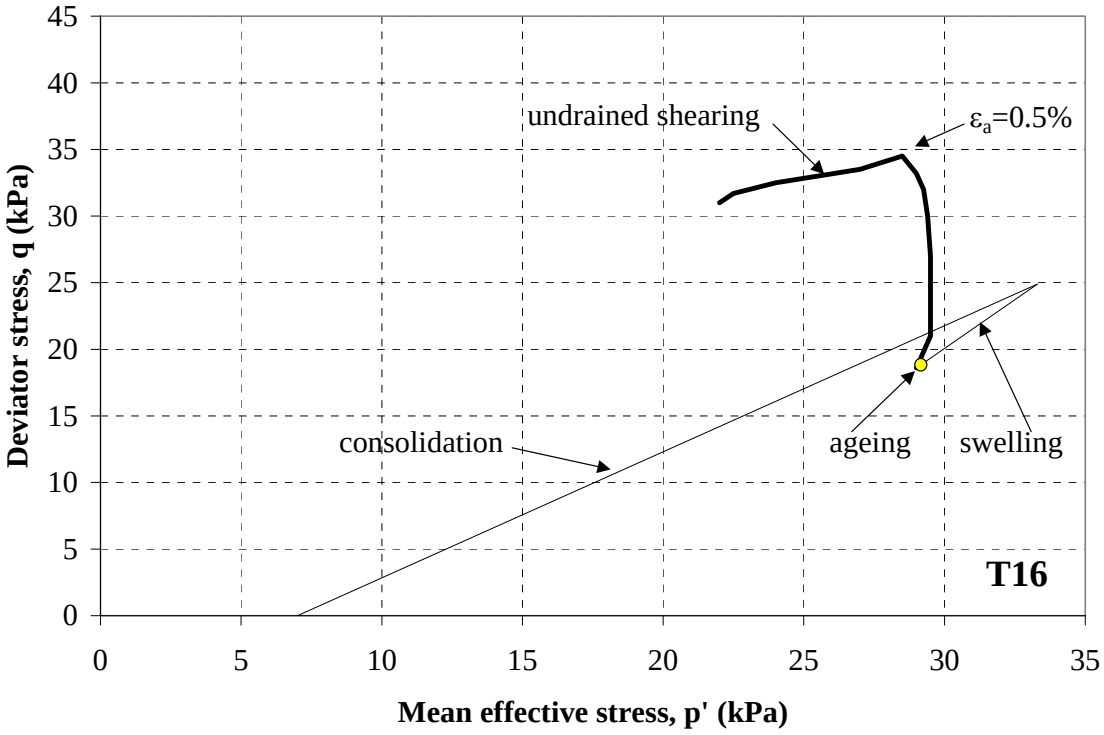

Figure 3-8 Typical q-p' CK_oUC stress path for lightly overconsolidated sleech

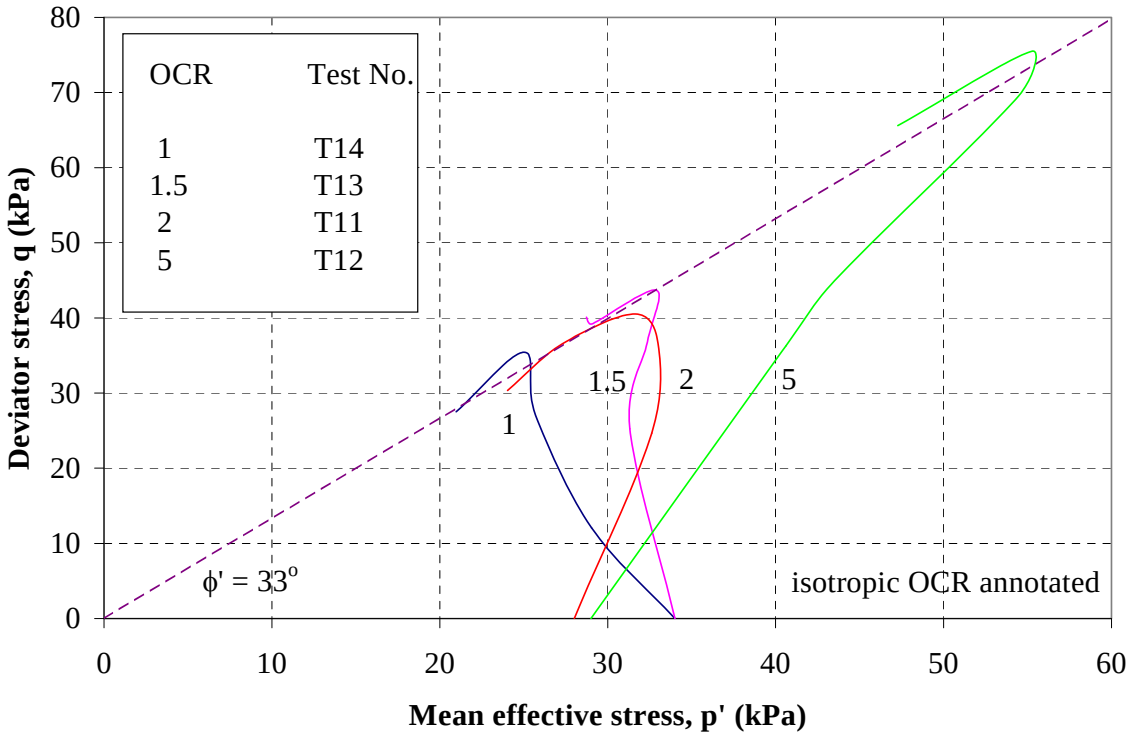

Figure 3-9 Typical CIU stress paths (T11-T14)

$$\frac{c_u}{\sigma'_{vo}} = \left(\frac{c_u}{\sigma'_{vo}}\right)_{nc} OCR^{0.8} = (0.3 \pm 0.05) OCR^{0.8}$$

Many of the measured undrained stress ratios, particularly those for the anisotropic tests and those at very low OCR (<1.2), appear to be somewhat higher than anticipated, but nevertheless are in keeping with values quoted by Crooks and Graham (1976).

Laboratory values of c_{utc} are typically 20±3 kPa and show no clear trend with depth. If an average yield stress of σ'_{vy}=55kPa is adopted (based on Figure 3-6), the ratio c_{utc}/σ'_{vy} is typically 0.3-0.4. Better quality block or Sherbrooke samples are likely to give slightly higher c_{utc}/σ'_{vy} ratios (while also yielding higher individual c_{utc} and σ'_{vy} values). These c_{utc} values agree quite well with the field vane test results (Figure 3-5) scaled by 0.85 (Bjerrum's correction for a plasticity index of ≈40%); such conformity was also found at the Bothkennar site.

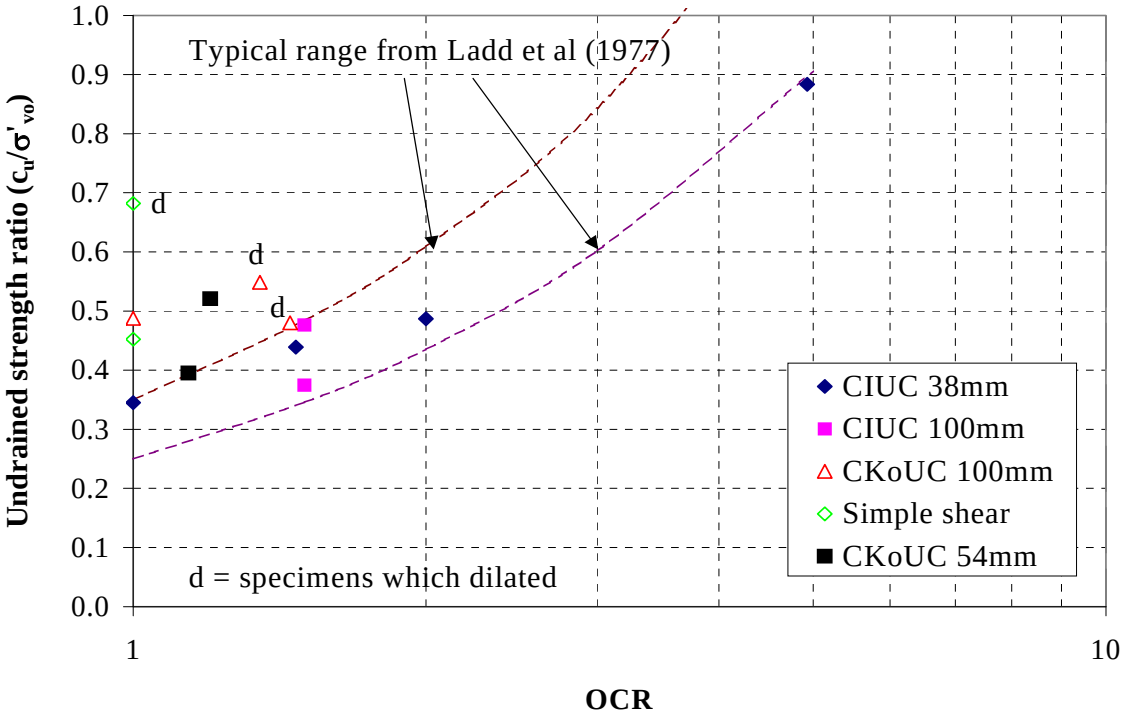

Figure 3-10 Undrained strength ratios for Stratum 3 material

3.8.2 Undrained Strength in Triaxial Extension

One CIUE test (T7) and one CK_oUE test (T17) was carried out. The q-p' stress paths for these tests are presented in Figure 3-11. They show:

- Values of c_{ute} are typically 13-15kPa and thus are lower than c_{utc} values.
- c_{ute}/σ'_{vo} values were found to be 0.28 (OCR=1.15) and 0.31 (OCR=1.5), both plot lower than the c_{utc}/σ'_{vo} values of Figure 3-10.

3.8.3 Rate Dependence of Undrained Strength

The dependence of the undrained strength of normally consolidated 'sleech' on axial strain rate was investigated in two further CIU tests performed on 54mm diameter samples[14] (between depths of 4m and 5m). These samples were isotropically consolidated to a mean effective stress (p'_i) of 100 kPa and each was then subjected to triaxial compression at initial lower axial strain rate and at a final faster axial strain rate.

[14] Tests not listed in Table 3-2.

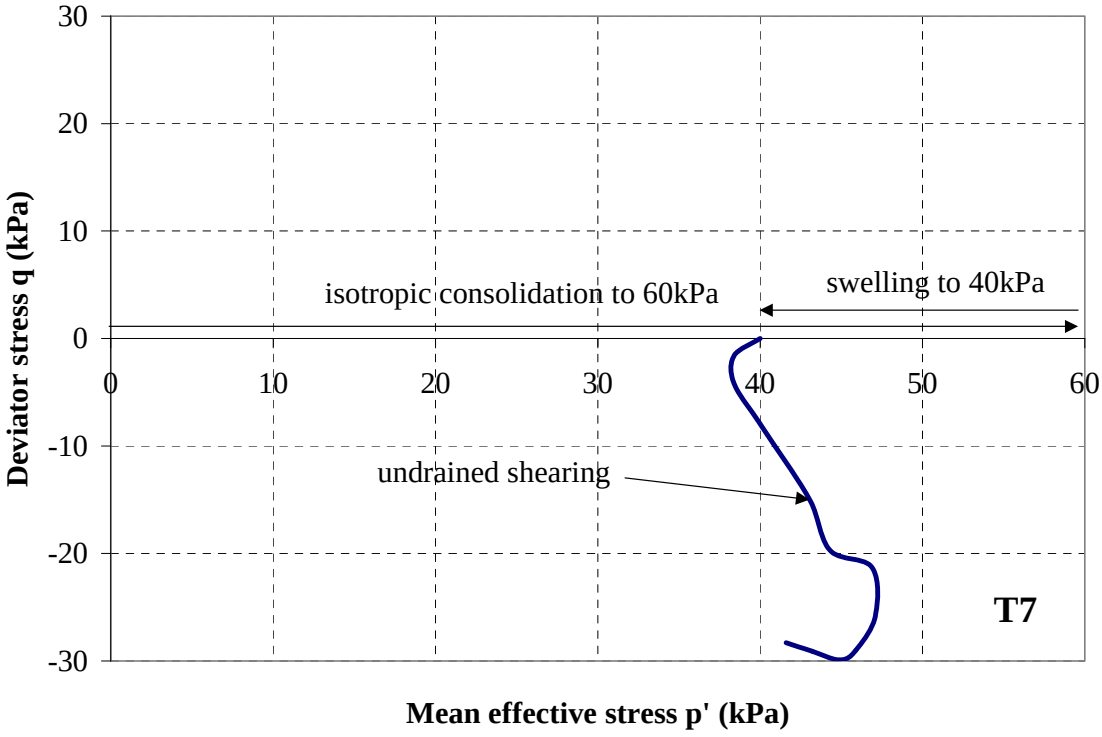

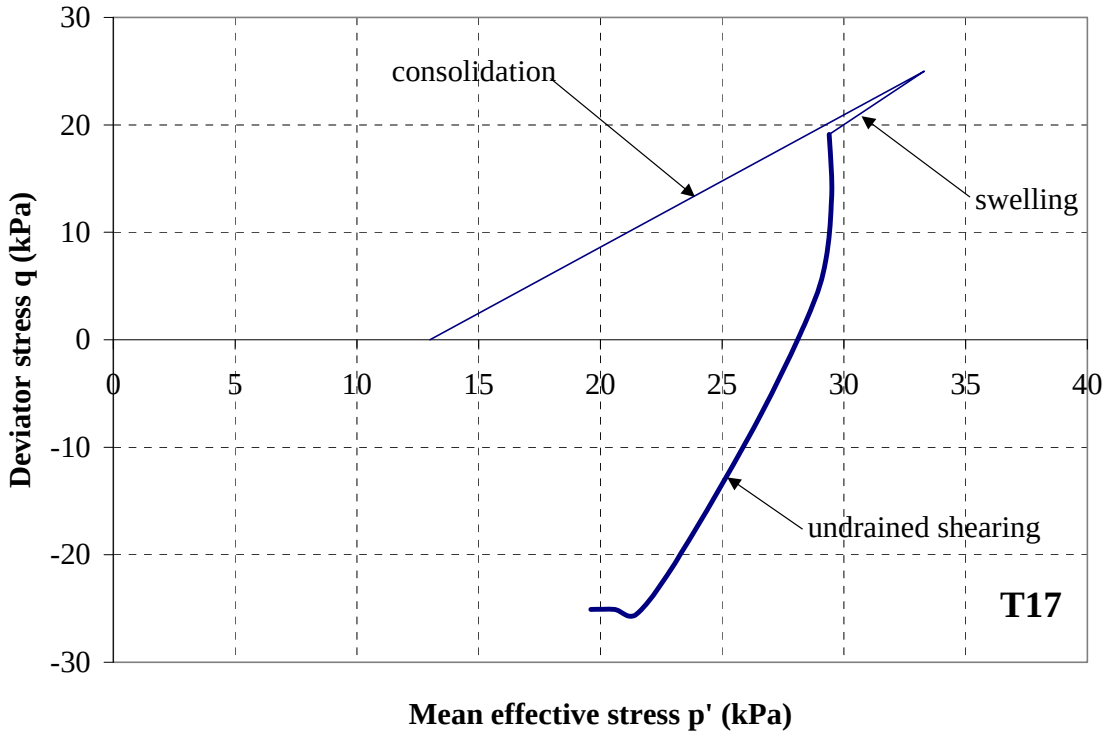

Figure 3-11 Triaxial extension q-p’ stress paths

The results from these tests are summarised on Figure 3-12, where it is evident that the c_u/p'_i ratios increase by a factor of 15% for each log cycle increase in strain rate[15].

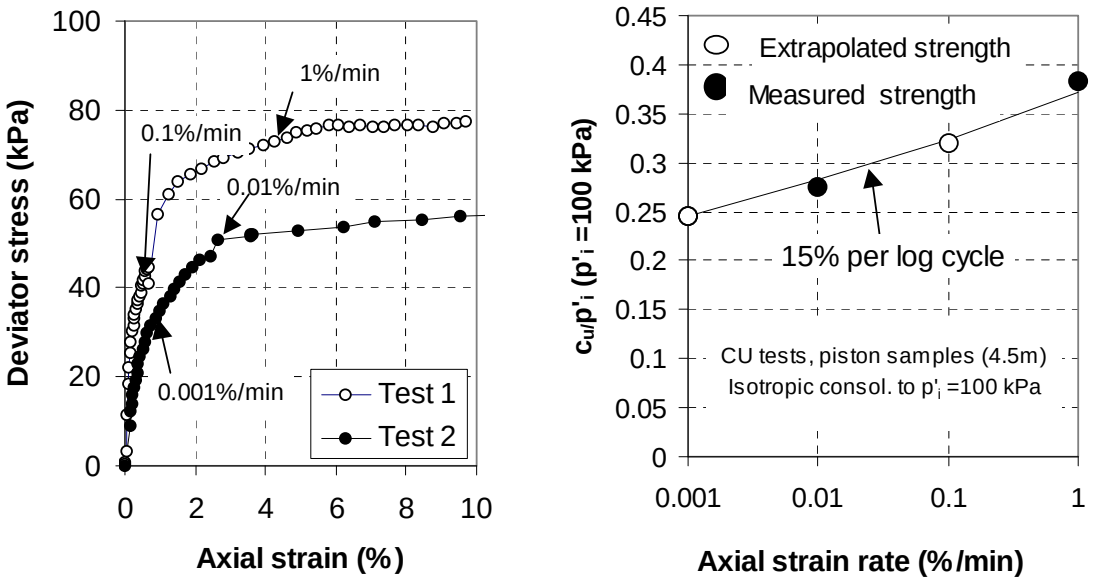

Figure 3-12 Rate dependence of undrained strength

Strain rate determinations on triaxial specimens by Crooks and Graham (1976) produce values in the range 8-17% per log cycle, with much of the data in the 10-12% range (for a plasticity index of ≈40%).

3.8.4. Effective Stress Strength

The effective stress strength parameters of Stratum 3 were derived from the consolidated undrained triaxial tests of Table 3-2 and a number of shear box tests reconsolidated to normal effective stresses between 50kPa and 200kPa. The values of stress invariants t and s' at ultimate conditions (≈10-20% axial strain) are plotted in Figure 3-13 for the CU triaxial tests.

[15]The 'extrapolated' c_u/p'_i ratios plotted on Figure 3.7 refer to ratios estimated from the initial slower rate adopted in each test.

The constant volume friction angle (ϕ'_{cv}) shows a relatively low sensitivity to the specimen's stress history, sample depth and sample quality. The ultimate strength in Stratum 3 is well represented by the effective stress strength parameters: c'=0 and ϕ'_{cv} =33.5^o. Noteworthy points regarding the constant volume friction angle include:

- This relatively high friction angle is comparable to that of the Bothkennar clay-silt (34^o), which has a slightly higher clay fraction, but lower percentage of clay minerals.
- This friction angle is more in keeping with the plasticity index of the material when the organics are removed than when the organics are present (as suggested by Padfield and Mair 1983).
- The variability in particle size distributions over the depth of Stratum 3 is not reflected in the ϕ'_{cv} values.

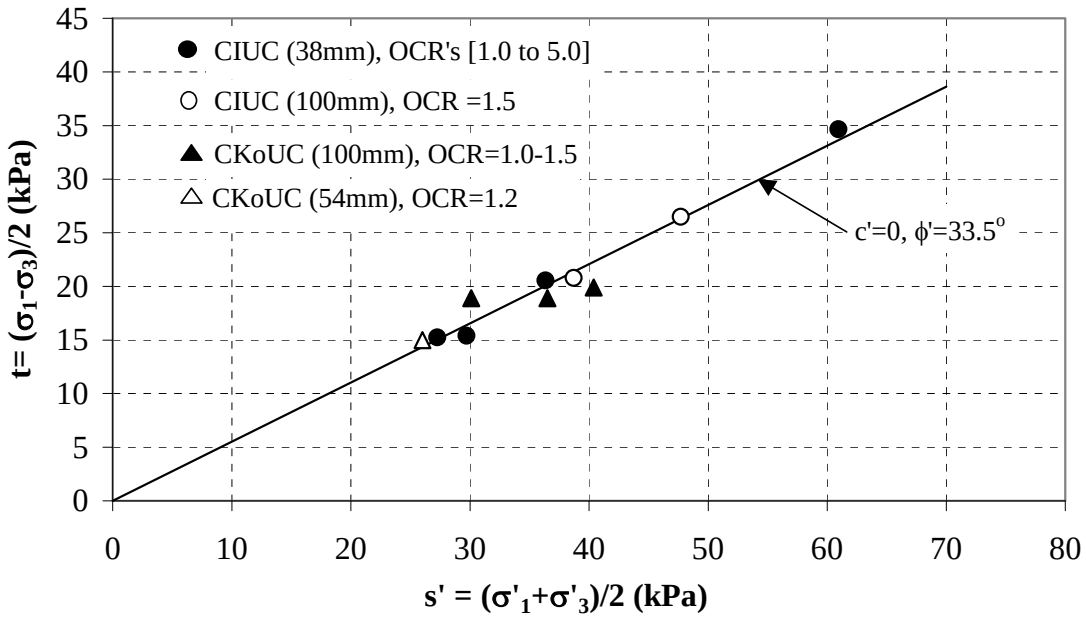

Figure 3-13 Constant volume friction angle for triaxial compression tests

Plots of shear stress against normal stress for the 60mm shear box specimens sheared at 0.0244mm/min (Figure 3-14) reveal the following:

- The shear stresses of 8-12kPa corresponding to zero normal stress are believed to be 'apparent' c' values which are a function of the testing apparatus. No such cohesion is evident in the triaxial data of Figure 3-13.

- Typical plots of vertical against horizontal displacement reveal the contractant behaviour typical of lightly overconsolidated materials (selected data in Appendix 3-8).
- The values of ϕ'_{cv} (calculated assuming c'=0 to be consistent with the triaxial data in Figure 3-13) vary from 33° at σ'_v=50kPa to 26° at σ'_v=200kPa. The former stress level is most representative of the in-situ stress state, which shows good agreement with ϕ'_{cv} measured in triaxial compression tests. As with the triaxial specimens, ϕ'_{cv} is invariant with depth.
- The slightly higher ϕ'_{cv} values in Stratum 2 reflect the lower water contents and higher sand content compared with Stratum 3.

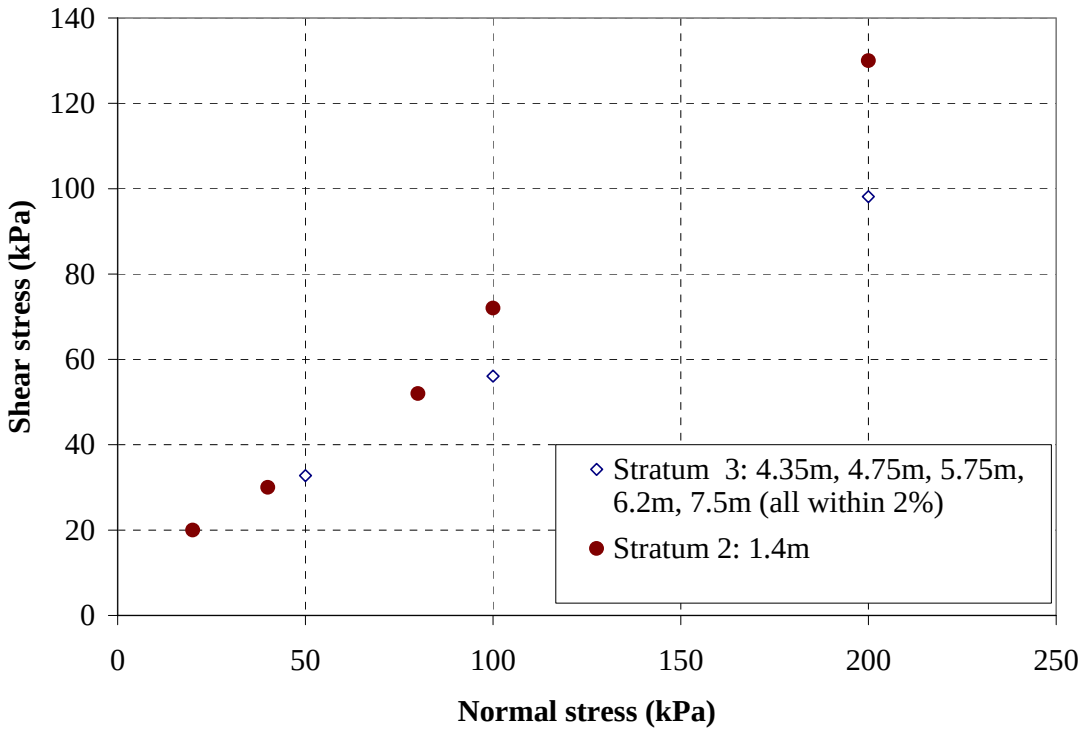

Figure 3-14 Shear box tests in Strata 2 and 3

Undrained constant-height simple shear tests were also performed (on intact samples consolidated to stresses near the preconsolidation pressure), some of which showed unusual τ-σ'_n stress paths[16] (Appendix 3-8). The measured values lay between 25° and 30°, 3.5° to 8.5° below those measured in triaxial compression. This falls roughly half

[16] Probably due to poor quality samples

way between the average ϕ'_{cv} in triaxial compression and extension. The c_{uss} values are in reasonable agreement with c_{utc} values (Figure 3-9).

3.9 Stiffness Properties of Sleech

Local strain measurements on the triaxial specimens were determined by:

- Two Hall effect transducers for tests T16 (compression) and T17 (extension)
- A Video Extensometer for T6 and T8 (both compression). This entailed the use of a high resolution video camera to remotely track the vertical movements of markers on the specimen's rubber membrane. (Appendix 3-9)

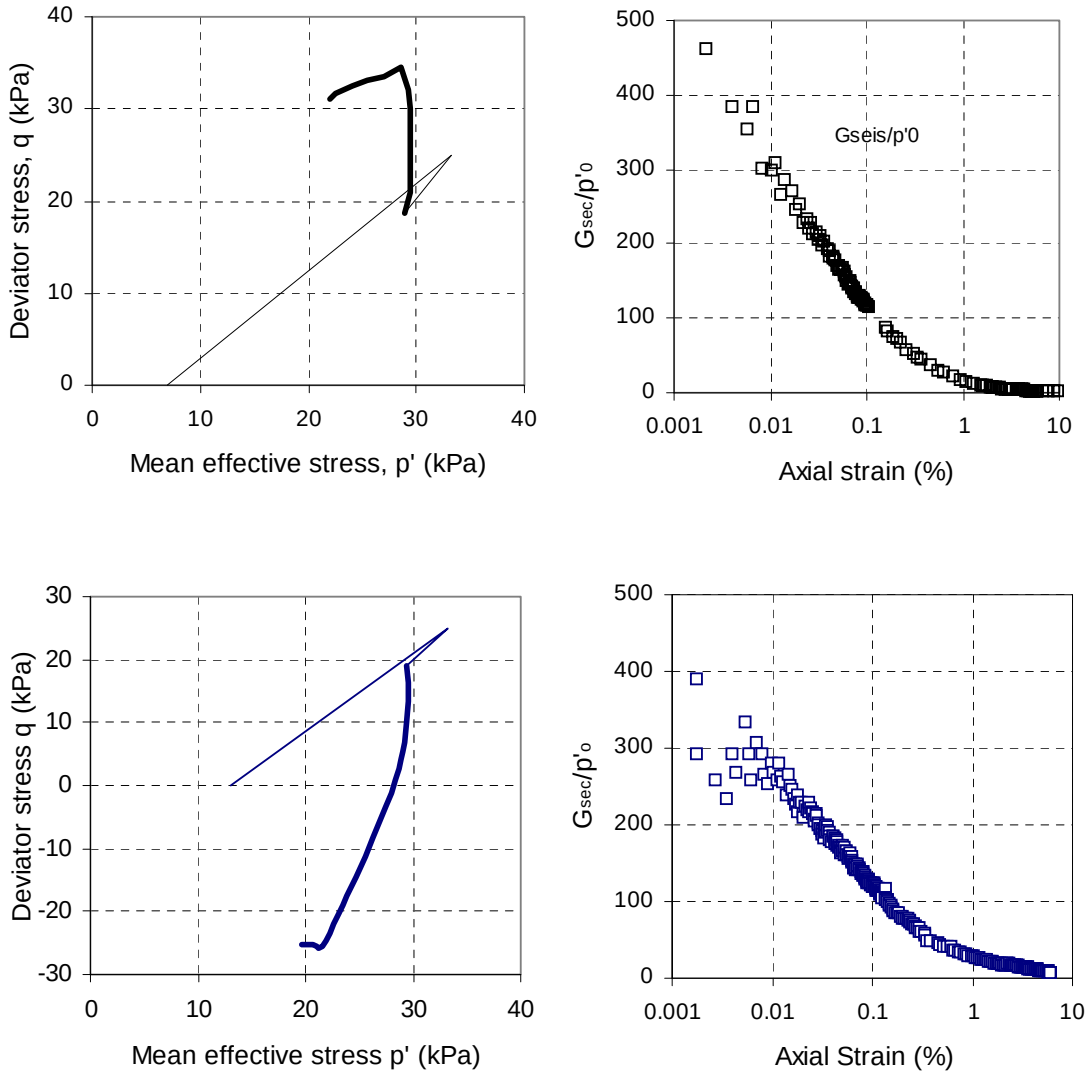

Figure 3-15 Small strain stiffness measurements for T16 (compression, above) and T17 (extension, below)

Typical small strain secant shear stiffness values G_{sec} (calculated from E_{sec} with υ=0.5 for undrained conditions) normalized by the initial mean effective stress at the beginning of undrained shearing p'_o are shown in Figure 3-15 (for T16 and T17) along with their corresponding stress paths. For the compression tests, stiffness measurements made for T8 agree very well with T16 for ε_a>0.01%.

Measured G_{sec} values show good agreement with comparable data for the Bothkennar clay silt (Hight et al 1992, Smith et al 1992). However, Figure 3-16 suggests that G_{sec}/p'_o values for the Belfast sleech are generally slightly lower than those measured for the Bothkennar clay-silt.

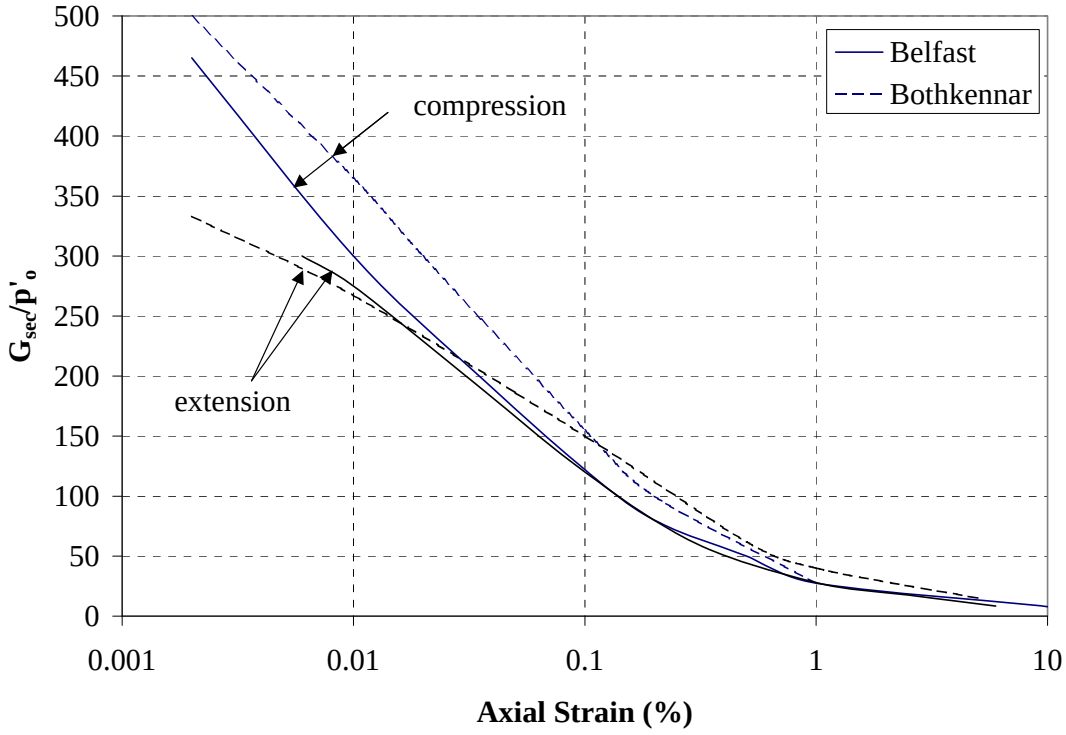

Figure 3-16 G_{sec}/p'_o values for Belfast and Bothkennar clays

3.10 Residual Strength

Soil-on-soil ring shear tests were performed on specimens of the sleech. Although not true interface tests (because the concrete pile wall was not simulated in the experiment), procedures adopted otherwise followed the recommendations of Jardine et al. (1998) for

ring shear testing performed for displacement pile design. Samples tested in the TCD Bromhead ring shear apparatus after consolidation were first subjected to a large displacement at the fast (undrained) shearing rate of 4.5mm/min to model pile installation. Samples were then sheared at a slow drained rate of displacement of 0.035mm/min after a peak and ultimate residual friction angles ($\phi'_{p,res}$, ϕ'_{res}) measured in this way and at normal effective stress of 100 kPa are plotted against depth on Figure 3-17. The difference between $\phi'_{p,res}$ and ϕ'_{res} is typically no greater than 1^{o}.

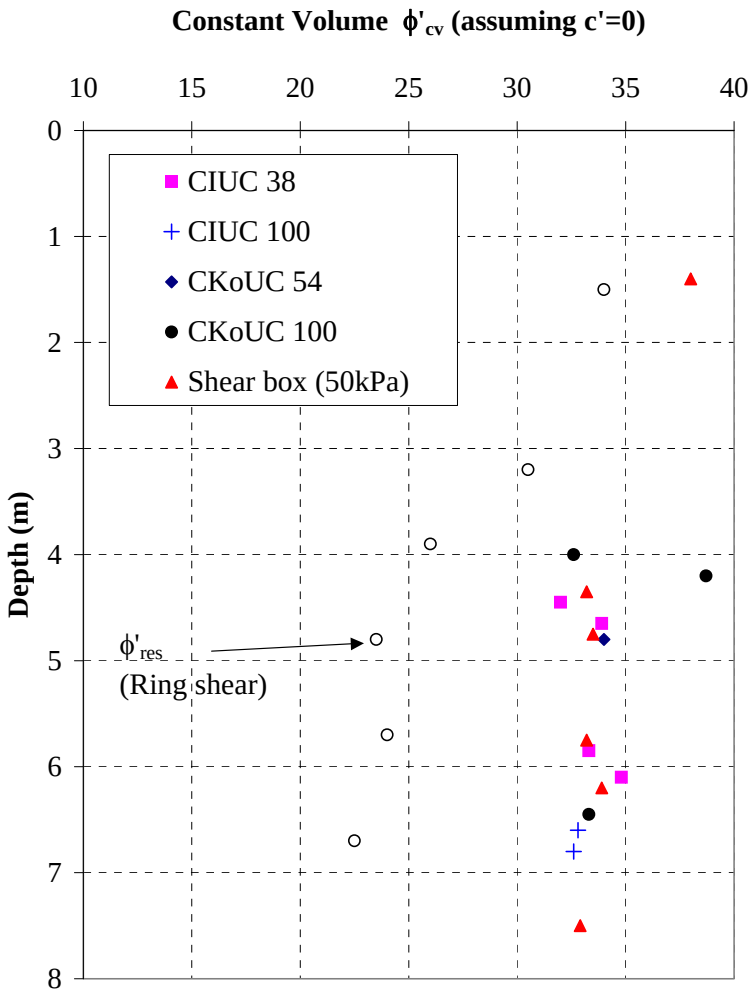

Figure 3-17 Residual friction angles for Belfast sleech

Despite the sparsity of data at depths shallower than 3m, it is clear that ϕ'_{res} falls only slightly below ϕ'_{cv} measured in triaxial compression and that the shearing mode is 'turbulent' in this region. However, below this depth, the difference is more significant

(with ϕ'_{res} lying between 19.5^{o} and 25.5^{o}) indicating a 'transitional' sliding mode, i.e. where both turbulent and sliding shear takes place in different parts of the shear zone. This shearing mode and the variability of the ϕ'_{res} angles measured is consistent with expectations based upon the composition described in Section 3-5.

Chapter 4

Experimental Procedures followed for the Field tests

4.1 Introduction

A comprehensive programme of piling research was carried out at the Kinnegar soft clay test bed between August 1997 and June 2001. The core experimental research of this Thesis concentrates upon a programme of axial static and one-way cyclic tests on friction piles, comprising single reference piles and five-pile groups. Laterally loaded pile tests on end bearing piles (Phillips 2002) were also performed at the same site.

A total of seven tests on four single piles and seven tests on four pile groups are presented in this Thesis. In order to distinguish between the individual piles and pile tests carried out on them, a labelling system was devised with two components:

Pile ID / Loading history

The Pile ID is identified by terms in the following order:

C or T: compression or tension loading

S or G: single pile or pile group

number1: the single pile or pile group (under the designated loading direction) being referred to

[number2]: applicable to pile groups only, identifying a particular group pile (3=centre, 1,2,4,5=corner).

For example, CS1 is the first compression single pile, TG2[5] is a corner pile of the second tension pile group.

When referring to a particular test on a single pile/pile group, the second (optional) loading history component may be added. This lists in chronological order (from first to last) the previous tests (if any) and the current test performed on a single pile/pile group (s=static, c=cyclic). For example, group TG2 was subjected to a virgin cyclic test (TG2/c), which was followed by a static test (TG2/cs). In this static test, the centre pile's behaviour is referred to by TG2[3]/cs.

A chronological list of the principal site events (relevant to all axial load tests) and the ID for the test piles is given in Table 4-1. The letters A to H refer to the pile test locations in the site plan of Figure 4-1. This Chapter details all of the major components of the fieldwork culminating with the full-scale pile tests.

Date	***Event***
18/8/1997	Installation of 9 no. pneumatic piezometers around proposed location of tension pile group
4/9/1997	Installation of tension 5-pile group TG1 *(A)*
December 1997	End of pneumatic piezometer readings
30/4/1998	Casting of 'instrumented' tension single pile at Mallusk TS1
12/6/1998	Installation of 'instrumented' tension single pile TS1 *(B)*, plus support piles for single pile and pile group platforms
August 1998	Casting of concrete support platforms for tension group and single pile tests
17/9/1998	Tension pile group static load test TG1/s *(A)*
19/9/1998	Tension single pile static load test TS1/s *(B)*
12/2/1999	Casting of 'instrumented' compression pile group at Mallusk CG1
29/4/1999	Installation of 'instrumented' compression group CG1 *(C)*
17/5/1999	Removal (from *(B)*) and re-installation (at *(D)*) of tension single pile for use in compression single pile test CS1
June 1999	Casting of concrete support platforms for compression group and single pile tests
5/8/1999	Compression pile group static load test CG1/s *(C)*
7/8/1999	Compression single pile static load test CS1/s *(D)*
September 1999	Driving of new tension single pile TS2 *(E)*
5/10/1999	Cyclic tension pile group test TG1/sc followed by static test TG1/scs *(A)*
14/12/1999	Tension single pile static load test TS2/s *(E)*
9/5/2000	Tension single pile static load re-test TS2/ss *(E)*
10/5/2000	Cyclic tension single pile test CTS1/sc *(D)*

Date	*Event*
11/5/2000	Tension single pile static load test CTS1/scs *(D)*
1/6/2000	Cyclic tension pile group test CTG1/sc *(C)*
22/6/2000	Installation of 5-pile compression group CG2 *(F)*
17/12/2000	Compression static load test on corner pile of group CG2[2]/s *(F)*
	Removal of same group from ground *(F)*
	Installation of 5-pile group TG2 *(G)* and single pile TS3 *(H)* for tension cyclic loading
8/5/2001	Cyclic TS3/c and static TS3/cs single pile tension test *(H)*
5/6/2001	Cyclic TG2/c and static TG2/cs pile group tension test *(G)*

Table 4-1 Sequence of piling events at Kinnegar

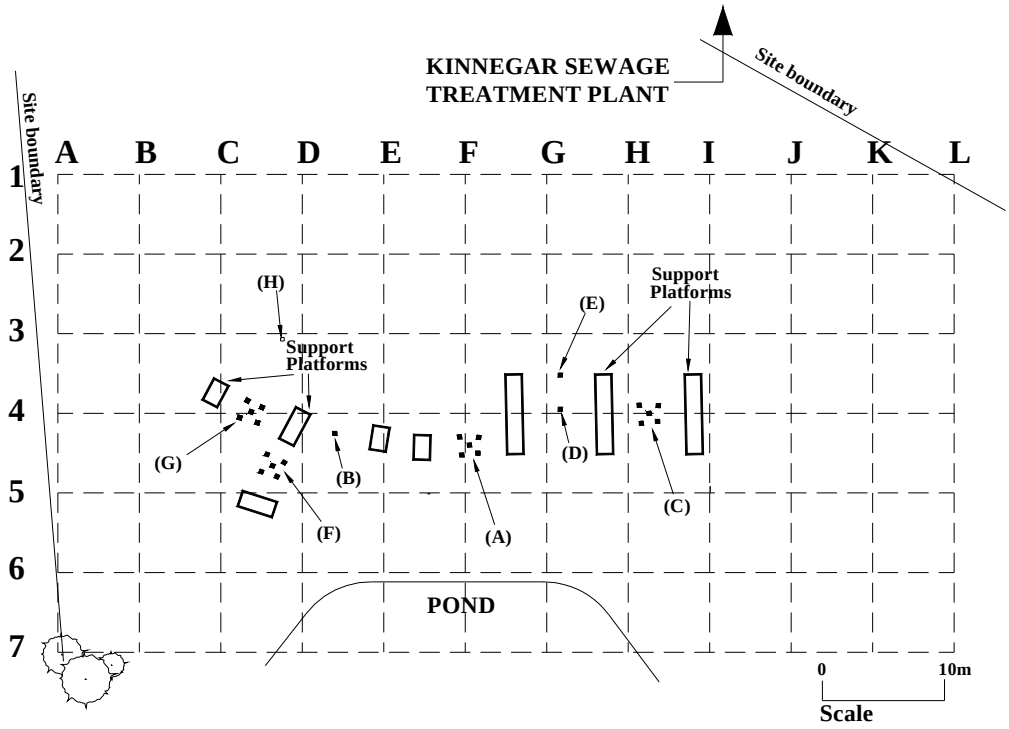

Figure 4-1 Kinnegar site plan identifying test locations

Figure 4-2 Lowering of the pile cap onto TG3

4.2 Pile cap design and assembly

The group piles were loaded together through a steel loading cap (shown in Figure 4-2 while being hoisted into position). The following subsections discuss the factors involved in its design and assembly.

4.2.1 Choice of material

Steel was selected because it offered the following advantages over concrete[1]:

- The ability to be reused for a number of different groups
- Could be manufactured off site and removed the need for steel fixing in the cap and exposing steel in the pile heads to provide continuity between piles and cap.

4.2.2 Pile Cap Design Approach

A suitable arrangement of steel was deemed to consist of two orthogonal rows of UC-sections (152×152×83), sandwiched by a steel plate (10mm thick) top and bottom. This symmetrical arrangement (i.e equal bending stiffness on all four sides of the cap) was

[1] Costs comparable for the size required for the 5-pile group.

important to 'discourage' bending in the course of the load tests originating from the pile cap geometry.

The arrangement of steel was required to provide the same bending stiffness (EI_{xx} value[2]) as a typical concrete cap 1.5m × 1.5m × 0.5m capable of safely resisting a central concentrated load of 1000kN (or 200kN/pile)[3]. An optimum solution involved the use of two orthogonal rows of 6 no. 152×152×83 UC sections, with 1.8m×1.8m×10mm plates top and bottom, offering an overall minimum weight of steel (for handling purposes).

4.2.3 Manufacture and assembly

The pile cap was built in two halves. One finished half was inverted and placed upon the other. Each half comprised a steel end plate with the six equally spaced and parallel UC rows welded on top. Each end plate was formed of two smaller ones welded together, with the UC sections positioned perpendicular to the weld. The two halves were joined so that the two sets of UC sections lay at right-angles to each other. Restricted welder access limited connection between the plates to along the periphery of the assembled unit. The potential for a gap to open in the centre had important implications for the tension group tests.

4.3 TCD Pile Head Load Cells

The expense of purchasing purpose-made load cells for the head of the single pile and group piles stretched beyond the project budget. Six load cells were fabricated in the laboratories at TCD, versatile for use in both the tension and compression pile tests. It was imperative that these cells allowed the applied load to be resolved to sufficient precision and were robust enough to respond repeatably under static and cyclic loads.

4.3.1 TCD Basic Load Cell Design

The basic load cell comprised a round hollow steel section, with an external diameter of 114mm and wall thickness of 4mm. A typical TCD load cell may be seen in Figure 4-3.

[2] E is the material Young's modulus, I_{xx} is the second moment of area about the horizontal neutral axis.
[3] Designed according to procedures in O'Brien and Dixon (1995)

Figure 4-3 TCD Pile head load cell

Two opposite faces of the cylinder were fitted with 350Ω electrical resistance strain (ERS) gauges (gauge factor = 2.10). A full (or Wheatstone) bridge *configuration* of gauges was bonded to a smooth zone on each face; this consisted of an arrangement of four gauges in a 'cross' formation (two orientated axially and two circumferentially). This composite arrangement provided stable output with minimal drift (including compensation for temperature fluctuations) and compensation for lateral strains (Poisson effect). Cables between the gauge and data logger input point were screened to reduce electrical 'noise'.

4.3.2 TCD Load Cell within Test Assembly

Modifications to the basic instrumented cylinder were necessary so that it could be both anchored to the pile head and produce a fixed connection with the steel pile cap. The load cell connection to the pile head and fixity with the pile cap is shown in Figure 4-4.

Anchorage to the pile head (Figure 4-4 top left)

A square steel plate (150mm x 150mm x 25mm thick) with a 30mm diameter hole at its centre was fixed to the base of each cylinder with a ring of weld inside and outside. This hole accommodated the dywidag anchorage bar grouted into the pile head (see Section 4.7).

Figure 4-4 Load cell fixity to pile head (top left), Load cell-pile cap welded connection (top right), Assembled test setup (bottom)

When in position, this bottom steel plate located itself flush on the pile head, with the dywidag bar protruding through the hole in the bottom plate. Threaded dywidag nuts were screwed tightly onto the protruding bar within the cylinder to secure the load cell (particularly crucial for the tension tests). The main issues addressed at the design stage

were the weld strength required to withstand applied tensile loads on the pile, and the plate thickness needed to prevent bearing failure over the region of contact of the dywidag nut.

Fixity with the pile cap (Figure 4-4 top right)

At the upper end of the cell, a further plate (25 mm thick) was welded to the cylinder. This had a centrally located hole to allow hand/spanner access to tighten the dywidag nut at the pile head. A further plate was located on top of this, to which the pile cap could be welded when in its final position. These two plates were bolted together near the four corners for ease of separation (load cells from cap) after testing.

Tension single pile loadcell

An alternative arrangement was developed for attaching the basic load cell to the head of the single tension pile (TS1/s). The required dywidag bar anchorage length within the pile head (see Section 4.8) could not be achieved with a central single bar, as instrument cables in this pile came within 200mm of the pile head. A second wider base plate was positioned below the first, incorporating six drilled holes to accommodate six shorter bars. The two base-plates are connected by a vertical piece of flat steel. Therefore the cylindrical part of the assembly is more elevated in relation to the pile head than is the case with the other cells, providing room beneath to tighten the dywidag nuts (see Figure 4-11 later).

4.3.3 Calibration of TCD load cells

Relationships between the voltage output from the bridge configuration and the applied load were obtained in calibration tests using certified loading apparatuses. Special accessories were required for calibrations in tension; the top plate (for welding to the pile cap) was replaced by a plate with a central hole. The hole at each end of the cell was fitted with a short length of dywidag bar, secured inside with dywidag nuts and outside in the clamping blocks of the Denison loading machine (Figure 4-5). Motorised separation of the clamping blocks induced tensile loading. A number of tests were performed in tension to eliminate a few start-up problems, including inadequate weld lengths and plate thicknesses. Compression calibrations were carried out in the machine's standard 'crushing' mode.

Figure 4-5 Calibration of pile head load cells in tension

General calibration procedure

The general calibration procedure consists of:

(i) Strain gauge excitation (10V) and a period of 30 minutes to 'warm' the gauges

(ii) Cycling (or 'working') the gauges slowly [0-200kN] to minimise hysteresis. Repeatable linear load-strain response emerged after two/three load/unload cycles.

(iii) Strain gauge output from the load cells (and output from the Mayes load cell[4]) corresponding to the certified applied load was recorded (either manually or digitally).

(iv) Every effort was made to ensure that the loading was balanced, i.e that the strains recorded on either side of the steel cylinder differed by no more than 20% at any

[4] The Mayes load cell was used in conjunction with the jacks in most field tests. The Mayes cell and TCD pile head cells could be mounted one on top of the other in the certified loading apparatus.

stage of loading. The calibration factor (λ) relates the applied load to the average of these two outputs; λ was found to lie in the range 0.35$\pm$0.03 kN/mV for all load cells (with linear regression coefficients r^2>0.990). Calibrations indicated that the pile loads would be accurate to 0.2kN.

4.4 Pile Instrumentation

A schematic representation of the complete *internal* instrumentation scheme used in the test piles is provided in Figure 4-6 (the letters identify the pile locations of Figure 4-1). Important details of all external and internal instrumentation are now summarised:

4.4.1 Linear Variable Differential Transformers (LVDTs)

Each LVDT had a total working range of 50mm. The main features of the LVDTs used include:

(i) Most devices used were of DC type, excited at 5V and logged to the *High Level Card* of the System 5000 data acquisition system. Devices using AC were excited at 4.0 mV/V/mm with an amplitude gain of unity and logged to the *LVDT Card*.

(ii) The resolution of each device was 0.005mm, with a perceived accuracy of 0.01mm.

(iii) Devices were mounted initially to ensure adequate travel was available for the expected displacements; sometimes devices were reset during a test. Care was taken to avoid a short non-linear[5] section (≈10mm) at each end of full range.

(iv) DC calibration factors were typically 0.0055$\pm$0.0002 mm/mV (5V excitation).

4.4.2 Acoustic Vibrating Wire (AVW type TR55) gauges

The vibrating wire gauges were attached to the reinforcing steel using two different methods:

(i) Each gauge's mounting blocks were screwed to another set of purpose-made steel blocks. The new blocks were pre-welded to the steel at a predefined spacing.

(ii) Special U-bolts were used which encircled the bar, passed through holes drilled in the mounting blocks, and secured with nuts (Figure 4-7). The inherent advantage of this system lies in the ability to preset the gauge period accurately within the range

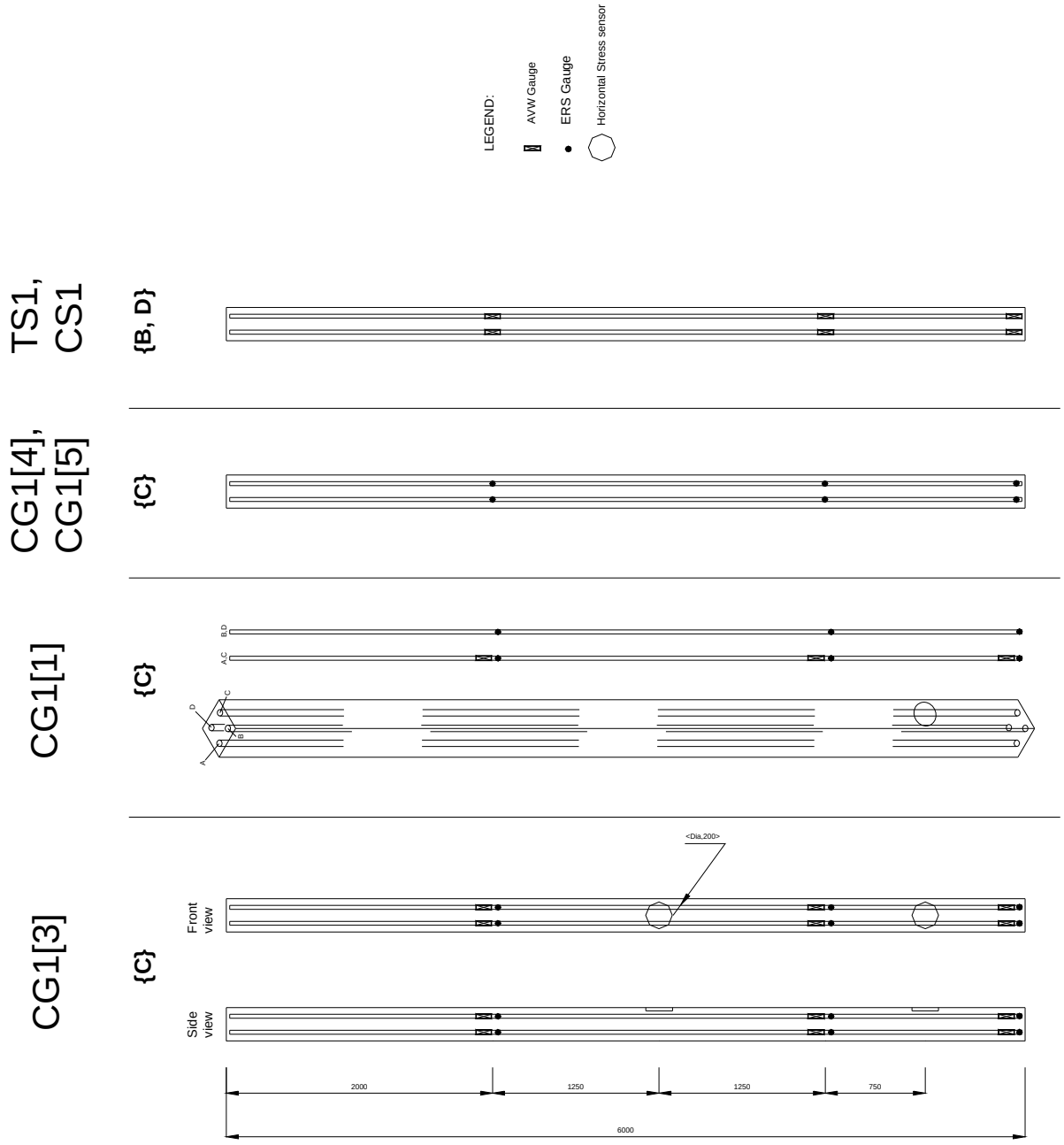

Figure 4-6 Internal instrumentation scheme for test piles

[5] A non-linear relationship between voltage output and displacement.

specified by the manufacturer, lowering the likelihood of occurrences such as creep and wire breakage.

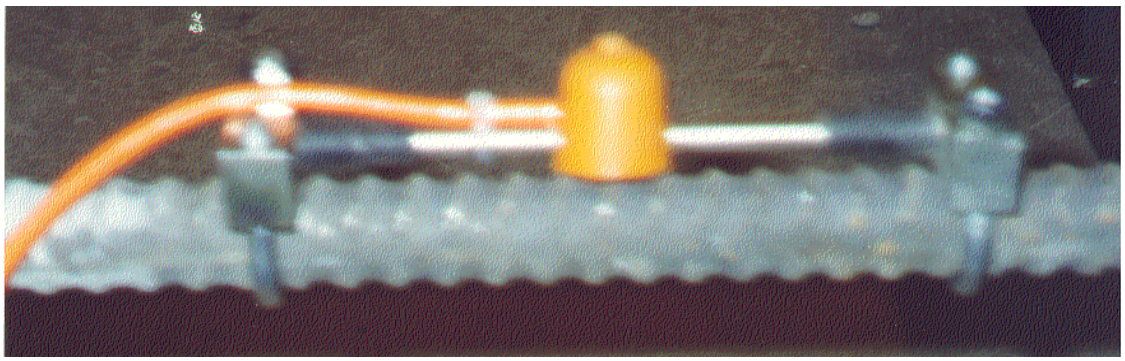

Figure 4-7 Attachment of VW gauges to reinforcement bars

A tight-fitting 50mm diameter, 175mm long section of PVC pipe was then slid over each VW gauge. The pipe ends were sealed with circular rubber pieces (with central holes for the reinforcement bar). Polyurethane sealant was injected through a small hole in the side of the pipe, with the dual purpose of preventing moisture ingress (especially during casting) and helping damp pile driving vibrations. Selected VW gauges were calibrated and checked with Gage Technique Limited specifications. The accuracy of the VW gauges was approximately $\pm 2\mu\varepsilon$.

4.4.3 Electrical Resistance Strain (ERS) /Foil Gauges

Standard ERS gauges of nominal resistance 350Ω and gauge factor of 2.08 were used. The gauges were bonded to a smooth surface on the reinforcing bar (achieved by angle-grinding) and covered with a neoprene water-proofing agent and silicone sealant prior to encasement in concrete. 'Ribbon' cables were soldered to the gauge for data acquisition.

Both System 5000 and Datascan software were used to record the strain gauge output; unfortunately, wiring faults meant that no data was obtained from those gauges connected to the Datascan in CG1/s. Calibration was carried out on identical gauges and these were accurate to $\pm 1\mu\varepsilon$.

4.4.4 Pressure Cells (Piezo-Resistive Pressure Transducers)

Three pressure transducers for use in aggressive environments (two in CG1[3]/s and one in CG1[1]/s) were cast flush with the pile surface to measure the horizontal total stress at the pile-soil interface. These are oil-filled flatjacks, 200 mm in diameter, 10 mm in thickness and with a working range of 0-500kPa. Pressure cell calibrations were found to be 5kPa/mV (for a 10V excitation), having an accuracy of ±2kPa.

4.4.5. Pneumatic piezometers

Prior to installation of TG1, nine pneumatic piezometers were installed at a variety of depths and radial displacements within and surrounding the zone designated for the group (Figure 4-8). A '*Minit Man*' boring device and a hand-auger were used to drill starter holes from the base of which the piezometers were pushed in using lengths of plastic tubing. The holes were then back-filled with a cement-bentonite grout. All porous stones were kept saturated in a de-airing chamber until the time of piezometer insertion. Initial 'free-field' hydrostatic pore pressure readings were read individually with a readout unit; pore pressures were also noted during and after installation of the tension group.

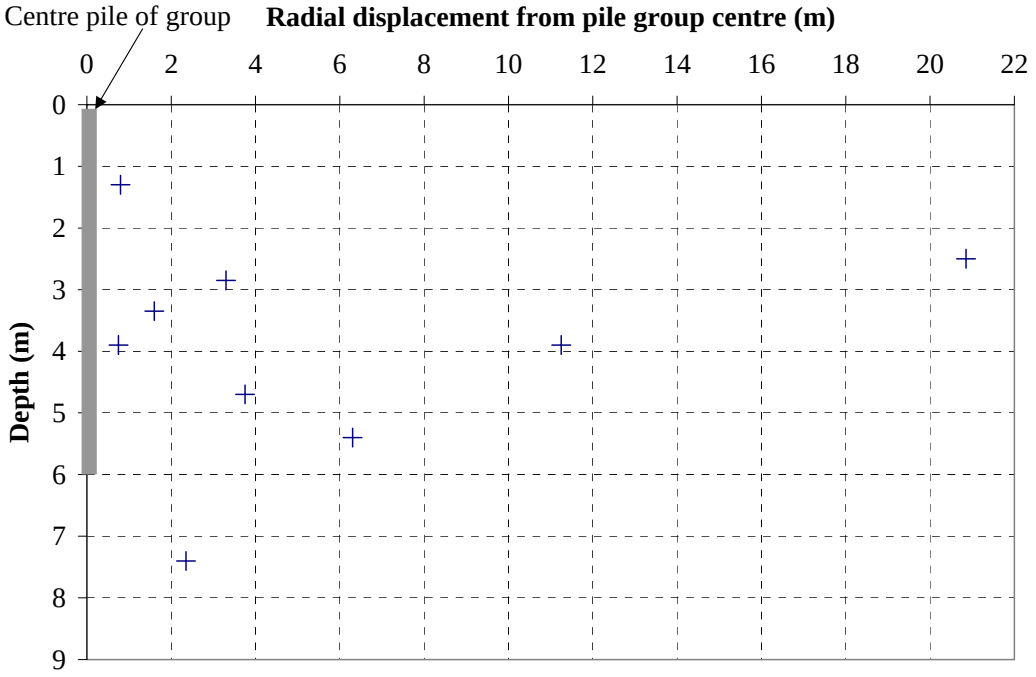

Figure 4-8 Spatial arrangement of piezometers around pile group

4.5 Casting of Concrete Piles

All piles tested in this programme are standard piles produced by Lowry Piling at their Mallusk casting yard, north of Belfast. The precast concrete piles have a characteristic cube strength of 50N/mm^2, are 7m long, 250mm square and reinforced with 4 no. T16 bars.

4.5.1 Instrumented piles

ERS and AVW strain gauges were attached to the T16 reinforcement bars (for the instrumented piles) at TCD's laboratory (see configuration in Figure 4-6). The standard 6m lengths of reinforcement bar were lapped with additional 1.1m lengths and were welded together (the 100mm overlap was eventually placed at the top end of the pile).

While affixing the links (continuous cage) to the reinforcement bars at the casting yard, great care was taken to prevent damage to the gauges and electrical cables. The cover to the longitudinal steel was sometimes slightly larger than for standard piles; in some places the cage had to surround the 50mm diameter PVC piping which housed the AVW gauges.

Each completed cage was inserted into a 250mm square casting bed, with all cables gathered up neatly along the centre of the cage, held in position by wire stirrups and emerging from the side of the pile towards the top end (allowing for subsequent trimming). Pressure cells were carefully positioned on the floor of the casting bed with active face down so as to finish flush with the hardened concrete surface. The pressure cell cables were also supported at the centre of the pile. The pile was cast longer (7.0m) than the required embedment depth (6.0m) for easier driving; some of the surplus free-standing length was subsequently trimmed for easier loading.

4.5.2 Instrument Readings at casting

AVW gauge readings were recorded with the cage in the casting bed before pouring the concrete. Further readings were taken during the pour (where practicable) and during the initial set period of approximately two hours afterwards. No ERS gauge readings or pressure cell readings were taken at the casting stage, due to the impracticality of using the necessary data-logger at this point. However, resistance checks using a pocket multimeter

confirmed proper working order of 90% of the ERS gauges and all pressure cells after confinement within the concrete.

4.5.3 General Concrete details

The piles were covered and steam cured overnight before being removed from the shuttering the following day. A minimum of 28 days was observed between casting and installation. 28-day cube strengths from 150mm concrete samples lay in the range 60±5 N/mm^2.

4.6 Test Pile and Support Pile Installation

4.6.1. General

A hydraulic hammer was used to install the piles (Figure 4-9). Once the pile bases penetrated below the filled material, the clay provided little resistance to driving and the piles were largely 'pushed' to 6.0m embedment. Installation was too rapid to deduce pile set from graduations were marked every 0.5m on the pile shaft. All five piles in the groups were driven within 20-25 minutes.

Figure 4-9 Installation of TG1

4.6.2 Pile group layout

The following points were common to the installation of all four pile groups (TG1, CG1, TG2, CG2):

(i) The centre pile was installed first (pile [3]), followed by the corner piles in anticlockwise order ([1], [4], [5], [2]). The soil heave caused by corner pile driving caused the centre pile to lift, so it was re-tapped by an amount varying from 3mm to 7mm.

(ii) The average centre-centre spacing was typically 750±20mm over all four groups; alternatively $2.92<s/B<3.08$ where B is the pile width or $2.59<s/D_{eq}<2.73$ where D_{eq}=282.1mm is the diameter of an equivalent circular pile of the same area.

4.6.3 Removal and reinstallation of single pile

The tension pile TS1 (already loaded to ultimate conditions at location B) was reinstalled (at D) as compression pile CS1. Excavation to approximately 0.75m depth around the head of TS1 was first necessary, allowing a heavy cable noose to then be tied around the top of the pile. The pile was then extracted by raising the drop hammer of the piling rig, which was chained to the pile head noose.

A spade and brush were used to clean the *sleech* adhered to the pile sides (up to 5mm thickness over the lower 4m of the pile) before reinstallation. A number of tiny cracks were observed encircling the pile, particularly between 1.0m and 3.0m from the pile head.

4.6.4 Installation measurements

Pneumatic piezometers/TG1

Despite being hampered by the position of the piling rig, with some piezometers less accessible than others, a set of installation pore pressures was obtained. The turnaround of ≈30 seconds in taking readings may have caused some of the peak excess pore pressures to have been missed; however this is not likely to have caused significant errors. The dissipation process was monitored for two months after installation until further readings were interrupted by vandalism to the plug connectors interfacing with the readout unit.

Pressure cells /CG1

All three pressure cells were logged at 1Hz during group installation (using the Datascan software), from 15 minutes before installation of the first pile CG1[3] until three hours after CG1[2] and all subsequently driven support piles (see Section 4.7.1) were in place. The pressure cell on CG1[1] did not function during installation[6]. Further readings were taken over the period between installation and load test CG1/s.

All CG1 piles were marked at intervals of 0.5m along their lengths with the intention of subsequently relating pressure cell output to the stage of pile embedment during installation. Unfortunately installation was too rapid and it should be noted that one pile plummeted ≈1.5m instantaneously during driving.

Vibrating Wire/Electrical Resistance gauges

The vibrating wire gauges were logged with a portable readout unit before driving, after driving and over the equalisation period for four piles CS1, TS1, CG1[3] and CG1[1]. Readings were taken between each CG1 pile was driven. The ERS gauges within CG[1], CG[3], CG[4] and CG[5] were not logged during installation due to the obvious difficulties associated with digital logging and pile-rig mounting/driving.

4.7 Further preparatory work in advance of pile load testing

4.7.1 Concrete Support Platforms

It was imperative that the reactions from the load test assembly (to be described in Section 4.8) had minimal effect on the soil in the vicinity of the test piles. A set of (two or three) slip-coated end bearing anchor piles were installed either side of the group/single pile[7]. These were located no closer than 12 pile widths from the group centre/single pile and served to transmit the reaction load to the competent sand stratum at 9.5m (3.5m below the toe depth of the piles)[8].

[6] But worked in load test CG1/s
[7] For pile load tests not involving the cone truck, see Section 4.8.5
[8] Figure 5-1 will show that driving the reaction piles (between 3.3 and 3.8 hrs) had negligible effect on the horizontal stress recorded at the centre pile location.

A concrete platform was constructed on top of the set of protruding anchor piles on each side of the test piles. The ground was levelled and concrete (30N/mm^2 characteristic strength with a 36 hour retarding agent) was poured onto a 50mm base layer of expanded polystyrene within the shuttering (preventing direct contact between the concrete and the ground). The platforms were unreinforced due to the small reaction stresses expected. However, the partial collapse of one of the forms during pouring meant that some sleepers were required to restore a level surface with the opposite platform, prior to building the test assembly.

The platforms used were of different sizes (see Figure 4-1):

(i) 1.5m long x 1.0m wide x 0.6m high, supported by 2 no. 350mm square piles: these were used for tension tests on TS1, TG1 and TG2 and the corner pile compression test CG2[2]. The platforms only needed to be long enough to accommodate the 880mm wide transfer beam.

(ii) 5.0m long x 1.0m wide x 0.6m high, supported by 3 no. 350mm square piles: these were used for compression tests. The longer support platforms were required to provide sufficient horizontal surface area for the grillage and Kentledge overhead. Three piles were provided to help the platform function as a unit only and provided a substantial redundancy in loading bearing capacity.

It may be seen that (i) some platforms are common to two pile test locations and (ii) both platforms used for tension group test TG1 were extended for adjacent tests CS1 and TG2. Tests on TS2 and TS3 and reload tests on CS1 did not require platforms as they were loaded using the cone truck.

4.7.2 Pile Head Trimming and Anchorage of Load Cells

The surplus free-standing length of pile (≈1m) after driving was trimmed using a con-saw to within 300-500mm of the ground surface. In addition to guaranteeing that all the pile heads were at exactly the same level, the free-standing length to which the piles were trimmed was important to ensure compliance of the whole test assembly (for example, that

the jack fitted between the pile cap and reaction beam in CG1) and for ease of access to the pile head instrumentation.

A 32mm hole was diamond-drilled into the head of each pile at its centre. High strength dywidag bars (25mm diameter) were grouted[9] into the holes leaving 100mm protruding as an anchorage point for the TCD load cells. The depth of each drilled hole was nominal for compression loading (≈100mm), with each dywidag bar serving merely as a location pin. However, for tension tests, a 1000mm bond length was required to safely resist the design pull-out load of 200kN per pile.

A 1000mm central hole was impossible in TS1 due to a bunch of AVW cables rising to within 200mm of (final) pile head level. The equivalent bond length was provided by 6 ×170mm deep holes; the base-plate of the tension single pile loadcell was modified to accommodate the increased number of anchorage points (see Section 4.3.2, Figure 4-11). In the process of uninstalling TS1 to redrive as CS1, the dywidag bars were displaced. These were replaced with one central locating pin penetrating to 100mm for CS1, so that a standard TCD load cell could be once again mounted on this pile.

Finally all pile heads were topped with a self-levelling cement-based screed to provide a smooth contact with the load cells.

4.8 Load Test Assemblies and Loading Mechanisms

4.8.1. Attachment of Load Cells and Pile Cap

The TCD load cells located themselves over the dywidag spigots protruding from the pile heads. Dywidag nuts were then screwed onto the bar within the cylinder to tighten the load cells to the pile head (Figure 4-4); this was crucial in the tension tests. At this stage, the top-plate is bolted to the head of the load cell.

For the group tests, the steel pile cap was then lowered centrally by crane onto the five load cells (Figure 4-2). Steel shims were inserted in a few locations between the top of the load

[9] With epoxy resin Fosroc Lokset S25

cell and the pile cap to ensure that the pile cap was level. The top-plates (and shims) of the five load cells were tack-welded to the underside of the pile cap. The pile cap was then lifted off and the bolts linking the two top-plates of the load cell were removed so that the upper set of plates came away with the pile cap. These plates were then properly welded to the pile cap; the length of weld required was more critical in tension than compression. Finally, the cap was repositioned and the bolts were reinserted (Figure 4-4).

Upon completion of the group test, the pile cap could be lifted once the bolts underneath were removed. The plates attached were subsequently burned away from the pile cap for reuse. The cap was reversed for later tests as the welding/burning started to roughen the surface of the pile cap.

4.8.2 Summary of Load Test Assemblies

The methods used to load test the piles are summarised in Table 4-2, which also highlights the relevant Figures to be referenced.

Assembly Type	Pile(s) tested	Section	Figures
Tension transfer beam	TS1 TG1, TG2	4.8.3	4-11 4-10
Full Kentledge arrangement	CG1	4.8.4	4-12
Mini-Kentledge arrangement	CS1, CG1	4.8.4	4-13
TCD GIU (‘cone truck’)	TS2, TS3, CTS1	4.8.5	4-14

Table 4-2 Load testing methods

4.8.3 Tension Pile Group and Single Pile Assembly

A 6m long, 880mm square, steel reaction beam spanned between the concrete platforms for both tension group and single pile tests. The purpose of this beam was to offer a load-path for the applied group load to the anchor piles. The effective level of the platforms was raised using concrete blocks to offer adequate clearance under the reaction beam for the pile cap and jacking assembly.

Figure 4-10 Tension Pile Group Assembly

Figure 4-11 Tension Single Pile Assembly

Pile group

A short 1.2m long beam was centred on top of the main reaction beam at right angles to it. Two 500kN jacks were seated near either end of the overhanging beam. The upper end of a high strength steel macalloy bar (diameter 40mm) passes through a void near each end of the short beam, through each hollow jack and is secured at the top of the jack with a macalloy nut. The lower end of the macalloy bar passes through purpose burned holes at the appropriate locations in the pile cap, and is secured to the pile cap's top and bottom plates with macalloy nuts (Figure 4-10). It should be noted that the position of these holes were based upon site practicalities and that these positions would influence the distribution of load among the group piles. Upward movement of the jack rams lifts the pile cap, which in turn applies tensile load to the individual group piles. A hydraulic T-piece hose ensures equal jack pressures, and a readout unit on the jack load cell is used as a site control.

Single pile TS1

The mechanism used differs only in that the pile cap is replaced by a light transfer beam above the pile head (Figure 4-11). This beam (1.2m long, consisting of back to back channel sections tied together by steel plates which maintain a 50mm gap between them) is linked to the jack with macalloy bars as before; these bars pass through the new beam and are secured top and bottom with nuts. This beam was welded to the single pile load cell.

4.8.4 Compression Pile Group and Single Pile Assembly

The concrete platform levels were raised with concrete blocks. Three sets of I-beam grillages (2 no. 6.4m x 1.6m, 1 no. 6.4m x 2.2m) spanned 4.5m between platforms.

Before placing the grillage, the 6m long transfer beam (already described) was mounted on secondary supports so that it ran parallel to the platforms and at right angles to the grillage beams. The heights of the supports were such that only a small gap existed between this beam and the placed grillage above prior to the load test. It was assumed that the applied loads would be dispersed by the piled platforms and not carried by these secondary supports. Once the grillage was in position, 19 Kentledge blocks amounting to 600kN reaction were craned onto the grillage (see Figure 4-12).

Figure 4-12 Compression Pile Group Assembly

Two jacks were positioned on the pile cap[10], in locations corresponding to the pulling points in the tension test. Compliance between the top of the jack ram and the bottom of the transfer beam required roughly 100mm of steel packing plates.

Simpler assemblies sufficed for all other compression tests. The ultimate load in single pile CS1 and corner pile CG2[2] (loaded alone) could be applied by jacking against the transfer beam (58 kN, now spanning *between* the piled platforms) with two Kentledge blocks on top (2 x 32 kN). This assembly is shown in Figure 4-13.

4.8.5. Loading single piles with the TCD Ground Investigation Unit

The TCD Ground Investigation Unit provides a 200kN reaction for cone insertion and could therefore be used as an economic means of testing tension single piles (experience showing single piles to have capacities of less than 100kN). The dywidag bar penetrating 100mm from the pile head was extended by coupling it with a further length of dywidag bar, so that it passed into the truck through the hole normally used for lowering the cone rods. The jack and load cell were both located within the truck, as shown in Figure 4-14. Six tests (TS2/s, TS2/ss, CTS1/c, CTS1/cs, TS3/c and TS3/cs) were carried out in this way.

4.8.6 Positioning of displacement measurement devices

Reference beams

It was imperative that the movements registered by the displacement transducers were true pile head displacements, isolated from disturbance induced in the soil immediately surrounding the pile(s). A stiff set of steel reference beams was used for this purpose.

For most of the pile tests, parallel scaffold frameworks were located on both sides of the group/single pile, approximately 2.5m apart, each supported only at the extremities of the 6m long frame (Figure 4-11). A number of poles and ratchet straps acting transversely served to stiffen both frames. A number of such poles passing close to the pile(s) provided an attachment point for the magnetic clamps and retort stands to locate the transducers.

[10] The pile cap was positioned before the transfer beam, grillage beams and Kentledge were added.

Figure 4-13 Compression Single Pile Assembly

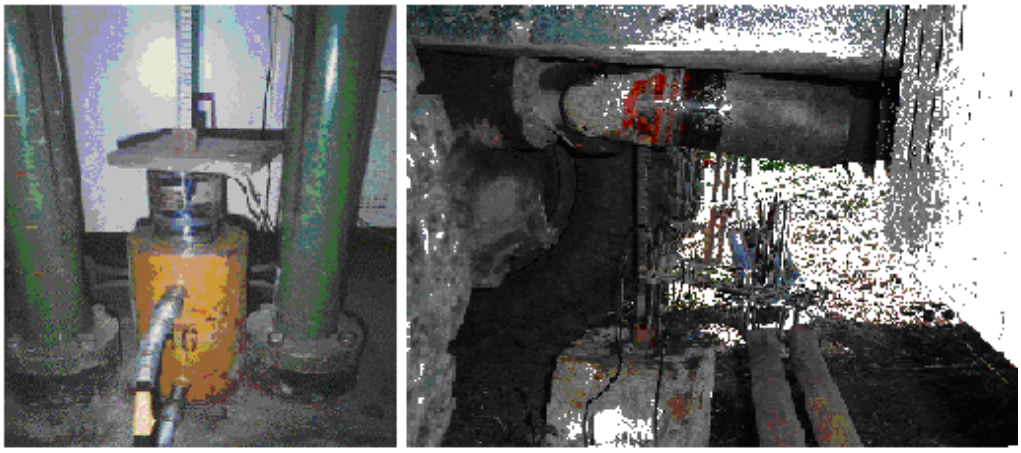

Figure 4-14 Single Piles loaded with TCD Ground Investigation truck

Where the cone truck was used to load the piles, one scaffold beam passed beneath the truck and was supported (i) by drilling into the formwork of the concrete support platforms 4.5m apart (TS2 and CTS1) or (ii) with independent supports, also 4-5m apart (TS3).

Displacement measurements

One LVDT was used at the head of each group pile, in addition to a dial gauge at the centre of the pile cap. Vernier scales were located on the sides of the pile cap in TG1/s and monitored with a surveying level to identify tilting. A pair of LVDTs were located on diagonally opposite sides of all single piles.

4.8.7 Load Application

A hand-pump was used to apply load in TS1/s and TG1/s. In the former test, difficulty arose in holding a constant load; this made monitoring pile head creep rates as a site control quite difficult. In all subsequent tests, a more satisfactory '*Power Team*' petrol driven pump was used to regulate load levels. A pressure release valve guaranteed load stability. This was particularly useful in the cyclic tests where the load could be raised and lowered very easily by turning a knob.

The readout unit for the jack load cell was used as a site control only, but the load cell output was logged to a PC.

4.9 Data Acquisition during Load Tests

4.9.1 Computer-logged data

Two different logging systems were used over the course of the test programme; both were used together when a lot of instruments were being logged (i.e 65 channels in CG1/s). Compatibility of both systems was confirmed in the laboratory[11]. In general, data was recorded as shown in Table 4-3. Devices which required an external excitation voltage (pressure cells and LVDTs) were monitored to ensure that the excitation was both correct and stable throughout testing.

Logger	**Devices**
2 × System 5000 units with Pentium P.C.	LVDTs, TCD & Mayes load cells, ERS gauges
4 × Datascan modules with laptop	Pressure cells, Mayes load cell, ERS gauges

Table 4-3 Use of Data Acquisition Software

The logging frequency used in static tests varied from 0.05Hz to 1Hz, depending on the pile head creep rate. Highest frequency logging was used to capture sudden output changes arising during and immediately after load increments, or during the displacement rate-controlled static tests. Slower frequencies sufficed towards the end of load holding spells. In the cyclic tests, the data frequency of 0.33Hz captured 20 datapoints per load cycle. All devices were allowed to log for at least 30 minutes before testing to 'warm' the device, to check for drift or other instrumentation malfunctions.

The TCD GIU was used to house the computer and data acquisition hardware and provided a useful location to analyse the results as they were recorded. All cables were fed through either the rear door or the cone hole in the floor. External power was provided continuously

[11] For ERS gauges and the Mayes load cell.

by either a petrol generator or the truck's battery. A typical arrangement of data acquisition hardware within the truck is shown in Figure 4-15.

Figure 4-15 Data acquisition for pile tests

4.9.2 Manually recorded data

Readings were taken manually for the AVW and dial gauges during the static tests (readings were most regular immediately after a load increment and least regular as the creep rate slowed down towards the end of a holding period). A switching box was used to speed up the data acquisition process for the twelve VW gauges of TS1/s and CS1/s, and the eighteen of CG1/s. During the cyclic tests, the dial gauges were used to get an indication of the amplitude and mean displacement of the piles. However, the turnaround between successive VW gauge readings was too slow to obtain much useful information during cyclic loading.

Particular care was taken to ensure that computer logged and manual data were recorded relative to the same time datum for subsequent data assimilation. Watches were therefore synchronised with the internal timer of the data acquisition package.

4.10 Load Test Procedures

The need to perform all related tests in a consistent manner gives rise to procedures for the static and cyclic tests which are detailed below:

4.10.1 Static Maintained Loading Tests

The core tests of this thesis were MLTs. The principal criteria are itemised below:

(i) It was endeavoured (as far as possible) to use similar load increments for corresponding single pile and pile group tests. These increments were smallest initially to capture pile stiffness at low displacements and small towards failure to capture the shape of the load-displacement curve with failure imminent. Moderate increments were imposed in between.

(ii) The criterium for applying a new increment of load was that the creep rate over the current load-holding period had dropped below a threshold of 0.24mm/hour. The length of the holding period varied from less than 5 minutes at low loads to several hours near 'failure'. Restrictions in the length of the working day sometimes meant that this was not always strictly adhered to (but subsequent corrections were applied, see Section 5.8).

(iii) Creep rates were generally checked over 10 minute intervals. Incremental load-displacement plots were generated as the test progressed to help choose the size of the next increment.

(iv) In additional to the overall applied load, the centre and one corner pile in each group were selected as controls for monitoring the rate of creep of the group.

(v) The pile(s) were unloaded when the plotted load-displacement response appeared to be forming an asymptote to some value of load (typically at a single pile displacement of 15mm or an average group displacement of 25mm). It is recognised that much more stringent criteria are required to define 'ultimate conditions'.

4.10.2 Static tests at constant rates of displacement

When the piles were fully unloaded[12] at the end of the maintained load static tests, the piles were rejacked at the faster rate of 1 ± 0.2 mm/min for approximately 10 minutes. The dial

[12] With the exception of TG1, which was not unloaded after the end of the maintained load test.

gauge provided the easiest way of controlling the displacement rate, as the correct rate may be achieved by loading the pile(s) so that the dial gauge pointer rotated in tandem with the second hand on a clock face.

4.10.3 Cyclic tests

The loading procedure for the cyclic tension tests was as follows:

(i) The piles were subjected to a very brief maintained load test[13] (to form an idea of what deformation might be expected under different ranges of cyclic loading) before complete unloading.

(ii) Piles were subjected to one-way cycles between a minimum cyclic load (Q_{min}) and a maximum cyclic load (Q_{max}) with a cyclic period of 60$\pm$2 seconds (easily related to a clockface)[14].

(iii) Q_{min} was typically 5-10kN per pile and was somewhat dependent upon pump control. If there was little accumulation of mean pile head displacement (δ_{mean}) or displacement amplitude (δ_{amp}) after a certain number of cycles, Q_{max} was usually raised to 'encourage' further cyclic degradation.

(iv) Tests were typically terminated once δ_{mean} (single pile or average group) exceeded 25-30mm (with the exception of TG1/sc after 512 cycles).

(v) Cyclic group test TG1/sc was followed within 30 minutes by a static MLT (TG1/scs). All other tests had an 'overnight' (<12hours) setup period between static and cyclic tests.

Problems specific to the cyclic group test CTG1/sc are detailed in Appendix 4-1.

[13] Never exceeding ≈3mm deformation for pile groups or ≈1.5mm for single piles

[14] Although the time from peak to trough was the same as from trough to peak, the cycles were sometimes slightly 'unsymmetrical', i.e the initial loading rate after the peak was faster than average and the initial loading rate after the trough was slower than average.

Chapter 5

Static Load Test Data for Single Piles and Pile Groups

5.1 Introduction

Measurements made during the Kinnegar pile tests are presented in this Chapter. Data pertaining to the pile installation and equalization processes are presented initially. All of the static load tests on single piles and closely spaced groups of five piles are then considered. Further relevant information is presented which provides a basis for accurate comparisons between each of the load tests.

The pile tests forming the subject of this Chapter are listed in Table 5-1, with details of their location (see Table 4-1, Figure 4-1). The notation introduced in Chapter 4 is used; in the case of group piles, the reader is reminded that [3] signifies the centre pile. The measured incremental load-displacement plots are shown in Appendix 5-1 and smoothed versions (representing a creep rate of 0.24mm/hour) are shown in this Chapter.

Single pile / pile group	**Description**	**Reference (Table 4-1, Figure 4-1)**
CS1/s	First compression single pile	(D)
TS1/s	First tension single pile	(B)
TS2/s	Second tension single pile	(E)
TS2/ss	Second tension single pile (reloaded)	(E)
CG1/s	First compression pile group	(C)
CG2/s	Second compression pile group	(F)
TG1/s	First tension pile group	(A)

Table 5-1 Static pile tests presented in this chapter

5.2 Pile installation

5.2.1 Horizontal total stress on centre pile of group

No horizontal total stress measurements were made on any of the single piles during their installation. The centre pile of compression group CG1 (referred to as CG1[3]) was equipped with a pair of horizontal total stress cells (at 3.25m and 5.25m). As the first pile

of the group to be driven, the centre pile effectively behaved as a single pile until the first of the corner piles entered the soil. One of the corner piles CG1[1] also contained a horizontal total stress sensor at 5.25m which failed to function properly during installation. The sensors were logged continuously from before the installation of CG1[3] until a few hours after the last corner pile CG1[2] was driven[1]. The variation in horizontal total stress (σ_h) over the entire installation period is shown in Figure 5-1. The delivery to site of the wrong pile accounts for the two hour interval between the driving of CG1[5] and CG1[2].

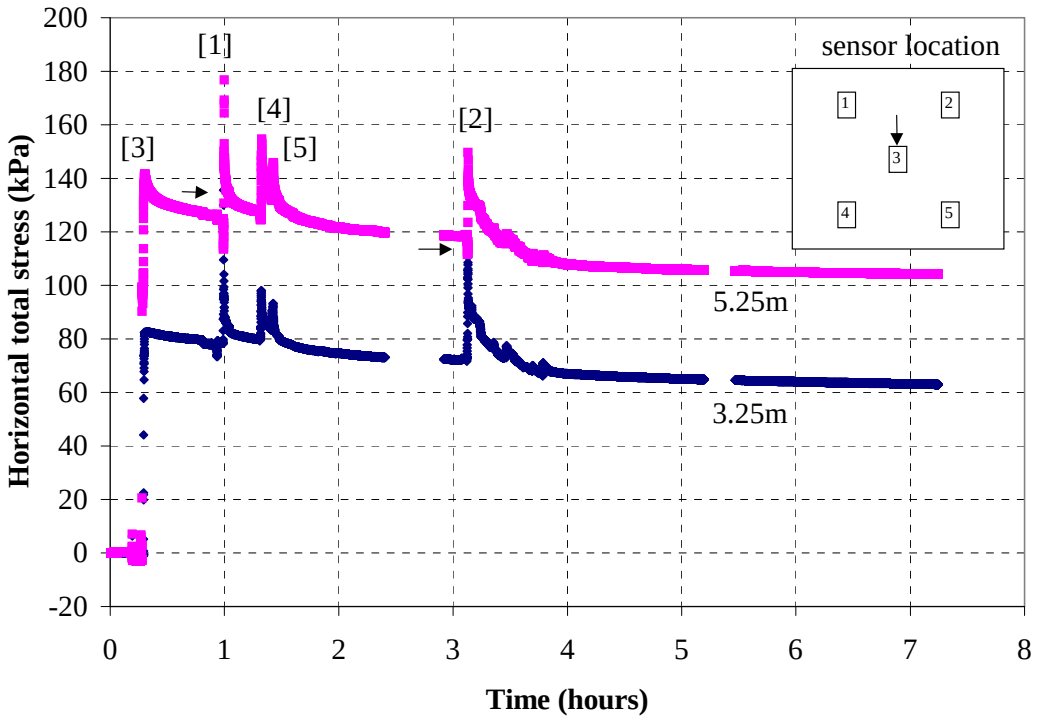

Figure 5-1 σ_h variations on CG1[3] during the installation of CG1

Attention is drawn to the following points:

(i) During the installation of the corner piles, overall σ_h values on the centre pile CG1[3] exceed those measured when CG1[3] was itself installed. The peak value for the group arises when the closest corner pile CG1[1] is installed and σ_h values at this time exceed the single pile values by ~60% at 3.25m and ~30% at 5.25m. The

[1] Sensors were also logged during equalisation

additional horizontal stress changes ($\Delta\sigma_h$) induced by each corner pile are smaller than σ_{hi} (maximum value) for the single pile, and each change clearly reflects the proximity of the pile being driven to the pressure sensors.

(ii) Each increase is very short-lived and significantly, there appears to be no accumulation of σ_h although a number of piles are being driven (this is particularly clear for CG1[4] and CG1[5] which are driven in closest succession at t = 1.4 hours). This suggests that σ_h on the centre pile soon after driving the group may not have differed if the five piles had been driven over a shorter period.

(iii) As each corner pile is driven, σ_h suddenly increases (from a value just before its driving of σ_{hb}). The maximum increase ($\Delta\sigma_{h\ max}$) is shown for each of the corner piles in Table 5-2 and reflects the proximity of the pile being driven to the sensor. It is of interest to note that when CG1[1] and CG1[2] are being driven, $\Delta\sigma_{h\ max}$ is relatively insensitive to the position of the sensor on CG1[3], but $\Delta\sigma_{h\ max}/\sigma_{hb}$ reflects the sensor position strongly.

(iv) An interesting feature of the measurements is the small drop in σ_h taking place immediately before the large increase in σ_h as the pile is installed. This drop also appears to be more pronounced at 5.25m. This phenomenon is highlighted in Figure 5-2 with zoomed up versions of the data for CG1[1], CG1[4] and CG1[5], although it also arises for the single/centre pile CG1[3]. This is believed to be due to 'cross-effects' on the pressure cells as they were subjected to large movements as the piles were installed; such effects were not considered during pressure cell calibration.

Corner Pile Identification	**Distance from sensor to centrepoint of corner pile**	**z = 5.25m**		**z = 3.25m**	
		$\Delta\sigma_{h\ max}$	$\Delta\sigma_{h\ max}/\sigma_{hb}$	$\Delta\sigma_{h\ max}$	$\Delta\sigma_{h\ max}/\sigma_{hb}$
CG1[1]	600 mm	51	0.411	57	0.731
CG1[2]	692 mm	33	0.271	40	0.548
CG1[4]	844 mm	26	0.203	18	0.223
CG1[5]	907 mm	13	0.097	9	0.107

Table 5-2 Increases in σ_h due to each corner pile installation

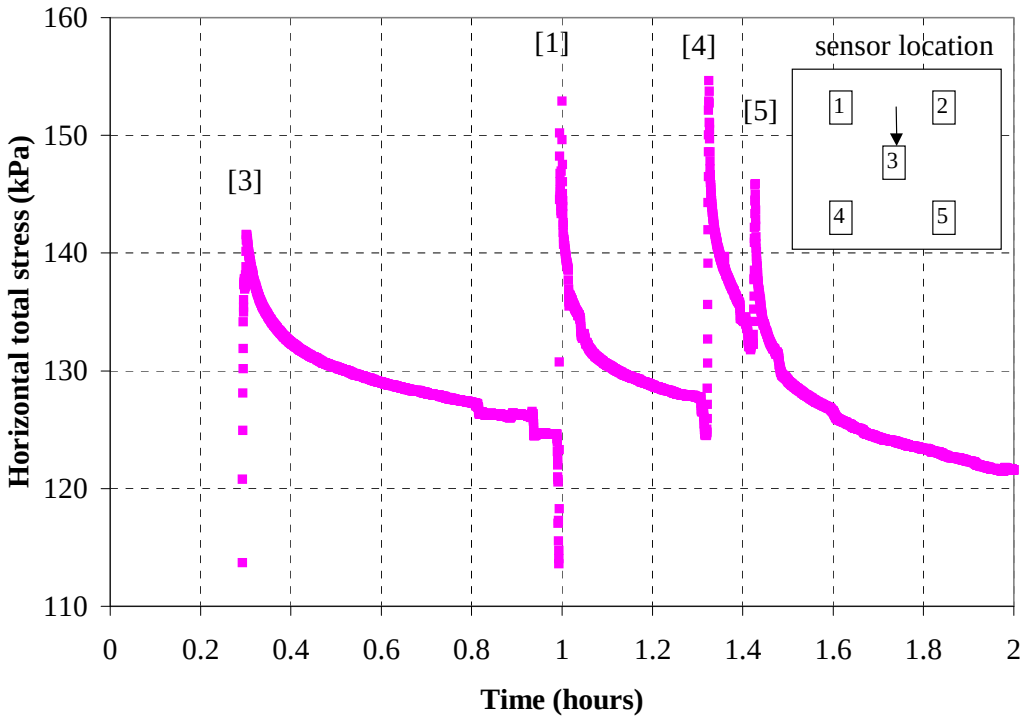

Figure 5-2 Zoomed plot showing initial σ_h drops when pile is installed (5.25m)

5.2.2 Maximum excess pore pressures around pile group

The excess pore pressures in the soil surrounding TG1 were monitored as the pile group was installed. A total of nine pneumatic piezometers[2] were used. The measured data is presented in Appendix 8-2.

Pore pressures measured before installation conform very well with the expected hydrostatic pore pressure distribution. The frequency of measurements was limited by access problems (when the rig was in position) and that only one piezometer could be monitored at a time; nevertheless relatively regular records were made from the time of installation of the first group pile TG1[3] until one hour after driving the final pile TG1[2]. It may be assumed that the value of Δu_{max} is at least equal to the maximum recorded during this time. The Δu_{max} distribution around TG1 is presented in Figure 5-3.

[2] The most useful piezometer (within the group) could not be inserted sufficiently below the water table and did not contribute any data.

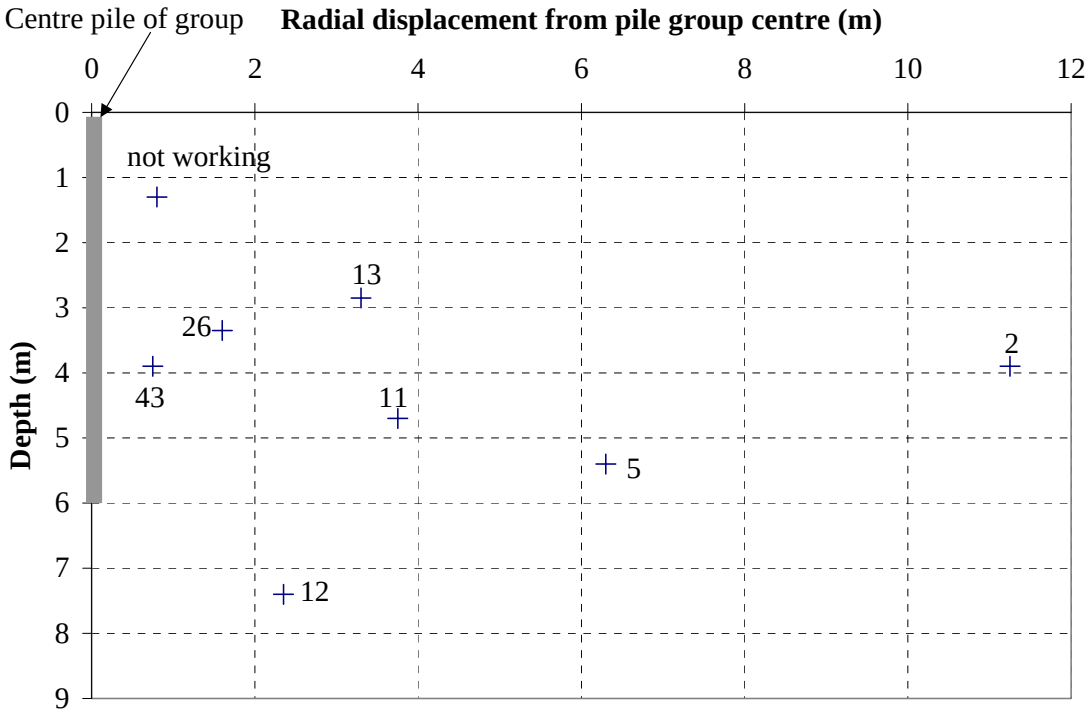

Figure 5-3 Distribution of maximum excess pore pressures (kPa) surrounding TG1

The maximum excess pore pressure ratio ($\Delta u_{max}/\sigma'_{vo}$) is plotted in Figure 5-4 as a function of the distance from the pile group centre normalised by the equivalent radius of one pile (r/R). No data are available for excess pore pressures within the pile group perimeter (r/R<5). However, beyond the pile group perimeter (r/R>5) and above pile base level, values of $\Delta u_{max}/\sigma'_{vo}$ reduce linearly with the logarithm of r/R. Only one piezometer (at r/R=16.7) lies *below* pile base level; this recorded the lower $\Delta u_{max}/\sigma'_{vo}$ value as expected.

5.3 Equalisation

5.3.1 Horizontal total stress on centre pile of group

Further measurements of σ_h on CG1[3] made after group installation and before load testing are presented in Figure 5-5. Insufficient measurements were taken to confirm unequivocally that full equalisation of the total stress had been reached, although a constant state of horizontal effective stress was believed to have been relatively close. Lehane (1992) suggests that as equalisation is close, excess pore pressure and total stress appear to

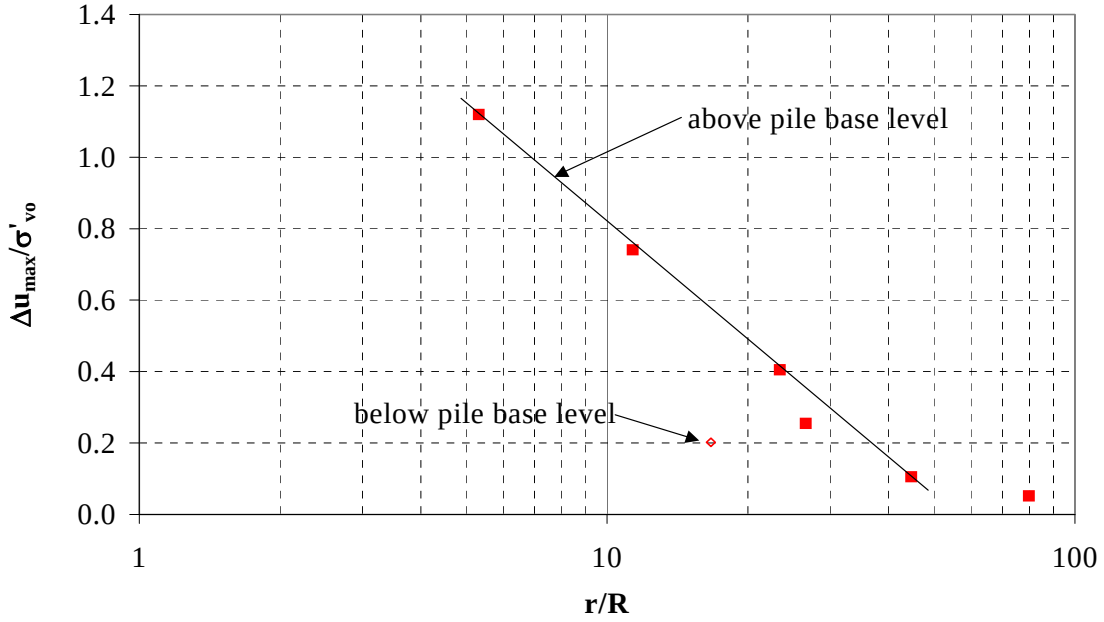

Figure 5-4 Decay of $\Delta u_{max}/\sigma'_{vo}$ with distance from the centre of TG1

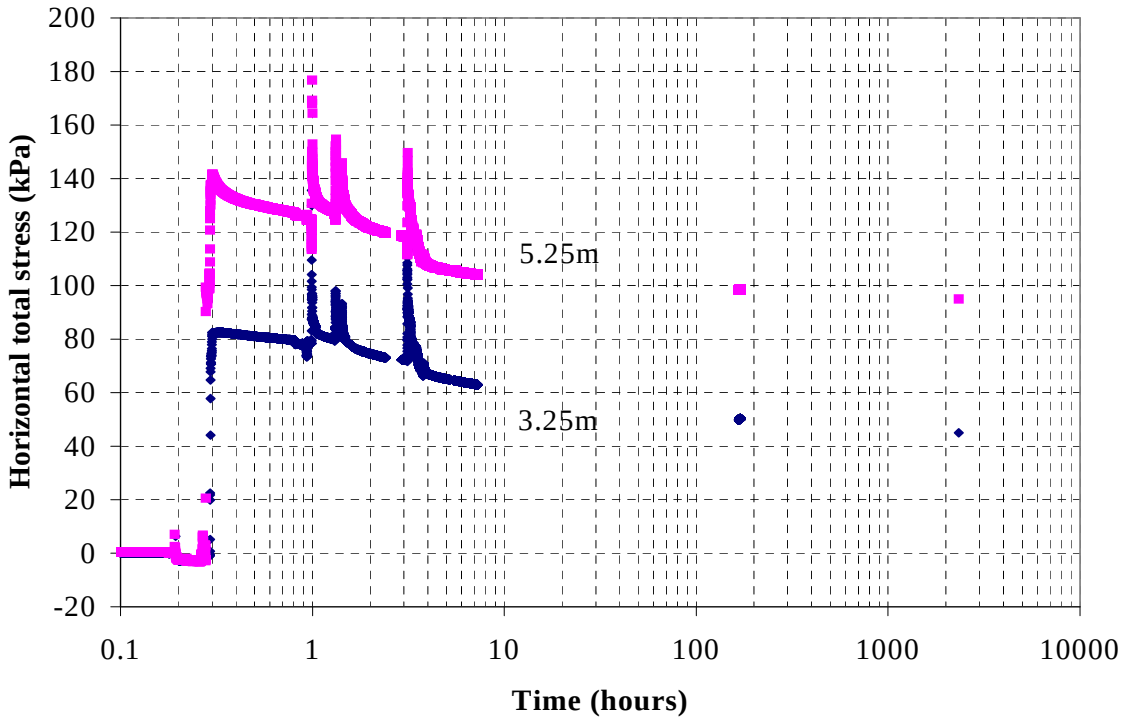

Figure 5-5 Horizontal total stress decay over the equalization period

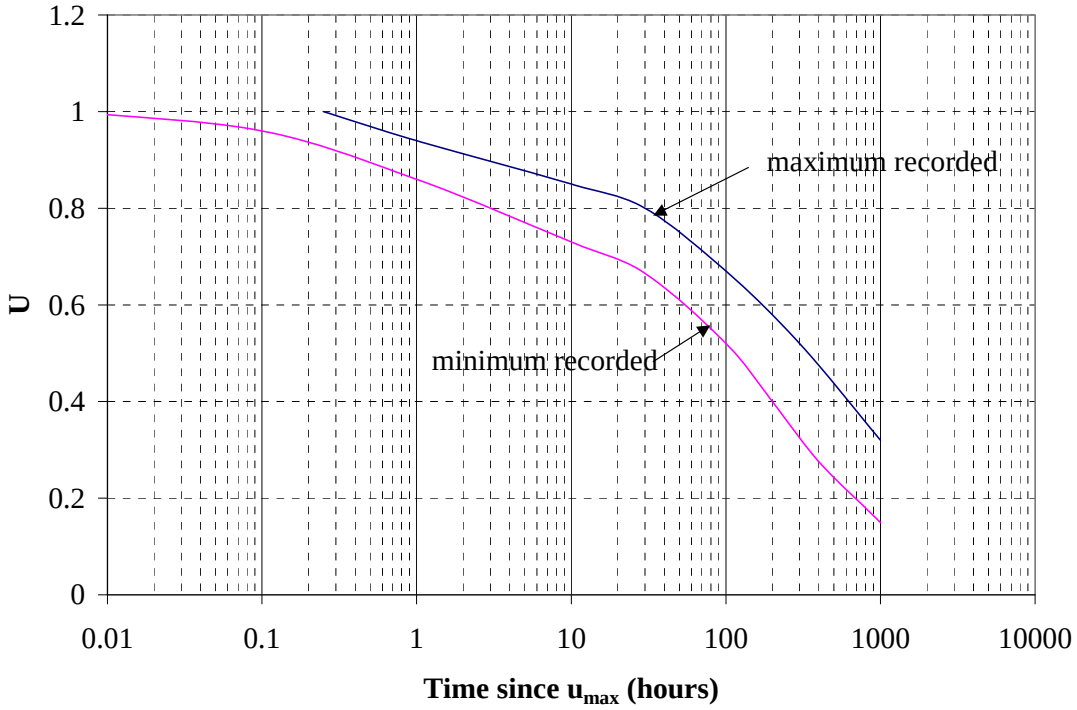

Figure 5-6 Range of the pore pressure dissipation curves
(uncorrected for seasonal rise in water table)

decay at the same rate, so that horizontal effective stresses reach a constant value before either total stresses or pore pressures do so individually.

5.3.2 Pore Pressure Dissipation around pile group

The pattern of pore pressure dissipation with time in the soil surrounding TG1 is shown in Figure 5-6. Pore pressure decay is represented by the degree of dissipation[2] U, for which u_{max} values are based upon the measured peak pore pressures. A representative decay curve is likely to lie closer to the lower bound[4] shown. Excess pressures at r/R>5 have at least halved within ten days of driving and at least 80% dissipation had occurred within six weeks. It should be noted that a seasonal water table rise of ≈0.2m was noted over this period; so the measured pore pressures that have been used to calculate U in Figure 5-5 will

[2] The degree of dissipation $U = (u-u_o)/(u_{max}-u_o)$
[4] Slow responses of the pneumatic piezometers may also cause the Δu_{max} values to be under-estimated

underestimate the amount of pore pressure dissipation that has taken place in response to pile driving. This is most pronounced with those piezometric locations recording least changes in pore pressure (see Appendix 8-2). A relatively narrow band exists for the value of U throughout equalization, within which no systematic dependence upon normalized vertical (z/R) or radial (r/R) position is identifiable.

5.3.3 Residual Loads

Vibrating wire gauges embedded in TS1, CS1, CG1[1] and CG1[3] were recorded after equalisation to determine residual loads in these piles (against a pre-installation datum). Unfortunately, long-term strain readings were erratic showing inconsistent fluctuations over a number of months.

5.4 Tension Single Pile Load Tests

Three tension single pile tests were carried out: virgin tests TS1/s and TS2/s and re-test TS2/ss. The smoothed load-displacement plots for the virgin tests are shown in Figure 5-7.

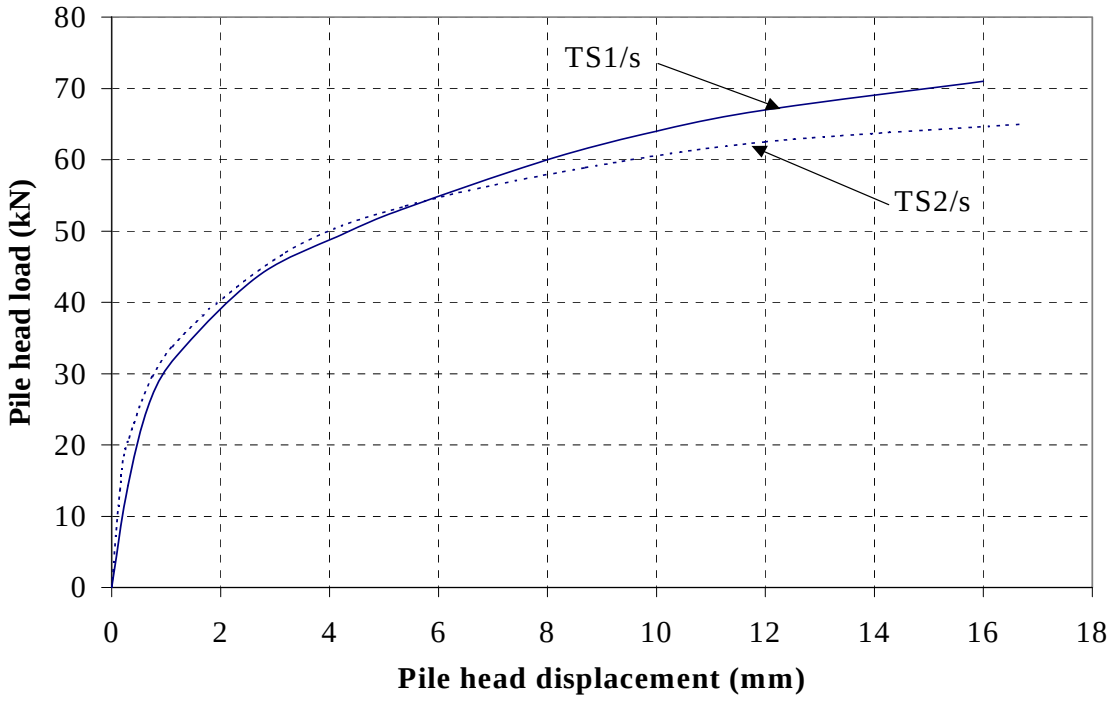

Figure 5-7 Smoothed load-displacement plots for TS1 and TS2

The stiffness of TS2 is slightly higher than TS1 at working loads (≈30kN) but becomes softer when ultimate conditions are imminent. Pile head loads of 71kN (TS1) and 64kN (TS2) were recorded at a pile head displacement of 16mm. CPT end resistance data near the two test locations suggest that local variations in soil consistency may contribute to this difference[5].

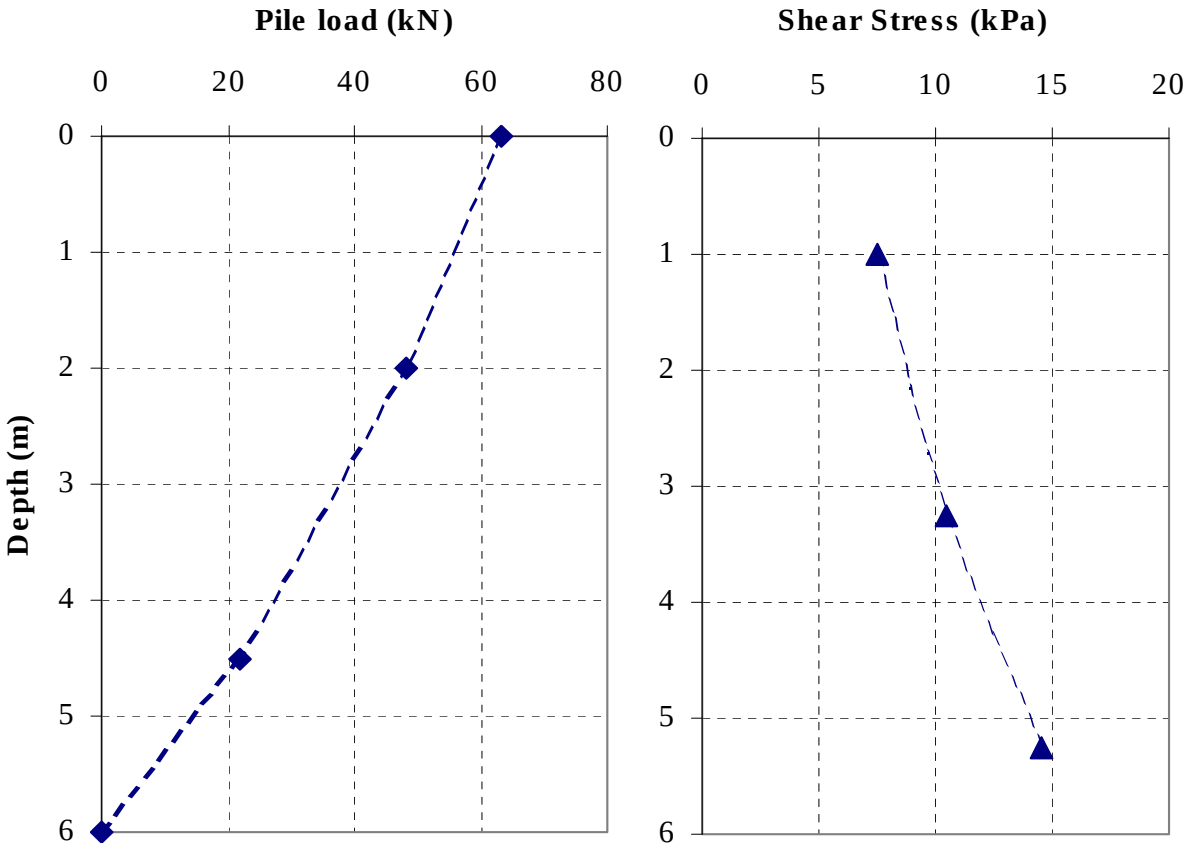

Figure 5-8 Load distribution and shear stress profiles for TS1/s (≈10mm)

Measured load and shear stress distributions in pile TS1/s are shown in Figure 5-8. Due to difficulties[6] in interpreting the strain gauges, only the measured load distribution corresponding to a pile head displacement of 10mm (4% of the pile width) is presented. This displacement is likely to be sufficient for peak shear stresses to have been *almost* fully mobilized.

[5] Specific CPT data referenced in Figure 3-1 may be see in Appendix 3-4
[6] The strain output with time showed an 'apparent' yield at a strain of approximately 10με .

TS2/s was carried out 85 days after installation and was retested (TS2/ss) 236 days after installation. The smoothed load-displacement curves for both tests are shown in Figure 5-9. Reloading appears to increase pile capacity by at least 25% over the period in question. Unfortunately, the exact peak load for TS2/ss (at a creep rate of 0.024mm/hour) was not determined since the pile failed prematurely as the load rose suddenly due to pump problems (shown as dotted). The response of TS2/ss appears to be much less non-linear than TS2/s and it is possible that pile 'failure' might have been more brittle in this instance. A load of 100kN appears to form a reasonable upper bound on the capacity of TS2/ss.

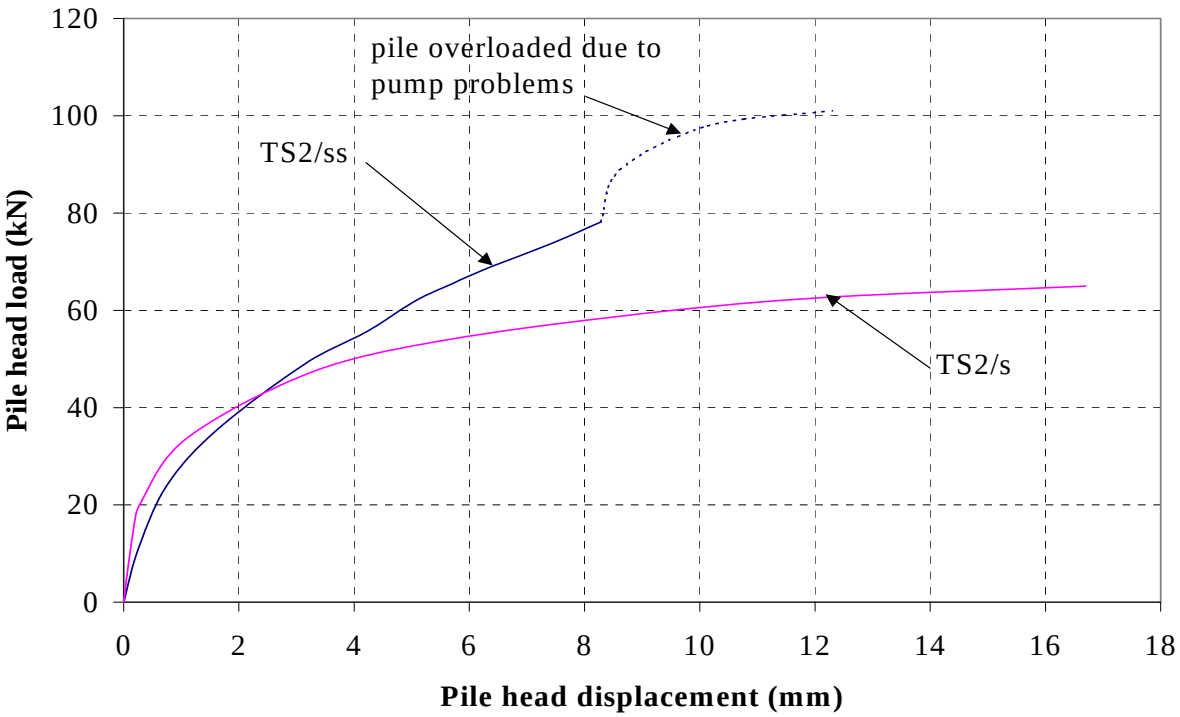

Figure 5-9 Comparison between TS2/s and TS2/ss

5.5 Compression Single Pile Load Test

One compression single pile CS1/s was tested during this programme. Unfortunately, the test was terminated earlier than would have been desirable in hindsight; the smoothed load-

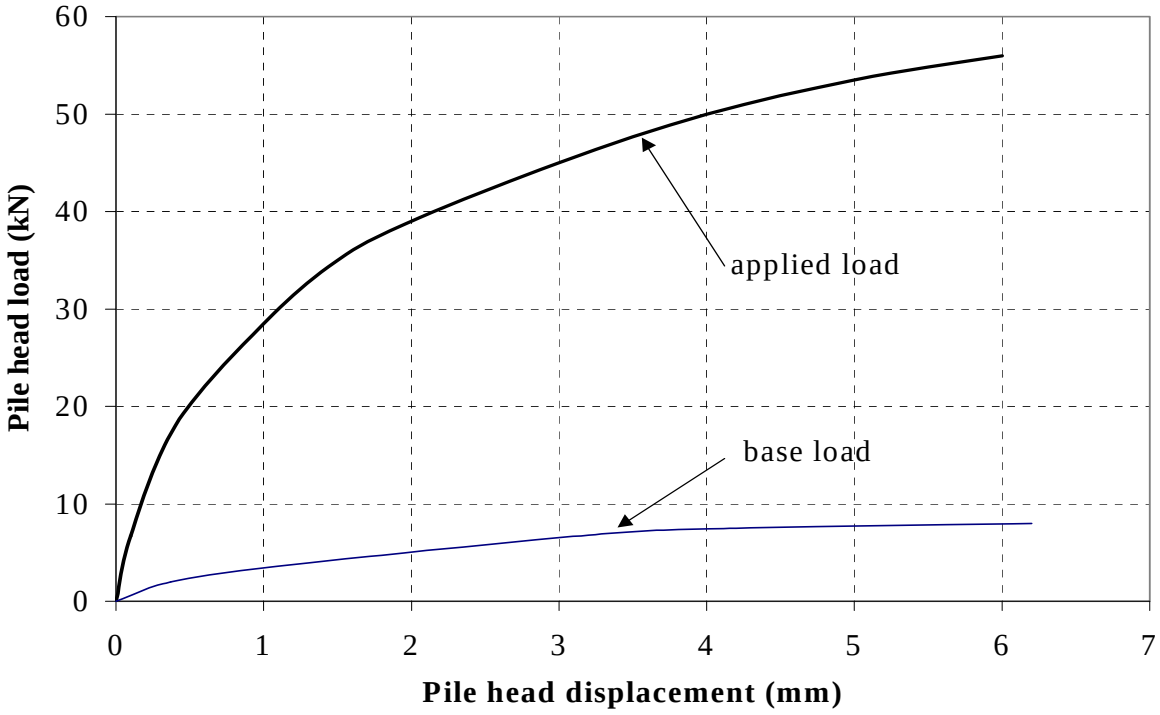

Figure 5-10 Load-displacement behaviour for CS1/s

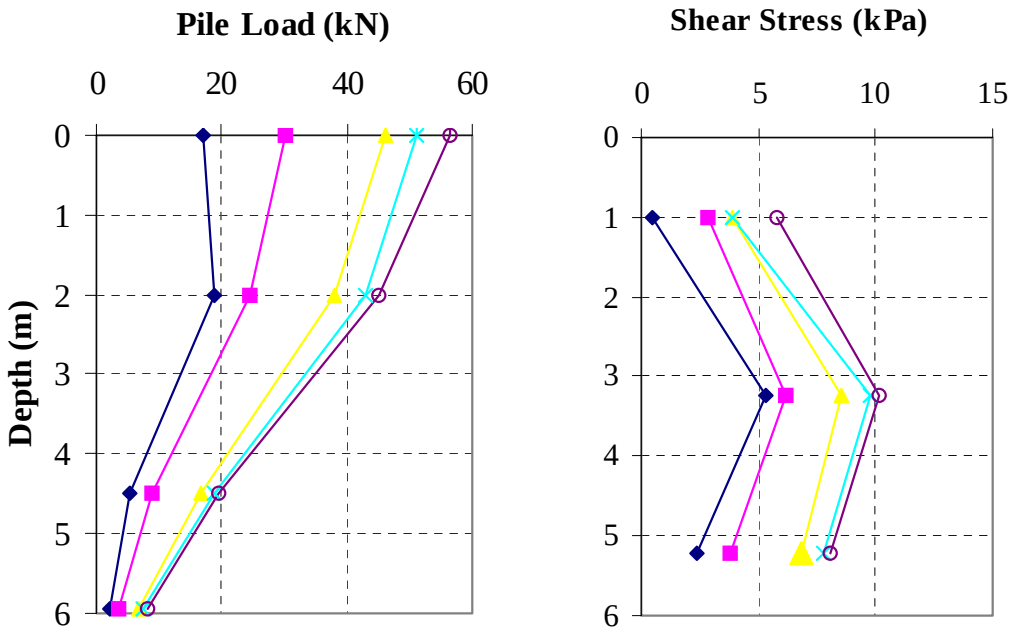

Figure 5-11 Load distribution and final shear stress profile for CS1/s (≈6mm)

displacement behaviour up to a pile head displacement of 6mm is shown in Figure 5-10. There appears to be little difference between the measured responses of CS1 and the average of TS1 and TS2 up to 6mm displacement. The best estimate of the pile base load (based upon strain gauges 50mm above the pile base) is also included in Figure 5-10. Figure 5-11 shows the load distribution of CS1/s at various stages of loading with the final shear stress profile in the pile (6mm displacement).

Low load transfer within the filled ground and greater load transfer within the sleech aligns with typical compression pile behaviour. Evidence from Figure 5-10 suggests that a pile head displacement of 6mm is insufficient to mobilize either shaft or base ultimate loads.

5.6 Tension Pile Group Load Test (TG1/s)

The maximum load applied to tension pile group TG1/s of 297kN required an average group displacement of 22.2mm. The smoothed load displacement plots for each of the five piles TG1[1] to TG1[5] are presented in Figure 5-12. An interesting feature of TG1/s is the behaviour of the pile cap, manifested in the variation of pile head loads (Figure 5-13) and displacements (Figure 5-14) as the test progresses. It is clear that from an early stage of the group test, the centre pile TG1[3]/s is at a more advanced stage of loading than any of the corner piles and has displaced further than the corner piles. The load sharing imbalance imparted to the piles is due to the flexibility of the pile cap under its applied load. However, by the time the *average* displacement of the five pile heads has reached ≈7mm, the loads in the piles have equalized, although TG1[3]/s continues to displace furthest.

Very little bending in the TCD pile head load cells (i.e. similar strains measured on both sides) offers secondary evidence of the flexible pile cap response.

The corner piles themselves do not all respond consistently as might be anticipated under vertical loading. It may be seen, particularly from the corner pile displacements in Figure 5-14, that the pile cap has tilted notably (about the axis [1]-[3]-[5]). Independent confirmation of pile cap tilt was obtained from tracking markers on the pile cap with a surveying level.

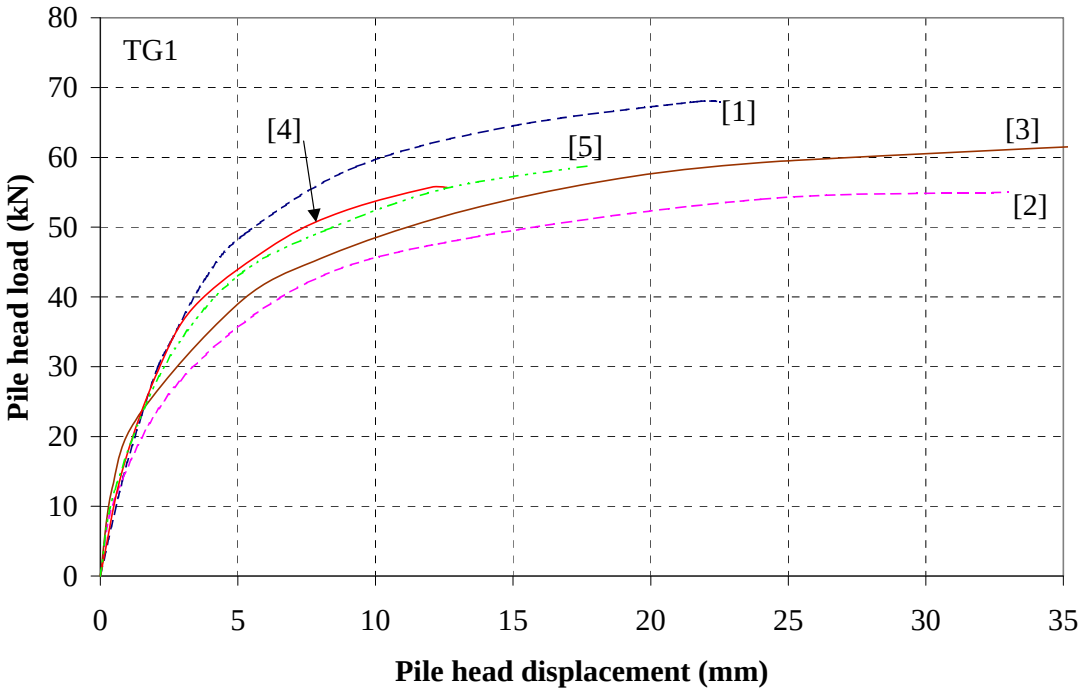

Figure 5-12 Load displacement behaviour of piles in TG1/s

5.7 Compression Pile Group load tests (CG1/s and CG2/s)

Two compression load tests were carried out on pile groups. CG1/s involved simultaneous loading of all five piles (like TS1/s), while in CG2/s, only one pile (corner pile CG2[2]/s) was loaded. In the latter test, displacement measurements were made on the load-free piles.

5.7.1 Full group test CG1/s

An average pile head displacement of 23.3mm was required to mobilise the maximum applied compression load in CG1/s of 311kN. The load-displacement responses of the individual piles are shown in Figure 5-15. The load cell at the head of CG1[4] failed to function during the load test; the load in CG1[4] may be estimated from the total group load (measured with the Mayes load cell at the jack location) less the sum of loads in the other four piles.

The pile cap behaved much more rigidly during CG1/s (than during TG1/s), causing all piles to settle by similar amounts. The displacements measured on the centre group pile and

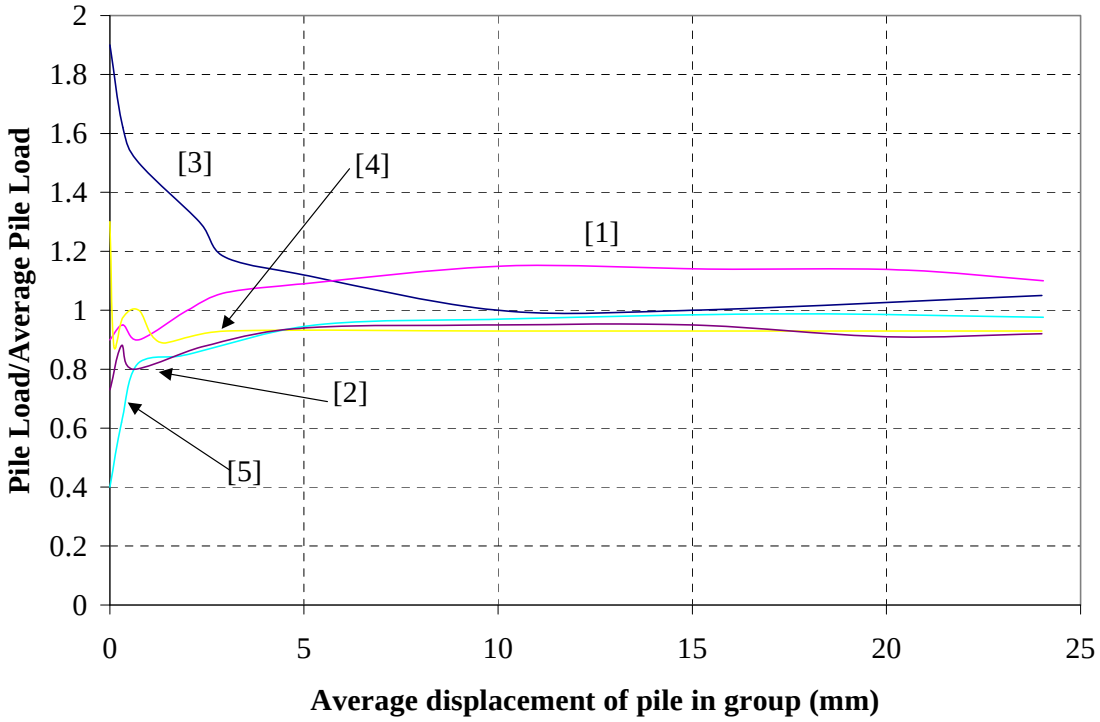

Figure 5-13 Load sharing among individual TG1/s piles

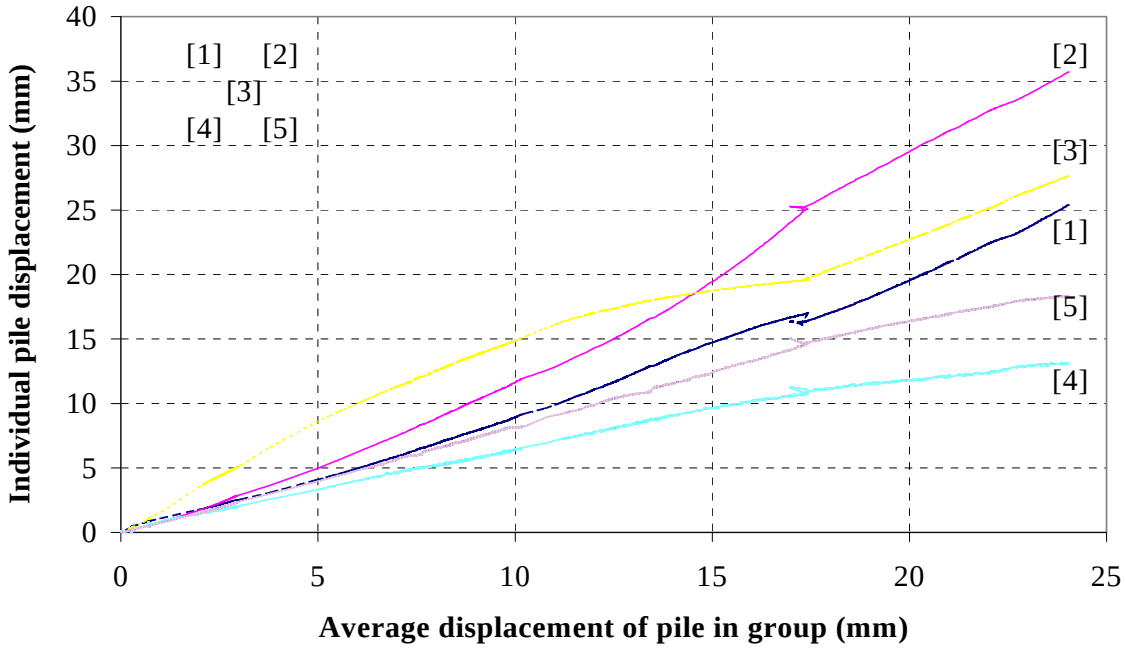

Figure 5-14 Relative displacements of individual TG1/s piles

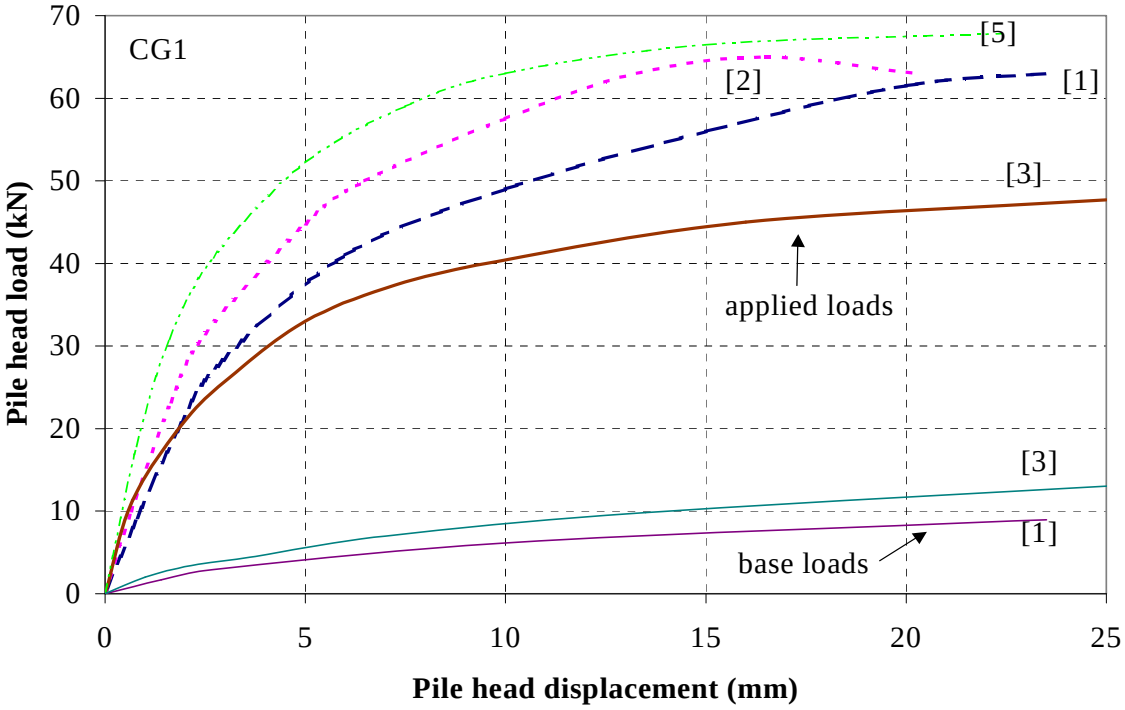

Figure 5-15 Load-displacement behaviour of piles in CG1/s

and average of the four corner piles are consistent throughout loading[7] (Figure 5-16). The TCD pile head load cells all exhibit some bending (most prominent in the corner piles), also indicative of uniform cap settlement.

There is approximately a factor of two variation between the measured 'working' stiffnesses of the corner piles in Figure 5-15 (an indication of pile cap tilt), but this has equalized as ultimate conditions approach and the corner piles all carry similar loads. The centre pile CG1[3] has started to assume lower loads than the average corner pile upon reaching an average group displacement of ≈1mm and lower than all the corner piles by ≈3mm. The centre pile load falls ≈25% below that of an average corner pile by 20mm average group displacement.

[7] Not surprising since the pile cap was designed to withstand compression rather than tension loading.

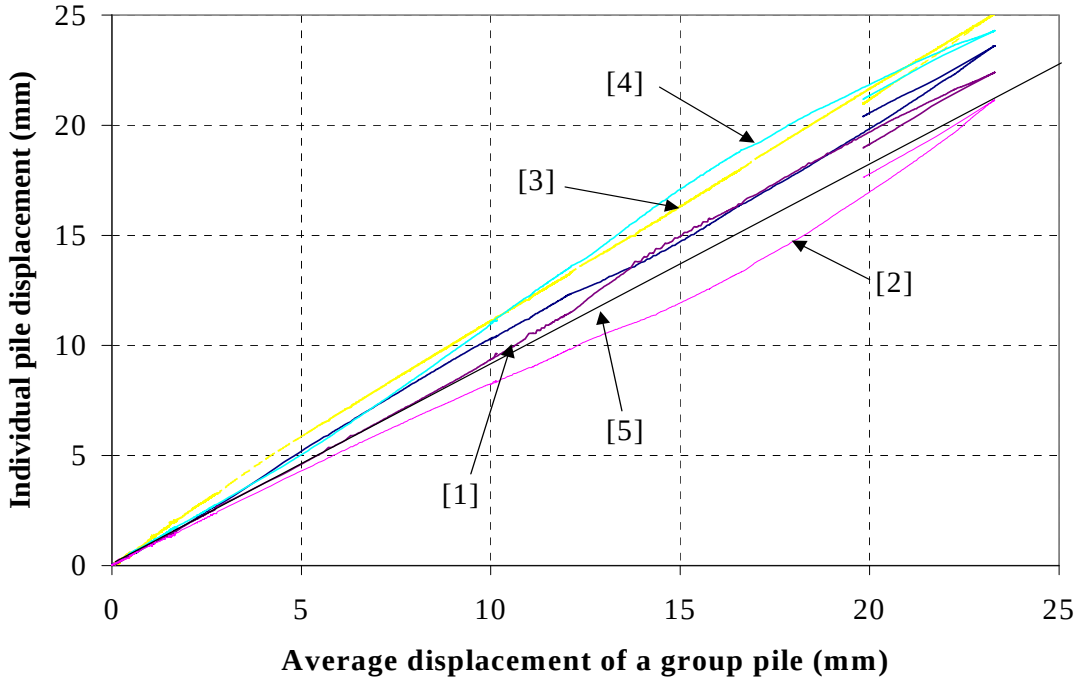

Figure 5-16 Relative displacements of individual CG1/s piles

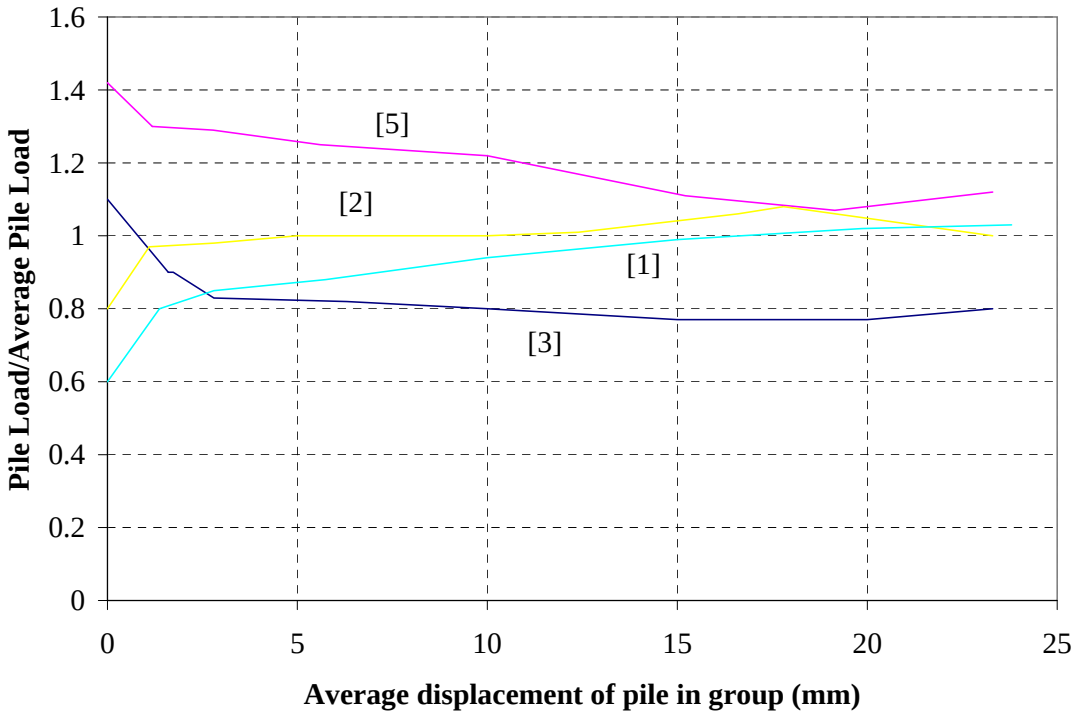

Figure 5-17 Load sharing among CG1/s piles

Load distributions

The compression group CG1 was heavily instrumented with strain gauges (see Appendix 4-1). All strain data is presented in Appendix 5-2. The main issues regarding the interpretation of these readings is summarized below:

(i) The single ERS gauge just below the head of CG1[3] showed excellent agreement with the output from the load cell at the pile head. This gave confidence in the accuracy of the gauges and reassurance that bending of the load cells was unlikely to hamper load interpretation.

(ii) Excellent agreement was found between the response of the VW and ERS gauges at the 2.0m level in CG1[3]. Good agreement was also found at 4.5m. Just above the pile base at 5.95m, some of the gauges did not show a clear response to load, so only those responding sharply to load increments were used to infer the pile loads.

(iii) Fewer gauges in CG1[1] made the interpretation slightly more difficult, with zero shifts identified in some cases. However comparison of the start zero, the end zero and an intermediate zeros arising from an unintentional unload reload loop, allowed the strain baseline to be known with some degree of confidence. No satisfactory interpretation was made of the VW gauges in CG1[5].

(iv) The ERS gauges in CG1[4] and CG1[5] were improperly wired to the Datascan system prior to the load test, so no strain data are available for these piles.

Load distribution patterns for corner pile CG1[1]/s and centre pile CG1[3]/s are shown in Figure 5-18 to within $\pm$2kN. The final distributions shown represent pile head displacements of close to B/10 and provide reasonable indications of the ultimate load distributions in the piles. These load distributions are compared in Figure 5-19 with a *projection* of the final load distribution in single pile CS1/s at a displacement of 25mm (based on the interpretation of Section 5-8). Compatible shear stress distributions are presented in Figure 5-20. The load transfer within the sleech (i.e. Stratum 2 and 3 material as defined in Section 3.5; from ≈2.0m to 6.0m at the pile locations) is of primary interest.

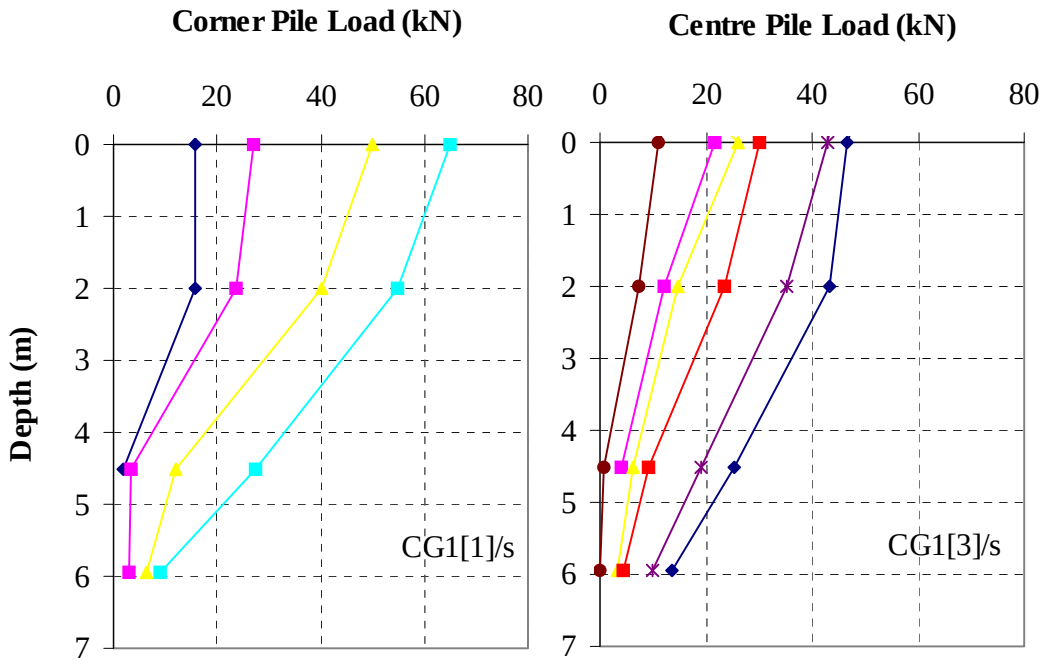

Figure 5-18 Load distributions in CG1[1]/s and CG1[3]/s

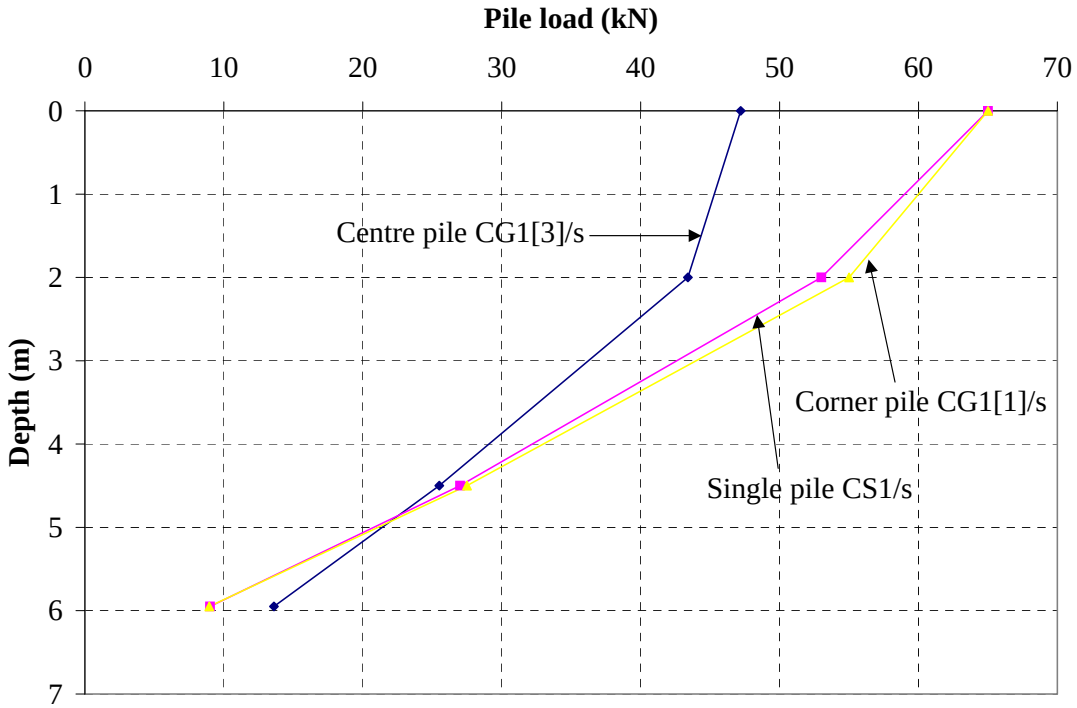

Figure 5-19 Load distributions in single, corner and centre piles (at B/10 displacement)

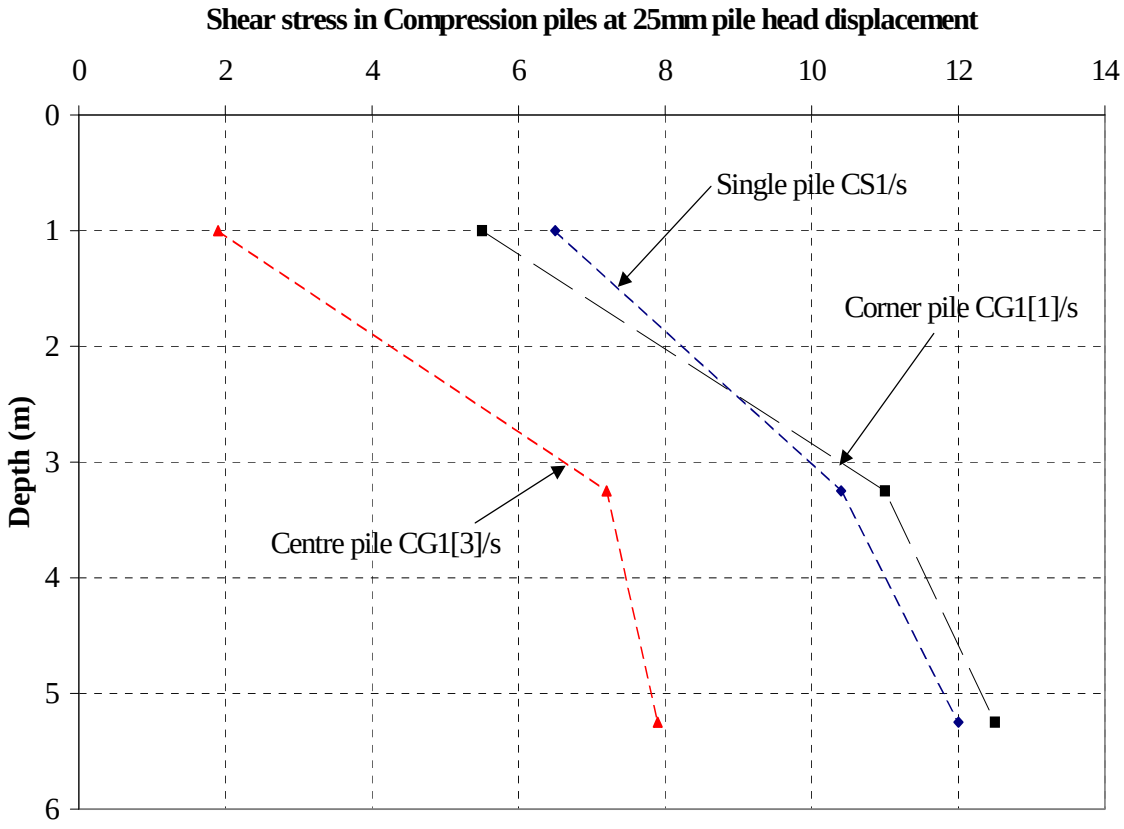

Figure 5-20 Distributions of shear stress in single, corner and centre piles

It is clear that:

- Not only are the corner and single pile capacities comparable but their 'final' load distributions at 25mm displacement are also very similar.
- Although the interpretation of base loads are somewhat approximate, it nevertheless appears that the centre pile carries more load at its base than an equivalent single pile. Piles subjected to external/interactive loading transmit more load to the soil at the lower part of the shaft and at the pile base than isolated piles.
- When the load carried by the portion of the pile embedded in *sleech* is considered, it is clear that the centre pile carries a much greater *proportion* of this load at its base than the single pile.
- Further interpretation of the shear stresses acting on the piles follows in Section 5.8.

Horizontal total stresses

Measurements of σ_h (on CG1[3] at depths of 3.25m and 5.25m, and on CG1[1] [8] at a depth of 5.25m) were made during the group load test (Figure 5-21). Relatively small increases in σ_h were registered at all three instrument positions as a result of group loading. The magnitudes of these changes are of the same order as the devices' accuracy, and do not show a sharp response to the applied load. The correspondence between the σ_h measurements at 5.25m on CG1[1] and CG1[3] is noteworthy.

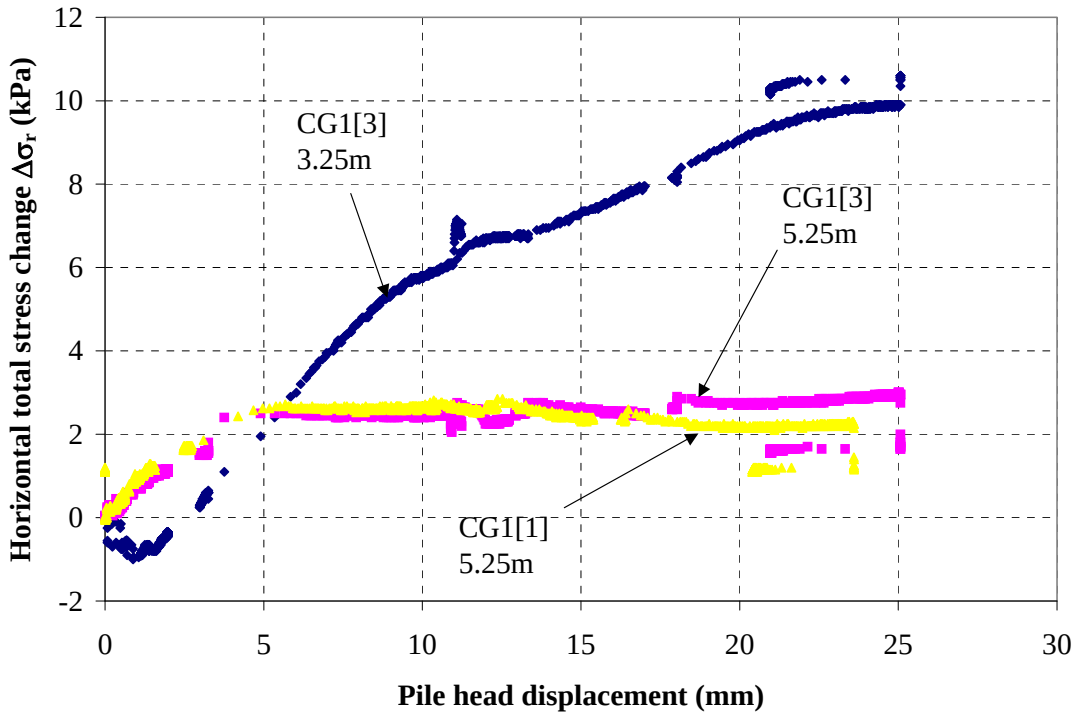

Figure 5-21 Changes in σ_h during loading of CG1

5.7.2 Corner Pile Load Test CG2/s

While categorized as a pile group test, corner pile CG2[2] was loaded alone and therefore was not subjected to interactive loads from the four remaining group piles. The pile was loaded to 42.5kN, at which point hydraulic problems within the jack/pump system caused the pile to be overloaded instantaneously. Figure 5-22 shows that the working stiffness of

[8] This instrument was found to operate during the load test CG1/s, although it did not respond during installation of the CG1.

CG2[2]/s (a corner group pile when loaded alone) is very similar to that of single pile CS1/s; slight differences are consistent with small q_c variations between the two test locations. On this basis (and in the absence of any load interaction), it is suggested that the installation of the four neighbouring piles had little or no effect upon the corner pile.

Displacements at the head of the load-free piles (due to the loading applied to corner pile CG2[2]) were also recorded and plotted as a function of the load in CG2[2] (Figure 5-23).

The significance of the 'interactive' displacements imposed on the load-free piles in relation to those measured on the loaded pile are shown in Figure 5-24. All measured displacements are plotted as a function of distance from the loaded pile (CG2[2]) normalized by the pile width (i.e. s/B; s/B=0 represents CG2[2]'s own displacement). Figure 5-24 captures how the influence of loaded piles in a group depends on how far apart they are spaced.

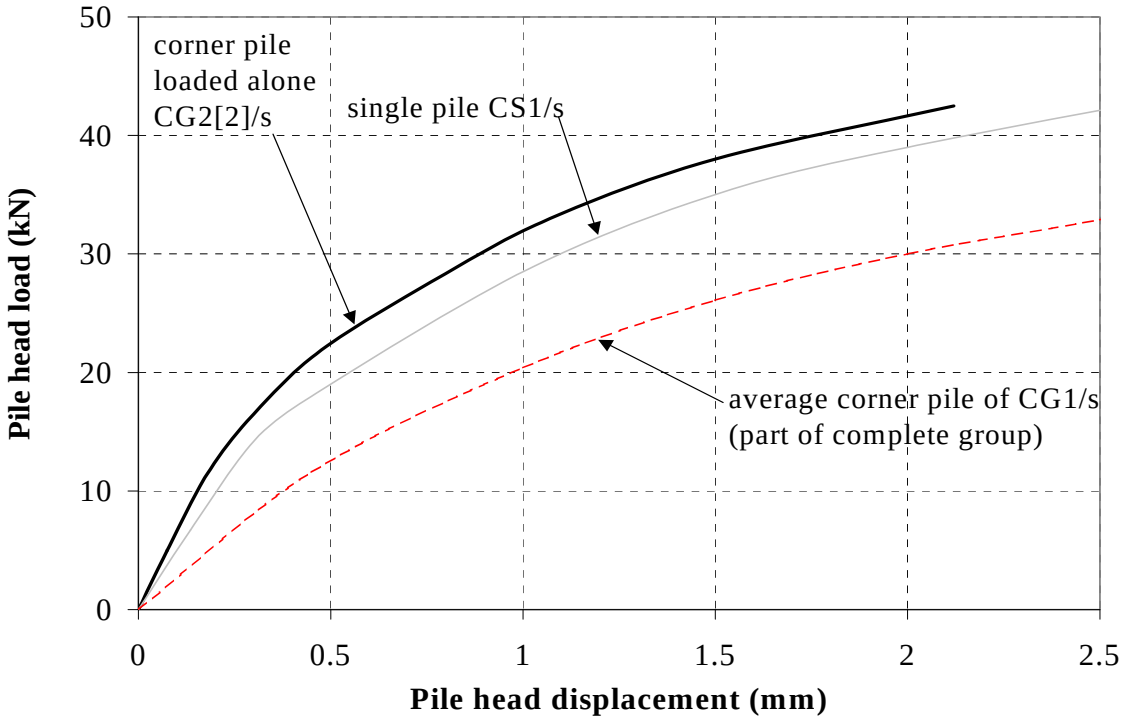

Figure 5-22 Corner pile load test CG2[2]/s

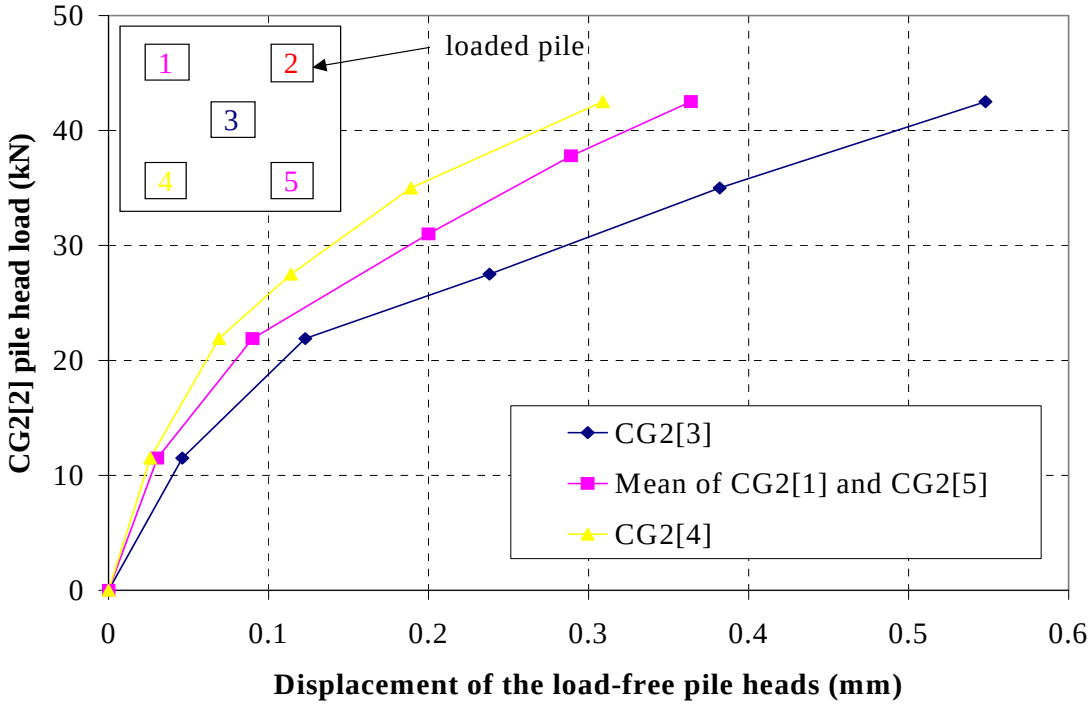

Figure 5-23 Interactive displacements on load-free piles (CG2/s)

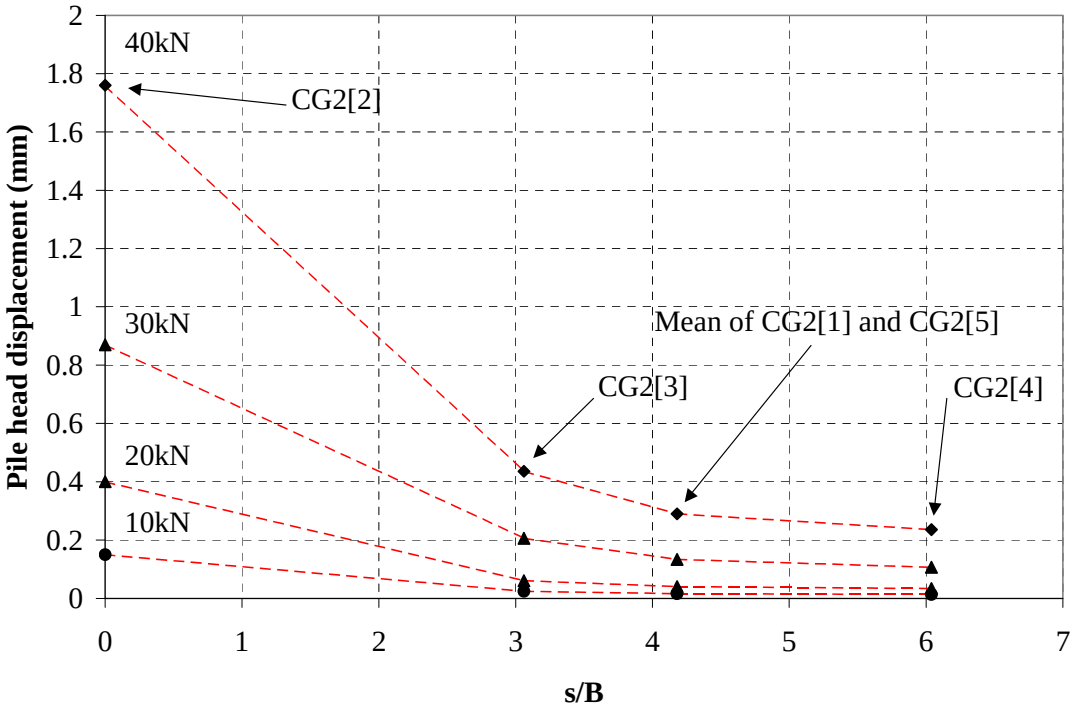

Figure 5-24 Variation of interactive pile displacements with spacing

It should be noted that greatest reliability is attached to the 'interactive' displacements on the non-loaded piles at loads in excess of 20kN; slight instability of the reference beam occurred at lower loads.

5.8 Reliable Assessments of Shaft Capacities

When interpreting the load test data presented in this Chapter, it is essential that the overall capacity of the single and group piles are known accurately, and that the shaft and base components of capacity can be separated. This enables valid comparisons to be made between the respective pile tests. This is particularly important given that the majority of maximum pile loads[9] measured in this Thesis fall within the narrow range of 45-75 kN.

5.8.1 Definition of Pile Capacity

The definition of pile 'failure' has long been a contentious issue, with a number of different definitions available. For the purposes of this Thesis, the following definitions are adopted:

- The ultimate capacity of a single pile is defined as the load required to displace the pile head by 10% of its width or diameter. However, it is likely that larger displacements are required to bring group piles to the same level of ultimate load mobilization of an equivalent single pile. Therefore all static group pile load-displacement curves were further extrapolated to the arbitrary figure of 50mm in an attempt to recognize the effects of group action.
- The load-displacement curves were standardized by ensuring that the creep rate at the end of each stage of maintained loading was 0.24mm/hour. All of the load-displacement curves already presented have been corrected (where necessary) so that they connect points of equal creep rate.

When a test was stopped before reaching 25mm (or 50mm) displacement, hyperbolic extrapolation (Chin 1972) was used to determine the single pile/pile group capacities:

$$\frac{\delta_1 - \delta_2}{\frac{\delta_1}{P_1} - \frac{\delta_2}{P_2}} = P_{ul}$$

[9] Maximum load reached in the test, not necessarily the failure load

where δ_1 and δ_2 are the displacements at loads P_1 and P_2 respectively and P_{ul} is a (hypothetical) load corresponding to infinite pile displacement. P_{ul} for a pile is found as the inverse slope of the straight line produced by plotting δ/P against δ over the entire test[10]. Extrapolated total pile capacities and pile base capacities are presented in Table 5-3.

TOTAL APPLIED LOADS			
Pile(s)	**Chin's P_{ul} (kN)**	**Load at 25mm (kN)**	**Load at 50mm (kN)**
CS1/s	68.6	66.0	
TS1/s	79.7	72.8	
TS2/s	68.1	64.8	
TS2/ss	123.1	n/a	n/a
CG1[1]/s	76.2	62.5	68.8
CG1[2]/s	76.8	68.8	72.6
CG1[3]/s	53.4	47.7	50.4
CG1[5]/s	74.8	69.6	72.1
CG1/s	334.3	311.5	322.5
TG1[1]/s	77.3	69.1	73.0
TG1[2]/s	60.7	53.5	56.8
TG1[3]/s	69.5	59.4	64.2
TG1[4]/s	68.2	61.6	64.7
TG1[5]/s	66.7	60.6	63.4
TG1/s	351.5	306.6	327.5
BASE LOADS			
CS1/s	10.4	9.5	-
CG1[1]/s	12.2	9.2	10.5
CG1[3]/s	18.2	12.5	14.8

Table 5-3 Loads extrapolated using hyperbolic model

[10] The hyperbola is a poor model for the reloaded single pile TS2/ss, which behaves in a more linear manner than any of the other piles. Chin's procedure predicts P_{ul} of 123kN, which is almost 50% larger than any other ultimate loads predicted at Kinnegar.

5.8.2 Pile Equilibrium and Shaft Capacity

The axial capacity of a pile or pile group is conventionally taken as the load, over and above the pile weight and the weight of the cap, which causes ultimate failure. This is a reasonable assumption in the majority of cases, where the weight of the pile and cap are quite low in relation to applied tensile or compressive loads. The weight of all piles tested in Kinnegar was 9kN (which is typically between 12 and 18% of the maximum applied pile loads) and the pile cap had the effect of adding a further 2 kN compression per group pile[11]; so the pile and cap weight cannot therefore be ignored for the Kinnegar tests.

A pile subjected to tension loading close to ultimate failure is in equilibrium due to the action of four forces. The applied tension load ($P_{app\ t}$) and the force due to pore pressure acting on the pile base (uA_b)[12] act upwards and must be balanced by the sum of the pile weight (W_p) and the load carried by shear stresses on the pile shaft ($Q_s = q_sA_s$) which act downwards, i.e.

$$P_{app_t} + uA_b = W_p + Q_s$$

The installation process may be thought of as effectively replacing a volume of soil with the same volume of concrete, so the resultant increase in load on the soil beneath the pile base after installation is given by:

$$(\gamma_c - \gamma_s)V \qquad or \qquad W_p - W_s$$

where γ_c and γ_s are the unit weights of concrete and soil respectively, V is the pile/displaced soil volume and W_s is the weight of the displaced soil volume[13]. This (relatively small) net increase in load acts in addition to an applied compression pile head load ($P_{app\ c}$) and must be in equilibrium with the shaft ($Q_s=q_sA_s$) and base ($Q_b=q_bA_b$) resistances. Therefore:

$$Q_s + Q_b = P_{appc} + (\gamma_c - \gamma_s)V$$

[11] It is assumed that each group pile carries one-fifth of the pile cap weight.
[12] It is assumed that, as the pile tests were effectively drained, there was sufficient time to allow water pressures to develop at the pile base.
[13] May be calculated from the unit weight profile in Figure 3-3.

The shaft capacities and corresponding ultimate shear stresses for compression single pile CS1/s and tension single piles TS1/s and TS2/s are presented in Table 5-4. The subscript '25' represents the ultimate capacity at 25mm displacement. It should be noted that all three piles were in the ground for similar periods before testing (see Table 5-7), so (potential) time related effects (discussed further in Section 5.9) are not variables in this comparison.

Pile	$P_{app\ 25}$ (kN)	W_p (kN)	W_s (kN)	$Q_{b\ 25}$ (kN)	uA_b (kN)[14]	Q_s (kN)	q_s (kPa)	
CS1/s	66.0	9.0	6.3	9.5	-	59.2	**9.9**	
TS1/s	72.8	9.0	-	-	3.1	66.9	**11.2**	*average*
TS2/s	64.8	9.0	-	-	3.1	58.9	**9.8**	*10.5*

Table 5-4 Summary of static single pile test data

Equivalent calculations are carried out for the pile groups CG1/s and TG1/s (Table 5-5). In this case, the subscript '50' refers to the group loads at 50mm displacement.

Pile	$P_{app\ 50}$ (kN)	W_p (kN)	W_s (kN)	Q_b (kN)	uA_b (kN)	Q_s (kN)	q_s (kPa)
CG1/s	322.5	55.0	31.5	57	-	289	**9.6**
TG1/s	327.5	55.0	-	-	15.6	288	**9.6**

Table 5-5 Summary of static pile group test data

5.8.3 Comparison of Capacities and Pile Group Capacity Efficiency

The following observations arise from Tables 5-4 and 5-5:

- The tension and compression single pile shaft capacities (at 25mm displacement) are approximately the same. The agreement is more convincing if the close proximity of the test locations of CS1/s and TS2/s (2m) is taken into consideration. Without considering pile weights and pore pressure base uplift, it could have been

[14] u based upon hydrostatic pore pressure distribution, water table at 1m depth.

concluded in error that the compression shaft capacity was in fact lower than in tension.

- Different ultimate average shear stresses in TS1/s and TS2/s reflect the slight gradient in soil consistency across the site (as evidenced by q_c measurements) and may also indicate slightly different levels of pore pressure dissipation around the piles[15]; the evidence of Figure 5-6 suggests that 100% equalization may not have been reached at this time.
- The tension and compression pile group shaft capacities (at 50mm displacement) are also the same. Since TG1/c was tested 378 days after installation and CG1/s was tested 101 days after installation, these results suggest that the effects of undisturbed aging are negligible over the period 3 months to 1 year after driving and that equalization of the pile groups was complete after 3 months. Undisturbed aging and other time related effects are discussed in Section 5.9.

Pile	**Overall Capacity Efficiency**				**SHAFT Capacity Efficiency**			
	P_{25g}/P_{25s}		P_{50g}/P_{25s}		P_{25g}/P_{25s}		P_{50g}/P_{25s}	
CG1 full group	0.94		0.98		0.96		0.98	
CG1 centre pile	0.72		0.76		0.69		0.74	
CG1 corner pile	1.00		(>1)		1.00		(>1)	
Reference pile	*TS1*	*TS2*	*TS2*	*TS2*	*TS1*	*TS2*	*TS1*	*TS2*
TG1 full group	0.84	0.94	0.90	(>1)	0.80	0.88	0.86	0.98
TG1 centre pile	0.82	0.92	0.88	(>1)	0.80	0.91	0.87	0.99
TG1 corner pile	0.84	0.94	0.89	1	0.83	0.94	0.88	0.99

Table 5-6 Capacity efficiency of CG1/s and TG1/s
(P_{25g} and P_{50g} are the group capacities at 25mm displacement and 50mm displacement respectively, P_{25s} is the single pile capacity at 25mm displacement)

[15] Piles TS1/s and TS2/s were loaded 99 and 85 days respectively after installation.

- The definition of capacity efficiency for group piles is not unique and depends on the relative displacements of group and single piles. Capacity efficiency is defined as the ratio of the applied[16] pile head load (leading to 25mm/50mm movement) of a group to the capacity (at 25mm movement) of a single pile. Table 5-6 summarises:
  (i) Capacity efficiencies for complete group, centre and average corner pile
  (ii) Overall and shaft efficiencies for these piles. Base loads are too low to determine base efficiencies accurately, but it is clear from Figure 5-19 that group action increases base efficiency.

It may be seen from Table 5-4 that the shaft capacity efficiency of a centre group pile is lower than that of a corner group pile, but this difference is not consistent for the two group tests shown, and depends upon the way in which the pile cap distributes load among the piles. The load was shared relatively evenly among the group piles in TG1/s, but favoured the corner piles in CG1/s. However, the overall capacity efficiency of both groups may differ slightly also, although both are typically no less than 90%.

The issue of pile group stiffness efficiency is considered in detail in Chapter 8.

5.9 Time-Related Influences on Pile Capacity

Not all of the load tests described in this Thesis (this Chapter and Chapter 6) were performed under identical conditions. Standardization of load-displacement data has already been discussed, but no mention has yet been made of the influence of time on pile capacity. Sufficient site-specific data is available from the pile tests to quantify a number of time-related factors which will enable more detailed comparison of the test results. These factors may be identified as:

(i) Effect of strain rate during pile loading.
(ii) Undisturbed Aging effects
(iii) Preloading effects

[16] Not including contributions from the other piles

5.9.1 Effect of strain rate during pile loading

The effect of displacement rate on the shear strength of soil is commonly accepted as 10±5% per log cycle increase in strain rate. Although the mode of shearing entailed in pile loading differs from that imposed in CIU triaxial tests, a strain rate effect of 12% per log cycle is estimated on the basis of the data presented in Section 3.8.3. The change in loading rate in Figure 5-9 induced pile failure too quickly to use this test as a basis for a reliable assessment of displacement rate effects. A figure of 12% per log cycle is used in subsequent interpretation.

5.9.2 Undisturbed Aging Effects

Undisturbed ageing effects have been defined in Section 2.5.1. The time elapsed between the installation and the load testing of all single piles/pile groups reported in this Thesis are listed in Table 5-7.

Pile test	Time since driving (days)	Pile test	Time since driving (days)
TS1/s	99	CS1/s	82
TS2/s	85	CG1/s	101
TS2/ss	236	CG2[2]/s[17]	178
TS3/c*	142	TG1/s	378
TS3/cs*	142	TG1/sc*	761
CTS1/sc*	358	TG1/scs*	761
CTS1/scs*	358	TG2/c*	170
		TG2/cs*	170

Table 5-7 Time between installation and loading (tests marked * in Chapter 6)

Assuming that the shaft capacity is the same under tension and compression loading (as illustrated for single piles in Section 5.8.3), then comparison of TG1/s and CG1/s suggests that ageing may be ignored over the period 3 months to 1 year after installation.

[17] CG2[2] was not loaded to failure.

5.9.3 The effect of soil preshearing/reloading

A number of the piles tested in this programme were re-tested at a later stage. Two distinct forms of retesting were conducted:

(i) When the piles were unloaded after the slow virgin static tests (Sections 5-4 to 5-7), all piles were immediately reloaded at a faster rate (typically ≈1mm/min). This process is subsequently referred to as short-term or *undrained reloading*, taking place without a significant setup period.

(ii) After the slow virgin static tests, the surrounding soil was allowed to re-equalise and age for a period before being re-loaded. The re-loading process is termed as *aged reloading* (Section 2.5.2). A feature of the current test programme is that retested piles exhibit higher capacities than measured in original tests. These differences appear to be entirely due to potential pre-shearing effects since undisturbed ageing has been shown not to be significant.

Undrained reloading

Capacity differences between slow static tests (0.004mm/min) and faster retests which follow immediately (of the order of 1mm/min) represent some combination of displacement rate effects and potential undrained reloading effects[18]. The magnitude of undrained reloading effects emerges through a comparison of the measured gain in capacity between the two tests with that predicted based upon rate effects alone (Table 5-8). The sensitivity of the outcome to the use of displacement rates of 10% and 12% per log cycle are shown.

In general, correction for loading rate alone overpredicts the percentage capacity increase; thus suggesting that undrained preshearing (i.e. without significant dissipation of pore pressure from the prior test) causes a 10-15% reduction in pile capacity, although the exact amount is difficult to project reliably.

Aged reloading

Information regarding *aged reloading* of piles (following re-equalisation and a period of ageing) may be obtained from the following pile tests; the corresponding intervals between

[18] No other time related effects arise (setup, ageing).

Test	Virgin Capacity [19] (kN)	Re-test Capacity (kN)	Re-test rate (mm/min)	Measured capacity increase (%)	Predicted capacity increase (%)		Approximate reloading effect (%)	
					10%	12%	10%	12%
CS1	66.0	74.0	1.14	**12.1**	**24.5**	**29.5**	**-9.9**	**-13.4**
TS1	72.8	78.5	0.91	**7.8**	**23.6**	**28.3**	**-12.8**	**-16.0**
TS2	64.8	71.0	1.00	**9.6**	**24.0**	**28.8**	**-11.6**	**-14.9**
TG1	306.6	~340	0.63	**10.9**	**22.0**	**26.4**	**-9.1**	**-12.3**
CG1	311.5	~360	0.83	**15.6**	**23.2**	**27.8**	**-6.2**	**-9.6**
						Average:	**-9.9**	**-13.2**

Table 5-8 Piles reloaded without time for ageing

installation and the two relevant static tests may be found in Table 5-5:

(i) The tension single pile test TS2/s, subsequently reloaded as TS2/ss.

(ii) The tension pile group test TG1/s, subsequently reloaded as TG1/scs. Although TG1 was subjected to low levels of cyclic loading in the intervening period, displacement measurements suggest that little cyclic *damage*[20] was caused, so that the difference between the static capacities provides a good estimate of aged reloading over that period.

Although a number of other static re-tests were performed; cyclic tests to ultimate conditions were conducted in between which will later be shown to have had an effect upon the subsequent static capacity.

It may be concluded from Figure 5-25 that prior testing accompanied by a pause of between 5 months and 1 year leads to a capacity gain in the region of 27%. A similar figure was identified in both tests, which suggests that this percentage is a tentative maximum and that

[19] Performed at a displacement rate of 0.004mm/min or 0.24mm/hr
[20] Refer to Chapter 8 for the cyclic pile load tests.

no further capacity can be developed with time[21]. The plotted time dependence of this capacity gain is conjectural, but is based on the fact that only 151 days were required for TS2 to increase in capacity by ≈27% while 383 days elapsed between TG1/s and TG1/scs. The magnitude of the aged reloading effect is comparable to the capacity gain discovered by Karlsrud and Haugen (1986) for first reloading (Section 2.5.2).

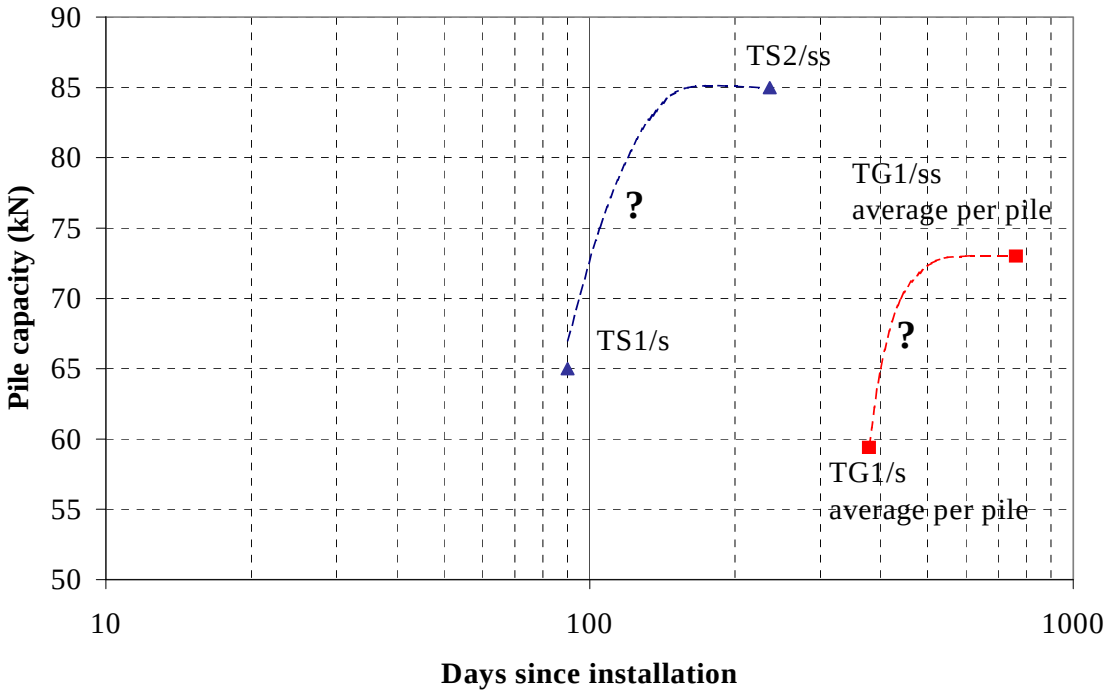

Figure 5-25 Aged reloading effect for Belfast piles

[21] There is some uncertainty regarding the accuracy of the value of 85kN derived for TS2/ss due to the testing problems identified in Chapter 5, although the potential error is believed unlikely to exceed 5kN.

Chapter 6

Cyclic Load Test Results for Single Piles and Pile Groups

6.1 Introduction

Data from a programme of cyclic tests, which were carried out as an adjunct to the principal static tests, are presented in this Chapter. The scope of the test programme may be summarized by the following points:

- All cyclic tests were carried out in one-way tension (no cyclic compression tests were performed)
- Cyclic tests were followed (within 12 hours) by a slow static test[1] (except CTG1/sc)
- Some of the cyclic tests were performed on virgin piles and others on piles which had previously been loaded. Details of these tests are presented in Table 6-1 and a load history of each pile test is provided where relevant. The reader is also referred to Table 4-1/Figure 4-1 for the test locations and Table 5-5 for the times between installation and load testing.

Single/group pile	**Previous test**	**Cyclic test**	**Static re-test**
Single piles	-	*TS3/c*	TS3/cs
	CS1/s	*CTS1/sc*	CTS1/scs
Groups	-	*TG2/c*	TG2/cs
	TG1/s	*TG1/sc*	TG1/scs
	CG1/s	*CTG1/sc*	-

Table 6-1 Cyclic and ensuing Static pile tests

6.2 Cyclic Single Pile Test Results

The cyclic single pile tests were conducted to establish the effects of cyclic loading on isolated piles and also to provide a reference for the cyclic group tests. Some pertinent details of each of the single pile tests, including time since installation and number of cycles imposed are provided in Table 6-2. The relative progress of each test in reaching the maximum applied load is compared in Figure 6-1.

[1] TG1/scs followed with 30 minutes of TG1/sc; all other static re-tests commenced typically 10-12 hours after the end of the cyclic tests.

	CTS1/sc	TS3/c
Previous test (time since installation)	CS1/s (88 days)	none
Current test: time since installation	358 days	142 days
Cyclic period	60 secs	60 secs
Total number of cycles	560	187
Number of cycles at each load level	276 (64 kN) 246 (72 kN) 38 (81 kN)	19 (56 kN) 30 (62 kN) 27 (67 kN) 111 (72 kN)
Maximum applied tension load in subsequent static test[2]	CTS1/scs 68 kN	TS3/cs 64 kN
Ultimate static shaft tension[3]	64.7 kN	57.5 kN

Table 6-2 Cyclic single pile tests

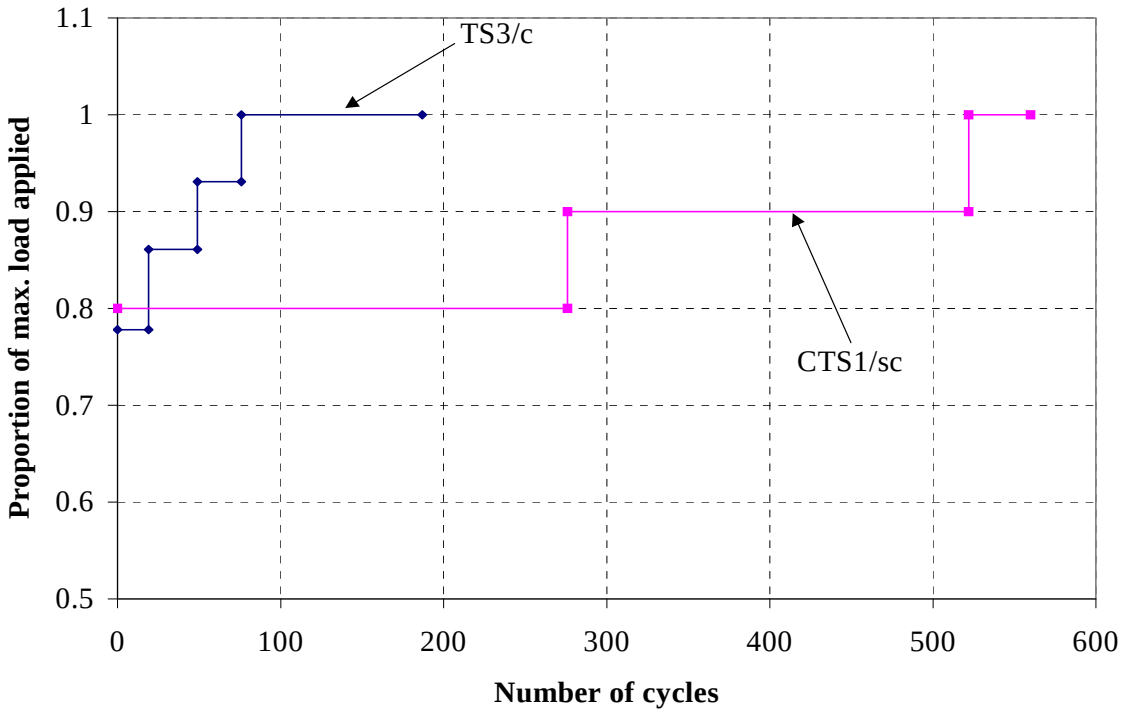

Figure 6-1 Relative progression of cycling in CTS1/sc and TS3/c

[2] Static loads not yet extrapolated to correspond with 25mm mean pile head displacement.
[3] Failure is defined as the point where the pile head displacement reaches 25mm (=B/10) with a drained creep rate of 0.004mm/min. Corrections are made for pile weight and pore pressure acting at the pile base.

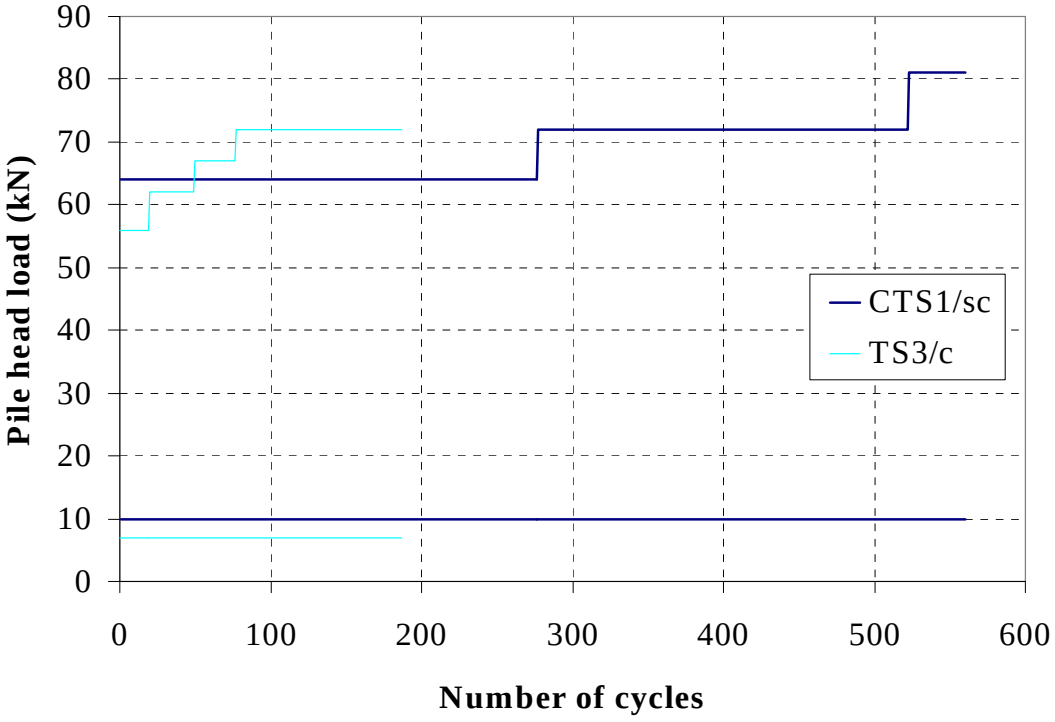

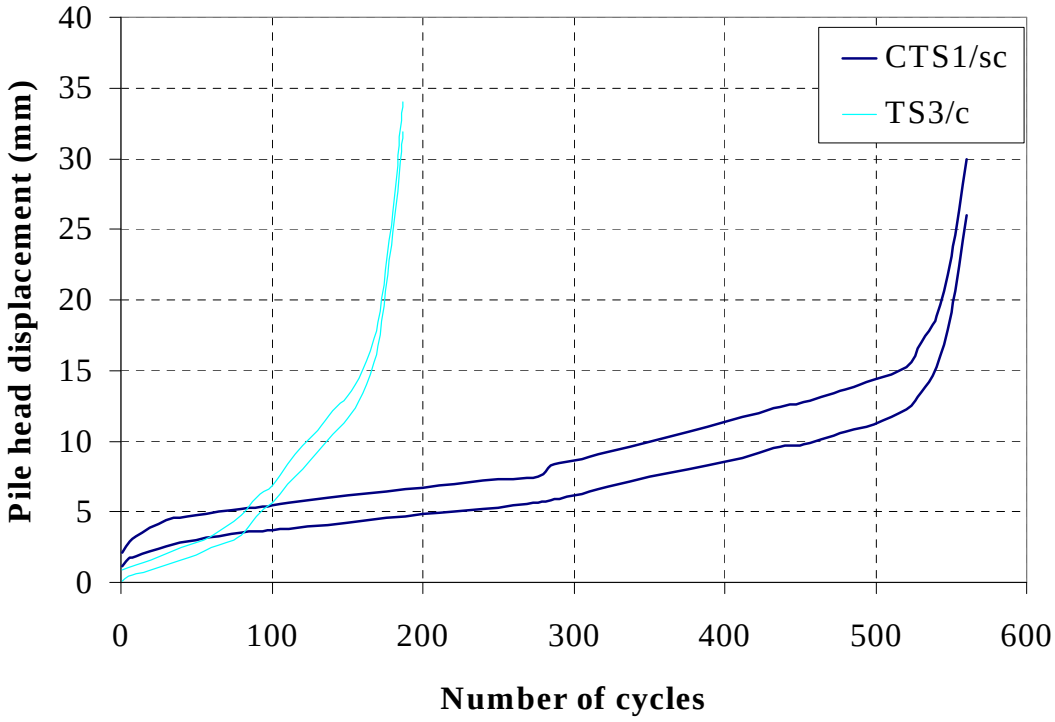

Figure 6-2 Maximum and minimum single pile cyclic loads and displacements

Fewer cycles were needed for TS3/c to reach a mean pile head displacement of 25mm; experience gained from CTS1/sc suggested that the magnitude of the load cycles should be increased when the rate of cyclic degradation was low. The tension load cycles and the corresponding mean pile head displacements are shown in Figure 6-2 for both TS3/c and CTS1/sc. The pile head displacement amplitudes (one half of the difference between minimum and maximum displacements on any one cycle) are shown in Figure 6-3.

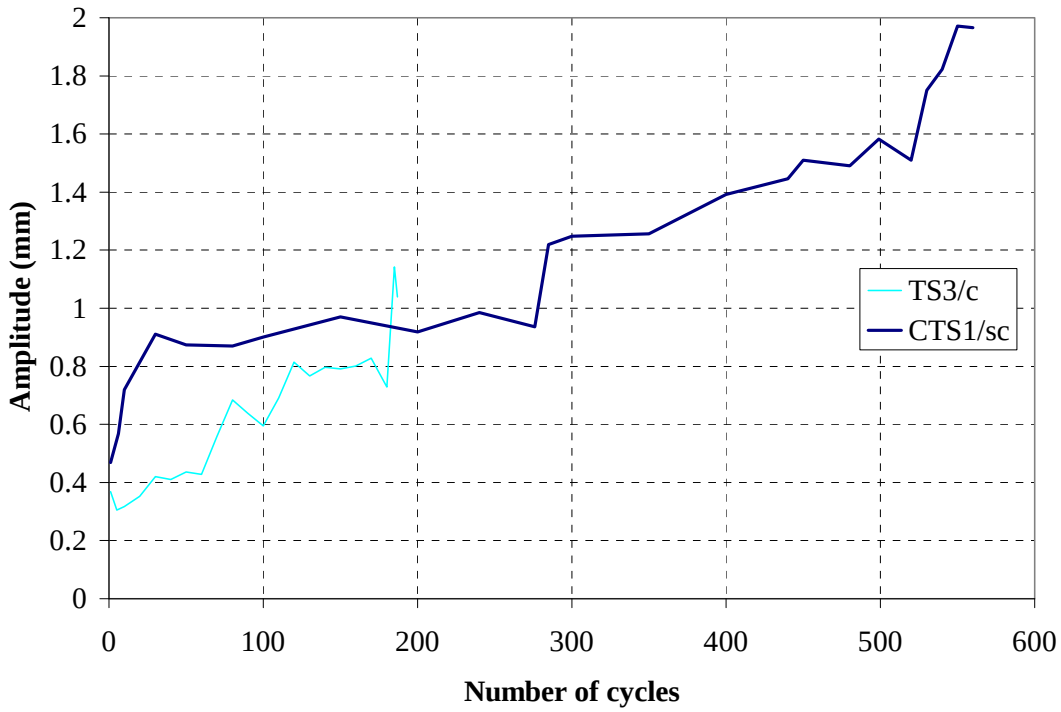

Figure 6-3 Displacement Amplitudes for single piles

6.3 Cyclic Pile Group Test Results

The details of tension tests on the virgin pile group (TG2/c) and a pair of reloaded pile groups (TG1/sc and CTG1/sc) are summarized in Table 6-3. The load cycles and pile head displacements for each individual pile of the group are presented in full in Appendix 6-1. In the interest of clarity, however, only the characteristic pile responses (centre and average corner) are presented in this Chapter, as the pile cap exhibited some tilt under load.

	TG1/sc	TG2/c	CTG1/sc
Prior test (days since installation)	TG1/s (378)	none	CG1/s (101)
Current test: days since installation	761	170	398
Cyclic period	60 secs	60 secs	60 secs
Total number of cycles	512	440	247
Number of cycles at each load level	512 (267 kN)	18 (174kN) 33 (189kN) 28 (200kN) 157 (220kN) 118 (232kN) 62 (244kN) 24 (261kN)	247 (260kN)
Maximum applied tension load in static test	TG1/scs 365 kN	TG2/cs 249kN	none
Ultimate static shaft friction	336 kN	220 kN	none

Table 6-3: Cyclic Pile Group Tests

The test data representing the responses of the characteristic group piles are presented in the following figures:

- Pile head load and mean pile head displacement against number of cycles for TG1/sc (Figure 6-4)
- Pile head load and mean pile head displacement against number of cycles for TG2/c (Figure 6-5)
- Displacement amplitudes for TG1/sc and TG2/c in Figures 6-6,
- Pile head load and mean pile head displacement against number of cycles for CTG1/sc in Figure 6-7 and displacement amplitudes in Figure 6-8.

Problems encountered with the testing apparatus during CTG1/sc are recounted in Appendix 4-1. When the test was terminated, four of the five piles were effectively either at

or close to cyclic failure while the fifth (CTG1[5]/sc) only experienced very low levels of cyclic loading. For the purposes of subsequent interpretation, it is therefore considered as a "triangular" 4-pile group. While this complicates an attempt to interpret group action effects, it is still possible to establish the whether or not cyclic degradation arises. Since the term 'average corner pile load' is no longer useful, the behaviour of all four piles is shown in Figures 6-7 and 6-8. It should be noted that the total pile group load less the sum of the loads in the functional piles is 20 ± 10 kN which is consistent with the low pile displacements in CTG1[5]/sc. Test TG1/sc was carried out at a constant magnitude of cyclic load without cyclic failure being reached. 'Failure' in TG2/c was encouraged by raising the maximum cyclic load when the rate of cyclic degradation was low.

6.4 Static Tests Results immediately after cycling

With the exception of the aborted group test (CTG1/sc), each of the cyclic tests was followed by a slow static test within 12 hours. Summary load-displacement plots for tests CTS1/scs, TS3/cs, TG1/scs and TG2/cs are shown in Figures 6-9, 6-10, 6-11 and 6-12 respectively. Data for each individual pile are given in Appendix 6-2. The following points should be noted:

- Due to time constraints, some of the static re-tests were carried out at a slightly faster strain rate than the standard static tests of Chapter 5 (creep rates up to ≈0.01mm/min). Therefore the measured load-displacement curves (in Figures 6-9 to 6-12) have been adjusted to represent the behaviour of the pile(s) had they been tested at the standard rate.
- Since each of the pile groups tested exhibited different pile cap flexibility, the data is summarized in terms of the performances of the centre and average corner piles of the group.

A prominent feature of all of the static re-tests after cycling (both single piles and groups) is that the load-displacement behaviour is significantly more linear and brittle than their virgin counterparts.

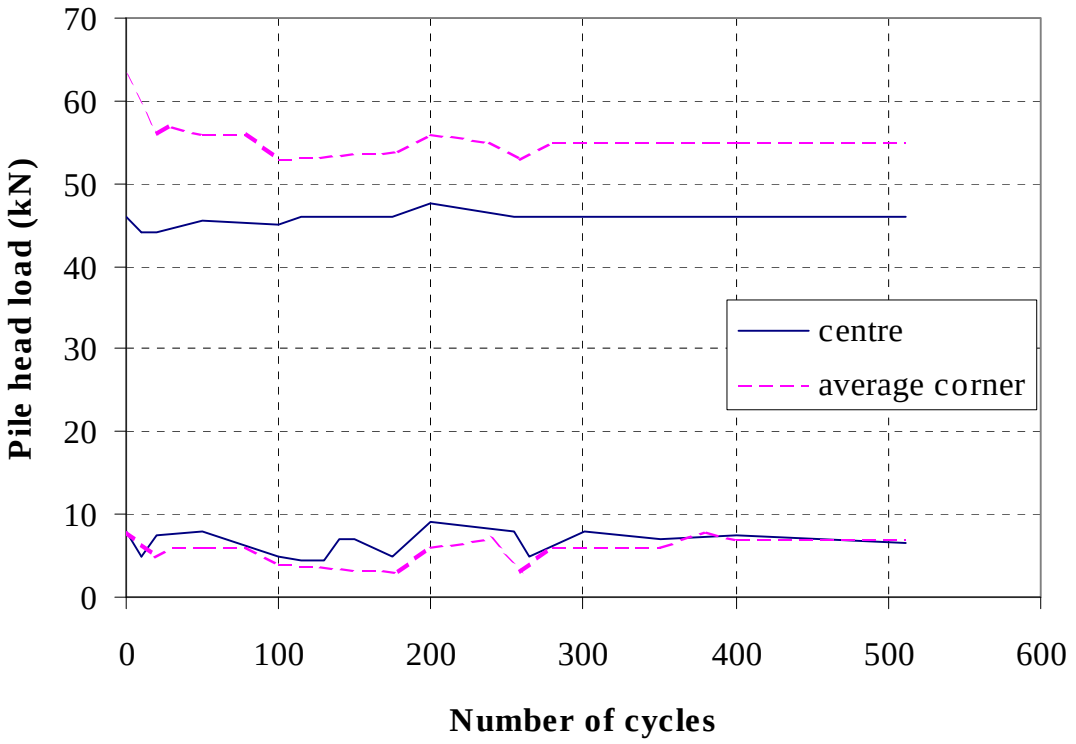

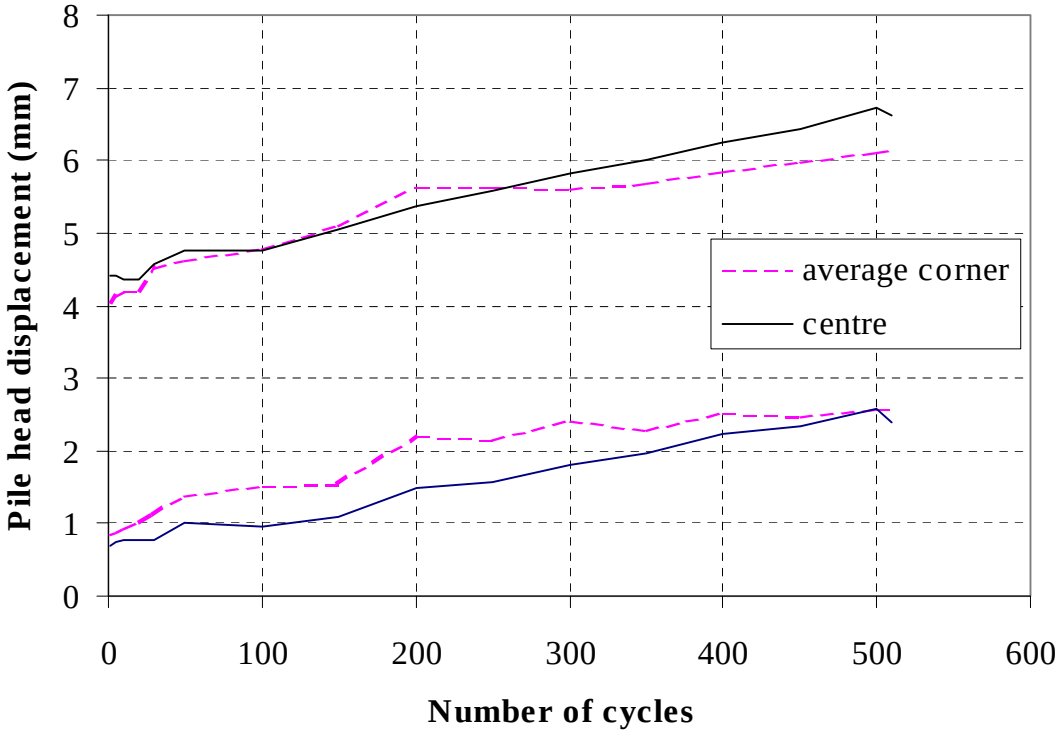

Figure 6-4 Maximum and minimum cyclic loads and displacements for TG1/sc

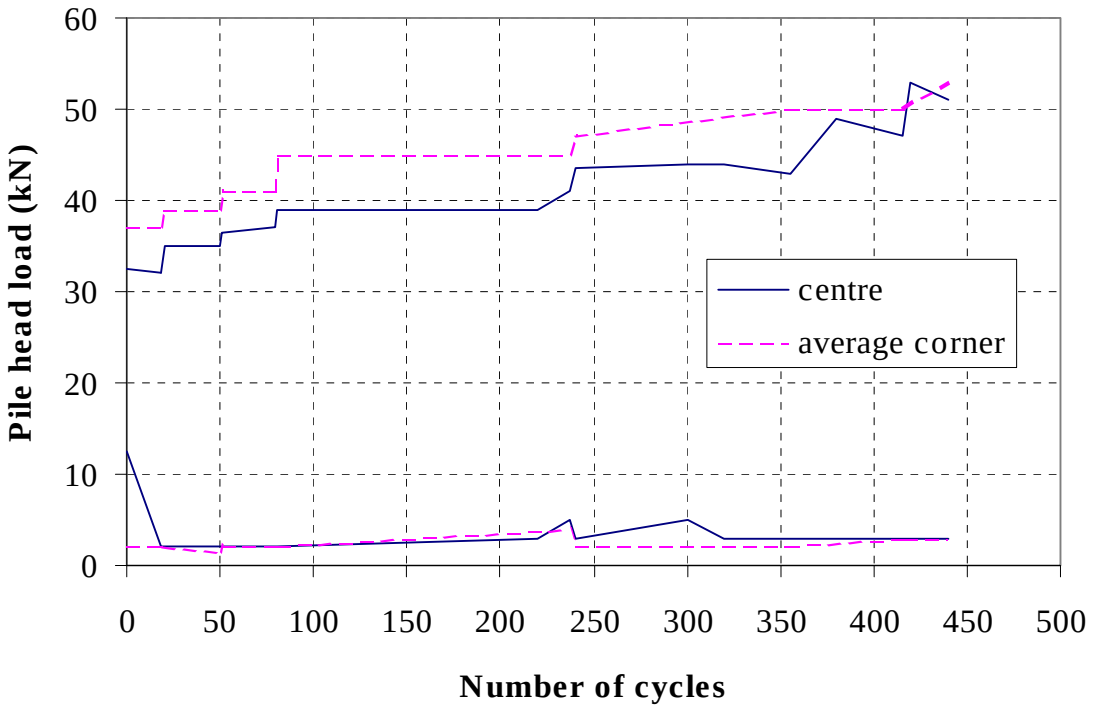

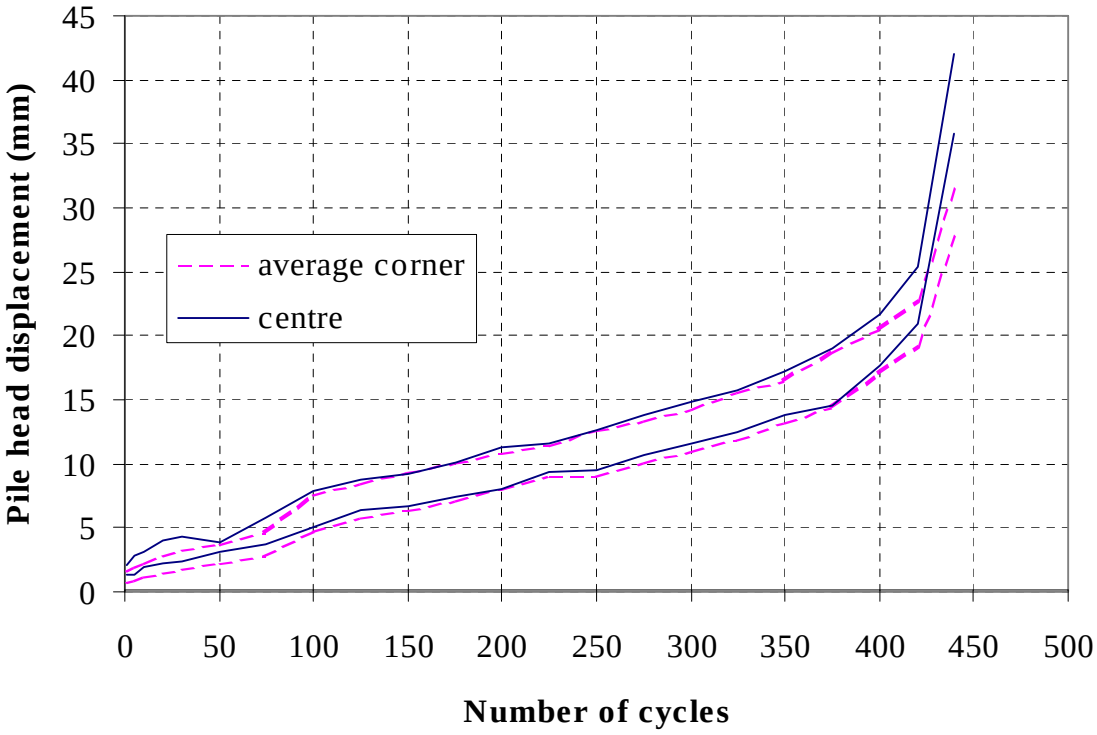

Figure 6-5 Maximum and minimum cyclic loads and displacements for TG2/c

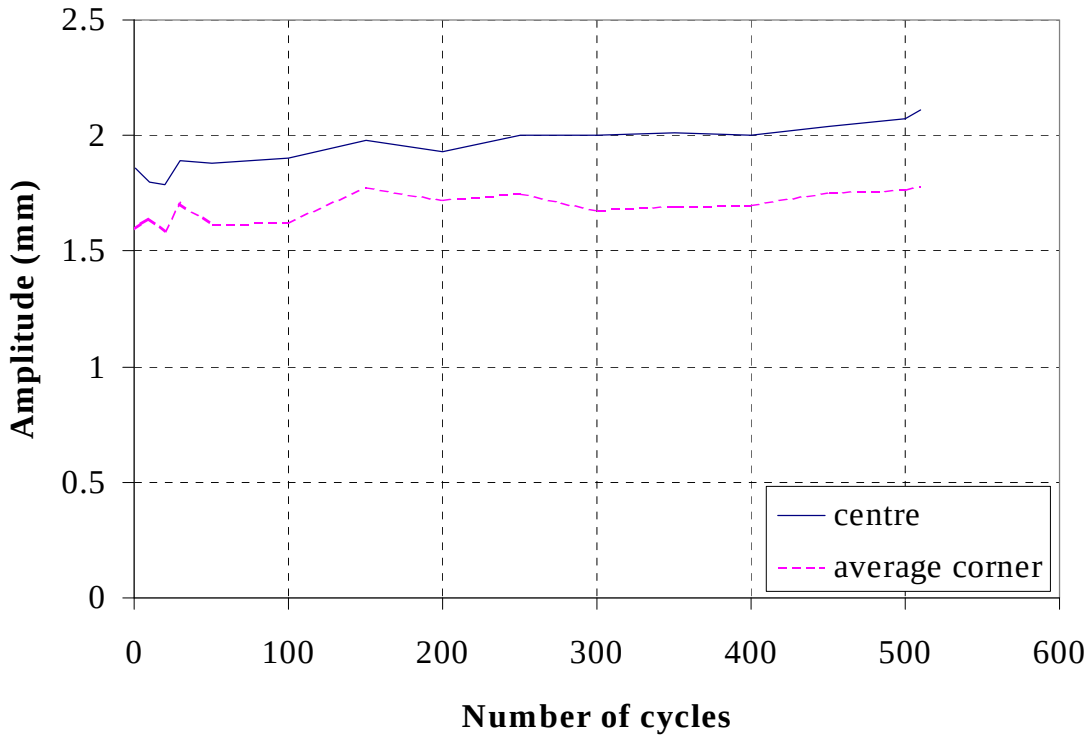

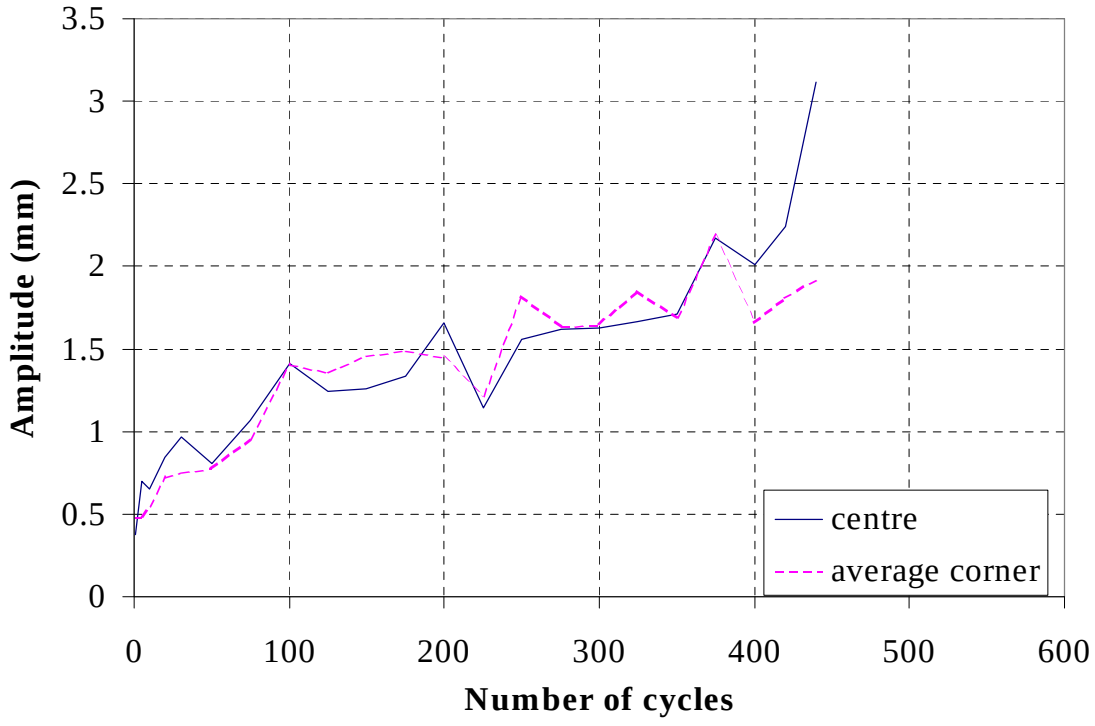

Figure 6-6 Displacement amplitudes for TG1/sc (top) and TG2/c (bottom)

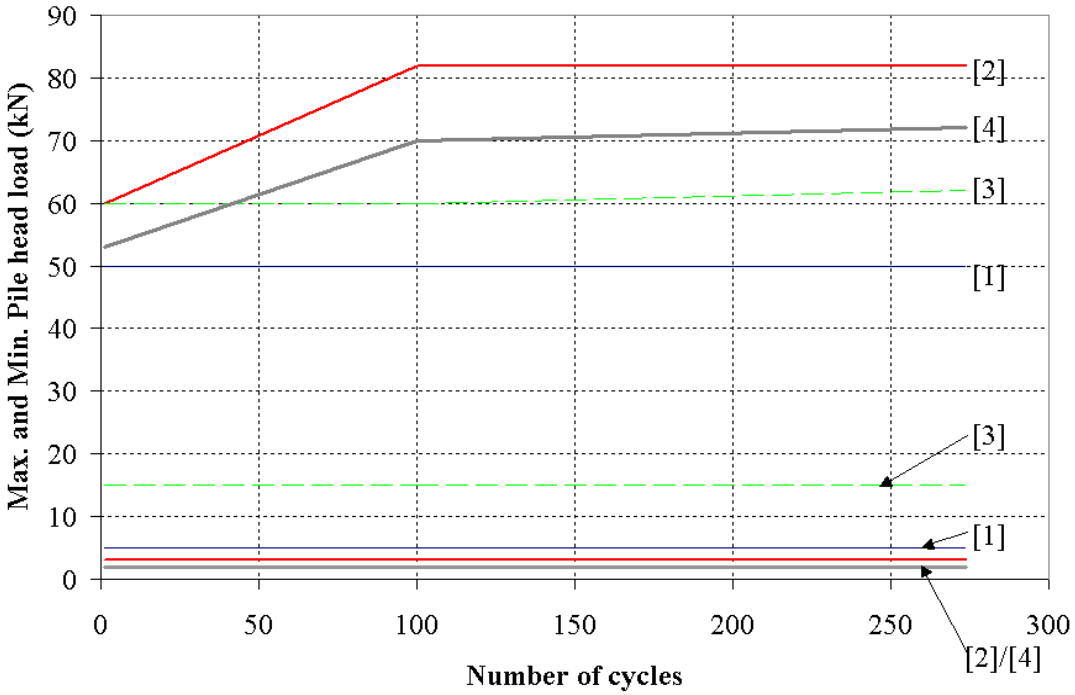

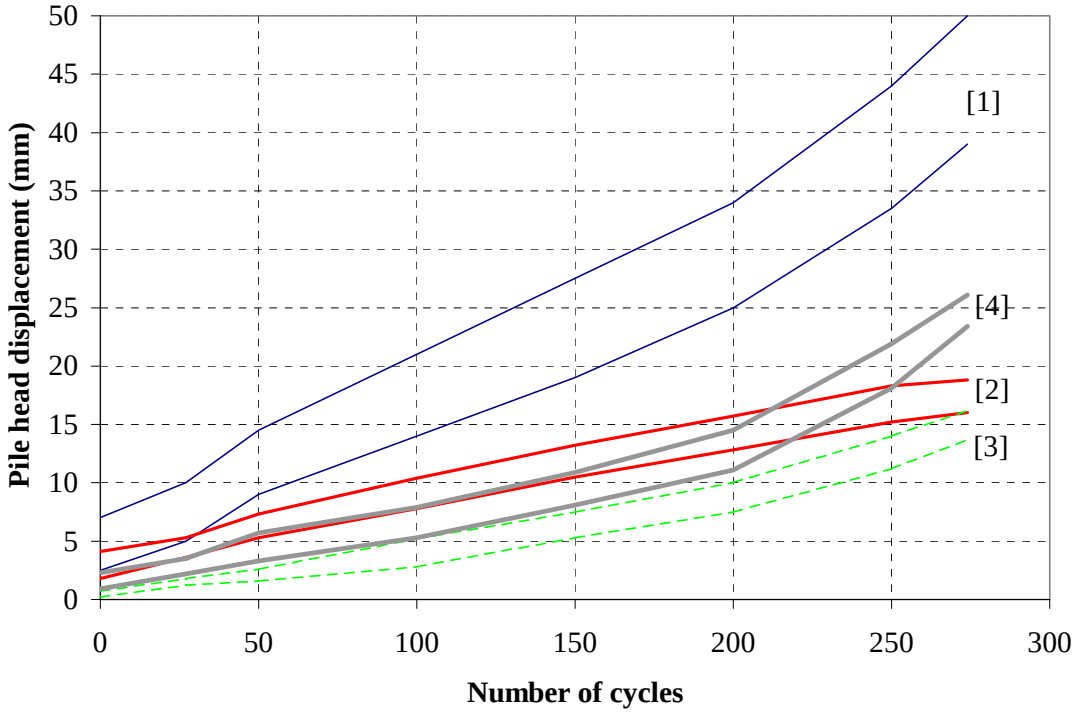

Figure 6-7 Maximum and minimum cyclic loads and displacements for CTG1/sc

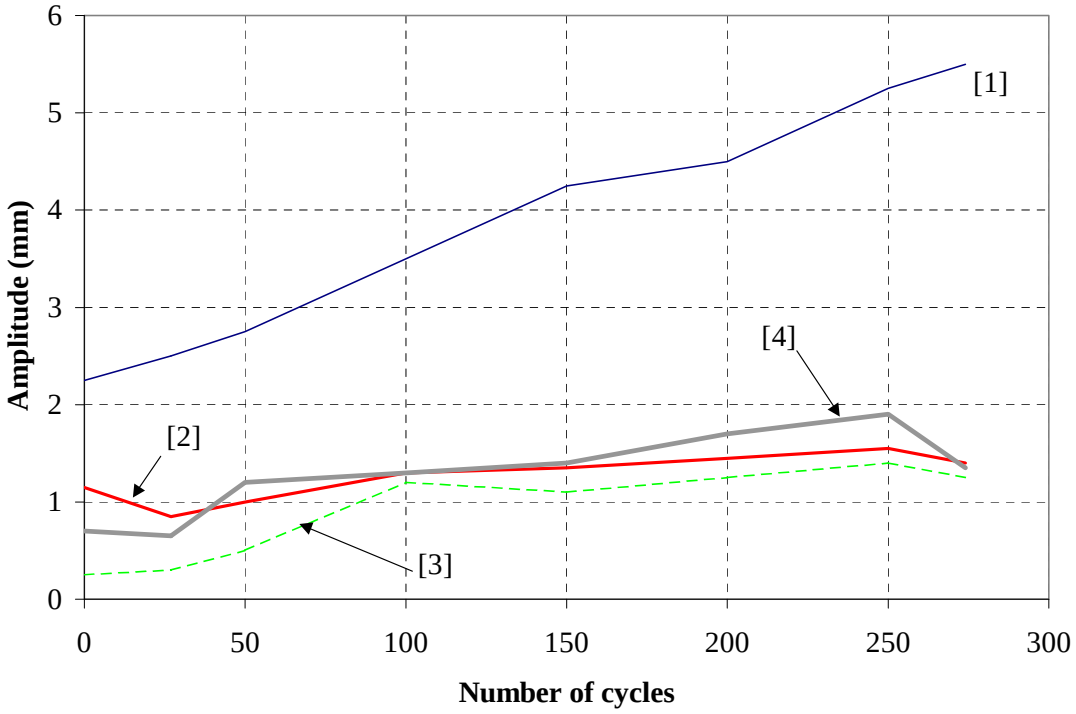

Figure 6-8 Displacement amplitude for CTG1/sc

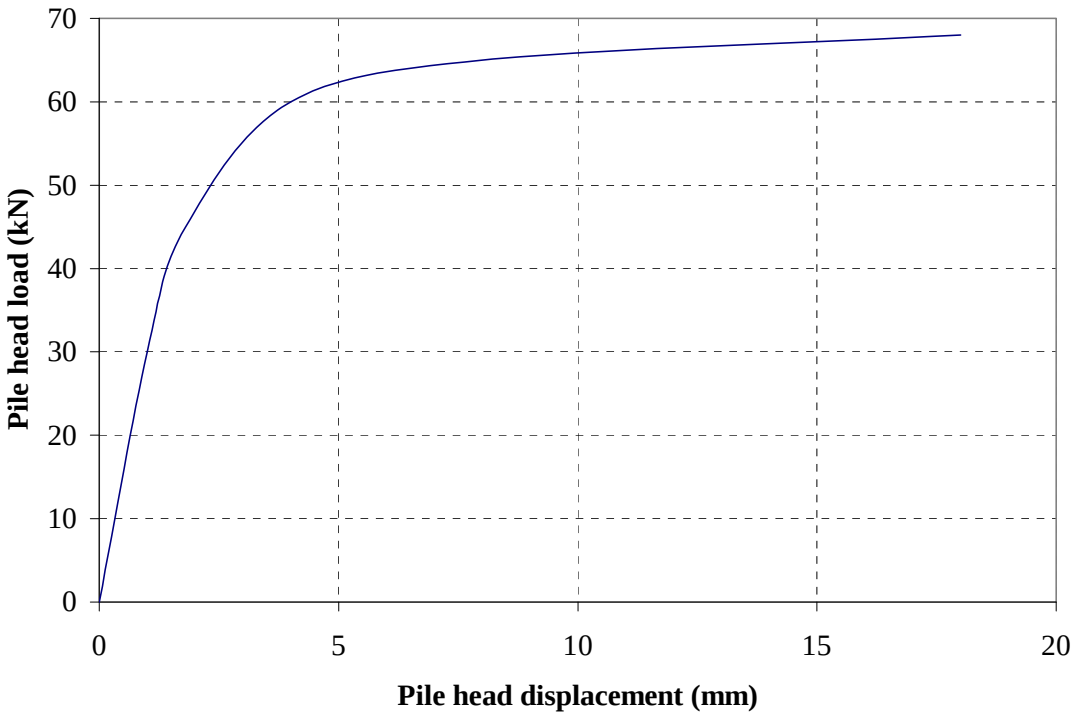

Figure 6-9 Load-displacement plot for CTS1/scs

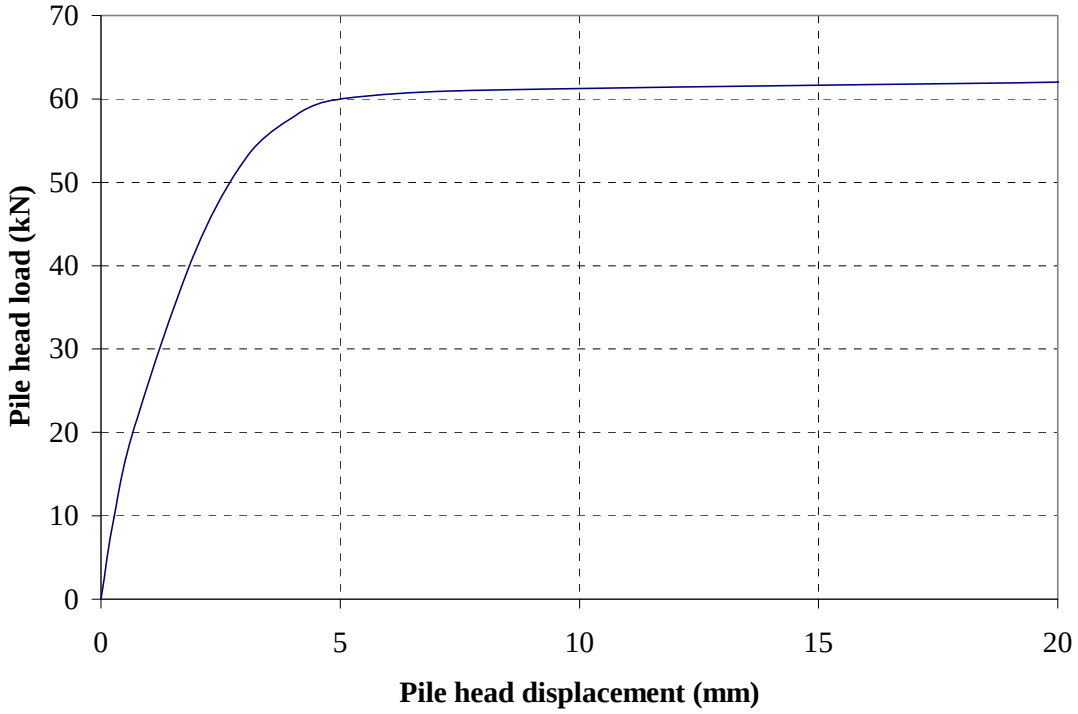

Figure 6-10 Load-displacement plot for TS3/cs

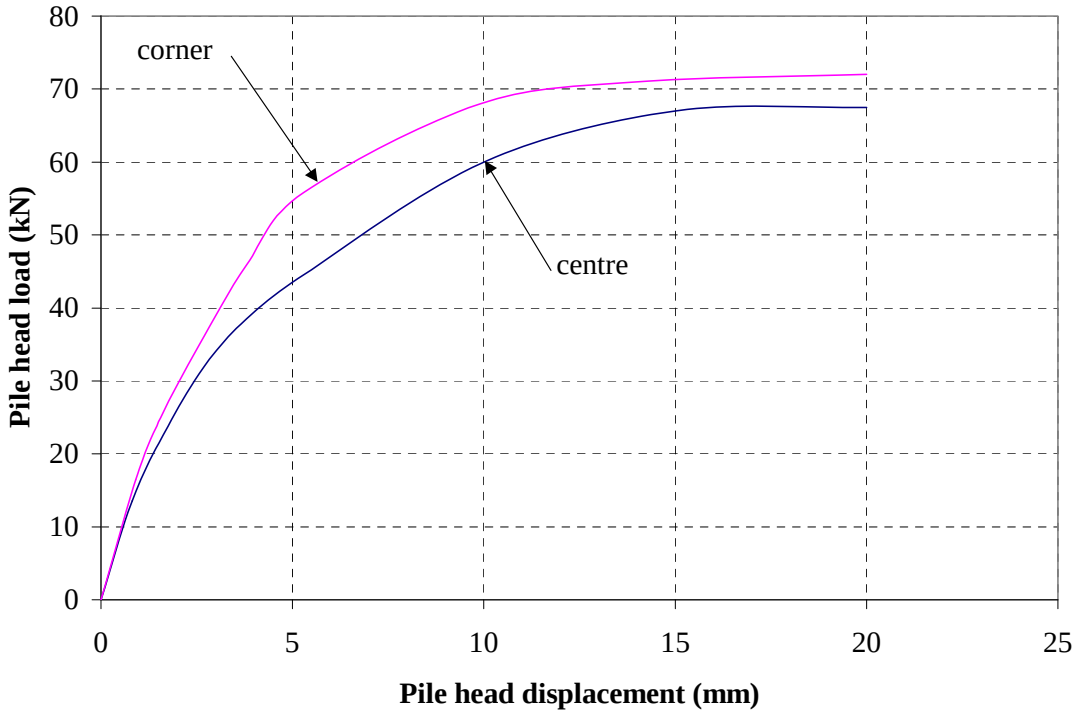

Figure 6-11 Load-displacement plot for TG1/scs

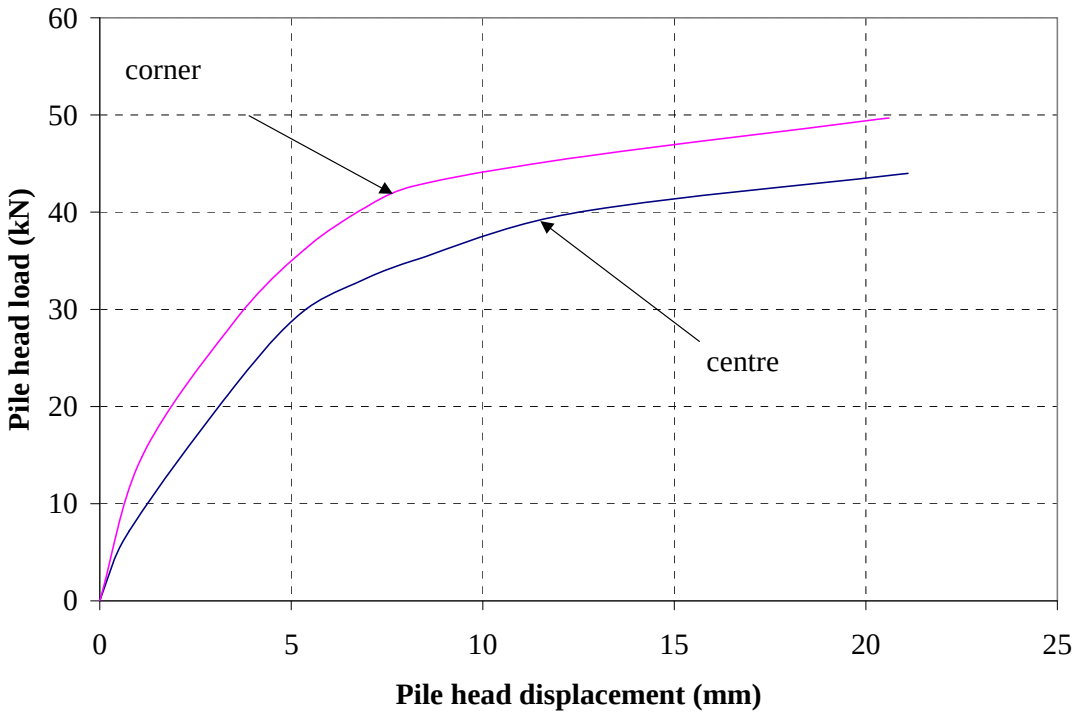

Figure 6-12 Load-displacement plot for TG2/cs

6.5 Mechanisms of Cyclic Failure

The term cyclic 'failure' is not globally defined; however, in a specific set of test circumstances, 'failure' will be induced within a small number of cycles when the maximum applied cyclic load is a high proportion of the expected static capacity (at the same rate). Lower load levels may also induce failure if sufficient cycles are provided. The current test programme suggests that the onset of cyclic 'failure' is linked to sudden increases in the mean pile head displacement, with much more modest displacement amplitude increases.

Features of the single and group pile cyclic load tests include:

- Tension loading at a constant cyclic *loading* amplitude induced permanent displacements (δ) which varied in an approximately linear fashion with the number of cycles (N):

$$\delta = kN$$

The value of k increases in accordance with the level of loading applied; a typical illustration of the increase in k (slope of the graph) with increased maximum cyclic load level may be seen for TS3/c in Figure 6-13. Cyclic tests on single tension piles by McAnoy et al (1983) in Cowden till show similar behaviour.

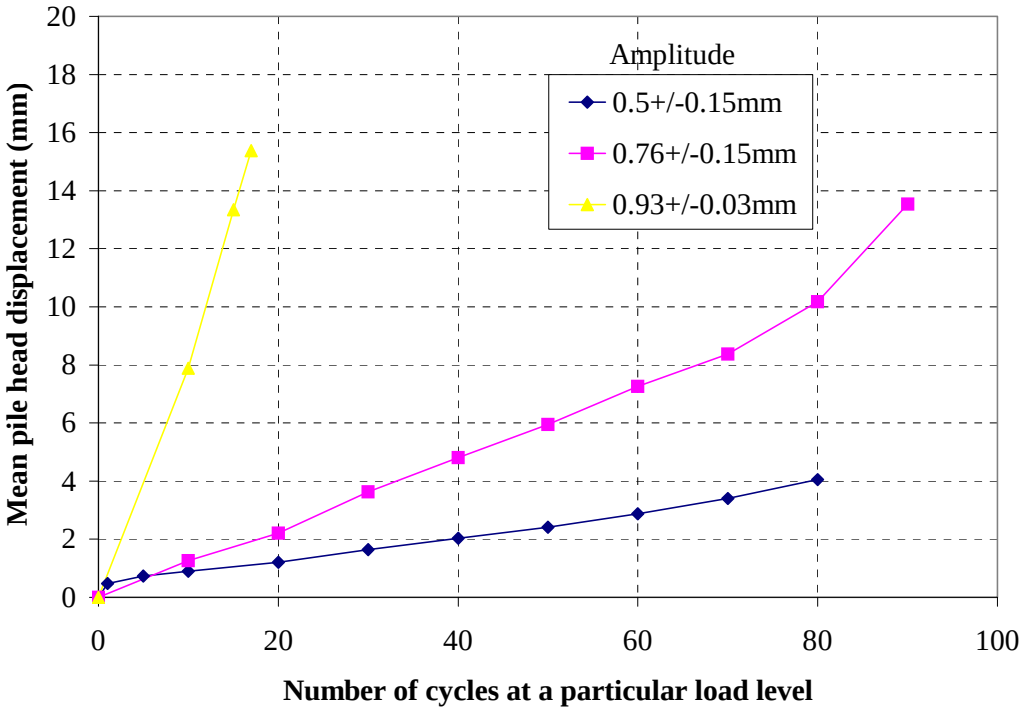

Figure 6-13 Mean pile head displacement against number of cycles for TS3/c

- Displacement amplitudes only increase marginally during cycling and are significantly lower than the mean displacements. One-way cyclic tension pile tests in Haga clay (Karlsrud and Haugen 1986) showed similar trends.
- The rate of increase in permanent pile head displacement ($\Delta\delta/\Delta N$) is low when peak cyclic loads are less than 70-80% of the dynamic[4] pile capacity, but increases dramatically as the peak cyclic load approaches this capacity. Alternatively, there appears to be a critical displacement level (also noted by Briaud and Felio, 1985) at which the mean effective stress drops rapidly causing sudden increases in mean

[4] static capacity at the same rate as the cyclic tests, defined in Section 6.6

displacement marking imminent cyclic failure. This critical displacement appears to be ≈12-15mm for single piles (Figure 6-2) and slightly greater (≈20-25mm) for pile groups (Figure 6-5).

- Δδ/ΔN is plotted as a function of the displacement amplitude for single piles and groups in Figure 6-14. Each data point represents a specific load amplitude. There is no unique relationship between the displacement amplitude imposed and the rate of accumulation of permanent displacement; the 'critical' amplitudes for the centre and corner piles of TG1/sc would be greater than shown by the single datapoints plotted, as 'failure' was not reached. Nevertheless, it is clear that the 'critical' amplitudes of group piles exceed those of single piles.

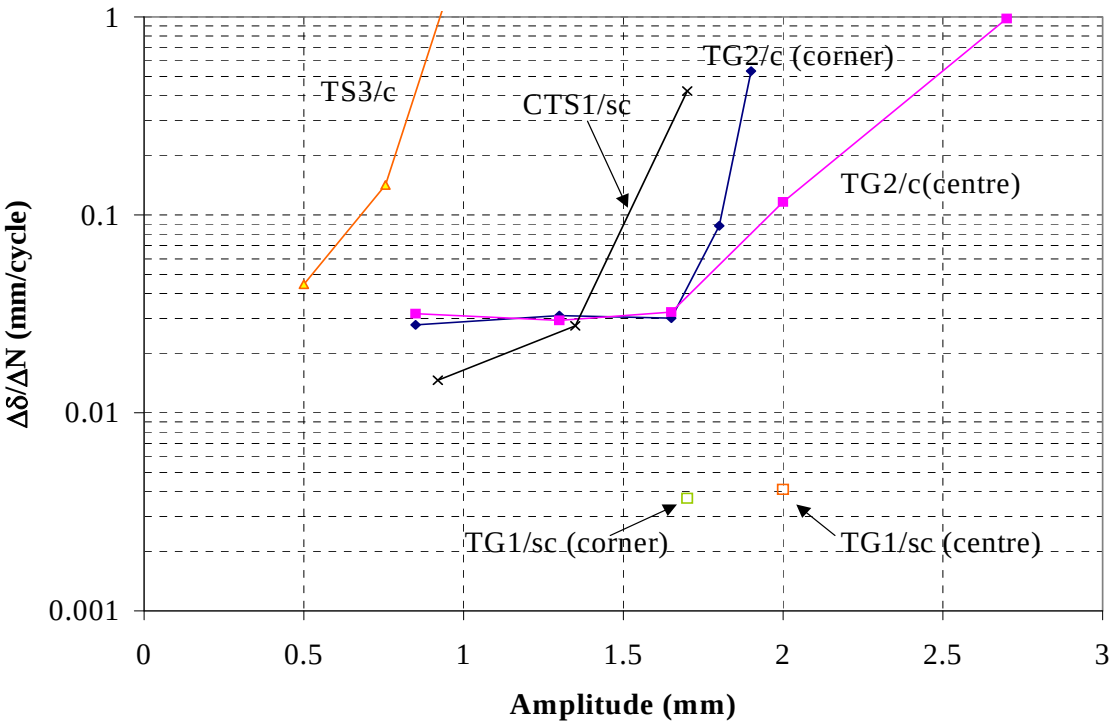

Figure 6-14 Variation of Δδ/ΔN with amplitude (all cyclic tests)

6.6 Effect of cyclic loading on pile shaft capacity

A key parameter for interpreting the cyclic test data is defined as $Q_{s\ bef}$; this is the anticipated static tension shaft capacity[5] based upon an 'imaginary' test conducted just before a particular cyclic test was carried out. This provides a suitable normalizing parameter by which the effects of cycling may be gauged. $Q_{s\ bef}$ could not be determined by direct testing without severely affecting subsequent cyclic tests, so the static test data ($Q_{s\ ref}$ values) of Chapter 5 with the time-related effects[6] quantified in Section 5.9 provide a basis for projecting $Q_{s\ bef}$. Other important definitions include:

- $Q_{s\ ref}$: An appropriate reference tension shaft capacity
- Q_{pcy}: The peak[7] axial load applied in the cyclic test (which was performed with a load period of 60 seconds).
- $Q_{d\ bef}$: The anticipated tension shaft capacity immediately before the cyclic test at the displacement rate employed in the cyclic test. This (dynamic capacity) is inferred from $Q_{s\ bef}$ with a strain rate correction applied (Section 5.9.1).
- $Q_{s\ aft}$: The measured static shaft capacity (usual definition) carried out *after* the cyclic test (reflecting cyclic degradation, if any)
- $Q_{d\ aft}$: The anticipated shaft capacity after the cyclic test at the displacement rate employed in the cyclic tests. This is inferred from $Q_{s\ aft}$ with a strain rate correction applied.

Corrections for pile weight and pore pressure acting at the pile base are also included (see Section 5.8.3). The above terms are applicable to both isolated piles and group piles. Useful comparisons include $Q_{pcy}/Q_{d,\ bef}$ which indicates the severity of cycling imposed and $Q_{s,\ aft}/Q_{s,\ bef}$ (= $Q_{d,\ aft}/Q_{d,\ bef}$) which shows whether prior cycling has any bearing upon static capacity. These comparisons are made for two single piles (C(T)S1 and TS3) and three *complete* pile groups (TG1, TG2 and CG1) in Table 6-4.

[5] Creep rate of 0.004mm/min and capacity defined by 25mm displacement.
[6] Aged or drained reloading of 27%, undisturbed aging considered insignificant.
[7] There is no *unique* cyclic capacity, as its value depends upon the loading history and number of cycles applied, so the term is not used in this discussion.

Pile(s)	**C(T)S1**	**TS3**	**TG1**	**TG2**	**C(T)G1**
Cyclic test (Virgin/ reloaded)	Reloaded	Virgin	Reloaded	Virgin	Reloaded
$Q_{s\ ref}$ (kN) (Test used)	59.2 (CS1/s)	66.9 (TS1/s)	267 (TG1/s)	267 (TG1/s)	278 (CG1/s)
$Q_{s\ bef}$ (kN)	75.2	66.9	339	267	353
$Q_{d\ bef}$ (kN)	101.1	87.8	459	363	480
Q_{pcy} (kN)	75.1	66.1	*237*[8]	232	237
$Q_{s\ aft}$ (kN)	64.7	57.5	336	219	
$Q_{d\ aft}$ (kN)	87.0	75.5	456	298	
$Q_{pcy}/Q_{d\ bef}$	**0.74**	**0.75**	0.52	**0.64**	**0.62**[9]
$Q_{s\ aft}/Q_{s\ bef}$ ($=Q_{d\ aft}/Q_{d\ bef}$)	**0.86**	**0.86**	**0.99**	**0.82**	

Table 6-4 Shaft capacity measurements and predictions (12%/log cycle rate effect)

6.6.1 General Trends

Trends evident from Table 6-4 for single piles and complete groups may be summarised as follows:

- Values of $Q_{pcy}/Q_{d\ bef} \approx 0.75$ appear typical for single piles, suggesting that cyclic loading degrades shaft capacity by ≈25%. Complete pile groups experience further degradation, with $Q_{pcy}/Q_{d\ bef} \approx 0.63$ measured. The full-scale tests suggest that group action is slightly more pronounced than indicated by two-way cyclic group tests in kaolin conducted by Hewitt (1988, see Figure 6-15).
- The level of tension cycling in TG1/sc was relatively light in relation to the other tests ($Q_{pcy}/Q_{d\ bef} = 0.52$) and resulting cyclic degradation was low. Therefore, well-designed piles (with a factor of safety on ultimate failure of greater than two) are unlikely to experience a reduction in their available capacity; this is confirmed by the results of the ensuing static test for which $Q_{s\ aft}/Q_{s\ bef} \approx 1$.
- Values of $Q_{s\ aft}/Q_{s\ bef}$ for piles brought to cyclic 'failure' are typically about 0.86 for the single piles and only marginally less for group TG2. Therefore, tension cycling

[8] 'Failure' did not occur in this cyclic test
[9] Taking into account that there were only four 'active' piles, ratio multiplied by 5/4

to ultimate conditions, at between 60 and 75% of the piles' dynamic capacity results in a reduction of ≈15% in the static capacity after cycling.

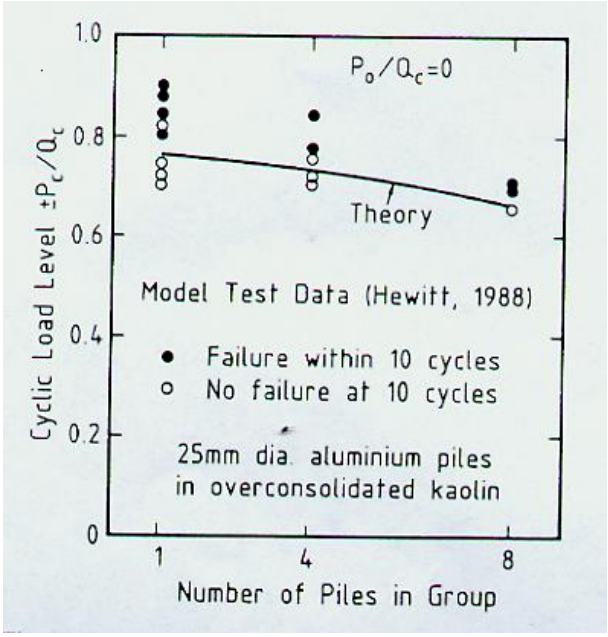

Figure 6-15 Cyclic tests on model pile groups in kaolin (Hewitt 1988)

- Immediate (undrained) reloading has been shown in Table 5-6 to cause an reduction in pile capacity of typically 10-15%. The fact that the $Q_{d\ aft}$ values exceed Q_{pcy} values (by amounts between 8-26%) is probably due in part to the 'overnight' setup of pore pressures between the cyclic and ensuing static tests. Therefore this 'reloading' may not fall into either undrained or drained reloading categories but represents a partially drained situation.

6.6.2 Centre Pile of Group

The extent of shear stress degradation on the centre pile of a group due to cyclic loading is more difficult to determine. The behaviour of the pile cap in the reference test may not correspond with its behaviour in the cyclic test, in which case $Q_{s\ ref}$ and Q_{pcy} are not directly comparable. The two cases TG1/sc and TG2/c are considered separately (and the relevant computations are outlined in Table 6-5:

CENTRE Pile(s)	**TG1[3]/sc**	**TG2[3]/c**
Cyclic test (Virgin/ reloaded)	Reloaded	Virgin
$Q_{s\ ref}$ (kN)	51.5	51.5
$Q_{s\ bef}$ (kN)	65.4	51.5
$Q_{d\ bef}$ (kN)	84.2	65.4
Q_{pcy} (kN)	38.1	42.1
$Q_{s\ aft}$ (kN)	63.1	38.3
$Q_{pcy}/Q_{d\ bef}$	0.45	0.64
$Q_{s\ aft}/Q_{s\ bef}$ ($=Q_{d\ aft}/Q_{d\ bef}$)	0.96	0.74

Table 6-5 Shaft capacity measurements and predictions (centre piles)

Comparison of Tables 6-4 and 6-5 shows that a centre group pile is more severely affected by cycling than a single pile. The reason for the differences in $Q_{pcy}/Q_{d\ bef}$ between the two tests (TG1[3]/sc and TG2[3]/c) lies in differences in pile cap behaviour between the cyclic test and its reference. For instance, Q_{pcy} for the centre pile of TG1/sc is ≈10kN below that of an average corner pile, although in the reference static test TG1/c, $Q_{s\ ref}$ for the centre pile and average corner pile are virtually the same. Q_{pcy} for the centre pile of TG2/c is virtually the same as for an average corner pile, so this gives a more honest reflection of centre pile behaviour. A maximum value of $Q_{pcy}/Q_{d\ bef}$ ≈0.66 is in keeping with the corresponding figure for the complete group.

An 'interaction diagram' is presented in Figure 6-16 which plots $Q_{s\ aft}/Q_{s\ bef}$ (a measure of the degradation of static capacity due to cycling) against $Q_{pcy}/Q_{d\ bef}$ (a measure of the severity of cycling imposed), showing data from single piles, complete groups and centre piles. Trendlines are deduced by inspection. Significant degradation of shaft capacity (arbitrarily chosen as 10%) occurs at $Q_{pcy}/Q_{d\ bef}$ ≈0.7 for an isolated pile and ≈0.45 for the centre group pile. Centre group piles clearly undergo further shaft capacity degradation than that experienced globally by the pile group. Since the short-term reduction in capacity following static pile failure has been estimated as 10-15%, failure under cyclic loading leads to a slightly weaker soil consistency adjacent to group piles than that induced by monotonic group failure (or by cyclic/static single pile failure).

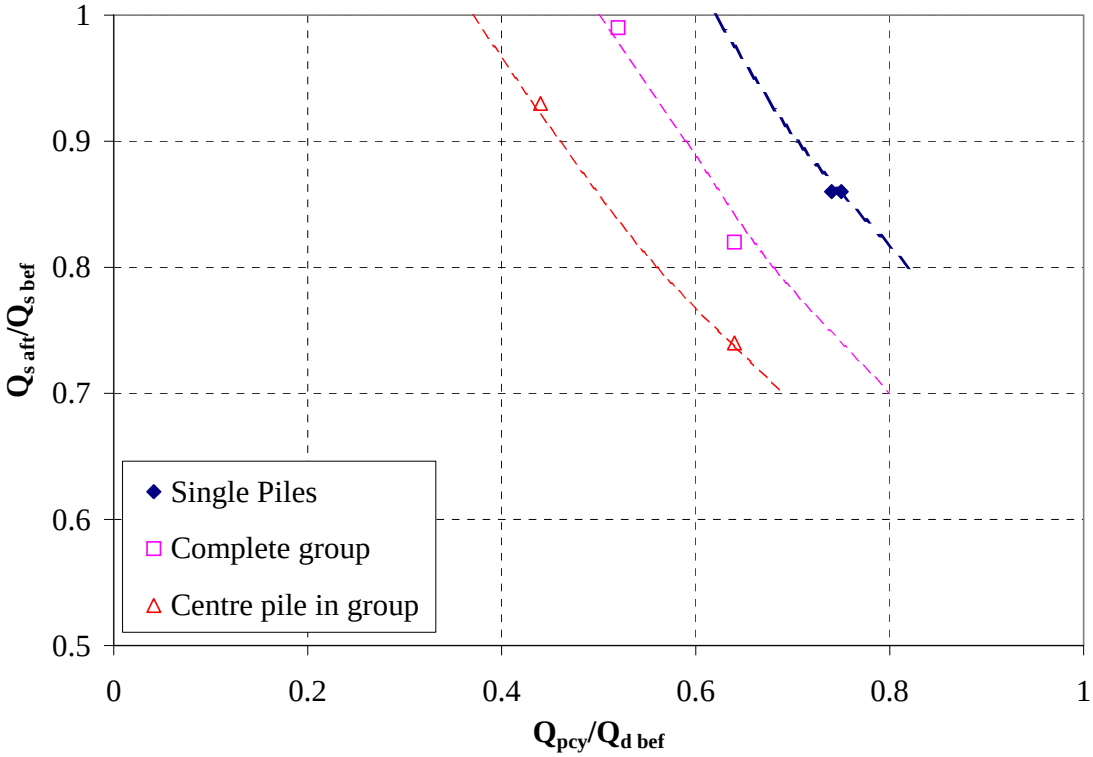

Figure 6-16 Plot of $Q_{pcy}/Q_{d\ bef}$ against $Q_{s\ aft}/Q_{s\ bef}$ for cyclic tests

An alternative interaction diagram is presented in Figure 6-17 which plots the cyclic load amplitude Q_c as a function of the average cyclic load Q_{ave} (both normalised by $Q_{d\ bef}$). The extent of cyclic degradation is indicated by how close the test path ventures to the $Q_{max}=Q_{d\ bef}$ line (i.e. no degradation if line is reached). It is also clear here that group centre piles experience further degradation that the single piles.

6.7 Modelling cyclic pile response using RATZ

The ability of RATZ[10] to model single pile behaviour under cyclic loading is considered. The steps involved in developing the RATZ model appropriate to the Belfast tests may be summarised as follows:

- Selection of suitable RATZ parameters which enable it to predict the static response of a single pile. The RATZ parameters used are given by Kieran (2001) and the level of

success at predicting the pile head load displacement response and measured t-z curves (see Chapter 8) at 3.25m and 5.25m are presented in Figures 6-18 and 6-19 respectively. The hyperbolic model was used (ζ=2).

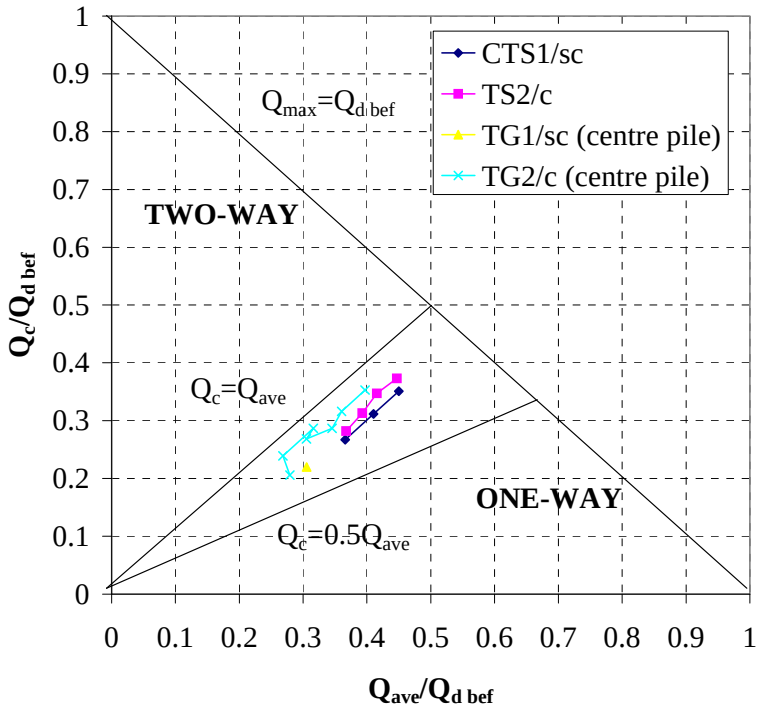

Figure 6-17 Standard interaction diagram for single and centre group piles

- The same soil/pile model (with some additional cyclic parameters supplied) was used to predict the pile behaviour when cyclic loads were imposed.

Initial investigation by Kieran (2001) suggests:

(i) The predicted variation of accumulated mean pile head displacement with number of cycles is particularly sensitive to the non-linearity of the soil model (i.e. the value of ζ)

(ii) Linear models (ζ=0) predict significantly less accumulated displacement than non-linear parabolic ones (ζ=1).

[10] Load transfer analysis for axially loaded piles; some details provided in Chapter 2.

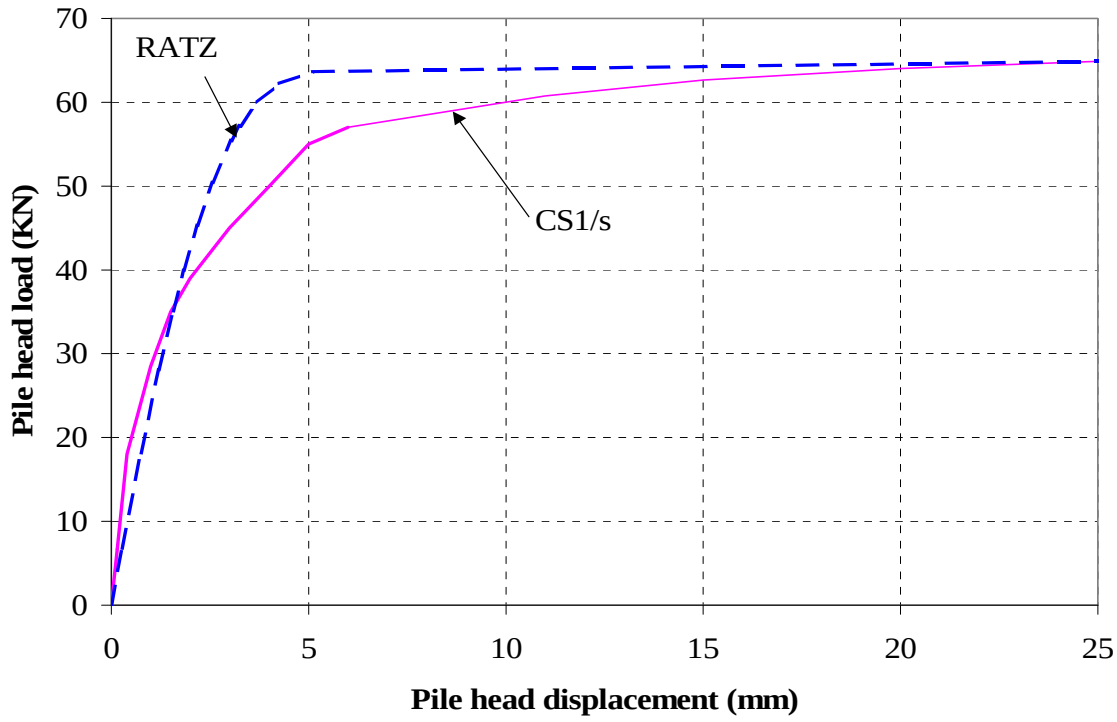

Figure 6-18 Measured and RATZ single pile load displacement plots

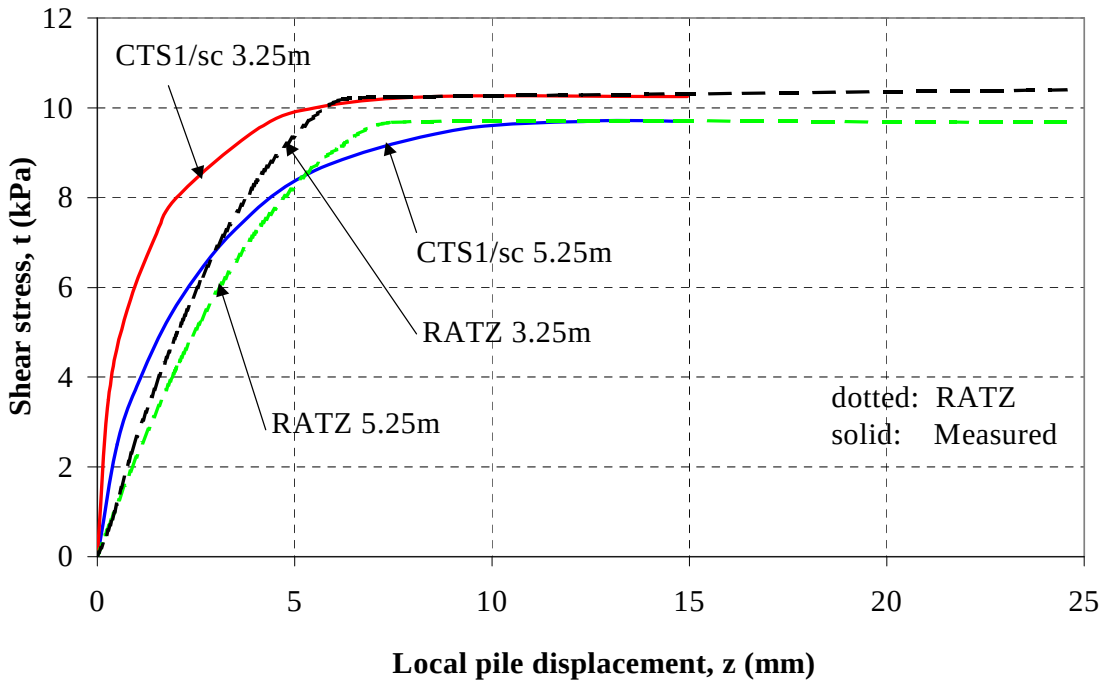

Figure 6-19 Measured and RATZ t-z curves at 3.25m and 5.25m

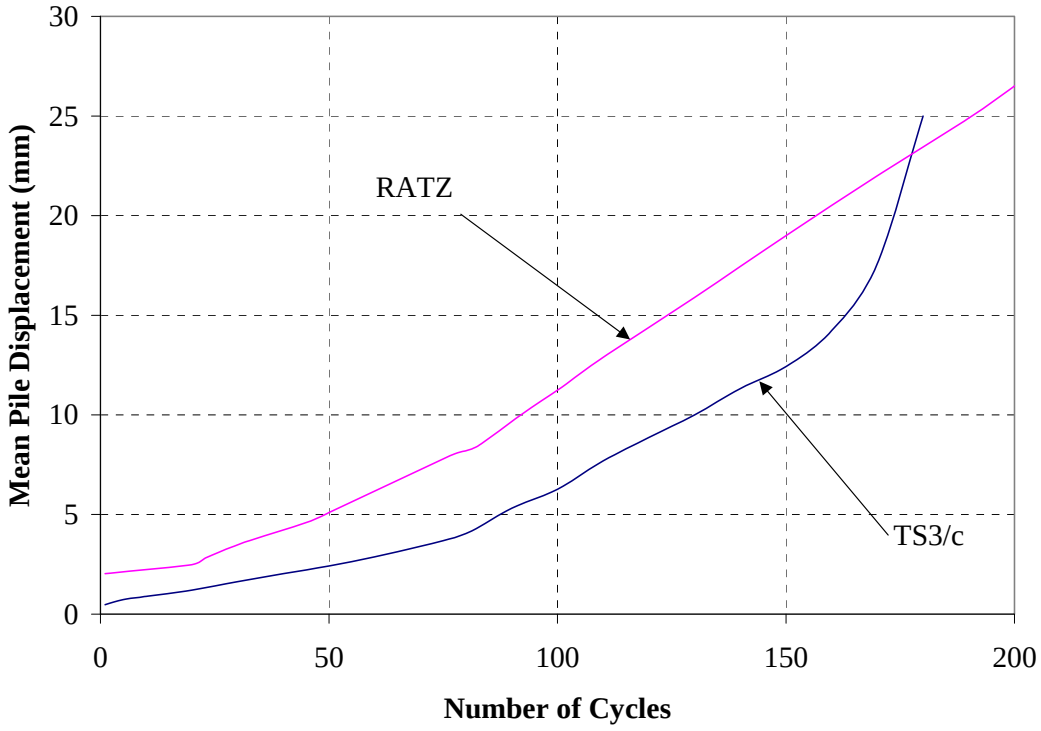

Figure 6-20 Variation of mean pile head displacement with number of cycles (RATZ and TS3/c)

(iii) Kieran (2001) suggests that the best match between RATZ predictions and field measurements is found by setting $\zeta = 0.7$. However in reality, the measured static t-z curves for the single pile are more non-linear than either the hyperbolic or parabolic models offered by RATZ, and so the use of $\zeta = 0.7$ is hardly representative of material behaviour.

(iv) RATZ overpredicts the gain in mean pile head displacement with number of cycles recorded in virgin test TS3/c (Figure 6-20), although it also responds to increases in peak cyclic load level. There is no evidence from the predictions of the critical strain/displacement threshold indicated by the single pile at 12mm mean pile head displacement.

Chapter 7

Numerical Model of Pile Group Behaviour

7.1 Introduction

Two numerical models are developed for use in Chapter 8 as a means to supplement and develop the pile group field measurements. These models are:

(i) An axisymmetric finite element analysis of the Belfast pile group configuration, using the OASYS SAFE program. This is used in conjunction with a soil model called BRICK which allows the essential features of the soil behaviour to be captured, particularly its stiffness non-linearity. The development of a Belfast-specific model is described in Sections 7-2 to 7-7. The theory of the SAFE and BRICK programs is summarized in Appendix 7-1.

(ii) A simple numerical model of a single pile, easily implementable in a spreadsheet format (Section 7-8). The soil displacement profile surrounding the loaded pile is obtained by integrating the soil strains over the radius of influence of the pile; these strains are calculated from the hyperbolic expression for soil stiffness proposed by Lee and Salgado (1999). Theoretical load transfer relationships for the pile developed in this way may be compared to measured t-z curves for CS1/s.

A feature of both of these models (more prevalent for the group analysis in (i) above) is that installation effects cannot be modelled, so the piles are effectively 'wished-in-place'. While neglecting the installation effect caused by the group piles is hardly desirable in practice, 'wished-in-place' analyses offer a useful analytical tool for this research since they provide a baseline by which the measured installation effects may be assessed. The stages of development and validation of each of these models is now described in detail.

7.2 SAFE mesh and load application

An axisymmetric analysis was devised in which the axis of the centre pile of the group[1] coincides with the axis of symmetry of the mesh. However, the nature of an axisymmetric analysis prevents discrete locations from being assigned to the corner piles. The net effect of loading four corner piles must be approximated by loading a circular annulus with centreline radius equivalent to the spacing between centre and corner piles (≈750mm). The magnitude of loading is described later.

[1] Effectively a single pile when no loading is applied to the corner piles.

The OASYS SAFE mesh adopted is shown in Figure 7-1. All elements have length to width ratios not exceeding 7. The far boundary was chosen sufficiently distant from the axis not to influence the results[2] and was restrained horizontally only. The lower boundary at the interface between sleech and sand (8.4m) was completely fixed, and the axis of symmetry was also confined horizontally.

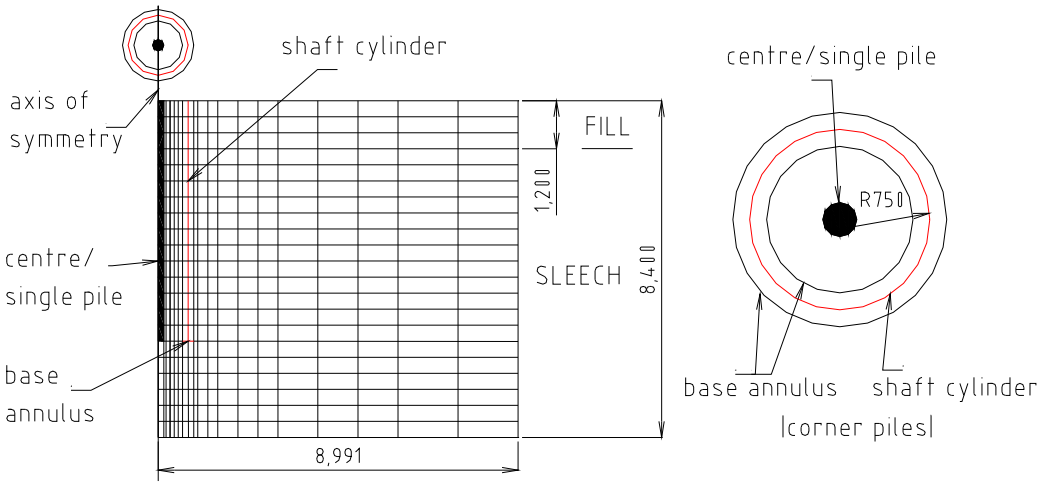

Figure 7-1 OASYS SAFE mesh for pile group analysis

Linear elastic reinforced concrete properties[3] were assigned to a row of elements along the axis of symmetry to represent the centre/single pile. The corner piles were not physically represented as concrete, although shear and base stresses could be applied *to the soil mass* in the manner described below:

- Shear stresses are applied to one side of an infinitely thin cylinder of soil (of radius s = 750mm, centred about the axis of symmetry. This cylinder has a height of 6m equivalent to the pile length. Since this cylindrical surface area exceeds that of the four rectangular pile shafts combined, applied shear stresses are scaled down by the correct Shaft Area Ratio[4] to generate the same load applied to the four discrete

[2] At which point, the absence or inclusion of vertical restraint made little or no difference.
[3] E=34kN/mm^2, υ=0.2
[4] Shaft Area Ratio = Surface area of cylinder/Sum of the shaft areas of all four corner piles

corner pile shafts. This loading is imposed via 'line elements' on the 2-D SAFE user-interface.

- Base stresses are assumed to act on a circular annulus with internal radius equal to (s - r) and external radius equal to (s + r). These must also be scaled down by the Base Area Ratio[5] in order to represent the same loading state as that applied to the four discrete corner pile bases.

The displacements computed around the 'imaginary' corner pile locations are unlikely to be representative of the discrete corner piles having modelled all four of them as one continuous unit. However, the overall (interactive) contribution of these displacements at the centre pile location is expected to be realistic. One objective of the linear elastic analyses described in Section 7.3 is to justify this assumption.

7.3 Validation of SAFE pile group analysis in Linear Elastic soil

Single pile and pile group analyses were carried out in linear elastic soil conditions with two main purposes:

(i) To ensure that the far boundary was sufficiently distant from the piles so that moving it further away would have negligible effect upon the calculated stresses and settlements within the soil mass

(ii) To assess the validity of representing the loads on the discrete corner piles as shear stresses on an equivalent cylindrical surface and base stresses on an equivalent annulus. In particular, it is important that the interactive displacements experienced at the centre pile due to corner pile loading were realistic.

The mechanisms used to conduct these checks are as follows:

(i) *Single pile LE analysis*: Comparison is made first of all with the analytical solution of Randolph and Wroth (1978)[6] shown in Section 2.3.1 which assumes that the pile is embedded in an infinite layer. Secondly, this is amended with a correction which accounts for the presence of a rigid layer at some depth (as used in GASGROUP, Guo and Randolph 1999) is applied to the solution of Randolph and Wroth (1978).

[5] Base Area Ratio = Area of base annulus/Sum of the base areas of all four corner piles

(ii) *Pile Group LE analysis*: The SAFE/LE results are compared with PIGLET predictions of a 5-pile group of the configuration used in Belfast. Although the pile cap is not physically modelled in the SAFE model, the extremes of rigidity and flexibility associated with pile cap behaviour are modelled by imposing conditions of uniform settlement and uniform loading respectively. PIGLET allows for both of these cases to be analysed.

For both FE and PIGLET analyses, the soil was assumed to have an equivalent linear elastic shear modulus (G_{sec}) of 3000kPa[7] (constant with depth) and a Poisson's ratio of 0.2.

7.3.1 Single Pile LE analysis:

Pressure loads were applied to the nodes at the head of the single pile. The single pile load-displacement responses predicted by the SAFE/LE model are compared with closed form solutions in Figure 7-2. Very good agreement may be observed between the SAFE/LE response and the closed form solution accounting for the rigid layer at 8.4m depth.

7.3.2 Pile Group LE Analysis

Pressure loads were applied to line elements at the head of the centre pile (as was the case for the single pile). However, application of load to the corner piles was achieved through the specification of separate shear stresses tangential to line elements and base stresses perpendicular to line elements. Thus an approximate load split between shaft and base was required. An expression following from the work of Randolph and Wroth (1978) serves this purpose for linear elastic conditions, where P_t is the total load, P_b is the base load:

$$\frac{P_b}{P_t} = \frac{\dfrac{4\eta}{(1-\upsilon)\xi}\dfrac{1}{\cosh \mu l}}{\dfrac{4\eta}{(1-\upsilon)\xi} + \rho\dfrac{2\pi}{\zeta}\dfrac{\tanh \mu l}{\mu l}\dfrac{l}{r_o}}$$

[6] Or alternatively, PIGLET used for a single pile.

[7] Based upon backfigured G_{sec} values from the single pile test CS1/s at ≈40% of single pile "capacity".

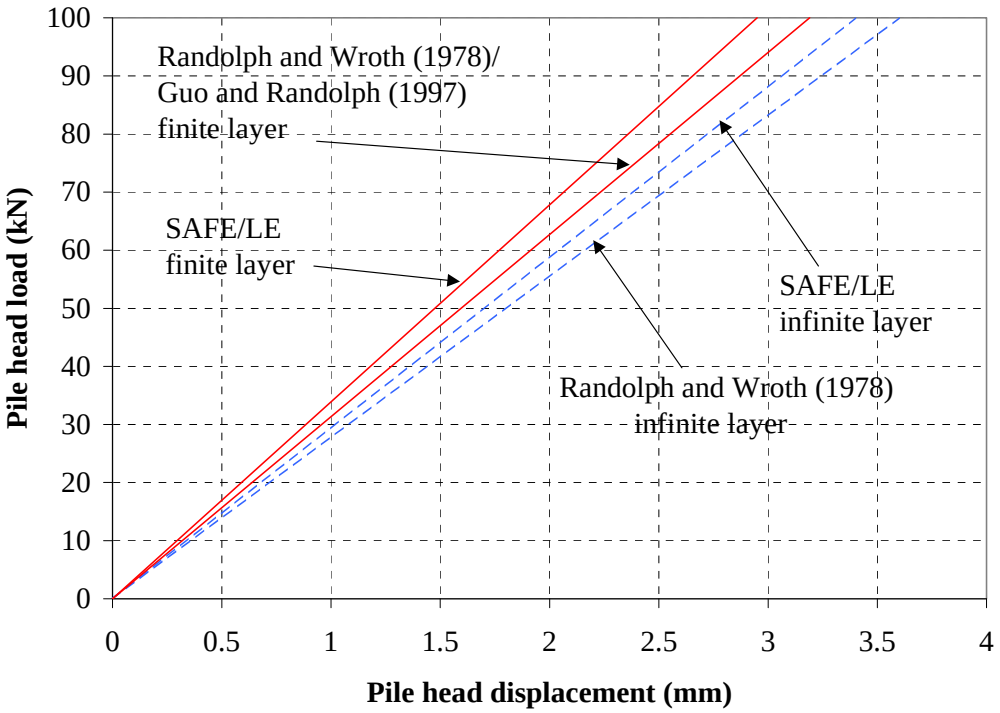

Figure 7-2 Validation of SAFE/LE analysis for single piles

It should be noted that the interactive settlements at the shaft of the centre pile are relatively insensitive to changes in P_b of $\pm$5%.

The approaches used to assess compatibility between SAFE/LE and PIGLET differ slightly for rigid and flexible pile caps. These are detailed below:

Rigid pile cap

(i) A 10mm displacement was imposed to the rigid cap in a PIGLET analysis and the corresponding distribution of load among centre and corner piles was recorded.

(ii) This same centre pile load was reapplied directly (to the line elements) at the head of the centre pile of the SAFE/LE model.

(iii) The PIGLET corner pile loads were split into appropriate shaft and base components, and the corresponding shear and base stresses were scaled down as already described before being applied to the SAFE/LE model.

(iv) The resulting centre pile displacement[8] in the SAFE/LE model and the original 10mm displacement applied in the PIGLET run are then compared. It is noted that the pile is virtually incompressible, so that all points from pile head to tip displace equally.

Flexible pile cap

Equal loading was applied to centre and corner piles in both SAFE/LE and PIGLET analyses and the resulting centre pile settlements were compared. PIGLET does not provide for the presence of a rigid layer, so compatibility between PIGLET and SAFE/LE could not be expected to be any better than that found through the single pile comparison. However, the agreement between the two models' predictions for the centre group pile is almost as good as for the single pile (Figure 7-3).

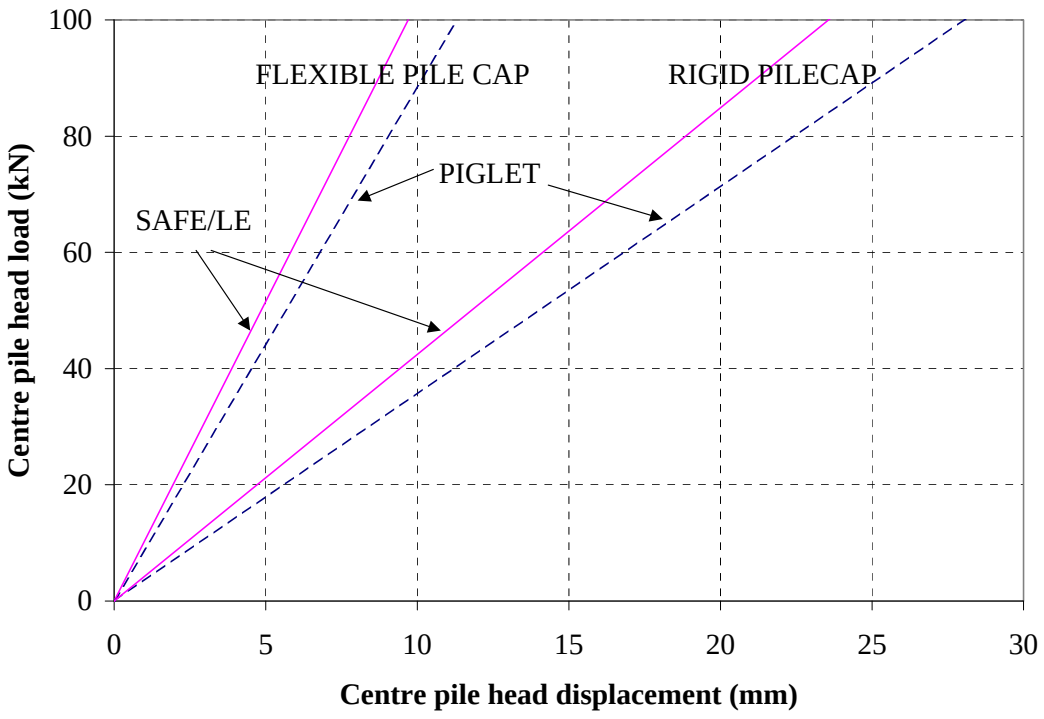

Figure 7-3 Validation of SAFE/LE analysis for centre pile of group

[8] The corner piles would be expected to settle by the same amount, but they are not expected to be reliable in the SAFE/LE analysis.

The outcome of the SAFE/LE analysis confirms that 9m is a sufficient distance to locate the mesh boundary and that furthermore, the use of a circular annulus to model the corner piles predicts relatively accurately the interactive displacements that they impose on the centre pile when they are loaded.

7.4 Development of a non-linear soil model using BRICK

A soil model is developed to capture the essential features of the behaviour of Belfast sleech, with particular emphasis on its pronounced stiffness non-linearity. OASYS BRICK (Simpson 1992, 1996), which is both a stand-alone program and an optional component of SAFE, was used for this purpose.

In advance of using BRICK in conjunction with SAFE (subsequently referred to as SAFE/BRICK), the BRICK parameters were validated alone for triaxial (CK_oUC, CK_oUE) conditions[9]. Relatively accurate predictions of stress path shape, undrained shear strength and stiffness (in terms of G_{sec}/p') were sought under each shearing condition.

7.4.1. BRICK input parameters

The BRICK input parameters are largely based upon the site investigation data of Chapter 3 and fall into three main categories:

(i) The stress/strain history to which the soil has previously been subjected
(ii) Variation of tangent shear stiffness (G_t) with shear strain (γ), subsequently referred to as the *string* data.
(iii) Indices derived from 1-D compression and triaxial tests.

Stress/strain history of the soil

The following chronological stress history is typical of that to which the sleech has been subjected:

[9] Examination of the soil response alone, irrespective of the piling.

(i) Natural consolidation (K_o=0.5) and swelling (K_o=0.6) to the current in-situ lightly overconsolidated state. An (isotropic) overconsolidation ratio of 1.2 was used as a representative average over the depth of the sleech layer.

(ii) Soil sampling causes the deviator stress to drop to zero and the mean effective stress p' to reduce from p_o' to values[10] in the range 5-10 kPa.

(iii) Reconsolidation and swelling to artificially restore the deviator and mean effective stresses to values close to those in (i) before the soil was sampled.

These 'pre-shearing' stress paths in q-p' space are shown in Figure 7-4. It should be noted that the subsequent behaviour of the soil when sheared was found not to be affected significantly by the modelling of sampling disturbance (i.e. (i) + (ii)). Undrained shearing is effected in BRICK by setting the volumetrical strain to zero and imposing an upper limit upon the shear strain.

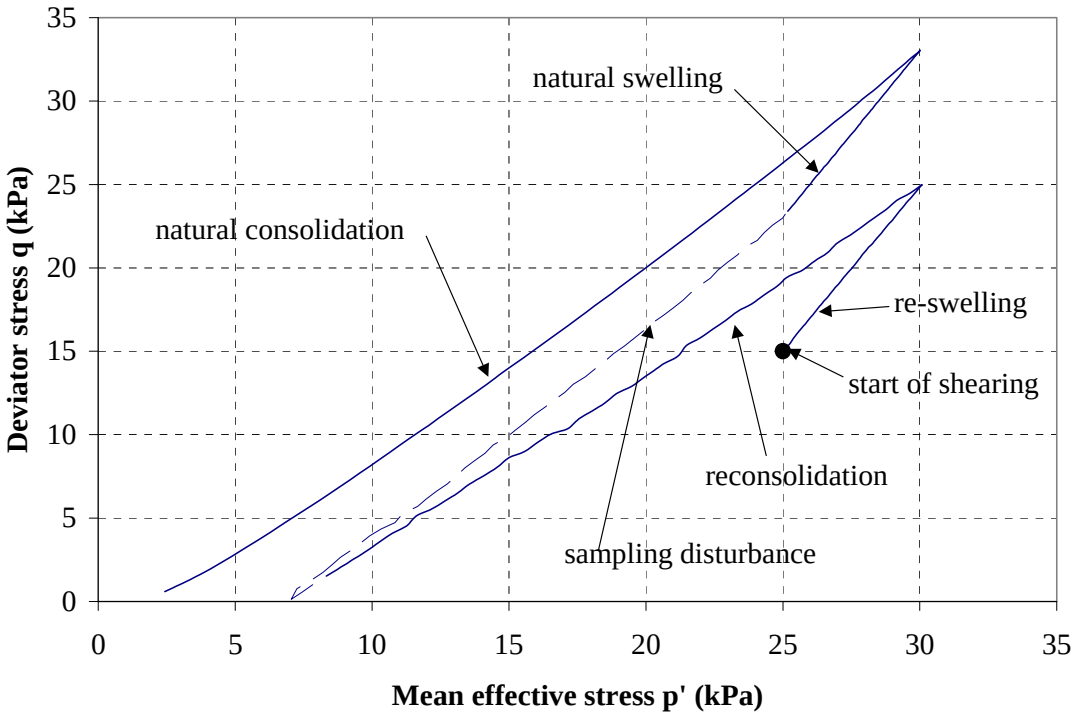

Figure 7-4 Reconstructed stress history of the sleech in q-p' space

String data

Simpson (1992) shows that the tangent stiffness response (G_{tan}) of a soil depends upon how much the direction of the current stress path has rotated in relation to the direction of the previous stress path. This angle is referred to as ϑ and a complete reversal in stress path direction ($\vartheta=180^o$) gives rise to the maximum possible stiffness the soil can exhibit. Lehane and Simpson (2000) illustrate this effect for Dublin Boulder Clay (see Figure 7-5). It is this maximum G_{tan} variation with γ that is required as input to the BRICK model and the area underneath this S-shaped curve governs the value of ϕ' (Simpson 1992).

While the stiffness corresponding to a complete stress reversal ($\vartheta=180^o$) has not been measured directly for the Belfast sleech, data from triaxial tests (for which $\vartheta=120^o$-150^o) provide a useful starting point. This input G_{tan}-γ data (string data) may be manipulated so that the model satisfactorily predicts the [G_{sec}/p']–γ trends measured in the triaxial tests.

The following steps were involved in this process:

(i) Basing a G_{tan}-γ S-shaped curved on small strain measurements (Section 3.9)

(ii) Representing the data in (i) in a stepped format (the string data)

(iii) Modification of these steps in order to predict the salient features of triaxial compression and extension behaviour, namely a reasonably good estimate of undrained strength and the variation of G_{sec}/p' with γ.

G_{sec}–γ relationship from measured data

The first stage was to produce a reasonable estimate of the dependence of secant shear modulus (G_{sec}) on shear strain (γ). There is some uncertainty regarding the variation of G_{sec} at γ<0.01%; this portion of the curve was tailored to tie in with G_{seis} (≈10500kPa) at γ<0.001%.

G_{sec}–γ and G_{tan}–γ relationships fitted by a standard curve

Fahey (2000) proposed the following distorted hyperbolic G_{sec}-γ relationship:

[10] Initial p' values were recorded in triaxial compression tests before the "B-check"

$$\frac{G_{sec}}{G_o} = \frac{1}{1+\left(\frac{\gamma}{\gamma_{ref}}\right)^g}$$

γ_{ref} is the strain when $G_{sec} = 0.5G_o$ and g defines the degree of non-linearity of the stress decay. Changes in the mean effective stress term p' during a triaxial compression test are assumed to be small and the dependence of G_o[11] on the current p' was not modelled. The curve provides a good fit to the measured data when g=0.88 and γ_{ref} = 0.045% (Figure 7-6).

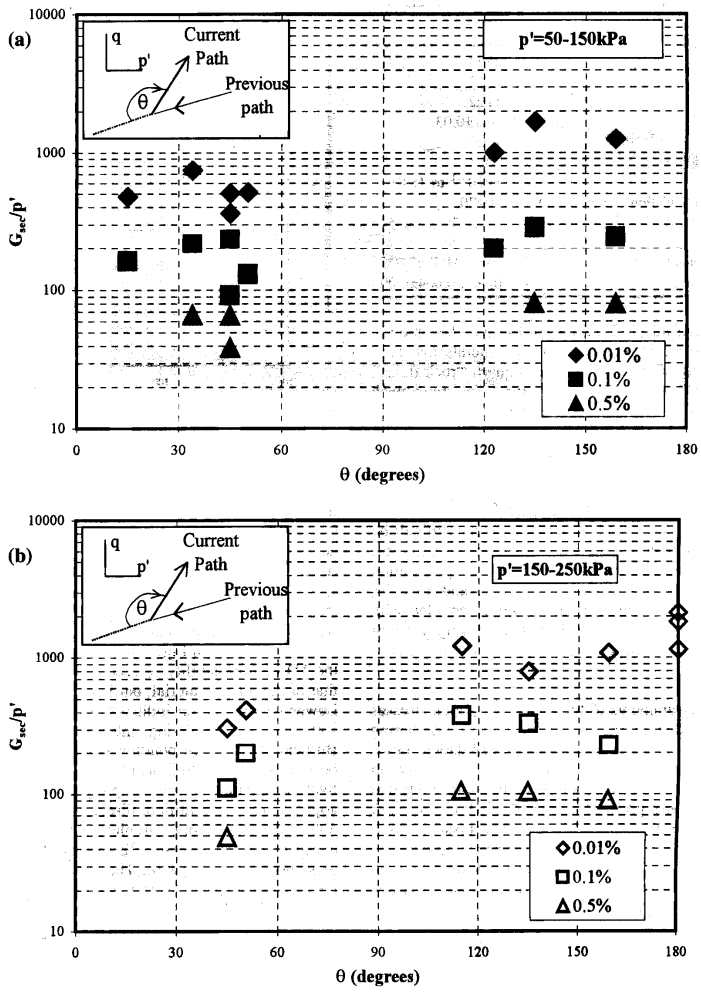

Figure 7-5 Effect of ϑ upon G_{tan} at different strain levels (Lehane and Simpson 2000)

[11] G_o is assumed to equal G_{seis}

G_{tan} may be determined most easily from the curve fit expression by differentiation, alternatively thought of the slope of the tangent to the q-γ (stress-strain) relationship. The derivative expression is given in the equation below and also plotted in Figure 7-6.

$$\frac{G_{\tan}}{G_o} = \left(\frac{G_{\sec}}{G_o}\right)^2 \left(1 + (1-g)\left(\frac{\gamma}{\gamma_{ref}}\right)^g\right)$$

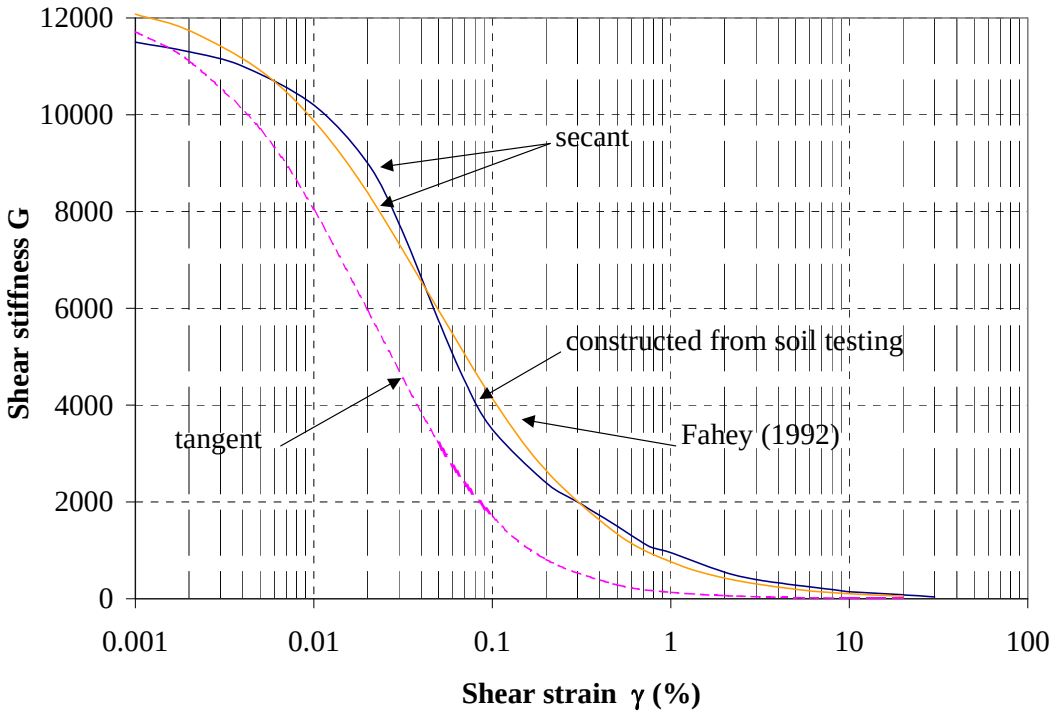

Figure 7-6 Variation of G_{sec} and G_{tan} with shear strain γ

G_{tan}-γ curve for ϑ=180°

Attempts to modify the G_{tan} curve of Figure 7-6 to correspond with ϑ=180° are aided by the work of Lehane and Simpson (2000) (see Figure 7-5). The dependence of G_{tan} on ϑ is stronger at low strains than at high strains, suggesting that 'stiffening' of the uppermost part of the S-shaped curve would be most appropriate. Some 'stiffening' of the portion of the curve corresponding to γ>0.1%, was also required to produce realistic output. The final curve is required in stepped format; these 'BRICK strings' are shown in Figure 7-7.

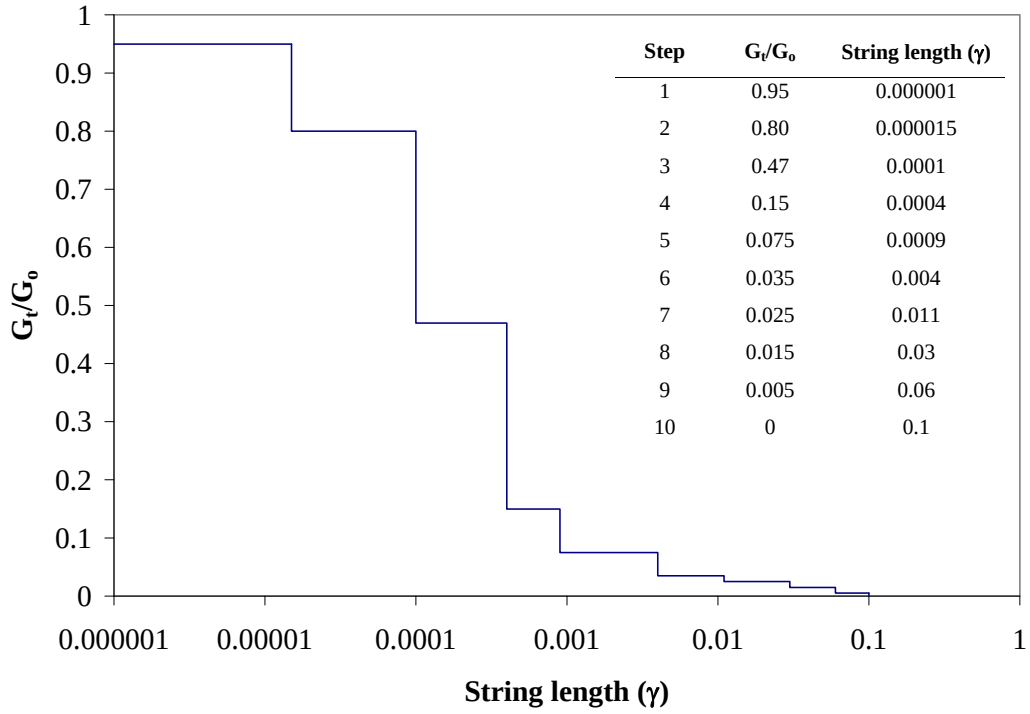

Step	G_t/G_o	String length (γ)
1	0.95	0.000001
2	0.80	0.000015
3	0.47	0.0001
4	0.15	0.0004
5	0.075	0.0009
6	0.035	0.004
7	0.025	0.011
8	0.015	0.03
9	0.005	0.06
10	0	0.1

Figure 7-7 BRICK string data

Parameter	Value	Details
ι	0.00165	ι is the small strain equivalent of λ, κ, defined as p'/K_{max}, calculated from G_o (seismic), controls ϕ'
$\kappa^* = \kappa/1+e$	0.020	κ determined from oedometer e-log σ'_v plots, e from natural moisture content
$\lambda^* = \lambda/1+e$	0.104	λ determined from oedometer e-log σ'_v plots, e from natural moisture content
υ	0.2	Poisson's ratio (assumed)
M	1.3	Drucker-Prager failure envelope definition
β_G	1	Effect of overconsolidation on soil stiffness
β_ϕ	1	Effect of overconsolidation on soil stiffness

Table 7-1 BRICK parameters

Consolidation and triaxial parameters

Many of the remaining BRICK input parameters are derived from triaxial or oedometer test data. These parameters are quantified and their selection is explained in Table 7-1. β_G and β_f were not measured, but the output was found to be relatively insensitive to their values.

7.5 Predicting Soil Response using BRICK

The ability of BRICK to predict soil behaviour under laboratory conditions concentrated upon three main areas:

(i) A reasonable prediction of the correct friction angle ϕ'

(ii) Stress path typical in shape of a lightly overconsolidated material and with a good estimate of undrained shear strength

(iii) Good estimate of G_{sec}/p' with γ for triaxial compression and extension.

The undrained shear strength predicted by BRICK of ~15kPa falls slightly below the values of ~20kPa typically recorded in the CK_oUC tests. Predicted triaxial compression and extension q-p' stress paths are presented in Figure 7-8. A comparison of the corresponding G_{sec}/p' predictions (over the range of $0.1\%<\gamma< 10\%$) with the measured stress paths of Figure 3-14 is shown in Figure 7-9. G_{sec}/p' values in compression are predicted very well but extension values are over-predicted for $\gamma<1\%$.

7.6 Stages of SAFE/BRICK analysis

The SAFE/BRICK analysis was carried out in a number of distinct stages to reproduce as closely as possible the sequence of events occurring at the site from soil deposition to loading. These stages are identified below:

(i) Deposition of the sleech (from ground level to the rigid boundary at 8.5m)

(ii) The sleech between ground level and 1.2m depth was transformed to 'filled ground'. This was modelled as an elastic Mohr Coulomb material with Young's modulus of 25000kPa and $\phi'=33^o$.

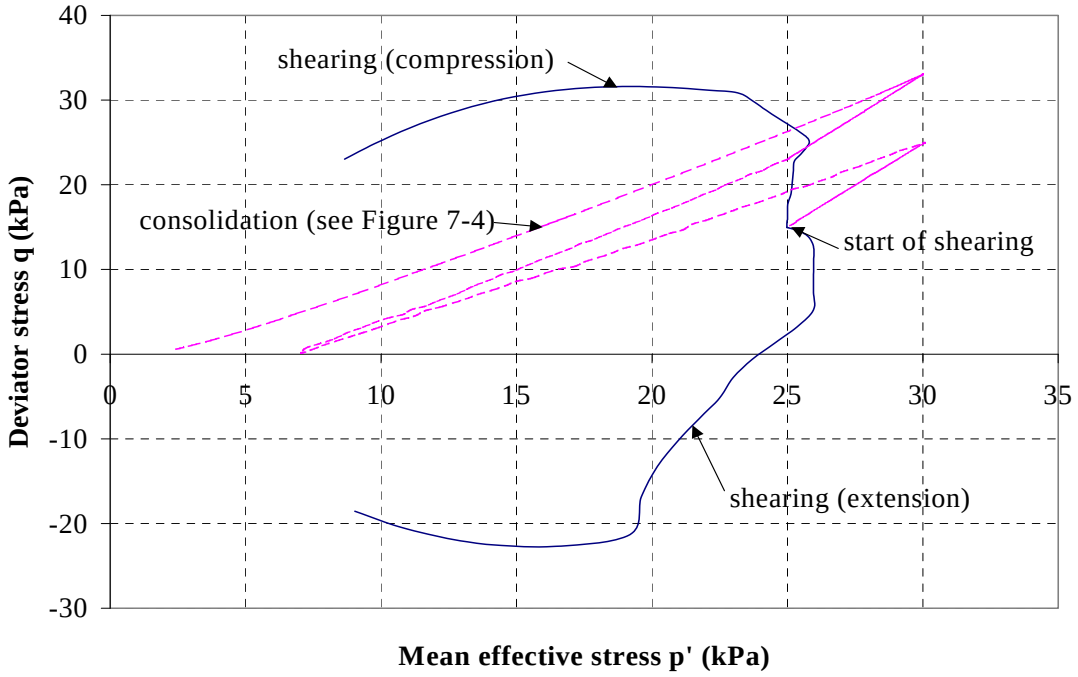

Figure 7-8 Predicted stress paths for triaxial compression and extension

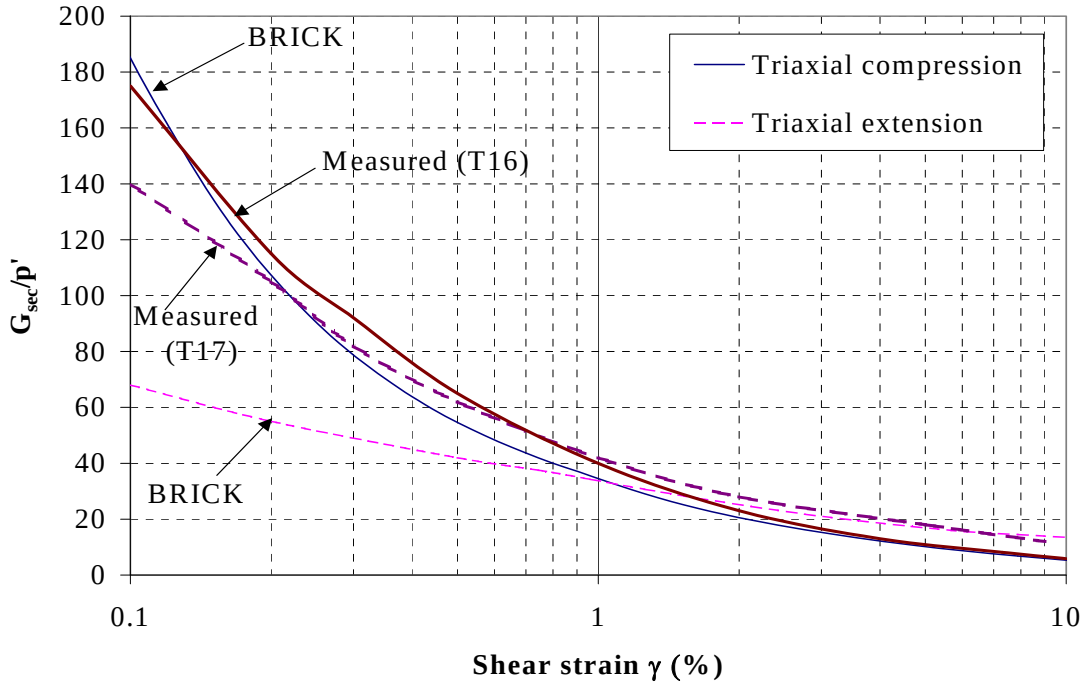

Figure 7-9 Predicted G_{sec}/p' variation for triaxial compression and extension [γ>0.1%]

(iii) Some of the 'filled ground' and sleech material adjacent to the axis of symmetry of the mesh was transformed into a linear elastic material with the properties of concrete.

(iv) The pile(s) were loaded in the manner described in Section 7.3.2. Two methods of loading were used for the head of the centre pile. The first method involved applying pressure loads on line elements and calculating the resulting displacements. Alternatively, fixed displacements could be imposed on the nodes (using the Restraint facility) and the stresses recorded at relevant Gauss points within elements. Both methods were found to give the same load-displacement response for the centre pile.

The displacements and stresses induced after each of the above stages (i) to (iv) were zeroed, and therefore the displacements computed in (v) pertain to the pile loading phase alone.

7.7 Results from SAFE/BRICK Analysis

7.7.1 Single Pile Prediction

While the stand-alone BRICK program predicts sleech behaviour reasonably well, it was also necessary to assess how well SAFE/BRICK could predict single pile behaviour in the same soil. Good agreement is shown in Figure 7-10 between CS1/s and the SAFE/BRICK single pile. Important observations include:

- The exactness of the agreement is somewhat fortuitous since SAFE/BRICK models wished-in-place piles
- The single pile stiffness is well predicted at working loads (of ≈40% of the single pile capacity)
- The loads corresponding to a pile head displacement of 15mm are in good agreement. The fact that the prediction disimproves at loads above 40kN may be related to the fact that the SAFE/BRICK model has no provision for the occurrence of slip between pile and soil (contact between the two is maintained at the pile soil

interface at all stages of loading). This will inevitably result in slight errors in predicting the pile capacity.

- The non-linearity of the sleech is captured in the pile behaviour, although Belfast sleech is slightly more non-linear than the prediction suggests.

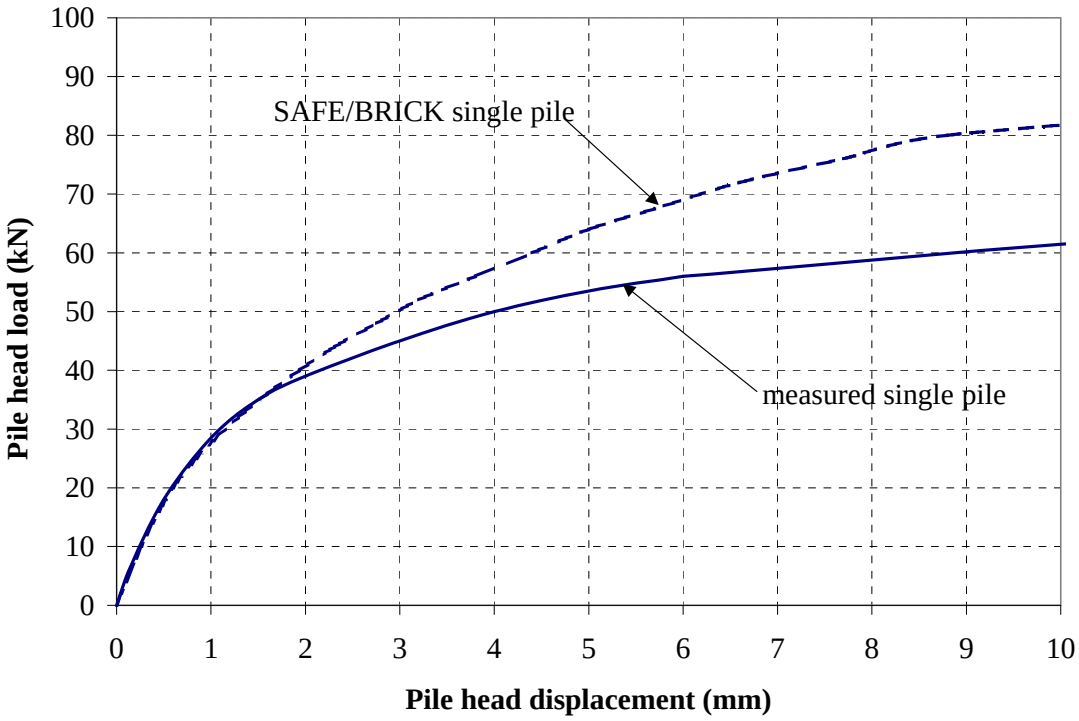

Figure 7-10 Comparison between SAFE/BRICK single pile and CS1/s

7.7.2 Centre Group Pile Prediction

The SAFE/BRICK prediction for the centre pile when loaded as part of the group is shown in Figure 7-11 and agrees very well with the measured response CG1[3]/s. The non-linearity of the centre pile's behaviour is captured as well as for the single pile. Although the piles modelled are 'wished-in-place' and the predicted stiffness values are not necessarily exact, the *relative* stiffnesses of the single and centre piles are well captured by SAFE/BRICK. This suggests that the model caters well for the effects of load interaction on the centre pile.

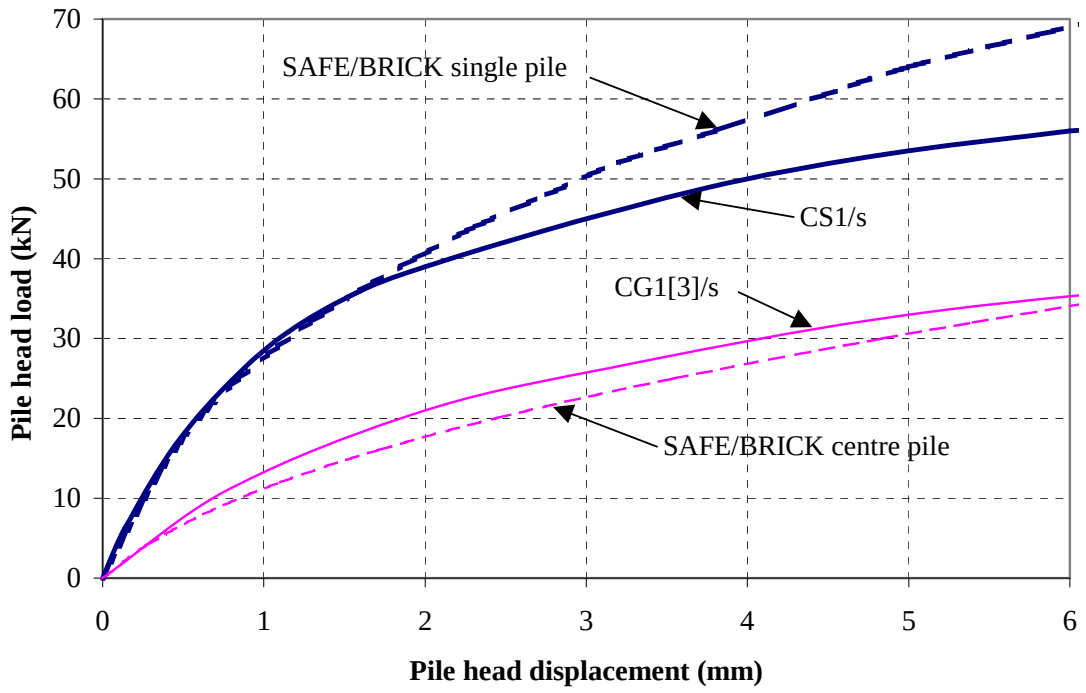

Figure 7-11 Comparison between SAFE/BRICK centre pile and CG1[3]/s

7.7.3 Predicted Settlement Profile surrounding a Single Pile

The ground settlement profile surrounding the loaded SAFE/BRICK single pile is shown in Figure 7-12. All settlement values (w) are normalized by the maximum value (w_{max}) which occurs at the pile-soil interface and therefore are typical 'interaction factors' as used to predict group behaviour. Values of w/w_{max} along the ground surface (at the top of the fill layer) suffered from some element distortion and are not presented. Observations include:

- At any pile spacing, w/w_{max} appears to reduce with depth (or possibly h/R)
- At any given pile spacing, w/w_{max} appear to reduce as the load level increases. However, Figure 7-11 suggests that the stiffness efficiency of the centre pile is relatively independent of load level.

Further SAFE/BRICK analyses were carried out to assess the validity of superposition and are presented in Figure 8-28.

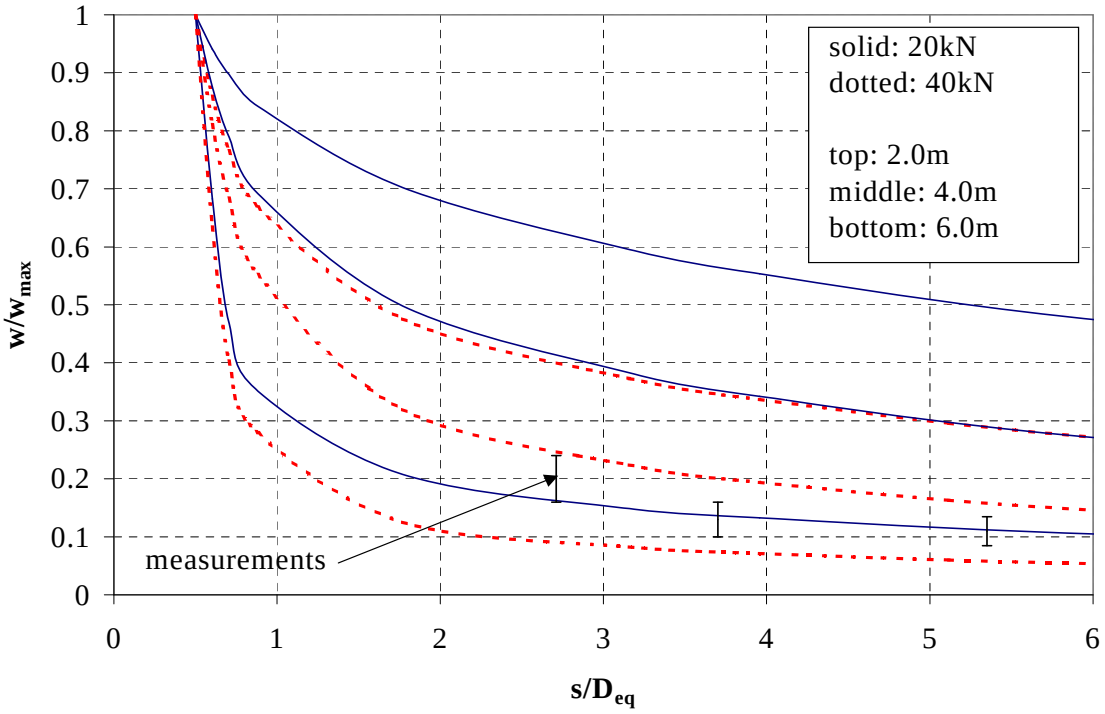

Figure 7-12 Normalized settlement profile around SAFE/BRICK single pile

7.8 Simple Numerical Model

The profile of ground settlement around a loaded pile may be predicted using a simple numerical approach which models the stresses and strains of the surrounding soil. Appropriate model parameters are chosen which offer a reasonably good match between the predicted t-z curves at the interface of pile and soil and those deduced from strain measurements for the single pile (CS1/s).

7.8.1 Soil model

The secant stiffness of the soil is assumed to vary according to the relationship of Lee and Salgado (1999):

$$G_{sec} = G_o\left(1 - f\left(\frac{\tau}{\tau_{max}}\right)^g\right)\left(\frac{p'}{p'_o}\right)^n$$

where G_o is the initial low-strain shear stiffness[12], τ is the shear stress in the soil, f and g are empirical curve fitting parameters[13], p' is the mean effective stress which has a far field value of p'_o, and n is a constant [0.5-1] whose value depends on strain level.

The shear stress (τ) is assumed to decay with distance from the pile in inverse proportion to the pile radius, according to:

$$\tau = \tau_{\max} \frac{r_o}{R}$$

where τ_{max} is the maximum shear stress at the pile soil interface, r_o is the pile radius and R is the distance from the pile shaft. The shear strains (γ) in the soil are calculated by combining the expressions above according to:

$$\gamma = \frac{\tau}{G_{\sec}}$$

Calculation of γ starts at the extreme boundary and propagates towards the pile. The corresponding downward settlement (w) of each element is calculated from:

$$w = \int_{r_o}^{200 r_o} \gamma dr \approx \sum_{r_o}^{200 r_o} \gamma \Delta r$$

where Δr is the width of the element at which the strain γ is calculated.

7.8.2 Implementation in spreadsheet format

The model was implemented in spreadsheet format through a number of steps; the solution obtained is based upon reasonable estimates of the soil parameters but is not unique:

- Values of f, g, G_o and the p' variation with radius were varied until the predicted t-z curves (i.e the τ-w relationships specific to the pile soil interface at $R = r_o$) produced the best match with measurements.

[12] G_o determined from seismic cone tests as 10000kPa.
[13] Best fit values: f = 0.95; g = 0.3.

- t-z curves were obtained by varying t in steps, up to t_{max}, and computing the corresponding value of z.
- The choice of radial variation of p' was important and is discussed in Section 7.8.3. The value of t_{max} is chosen to follow p' in tandem, according to:

$$\frac{t_{max}}{p'} = \sin\phi'$$

  with t_{max} at $R=r_o$ determined from the single pile t-z curve.
- Once the best match t-z curve is found (with measured curves at 3.25m and 5.25m depth), the resulting soil settlement profile may be plotted as a function of radius.

7.8.3 Variation of p' with distance from the pile shaft

Predictions of how equalized p' values vary with distance from the shaft of a single pile in Bothkennar clay are presented by Whittle (1991). Figure 7-13 illustrates Class A predictions (made in advance of the load test) of p'/σ'_{vo} as a function of r/R by Modified Cam Clay and SPM MIT-E3 models. Both indicate constant p' values between the pile shaft and r/R=4, a transition period 4<r/R<10 and *virtually* free field values at r/R>10. However, the models disagree regarding whether p' reduces or increases near the pile shaft.

The sensitivity of the model to three different p'/p'_o [14] variations with radius (Figure 7-14) was assessed. Figure 7-15 shows that while none produced a particularly strong match (perhaps because the soil model did not capture the strong non-linearity of the Belfast clay), the variation showing lowest p' at the pile shaft provided the best match.

7.8.4 Results from Simple Numerical model

Settlement profiles surrounding the single pile are shown in Figures 7-16 (3.25m) and 7-17 (5.25m) at a number of load levels (or proportions of t_{max}). It may be concluded that:

- As with the SAFE/BRICK model, w/w_{max} reduces as the applied load is increased.
- There is little apparent variation of w/w_{max} with depth, although the interface between soil and pile is not defined as clearly as with the SAFE/BRICK model.

[14] $p'/p'_o = p'/0.75\sigma'_{vo} = 1.33\ p'/\sigma'_{vo}$ (Figure 7-13 and 7-14)

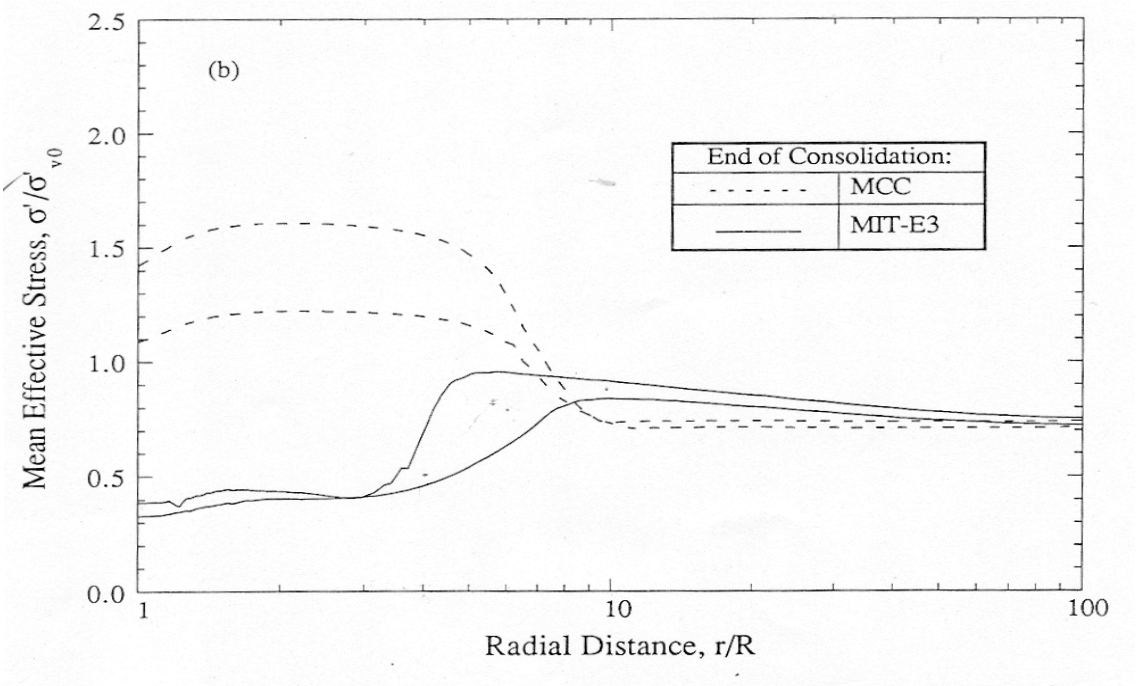

Figure 7-13 SPM MIT-E3 and MCC p' predictions for Bothkennar single pile

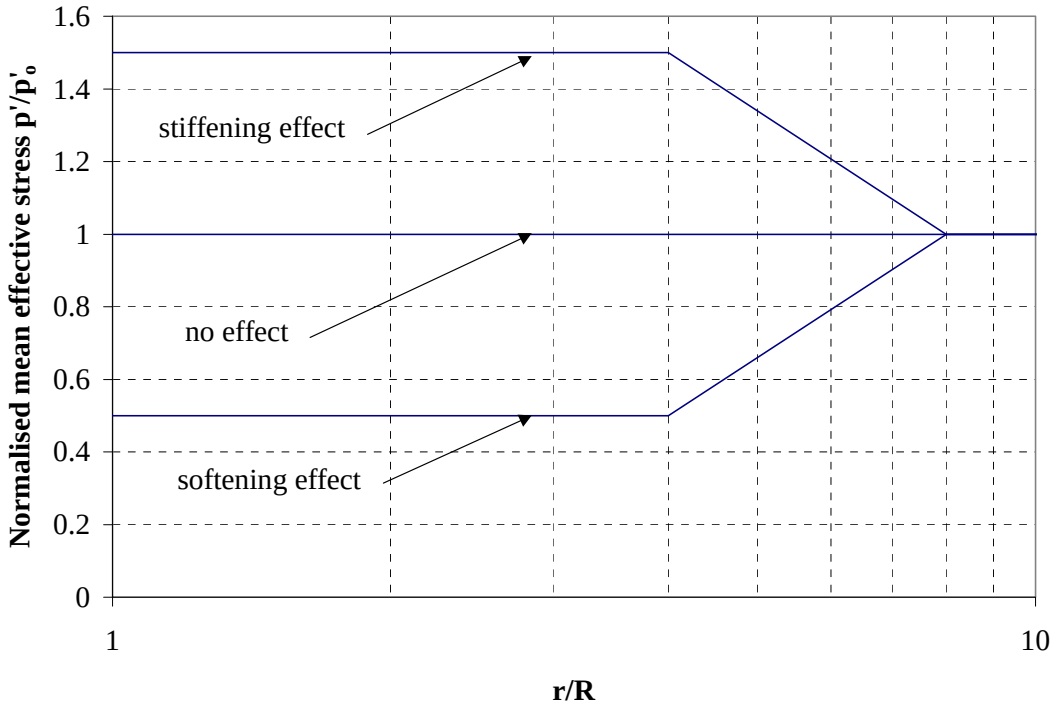

Figure 7-14 Assumed p' variation (after full equalization) for sensitivity analysis

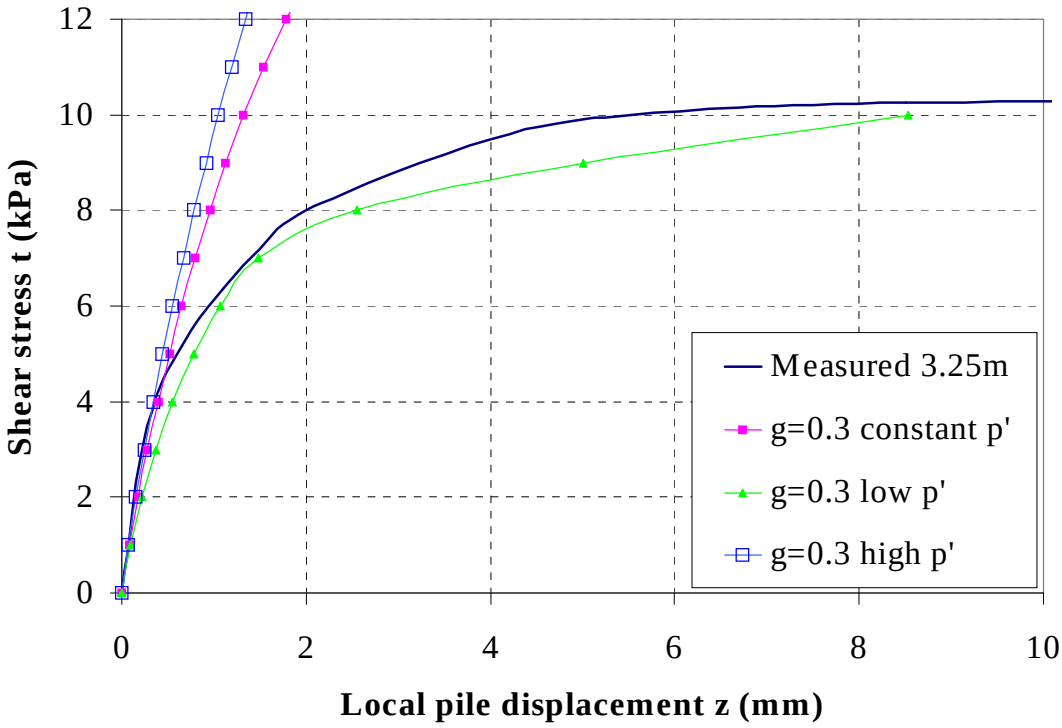

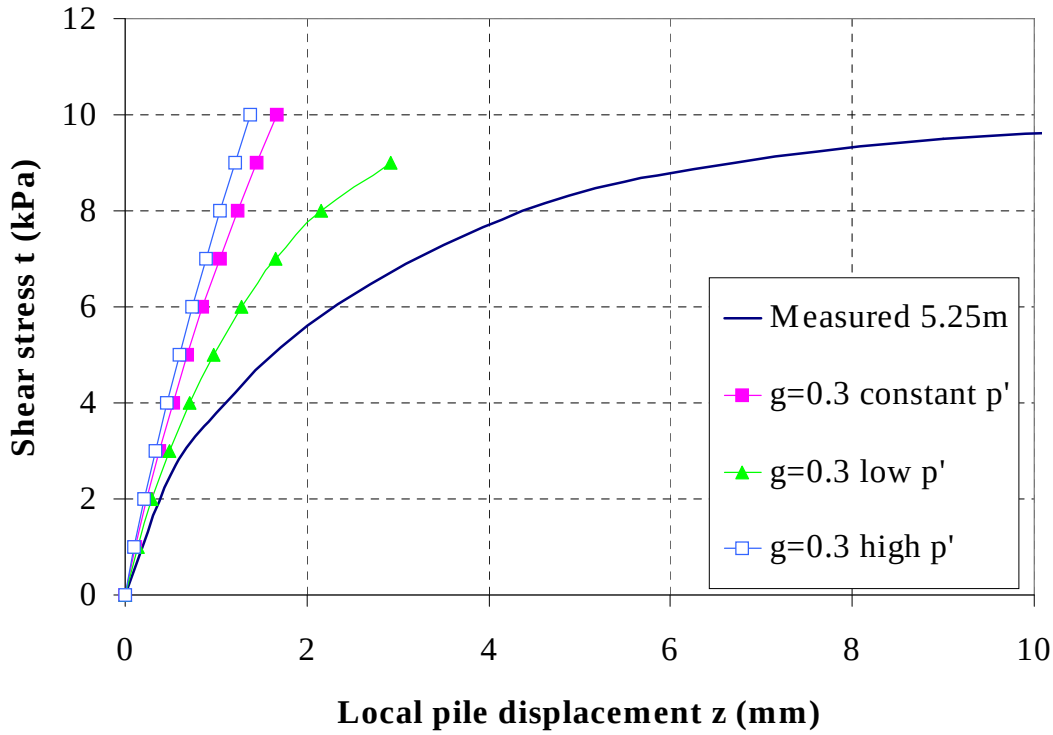

Figure 7-15 Predicted t-z curves: 3.25m (above) and 5.25m (below)

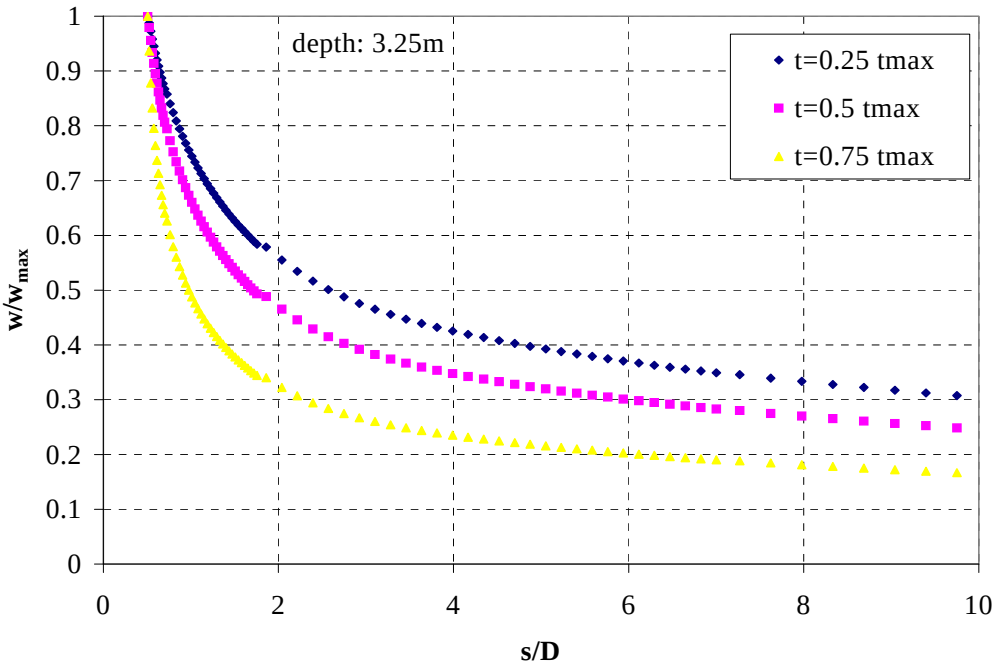

Figure 7-16 Normalized settlement profile around single pile 3.25m

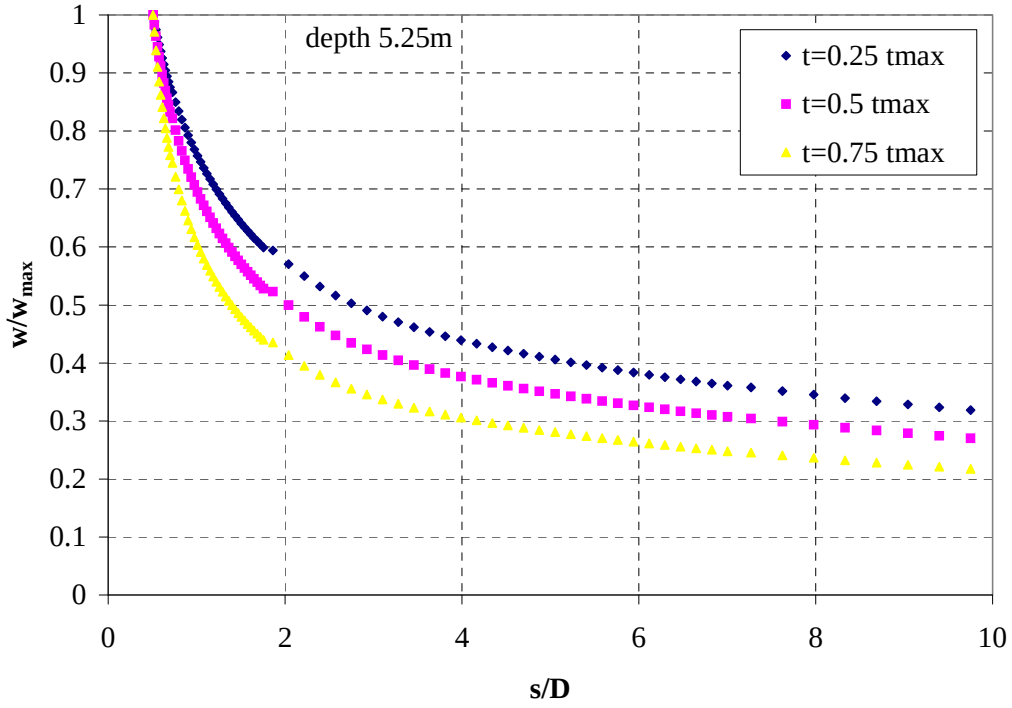

Figure 7-17 Normalized settlement profile around single pile 5.25m

Chapter 8

Discussion

8.1 Introduction

The discussion in this Chapter places greatest emphasis on the installation/equalization measurements and static load test data (presented in Chapter 5) with a view to highlighting some important features of group action in piles. These results provide the basis for discussion topics which include:

- Comparison of measured single pile capacities with standard prediction methods
- Total stress and pore pressure measurements pertinent to installation, equalization and pile loading[1]
- Stiffness and stiffness efficiency of small pile groups
- The role of soil non-linearity in predicting the stiffness of group piles
- Self-contained predictions of pile group load-displacement response based on field measurements
- Examination of the Belfast group data in the context of some other case histories of driven pile groups in soft clay.

Supplementary information used in the interpretation includes:

(i) Some standard empirical and numerical approaches used in single pile and group analysis.

(ii) Results of the SAFE/BRICK finite element analysis and the simple numerical model based upon the stress-strain relationship of Lee and Salgado (1999), both presented in Chapter 7.

(iii) Predicted and measured interaction factors from Jardine et al (1986) and Pellegrino (1983) respectively.

8.2 Single Pile Capacity Predictions

There are several single pile design approaches available, correlating shaft friction with a suitable soil parameter. The applicability of some of these shaft and base capacity prediction methods to the Belfast conditions is now assessed. Measured shaft and base

[1] A number of stress ratios (based upon horizontal total stress and pore pressure measurements) and other terms used in this Chapter are defined in Appendix 8-1.

stresses extrapolated to 25mm pile head displacement have already been presented in Table 5-2.

8.2.1 Shaft Capacity Predictions

Comparisons between predictions and measurements of the shaft friction q_s are limited to the lower-half of the pile (3.0m-6.0m)[2], since the q_c profiles in the upper 2.5m show considerable variation across the site (Figure 3-5). Table 8-1 compares $q_{s\ meas}$ (CS1/s) with $q_{s\ pred}$ determined by the α- and β- methods[3]. Quoted values for $q_{s\ meas}$ incorporate corrections for pile weight. Both methods result in similar degrees of over-prediction of the value of q_s.

Method	$\mathbf{q_{s\ pred}}$ **(kPa)**	$\mathbf{q_{s\ meas}}$ **(kPa)**	$\mathbf{q_{s\ pred}/q_{s\ meas}}$
$q_{s\ pred}=\alpha c_u$	16	$\approx$10.5	$\approx$1.5
$q_{s\ pred}=\beta(\sigma'_{vo})_{av}$	15$\pm$4	$\approx$10.5	$\approx$1.4$\pm$0.4

Table 8-1 Single pile shaft capacity predictions using the α– and β– methods

Improved predictions are provided by semi-empirical methods, such as those of Bustamante and Gianeselli (1982) and Almeida et al (1996), which relate q_s to a CPT parameter. A large database of instrumented piles led Bustamante and Gianeselli (1982) to derive α-values which enable the following relationship[4]:

$$q_s = \frac{q_c}{\alpha}$$

α=30 is recommended for driven precast piles in soft clay or mud, which leads to $q_{s\ pred}$=8.3kPa (or $q_{s\ pred}/q_{s\ meas}$=0.8). The method of Almeida et al (1996) is slightly more refined; q_s is related to q_{net}, where:

[2] Slightly higher q_s values than quoted for CS1/s in Table 5-4 as these relate to the lower half of the pile.
[3] API RP2A (1989) recommend $\alpha\approx$0.8 for c_u/σ'_{vo}=0.4. The expression of Flaate and Selnes (1977), which corrects empirically for pile length, arrives at β=0.36$\pm$0.09.
[4] These α values are not specific to a particular soil type, but depend on pile production and placement methods.

$$q_s = \frac{q_{net}}{k_1} \qquad q_{net} = q_T - \sigma_{vo}$$

and q_T is the cone tip resistance corrected for pore pressure at the cone shoulder[5]. The authors' design line suggests that k_1=20[6] for the Belfast sleech, giving a further improved prediction q_s= 9.5kPa ($q_{s\ pred}$ /$q_{s\ meas}$ ≈ 0.9).

The approach of Lehane et al (2000) incorporating the influence on q_s of q_T and other factors (such as h/R, the relative void index I_{vr}, and the plasticity index I_p) is displayed in Table 8-2.

Depth (m)	σ'_{v0} (kPa)	q_T (kPa)	h/R	w	LL	I_p (%)	e	e_L	I_{vr}	tan δ_f	f_L	q_s (kPa)
3.25	34.5	220	19.5	0.6	0.7	35	1.62	1.890	0.524	0.62	0.8	13.7
3.75	37.5	240	16.0	0.5	0.675	36	1.35	1.823	0.800	0.51	0.8	11.8
4.25	40.5	250	12.4	0.67	0.75	42	1.81	2.025	0.772	0.47	0.8	12.1
4.75	43.5	260	8.9	0.67	0.72	42	1.81	1.944	0.947	0.45	0.8	12.5
5.25	46.5	290	5.3	0.64	0.72	40	1.73	1.944	0.799	0.45	0.8	15.9
5.75	49.5	295	1.8	0.64	0.72	40	1.73	1.944	0.826	0.45	0.8	20.5

Table 8-2 Single pile capacity predictions using Lehane et al (2000a)

- The angle of interface friction δ_f is assumed to be equivalent to ϕ'_{res} (Figure 3-17); the difference between the friction characteristics of sleech on sleech and concrete on sleech shearing is believed to be small.
- This method gives a very good prediction of both the magnitude and distribution of load along the pile shaft over the range [3.0m-6.0m], for both tension and compression conditions. $q_{s\ pred}$ /$q_{s\ meas}$ is typically no greater than 1.2 over this portion of the pile.

[5] Values of k_1 result from backanalysis of 43 load tests (on driven and jacked piles) at 8 clay sites having piezocone data.
[6] q_{net}/σ'_{vo} averages 4.4 over length of pile between 3.0m and 6.0m depth.

- Lehane et al (2000b) shows that the method captures the *relative* values of skin friction on Belfast and Bothkennar (Lehane 1992) tension single piles, highlighting primarily the importance of accounting for δ_f in design calculations.

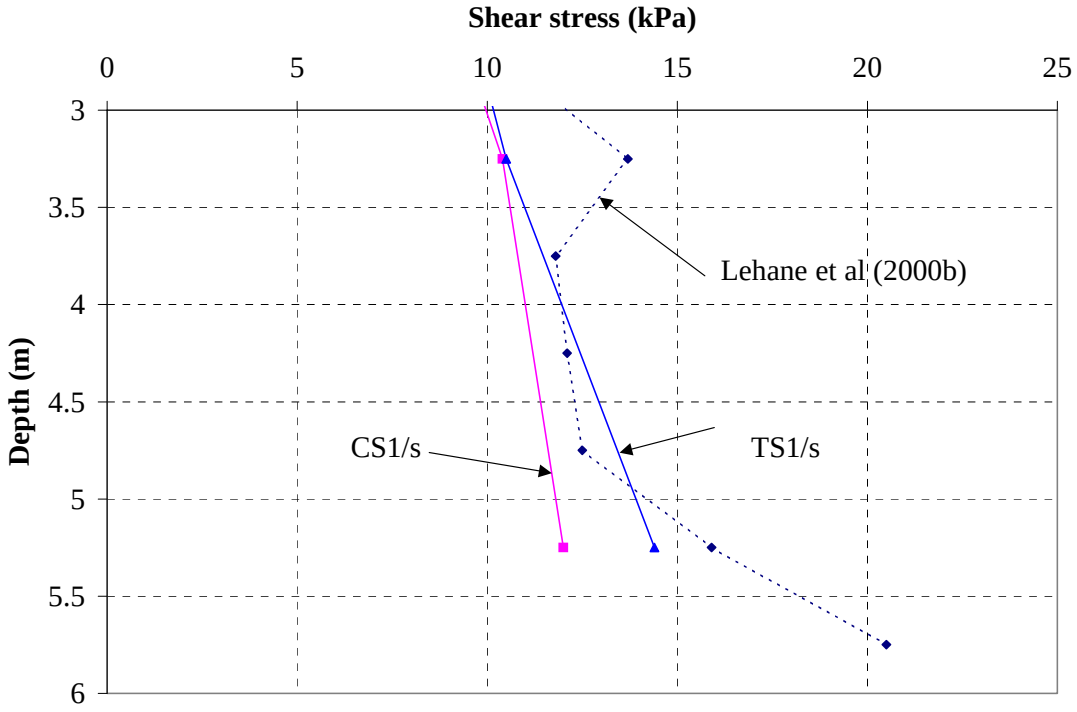

Figure 8-1 Comparison of $q_{s\ meas}$ and $q_{s\ pred}$ (Lehane et al 2000b) at Belfast

8.2.2 Base Capacity Predictions

The base loads measured in this Thesis were relatively low and difficult to measure accurately, so the accuracy of predictions is more difficult to assess. If the contribution of end bearing is assessed from bearing capacity theory:

$$q_b = N_c c_{uo} + \sigma_{vo}$$

with N_c=9 (Skempton 1951), the computed base stress of 180kPa is consistent with measurements (Figure 5-10). The method of Jardine and Chow[7] (1996), which suggests that

[7] q_c* is the value of q_c averaged 1.5 pile diameters above and below the pile base; q_c* ≈285kPa.

q_b/q_c* =0.8 for undrained loading, slightly overpredicts q_b (at 25mm displacement). Evidence from Figure 5-6 suggests that the load tests are likely to be partially drained, although much closer to the undrained than the fully drained situation.

From the discussion in Section 8.2, it may be concluded that the behaviour of single piles in *sleech* is consistent with expectations and that shear stresses on the pile shaft are predicted accurately by the more considered design approaches.

8.3 Total Stress and Pore Pressure Measurements

Group action on any pile may be regarded as the combination of the separate effects of driving and loading of adjacent piles. Measurements of stresses at the shaft of group piles over the installation and equalization periods (and comparison with single pile expectations) provide a means of assessing the effect of neighbouring pile installations. In this section, emphasis is placed on interpreting the σ_h and Δu measurements made during the test programme. A number of terms used in this discussion are explained in Appendix 8-1.

Instrument depth (m)	h/R	σ_{ri} (kPa)	H_i	H_i/K_o[8]	$\Delta u_{max}/\sigma'_{vo}$	YSR
3.25	19.5	82	1.74	3.5	1.64	1.5
5.25	5.3	141	2.13	4.8	2.02	1.1

Table 8-3 Single pile installation measurements

8.3.1 Total Stress Measurements for a single pile

The measured peak σ_h values in Figure 5-1 corresponding to the installation of CG1[3] are single pile values since this was the first of the group piles to be driven. H_i values are shown in Table 8-3 and they reduce with distance from the pile tip (h/R) as suggested by tests with the Imperial College Pile. H_i values measured in other clays have been reported by Lehane et al (1994) at h/R>20; Figure 8-2 confirms that the Belfast value compares favourably with other lightly overconsolidated clays.

[8] K_o is calculated using the well-known expression: $K_o = (1-\sin\phi')\ OCR^{\sin\phi'}$

Values of $\Delta u_{max}/\sigma'_{vo}$ shown in Table 8-3 are estimated from measurements of σ_h. Instrumented single pile tests in lightly-overconsolidated clay (Koizumi and Ito 1967, Karlsrud and Haugen 1985, Lehane 1992, Karlsrud, Kalsnes and Nowacki 1992) suggest that K falls from its ambient[9] K_o value to K_i values which are near zero during pile installation. A value of K_i=0.1 was used[10] to estimate the values of excess pore pressures reflected in Table 7-1. These are broadly consistent with $\Delta u_{max}/\sigma'_{vo} \approx 2.1$ measured on the shaft of a steel pile driven in St. Alban's clay by Roy et al (1981), another sensitive lightly overconsolidated clay.

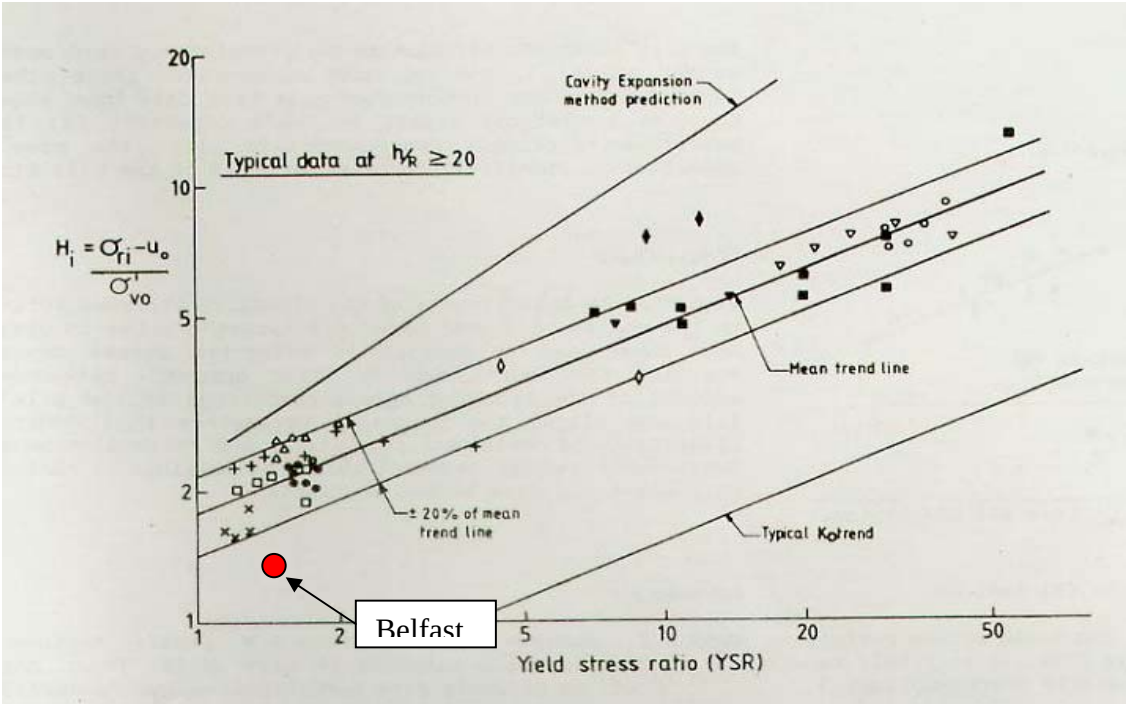

Figure 8-2 Database of H_i measurements at h/R>20 (Lehane et al 1994)

8.3.2 Excess Pore Pressure Fields surrounding a Single Pile and Pile Group

The distribution of installation excess pressures surrounding a single pile and pile group are compared in Figure 8-3. Not all of the trends shown are based on measurements, so the data shown is compiled from:

[9] Over the length of the pile embedded in sleech, K_o lies within the range 0.45-0.55

[10] Values of the excess pore pressure ratio ($\Delta u_{max}/\sigma'_v$) deduced are relatively insensitive to the choice of K_i between 0 and 0.2.

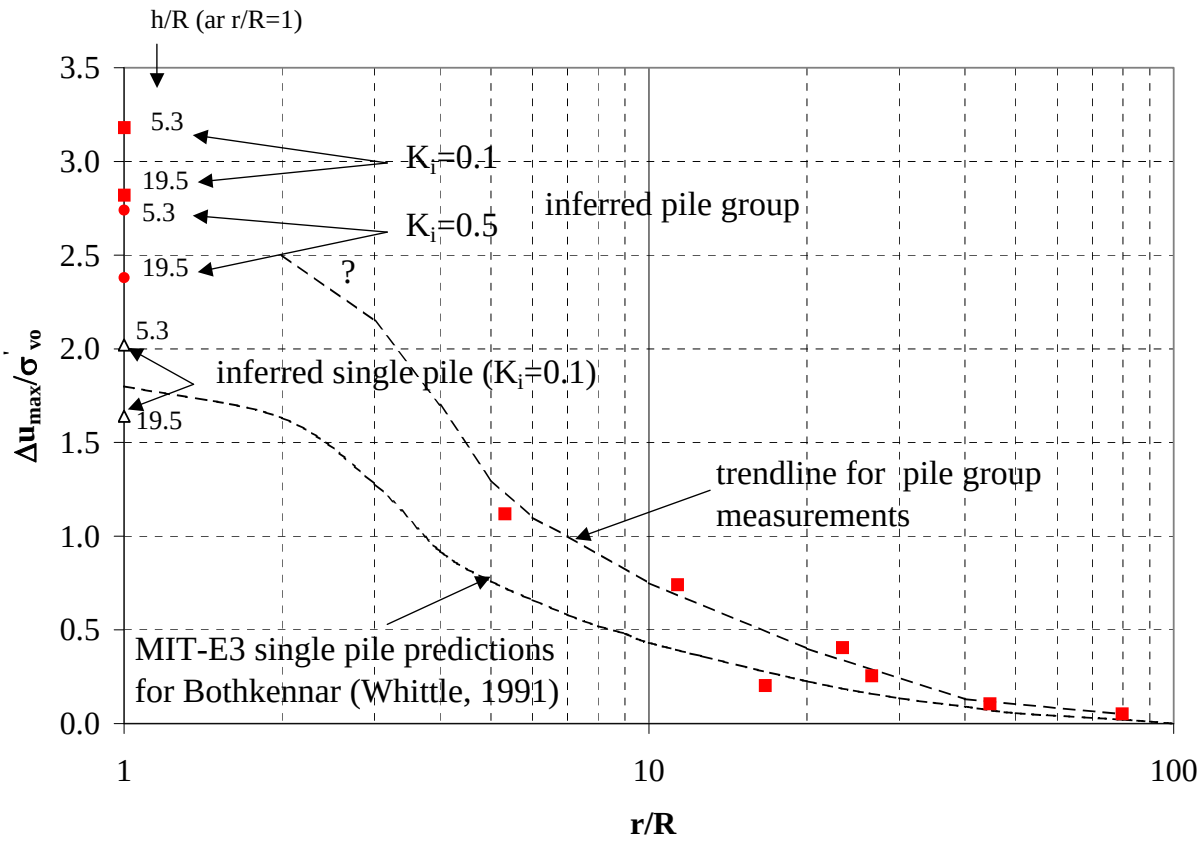

Figure 8-3 Distribution of installation excess pressures around single pile and pile group

(i) Single pile $\Delta u_{max}/\sigma'_{vo}$ values at r/R=1 from Table 8-3.

(ii) Pile group $\Delta u_{max}/\sigma'_{vo}$ values at r/R=1 (at the shaft of the centre pile) are estimated from the maximum σ_h value reached during the installation of the group (i.e. corresponding with the installation of corner pile CG1[1], see Figure 5-1). The value of K at the centre pile during the driving of CG1[1] is unknown. The sensitivity of the solution to K in the range [0.1-0.5] is therefore shown.

(iii) The decay of $\Delta u_{max}/\sigma'_{vo}$ with r/R for the single pile is based upon SPM MIT-E3 Class A predictions (Whittle, 1991) for driven single piles in Bothkennar clay. Good agreement is found between (ii) and (iii) at the single pile shaft (r/R=1).

(iv) The decay of $\Delta u_{max}/\sigma'_{vo}$ with r/R for the pile group is based upon pneumatic piezometer readings around TG1 for r/R>5.

The following observations may be made from Figure 8-3:

(i) Regardless of the K_i value used to infer $\Delta u_{max}/\sigma'_{vo}$ at the shaft of the centre pile, it emerges that the maximum excess pore pressures generated by group driving are everywhere greater than for a single pile, at least to a radial extent of r/R≈30.

(ii) It is noted that, although increases in σ_h due to driving are clearly transient, it does not necessarily follow that the pore pressure increases are also short-lived.

Predictions of c_h around TG1 based on the piezometer data is described in Appendix 8-2.

8.3.3 Equalisation of Total Horizontal Stress for centre pile and single pile

The capacity of a pile depends upon the equalized horizontal effective stress (σ'_{hc}). It is therefore of interest to compare σ_h for a single pile and centre pile over the equalization period to establish whether the installation of the corner piles will have an effect on the subsequent performance of the centre pile. The resulting variation from pile to pile of the soil stiffness[11] at the pile-soil interface provides the initial soil conditions for the load test.

The measured σ_h decay on the centre pile (Figure 5-1) arising from the installation of all five piles is compared with corresponding measurements for a driven isolated pile made by Lehane (1992, see Figure 8-4) at Bothkennar. Both trends are conveniently compared[12] in Figure 8-5 by plotting H/H_i as a function of the time factor T:

$$T = \frac{c_h t}{R^2}$$

When the measured decay of σ_h (both at h/R=5.3 and h/R=19.5) is examined over the period between the installation of the centre group pile and the first of the corner piles (i.e. while effectively a single pile), some inconsistencies arise between the two for which some reasonable adjustments have been recommended in Appendix 8-3.

[11] Soil shear modulus (G) depends on the mean effective stress level (p'), of which σ'_h is a component.

[12] The average field value of c_h at Bothkennar appropriate to driven piles has been established as ≈30m^2/year and the pile radius is 50.8mm.

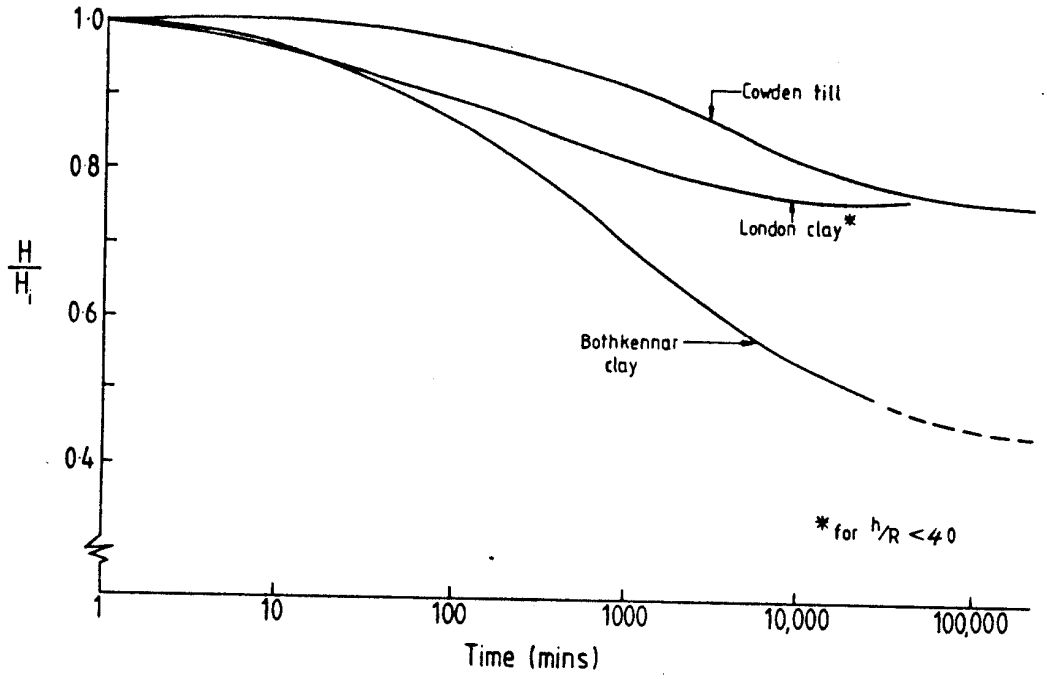

Figure 8-4 Variation of H/H_i for piles at Bothkennar (Lehane 1992)

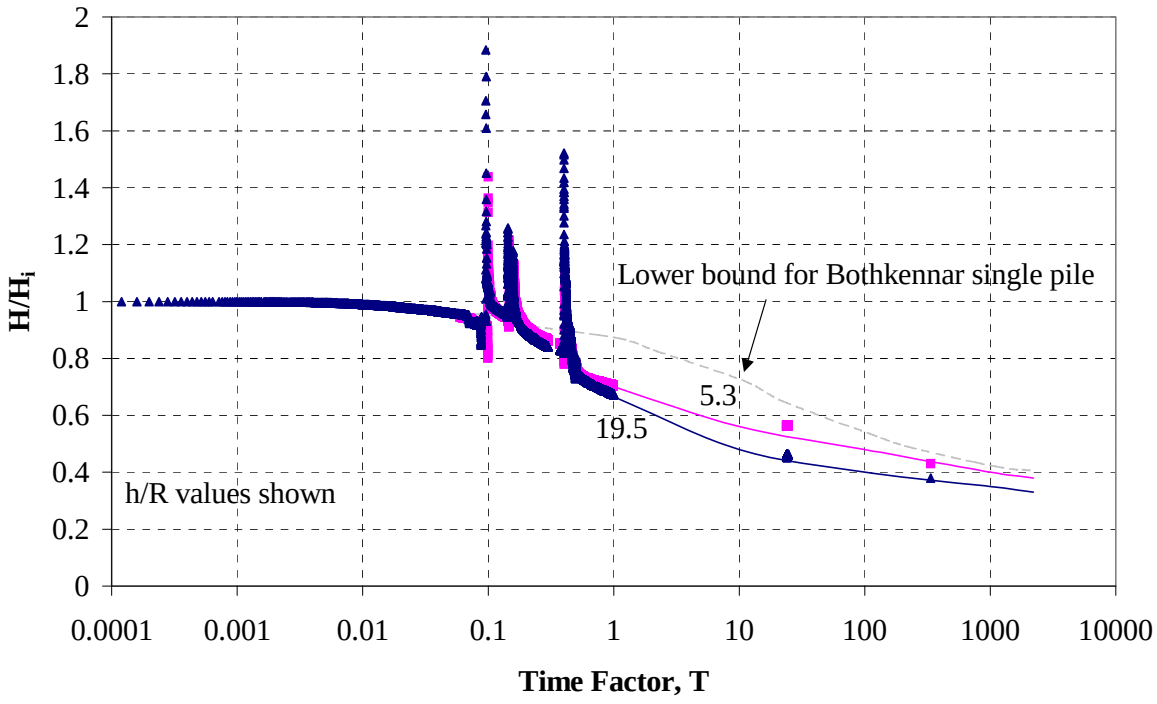

Figure 8-5 H/H_i decay for single pile (Lehane 1992) and centre group pile CG1[3]

A number of important points arise from the comparison of H/H_i decay for isolated and group piles (Figure 8-5):

- Shortly after driving all five group piles, H/H_i measured on the centre pile is significantly lower than that predicted for an isolated pile. The H/H_i value of the group's centre pile remains lower (than that estimated for the isolated pile) throughout the period required for equalization.
- At the time of the load test[13], H/H_i for the group appears to be slightly lower than that expected for a single pile. While this difference between the two is difficult to quantify exactly due to limited accuracy of the horizontal stress sensors, it is likely that the relaxation coefficient K_c/H_i for a pile group ($s/B \approx 3$) would be similar to, or fall only slightly below, that expected for a comparable single pile. This contradicts the commonly-held belief that adjacent pile driving serves to stiffen the soil in the vicinity of any group pile and enhance its subsequent performance under load.
- Values of the group relaxation coefficient (H_c/H_i or K_c/H_i) lie in the range 0.3-0.4. While comparable to or perhaps slightly lower than those measured by Lehane (1992) for single piles, they compound Lehane's observation that the relaxation coefficient is lower in lightly overconsolidated materials than in heavily overconsolidated materials (refer to Figure 8-3).
- Group K_c values of 0.57 (at z=3.25m, h/R =19.5) and 0.81 (at z=5.25m, h/R=5.3) exceed K_o, the coefficient of earth pressure at rest.
- In the research of Phillips (2002), values of $K_c \approx 0.6$ were measured at $h/R>34$ ($z<3.5$m) for a single end-bearing pile in the Belfast clay. These provide further evidence that K_c values pertinent to the centre group pile are *no greater* than corresponding single pile measurements.

8.3.4 Changes in Horizontal Total stresses during Load Test

Research by Imperial College London with the IC pile has shown that the radial/horizontal effective stress at ultimate conditions (σ'_{hf}) in a load test is ≈20% lower than that in existence at the end of equalization, or alternatively:

[13] by which time at least 85% of all excess pore pressures should have dissipated (Figure 5-6).

$$\frac{\sigma'_{hf}}{\sigma'_{hc}} = \frac{K_f}{K_c} \approx 0.8$$

This stress reduction factor is incorporated into the recommended single pile design method of Jardine and Chow (1996). Without pore pressure sensors on the group piles during loading, K_f is unknown for the partially drained situation relevant for the Belfast load tests. However, two total stress sensors on the centre pile and one on a corner pile of CG1/s suggested that the total stress changes very little as the pile group is loaded (Figure 5-21), i.e $H_f \approx H_c$. Further pore pressure measurements (at the pile shaft) would help to discern whether K_f/K_c for a group pile exceeds 0.8. It may be the case that the slightly lower K_c/H_i value reported for the group pile may be counteracted by a slightly greater K_f/K_c value, so that the net group installation effect K_f/H_i is approximately the same as for a single pile.

8.4 Group Pile Stiffness and Stiffness Efficiency in Load Tests

8.4.1 Definition of pile stiffness

Pile stiffness, a term often used for single piles, is defined as the ratio of the load applied at the head of the pile ($P_{s,app}$) to the corresponding pile head displacement (w_s). Elastic shortening of the single pile aside, the load applied at the pile head is the only source of movement.

$$k_s = \frac{P_{s,app}}{w_s}$$

The definition of the stiffness of a pile within a group is not as straightforward. In accordance with the discussion of Section 2.6.1, the stiffness of a group pile (k_g) is defined as the applied pile head load ($P_{g,app}$) divided by the total pile head displacement ($w_{g,\,tot}$). This displacement is in response to the *absolute* load on the pile; it is not solely due to $P_{g,app}$ but also reflects loads from interacting piles. This 'group' ratio will subsequently be referred to as the equivalent group pile head spring stiffness.

$$k_g = \frac{P_{g,app}}{w_{g,tot}}$$

The 'stiffness efficiency' (η_g) of an entire pile group or of any specific (or characteristic) pile within a group is given by:

$$\eta_g = \frac{k_g}{k_s}$$

which amounts to the ratio of the group pile to single pile settlement at a typical working load, such as ≈40% of the single pile capacity.

An 'equivalent' term for k_s applicable to one-way cyclic loading is $k_{s\ cyc,}$ the cyclic pile head spring stiffness. If in any one cycle, the applied cyclic load varies between $P_{s,min}$ and $P_{s,max}$ causing a displacement variation between $w_{s,\ min}$ and $w_{s,\ max}$, then $k_{s\ cyc}$ is defined as:

$$k_{s\,cyc} = \frac{P_{s,\max} - P_{s,\min}}{w_{s\,\max} - w_{s\,\min}}$$

The corresponding group term for cyclic loading is $k_{g\ cyc}$. Given that there is no unique definition of cyclic capacity (for either single piles or groups), a unique value of η_{cyc} cannot be determined.

8.4.2 Equivalent Raft and Pier Methods

These methods (Section 2-7) are widely used to estimate the k_g value of a complete pile group. Intuitively, the equivalent raft method is most suited to pile groups having a low aspect ratio[14], but becomes less justifiable as the pile length increases in relation to the plan dimensions of the group. Randolph and Clancy's (1993) aspect ratio parameter (R) for square groups (as defined in Section 2.7.2) recommends the use of the equivalent pier for the Belfast configuration (R<1), although the formula quoted for R is not particularly relevant to small groups which are not laid out in the simple N×N format.

The equivalent raft and pier approaches are evaluated against the CG1/s load-displacement response. Both methods require an estimate of the soil's Young's Modulus at a prescribed

[14] Pile length/group width

working group load (chosen arbitrarily as 25kN per pile or ≈40% of ultimate single pile capacity). The value of E_s=6000kPa used is back-figured from the single pile (CS1/s) load test (using Randolph and Wroth, 1978). The predicted equivalent spring stiffnesses for the five pile group are compared with CG1/s in Figure 8-6 and indicate:

- The equivalent raft method (for s/D_{eq}=2.7) implicity assumes greater pile-pile interaction than has been measured in the group tests. It is unlikely that the operational E_s around the pile group (i.e. averaged over five piles) is half of that for the single pile.
- The equivalent pier method produces a slightly better prediction, but nevertheless is very conservative for the Belfast tests.
- It may be the case that there are pile group configurations that do not fit conveniently into either of the above categories.

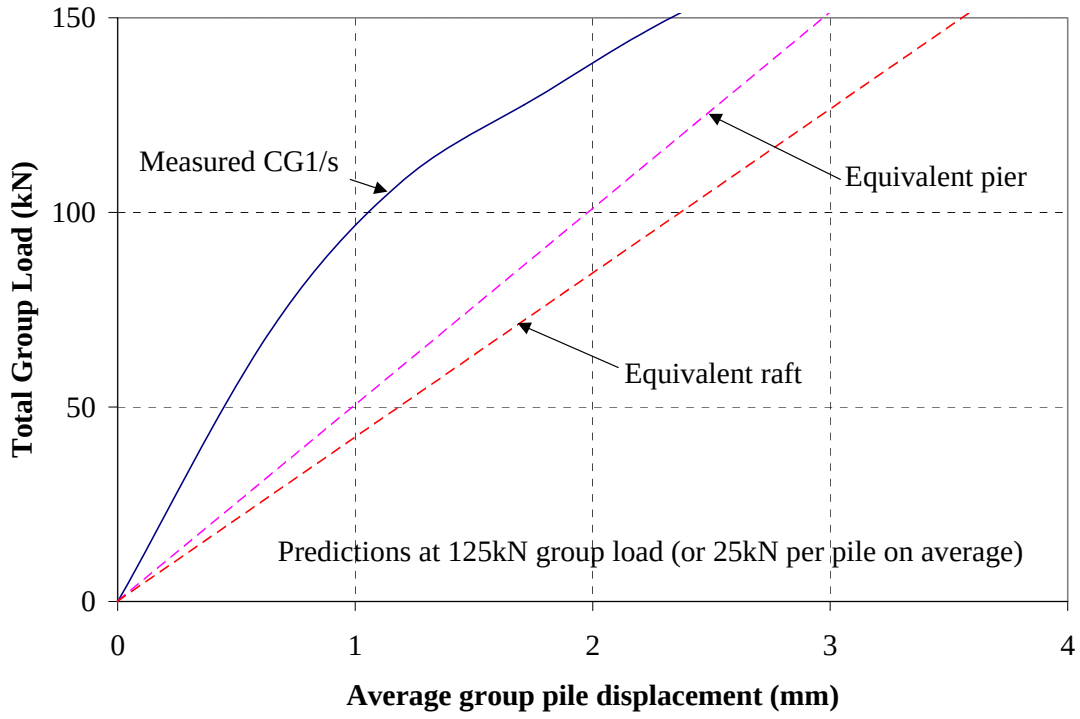

Figure 8-6 Comparison of Equivalent Pier and Raft methods with CG1/s (at 25kN/pile)

8.4.3 The overall Stiffness Efficiency of a 5-Pile Group (s/B=3)

The global stiffness efficiency of a group of piles (η_g) is independent of how the load is shared among each of the individual piles. The variation of η_g with the level of working load (alternatively represented as the factor of safety upon single pile capacity) is shown in Figure 8-7 for both tension group TG1/s and compression group CG1/s. It may be seen that:

- For a group of five piles spaced at s/B≈3, η_g lies in the range 40-50% (i.e. the stiffness of an *average* group pile is less than half of that for corresponding single pile) and appears relatively independent of load level.
- η_g is virtually the same whether group loading is in tension or compression.
-

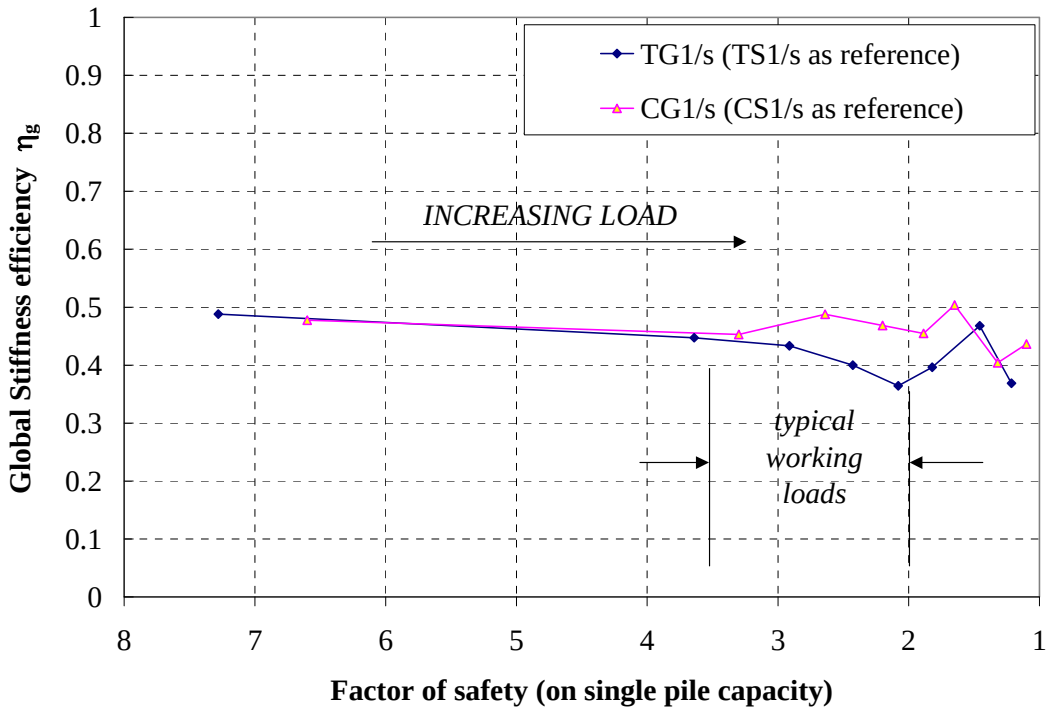

Figure 8-7 Stiffness efficiency as a function of safety factor on single pile capacity

8.4.4 The Stiffness and Stiffness Efficiency of the individual group piles

Details of the inconsistent behaviour of the pile cap and its effect on the loads and movements of each of the group piles have been illustrated in Sections 5.6 and 5.7. As in

Chapter 6, the performance of the group is analysed in terms of its centre pile and the average of its four corner piles. The load-displacement relationships of these 'characteristic' piles (i.e. single, average corner and centre) are compared in Figures 8-8 and 8-9 for compression and tension loading respectively.

The following points are noteworthy:

(i) The '*characteristic*' compression piles illustrate a reduction in stiffness associated with increased load interaction (Figure 8-8). This conforms with the expected behaviour of a rigidly capped group.

(ii) While the tension single pile is significantly stiffer than the tension group piles, the distinction between the centre and average corner piles is not so clearcut. Despite experiencing further interaction, the centre pile *appears* to be stiffer than an average corner pile at pile head displacements up to ≈2mm. However Figure 8-9 is a misleading gauge of interaction effects when all piles are not all at an equally advanced stage of loading. The influence of the pile cap in TG1 (already discussed in Section 5-6) is shown in Figure 8-10 in which the links between corner and centre pile load-displacement curves represent (selected) time contours.

(iii) Load interaction effects emerge more clearly once the centre and corner pile equivalent spring stiffnesses are plotted as a function of the *average displacement of the group*, a term which unifies the piles' performance in terms of time or stage of loading (Figure 8-11). At any stage of loading (for both tension and compression groups), the centre pile equivalent spring stiffness clearly falls below that of an average corner pile over the working load range. Furthermore, the magnitudes are relatively consistent between the tension and compression tests. While Figure 8-9 is useful in distinguishing between the performances of the group piles, direct determinations of η from this plot are precluded.

(iv) Although the true effects of interaction (or stiffness efficiency) of a group pile may be disguised by the behaviour of the pile cap, its influence may be uncoupled relatively easily from the measured load-displacement plots.

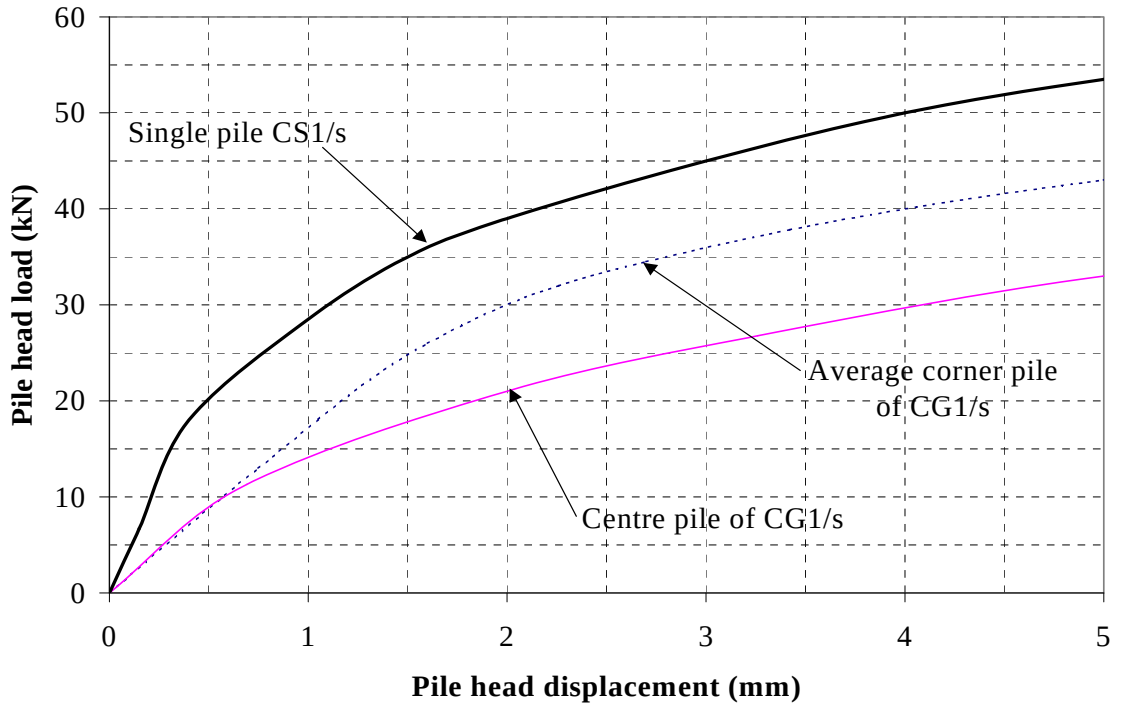

Figure 8-8 Equivalent spring stiffnesses of 'characteristic' compression piles

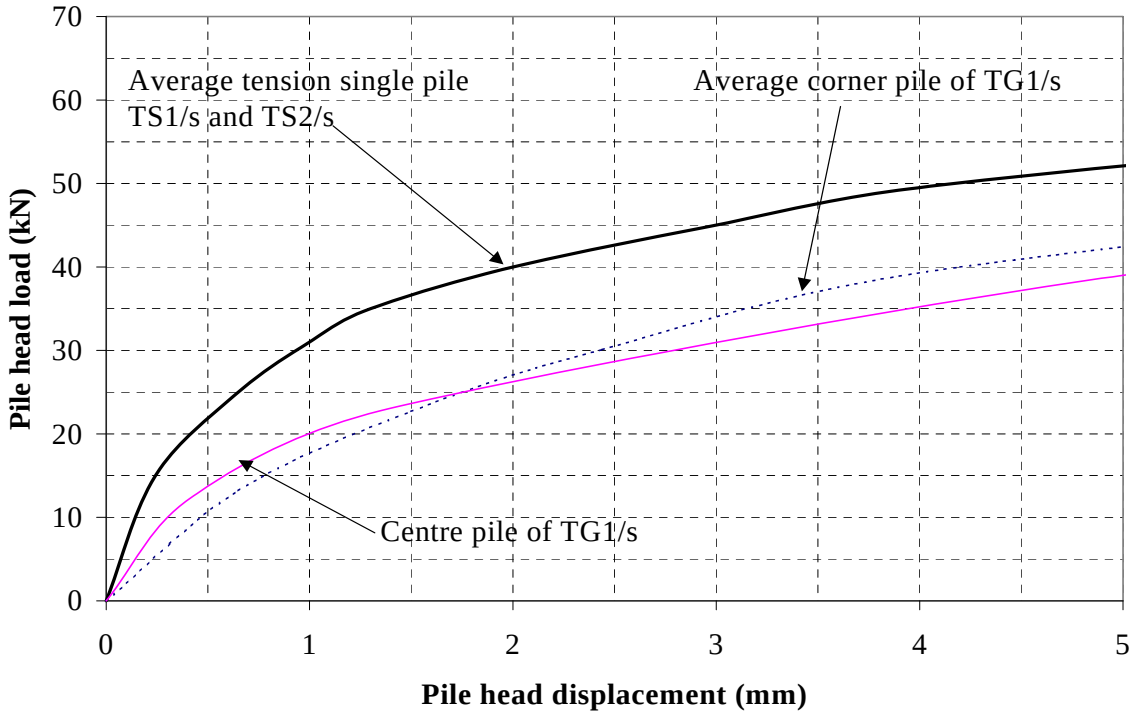

Figure 8-9 Equivalent spring stiffnesses of 'characteristic' tension piles

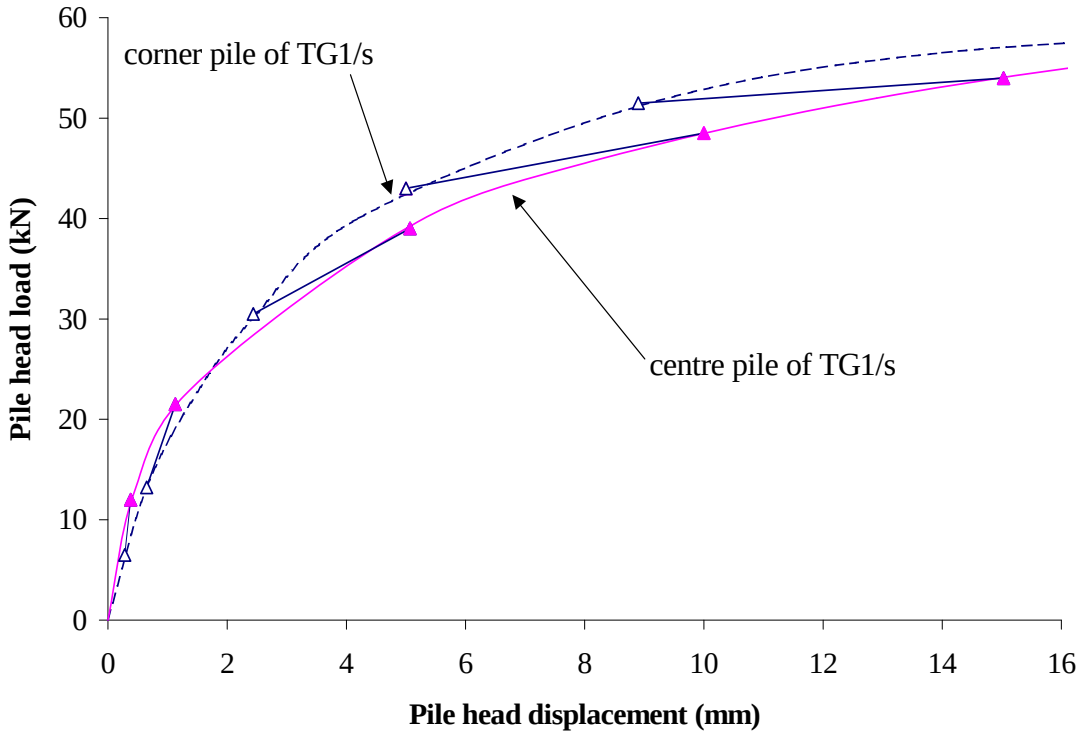

Figure 8-10 Relative loading progression of TG1/s piles

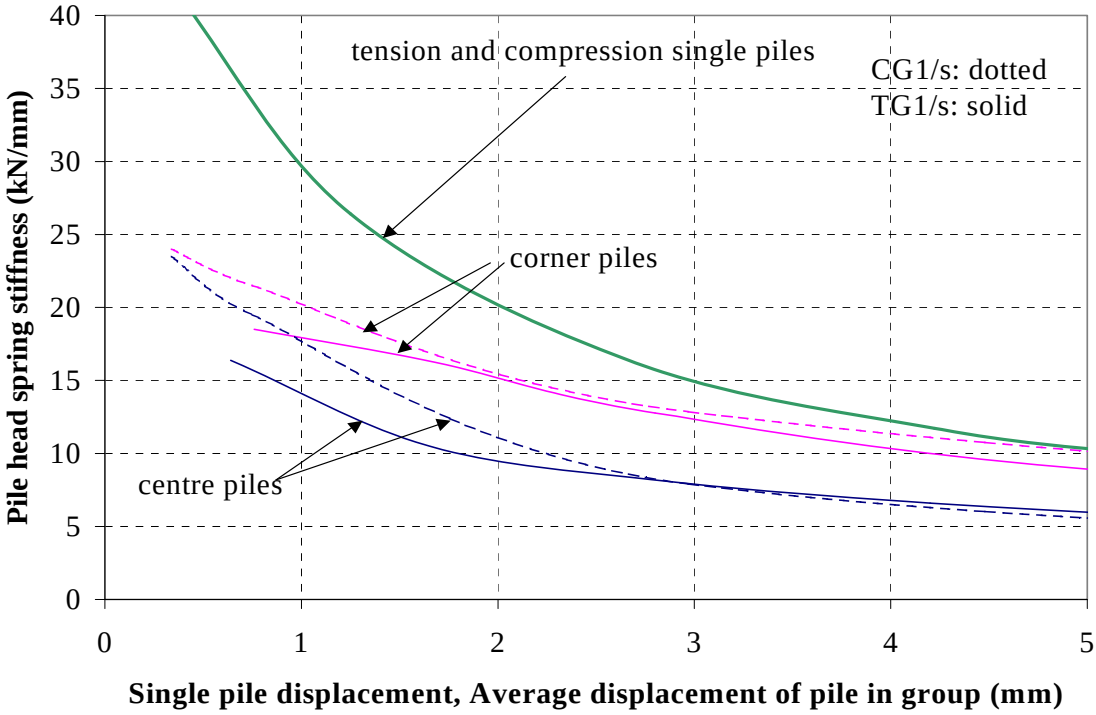

Figure 8-11 True load interaction effects uncoupled from pile cap behaviour

Similar trends arise in the one-way cyclic tension group load tests (TG1/sc and TG2/c), when $k_{g,\ cyc}$ for the centre and corner piles are plotted against the mean accumulated displacement averaged over the five piles. At any displacement, $k_{g,cyc}$ values fall below $k_{s,cyc}$ values as expected and the corner pile is stiffer than the centre pile, and thus are qualitatively consistent with the static tests. However, the difference between single and corner pile k_{cyc} values in the cyclic tests appears to be greater than the corresponding difference in static k values of Figure 8-11. Differences between k_{cyc} magnitudes in Figures 8-12 and 8-13 may be explained by the different loading histories experienced by the piles.

8.4.5 Pile Stiffnesses from Site Specific t-z curves

Site-specific t-z curves (tracking the development of shear stress[15] (t) at the interface of pile and soil with local[16] pile displacement (z)) have been developed from the measured load distributions in the characteristic piles. All single pile and group pile t-z curves are presented in Appendix 8-4. Comments pertinent to pile *stiffness* include:

(i) Although the measured single pile t-z curves are more strongly non-linear than those recommended by API RP2A (1993), the recommended values provide a reasonable 'average' or 'typical' estimate of the local pile stiffness over the length of the pile at a working load corresponding to $t=0.4t_{max}$ (a factor of safety of 2.5 on single pile capacity) (Figure 8-14).

(ii) At this working load level, API RP2A (1993) recommendations would grossly over-predict the equivalent spring stiffness of the centre pile of a five-pile group. The comparative t/t_{max}-z curves are presented in Figure 8-15.

(iii) The t-z curves illustrate that pile stiffness is greater at 3.25m than at 5.25m, and this applies to both the single and centre piles (Figure 8-16). The local value of η (at t=4kPa) is greater[17] at 5.25m than at 3.25m, also reflecting the greater transfer of load towards the lower part of the pile characteristic of group piles (already presented in Figure 5-19).

[15] Relative to the shear stress in existence at the start of the test; residual loads are unknown.
[16] Accounting for the elastic shortening of the pile.
[17] The stiffness efficiency is ≈15% at 3.25m and ≈22% at 5.25m.

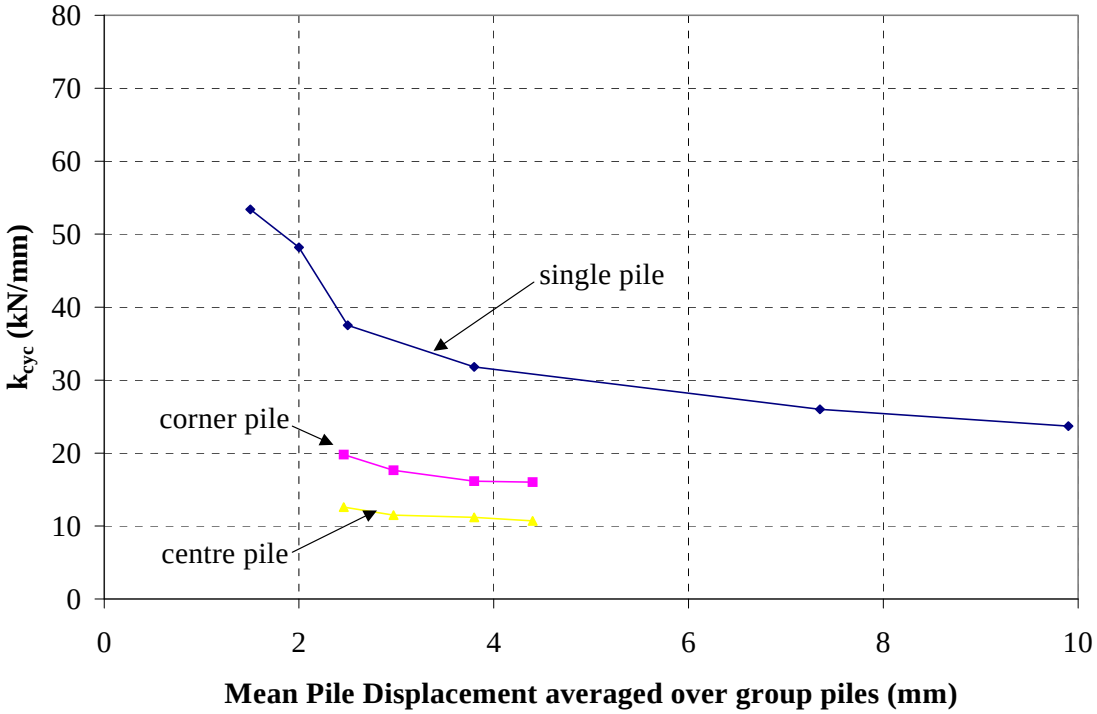

Figure 8-12 Reduction in k_{cyc} with average group displacement for TG1/sc

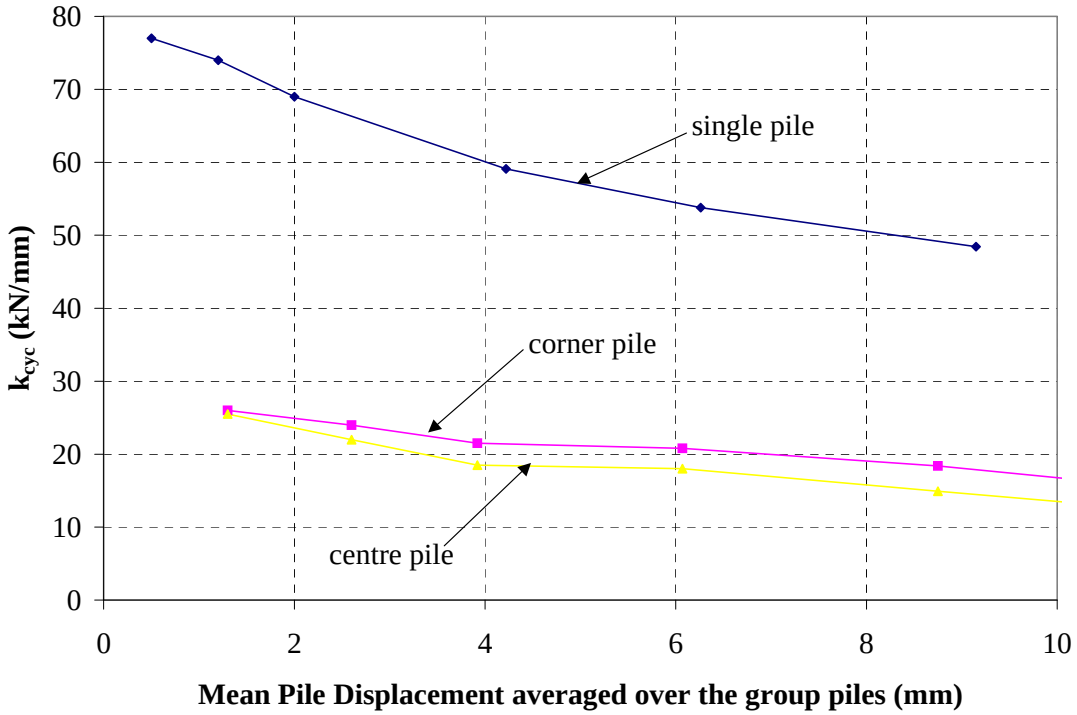

Figure 8-13 Reduction in k_{cyc} with average group displacement for TG2/c

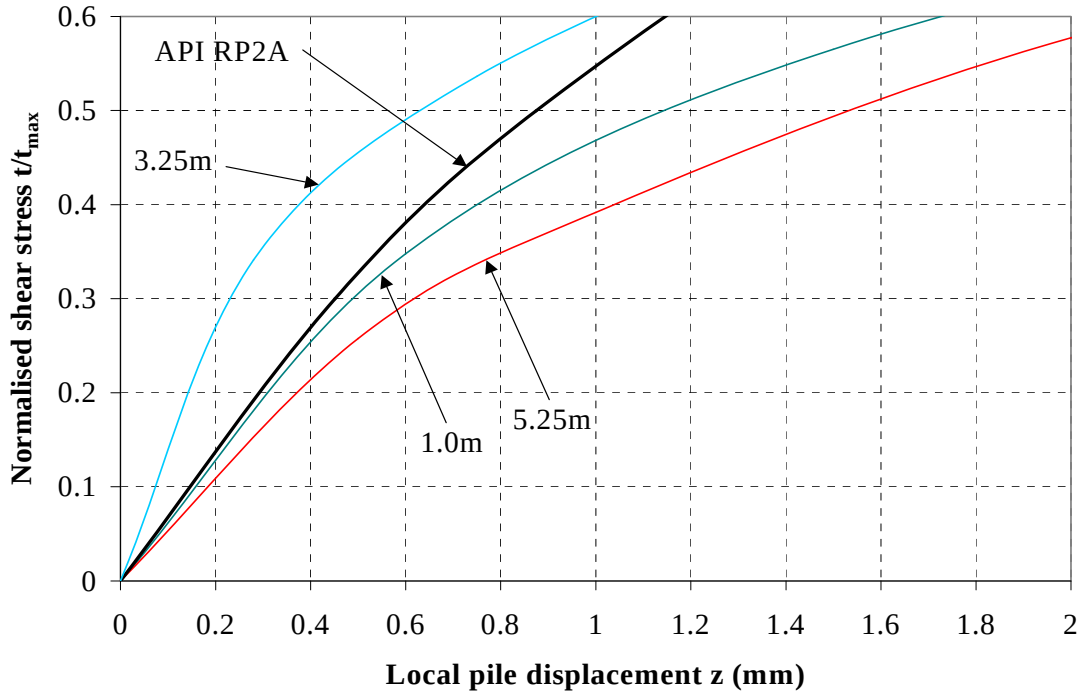

Figure 8-14 Measured single pile t-z curves compared with API RP2A recommendations

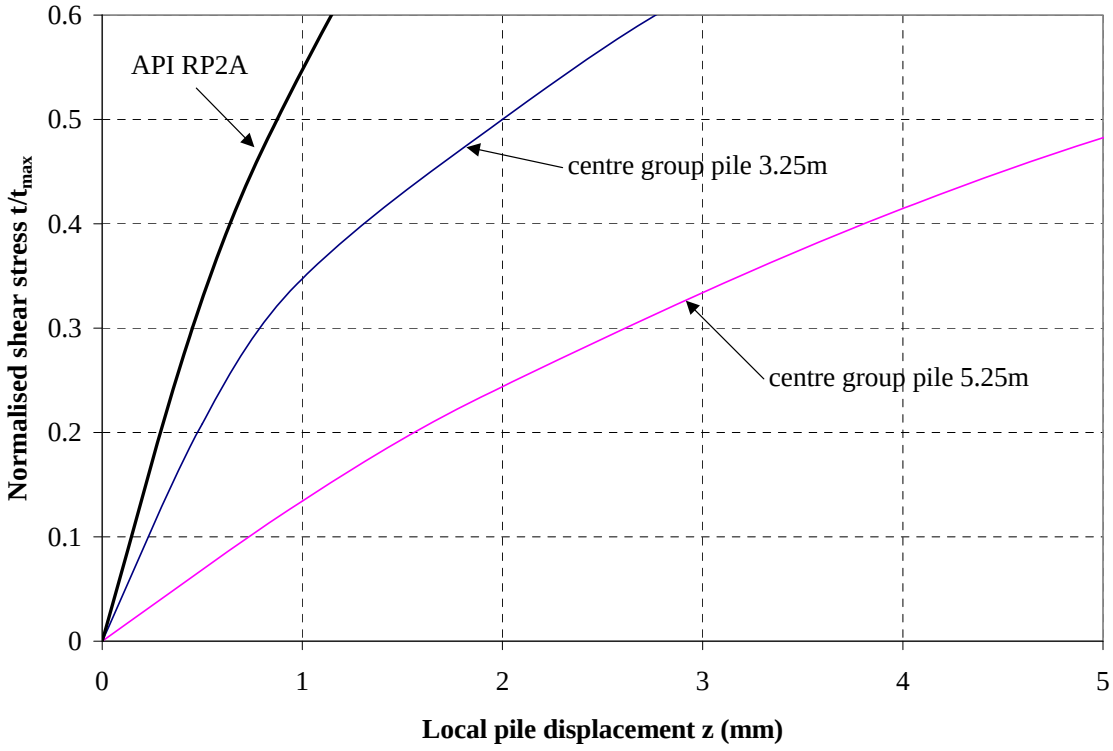

Figure 8-15 Comparison of measured centre group pile t-z curves with API RP2A (1991)

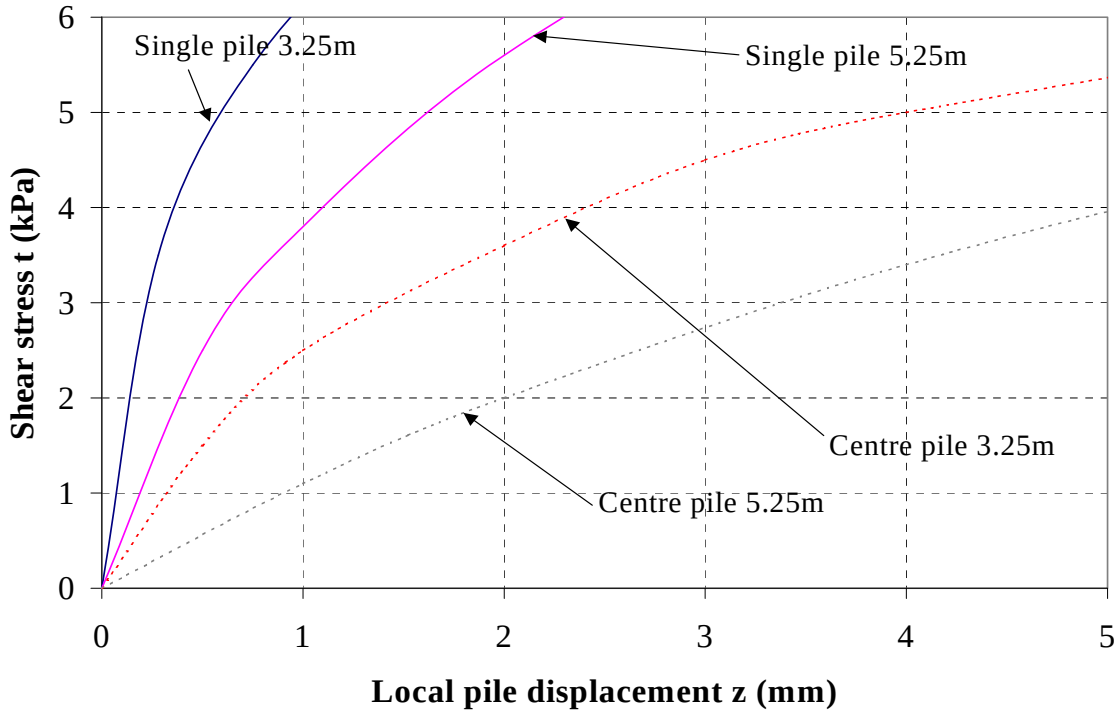

Figure 8-16 Comparison of measured single and centre pile t-z curves

8.4.6 Variation of Stiffness Efficiency with Pile Spacing

Individual group piles may behave as single piles (η_g =1) if they are spaced sufficiently far apart. However, for most practical situations, η_g reduces with closer pile spacing (i.e as s/B reduces). A projection[18] of this variation is presented (Figure 8-17) based upon the following information:

- Measured η_g values for groups with s/B=3 (TG1/s and CG1/s, Figure 8-7)
- Predictions of η_g for groups with s/B= 4.2 and 6.0. These predictions are based upon superimposing w/w_{max} values[19] derived from Figure 5-24 onto a single pile load-displacement plot[20]. These values are used to 'guide' the location of the η_g curve; and arise from the discussion on non-linear superposition follows in Section 8-6.

[18] based upon the Belfast 5-pile configurations and measured data
[19] The displacement of any non-loaded pile head (w) divided by the displacement at the head of the loaded pile (w_{max}).
[20] s/B=4.2 and s/B=6.0 correspond with distances from a corner pile to a near corner and the far corner respectively.

- Predictions from the equivalent pier method (for closely spaced piles)
- An assumption that group piles effectively behave as single piles if spaced at s/B>10.

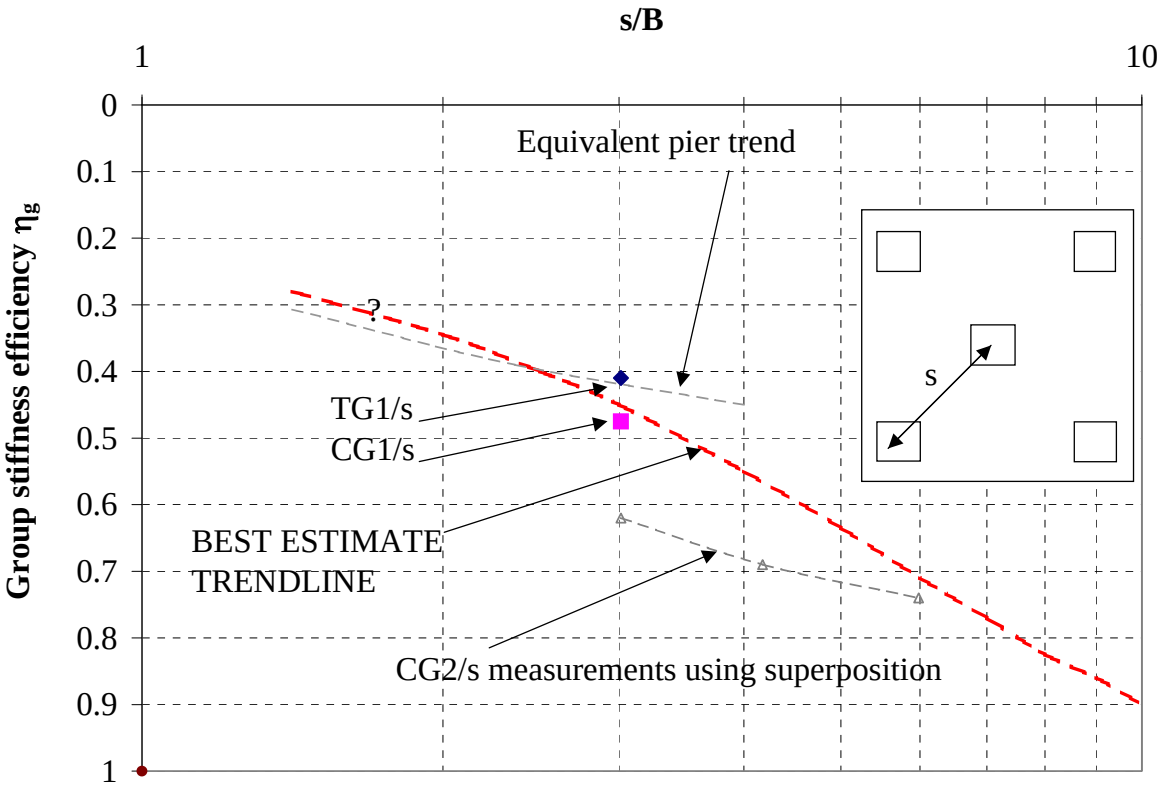

Figure 8-17 Variation of η_g with s/B for the Belfast test configuration

This function[21] provides a very useful estimate of the implications of choosing a particular pile spacing for the performance of a small pile group at working loads. For example, loading a group of five piles spaced at s/B=6 will only give rise to 50% of the settlement that the same piles would have if they were spaced at s/B=2. However, an 'optimum' spacing for the piles cannot be chosen on the basis of Figure 8-17 alone, since the cost of constructing the piles and pile cap is also an important consideration. The choice of pile spacing is not always prioritized in piling projects and the Belfast data provides an opportunity to assess whether this is a critical omission.

[21] Best fit curve (R^2=1): $\eta_g = 0.106444 + 0.127659(s/B) – 0.00384(s/B)^2 - 0.00011(s/B)^3$

The ideal spacing for piles in a group may be found by optimizing the stiffness efficiency of the group (η_g) per unit cost associated with the pile driving and casting the pile cap. The cost of driving a group of five piles (each 6m long) is independent of spacing, but the volume of reinforced concrete required for the pile cap increases with pile spacing and is the principal cost variable. The cost of the combined work (C) is given by:

$$C = (K_1 \times 6 \times 5) + (K_2 \times (s\sqrt{2} + 2B)^2)$$

where K_1 is the cost of driven piles per linear metre, K_2 is the cost per cubic metre of reinforced concrete (the pile cap is assumed to be 0.5m thick and overhangs the piles by B on each side) and s is the centre to corner pile spacing. Current Irish rates for K_1 and K_2 are 35 euro/m and 170 euro/m^3 respectively. The stiffness efficiency per unit construction cost η_g/C (normalized by its maximum value) is plotted as a function of s/B for the Belfast configuration in Figure 8-18.

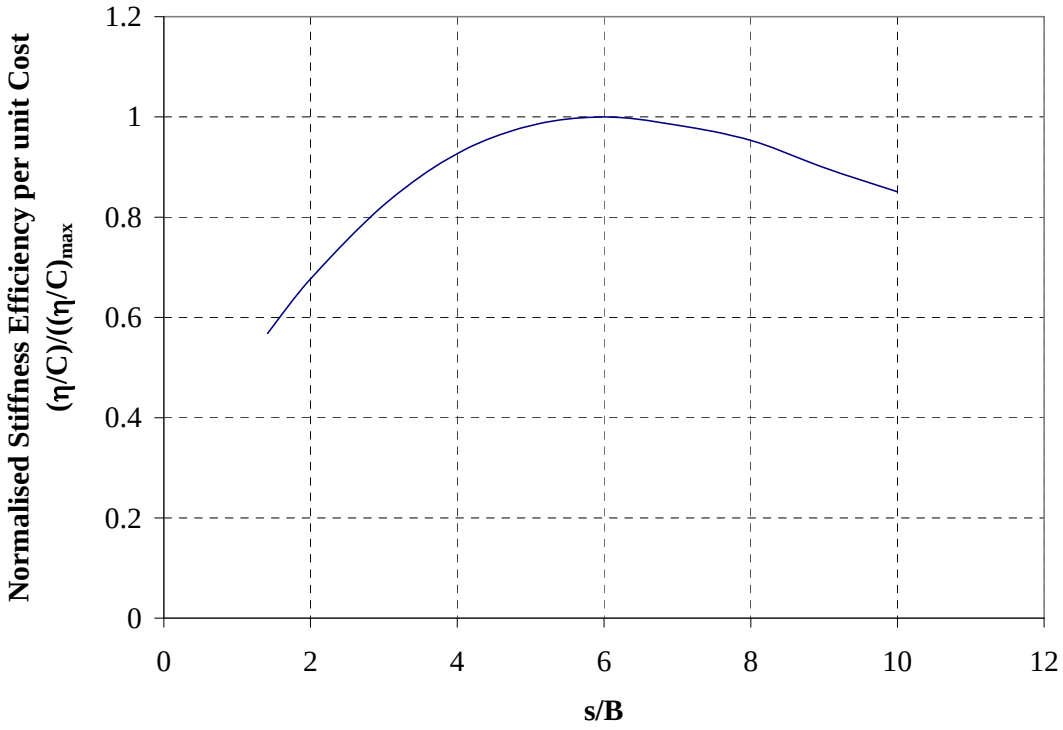

Figure 8-18 Stiffness Efficiency per unit Construction Cost as a function of pile spacing

Observations regarding optimum spacing of piles include:

(i) Small pile groups are most economically deployed with s = 6B±B.

(ii) Economy drops dramatically for piles spaced more closely than 4B.

(iii) The economy of the design appears much less sensitive to the use of spacings wider than optimum than it is to spacings closer than optimum.

(iv) Although the exact solution is sensitive to the relative values of K_1, K_2 and the η_g variation assumed, pile spacings less than 4B are not recommended for the Belfast conditions. However, no appreciable effects of adjacent pile installations have been observed in Belfast sleech. In situations where adjacent pile installations stiffen the soil around any group pile, it may then be preferable to space the piles more closely.

(v) Parametric studies with η_g values determined from PIGLET analyses (and cost functions of the form already proposed) indicate that the optimum pile spacing is insensitive to the number of piles (for small groups). However, the optimum pile spacing increases in accordance with an increase in pile aspect ratio (L/D).

8.5 The influence of stiffness non-linearity on pile group behaviour

8.5.1 Predictions of the load-displacement behaviour of group piles

The influence of soil stiffness non-linearity upon group pile load-displacement predictions emerges clearly from a comparison of a widely used linear elastic analysis method (PIGLET) and the non-linear SAFE/BRICK model[22] described in Chapter 7.

A value of G/c_u =140 for the *sleech* calibrates the PIGLET single pile response to match that of CS1/s at ≈30kN and reflects both installation disturbance and the additional strain due to loading. When the same value of G/c_u =140 is used for the group analysis, the group pile (spring) stiffnesses are grossly underestimated (Figure 8-19). In particular, the *relative* stiffnesses of the single and centre piles are predicted more realistically by the non-linear SAFE/BRICK model (Figure 7-10); this reflects the tendency of linear elastic soil models to overestimate interactive displacements. The discrepancy in the PIGLET predictions is likely to be greater for larger pile groups.

[22] Both assuming rigid pile caps

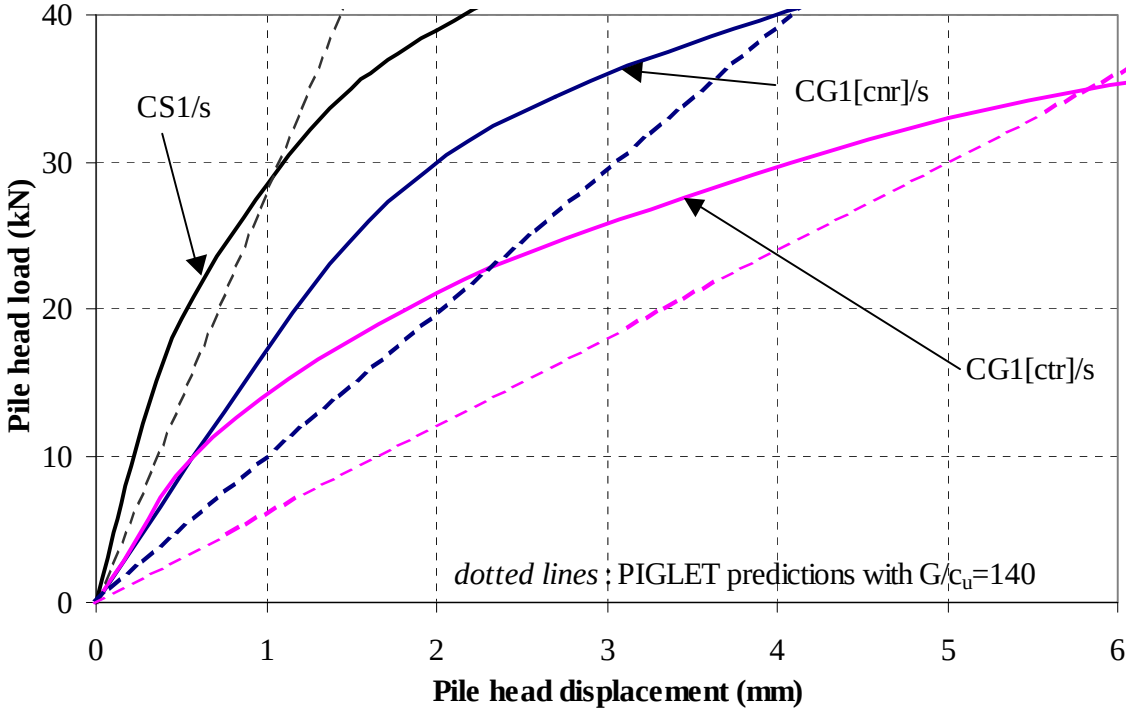

Figure 8-19 PIGLET predictions of the behaviour of CG1

8.5.2 Normalized settlement profiles/Interaction factors

The role of soil stiffness non-linearity may be represented alternatively through normalized settlement profiles (w/w_{max}) around a single pile (or preferably interaction factors) plotted as a function of s/D_{eq} (D_{eq} is the equivalent pile diameter; D_{eq}=1.128B).

A number of typical 'interaction factor' predictions for the Belfast piles are presented in Figure 8-20 as a basis of comparison with the measured interaction factors[23] (derived from Figure 5-24). The w/w_{max} predictions shown (representing the range of loads not exceeding 50% of the single pile capacity) are derived from:

- PIGLET's linear elastic expressions
- SAFE/BRICK single pile analysis (Figure 7-11)
- Simple numerical model single pile analysis (Figures 7-15 and 7-16)

[23] The error bars shown reflect the accuracy of the Belfast interaction factor measurements

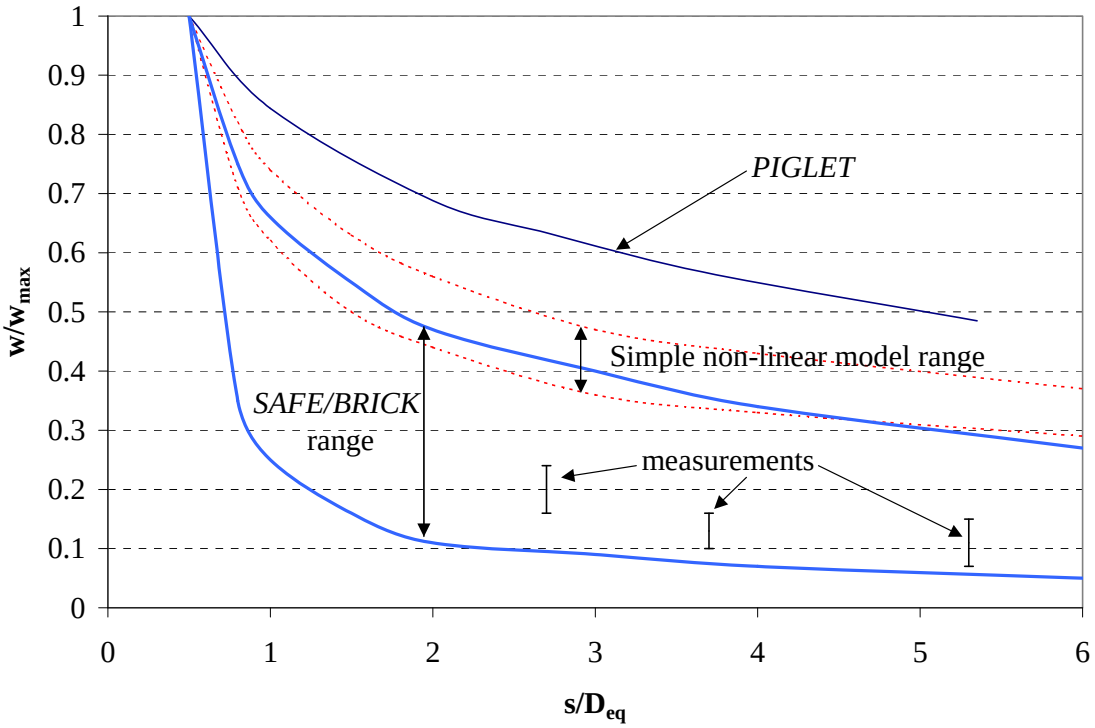

Figure 8-20 w/w_{max} predictions for Belfast piles

Important observations from Figure 8-20 include:

- The measured w/w_{max} values suggest that the ground settlement due to pile loading appears to be concentrated close to the pile shaft and has reduced significantly by $s/D_{eq} \approx 2.5$. The non-linear soil models capture this phenomenon better than PIGLET.
- At common pile spacings ($2.5 < s/D_{eq} < 6$), PIGLET overpredicts the measured interactive settlements by a factor of 3 to 5.
- Neither SAFE/BRICK nor the simple numerical model fully capture the degree of stiffness non-linearity exhibited by the sleech (although SAFE/BRICK is better), and thus may still slightly over-predict the interactive settlements. However, they provide much more realistic predictions than linear elastic analyses and suggest that even the simplest of non-linear analyses is likely to be much more informative than linear elastic ones.

The measured Belfast 'interaction' factors are compared in Figure 8-21 with typical interaction factors from other sources, which include:

- Settlements on non-loaded piles due to adjacent pile loading (Pellegrino 1983, Figure 2-26). The ranges shown represent the reduction in the value of w/w_{max} as the load increases.
- FE prediction of w/w_{max} around a single pile using the LPC2 soil model (Jardine et al 1986) which is strongly non-linear.

Despite differences in pile dimensions and subsoil conditions, all three sets of data are strongly consistent and serve to emphasise the importance of modelling the soil as a non-linear material if appropriate group predictions are sought. In addition, this data shows that interactive displacements may have diminished substantially by $s/D_{eq} \approx 3$.

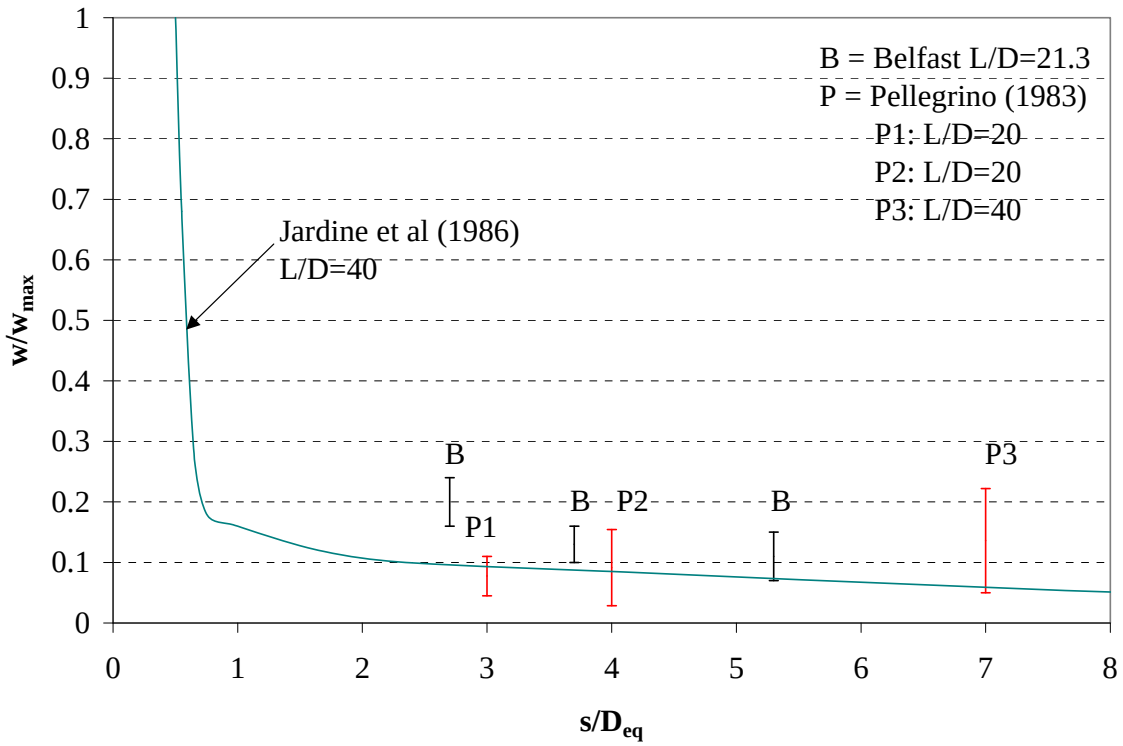

Figure 8-21 Normalized settlement profiles for non-linear soils/soil models

In this instance, the method of Caputo and Viggiani (1984)[24] (in which each pile's own load-displacement behaviour is non-linear but interactive displacements are linear elastic) may provide an acceptable estimate of group performance in certain cases. Once such case might be if group piles were subjected to a strong positive installation effect[25]; interaction would be reduced due to soil stiffening within the group perimeter, leading to the assumptions of this method being more plausible.

8.5.3 Factors influencing Settlement Profiles/Interaction Factors

The accuracy of the measured Belfast interaction factors was such that the dependence of w/w_{max} on the level of applied load was not obvious; it would be reasonable to assume it to be relatively constant with load level. However, SAFE/BRICK and the simple numerical model predictions (based upon non-linear *sleech* behaviour) and Pellegrino's measured interactive settlements (Figure 2-26) suggest that the greater the load applied to the group piles, the less the piles interact. However, such a relationship between load level and interaction may not be unique.

In the case of driven piles, any interaction factor predictions based upon settlement fields around single piles cannot account for 'local' modifications to w/w_{max} due to intervening piles. Based upon a comparison between the measured Belfast data and predictions by Jardine et al (1986) in Figure 8-21, it is tentatively suggested that the measured w/w_{max} value at $s/D_{eq}=2.7$ ($s/B=3$) is slightly higher than might be expected. One possible explanation would be that the datapoint at $s/D_{eq}=2.7$ represents a settlement measurement at the head of the load-free centre pile around which the soil may have been softened most by installation. This remains conjectural given the accuracy of the measured w values.

8.6 'Self-contained' predictions of pile group behaviour

Sufficient data has been assimilated from the test programme (single pile tests, corner group pile loaded alone and full group tests) to investigate some potential (self-contained) approaches to predicting pile group response. Two approaches are suggested:

[24] used in GRUPPALO
[25] not the case for pile groups driven in Belfast clay

- A simple model of how shear stress is transmitted radially through the soil around a pile
- Superposition of non-linear load-displacement curves

8.6.1 Simple interaction model

The simple interaction model applies to identical piles embedded in homogeneous soil (i.e. no differential driving effects within the group perimeter). When load is applied to the head of a pile, shear stresses are transmitted outwards from the pile shaft in all directions into the surrounding soil. Neighbouring piles therefore assume a proportion of this load; the proportion is determined by the angle subtended from the loaded pile to the load-free pile (A) and calculated as $A/360^o$ (Figure 8-22).

The model makes the distinction between the *overall* capacity of a group pile (the same as that of a single pile) and the amount of load that is applied *directly* to the pile to bring it to ultimate conditions (see Section 2.6.1). The difference is due to load interaction. The source of the interactive loading on the centre and a corner pile is shown schematically in Figure 8-23. If the (average) *applied* load on one corner pile is P_E and the applied load on the centre pile is P_C:

(i) The extra load on the centre pile due to the corner piles being loaded is:

$$0.295P_E$$

(ii) The extra load on a corner pile due to the centre pile and other three corner piles being loaded is:

$$0.074P_C + 0.122P_E$$

These interactive displacements are added to the centre and corner pile responses measured in TG1/s and CG1/s and compared with the measured single pile behaviour (at a particular displacement). The corner and centre pile reconstructions are shown in Figures 8-24 and 8-25 respectively. When carrying out these reconstructions, due account was made for the fact that the centre and corner piles were at different stages of loading throughout the group tests (i.e. P_C is not necessarily equal to P_E at any stage of testing).

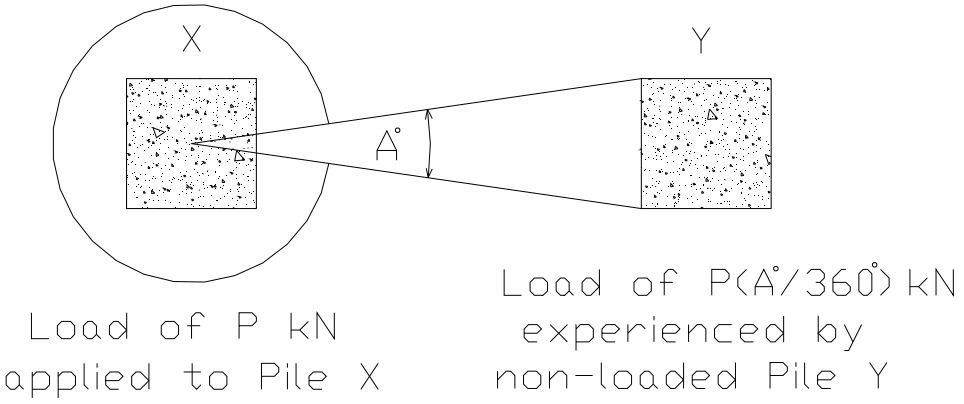

Figure 8-22 Simple interaction model for a pile pair

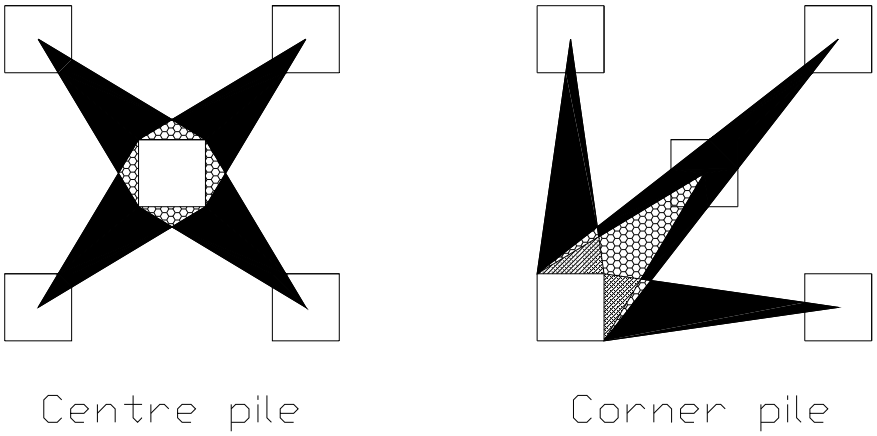

Figure 8-23 Simple interaction model for centre and corner piles

TS1/s and CS1/s provide the relevant single pile comparisons. On the basis of these figures, the following observations may be made:

(i) If single pile capacity is known/estimated from a load test on a contract pile, the simple interactive model is likely to provide a good estimate of the capacity of the centre and average corner group piles (i.e the reconstruction process used in

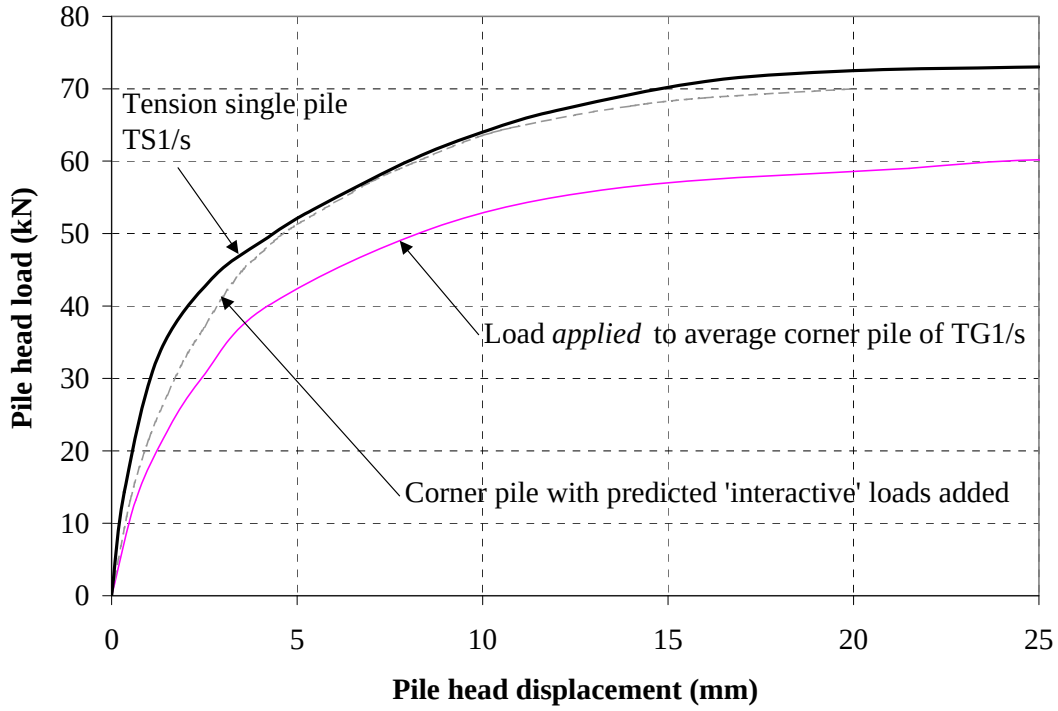

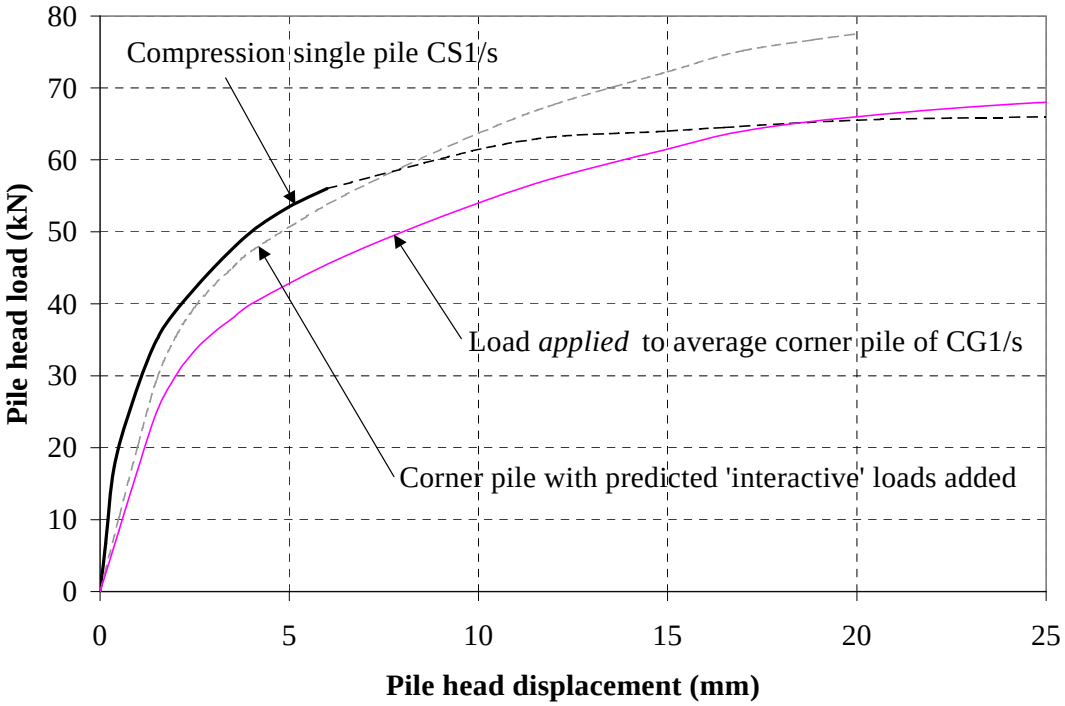

Figure 8-24 Interaction model applied to corner piles

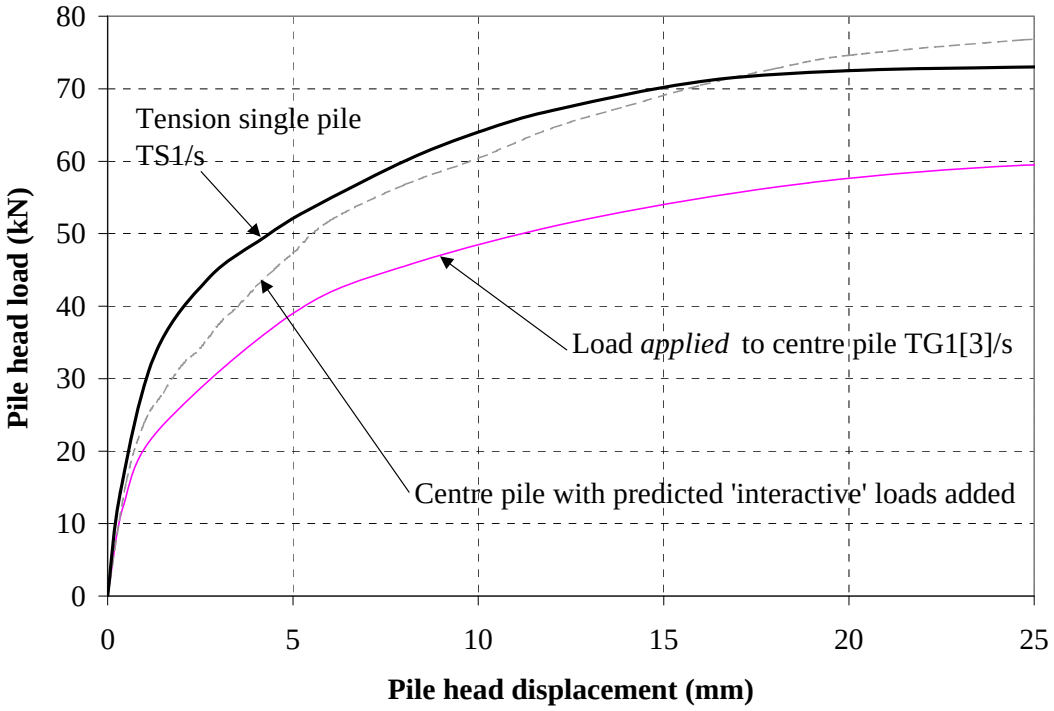

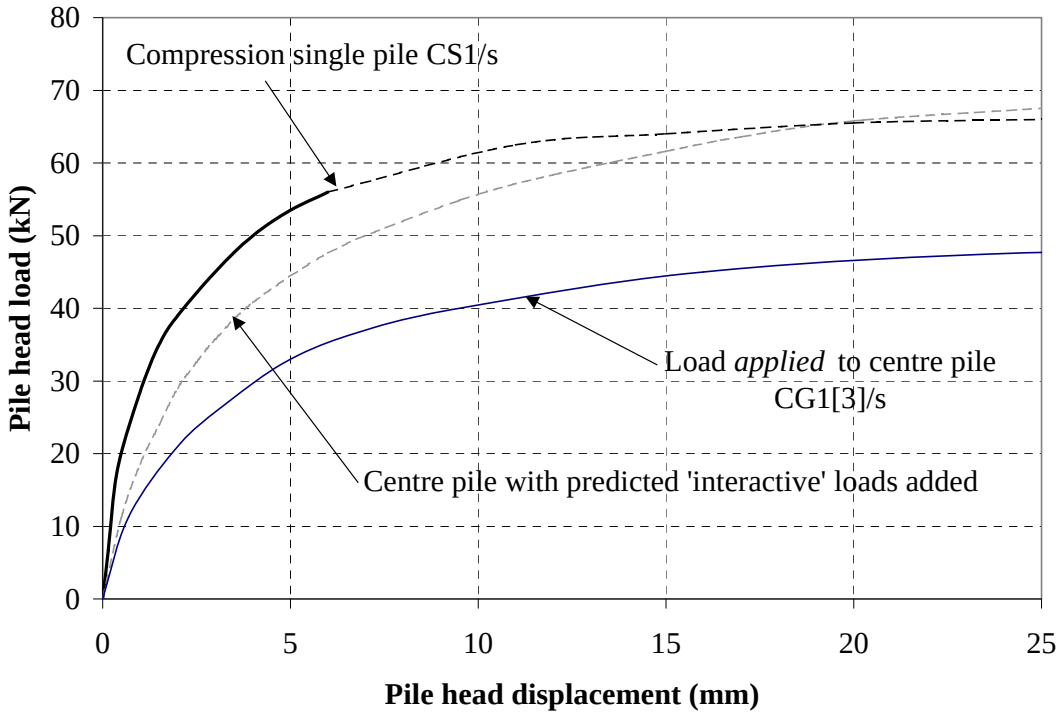

Figure 8-25 Interaction model applied to centre piles

reverse). However, the ‘equivalent spring stiffness’ of the group piles would be over-predicted at typical working loads.

(ii) The capacity of the compression group corner pile is poorly predicted by this method. This is due to the fact that the measured corner pile ‘capacity’ is high in relation to the reference single pile. Potential anomalies with pile ‘capacity’ are discussed in Section 8.7.

The interaction model described does not consider the bearing that adjacent pile driving may have on the performance of a group pile under load. However, Figure 5-22 probably suggests that there are no such installation effects for a corner group pile and this is borne out in the success of the predictions presented. The success of the centre pile predictions may also indicate that installation effects on the centre pile differ little from that expected for a single pile, and therefore that group action in a soft sensitive lightly overconsolidated clay is governed predominantly by load interaction and not installation effects.

8.6.2 Group Settlement estimates based on Superposition

Linear superposition is a theoretically justifiable technique used in many branches of engineering. Programs such as PIGLET and GASGROUP superimpose interactive displacement predictions (from neighbouring piles) onto single pile load-displacement curves as a basis of group settlement prediction. Superposition is also used in conjunction with elastic-plastic soil models (i.e. DEFPIG) but is only valid until yield takes place for the first time at the shaft of one of the group piles.

However, the use of superposition with real non-linear soil has no theoretical basis. While the non-linear load transfer curves used in PILGP1, for example, may represent single pile behaviour well, superposition of such non-linear data is strictly incorrect. Tests on a row of two and three driven piles by Cooke et al (1979) suggests that superposition is a successful way of anticipating the rows’ performance under load. Measurements from this Thesis enable the suitability of superposition to be assessed for small groups of closely spaced piles displayed marked non-linearity.

For any given *applied* pile load, Figure 8-26 presents a comparison of (i) and (ii) below:

(i) The displacement of a corner pile when loaded alone (CG2[2]/s) added to estimated displacement contributions due to the other four (centre and three corner) piles[26]. Figure 5-24 shows the displacements on the non-loaded piles when CG2[2] was loaded; a reciprocal relationship is assumed for each pile-pair whereby the extra displacement on CG2[2] when another pile is loaded is also assumed to be that in Figure 5-24.

(ii) The actual displacement of a corner pile (average corner pile of CG1/s) when loaded as part of the group.

The use of non-linear superposition in this case results in an under-prediction of the corner group pile settlement, or alternatively an over-prediction of its equivalent spring stiffness.

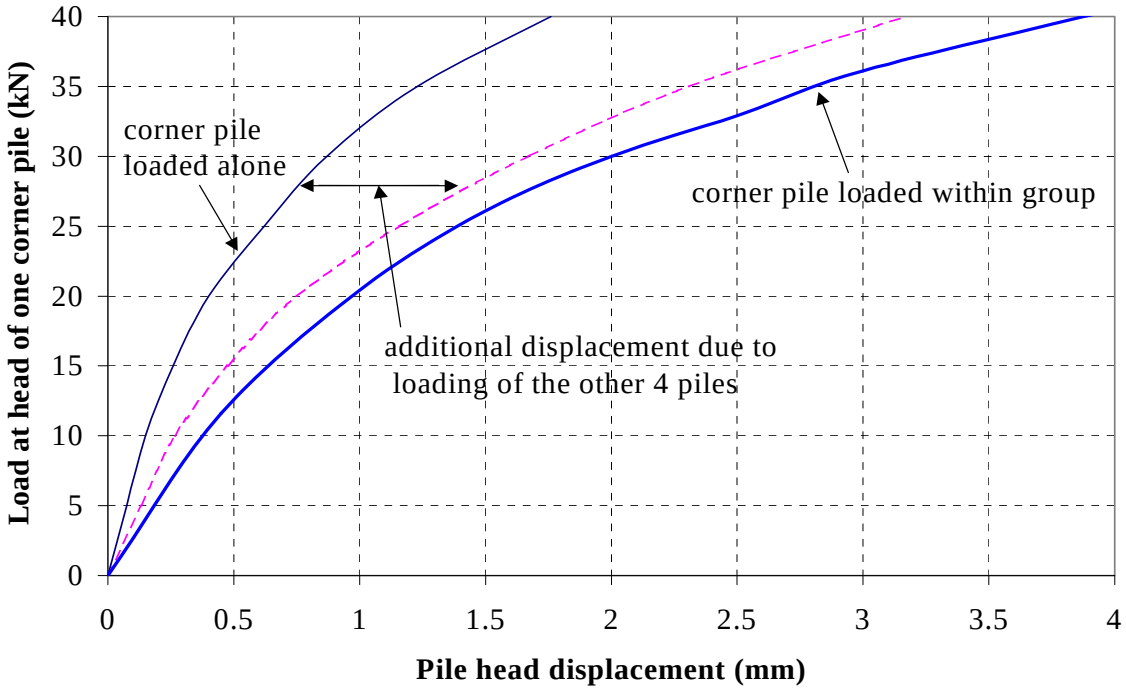

Figure 8-26 Non-linear superposition for corner pile of compression group

[26] Flexible pile cap assumed

An equivalent 'reconstruction' is presented for the centre pile of the group in Figure 8-27. In this instance, the centre pile was not loaded alone so the CG2[2]/s load-displacement curve is used as a substitute[27]. While the outcome remains the same (i.e. superposition underpredicts interactive settlements), the discrepancy is greater than that in Figure 8-26. While it is unlikely that the error in superposition is 'consistent', it is also possible that the zone around the centre pile may be slightly softer than around the corner pile (in which case a softer response for the centre pile loaded alone would have been more appropriate).

Non-linear superposition is inappropriate for small pile groups (which have neutral or small negative installation effects) and such predictions are likely to worsen as the scale of the group grows. However, the error entailed is likely to reduce as the piles are spaced further apart (and may become plausible at wide spacings) and this has been exploited in developing the η-s/B relationship of Figure 8-17.

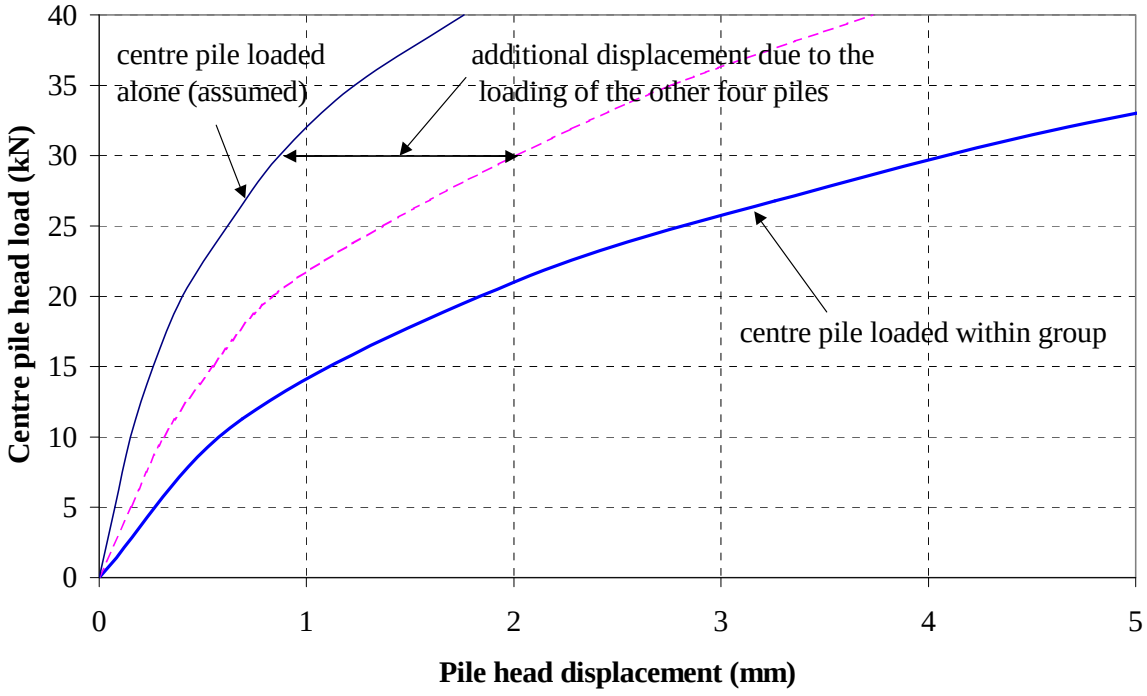

Figure 8-27 Non-linear superposition for centre pile of compression group

[27] This is valid if the soil surrounding the corner and centre piles of the group is affected *equally* by the installation of the group.

The SAFE/BRICK model devised in Chapter 7 provides a useful alternative for checking non-linear superposition, but without the complication of 'differential' installation effects on soil stiffness within the pile group. Installation effects cannot be modelled so the soil stiffness surrounding the piles is effectively homogeneous (i.e. bored piles). The components of Figure 8-28 include:

(i) The pile head load-displacement behaviour of the centre pile of the group when loaded alone (effectively a single pile prediction) *plus* the additional displacements at the head of the centre pile due to loading of all corner piles alone.

(ii) The pile head load-displacement behaviour of the centre pile when the centre and corner piles are loaded simultaneously. The same loads are applied to all piles.

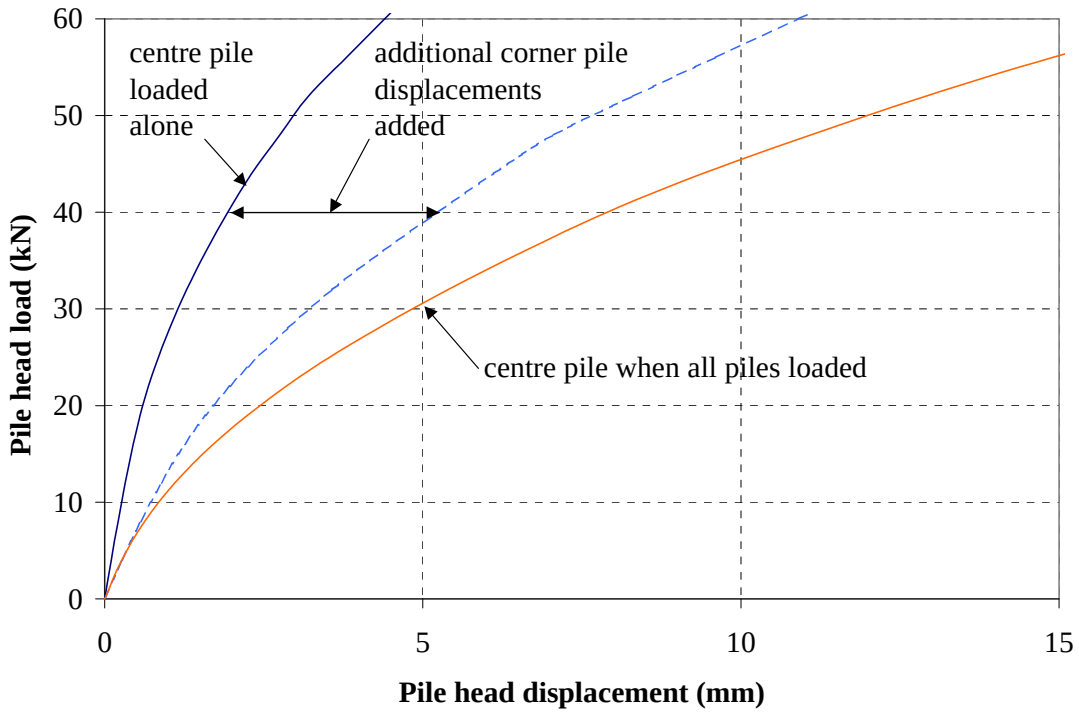

Figure 8-28 Non-linear superposition using SAFE/BRICK

The model findings are consistent with those from the measured data. The four corner piles have been idealized as a uniform cylindrical annulus in the SAFE/BRICK model; for real non-symmetrical groups, the disparity of Figure 8-28 may in fact be worse.

8.7 Examination of the Belfast data in the context of case histories

Some of the findings from the Belfast field tests are examined in the context of a number of case histories of driven and bored (friction) pile groups in clay soils.

8.7.1 The effect of neighbouring pile installations

The soil immediately surrounding the centre pile of a group is clearly modified by that pile's own installation. However, this Thesis is a source of information (both measurements and predictions) to indicate whether the driving of the adjacent corner piles exert any further changes to the state of the soil around the centre pile.

The following evidence has arisen:

- The value of σ_{hc} measured on the centre pile of CG1/s falls slightly below that predicted for an equivalent single pile (Section 8-3) and σ_h does not change appreciably during loading. It is therefore reasonable to suggest that adjacent installations may cause either a neutral to small negative effect on the soil stiffness around the centre pile.
- The measured w/w_{max} value at the centre pile location s/D_{eq}=2.7 (Figure 8-21) appears high in relation to the trend indicated by the other two (corner pile) datapoints. A slightly softer zone of material surrounding the centre pile would be compatible with this observation.
- The poor success of non-linear superposition in predicting the centre pile performance (Figure 8-27) may suggest that had the centre pile been loaded alone, it might have behaved less stiffly than the measured corner pile response. This, again, is in keeping with above observations.
- Pile capacities predicted by the load interaction model (Section 8.6.1) show no evidence of an installation effect over and above that expected for a single pile.

Supporting evidence may be found from Figure 5-22, which suggests that the corner pile of a group is not significantly affected by neighbouring installations.

Overall evidence suggests that the neutral to small negative installation effect is quite small in relation to the effects of load interaction, which defies the commonly held belief that adjacent pile driving stiffens the soil within the perimeter of a group leading to enhanced performance under load. Fleming et al (1992) suggest that group piles in sensitive clay may be subjected to 'negative' installation effects, but evidence of this Thesis and Section 2.13.1 suggests that the effect of adjacent pile installations is not solely a function of the sensitivity. For instance, Koizumi and Ito (1967) and O'Neill et al (1982) report neutral installation effects in overconsolidated clay, with high soil sensitivity noted in the former case. However, although the pile tests of Brand et al (1972) were conducted in lightly overconsolidated sensitive marine clay, neighbouring pile installations appear to have a stiffening effect on the soil prior to loading.

8.7.2 Pile Capacity

Some examples presented in Section 2.13.1 have served to highlight the difficulties faced by designers endeavouring to predict the capacity of group piles. There appear to be certain inconsistencies between pile types and soil conditions, i.e. bored pile groups by Franke et al (1994) and Cooke et al (1981) in similar overconsolidated soil conditions (Frankfurt and London Clays respectively) lead to very diverse outcomes in terms of capacity efficiency.

In addition, the Belfast tests show how a pile cap can dictate the load sharing among piles. The capacity of the centre pile of ('rigidly' capped) CG1/s was found to be ≈25% lower than a compression single pile, while the capacity of the centre pile of ('flexibly' capped) TG1/s was ≈12% lower than the (most comparable) tension single pile, despite equally spaced piles in both instances. Other impediments to comparison of single pile and group capacities lie in the absolute (or relative) definition of capacity in each instance. The Belfast tests and other data show that group piles require greater displacements to mobilize peak shaft and base stresses and some account must be made for this when predicting group pile capacities.

8.7.3 Pile Stiffness

The case histories provide little guidance in providing an overview of the factors affecting pile capacity, and many anomalies and inconsistencies emerge. However, the same database provides a much more consistent measure of the effects of group action through the load-displacement data at working loads. The pile tests of this Thesis and those listed in

Author(s)	Soil Conditions	Type[28]	N	L (m)	D (mm)	L/D_{eq}	s/D_{eq}
McCabe (2002)	LOC soft organic clayey silt	D	5	6	250sq	21.3	2.7
Thorburn et al (1983)	LOC soft very silty clay	D	55	27	250sq	102.8	7.1
Brand et al (1972)	LOC Bangkok soft sensitive marine clay	D	4	6	150	40	2
		D	4	6	150	40	2.5
		D	4	6	150	40	3
Koizumi & Ito (1967)	Sensitive OC organic silty clay	D	9	5.55	900	18.5	3
Trofimenkov (1977)	Stiff silty clay	B	6	12	1000	12	2
		D	7	4.5	338.5	30.4	1.8
		D	9	12	395	13.3	3.35
Cooke et al (1980)	OC London Clay	J	3	5	168	29.8	3
Cooke et al (1981)		B	351	13	450	28.9	3.6
Tortsman (1973)	OC Frankfurt Clay	D	430	nr	nr	nr	nr
Franke et al (1994)		B	40	30	nr	nr	nr
Goossens and van Impe (1991)	Interbedded stiff clays and sands	B	697	13.4	520[29]	25.77	4

Table 8-4 Some published case histories of friction pile groups in clay (nr = data not reported, OC = overconsolidated, LOC =lightly overconsolidated)

[28] B=Bored, D=Driven, J=Jacked
[29] 800mm diameter under-ream

Table 8-4 (and Figure 8-29) all indicate that a group pile settles further than a single pile at the adopted/expected working load levels (i.e $\eta_g<1$), irrespective of where its capacity lies in relation to that of a single pile.

Moreover, it has been shown in Section 8-4 that the extent of load interaction on any pile may be clearly reflected by its stiffness at working loads once the pile cap flexibility is taken into account. However, the distribution of load among the group piles at ultimate conditions (i.e capacity) is directly linked to the structural performance of the cap.

Accordingly, the load-displacement behaviour of ten driven/jacked and four bored friction pile groups in clay listed in Table 8-4 are examined. The global group stiffness efficiency η_g (as defined in Section 8.4.1/8.4.3) is plotted in Figure 8-29 as a function of the proportion of single pile capacity[30] mobilized per pile in the group. For any case history, several data points are plotted where complete group load-displacement curves have been made available, and one point is given where only working load settlements have been reported. A few of the case histories relate to piled raft foundations; in these situations, the data reported allowed the load carried by the piles to be isolated from the total load (including that carried by soil contact pressures beneath the raft).

Observations from Figure 8-29 include:

- Quite a large range of η_g values exist ($0<\eta_g<1$) which reflect in part the number of piles in each group.
- The Belfast data (average of Figure 8-7) and other case histories with continuous group data suggest that η_g remains relatively constant with load. On the other hand, the group tests of Koizumi and Ito (1967) show that the relative non-linearity of single and group piles differ.

The 'capacity' efficiency of a pile group is believed to be related to some power of N, the number of piles in the group. Fleming et al (1992) suggests that this power is [0.3-0.5] for friction piles and Poulos (1989) suggests [0.4-0.6]. A parametric study using the linear

[30] Reasonable estimates are made or error bars are shown where the single was not loaded to 'failure'.

elastic interaction factors of PIGLET suggest that η_g is inversely proportional to $N^{0.5}$. $N^{0.5}\eta_g$ replaces η_g in Figure 8-30 and the following observations may be made:

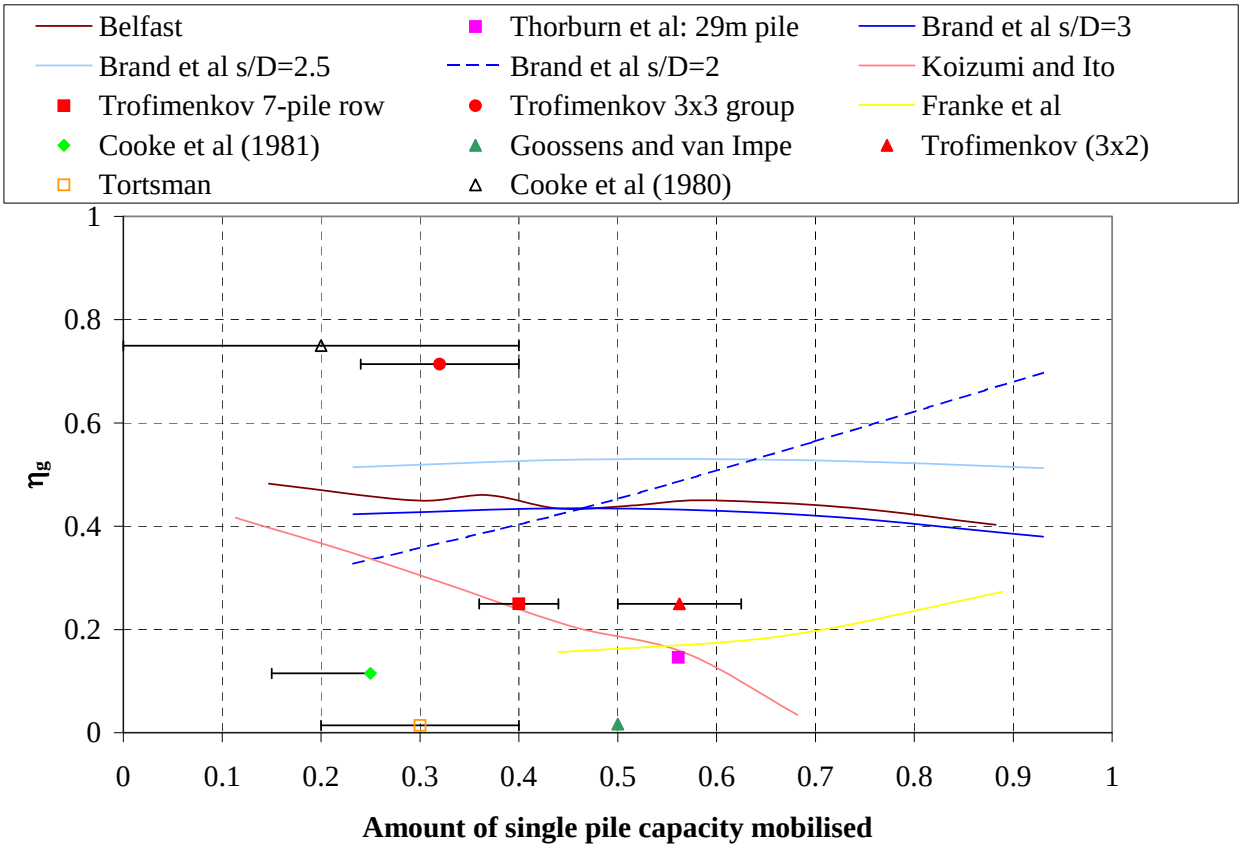

Figure 8-29 Values of η_g for pile group case histories in clay

(i) The large range of η_g values in Figure 8-29 is condensed considerably within the $N^{0.5}\eta_g$ framework, particularly at working loads of 30-50% of single pile capacity.

(ii) A preliminary design estimate of the settlement of a group of piles under working load may be given by:

$$w_g = (0.8 \pm 0.3) w_s \sqrt{N}$$

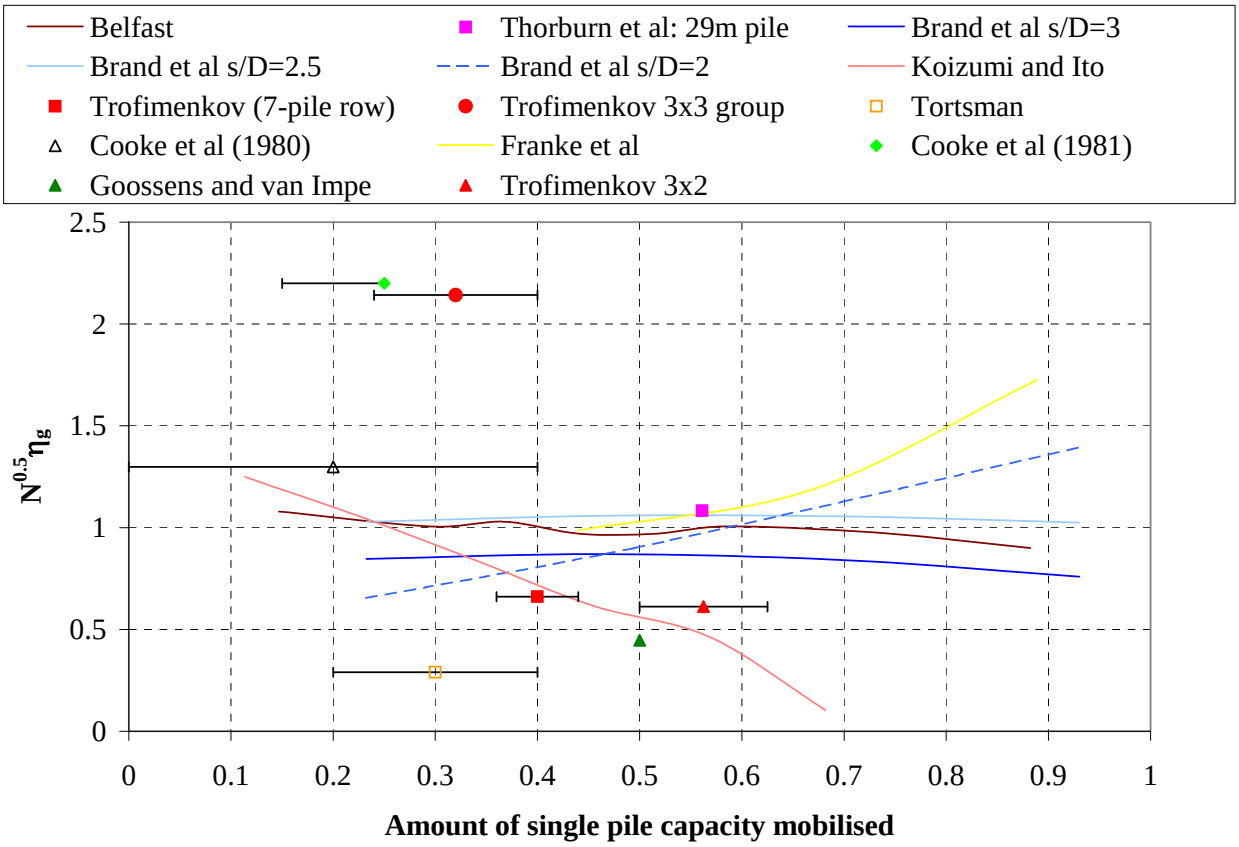

Figure 8-30 Values of $N^{0.5}w_s/w_g$ for pile group case histories in clay

The results of the Belfast pile groups TG1/s and CG1/s are typical of the range of values bounded by the above equation.

(iii) Careful analysis of the dataset has shown there to be no obvious systematic dependence upon other factors such as s/D[31], L/D (including under-reaming), pile compressibility or the installation method. Further refinement would also require a detailed understanding of the soil behaviour.

[31] The majority of s/D values in the database were similar [2.5-4]

Chapter 9

Conclusions

The static and cyclic pile load tests described in this Thesis form part of an ongoing research programme to investigate driven pile behaviour in the soft clay at Kinnegar near Belfast. Extensive site investigation data has been assimilated for this purpose by Trinity College Dublin since 1997, which reveals the Belfast *sleech* to be quite similar in consistency to the clay/silt at the National Soft Clay Test Site at Bothkennar, Scotland. The bulk of the *sleech* deposit consists of a soft sensitive clayey silt of estuarine origin, which is very lightly overconsolidated material and exhibits medium to high plasticity. Some notable differences between the Belfast and Bothkennar materials include different clay fraction compositions and different residual friction angles (ϕ'_{res}); the latter explains the greater maximum shear stresses at Bothkennar than at Belfast.

A proper and consistent interpretation of the pile test data required knowledge of some time-related influences on pile capacity specific to the Belfast deposit. Information presented in this Thesis indicates:

- The absence of undisturbed aging effects (after full equalization of the horizontal effective stresses caused by driving) unlike other clay sites such as Haga in Norway. Therefore, there are no apparent economic benefits to be gained by early mobilization of the piling rig to site for Belfast projects.
- Two distinct effects of pile reloading: (a) immediate (undrained) reloading before setup of pore pressures takes place causes a 10-15% reduction in pile capacity, (b) long-term (drained) reloading (observing between four months and one year from initial shearing) causes a capacity gain which is typically ≈27%.

The uniqueness of the current test programme lies in the fact that full-scale groups were brought beyond typical working loads close to ultimate conditions, complete load-displacement curves have been measured for single and individual group piles, and direct measurements of interactive settlements have been made. Radial horizontal stress measurements and shear stress distributions provide further insight into the mechanisms of group action.

It is commonly assumed that the ground is stiffened by neighbouring pile installations, so that the loss in capacity efficiency accountable to load interaction may be somewhat counteracted in advance by positive installation effects. Data presented in this Thesis, particularly measurements of σ_h for a centre group pile, suggest that surrounding piles (at s/B=3) have a neutral or perhaps a small negative effect (<10%) on pile capacity. In either case, the effects of load interaction between the piles is the dominant source of 'group action' in this instance. Evidence from testing a corner pile alone suggests that the effect of adjacent pile driving on the corner pile performance is insignificant. Further informative work would include a load test on the centre pile of a group alone (not performed for this Thesis) for evidence of reduced/unchanged capacity compared with a single pile. Similar exercises could be performed for groups with more than two characteristic piles (i.e 3^2 groups).

When a group of closely spaced piles is installed, the maximum total stresses and peak excess pore pressures at the group centre are greater than expected for an equivalent isolated pile. However, the total stresses are transient and return very quickly to values *below* single pile values, suggesting that there is no 'accumulation' of total stress due to multiple installations. This total stress deficit immediately after group installation has diminished by the time the soil has fully equalized.

The strong parallels between tension and compression loading are an interesting feature of the Belfast load test programme. Once appropriate corrections have been made to the measured load-displacement responses, the ultimate shaft capacities of (adjacently positioned) tension and compression single piles at 25mm displacement were found to be the same. Pile stiffnesses at working loads are very similar. Similarities in terms of pile group behaviour include:

- Comparable shaft capacities of the groups (at an arbitrary displacement of 50mm)
- The *stiffness* efficiencies of tension and compression groups were found to be consistent with each other and lie between 40% and 50%, regardless of load level.
- The stiffnesses of the *characteristic* piles of the tension and compression groups are also very similar when considered as a function of the average group displacement

reflecting the stage of loading. Although the pile cap did not behave consistently from test to test, it has been shown nevertheless that the effect of load interaction is independent of loading direction.

- The stiffness of the centre pile in a group is typically 35-40% of that of a single pile (at a factor of safety of 2.5 on ultimate conditions).

Groups of the scale tested in this Thesis are typically used as support for columns, in which case the exact spacing of these piles is of interest. A best estimate of how the stiffness efficiency of a five-pile group varies with the spacing to width ratio has been made ($2B<s<10B$). For instance, this curve indicates that piles spaced at s/B=6 settle by half the amount that they would if spaced at s/B=2. However, the choice of an optimum spacing for the pile group must also consider the cost of pile driving and cap construction. For piles in soil with no appreciable installation effect, piles should be spaced no closer than s/B=4, with little variation in the economy associated with any choice of spacing between s/B=4 and s/B=8. Closer pile spacing may be preferable in soil which is stiffened (i.e positive installation effects) by adjacent pile driving.

Stiffness efficiency provides a good gauge of pile group performance, but capacity efficiency may be more difficult to predict; being largely influenced by the flexibility of the pile cap and relative displacements of the single and group piles.

Arguably the most important step in modelling the behaviour of a group of piles is the choice of an appropriate non-linear soil model. In reality, the effect of pile loading in real soil is concentrated close to the pile shaft, and soil displacements have diminished considerably by $s/D_{eq}=2$. Linear elastic methods do not predict this sharp decay, with the result that interaction is strongly overpredicted, and load sharing within the group may be unrealistically biased towards the corner piles[1]. PIGLET predicts interaction factors which are at least three times as great as the Belfast measurements over the range of commonly deployed spacings, although not all soils exhibit the same degree of non-linearity as the *sleech*. Although the BRICK non-linear soil model developed in the course of this Thesis

[1] Assuming a rigid cap

has been based upon limited small strain stiffness measurements, its success shows that even unsophisticated attempts at representing non-linearity (i.e. a multi-linear model) may be much more fruitful than linear elastic predictions.

Although the use of non-linear soil models is encouraged when predicting pile group behaviour, the use of non-linear superposition is not suitable for closely spaced pile groups. It may however, provide a reasonable estimate for pile groups for which s/B>6. The capacity of small pile groups may be predicted reasonably well by a simple model which computes the interactive load transmitted to any group pile by the angle subtended between each pile pair.

The interaction factors corresponding to any pile spacing are commonly assumed to be independent of load level or horizon along the pile shaft. Evidence from the SAFE/BRICK model suggests that neither effect may be true, but the significance of this finding will depend upon the spacing of the pile adopted and the extent of non-linearity of the soil. Further tests of the type conducted in this Thesis (i.e. the corner pile load test) would help investigate this further.

A small database of friction pile groups in clay provide information on the stiffness efficiencies of pile groups at working loads. The range of measured stiffness efficiencies is quite large but condenses considerably when account is taken for the size of the group. The degree of interaction was assumed to be proportional to the square root of the number of piles in the group. Further attempts to refine the scatter were unsuccessful, as no systematic dependence was found between the stiffness efficiency and parameters such as the pile spacing, pile aspect ratio, pile compressibility and pile construction/installation method (bored or driven). However, the data allows a reasonable first attempt to be made at estimating the stiffness efficiency of a pile group. Strong emphasis should be placed upon expanding the database of available case histories as this provides the only true method of appraising and developing group prediction methods.

The results of one-way tension cyclic load tests on single piles and pile groups may be summarized as follows:

- Cyclic tension loading leads to a degradation in the available shaft capacity of single piles and pile groups. The level of this degradation depends on the peak cyclic tension loads applied; however it is not significant when this peak tension load is less than ≈50% of the static tension capacity of the piles. Well-designed piles (with a factor of safety in excess of 2 against ultimate failure) are therefore not likely to experience a reduction in their available shaft capacity.
- Piles that are brought to failure by the application of high levels of cyclic loading (i.e. with peak loads greater than about 50-70% of the tension capacity) suffer a reduction in shaft capacity; reductions of up to ≈25% for single piles and up to ≈35% for group piles were inferred from the test results. The higher level of degradation for the group piles is notable and is worthy of further research.
- The rate of accumulation of permanent pile displacements during cycling is also strongly related to the peak cyclic load level. Rates of accumulation increase dramatically as the peak cyclic load approaches the (dynamic) pile capacity.

References

Almeida, M., Danziger, F., and Lunne T. (1996) The Use of the Piezocone Test to Predict the Axial Capacity of Driven and Jacked Piles, *Canadian Geotechnical Journal*, 33, 23-41

American Petroleum Institute (API) (1993) RP2A: Recommended Practice of Planning, Designing and Constructing Fixed Offshore Platforms, *Working Stress Design, 20th Edition, Washington* 59-61

Baligh, M.M. (1985) Strain Path Method, *Journal of Geotechnical Engineering Division*, ASCE 111, No. GT9, 1108-1136

Banerjee, P.K. and Driscoll, R.M (1976). Program for the analysis of pile groups of any geometry subjected to horizontal and vertical loads and moments, PGROUP(2.1). *Department of Transport, London HECB/B/7*.

Bell, A. (1977) Laboratory Studies of the Belfast Estuarine Deposits. *PhD Thesis, Queen's University of Belfast.*

Berezantzev, V.G., Khristoforov, V. and Golubkov, V. (1961) Load bearing capacity and deformation of piled foundations. *Proceedings 5th ICSMFE, Paris*, 2, 11-15.

Boussinesq, J. (1885) Applications des Potentiels a L'etude de L'equilibre et du Mouvement des Solides Elastiques, *Gauthier-Villars*, Paris.

Bowles, J.E. (1988) Foundation Analysis and Design, *4th Edition, Civil Engineering Series, McGraw-Hill International Edition*

Brand, E.W., Muktabhant, F. and Taechathummarak, A., (1972) *Proceedings of Conference on Performance of Earth and Earth Supported Structures*, Vol 1, No. 2 903-928.

Briaud, J.L.& Felio, G.Y. (1986). Analysis of Existing Cyclic Vertical Load Tests in Clay, *Proceedings of the 18th Annual Offshore Technology Conference, Houston, Texas*, 31-40.

Briaud, J.L., Tucker, L.M. and Ng, E., (1989). Axially Loaded Five Pile Group and Single Pile in Sand. *Proc. 12th ICSMFE, Rio de Janeiro*, Vol 2, 1121-1124.

Burland, J.B. (1990) On the Compressibility and Shear Strength of Natural Clays, *Geotechnique*, 40, No.3, 327-378

Bustamante, M. and Gianeselli, L. (1982). Pile bearing capacity prediction by means of static penetrometer CPT. *Proceedings of the 2nd European Symposium on Penetration Testing*, Amsterdam Vol. 2, 493-500

Butler, F.G., (1974) Review paper: Heavily Over-consolidated Clays, *Proceedings of the Conference on Settlement of Structures*, Pentech Press, Cambridge, 531-578

Butterfield, R. and Banerjee, P.K. (1971). The elastic analysis of compressible piles and pile groups. *Geotechnique* 21, No.1, 43-60.

Caputo, V., Mandolini, A. and Viggiani C. (1991) Settlement of a piled foundation in pyroclastic soils. *Proceedings XI ECSMFE Florence*, Vol. 1, 353-358.

Caputo, V. and Viggiani, C., (1984) Pile foundation analysis: a simple approach to nonlinearity effects. *Rivista Italiana Di Geotecnica*, Vol. 18, No. 2, 32-51

Carter, J.P., and Kulhawy, F.H, (1988) Analysis and Design of Drilled Shaft Foundations Socketed into Rock, *Report to Electric Power Research Institute, EL-5918, Research Project* 1493-4

Cooke, R.W., Bryden-Smith, D.W., Gooch, M.N., and Sillett, D.F. (1981), Some observations of the foundation loading and settlement of a multi-storey building on a piled raft foundation in London clay. *Proc. Instn. Civ. Engrs*, Part1, 70, 433-460

Cooke, R.W., Price G. and Tarr, K. (1979) Jacked piles in London clay: a study of load transfer and settlement under working conditions. *Geotechnique* 29, No.4, 461-468.

Cooke, R.W., Price G. and Tarr, K. (1980) Jacked piles in London clay: interaction and group behaviour under working conditions. *Geotechnique* 30, No.2, 97-136.

Coyle, H.M., and Reese, L.C., (1966) Load Transfer for Axially Loaded Piles in Clay, *Journal of the Soil Mechanics and Foundations Division*, ASCE, Vol. 92, No. SM2, 1-26.

Chin, F.K. (1970) Estimation of the Ultimate Load of Piles not Carried to Failure, *Proceedings 2nd SE Asian Conference on Soil Engineering, Singapore,* 81-92.

Chin, F.K. (1972) The Inverse Slope as a Prediction of Ultimate Bearing Capacity of Piles, *Proceedings 3rd SE Asian Conference on Soil Engineering, Hong Kong,* 83-91.

Chow, F.C. (1997) Investigations into the Behaviour of Displacement Piles for Offshore Foundations. *PhD thesis*, Faculty of Engineering, Imperial College of Science, Technology and Medicine, University of London.

Chow, F.C. (1995) Field Measurements of Stress Interactions between Displacement Piles in Sand, Cooling Prize Winner, *Ground Engineering*, July/Aug, 36-40

Chow Y.K. (1986) Analysis of Vertically Loaded Pile Groups. *International Journal for Numerical and Analytical Methods in Geomechanics*, 10, No. 1, 59-72.

Chow Y.K. (1987) Iterative Analysis of Pile-Soil-Pile Interaction, *Geotechnique*, Vol. 37, No. 3, 321-333.

Christian J.T., and Carrier W.D. (1978) Janbu, Bjerrum and Kjaernsli's Chart Reinterpreted, *Canadian Geotechnical Journal*, 15, 123-128

Crooks, J.H.A. and Graham, J. (1972) Stress-strain Properties of Belfast Estuarine Clay. *Engineering Geology, 6*: 275-288.

Crooks, J.H.A. and Graham, J (1976) Geotechnical Properties of the Belfast Estuarine Deposits. *Geotechnique 26, No. 2*, 293-315.

Desai, C.S. and Holloway, D.M. (1972) Load Deformation Analysis of Deep Pile Foundations, Proceedings of the Conference on the Applications of the Finite Element Method in Geotechnical Engineering, *U.S. Army Engineers, Waterways Experiment Station, Vicksburg, Mississippi.*

DiMillio A.F., Ng, E.S., Briaud, J.-L. and O'Neill, M.W. (1987) Pile Group Prediction Symposium: Summary, Volume I, Sandy Soil. *Report No. FHWA-TS-87-221 Federal Highway Administration, McLean Virginia, USA.*

Ekstrom, J., (1989) A Field Study of Model Pile Group Behaviour in Non-Cohesive Soils: Influence of Compaction due to Pile Driving, *Dissertation, Department of Geotechnical Engineering, Chalmers University of Technology, Gothenberg.*

Fahey, M. (1992) Shear modulus of cohesionless soil: variation with stress and strain level. *Canadian Geotechnical Journal*, 29, 157-161.

Fahey, M. and Carter, J.P. (1993) A Finite Element Study of the Pressuremeter Test in Sand using a Non-Linear Elastic-Plastic Model. *Canadian Geotechnical Journal, Vol. 30*, 348-362.

Flaate, K., and Selnes, P. (1977) Side Friction of Piles in Clay. *Proceedings of the Ninth International Cinference on Soil Mechanics and Foundation Engineering, Tokyo,* Vol. 1 517-522.

Fleming, W.G.K., (1992) A New Method for Single Pile Settlement Prediction and Analysis, *Geotechnique 42*, 411-425

Fleming, W.G.K., Weltman, A.J., Randolph, M.F. and Elson, W.K. (1992). Piling engineering, 2nd Edition. *Surrey University Press*.

Focht, J.A. and Koch, K.J. (1972) Rational Analysis of the Offshore Performance of Pile Groups, *Proceedings of the 5th Offshore Technology Conference, Houston, Texas*, 2, 701-708

Fox, E.N. (1948) The Mean Elastic Settlement of a Uniformly Loaded Area at a Depth Below the Ground Surface, *Proceedings of the 2nd International Conference on Soil Mechanics*, Rotterdam 1948, Vol. 1 129-132

Franke E., Lutz B. and El-Mossallamy (1994) Measurements and Numerical Modelling of High Rise Building Foundations on Frankfurt Clay, *Geotechnical Special Publication No. 40*, Vol. 2 1325-1336.

Georgiannou, V.N., Burland, J.B. and Hight, D.W. (1990) The undrained behaviour of clayey sands in triaxial compression and extension. *Geotechnique* 40, No. 3, 431-449.

Gill, D.R., (1999) Experimental and Numerical Investigations of Undrained Penetrometer Installation. PhD Thesis, Department of Civil, Structural and Environmental Engineering, Trinity College Dublin.

Goossens, D. and Van Impe, W.F. (1991). Long Term Settlements of a Pile Group Foundation in Sand, overlying a Clayey layer. *Proc. 10th ECSMFE, Florence* 1, 425-428.

Greenfield, F.C. (1971) Early Settlement of Tall Buildings founded on Piles in London Clay. *Proceedings Conference on Behaviour of Piles, ICE, London* 71-78.

Guo, W.D. and Randolph M.F., (1997) Vertically Loaded Piles in Non-homogeneous media. *Int. J. Numer. Anal. Methods Geomech*. 21, 507-532

Guo, W.D. and Randolph M.F., (1998) Rationality of Load Transfer Approach for pile analysis, *Computers and Geotechnics* 23, 85-112.

Guo, W.D. and Randolph M.F., (1999) An Efficient Approach for Settlement Prediction of Pile Groups, *Geotechnique* 49, No. 2, 161-179.

Hansbo, S., (1993) Interaction Problems Related to the Installation of Pile Groups, *Conference on Deep Foundation on Bored and Auger Piles, Balkema, Rotterdam, 59-66.*

Hewitt, C.M. (1988) Cyclic Response of Offshore Pile Groups, *PhD thesis*, University of Sydney, Australia.

Hight, D.W., Bond, A.J. and Legge, J.D. (1992) Characterization of the Bothkennar clay: an overview. *Géotechnique*, Vol. 42, No. 2, 303-347.

Hooper, J.A. (1973) Observations on the Behaviour of a Piled Raft Foundation in London Clay. *Proceedings Institution of Civil Engineers London, Part 2, Result and Theory,* Vol. 55, 855-877

Houlsby, G.T. and Teh C.I. (1988) Analysis of the Piezocone in Clay, *Conference on Penetration Testing, Balkema, Rotterdam,* 777-783

Jardine, R.J., and Chow, F.C. (1996) New Design Methods for Offshore Piles, *MTD Publication 96/103, Marine Technology Directorate, London*

Jardine, R.J., Chow, F.C., Matsumoto, T. and Lehane, B.M. (1998) A New Design Procedure for Driven Piles and its Application to Two Japanese Clays. *Soils and Foundations*, Vol. 38, No. 1, 207-219.

Jardine, R.J., Potts, D.M., Fourie, A.B. and Burland, J.B. (1986) Studies of the influence of non-linear stress strain characteristics in soil-structure interaction. *Geotechnique* 36, No. 3, 377-396.

Karlsrud, K. and Haugen, T. (1985) Axial Static Capacity of Steel Model Piles in Overconsolidated Clay. *Proceedings of the 11th International Conference on Soil Mechanics and Foundation Engineering, San Francisco,* Vol. 3, 1401-1406

Karlsrud, K. and Haugen, T. (1986) Behaviour of Piles in Clay under Cyclic Axial Loading – Results of Field Model Tests. *Norwegian Geotechnical Institute,* Publication No. 166

Karlsrud, K., Kalsnes, B. and Nowacki, F. (1992) Response of Piles in Soft Clay and Silt Deposits to Static and Cyclic Axial Loading Based on Recent Instrumented Pile Load Tests, *Norwegian Geotechical Institute*, Publication 188.

Kieran, P. (2001) Axial Cyclic Loading of Piles in Soft Clay. *MSc Dissertation*, Trinity College Dublin.

Koerner, R.M. and Partos, A. (1974). Settlement of Building on Pile Foundation in Sand. *J. Geotech. Engng Div.,* ASCE 100, No. 3, 265-278.

Koizumi, Y. and Ito, K., (1967) Field Tests with Regard Pile Driving and Bearing Capacity of Piled Foundations. *Soils and Foundations* 7, No. 3, 30-53.

Konrad, J.-M. and Roy, M. (1987) Bearing Capacity of Friction Piles in Marine Clay. *Geotechnique* 37, No. 2, 163-175.

Kraft, L.M., Ray, R.P., and Kagawa, T (1981) Theoretical t-z Curves, *Journal Geotechnical Engineering Div*., ASCE 107(11) 1543-1561

Ladd, C.C., Foott, R., Ishihara K., Schlosser F., and Poulos H.G. (1977) Stress-Deformation and Strength Characteristics, *Proceedings of the 9th International Conference on Soil Mechanics and Foundation Engineering*, Tokyo, Vol. 2, 421-494.

Lee C.Y. and Small, J.C. (1991) Finite Layer Analysis of Axially Loaded Piles, *Journal of Geotechnical Engineering, ASCE*, Vol. 117, No. 11, 1706-1722

Lee, J. and Salgado, R. (1999). Determination of Pile Base Resistance in Sands. *Journal of Geotechnical and Geoenvironmental Engineering*, ASCE, August.

Lehane, B.M. (1992) Experimental Investigations of Pile Behaviour using Instrumented Field Piles. *PhD Thesis, University of London (Imperial College), England*.

Lehane, B.M., Chow, F.C., McCabe B.A. and Jardine R.J., (2000a) Relationships between the shaft capacity of driven piles and CPT end resistance. *Proceedings Institution of Civil Engineers Geotechnical Engineering, 143, Apr., 93-101*.

Lehane, B.M., Jardine, R.J., Bond A.J. and Chow, F.C. (1994) The Development of Shaft Resistance on Displacement Piles in Clay, *XIII International Conference on Soil Mechanics and Foundation Engineering, New Delhi*, 473-476

Lehane, B.M., and McCabe, B.A (1999) Interaction Effects in Laterally Loaded Pile Groups, *Advances in Civil and Structural Engineering Practice*, Edinburgh 1, 393-399

Lehane B.M., McCabe B.A. and Phillips D.T. (2000b) Instrumented Single and Group Piles in Belfast Soft Clay, *Australian Geomechanics News*, 35:4, pp 33-45

Lehane B.M., McCabe B.A., Phillips D.T., Jardine R.J., Paul T.S. and Horkan E., (1998/99) Piling Research in Belfast's soft clay, *Trans. Inst. Of Engrg of Ireland*, 122.

Lehane B.M., and Simpson B., (2000) Modelling Glacial Till under Triaxial Conditions using a BRICK Soil Model, *Canadian Geotechnical Journal*, Vol. 37, 1078-1088

Leroueil, S., Lerat, P., Hight, D.W. and Powell, J.J.M. (1992) Hydraulic Conductivity of a Recent Estuarine Silty Clay at Bothkennar, Scotland. *Geotechnique* 42, 2, 275-288

Liu, J.L., Yuan, Z.L., Zhang K.P. (1985) Cap-pile-soil Interaction of Bored Pile Groups *Proceedings XXI International Conference on Soil Mechanics and Foundation Engineering, Balkema, Rotterdam.* Vol. 3, 1433-36.

Mandolini, A. and Viggiani, C. (1992) Settlement Predictions for Piled Foundations from Loading Tests on Single Piles. *Proceedings Wroth Memorial Symposium on Predictive Soil Mechanics, Oxford* 464-482

Mandolini, A. and Viggiani, C. (1997) Settlement of Piled Foundations. *Geotechnique* 47, 791-816.

Manning, P.I., Robbie, J.A. and Wilson, H.E., (1972) Geology of Belfast and the Lagan Valley, *HMSO, Belfast*

McAnoy, R.P.L., Cashman, A.C., and Purvis, D. (1982) Cyclic Tensile Testing of a Pile in Glacial Till, *Proceedings of Recent Developments in the Design and Construction of Offshore Structures, Institute of Civil Engineers, London*

Mindlin, R.D (1936). Force at a Point in the Interior of a Semi-infinite Solid. *Physics* 7, 195-202

Mitchell, J.K (1976) Fundamentals of Soil Behaviour, 1st edition, *London: Wiley*.

Movius, H.L. (1953) Curran Point, Larne, Co. Antrim - The Type Site of the Irish Mesolithic, *Proceedings of the Royal Irish Academy*, 56B, 1-195

O'Brien, E.J., and Dixon, A.S. (1995) Reinforced and Prestressed Concrete Design – The Complete Process, *Longman Scientific and Technical.*

O'Loughlin, C.D., (2001) The One-dimensional Compression of Fibrous Peat and other Organic Soils, *PhD Thesis*, Trinity College Dublin

O'Neill, M.W (1983) Group Action in Offshore Piles. *Proceedings American Society of Civil Engineers Conference: Geotechnical Practice in Offshore Engineering, Austin* 25-64.

O'Neill, M.W., Ghazzaly O.I. and Ha, H.B. (1977) Analysis of Three-Dimensional Pile Groups with Non-Linear Soil Response and Pile-soil-pile Interaction. *Proceedings of the 9th Offshore Technology Conference, Houston*, 1977, 245-256

O'Neill, M.W., Hawkins R.A. and Audibert, J.M.E (1982) Installation of Pile Group in Overconsolidated Clay. *Journal Geotechnical Engineering Division, ASCE*, Vol 108, No. GT11

Ottaviani, M. (1975) Three-dimensional Finite Element Analysis of Vertically Loaded Pile Groups. *Geotechnique*, 25, No. 2, 159-174.

Ove Arup and Partners (1996) OASYS: Geotechnical Programs Manual. *Ove Arup and Partners, London, U.K.*

Paul, M.A., Peacock, J.D. and Wood, B.F. (1992). The engineering geology of the Carse clay at the National Soft Clay Research Site, Bothkennar. *Geotechnique 42*, No. 2, 183-198.

Pellegrino, A. (1983) Personal Communication of Caputo and Viggiani (1984)

Phillips, D.T., Personal Communication.

Phillips, D.T., (2002). The Behaviour of Concrete Piles under Lateral Loading. *PhD Thesis*, Department of Civil, Structural and Environmental Engineering, Trinity College Dublin.

Poulos, H.G. (1968). Analysis of the Settlement of Pile Groups. *Geotechnique* 18, No. 4, 449-471.

Poulos, H.G. (1971). Behaviour of Laterally Loaded Piles: II-Pile Groups. *Proceedings of the American Society of Civil Engineers*, 97 (SM5) 733-751

Poulos, H.G. (1988). Cyclic Stability Diagram for Axially Loaded Piles. *Journal of Geotechnical Engineering*, Vol. 114, No. 8, 877-895

Poulos, H.G. (1989). Pile behaviour – Theory and Application. Rankine Lecture. *Geotechnique* 39, No. 3, 365-415.

Poulos H.G. and Davis, E.H. (1980) Pile Foundation Analysis and Design, *Wiley*

Poulos, H.G. and Randolph, M.F. (1983) Pile Group Analysis: a Study of Two Methods. *Journal of Geotechnical Engineering*, Vol. 109, No. 3, 355-372

Randolph, M.F., (1977) A Theoretical Study of the Performance of Piles, *PhD Thesis, Cambridge University.*

Randolph, M.F., (1986) RATZ- Load Transfer Analysis of Axially Loaded Piles. *Report GEO 86033, Department of Civil and Resource Engineering, UWA.*

Randolph, M.F., (1987) PIGLET A Computer Program for the Analysis and Design of Pile Groups. *Report GEO 87036, Department of Civil and Resource Engineering, UWA.*

Randolph, M.F. (1994). Design Methods for Pile Groups and Piled rafts. *XIII ICSMFE, New Delhi* 5, 61-82.

Randolph, M.F. and Clancy, P. (1993) Efficient Design of Piled Rafts, *Proceedings of 2nd International Geotechnical Seminar on Deep Foundations on Bored and Auger Piles*, Ghent 119-180.

Randolph, M.F. and Clancy, P. (1994) Design and Performance of a Piled Raft Foundation. *Geotechnical Special Publication No. 40, Vertical and Horizontal Deformations of Foundations and Embankments, ASCE, Texas* 314-324.

Randolph, M.F. and Wroth, C.P. (1978) Analysis of deformation of vertically loaded piles. *J. Geotech. Engng Div*., ASCE 104, No. 12, 1465-1488.

Randolph, M.F. and Wroth, C.P. (1979) An Analysis of the Vertical Deformation of Pile Groups. *Geotechnique* 29, No. 4, 423-439

Reese, L.C., Wang, S.-T. and Reuss, R (1993) Test of Auger Piles for Design of Pile-Supported Rafts. *Deep Foundations on Bored and Auger Pile 11, Balkema, Rotterdam*, 343-346.

Shen, W.Y., Chow, Y.K. and Yong K.Y. (1999) Variational Solution for Vertically Loaded Pile Groups in an Elastic Half-space. *Geotechnique* 49, No. 2 199-213

Simpson, B. (1992) Retaining Structures: Displacement and Design: 32nd Rankine Lecture, *Geotechnique*, 42, No. 4, 541-576

Skempton, A.W. (1951) The Bearing Capacity of Clays, *Building Research Congress*, Div I, 180

Smith, P.R., Jardine, R.J. and Hight, D.W. (1992) The Yielding of Bothkennar Clay, *Geotechnique* 42, No. 2, 257-274

Sommer, H., Wittmann, P. and Ripper, P. (1985) Piled raft foundation of a tall building in Frankfurt clay. *Proceedings XI ICSMFE*, Vol. 4, 2253-2257.

Stephens, N. and Synge, M. (1966) Pleistocene Shorelines (in *Essays in Geomorphology*), *editor G.H. Dury, Heinemann*.

Thorburn, S., Laird, C and Randolph, M.F. (1983). Storage tanks founded on soft soils reinforced with driven piles. *Proceedings of the Conference on Recent Advances in Piling and Ground Treatment*, ICE, London, 157-164.

Tomlinson, M.J.(1995) Foundation Design and Construction, 6th Edition, *Longman Press*

Tortsman, B.A. (1973) The Behaviour of a Cohesionless Pile Group in Soft Clay. *Proceedings XIII ICSMFE Moscow*, Vol. 1, 237-242.

Trofimenkov, J., (1977) Panel Contributions Session 2 *Conference of Behaviour of Foundation and Structures*, Vol. 3 370-371

Van Impe, W.F., (1996) Case Histories of Pile Supported Rafts (Draft), *Report of ISSMFE Technical Committee No. 18*.

Vesic, A.S. (1968) Load Transfer, Lateral Loads and Group Action of Deep Foundations, *Performance of Deep Foundations, ASTM STP 444, American Society for Testing and Materials*, 5-14

Vijayvergiya, V.N., (1977) Load-Movement Characteristics of Piles, *Proceedings of the Ports '77 Conference, Long Beach, California*

Whitaker, T. (1957) Experiments with Model Piles in Groups, *Geotechnique 7*, No. 4, 147

Whittle, A.J., (1991) Prediction of Instrumented Pile Behaviour at the Bothkennar Site, *School of Engineering Report, Massachusetts Institute of Technology, USA.*

Wilson, H.E. (1972) Recent Geology of Northern Ireland, *HMSO, Belfast.*

Yamasita, K., Kakurai, M., Yamada, T. and Kuwabara F. (1993) Settlement behaviour of a five-storey building on a piled raft foundation, *Proceedings of the 2nd International Geotechnical Seminar on Deep Foundations on Bored and Auger Piles, Ghent* 351-356.

Appendix 2-1

Relationship between shaft capacity of driven piles and CPT end resistance (Lehane et al 2000)

Relationships between shaft capacity of driven piles and CPT end resistance

B. M. Lehane, BE, DIC, PhD, MIEI, F. C. Chow, MSc, DIC, PhD, CEng, MICE, B. A. McCabe, BA, BAI, MIEI and R. J. Jardine, MSc, DIC, PhD, CEng, MICE

Proc. Instn Civ. Engrs Geotech. Engng. 2000, **143**, Apr., 93–101

Paper 11973

Written discussion closes 31 August 2000

Manuscript received 17 March 1999; revised manuscript accepted 23 September 1999

Potential relationships between the shaft capacity of a pile driven in clay and the cone penetration test (CPT) end resistance are investigated using results from recent field research on displacement piles. It is shown that a relatively good correlation between shaft capacity and cone end resistance may be achieved if other influential parameters such as interface friction angle, clay sensitivity and relative depth of the pile tip are taken into account. The proposed approach is seen to provide good predictions for a range of pile test results and is both compatible with, and an improvement on, existing CPT-based methods.

Keywords: piles & piling; geotechnical engineering; design methods & aids

Notation

β	empirical factor relating CPT end resistance and ultimate shaft shear stress
C_c^*	compression index for normally consolidated reconstituted material
c_u	undrained shear strength
c_{utc}	undrained strength in triaxial compression
COV	coefficient of variation (standard deviation divided by mean)
D	pile diameter
e_0	*in situ* void ratio
e_{ICL}	void ratio of reconstituted material at $\sigma'_v = \sigma'_{v0}$
e^*_{100}	void ratio of reconstituted material at $\sigma'_v = 100$kPa
e_L	void ratio at liquid limit
f_L	loading coefficient ($\sigma'_{rf}/\sigma'_{rc}$)
h	height above the pile tip
I_p	plasticity index
I_{vr}	relative void index (equation (10))
K_c	earth pressure coefficient after equalization ($\sigma'_{rc}/\sigma'_{v0}$)
L	pile length
L_{max}	maximum pile length used in a given experimental programme in Table 2
N_{kt}	cone factor
Q_s	pile shaft capacity
q_s	ultimate average pile shaft shear stress
q_c	CPT end resistance
q_t	CPT end resistance, with pore pressure correction for piezocones
q_n	net cone resistance = $q_t - \sigma_{v0}$
R	pile radius
R_o	outer pile radius for pipe pile
R_i	inner pile radius for pipe pile
R^*	$(R_o^2 - R_i^2)^{0.5}$
S_t	clay sensitivity
u_c	pore pressure measured by piezocone
YSR	yield stress ratio (yield stress determined in oedometer test divided by σ'_{v0})
β	empirical factor relating CPT end resistance and ultimate shaft shear stress
δ_f	pile–soil interface friction angle at maximum shear stress
δ_p	peak interface friction angle
δ_{ult}	ultimate interface friction angle
σ'_{rc}	radial effective stress on shaft after equalization
σ'_{rf}	radial effective stress at maximum shear stress
σ'_{v0}	free field vertical effective stress
σ_{v0}	free field vertical total stress
τ_f	maximum shear stress on pile shaft
ψ	ratio defined by equation (18)
ΔI_{vy}	$\log_{10} S_t$

Introduction

The similarity between the mode of penetration of a driven pile and a cone penetrometer has prompted the development of many empirical formulae relating cone parameters to the capacity of driven piles. Briaud and Tucker[1] evaluated six such CPT-based methods against a large independent database and found that the method proposed by Bustamante and Gianeselli[2] gave the best predictions. This method, which is also referred to as the Laboratoire Central des Ponts et Chaussées *(LCPC) approach, relates the ultimate average* shear stress (q_s) to the CPT end resistance (q_c) averaged over the depth of the pile using an empirical factor, β:

$$q_s = (q_c)_{mean}/\beta \qquad (1)$$

Recommended β values and upper limits to q_s for full displacement piles in clay are provided in Table 1.

2. While the LCPC approach and other popular CPT-based methods (e.g. by De Ruiter and Beringen[3]) have been relatively successful, Briaud and Tucker[1] show that their reliability is not high and that estimates of capacity can, at best, only be expected to be within 40% of actual capacities. This paper uses the results from recent displacement pile research to

B. M. Lehane, Trinity College, Dublin

F. C. Chow, Geotechnical Consulting Group, London

B. A. McCabe, Trinity College, Dublin

ascertain if more reliable relationships between the cone end resistance and q_s for closed-ended piles in clay can be established. Following the recommendations of Campanella *et al.*,[4] and others, the cone end resistance, corrected for pore pressure acting on the filter stone of piezocones (i.e. q_t), is used in place of q_c as the definitive measure of end resistance.

3. Recent investigations using instrumented piles have greatly improved our understanding of the factors governing the shaft capacity of driven piles in clay. The findings of this research have been synthesized by Lehane *et al.*,[5] Jardine and Chow[6] and Jardine *et al.*[7] into effective stress design approaches which recognize the strong influence of the clay's yield stress ratio (YSR) on the stresses developed on the pile shaft; note that YSR is the overconsolidation ratio indicated by high-quality samples in oedometer tests. An extension of these methods is explored in the following by employing the CPT q_t value rather than YSR as a measure of clay consistency. One advantage of such an approach is that it does not rely on the interpretation of a YSR profile at a given site.

4. The framework adopted in the approaches of Lehane *et al.*[5] and Jardine and Chow[6] is outlined initially. These approaches establish expressions which relate the radial effective stresses acting on driven piles after full equalization (σ'_{rc}) to the clay's YSR. The same database as that used in the derivation of these expressions is employed here to investigate an equivalent relationship for σ'_{rc} which includes q_t as one of the governing parameters. The resulting formulation for pile shaft capacity is then examined against (*a*) a small, but independent, database of pile tests on closed-ended piles, and (*b*) existing correlations between q_t and shaft capacity.

Framework for evaluating shaft capacity in clays

5. Organizations such as MIT, Oxford University, NGI and Imperial College (IC) have, over the past 15 years, performed tests on high-quality instrumented displacement piles in a large range of clay soils. Some of the major features that have emerged are described by Jardine and Chow,[6] who also provide a full bibliography of relevant publications. Taking the results of the combined research, Jardine and Chow[6] proposed new methods for the design of driven piles in sand and clay. The framework for evaluating pile shaft capacity in clays is now described.

6. Shaft capacity (Q_s) is the integral, along the pile shaft area, of the local shear stresses at failure (τ_f). Q_s for a pile of diameter D and length L is given by

Table 1. β and q_s(max) recommended by Bustamante and Gianeselli[2]

Soil type	q_c: MPa	β for driven/jacked concrete piles	β for driven/jacked metal piles	q_s(max): kPa
Soft clay	<1	30	30	15
Firm–stiff clay	1–5	40	80	35
Stiff–hard clay	>5	60	120	35

$$Q_s = \pi D \int^L \tau_f \, dz \qquad (2)$$

7. The peak local shear stress is controlled by the magnitude of the radial effective stress at failure (σ'_{rf}) and may be described by the simple Coulomb failure criterion

$$\tau_f = \sigma'_{rf} \tan \delta_f \qquad (3)$$

The angle of interface friction at failure (δ_f) depends on many factors but can be assessed from ring shear interface experiments that model (*a*) the properties of the pile surface, (*b*) the displacement and rate history of soil adjacent to the shaft, and (*c*) the normal effective stress levels.

8. The magnitude of σ'_{rf} is typically 80% of the radial effective stress acting against the pile shaft prior to loading and after pile installation and equalization. σ'_{rf} may be written as $[f_L \sigma'_{rc}]$, where f_L is referred to as the loading factor. The IC instrumented pile tests indicated that f_L is $0{\cdot}8 \pm 0{\cdot}05$ in both compression and tension loading; this value is adopted when assessing load test results in the following.

9. σ'_{rc} can be expressed as a product of the free field vertical effective stress (σ'_{v0}) and an earth pressure coefficient K_c, so that

$$\tau_f = f_L K_c \sigma'_{v0} \tan \delta_f \qquad (4)$$

10. Results from high-quality instrumented pile tests in a large variety of clays show that K_c depends most strongly on the soil consistency (as expressed through YSR), the clay's sensitivity, the strain paths imposed during jacking or driving and the distance from the pile tip. With these factors in mind, Lehane *et al.*[5] conducted a statistical analysis of the database of radial effective stress measurements on closed-ended piles in clay and proposed the following expression for K_c (which had a coefficient of variation, COV, of predicted to measured K_c of 0·28):

$$K_c = \sigma'_{rc}/\sigma'_{v0} = [2 - 0{\cdot}625 I_{vr}] \mathrm{YSR}^{0{\cdot}42} (h/R)^{-0{\cdot}2} \qquad (5)$$

where

h/R = distance above the pile tip normalized by the pile radius
$I_{vr} = (e_0 - e_{ICL})/C_c^*$
e_0 = *in situ* void ratio
e_{ICL} = void ratio of the reconstituted material at $\sigma'_v = \sigma'_{v0}$
C_c^* = slope of the virgin consolidation line

R. J. Jardine, Imperial College, London

Table 2. Sites used in database

Clay	D: mm	L_{max}: m	Typical I_p: %	Reference	Symbol
Boston Blue (MIT)	38	40	20	Morrison[9]	●
Boston Blue (Saugus)	38	40	20	Morrison[9]	□
Bothkennar	102	6	50	Lehane[10]	▲
London Clay	80	6	45	Bond[11]	■
Cowden till	102	6·4	20	Lehane[10]	◆
Empire	38	75	50	Azzouz and Lutz[12]	△
Gault	80	9	50	Coop[13]	×
Haga	153	5	15	Karlsrud and Haugen[14]	✳
Huntspill	80	9	30	Coop[13]	⬕
Lierstranda	219	35	15	NGI[15]	+
Mortaiolo	457	57	10	Totani *et al.*[16]	○
Onsøy	219	35	10	NGI[17]	◇
Pentre (ICL and NGI)	102	19	20	Chow,[8] NGI[18]	◐◑
Rio de Janeiro	220	6.7	60	Soares and Dias[19]	⬗
Tokyo	300	5.6	55	Koizumi and Ito[20]	◧
Belfast	350	9.5	40	Lehane and Phillips[21]	◮

of the reconstituted material in $(e, \log_{10}\sigma'_v)$ space

11. Jardine and Chow[6] postulated that K_c values for open-ended piles may be estimated from equation (5) by using an equivalent pile radius (R^*) in place of pile radius (R) in the h/R term; R^* is given by $(R_o^2 - R_i^2)^{0.5}$, where R_o and R_i are the outer and inner pile radii respectively. This substitution has been shown by Chow[8] to lead to good estimates of shaft capacities of open-ended piles.

12. The influence of clay sensitivity (S_t) on K_c is incorporated in an indirect way in equation (5) by the relative void index term (I_{vr}), which is a measure of both S_t and YSR; for example, it may be shown that $I_{vr} \approx \log_{10}(S_t/YSR)$ in lightly overconsolidated clays. Jardine and Chow[6] separated the effects of S_t from YSR and proposed the following alternative expression to equation (5):

$$K_c = [2{\cdot}2 + 0{\cdot}016\text{YSR} - 0{\cdot}870\Delta I_{vy}] \times \text{YSR}^{0.42}(h/R)^{-0.2} \quad (6)$$

where

$$\Delta I_{vy} = \log S_t \quad (7)$$

Although this format provides a clearer indication of the relative influence of the parameters affecting K_c, it proved more expedient in the following to use equation (5) as the basis for the development of a K_c expression involving the CPT q_t value.

The instrumented pile database

13. Table 2 lists the sites at which radial effective stresses acting on the shafts of closed-ended displacement piles in clay have been measured with a high degree of accuracy. These measurements, which were also used in the development of equations (5) and (6), are used to investigate possible relationships between K_c and the CPT q_t value. Table 2 also details the pile diameters and maximum pile tip depths (L_{max}) employed in the various test programmes and lists typical plasticity indices (I_p) for the clays at each test site.

Development of correlation for K_c

14. The existence of a relationship between K_c and q_t was prompted by measurements such as those shown in Fig. 1, which displays σ'_{rc} and q_t data recorded in the glacial till at Cowden and in the soft Bothkennar clay.[22,23] It is evident that σ'_{rc} is typically about one-fifth of q_t at both sites. Closer examination of these and other measurements indicated that higher values of σ'_{rc} were developed in areas of high local q_t resistances and that σ'_{rc} recorded at any fixed depth was larger on shorter piles.

15. In keeping with these trends and that implied by equation (5), a relationship of the following form was investigated:

$$\sigma'_{rc} = f(q_t, h/R, \sigma'_{v0}, I_{vr}) \quad (8)$$

When piezocones were employed at the test sites listed in Table 2, q_t was derived from the measured end resistance in accordance with the standard correction proposed by Campanella *et al.*[4]

16. Given that q_t is generally assumed to vary linearly with the undrained strength of a clay (c_u), and that the undrained strength ratio (c_u/σ'_{v0}) varies with YSR (e.g. Ladd *et al.*[24]), it follows that a suitable term to use in place of the YSR term in equation (5) is the ratio q_t/σ'_{v0}, that is

$$K_c = f(q_t/\sigma'_{v0}, h/R, I_{vr}) \quad (9)$$

17. Values of q_t, I_{vr}, h/R and σ'_{v0} corresponding to all K_c measurements were determined with a view to establishing the best-fit format of the function in equation (9). Two of the 16 case histories listed in Table 2 could not be used (Tokyo and Rio de Janeiro), as they did

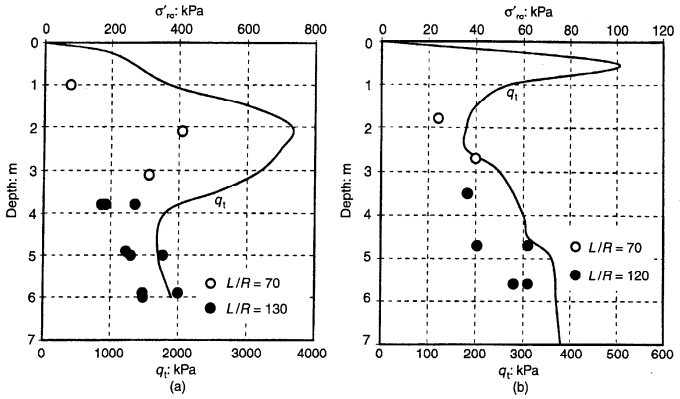

Fig. 1. Comparison of q_t profiles with equalized radial effective stresses measured in (a) Cowden and (b) Bothkennar

not report CPT profiles, while the K_c values recorded in the somewhat atypical Pentre and Lierstranda clay-silts will be examined separately.

18. Although I_{vr} values have been determined directly for some of the soils in the database (by conducting oedometer tests on reconstituted samples), in the interest of consistency, it was decided to determine I_{vr} for all sites in this study using Burland's[25] empirical correlations with the void ratio at the liquid limit (e_L), that is

$$I_{vr} = (e_0 - e_{ICL})/C_c^* \quad (10)$$

$$e_{ICL} = e_{100}^* - C_c^* \log_{10}(\sigma'_{v0}/100), \sigma'_{v0} \text{ in kPa} \quad (11)$$

$$e_{100}^* = 0{\cdot}109 + 0{\cdot}679e_L - 0{\cdot}089e_L^2 + 0{\cdot}016e_L^3 \quad (12)$$

$$C_c^* = 0{\cdot}256e_L - 0{\cdot}04 \quad (13)$$

19. The statistical analysis first assumed the same dependence of K_c on I_{vr} and h/R as predicted by equation (5) and that the YSR term in this equation could be replaced by a q_t/σ'_{v0} term. The resulting best-fit expression was

$$K_c = 0{\cdot}27[2 - 0{\cdot}625I_{vr}](q_t/\sigma'_{v0})^{0{\cdot}7}(h/R)^{-0{\cdot}2} \quad (14)$$

20. Equation (14), which is plotted with the database used in Fig. 2, has a coefficient of variation (COV) of $[(K_c)_{predicted}/(K_c)_{measured}]$ equal to 0·35. This COV is, in statistical terms, significantly larger than the COV of 0·28 found for equation (5), thereby providing indirect confirmation that K_c is more uniquely related to YSR than q_t/σ'_{v0}.

21. Chen and Mayne[26] show that an improved correlation between YSR and the cone end resistance is obtained if YSR is related to q_t less the pore pressure measured at the face or the shoulder of the cone (u_c). It is therefore likely that K_c would show a more systematic relationship with $(q_t - u_c)/\sigma'_{v0}$ than with q_t/σ'_{v0}.

22. Unfortunately, u_c profiles were not available for many of the sites in the instrumented pile test database and it was therefore necessary to examine the most important factors influencing the relationship between YSR and q_t/σ'_{v0} and incorporate these in the proposed function for K_c. A review of available correlations between q_t/σ'_{v0} and other clay parameters (e.g. Rasmussen *et al.*[27]) indicated that, while q_t/σ'_{v0} shows a strong dependence on YSR, it also increases with clay plasticity and reduces with clay sensitivity (S_t), that is

$$q_t/\sigma'_{v0} \approx f(\text{YSR}, I_p, S_t) \quad (15)$$

23. Given that the relative void index (I_{vr}) is a measure of S_t and YSR, and increases with reducing YSR and increasing S_t, one logical extension of equation (9) is that

$$K_c = f(q_t/\sigma'_{v0}, h/R, I_{vr}, I_p) \quad (16)$$

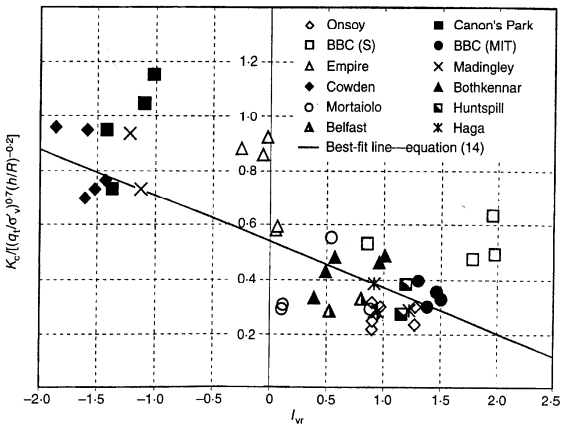

Fig. 2. K_c measurements plotted as a function of $(q_t/\sigma'_{v0})^{0{\cdot}7}$, $(h/R)^{-0{\cdot}2}$ and I_{vr}

where the dependence of K_c on I_{vr} differs from that of equation (5).

24. Various forms of functions for K_c were explored, and independent assessments of the effect of each of the parameters in equation (16) showed that it could be simplified to

$$\psi = K_c/[(q_t/\sigma'_{v0})^{0.6}(h/R)^{-0.2}] = f(I_{vr}, I_p) \quad (17)$$

25. The values of ψ are plotted against I_{vr} in Fig. 3, which also classifies the K_c measurements on the basis of I_p, that is data points obtained for high-plasticity clay ($I_p \geq 35\%$) are distinguished from those recorded in low- and medium-plasticity clays ($I_p < 35\%$). It may be seen that ψ generally reduces with increasing I_{vr} but that the form of the reduction depends on whether the material is of high or low to medium plasticity. There is clearly a scarcity of data, particularly in the moderately and heavily overconsolidated clays ($I_{vr} < 0$). The available data suggest the following best-fit exponential forms for ψ:

$$\psi = K_c/[(q_t/\sigma'_{v0})^{0.6}(h/R)^{-0.2}] = 0.3 + 0.3e^{-Ivr} \quad \text{for } I_p \geq 35\% \quad (18a)$$

$$\psi = K_c/[(q_t/\sigma'_{v0})^{0.6}(h/R)^{-0.2}] = 0.45 + 0.15e^{-Ivr} \quad \text{for } I_p < 35\% \quad (18b)$$

Given the somewhat arbitrary decision to adopt the I_p value of 35% as the boundary between high-plasticity clays and other clays, it is suggested that, in the absence of further information, an average value of ψ is obtained from equations (18a) and (18b) when I_p is close to 35%.

26. These equations, which are plotted on Fig. 3, have a COV in $[(K_c)_{predicted}/(K_c)_{measured}]$ of 0·26; this value represents a considerable improvement on that of equation (14) and suggests that both equation (18) and the YSR formulation for K_c (i.e. equation (5)) have a comparable reliability. Further instrumented pile test data would clearly assist in refining these expressions.

Checking the $K_c - q_t$ correlation against other K_c data

Sites at which q_t data were not available

27. The validity of equation (18) can be examined directly for the sites at which K_c measurements were obtained, but where CPT data were not available, by assuming that q_t can be related, via a cone factor (N_{kt}), to the undrained strength measured in triaxial compression c_{utc}:

$$q_n = q_t - \sigma_{v0} = N_{kt}c_{utc} \quad (19)$$

28. A comparison of measured K_c values with those predicted using equations (18) and (19), assuming a typical cone factor (N_{kt}) of 15, is provided in Fig. 4. It is evident that K_c values are predicted to within 20% in both the Rio de Janeiro and Tokyo clays.

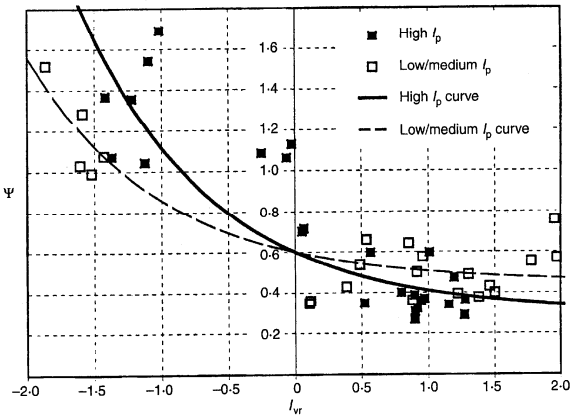

Fig. 3. Influence of I_{vr} and I_p on ψ (equation (18))

K_c measurements at Pentre and Lierstranda

29. The K_c measurements made in the low-plasticity clayey silts at Pentre and Lierstranda were significantly more variable than those measured at other sites. This variability is apparent in Fig. 5, which compares K_c measurements at the two sites with those predicted using equation (18).

30. Karlsrud *et al.*[28] suggest that the low K_c values measured by NGI were due to cylindrical arching effects sustained by these silty materials, while Chow's[8] database of tests at Pentre indicated that the large range of K_c values measured at Pentre was due to the highly laminated nature of the deposit. In any case, it appears that equation (18) does not capture all of the significant factors affecting K_c in high-permeability silts.

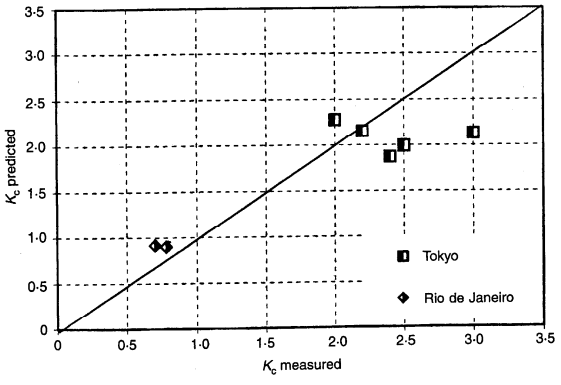

Fig. 4. K_c predictions at sites with no CPT data

Expression for shaft capacity

31. The ultimate average shear stress (q_s) and shaft capacity (Q_s) of a driven pile in clay is determined by combining equation (18) with equations (2) and (4), that is

$$q_s = Q_s/\pi DL = (1/L)\int^{L} [f_L K_c \sigma'_{v0} \tan \delta_f]\, dz \quad (20)$$

32. The interface friction angle (δ_f) is typically slightly less than the clay's residual angle and, depending on the relative displacement between the shaft and the soil during loading, may be a peak (δ_p) or ultimate (δ_{ult}) value. Jardine and Chow[6] propose that approximate design δ_p and δ_{ult} values for steel piles may be estimated using Fig. 6. Ramsey *et al.*[29] show that the guidelines on Fig. 6 provide reasonable lower-bound values but conclude that, because possible variations of δ are large, ring shear interface tests should be used to obtain direct measurements.

Validation of approach

33. The validity and reliability of the proposed approach is examined by comparing predictions for q_s using equations (18) and (20) with ultimate average shaft shear stresses recorded in some typical pile tests included in the database employed by Jardine and Chow[6] and Chow[8]. The approach is also compared with other standard CPT-based methods.

Data from case histories

34. q_s measurements for piles installed in six different soil types are summarized in Table 3. This group of tests was selected because of the availability of q_t profiles, δ angles and classification data at the test sites and also because the tests were not used in derivation of equation (18).

35. Values of K_c along the shaft of each pile were calculated from equation (18) using the w and LL data in conjunction with equations (10)–(13) to estimate I_{vr} values. The q_s value was then derived using equation (20), assuming an f_L value of 0·8 and the δ_f value given in Table 3; Chow[8] provides full justification for the selected δ_f angles.

36. Predicted q_s values are seen in Table 3 to be generally within 20% of measured values.

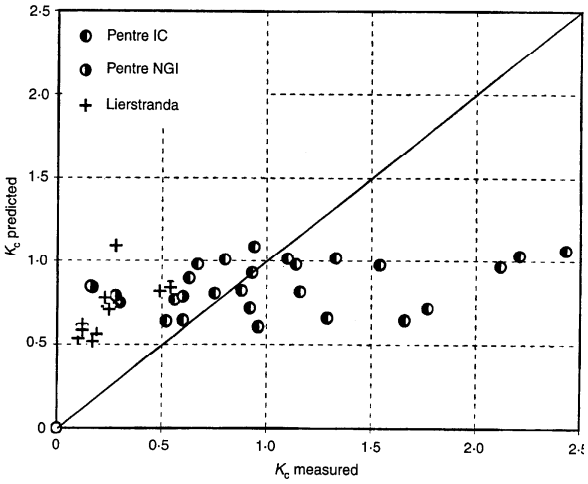

Fig. 5. K_c predictions for clay-silts

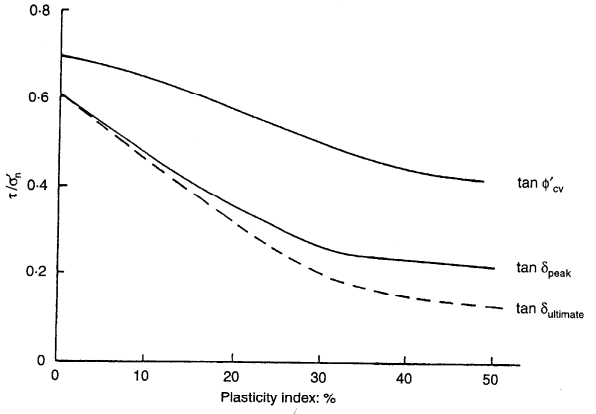

Fig. 6. Proposed design δ values after Jardine and Chow[2]

The margin of error, which is compatible with that of equation (18), is relatively small given the range of soil types examined. The error margin is also consistent with the anticipated reliability of the YSR approach (i.e. equation (5)); see Chow.[8]

Table 3. Predicted versus measured shaft capacities for selected database

Soil type	Reference	Embedded depth: m	D: m	Comp./tens.	δ: degrees	$(qs)_{meas}$: kPa	$(qs)_{pred}$: kPa	$(qs)_{pred}/(qs)_{meas}$
London Clay	Wardle *et al.*[30]	2–6·5	0·17	Comp.	14	61	77	1·26
St Alban Clay	Konrad and Roy[31]	1·3–7·6	0·22	Comp.	25	17	12·4	0·73
San Francisco Bay Mud	Kraft[32]	0–12·2	0·11	Comp.	26	11	10·7	0·97
Lowestoft Till	Karlsrud *et al.*[33]	3–12·9	0·22	Tens.	17	180	169	0·94
Oxford Clay	Karlsrud *et al.*[33]	17·5–25·6	0·22	Tens.	21	298	329	1·10
Onsoy marine clay	NGI[17]	12·5–22·5	0·22	Tens.	18	23	19	0·83

Comparison with existing CPT correlations

37. Bottiau,[34] and others, reviewed correlations for β (as given by equation (1)) and found that β generally increased with q_c and was typically between 20 and 60; for example, see Table 1. A recent systematic study of the variation of β with q_s is reported by Almeida *et al.*,[35] who examined the results from 43 pile load tests on driven and jacked steel piles at eight clay sites and found, as shown in Fig. 7(a), that β (defined in terms of q_t and referred to as k_1) varied between 15 and 47. Almeida *et al.* deduced that improved reliability would be obtained if β was assumed to vary with $(q_t - \sigma_{v0})/\sigma'_{v0} = q_n/\sigma'_{v0}$; their suggested design line and bounds for β are also shown in Fig. 7(a).

38. Equations (18) and (20) can be rearranged to check their consistency with the trends indicated in Fig. 7(a). If, for simplicity, it is assumed that β is to be derived for a uniform material with constant values of (q_t/σ'_{v0}), I_{vr} and δ_f and where σ'_{v0} increases linearly with depth, integration of a combination of equations (18) and (20) gives

$$\beta = (q_t)_{mean}/q_s = 0{\cdot}72[(q_t/\sigma'_{v0})^{0{\cdot}4}(L/R)^{0{\cdot}2}]/[f_L \psi \tan\delta_f] \qquad (21)$$

39. Equation (21) indicates that, in addition to q_t/σ'_{v0}, β also varies strongly with I_{vr}, δ_f and L/R. However, for the purposes of comparison with Fig. 7(a), an average L/R ratio of 80 is assumed and typical I_{vr} values for lightly and heavily overconsolidated clays of 1·0 and −1·0 respectively are adopted (see Figs 2 and 3). It is also assumed that f_L is equal to 0·8 and that $\tan\delta_f$ varies from 0·2 in high-plasticity clay to 0·45 in low–medium-plasticity clay (see Fig. 6). The β variations with q_t/σ'_{v0} obtained using these substitutions are plotted in Fig. 7(b).

40. It is clear by comparison of Fig. 7(a) with Fig. 7(b) that there is general compatibility between equation (21) and the upper- and lower-bound β values proposed by Almeida *et al.*[35] This comparison serves to highlight the dependence of β on the parameters given in equation (21) and explains the range in measured β values in Fig. 7(a).

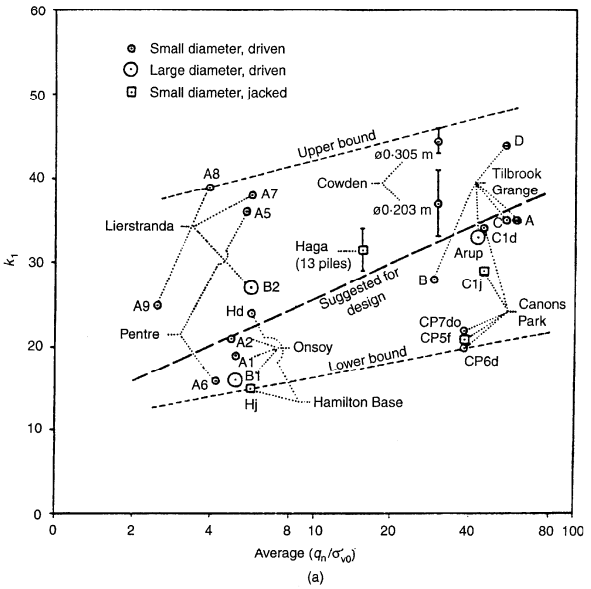

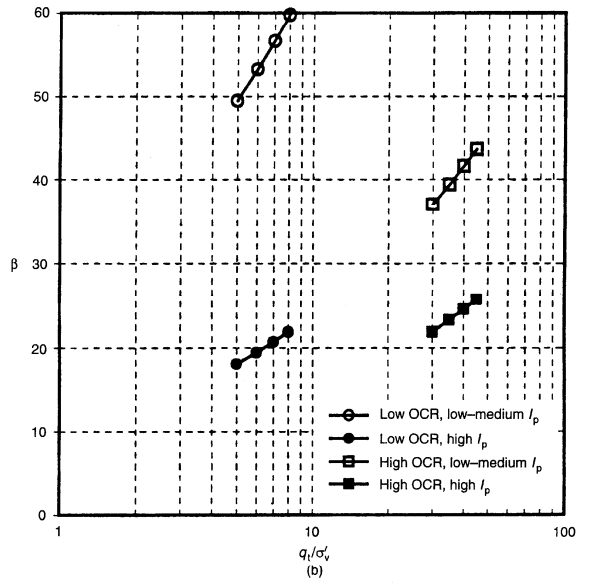

Fig. 7. (a) Database of Almeida et al. (b) Typical predictions given by new approach

Conclusions

41. High-quality instrumented pile tests have greatly assisted our understanding of the factors affecting the ultimate shear stress developed at a given location on the shaft of a closed-ended pile in clay. The investigation presented in this paper has shown that these shear stresses correlate well with the CPT q_t value but that other factors also need to be incorporated in a design approach; these factors include the interface friction angle between the soil and pile, the clay's sensitivity and the relative depth of the pile tip. Additional factors control the skin frictions developed on piles driven in silts and clayey silts.

42. The proposed approach differs from that presented in Jardine and Chow[6] by including q_t rather than YSR in the formulation. Although the YSR appears to be a controlling parameter

affecting the development of radial stresses on a pile, the alternative approach of using q_t in the manner presented in this paper has clear practical advantages and has a reliability comparable to that of the YSR formulation. Refinement of the approach described should be possible as the reporting of piezocone tests at driven pile test sites becomes more commonplace.

References

1. Briaud J. L. and Tucker L. M. Measured and predicted axial response of 98 piles. *Journal of Geotechnical Engineering*, ASCE, 1988, **114**, No. 9, 984–1001.
2. Bustamante M. and Gianeselli L. Pile bearing capacity prediction by means of static penetrometer CPT. *Proceedings of the 2nd European Symposium on Penetration Testing*, Amsterdam, 1982, vol. 2, 493–500.
3. De Ruiter J. and Beringen F. L. Pile foundations for large North Sea structures. *Marine Geotechnology*, 1979, **3**, No. 3, 267–314.
4. Campanella R. G., Gillespie D. and Robertson P. K. Pore pressures measured during cone penetration testing. *Proceedings of the 2nd European Symposium on Penetration Testing*, Amsterdam, 1982, vol. 2, 507–512.
5. Lehane B. M., Jardine R. J., Bond A. J. and Chow F. C. The development of shaft resistance on displacement piles in clay. *Proceedings of the 13th International Conference on Soil Mechanics and Foundation Engineering*, New Delhi, 1994, vol. 2, 473–476.
6. Jardine R. J. and Chow F. C. *New Design Methods for Offshore Piles*. MTD publication 96/103, 1996, HSE Books, London.
7. Jardine R. J., Chow F. C., Matsumoto T. and Lehane B. M. A new design procedure for driven piles and its application to two Japanese Clays. *Soils and Foundations*, 1998, **38**, No. 1, 207–219.
8. Chow F. C. *Investigations into the Behaviour of Displacement Piles for Offshore Foundations*. PhD thesis, Imperial College London, 1997.
9. Morrison M. J. *In Situ Measurements on a Model Pile in Clay*. PhD thesis, Massachusetts Institute of Technology, 1984.
10. Lehane B. M. *Experimental Investigations of Pile Behaviour Using Instrumented Field Piles*. PhD thesis, Imperial College London, 1992.
11. Bond A. J. *Behaviour of Displacement Piles in Overconsolidated Clays*. PhD thesis, Imperial College London, 1989.
12. Azzouz A. S. and Lutz D. G. Shaft behaviour of a model pile in plastic Empire clays. *Journal of Geotechnical Engineering*, ASCE, 1986, **112**, No. 4, 389–406.
13. Coop M. R. *The Axial Capacity of Driven Piles in Clay*. DPhil thesis, University of Oxford, 1987.
14. Karlsrud K. and Haugen T. Axial capacity of steel model piles in overconsolidated clay. *Proceedings of the 11th International Conference on Soil Mechanics and Foundation Engineering*, San Francisco, 1985, vol. 3, 1401–1406.
15. Norwegian Geotechnical Institute. *Summary, Interpretation and Analysis of the Pile Load Tests at the Lierstranda Test Site*. NGI report 52523-26. Rev. 1, July 1988.
16. Totani G., Marchetti S., Calabrese M. and Monaco P. Field studies of an instrumented full-scale pile driven in clay. *Proceedings of the 13th International Conference on Soil Mechanics and Foundation Engineering*, New Delhi, 1994, vol. 2, 695–698.
17. Norwegian Geotechnical Institute. *Summary, Interpretation and Analysis of the Pile Load Tests at the Onsøy Test Site*. NGI report 52523-23, Rev. 15, March 1988.
18. Norwegian Geotechnical Institute. *Summary, Interpretation and Analysis of the Pile Load Tests at the Pentre Test Site*. NGI report 52523-27, Rev. 16, August 1988.
19. Soares M. M. and Dias C. R. R. Behaviour of an instrumented pile in the Rio de Janeiro clay. *Proceedings of the 12th International Conference on Soil Mechanics and Foundation Engineering*, Rio de Janeiro, 1990, vol. 1, 319–322.
20. Koizumi Y. and Ito K. Field tests with regard to pile driving and bearing capacity of piled foundations. *Soils and Foundations*, **7**, No. 3, 30–53.
21. Lehane B. M. and Phillips D. P. *Instrumented Displacement Piles Subjected to Lateral and Combined Lateral and Axial Loading*. Department of Civil Engineering, Trinity College Dublin, 1996, report BL-DPP-1999(2).
22. Lehane B. M. and Jardine R. J. Displacement pile behaviour in glacial clay. *Canadian Geotechnical Journal*, 1994, **31**, No. 1, 79–90.
23. Lehane B. M. and Jardine R. J. Displacement pile behaviour in a soft marine clay. *Canadian Geotechnical Journal*, 1994, **31**, No. 2, 181–191.
24. Ladd C. C., Foott R., Ishihara K., Schlosser F. and Poulos H. G. Stress–deformation and strength characteristics. *Proceedings of the 9th International Conference on Soil Mechanics and Foundation Engineering*, Tokyo, 1977, vol. 2, 421–494.
25. Burland J. B. On the compressibility and shear strength of natural clays. *Géotechnique*, 1990, **40**, No. 3, 327–378.
26. Chen B. S. and Mayne P. W. Type 1 and 2 piezocone evaluations of overconsolidation ratio in clays. *Proceedings of the International Symposium on Cone Penetration Testing*, Linkoping, 1995, vol. 2, 143–148.
27. Rasmussen J. L., Feld T. and Gravgaard J. H. Comparison between cone factor, activity index and OCR for clay. *Proceedings of the International Symposium on Cone Penetration Testing*, Linkoping, 1995, vol. 2, 283–287.
28. Karlsrud K., Kalsnes B. and Nowacki F. Response of piles in soft clay and silt deposits and cyclic loading based on recent instrumented pile load tests. *Proceedings of a Conference on Offshore Site Investigation and Foundation Behaviour*. Society for Underwater Technology, Kluwer, London, 1992, pp. 549–584.
29. Ramsey N., Jardine R. J., Lehane B. M. and Ridley A. A review of soil–steel interface testing with the ring shear apparatus. *Proceedings of a Conference on Offshore Site Investigation and Foundation Behaviour*. Society for Underwater Technology, Kluwer, London, 1998, pp. 237–258.
30. Wardle I. F., Price G. and Freeman T. J. Effect of time and maintained load on the ultimate capacity of piles in stiff clay. *Proceedings of the*

Conference on Piling in Europe. Thomas Telford, London, pp. 92–99.
31. KONRAD J. M. and ROY M. Bearing capacity of friction piles in marine clay. *Géotechnique*, 1987, **37**, No. 2, 163–175.
32. KRAFT L. M. Effective stress capacity model for piles in clay. *Journal of the Geotechnical Engineering Division*, ASCE, 1982, **108**, No. 11, 1387–1404.
33. KARLSRUD K., BORG HANSEN S., DYVIK R. and KALSNES B. NGI's pile tests at Tilbrook and Pentre—review of testing procedures and results. *Proceedings of the Conference on Large Scale Pile Tests in Clay*. Thomas Telford, London, 1992, pp. 405–429.
34. BOTTIAU N. Comparative assessment of bearing capacity from CPT results. *Proceedings of the International Symposium on Cone Penetration Testing*, Linkoping, 1995, vol. 2, 399–406.
35. ALMEIDA M., DANZIGER F. and LUNNE T. The use of the piezocone test to predict the axial capacity of driven and jacked piles. *Canadian Geotechnical Journal*, 1996, **33**, 23–41.

Please email, fax or post your discussion contributions to the secretary: email: wilson_l@ice.org.uk; fax: +44 (0)20 7799 1325; or post to Lesley Wilson, Journals Department, Institution of Civil Engineers, 1–7 Great George Street, London SW1P 3AA.

Appendix 2-2

Typical trends shown by Pile Group Analysis Methods of Sections 2.8-2.10

Introduction

Poulos (Rankine Lecture, 1989) provides an excellent summary of the factors which govern the behaviour of pile groups, based upon broad experience with many of the analytical techniques described earlier in Sections 2-8, 2-9 and 2-10 and other work. These analytical techniques are not always applied directly in practice, but form the basis of convenient design curves and charts. These charts offer a qualitative indication of the likely effect of the controlling parameters on foundation performance. However, many are based on linear elastic theory and should be used with caution for quantitative analysis.

Interaction factors

O'Neill (1983) suggests that the interaction between a pair of piles is influenced by the characteristics of piles and soil, in addition to the pile and group geometry of each pile and the group. Interaction increases with increased pile compressibility ($\lambda = E_p/E_s$). Interaction reduces with an increase in ρ, the ratio of the soil's Young's modulus below the pile base to that above the pile base ($\rho=E_b/E_{sh}$). End bearing piles interact less strongly than friction piles. The variation of E_s with depth also influences interaction, piles in Gibson soil (linear stiffness-depth variation) interact less than piles in a homogeneous medium. The effects of each of these parameters on a two-pile interaction factor (α) may be seen in Figure A2-2.1.

It is very significant that early published solutions for interaction factors assumed that the piles were friction piles ($E_b/E_s=1$) which were incompressible ($K= \infty$) and located in a homogeneous soil. It is clear from Figure A2-2.1 that the combination of all three extremes explains the tendency to overestimate group settlements.

The geometrical factors governing interaction are the pile spacing and pile length, usually given as a proportion of the pile diameter (s/D and L/D respectively) and the number of piles N. The L/D dependence shown in Figure A2-2.2 is perhaps the least obvious of these. This has most relevance for the design of stocky piles but develops minor

importance for piles with L/D>25, so its effect is not pronounced for the vast majority of service piles.

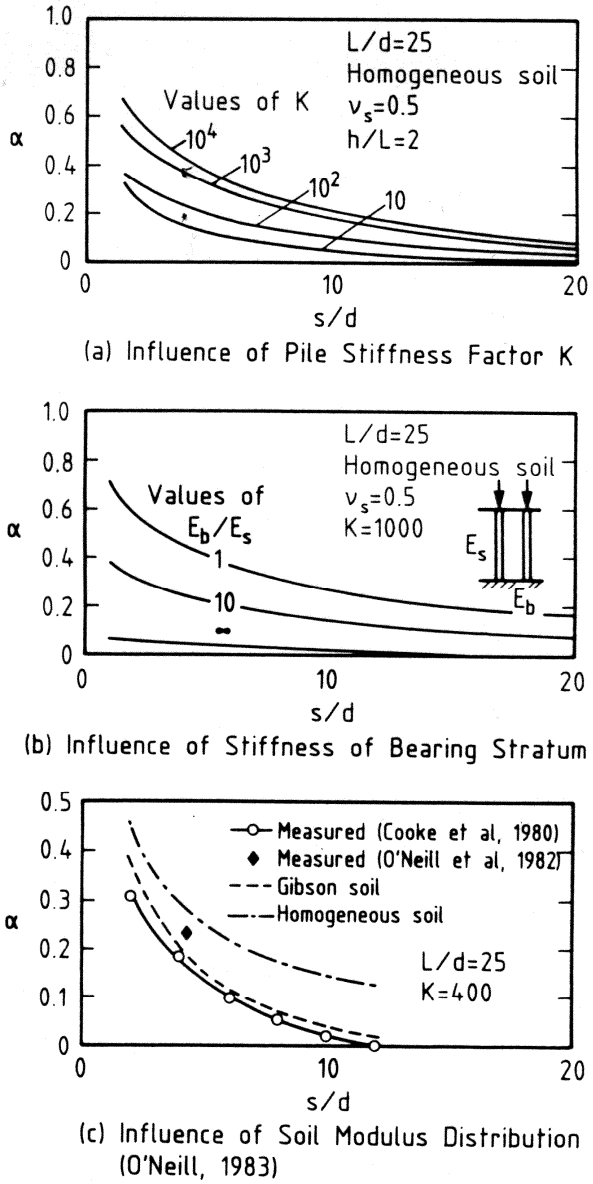

Figure A2-2.1 Non-geometrical factors governing two pile interaction (O'Neill 1983)

Normalised Expressions for Group Stiffness Definitions

In order to compare different pile groups (and individual piles within a group), dimensionless stiffness parameters have been adopted as a framework for assessing the effects of different variables in the analysis.

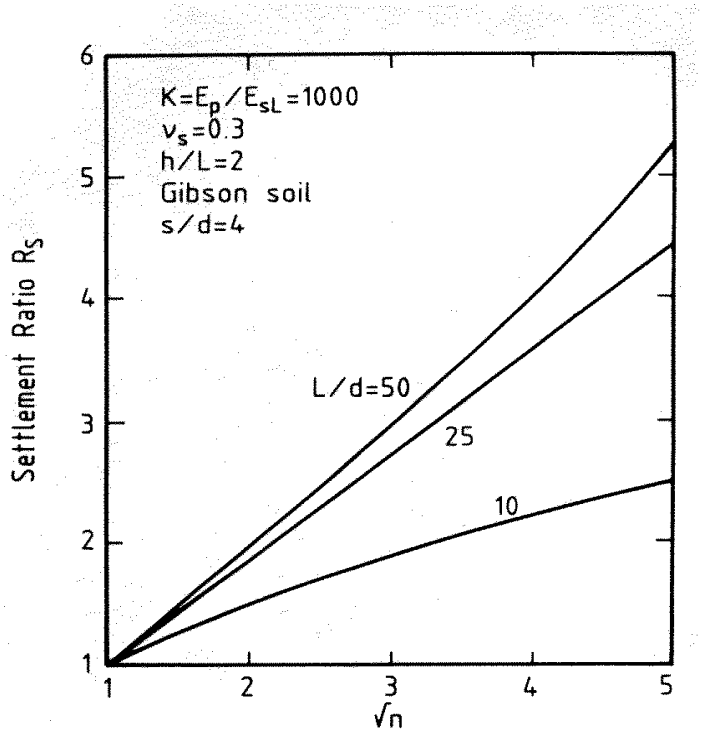

Figure A2-2.2 Influence of pile aspect ratio (L/D) upon interaction

These consist of terms reflecting the load-displacement 'stiffness' of a complete group/group pile normalized by a term defining the stiffness of the soil.

Randolph and Wroth (1978)

The most widely used dimensionless coefficient stems from the single pile load-transfer hypothesis of Randolph and Wroth (1978) as described in Section 2.3:

$$\frac{P}{G_L r_o w}$$

P is redefined as the average load on a group pile imposing an average group settlement of w. An example of its use is taken from Guo and Randolph (1999) where the normalised stiffness term is plotted as a function of L/r_o. Within this framework, it may be seen that:

- The normalized stiffness of a complete group decreases as a function of pile group size (Figure A2-2.3)

- The normalized stiffness of an individual group pile is shown to depend strongly upon its location within the group and also depends on the variation of G_L with depth (Figures A2-2.4 and A2-2.5 respectively)

The stiffness variation with position within the group (Figures A2-2.4 and A2-2.5) predicted by GASGROUP appears to be unrealistically skewed; highlighting the tendency of linear elastic analyses to overpredict interaction effects. The GASGROUP predictions appear to be in reasonable agreement with Butterfield and Banerjee (1971).

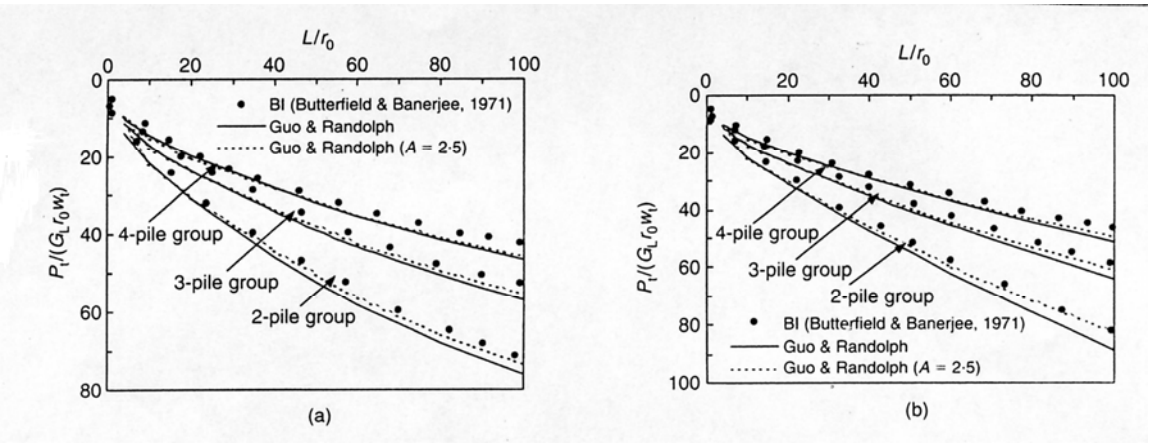

Figure A2-2.3 GASGROUP predictions of pile head stiffness for 3 groups in homogeneous soil (a) λ=6000, s/r_o=5, υ=0.5; (b) λ=∞, s/r_o=5, υ=0.5 (Guo and Randolph 1999)

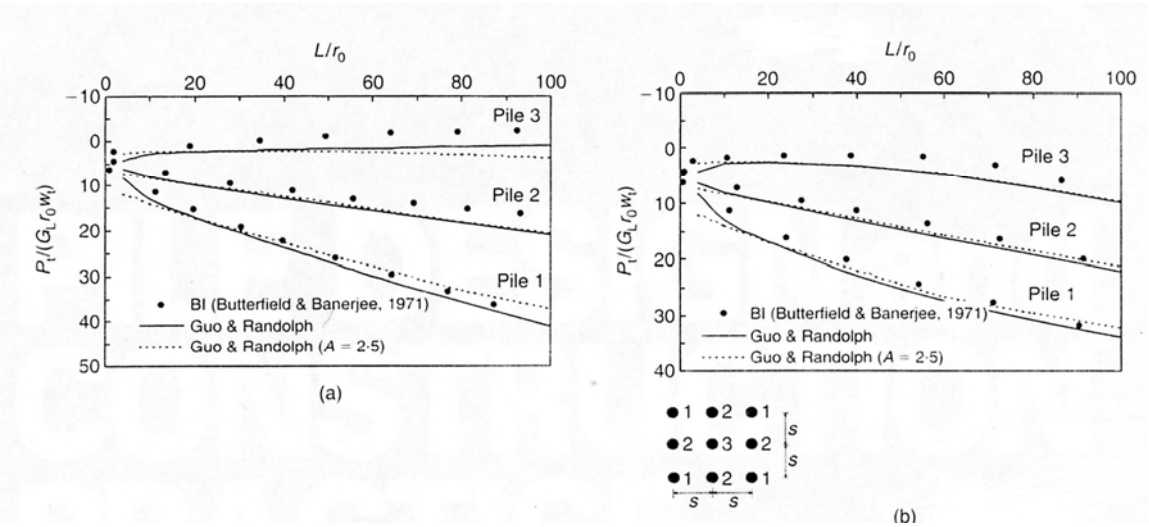

Figure A2-2.4 GASGROUP predictions of pile head stiffness in homogeneous soil (a) λ=6000, s/r_o=5, υ=0.5; (b) λ=∞, s/r_o=5, υ=0.5 (Guo and Randolph 1999)

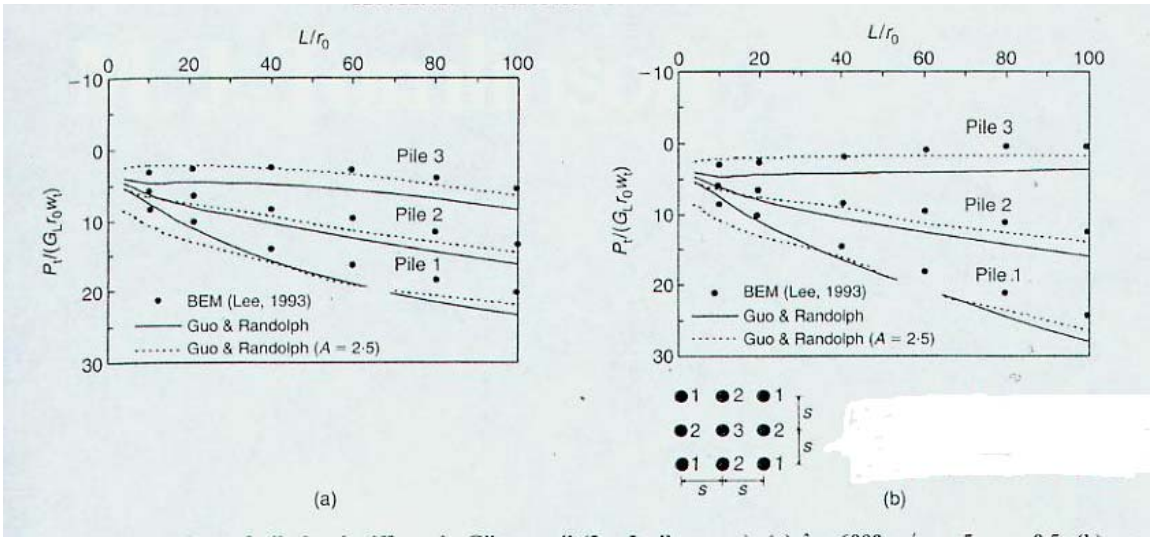

Figure A2-2.5 GASGROUP predictions of pile head stiffness in Gibson soil (a) λ=6000, s/r_o=5, υ=0.5; (b) λ=∞, s/r_o=5, υ=0.5 (Guo and Randolph 1999)

Randolph (1994)

An alternative non-dimensional coefficient more pertinent to pile groups incorporates pile spacing (s) and number of piles (n) (Randolph 1994):

$$\frac{k_p}{\sqrt{n}sG_L}$$

where k_p is defined as the total group pile divided by the average pile displacement.

The relative merits of five of the analysis approaches described (PIGLET, DEFPIG, GRUPPALO, PGROUP and PGROUPN) are readily seen when used within this framework (Figure A2-2.6). The variation of the normalised group stiffness term with group size is shown for square groups of piles (L/D=25, E_p/G=1000 and υ=0.5). Not surprisingly, good agreement is obtained between the methods for single piles and very small pile groups. However, as group sizes increase to practical proportions, estimates of load interaction diverge. GRUPPALO compares relatively well with PGROUP and PGROUPN, the more rigorous of the five methods. However, PIGLET and DEFPIG predictions are quite poor and differ by at least a factor of two for groups of 20×20 piles.

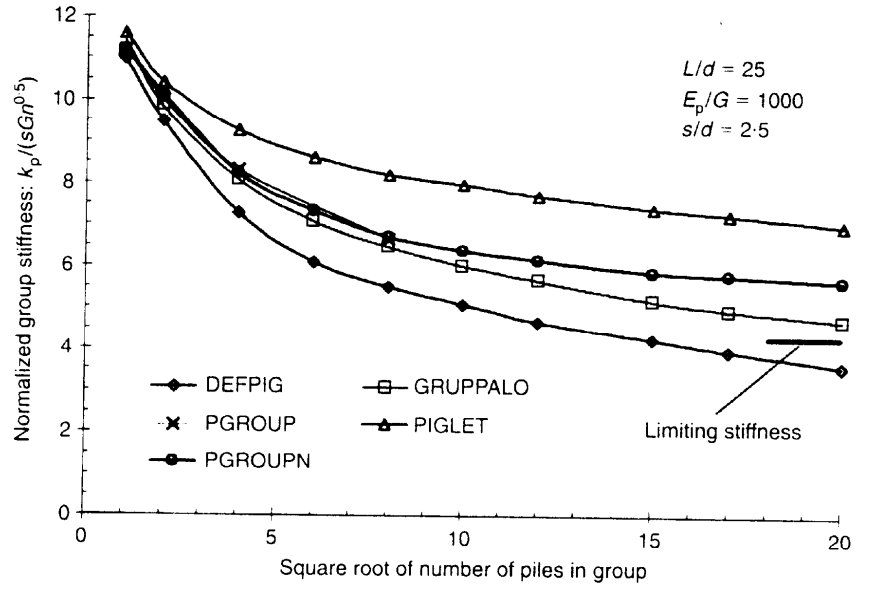

Fig. 2. Comparison of different pile group analysis methods for: (a) $s/d = 2{\cdot}5$; (b) $s/d = 5$

Figure A2-2.6 Comparison of different pile group analysis methods (Basile 1999)

While both DEFPIG and GRUPPALO are both classified as SBE Methods, GRUPPALO's more realistic prediction reflects that interaction effects are modelled more appropriately using the technique of Caputo and Viggiani (1984) than the approach of Poulos (1971). In addition, Poulos (1989) notes that if the standard DEFPIG interaction factors were substituted by those in PIGLET, both approaches would essentially yield the same output.

When the scale of a pile group becomes extremely large, then the corresponding normalised stiffness approaches that of a shallow foundation. When plotted within the framework described, Guo and Randolph (1999) show that GASGROUP predictions converge towards those for a shallow foundation at s/D=2.5, but become lower than that of a shallow foundation at s/D=5. The authors cite Cooke (1986) who notes that different mechanisms pertain to widely and densely spaced pile groups.

Poulos (1989)

Poulos (1989) proposed an equivalent parameter to that of Randolph and Wroth (1978), but expressed as a normalised flexibility term called a settlement influence factor (I_G):

$$I_G = \frac{w_G dE_L}{P_G}$$

where P_G is the load exerted on the pile group, w_G is the settlement of the pile group, d is the pile diameter and E_L is the soil's Young's modulus at the pile tip level. Guo and Randolph's (1999) plots of I_G against number of piles show reasonable consistency over a number of approaches. For any given spacing, there appears to be a limiting number of piles beyond which I_G remains constant with increased group scale.

Settlement Ratio

Arguably the simplest non-dimensional coefficient for group interpretation is the settlement ratio (R_s). R_s is defined as the ratio of the settlement of a pile group to that of a single pile corresponding to the same average load per pile. Since R_s does not include a measure of soil stiffness, different groups in different soil types are not directly

comparable. However, single and group pile behaviour in the same material may be related easily to one another.

Chow (1986) shows that R_s increases as the pile spacing reduces, showing a marked increase at s/D ≈4. At any given spacing, R_s depends strongly upon the number of piles. The prediction in Figure A2-2.8 corresponds with L/r_o = 40, λ = ∝ and υ = 0.5. The agreement between Chow's work and the boundary integral method solution of Butterfield and Banerjee is probably misleading given the small pile groups considered.

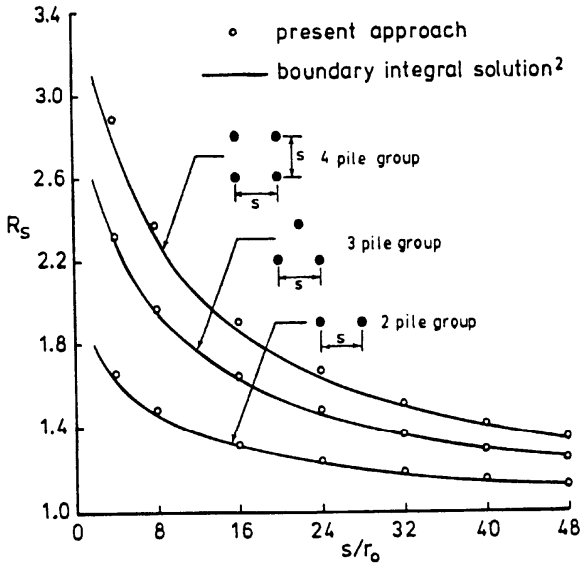

Comparison of settlement ratios for pile groups ($l/r_0 = 40$; $\lambda = \infty$; $\nu = 0{\cdot}5$)

Figure A2-2.8 Variation of R_s as a function of pile spacing (Chow 1986)

Consolidation Settlement

The immediate settlement of a pile group is determined by using undrained soil parameters, while total settlement (i.e. once the soil around the pile group has consolidated) may be estimated from drained values. Poulos (1989) suggests that the *proportion* of long-term or creep settlement to total settlement increases with the number of piles in the group.

Appendix 3-1

Chemical Tests on Sleech samples

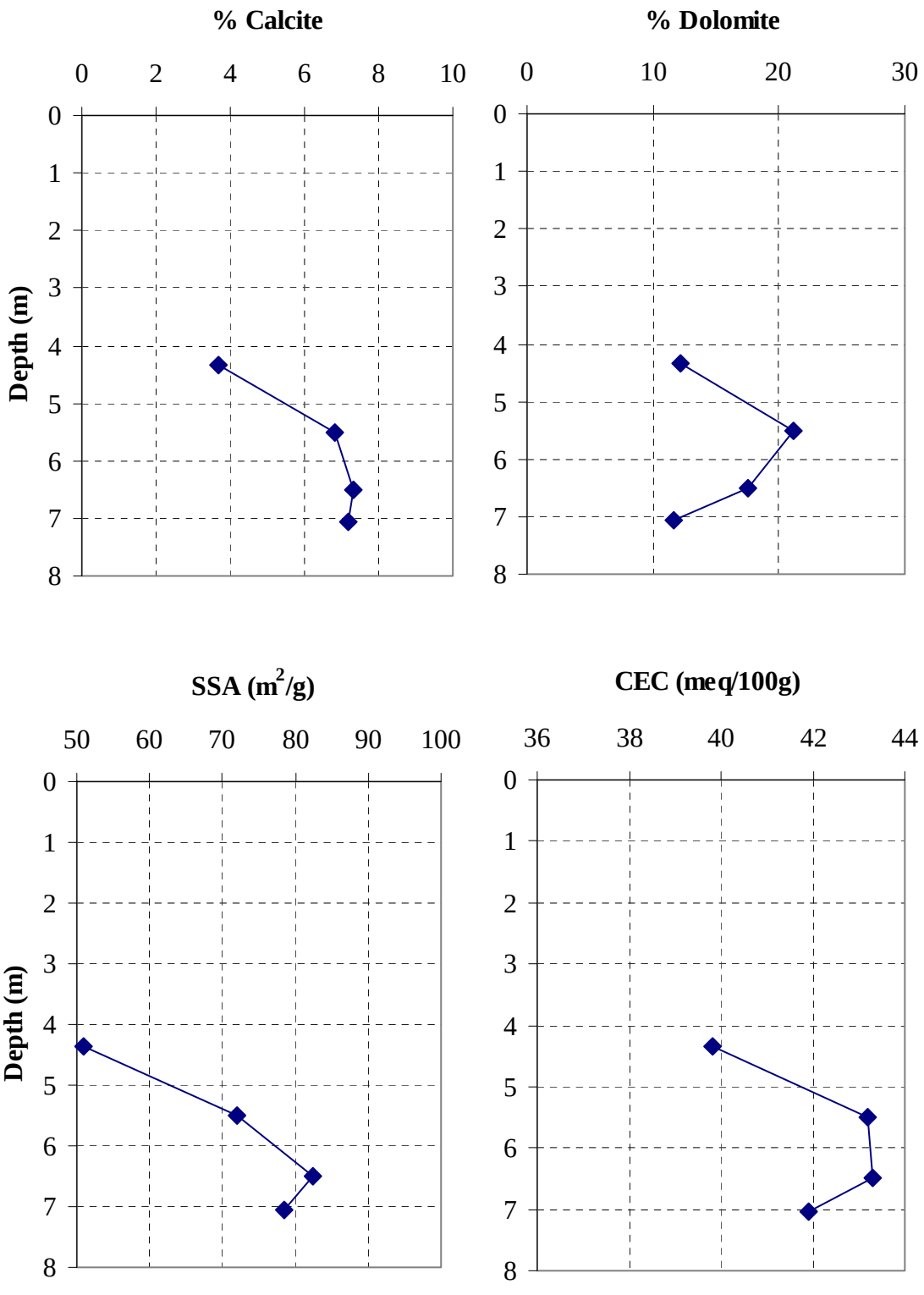

Chemical tests on sleech (carried out at University of Massachusetts, Amherst, USA)

Appendix 3-2

X-Ray Diffractograms on sleech samples

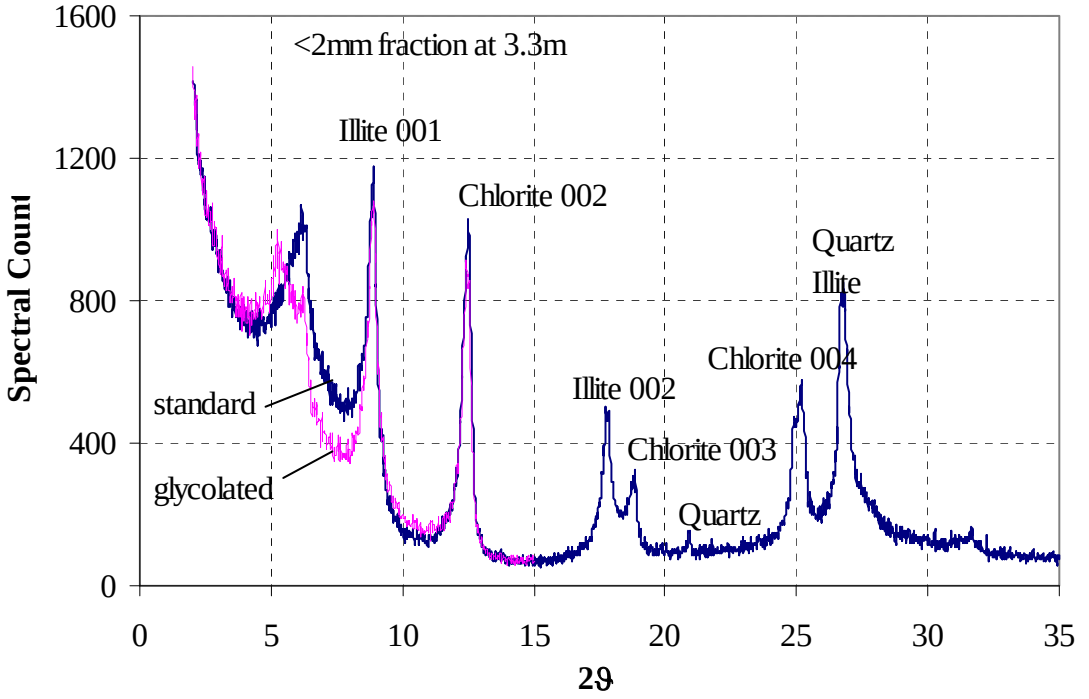

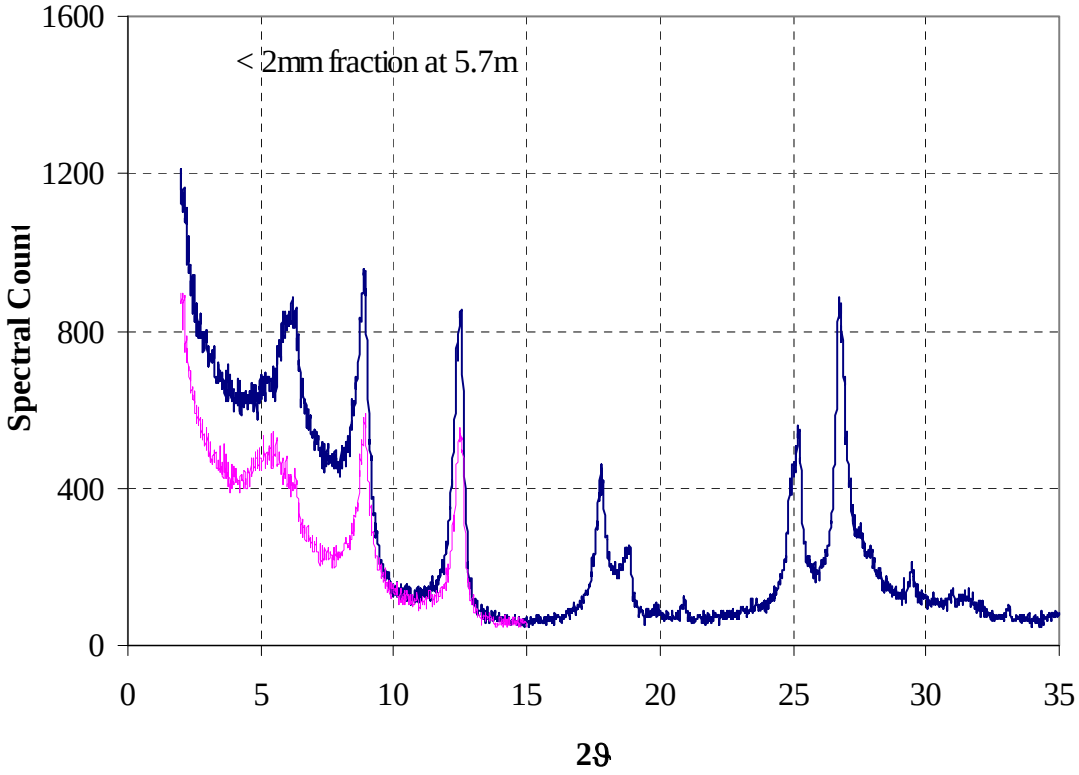

X-Ray Diffraction Spectra of Sleech clay fraction

Appendix 3-3

Selected Scanning Electron Microscope (SEM) Images of Sleech

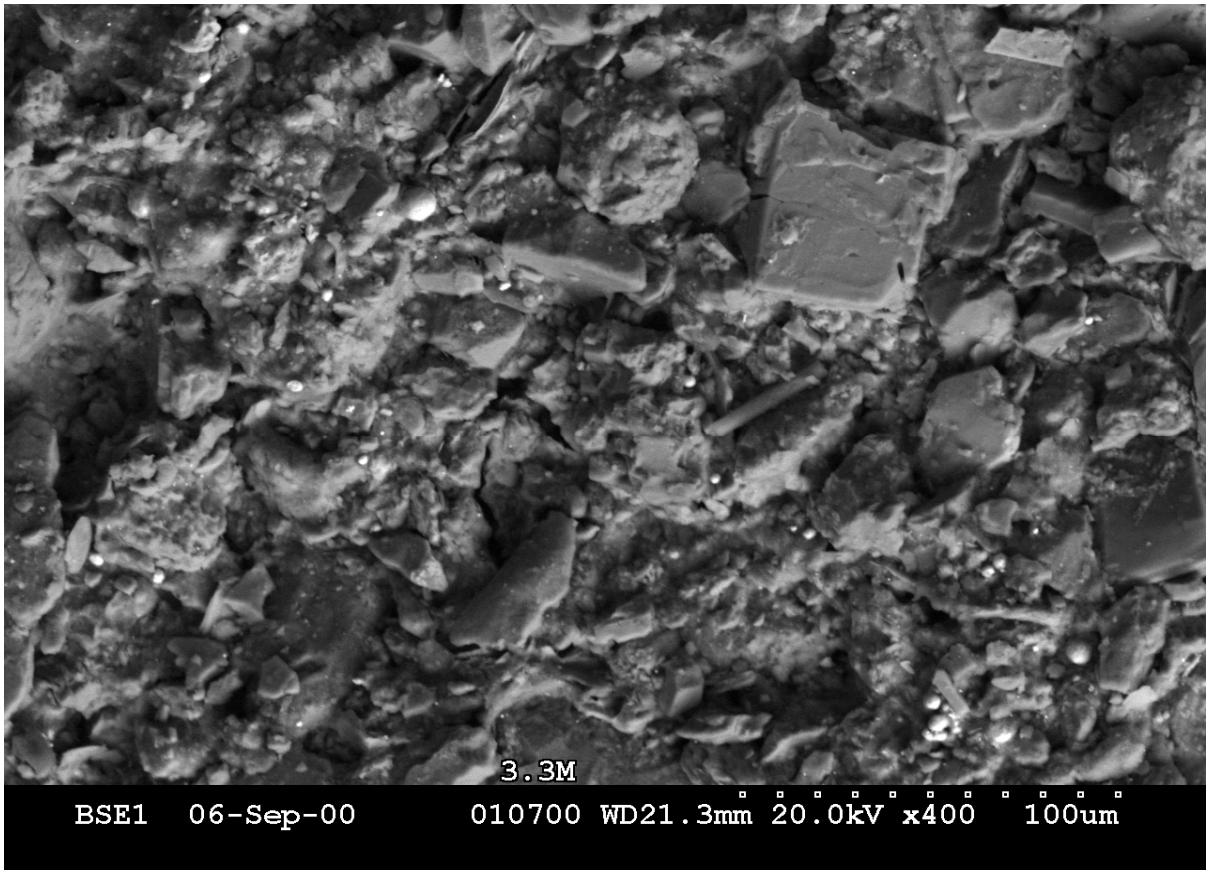
3.3M
BSE1 06-Sep-00 010700 WD21.3mm 20.0kV x400 100um

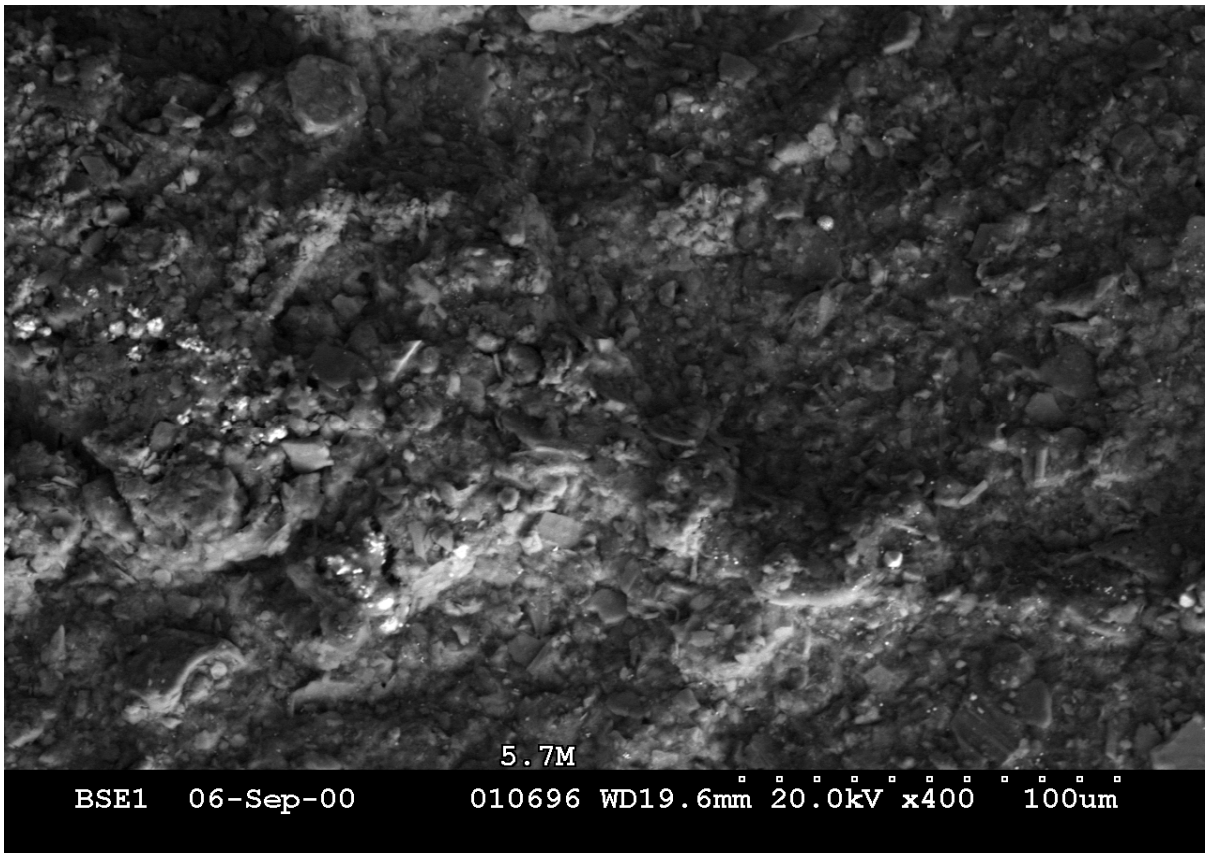
5.7M
BSE1 06-Sep-00 010696 WD19.6mm 20.0kV x400 100um

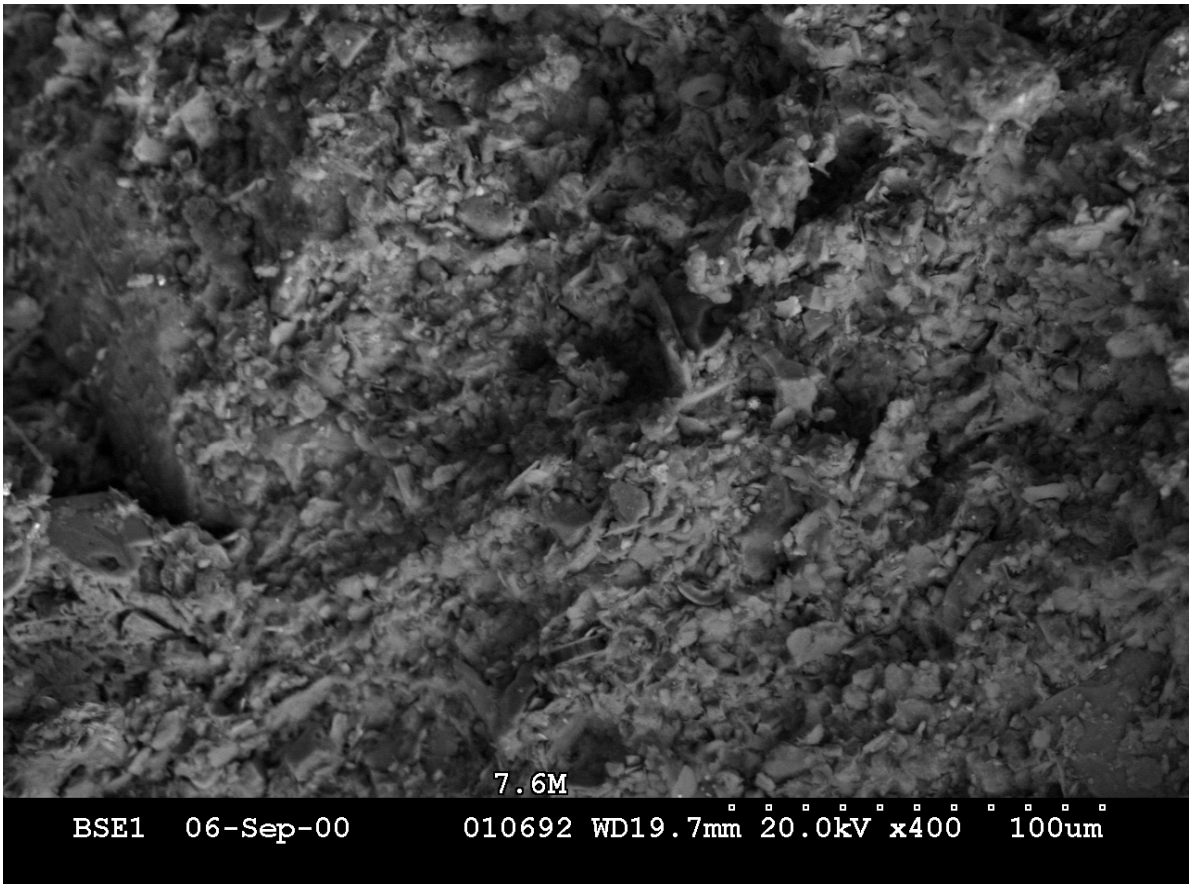
7.6M
BSE1 06-Sep-00 010692 WD19.7mm 20.0kV x400 100um

Appendix 3-4

Selected Cone Penetration Tests and Robertson's Charts

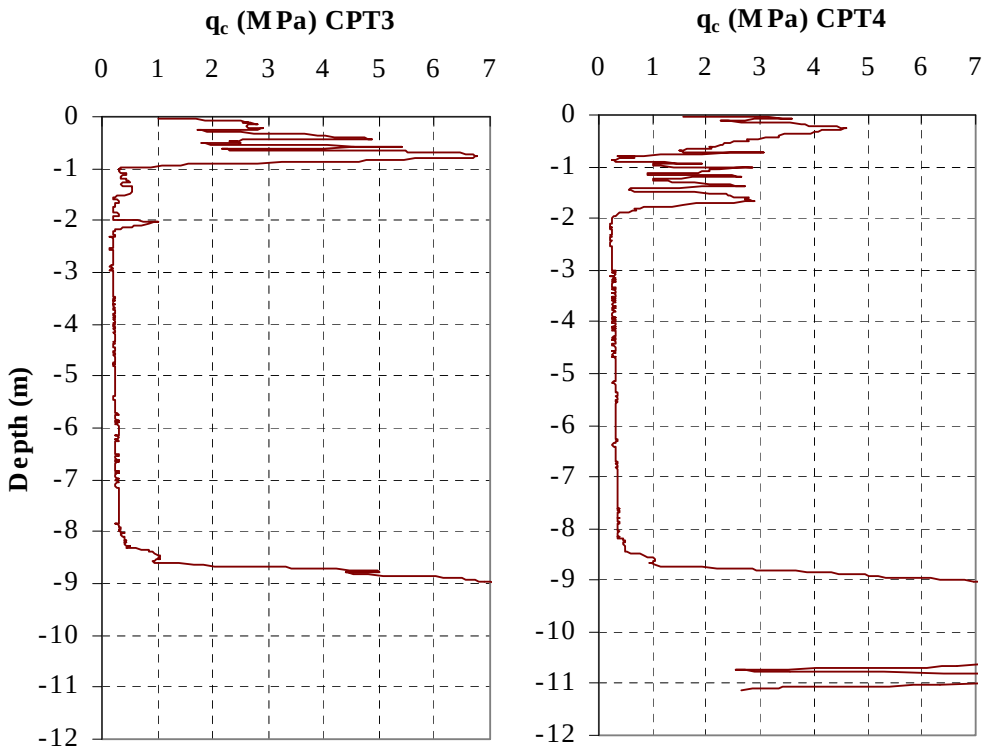
q_c (MPa) CPT3
0 1 2 3 4 5 6 7
0 -1 -2 -3 -4 -5 -6 -7 -8 -9 -10 -11 -12
Depth (m)

q_c (MPa) CPT4
0 1 2 3 4 5 6 7
0 -1 -2 -3 -4 -5 -6 -7 -8 -9 -10 -11 -12

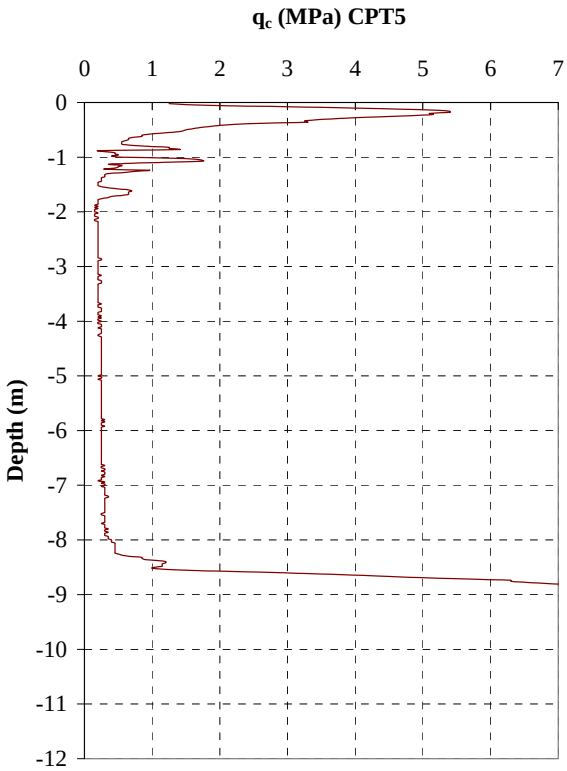
q_c (MPa) CPT5
0 1 2 3 4 5 6 7
0 -1 -2 -3 -4 -5 -6 -7 -8 -9 -10 -11 -12
Depth (m)

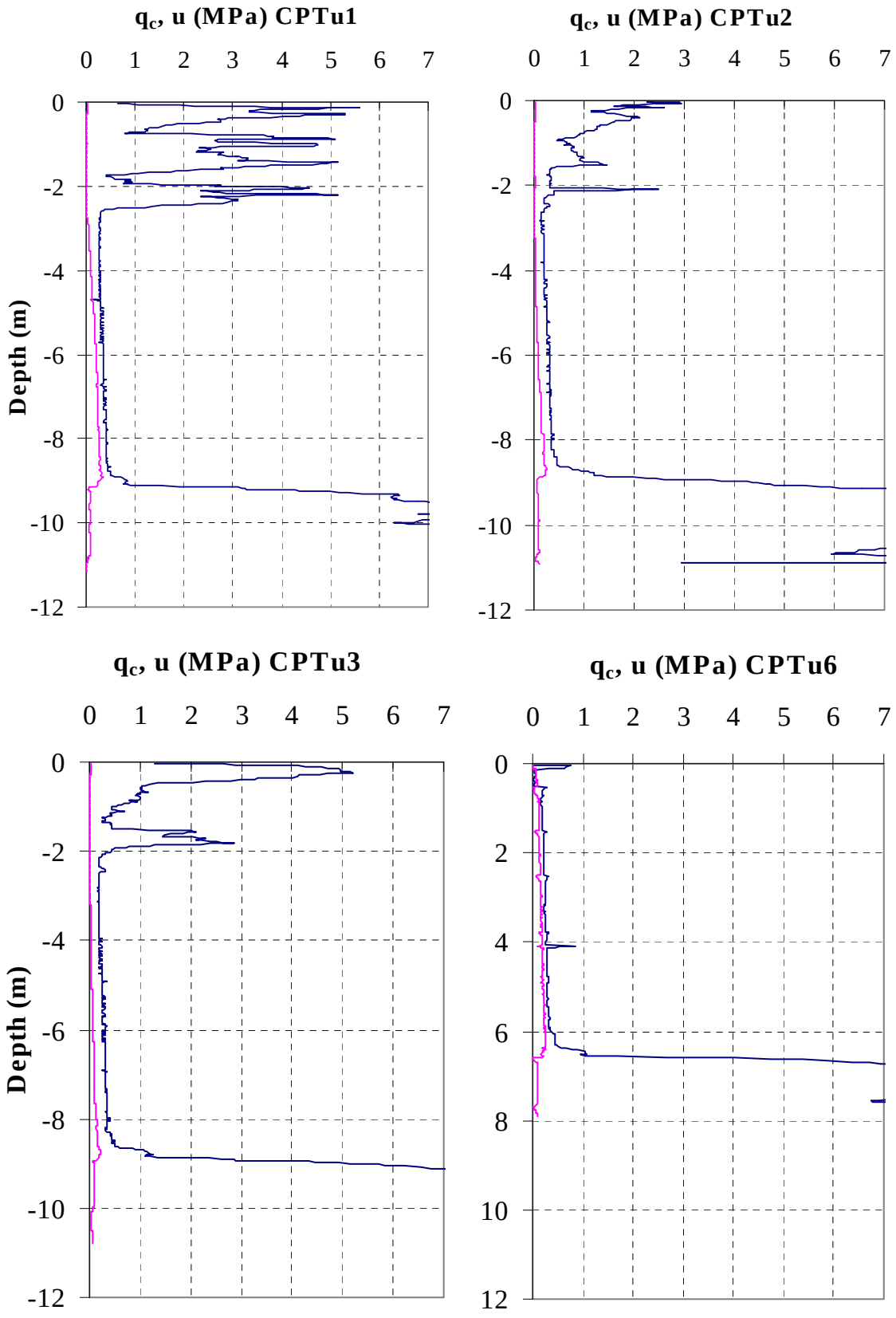
qc, u (MPa) CPTu1
0 1 2 3 4 5 6 7
0 -2 -4 -6 -8 -10 -12
Depth (m)
qc, u (MPa) CPTu2
0 1 2 3 4 5 6 7
0 -2 -4 -6 -8 -10 -12
qc, u (MPa) CPTu3
0 1 2 3 4 5 6 7
0 -2 -4 -6 -8 -10 -12
Depth (m)
qc, u (MPa) CPTu6
0 1 2 3 4 5 6 7
0 2 4 6 8 10 12

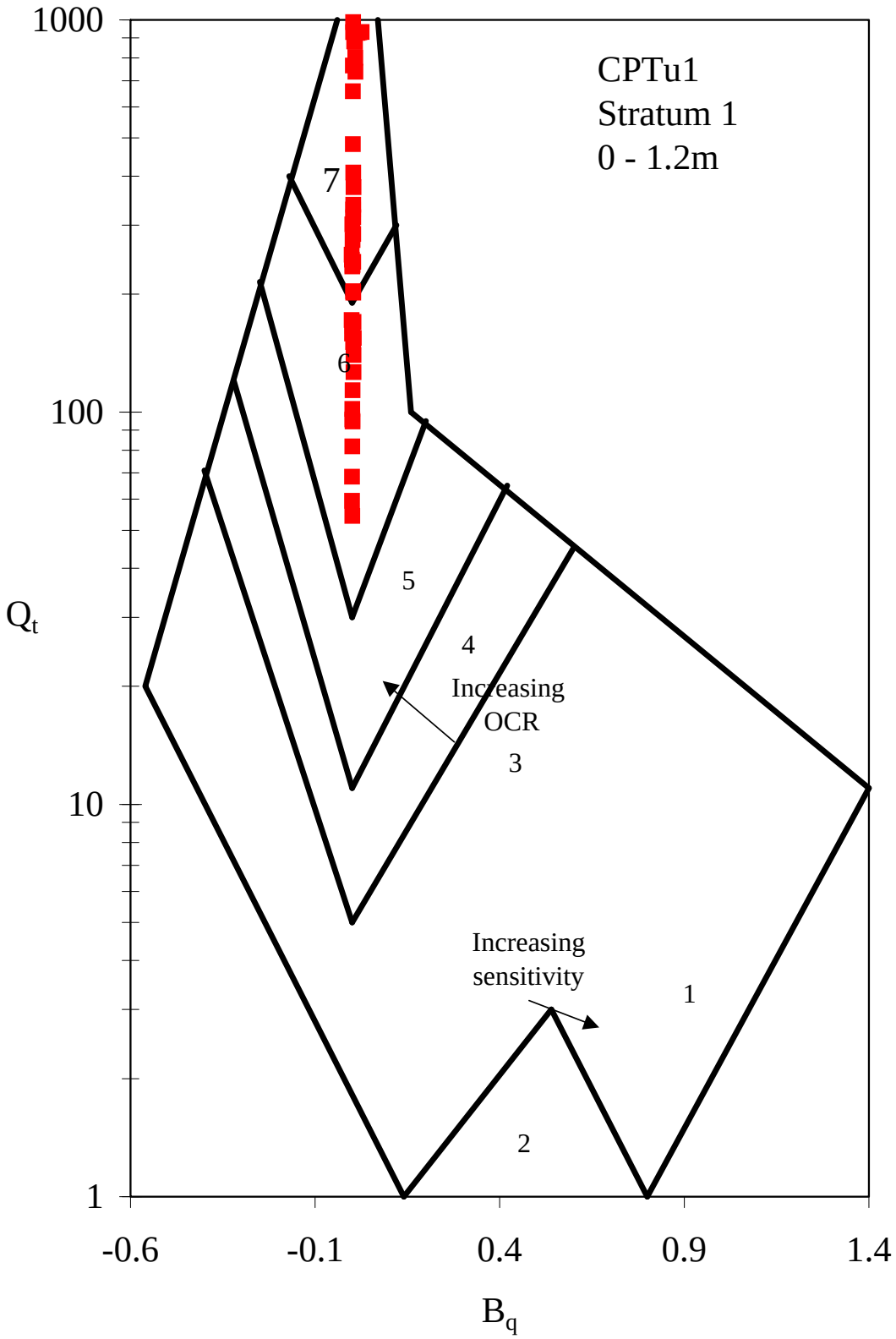
CPTu1
Stratum 1
0 - 1.2m
1000
100
10
1
Q_t
-0.6
-0.1
0.4
0.9
1.4
B_q
7
6
5
4
3
2
1
Increasing
OCR
Increasing
sensitivity

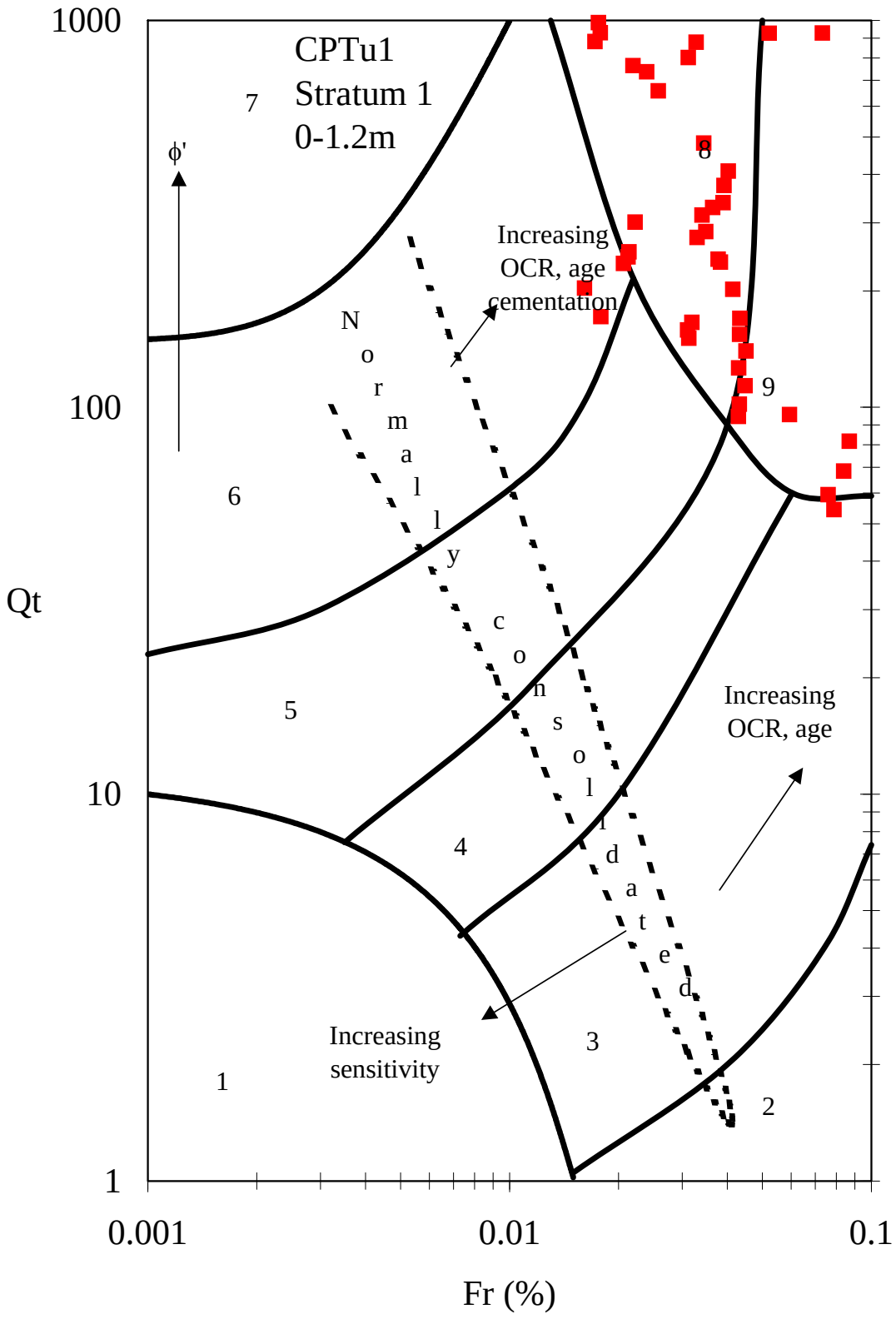
1000
100
10
1
Qt
0.001
0.01
0.1
Fr (%)
CPTu1
Stratum 1
0-1.2m
ϕ'
Increasing
OCR, age
cementation
Normally consolidated
Increasing
OCR, age
Increasing
sensitivity
1
2
3
4
5
6
7
8
9

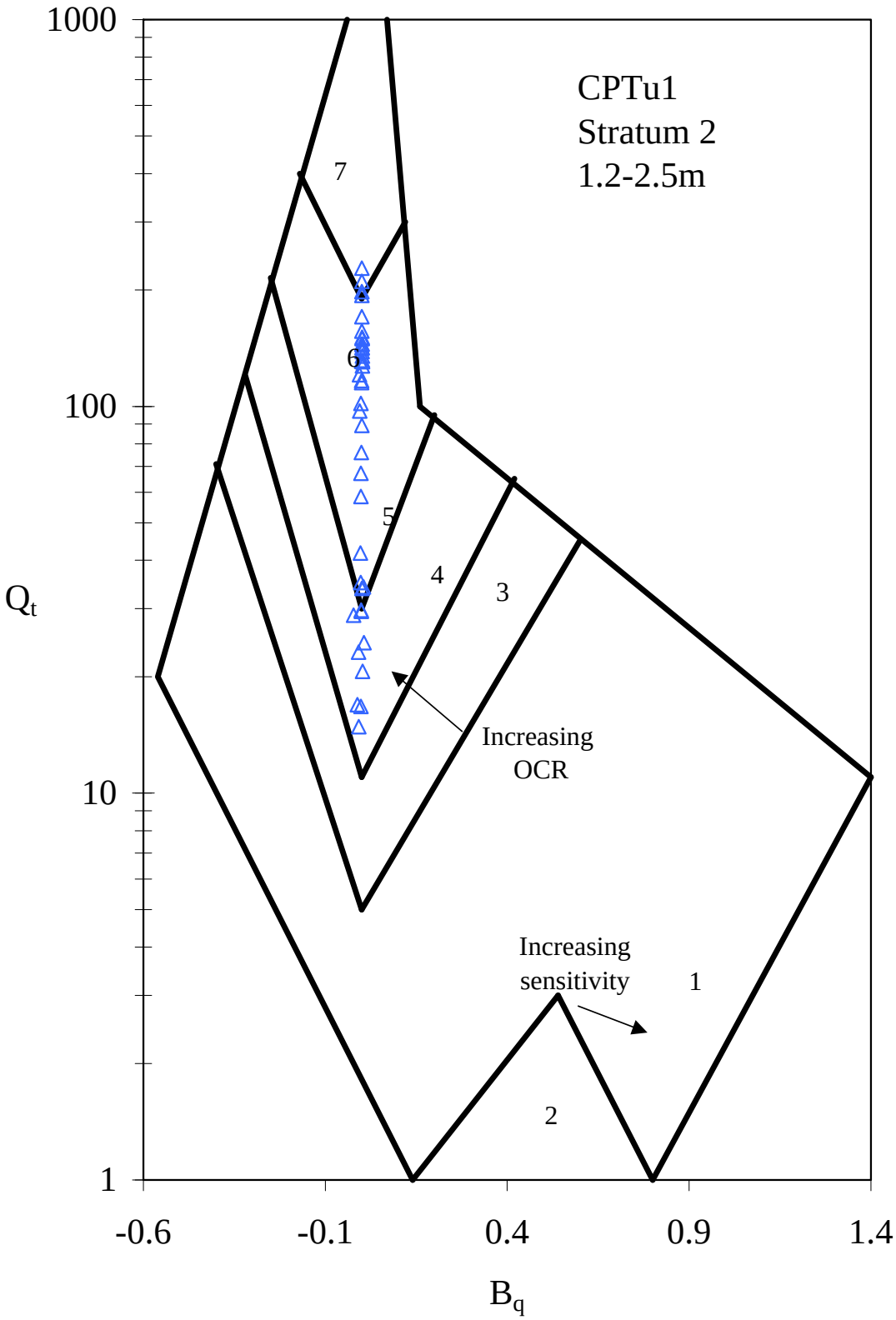
CPTu1
Stratum 2
1.2-2.5m
1000
100
10
1
Qt
-0.6
-0.1
0.4
0.9
1.4
Bq
7
6
5
4
3
2
1
Increasing
OCR
Increasing
sensitivity

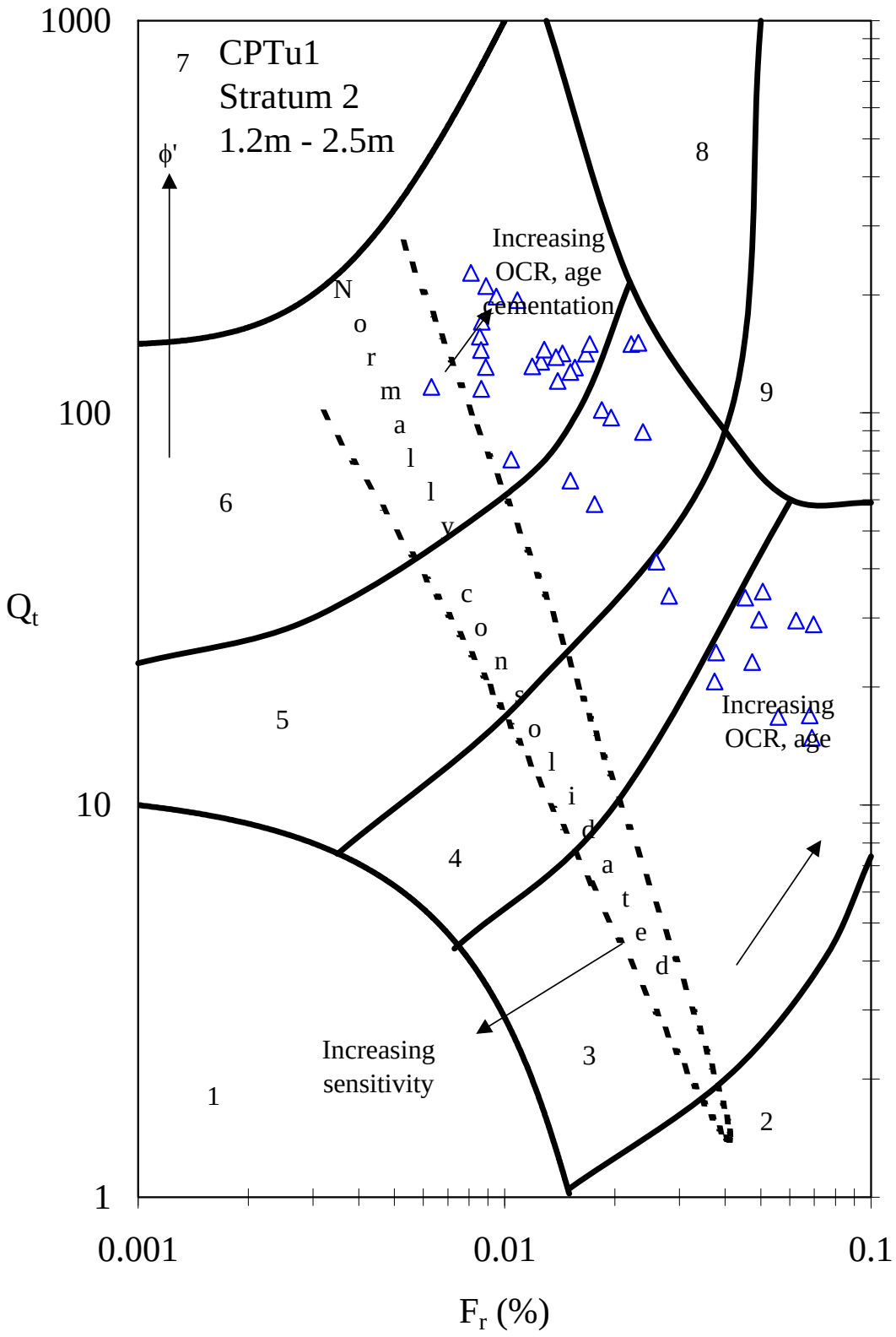
1000
100
10
1
0.001
0.01
0.1
Q_t
F_r (%)
CPTu1
Stratum 2
1.2m - 2.5m
ϕ'
7
8
9
6
5
4
3
2
1
Normally consolidated
Increasing OCR, age cementation
Increasing OCR, age
Increasing sensitivity

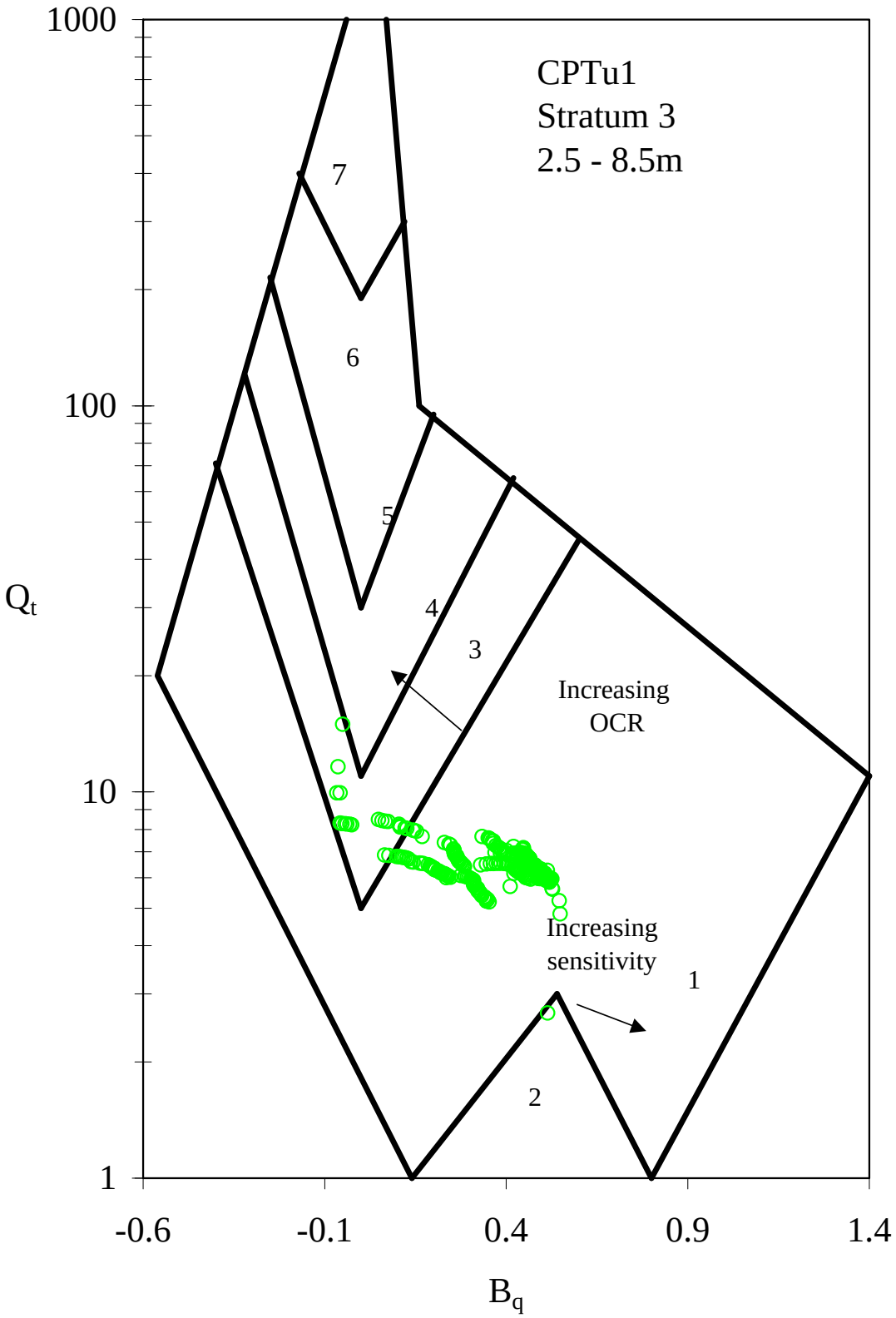
CPTu1
Stratum 3
2.5 - 8.5m
1000
100
10
1
Qt
-0.6
-0.1
0.4
0.9
1.4
Bq
7
6
5
4
3
2
1
Increasing
OCR
Increasing
sensitivity

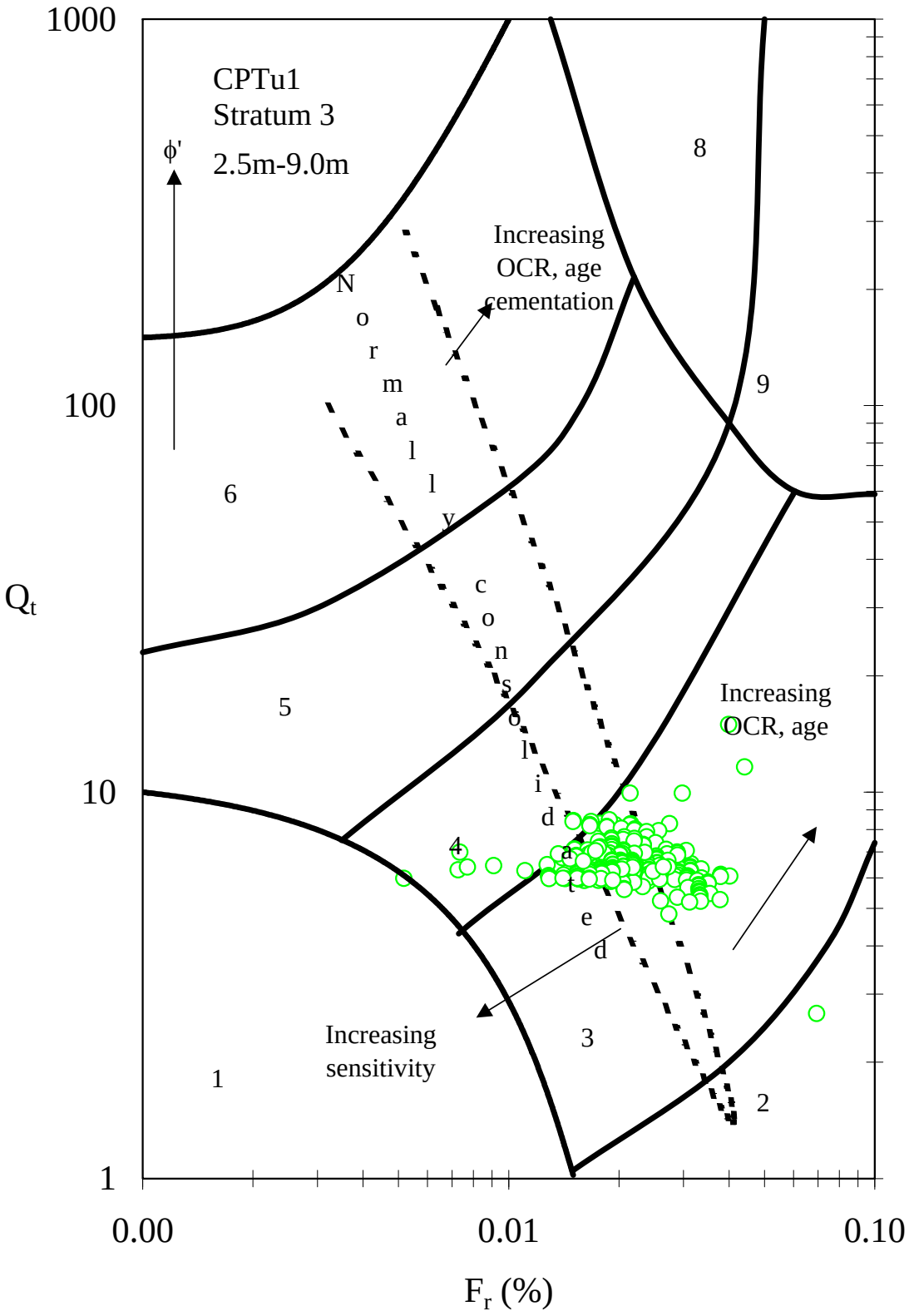
1000
100
10
1
Q_t
0.00
0.01
0.10
F_r (%)
CPTu1
Stratum 3
2.5m-9.0m
ϕ'
Increasing
OCR, age
cementation
Normally consolidated
Increasing
OCR, age
Increasing
sensitivity
1
2
3
4
5
6
8
9

Appendix 3-5

e-log σ'_v *Oedometer Curves*

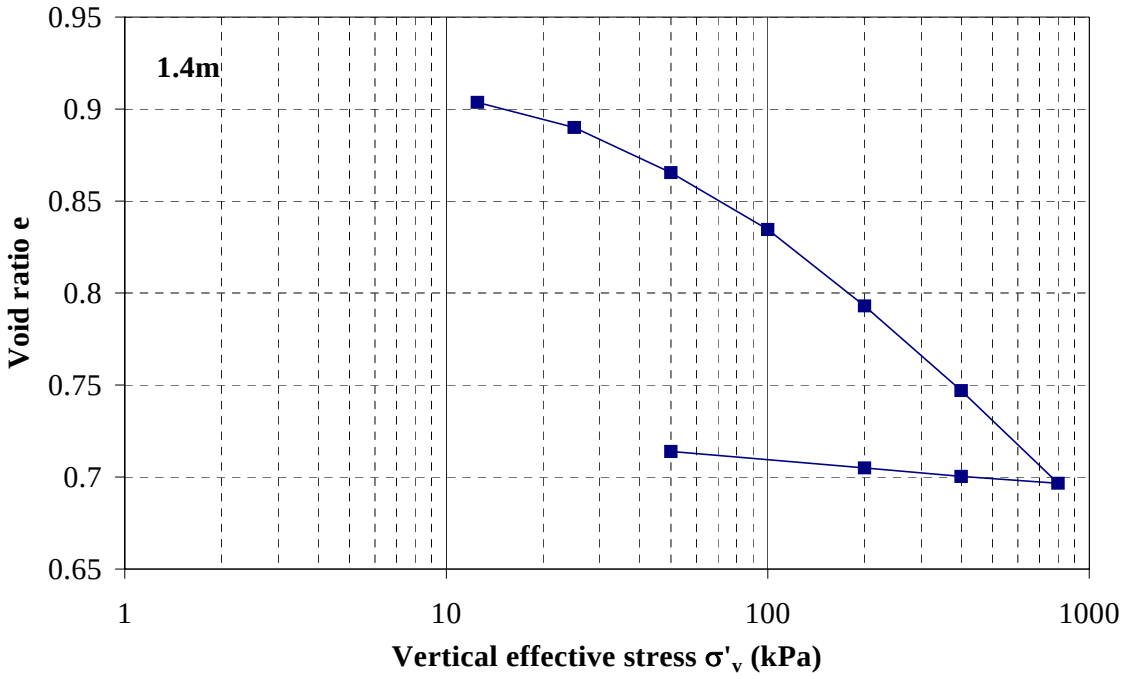
1.4m
Void ratio e
0.95
0.9
0.85
0.8
0.75
0.7
0.65
1
10
100
1000
Vertical effective stress σ'v (kPa)

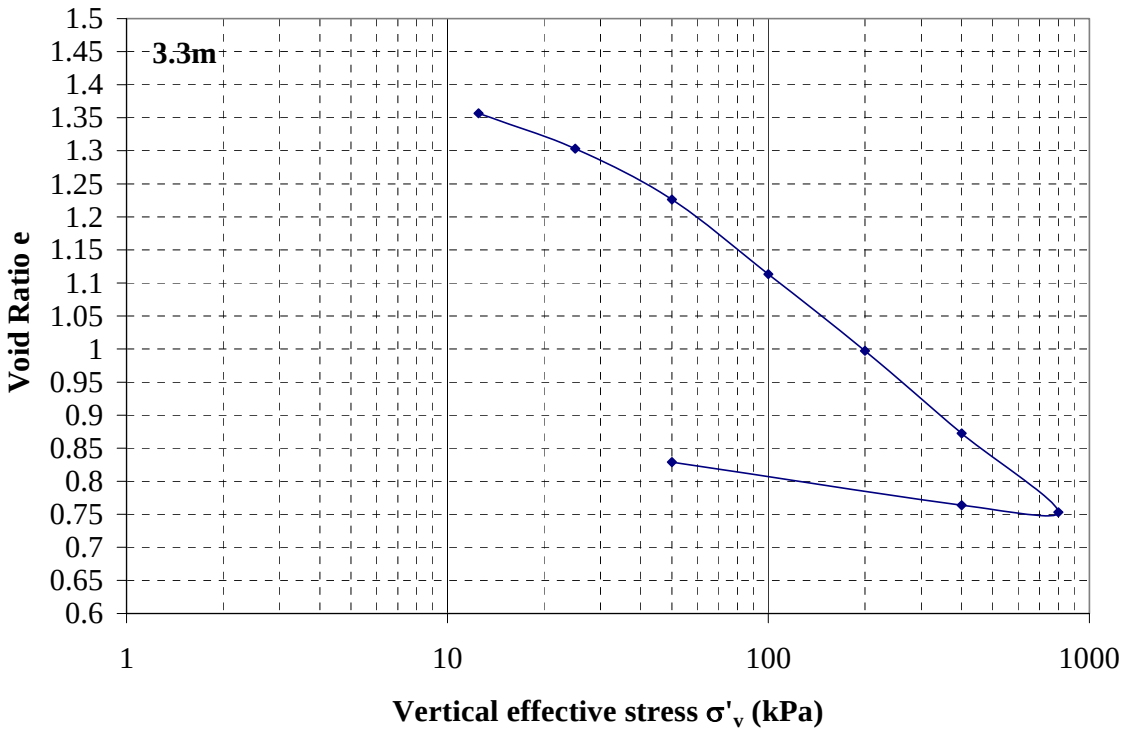
3.3m
Void Ratio e
1.5
1.45
1.4
1.35
1.3
1.25
1.2
1.15
1.1
1.05
1
0.95
0.9
0.85
0.8
0.75
0.7
0.65
0.6
1
10
100
1000
Vertical effective stress σ'v (kPa)

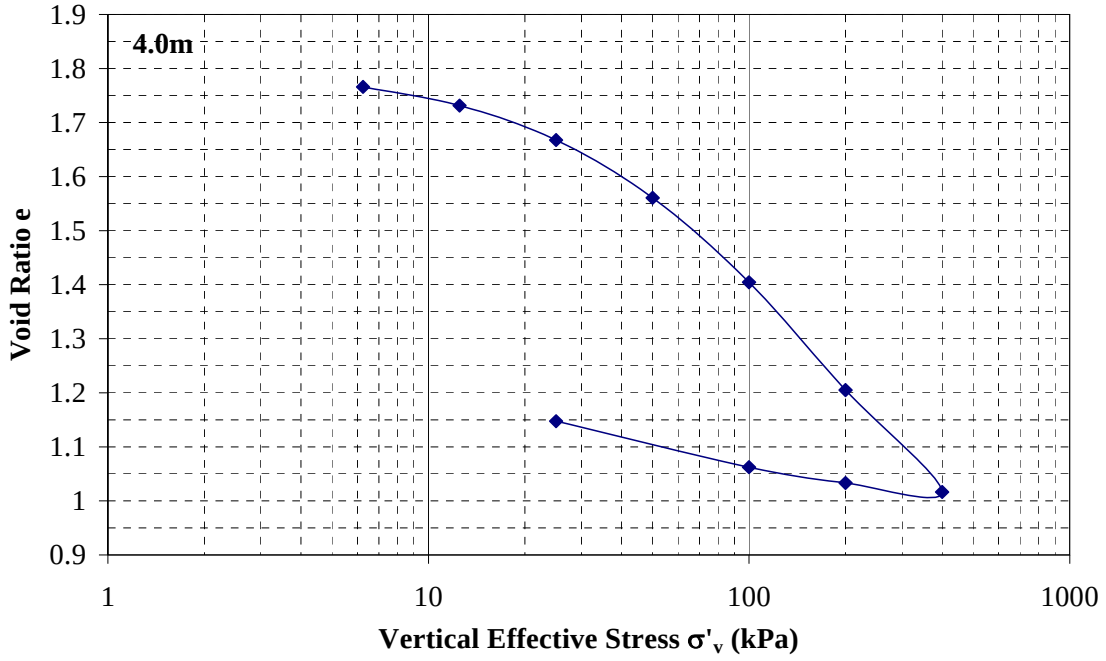
4.0m
Void Ratio e
1.9
1.8
1.7
1.6
1.5
1.4
1.3
1.2
1.1
1
0.9
1
10
100
1000
Vertical Effective Stress σ'v (kPa)

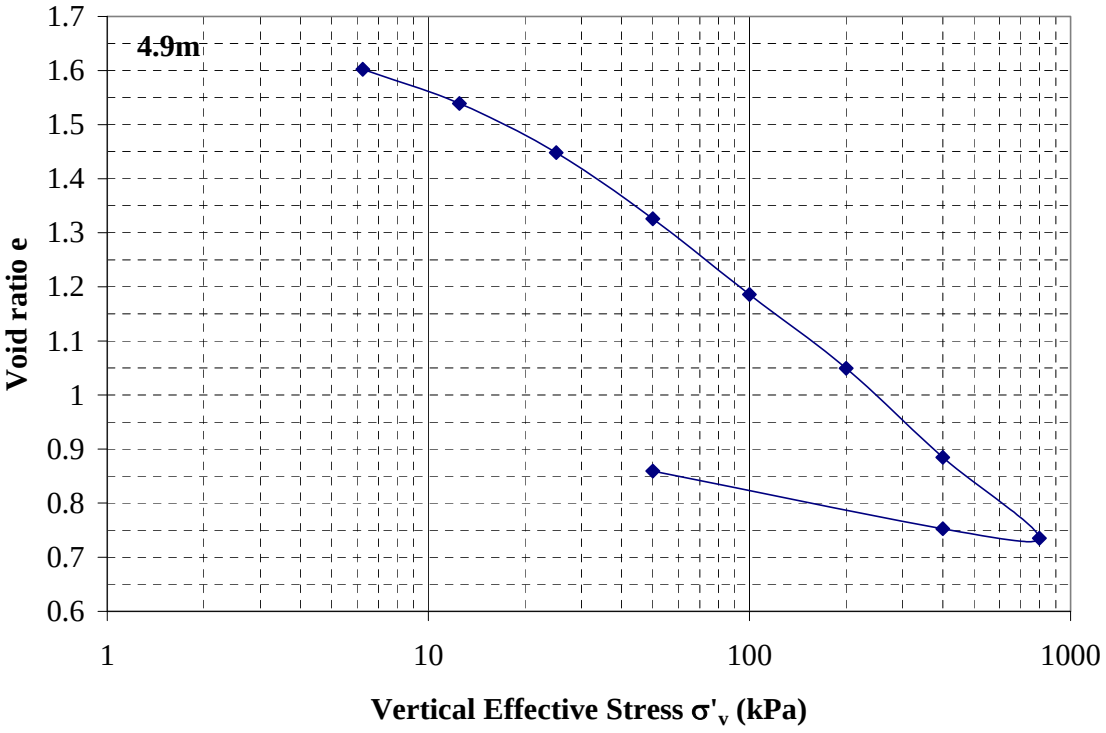
4.9m
Void ratio e
1.7
1.6
1.5
1.4
1.3
1.2
1.1
1
0.9
0.8
0.7
0.6
1
10
100
1000
Vertical Effective Stress σ'v (kPa)

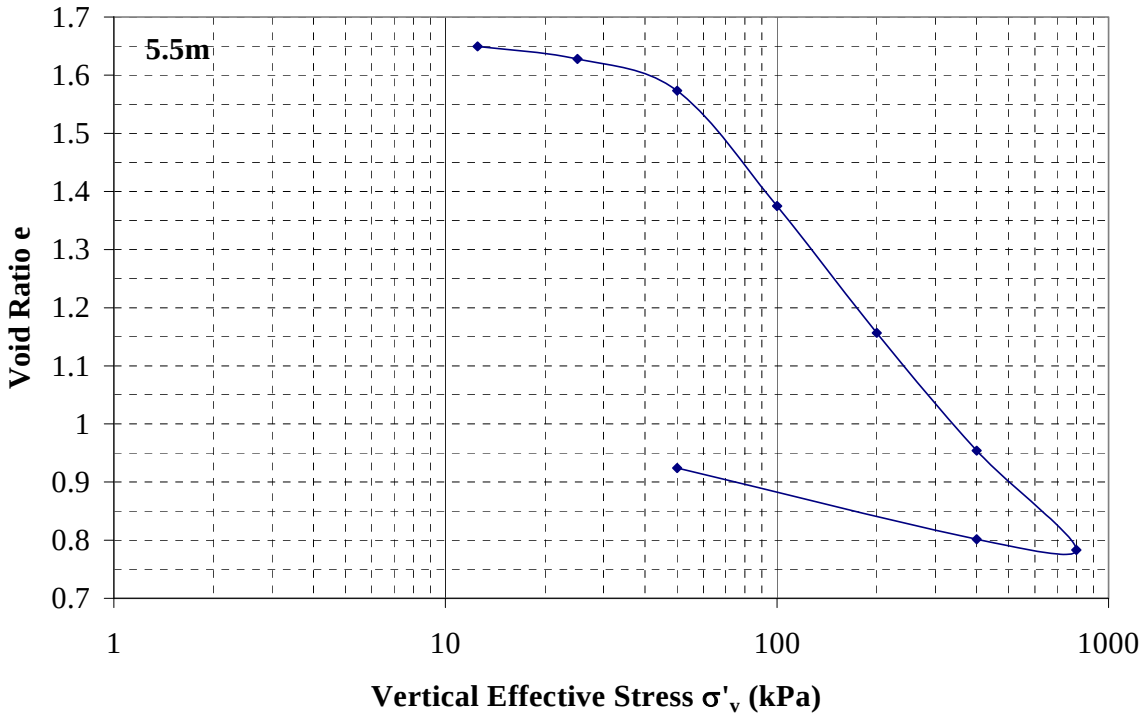
5.5m
Void Ratio e
1.7
1.6
1.5
1.4
1.3
1.2
1.1
1
0.9
0.8
0.7
1
10
100
1000
Vertical Effective Stress σ'v (kPa)

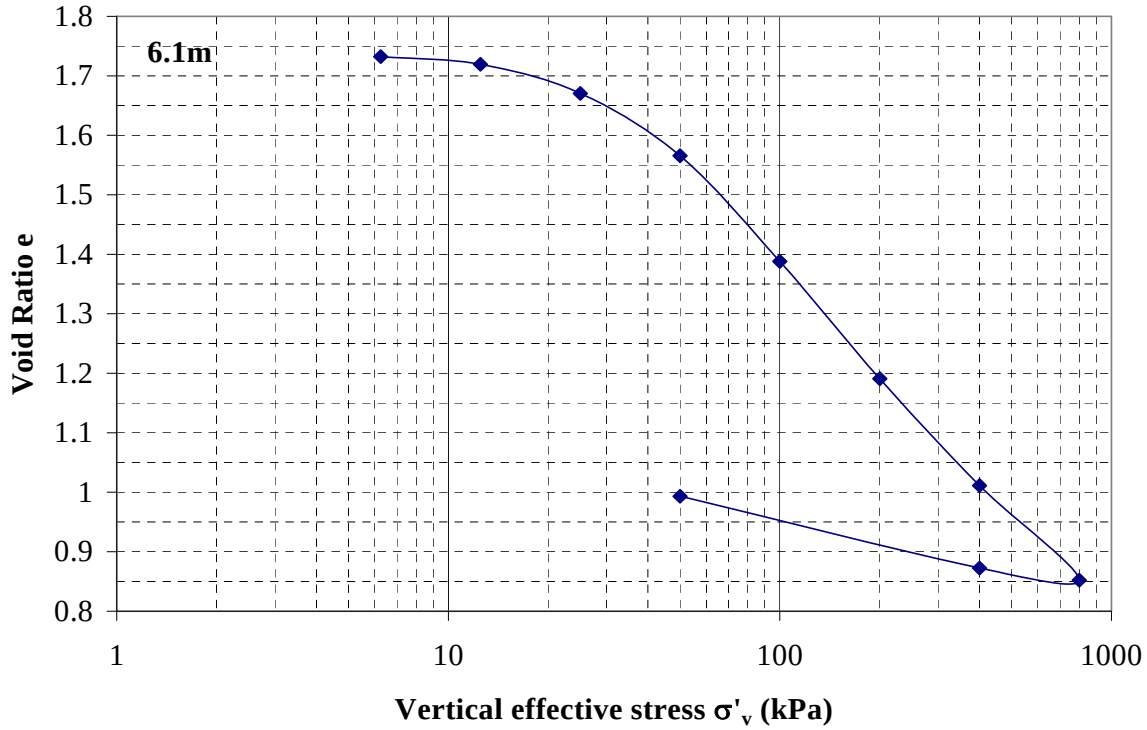
6.1m
Void Ratio e
1.8
1.7
1.6
1.5
1.4
1.3
1.2
1.1
1
0.9
0.8
1
10
100
1000
Vertical effective stress σ'v (kPa)

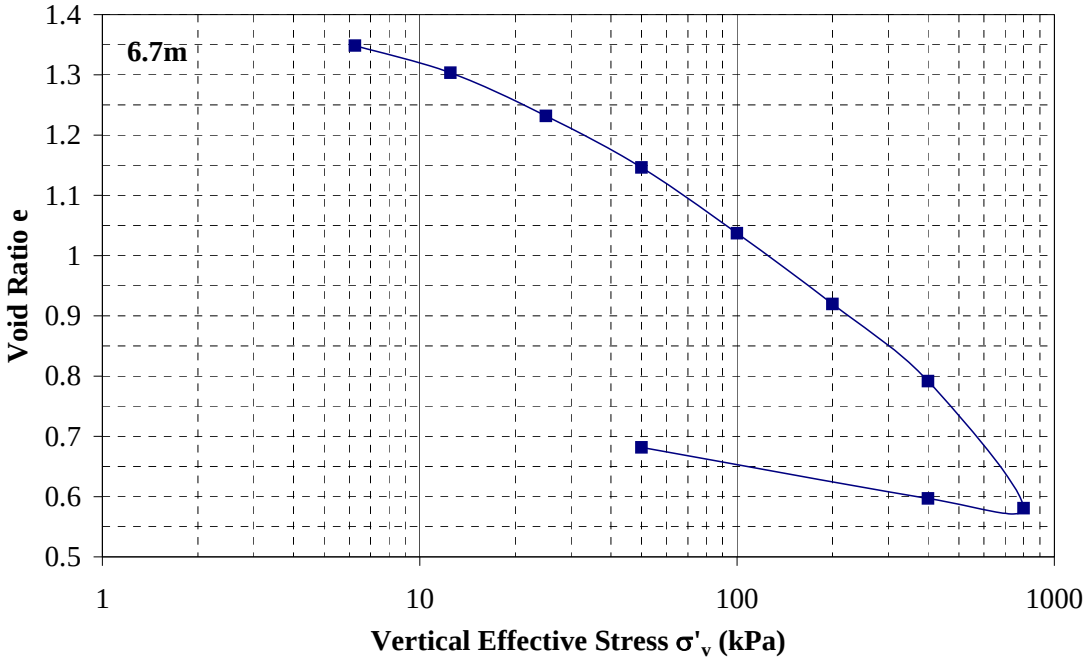
6.7m
Void Ratio e
1.4
1.3
1.2
1.1
1
0.9
0.8
0.7
0.6
0.5
1
10
100
1000
Vertical Effective Stress σ'v (kPa)

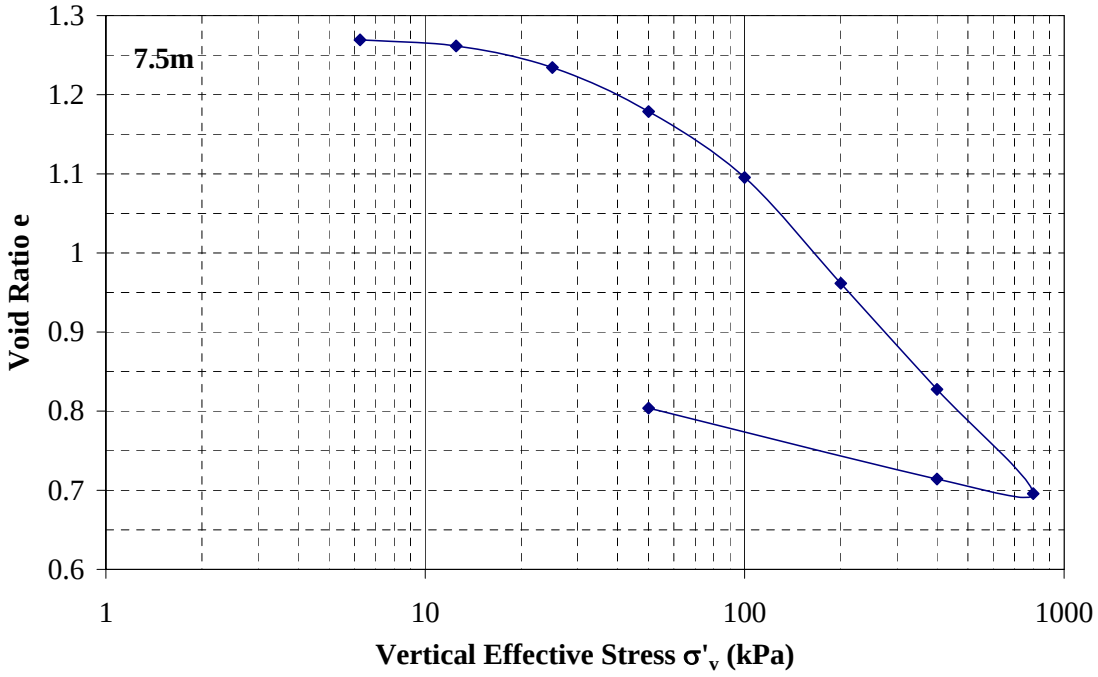
7.5m
Void Ratio e
1.3
1.2
1.1
1
0.9
0.8
0.7
0.6
1
10
100
1000
Vertical Effective Stress σ'v (kPa)

Appendix 3-6

C_V, C_α and permeability values for sleech

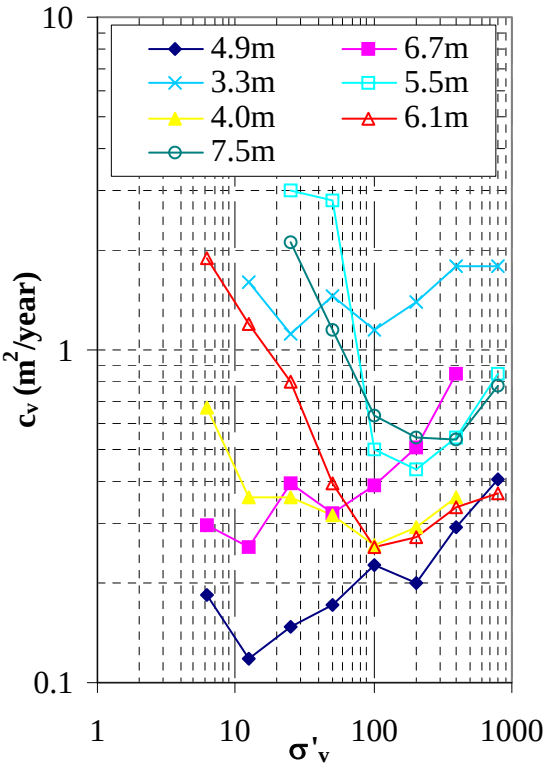
4.9m
6.7m
3.3m
5.5m
4.0m
6.1m
7.5m
10
1
0.1
1
10
100
1000
σ'v
cv (m2/year)

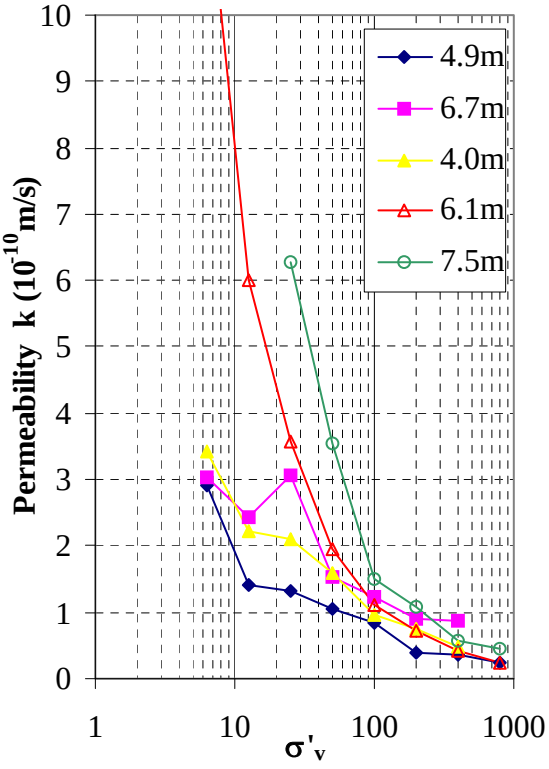
4.9m
6.7m
4.0m
6.1m
7.5m
10
9
8
7
6
5
4
3
2
1
0
1
10
100
1000
σ'v
Permeability k (10-10 m/s)

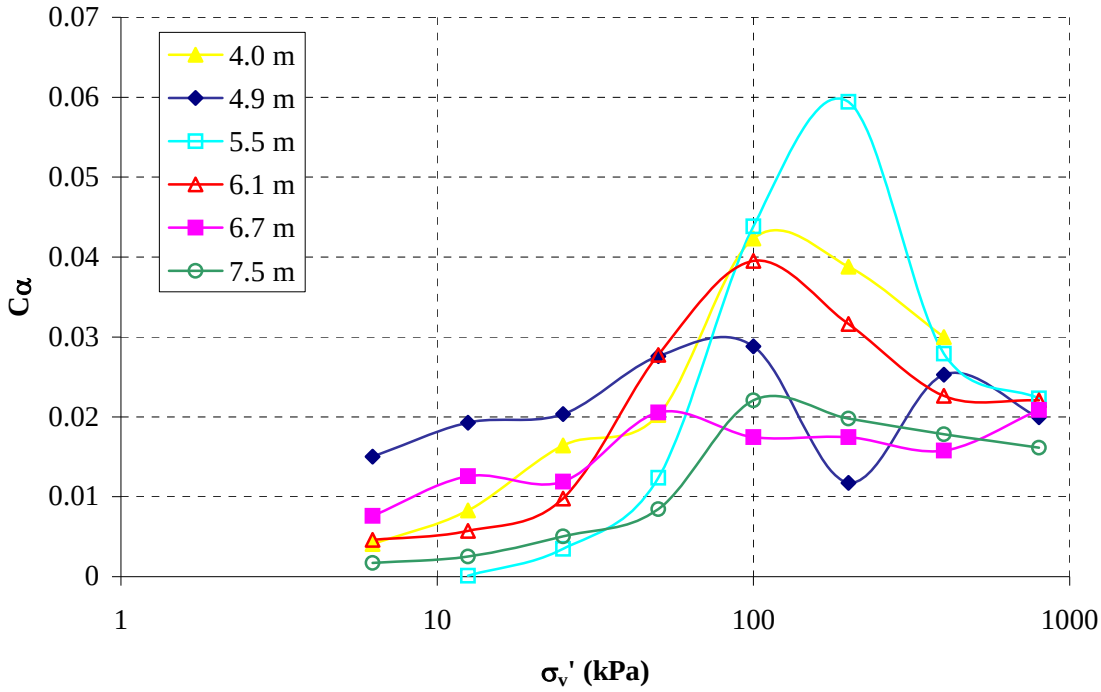
4.0 m
4.9 m
5.5 m
6.1 m
6.7 m
7.5 m
0.07
0.06
0.05
0.04
0.03
0.02
0.01
0
1
10
100
1000
σv' (kPa)
Cα

Appendix 3-7

Selected CIU and CK_oU Stress Paths

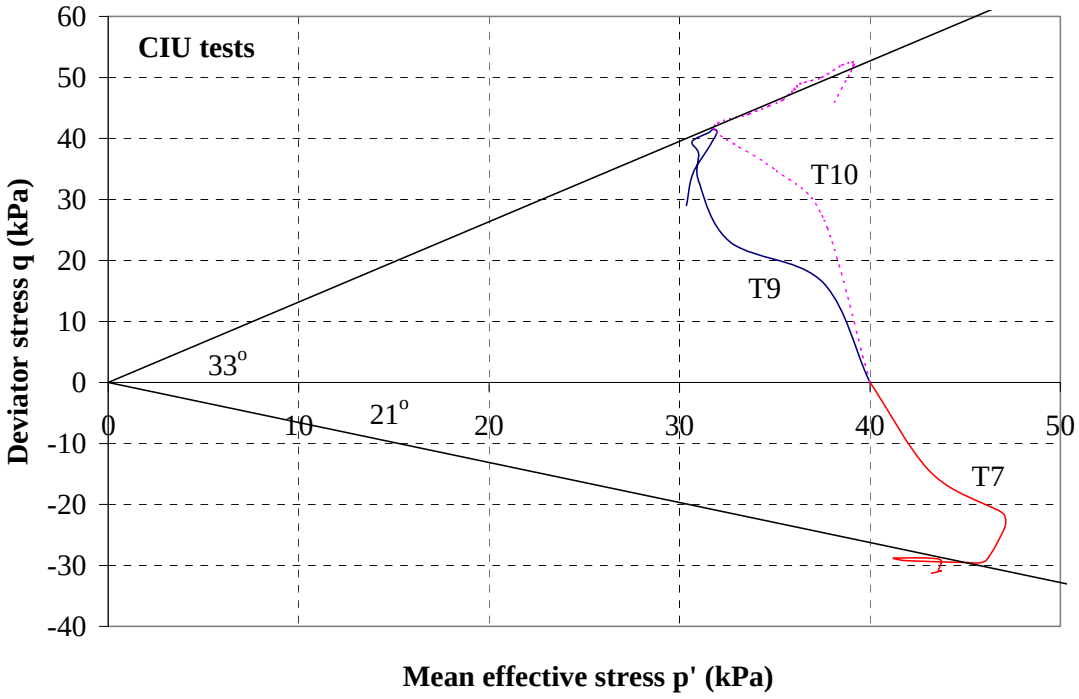
CIU tests
Deviator stress q (kPa)
Mean effective stress p' (kPa)
T10
T9
T7
33°
21°
60
50
40
30
20
10
0
-10
-20
-30
-40
0
10
20
30
40
50

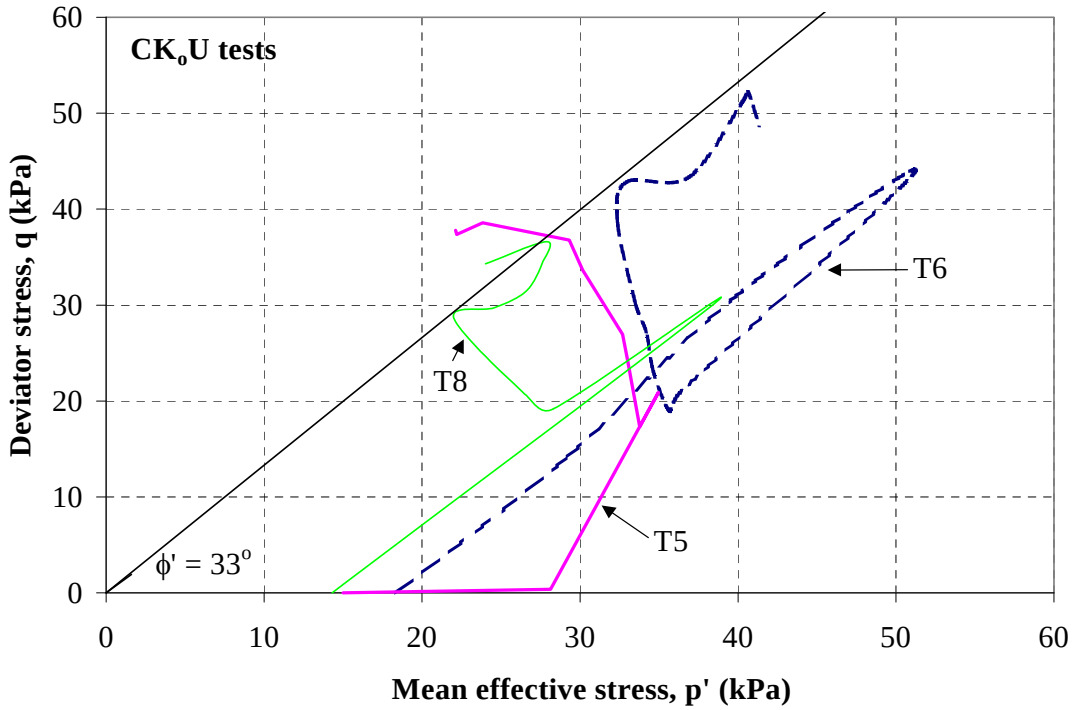
CK$_o$U tests
Deviator stress, q (kPa)
Mean effective stress, p' (kPa)
T6
T8
T5
ϕ' = 33°
60
50
40
30
20
10
0
0
10
20
30
40
50
60

Appendix 3-8

Shear Box and Simple Shear Tests

4.35m

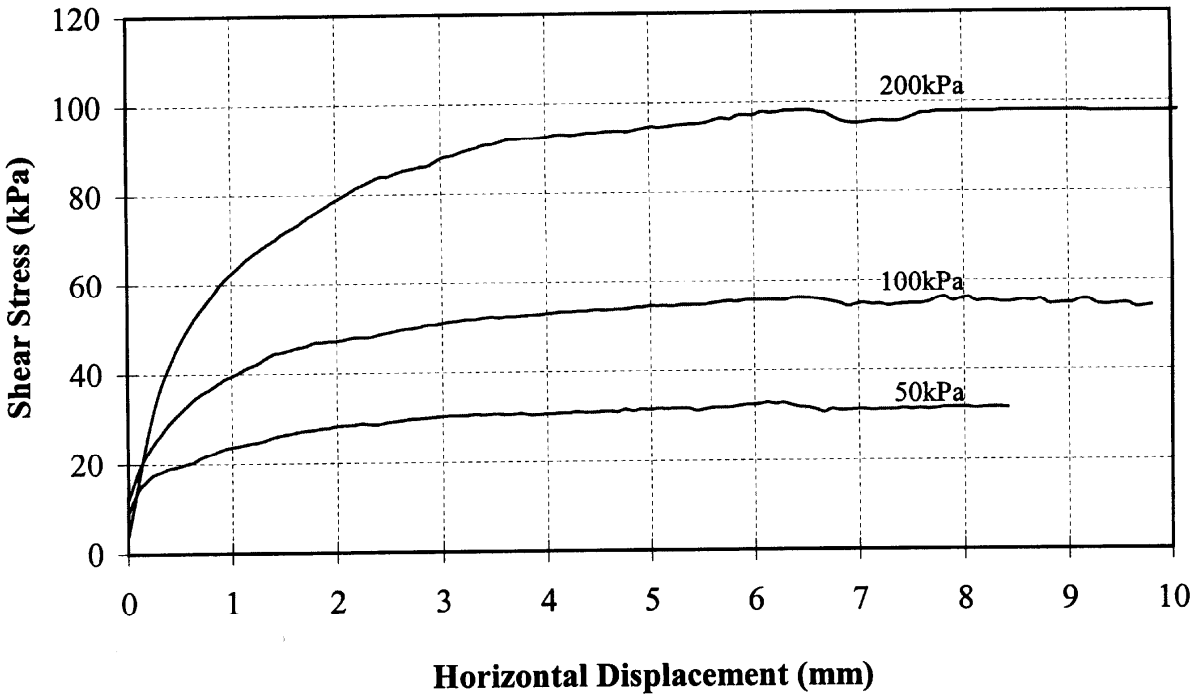
120
100
80
60
40
20
0
Shear Stress (kPa)
200kPa
100kPa
50kPa
0
1
2
3
4
5
6
7
8
9
10
Horizontal Displacement (mm)

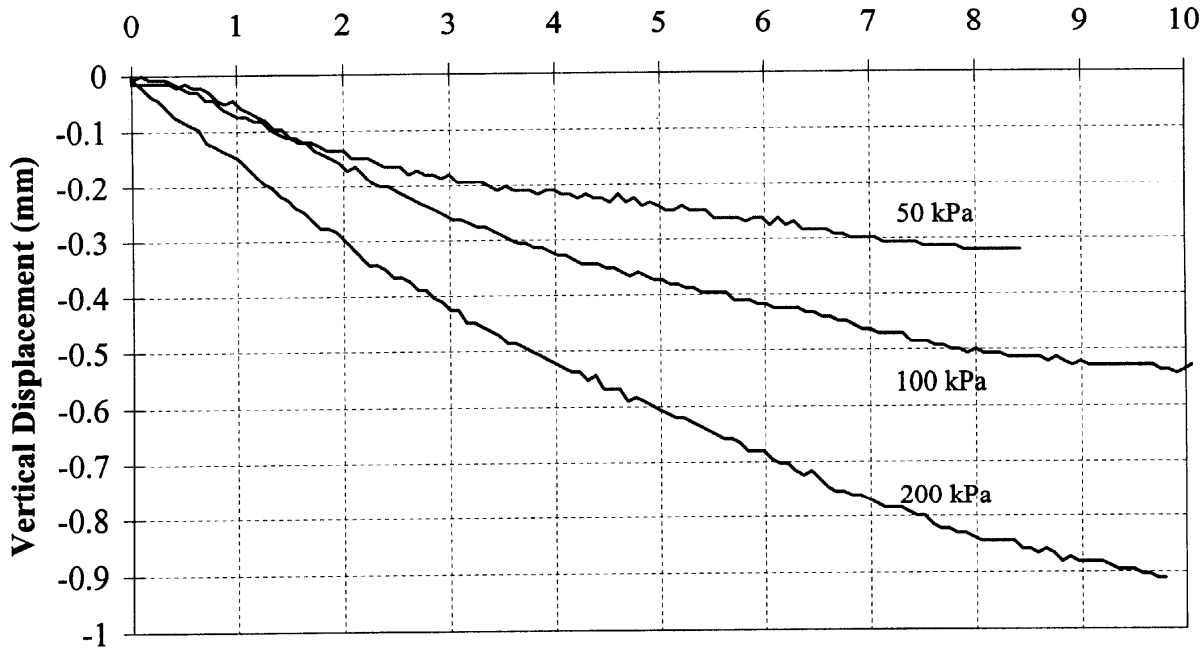
0
1
2
3
4
5
6
7
8
9
10
0
-0.1
-0.2
-0.3
-0.4
-0.5
-0.6
-0.7
-0.8
-0.9
-1
Vertical Displacement (mm)
50 kPa
100 kPa
200 kPa

4.75m

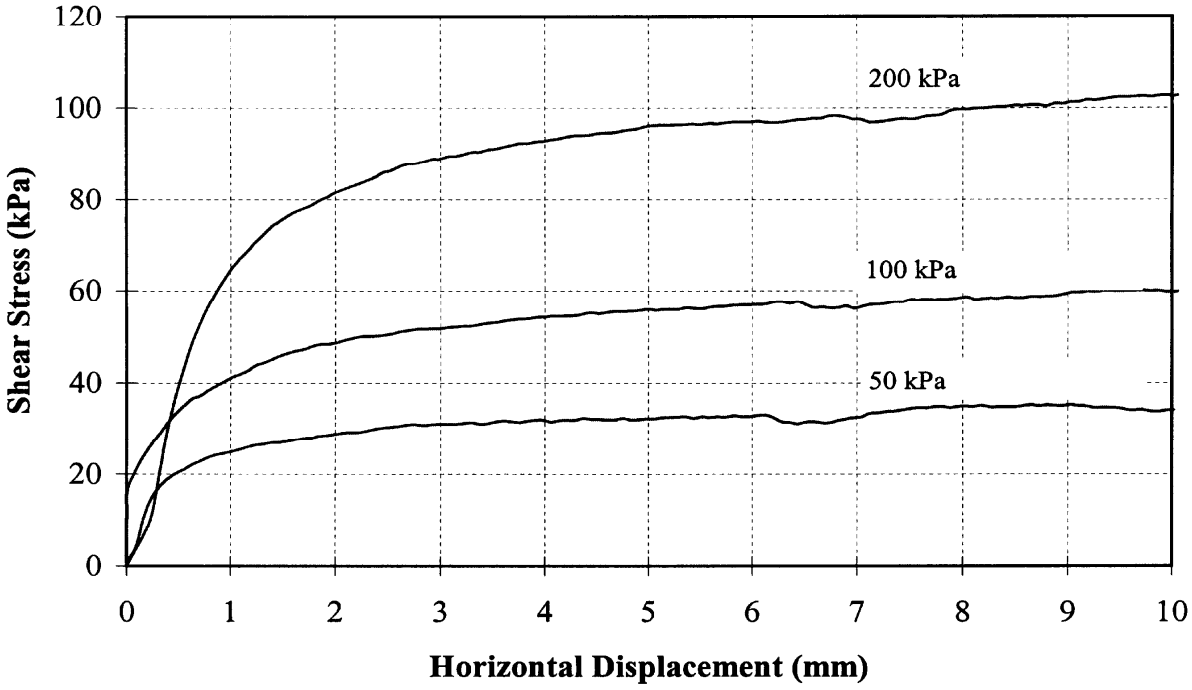
120
100
80
60
40
20
0
Shear Stress (kPa)
200 kPa
100 kPa
50 kPa
0
1
2
3
4
5
6
7
8
9
10
Horizontal Displacement (mm)

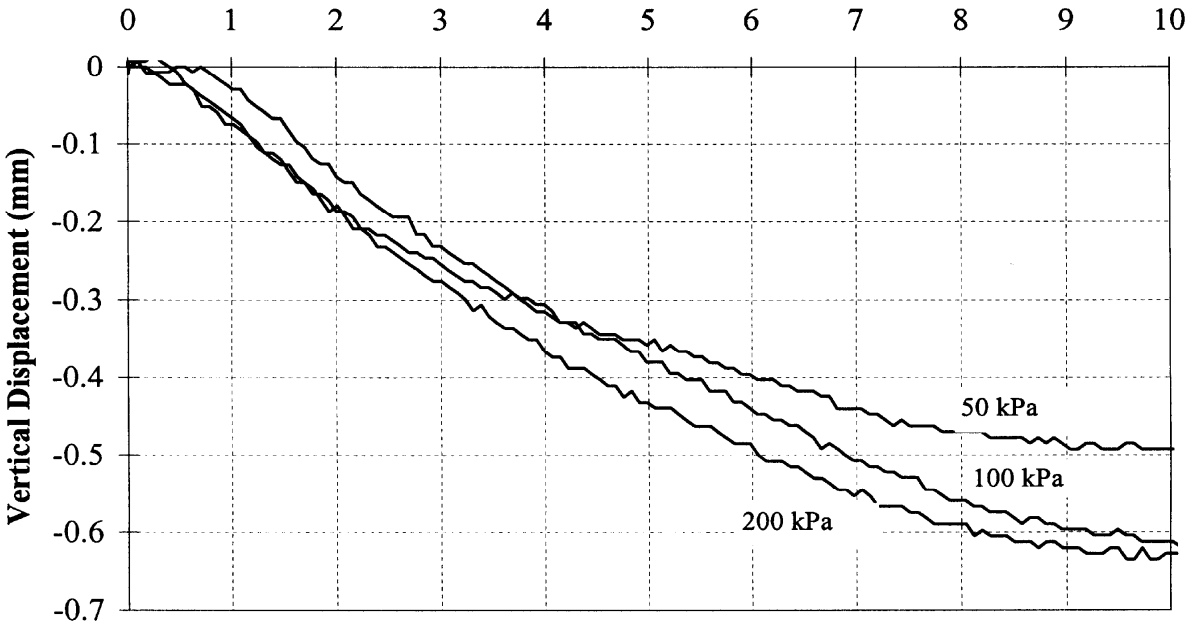
0
1
2
3
4
5
6
7
8
9
10
0
-0.1
-0.2
-0.3
-0.4
-0.5
-0.6
-0.7
Vertical Displacement (mm)
50 kPa
100 kPa
200 kPa

5.75m

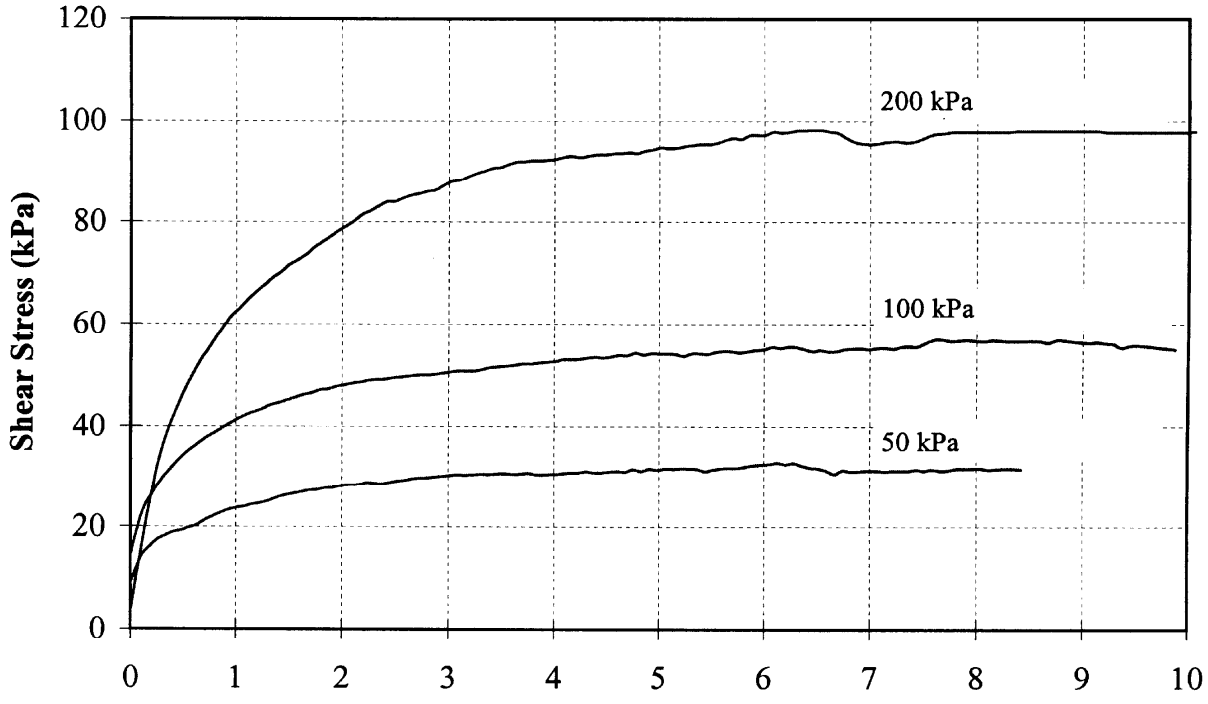
Shear Stress (kPa)
120
100
80
60
40
20
0
0
1
2
3
4
5
6
7
8
9
10
200 kPa
100 kPa
50 kPa
Horizontal Displacement (mm)

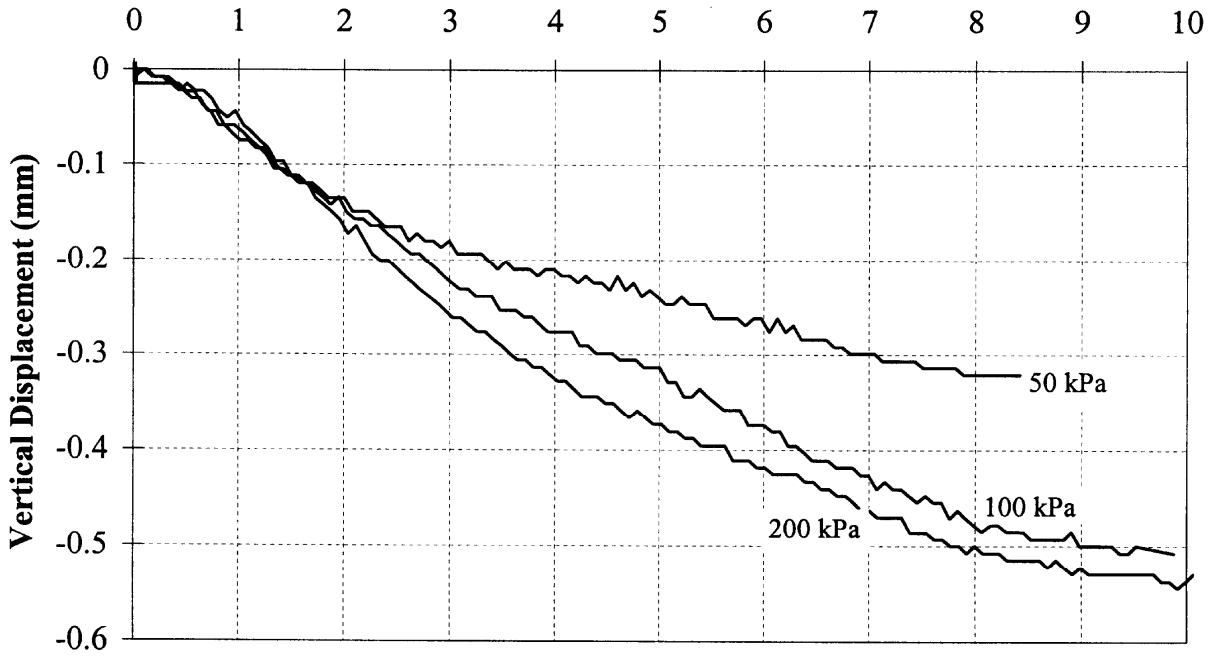
0
1
2
3
4
5
6
7
8
9
10
Vertical Displacement (mm)
0
-0.1
-0.2
-0.3
-0.4
-0.5
-0.6
50 kPa
100 kPa
200 kPa

6.2m

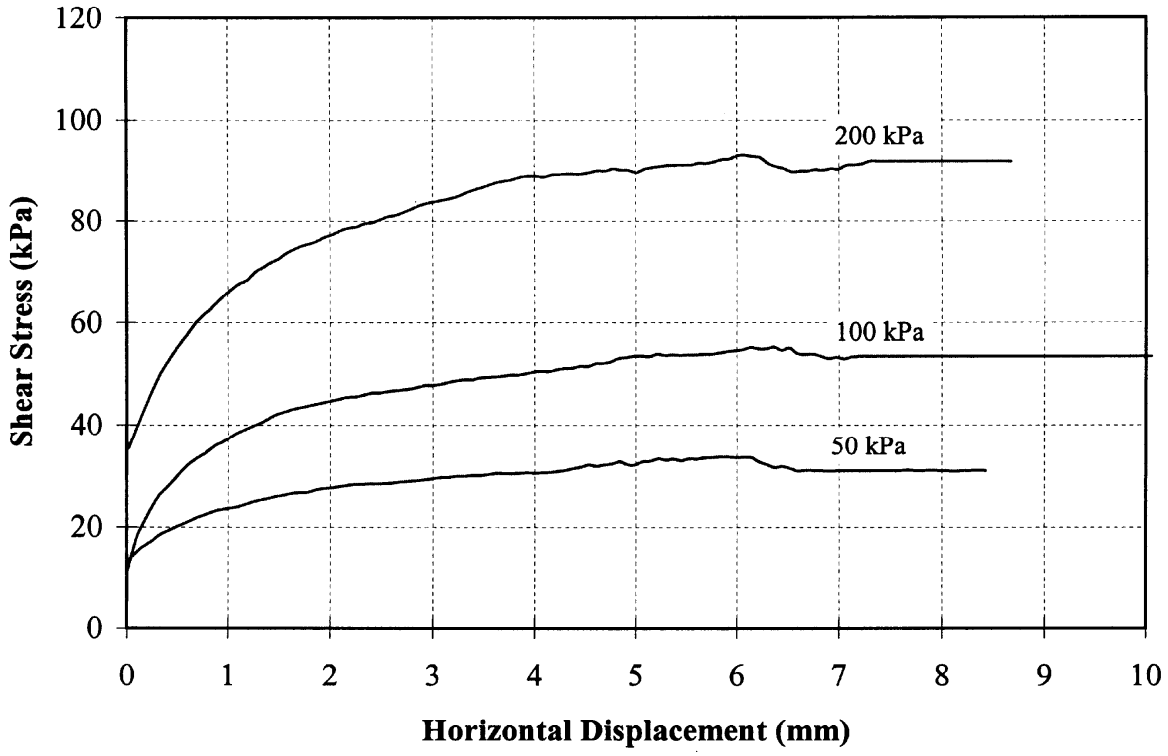
120
100
80
60
40
20
0
Shear Stress (kPa)
200 kPa
100 kPa
50 kPa
0
1
2
3
4
5
6
7
8
9
10
Horizontal Displacement (mm)

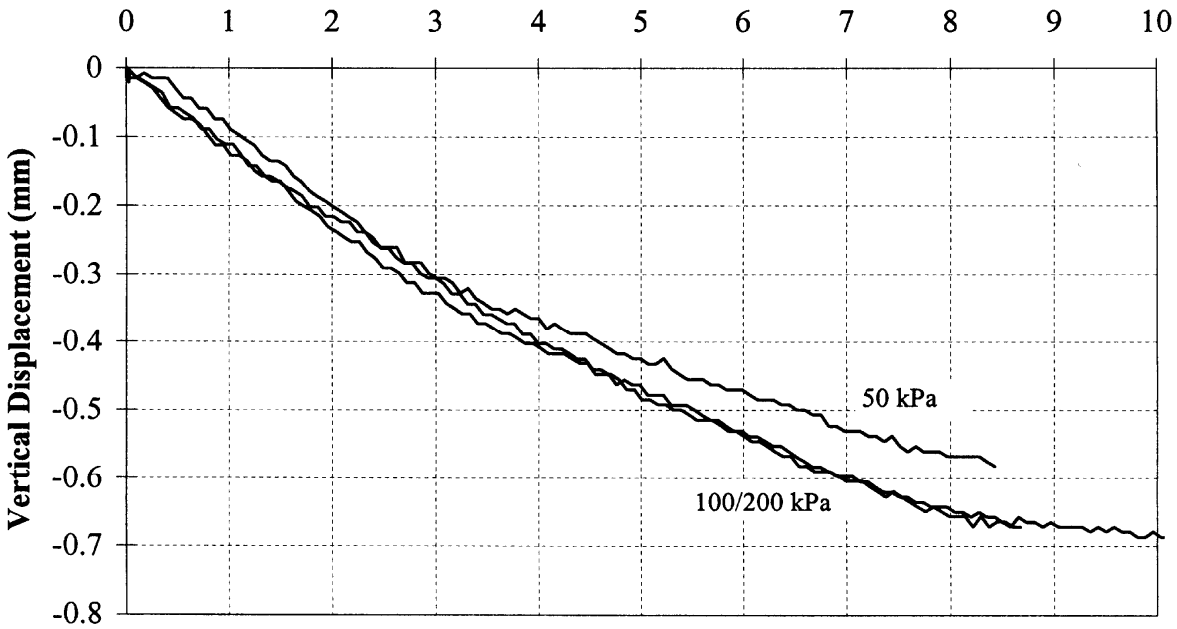
0
1
2
3
4
5
6
7
8
9
10
0
-0.1
-0.2
-0.3
-0.4
-0.5
-0.6
-0.7
-0.8
Vertical Displacement (mm)
50 kPa
100/200 kPa

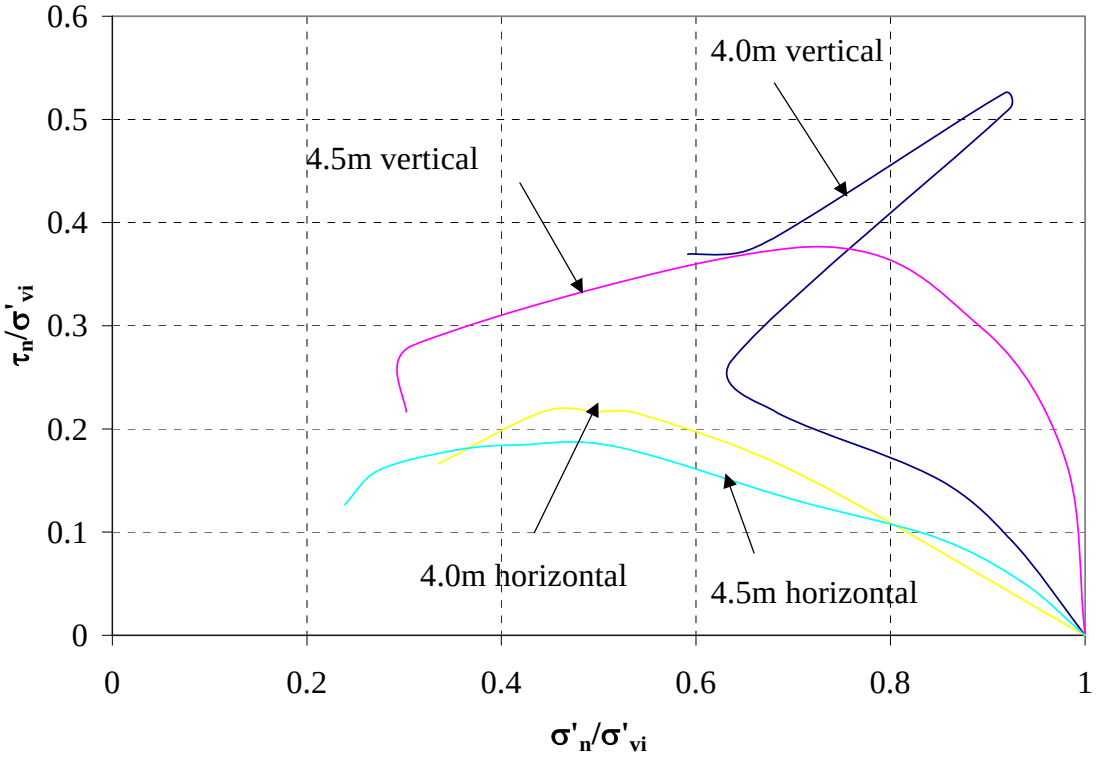

Simple shear tests

Appendix 3-9

Small strain stiffness determination using video extensometer

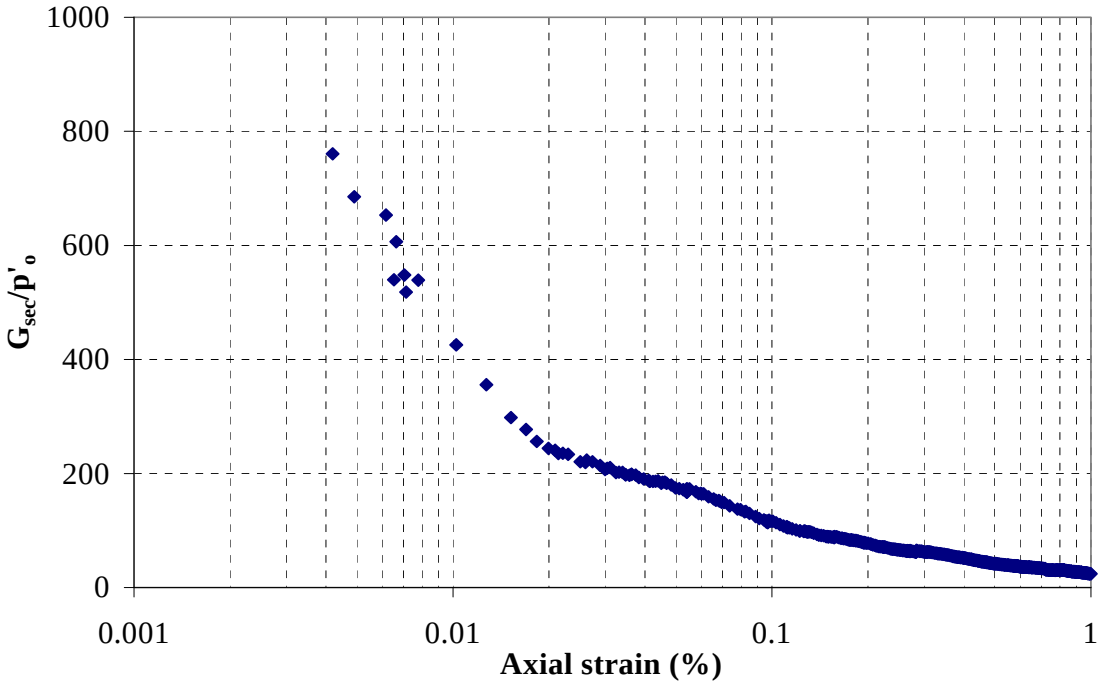

Small strain stiffness data for T8 (using video extensometer)

An alternative method of local strain measurement was used at TCD to determine the small strain stiffness of soil specimens in the triaxial apparatus. A video extensometer[1] was positioned remotely and was used to track (through the Perspex cell) the movement of points marked on the specimen's membrane. Some points on the membrane out of direct camera view were picked up with a mirror. The position of each point was typically recorded to a PC at a frequency of 0.2Hz (strain rate 4.5%/hour).

The accuracy of the data depends strongly on the care taken in setting up the video extensometer, and a full discussion on the necessary precautions is given by Gill (1999). In particular, it is essential that the point markers are well illuminated with light of uniform intensity[2] to provide a sharp contrast between the (black) marker and its (white) background. Local vertical strains may be calculated from the vertical movements, but

[1] High resolution camera
[2] To drown out fluctuations in natural light which would disimprove camera accuracy.

horizontal movements are distorted by the curvature of the cell. Light reflection from the cell provides the main obstacle to accurate measurements. Several points were monitored at the same height on the membrane so that any bending in the sample may be averaged out. All points were no closer than 50mm from the top or bottom of the 200mm long specimen in each of the tests.

The video extensometer was used in conjunction with tests T6 and T8 (see Table 3-2). The normalized small strain stiffness profile (G_{sec}/p_o') deduced from T8 is consistent with that measured by Hall effect sensors in T16 (both CK_oUC tests, T16 shown in Figure 3-14) and provides data to an axial strain of ≈0.005%. G_{sec}/p_o' values obtained in T6 are compatible but become unreliable at axial strains lower than 0.02-0.03%.

Appendix 4-1

Problems encountered in CTG1/sc

Although certain aspects of the results of CTG1/sc are reported in Chapter 6 on cyclic loading, problems were encountered from an early stage of this load test.

The pile head dywidag anchors used in the previous test CG1/s (100mm embedment) were deemed insufficient for a cyclic tension test. These short bars were removed and the pile heads were chipped back to expose the tops to the reinforcing steel. A steel plate was welded to the four bars and the dywidag 'stub' was repositioned at the centre of this plate by welding. However, the heat treatment during welding embrittled all bars and caused that on CTG1[4]/sc to fail after only 29 cycles of CTG1/sc. Up to this time, the load cell on CTG1[5]/sc was found to be moving relative to the pile head, while the pile's displacement was extremely low in relation to the other piles. It was also noted that the diagonally opposite corner pile CTG1[1]/sc was displacement much more than average.

Once the snapped bar was repaired, a further 247 cycles were imposed bringing the group close to 'failure' before two more dywidag bars gave way. The pattern of the second part of the test followed the first part quite closely. The test was terminated at this point.

Data from four of the five piles are satisfactory, so they are interpreted in Chapter 6 in the context of a four-pile triangular group. Only maximum cyclic pile loads and not the pile load-displacement behaviour are considered.

Appendix 5-1

Static Pile Test Load-Displacement plots

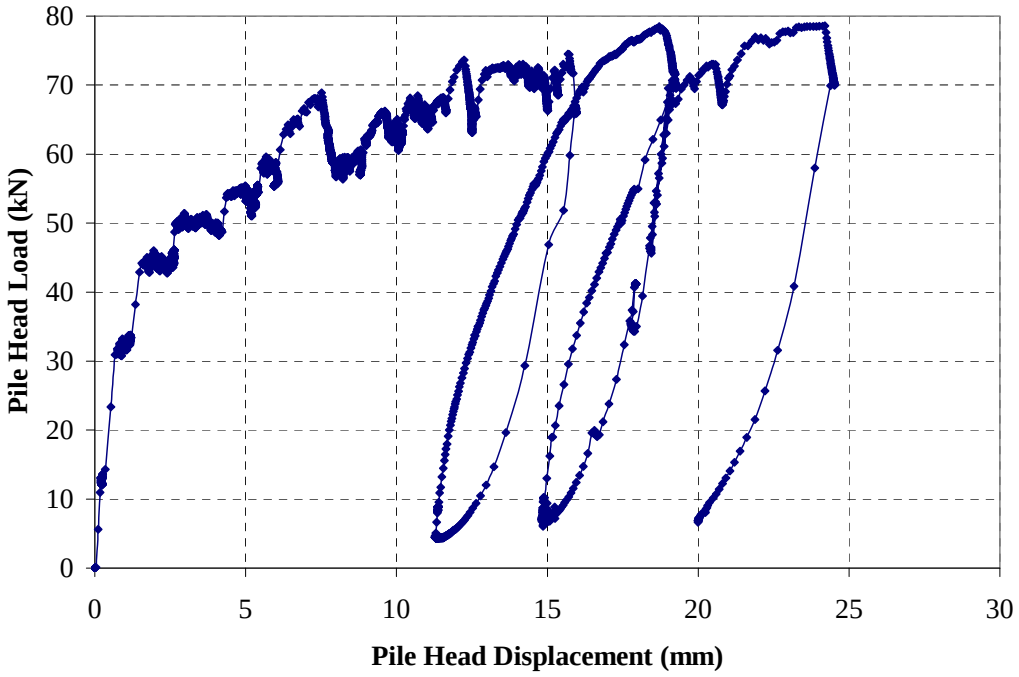
Pile Head Load (kN)
0
10
20
30
40
50
60
70
80
0
5
10
15
20
25
30
Pile Head Displacement (mm)

TS1/s

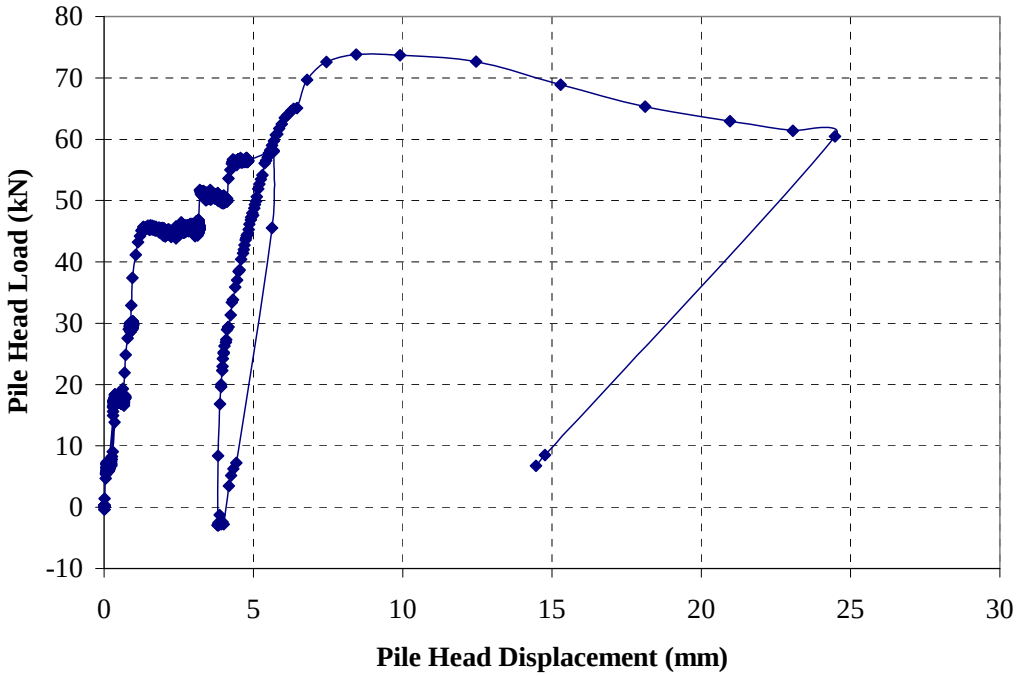
Pile Head Load (kN)
-10
0
10
20
30
40
50
60
70
80
0
5
10
15
20
25
30
Pile Head Displacement (mm)

CS1/s

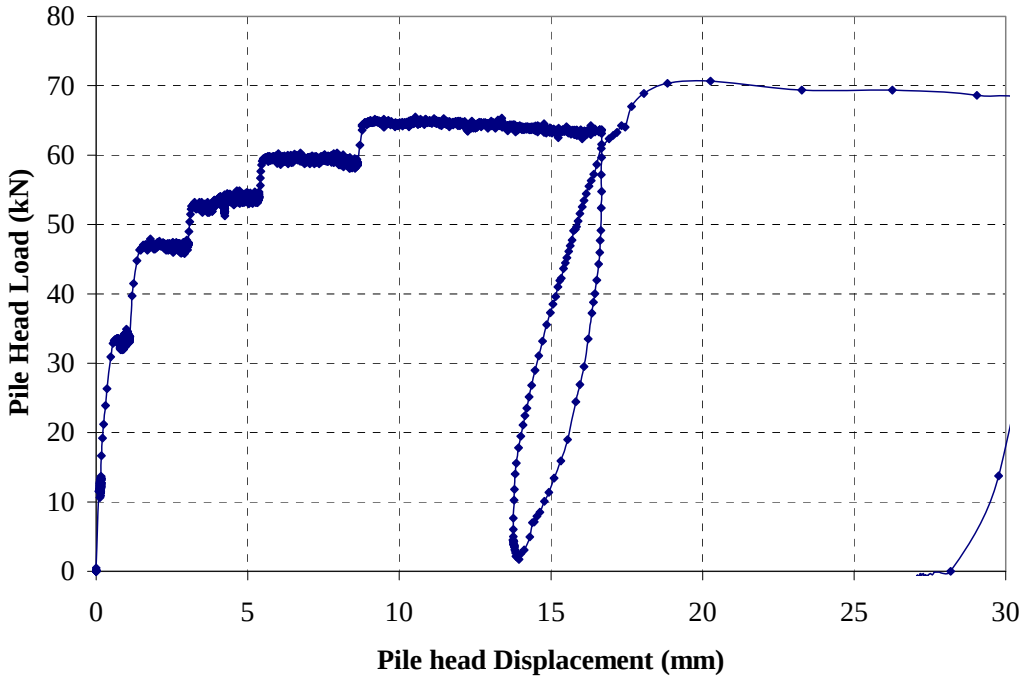
Pile Head Load (kN)
80
70
60
50
40
30
20
10
0
0
5
10
15
20
25
30
Pile head Displacement (mm)

TS2/s

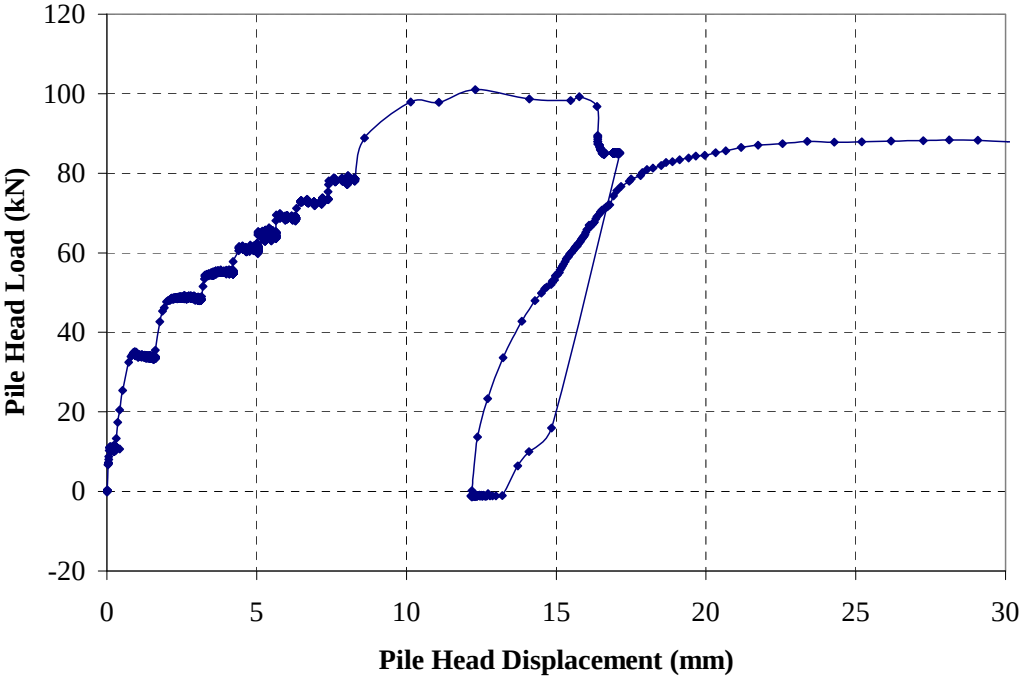
Pile Head Load (kN)
120
100
80
60
40
20
0
-20
0
5
10
15
20
25
30
Pile Head Displacement (mm)

TS2/ss

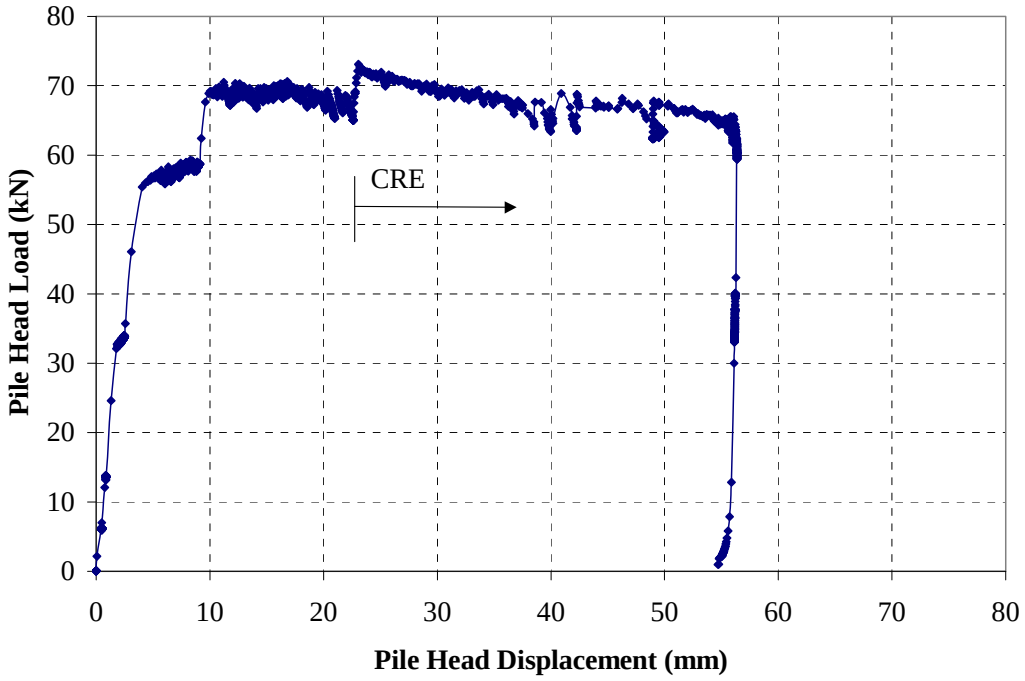
Pile Head Load (kN)
0
10
20
30
40
50
60
70
80
CRE
0
10
20
30
40
50
60
70
80
Pile Head Displacement (mm)

TG1[1]/s

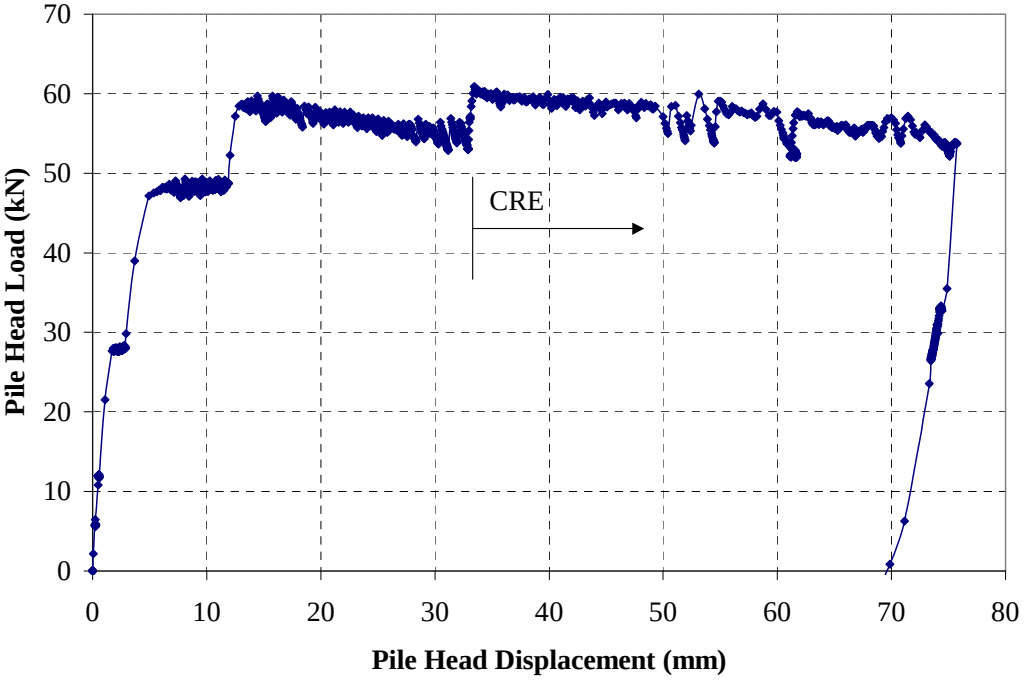
Pile Head Load (kN)
0
10
20
30
40
50
60
70
CRE
0
10
20
30
40
50
60
70
80
Pile Head Displacement (mm)

TG1[2]/s

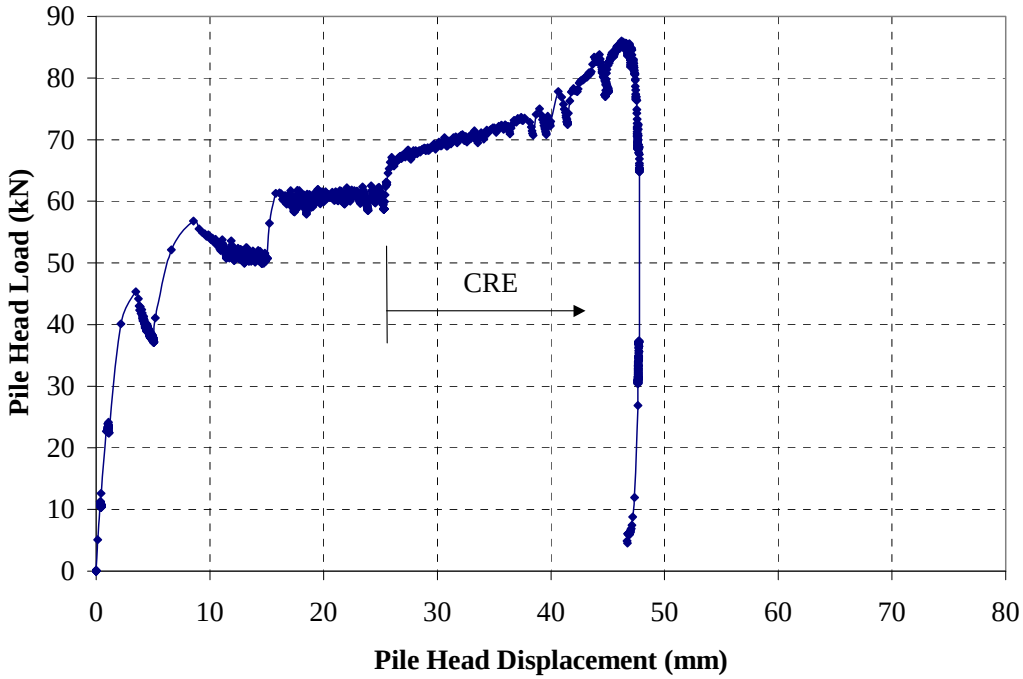
Pile Head Load (kN)
Pile Head Displacement (mm)
CRE
0
10
20
30
40
50
60
70
80
90

TG1[3]/s

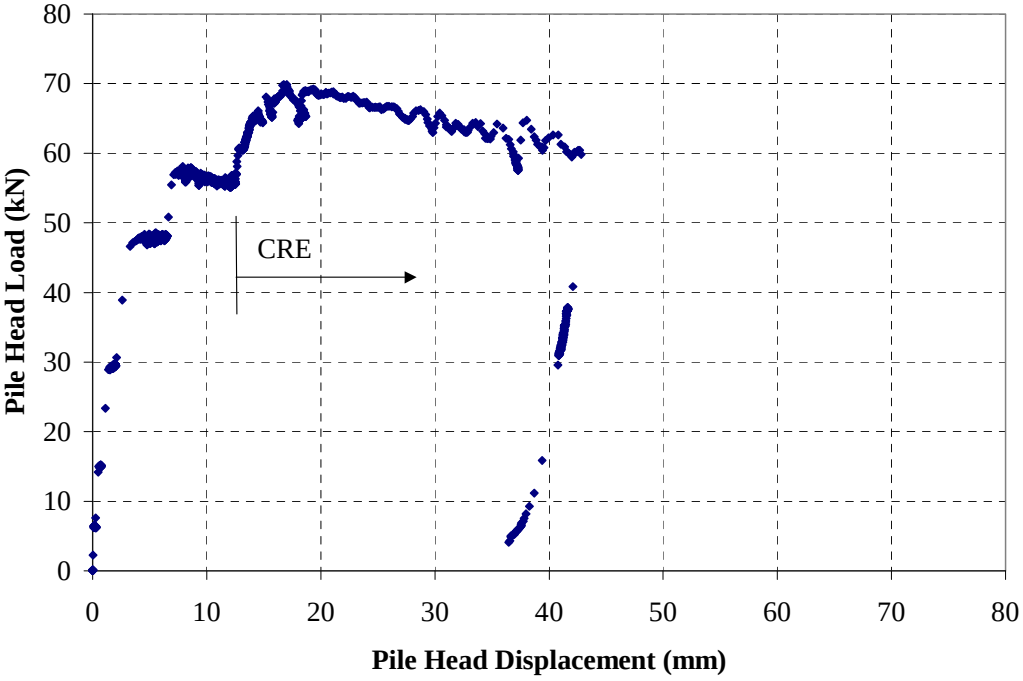
Pile Head Load (kN)
Pile Head Displacement (mm)
CRE
0
10
20
30
40
50
60
70
80

TG1[4]/s

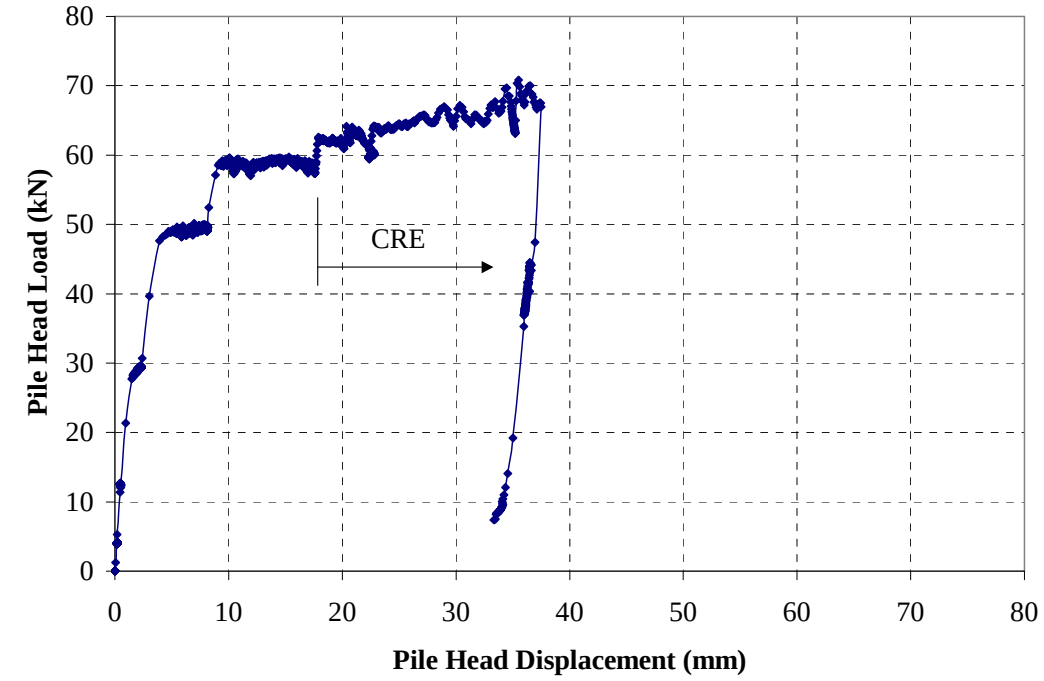
Pile Head Load (kN)
Pile Head Displacement (mm)
CRE
0
10
20
30
40
50
60
70
80

TG1[5]/s

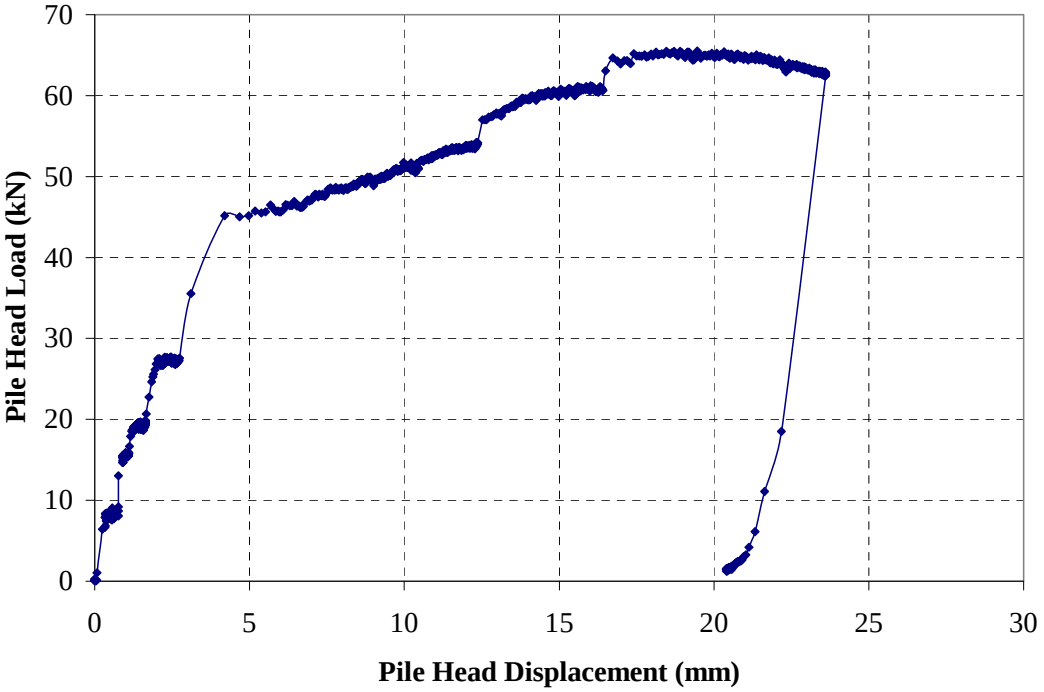
Pile Head Load (kN)
Pile Head Displacement (mm)
0
5
10
15
20
25
30
40
50
60
70

CG1[1]/s

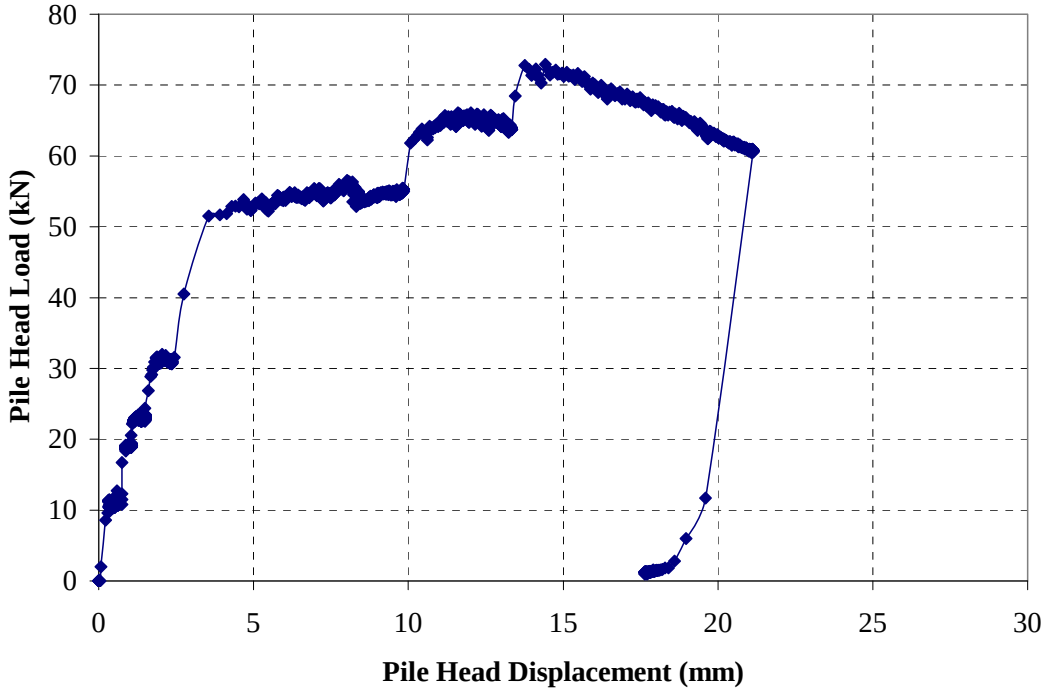
Pile Head Load (kN)
0
10
20
30
40
50
60
70
80
0
5
10
15
20
25
30
Pile Head Displacement (mm)

CG1[2]/s

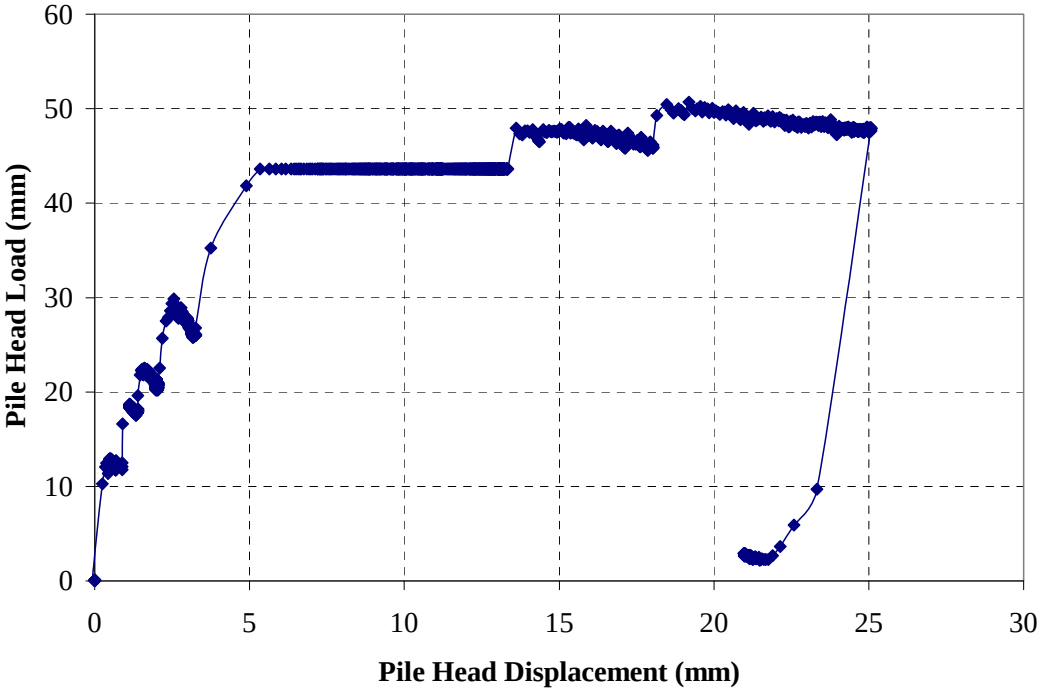
Pile Head Load (mm)
0
10
20
30
40
50
60
0
5
10
15
20
25
30
Pile Head Displacement (mm)

CG1[3]/s

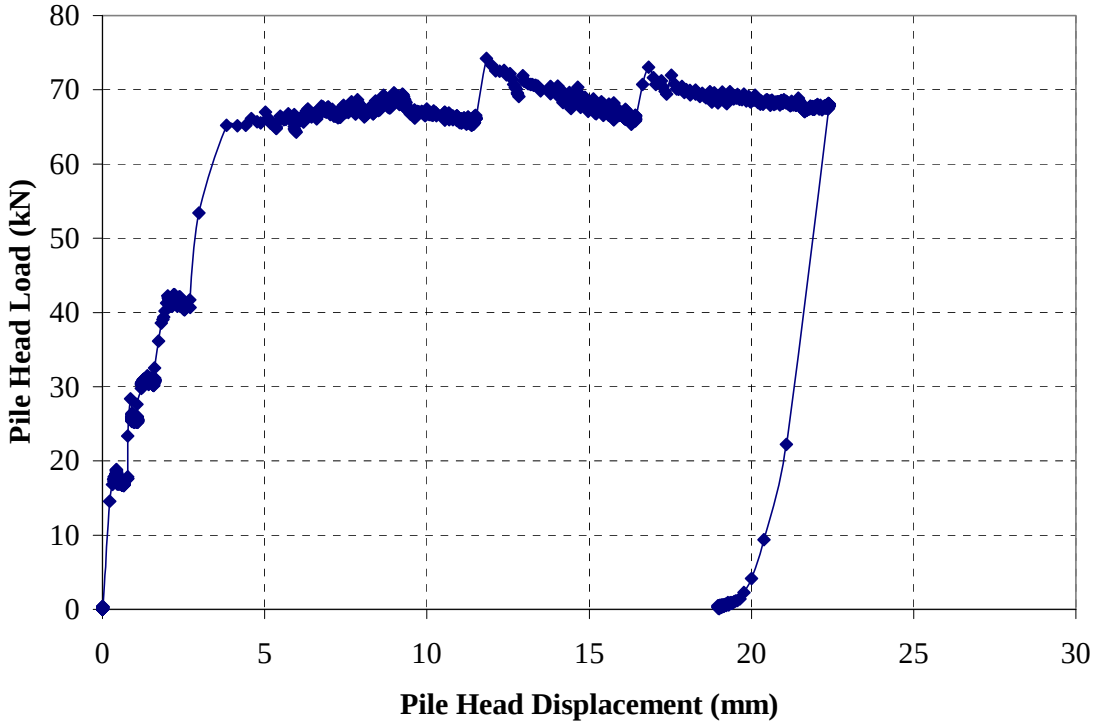
Pile Head Load (kN)
80
70
60
50
40
30
20
10
0
0
5
10
15
20
25
30
Pile Head Displacement (mm)

CG1[5]/s

Appendix 5-2

Strain Gauge Data

Strains measured on Pile Reinforcement

Vibrating wire and electrical resistance strain gauges were affixed to the surface of the reinforcement within the precast concrete piles. Since both the steel and interfacing concrete may be assumed to undergo equal straining, then the strain measurements may be used to infer the total load carried by the pile at the level of the gauges.

Pile load may be calculated from strain measurements by considering the section properties (cross sectional area and Young's modulus of steel and concrete) according to:

$$F\ (kN) = [E_{conc}A_{conc}+E_{st}A_{st}]\ \varepsilon \approx 2.27\ \mu\varepsilon$$

In general, this approach yielded plausible load distributions in the piles. Good agreement was found between electrical resistance and vibrating wire gauges where both were present at the same level within a pile (at the 2.0m and 4.5m locations). The reliability of pile base loads (interpreted from the gauges at 5.95m) was obviously much less where maximum strains of the order of 5με were recorded. Readings that did not respond sharply to the applied load were disregarded.

Where small amounts of drift was observed in the gauges, comparison of start and end 'zero' strain readings aided the interpretation. In a few cases, (unintentional) unload-reload loops occurring during the load test provided an intermediate 'zero' strain reading which also contributed to the interpretation. Some of the clearest data is presented in Appendix 5-2; strain data from both single piles (TS1/s and CS1/s) required significant interpretation and the raw data is not presented here.

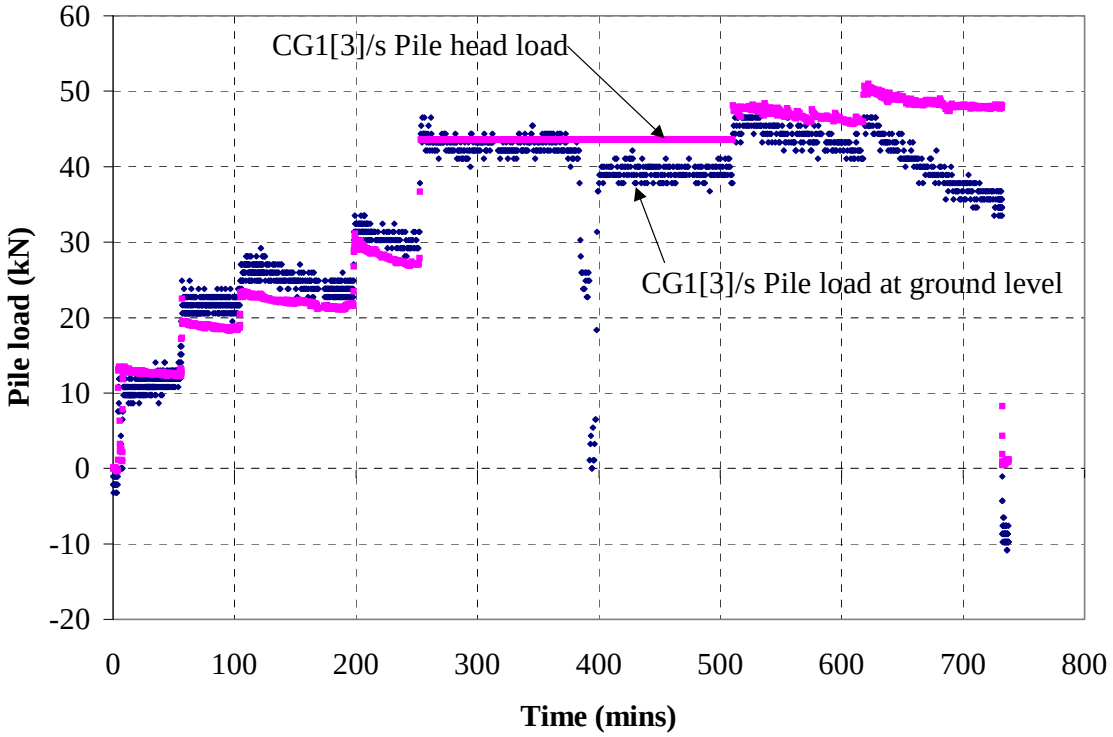

CG1[3]/s Correlation between pile head load and load at ground level

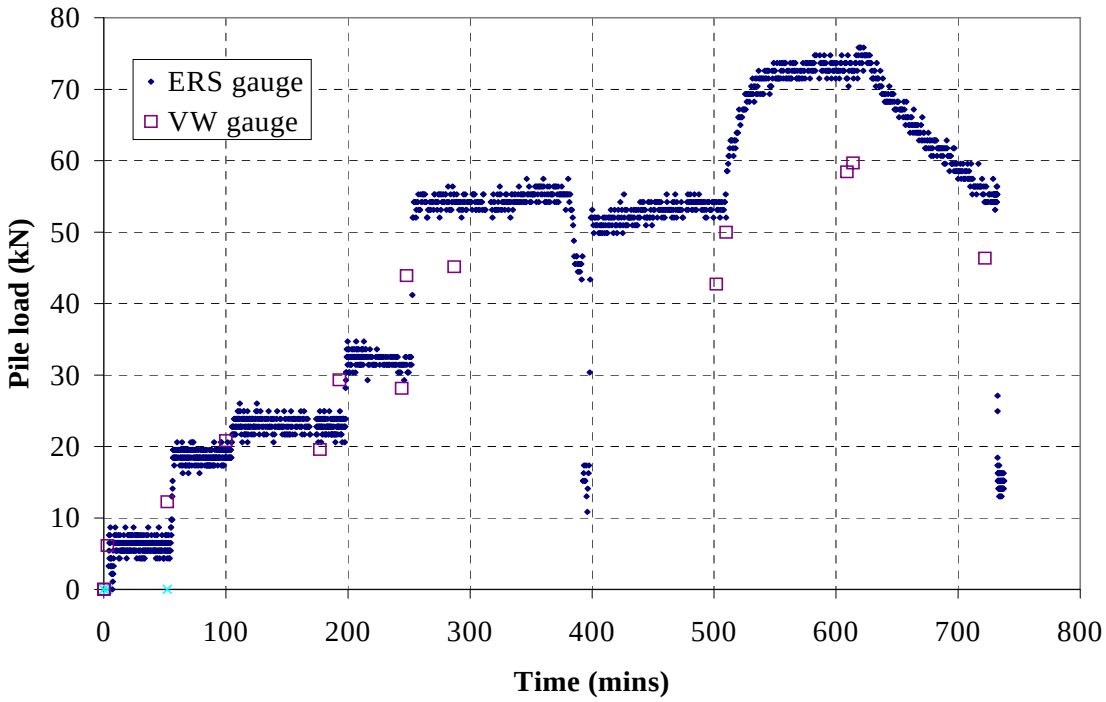

CG1[3]/s: Loads at 2.0m (Bar A)

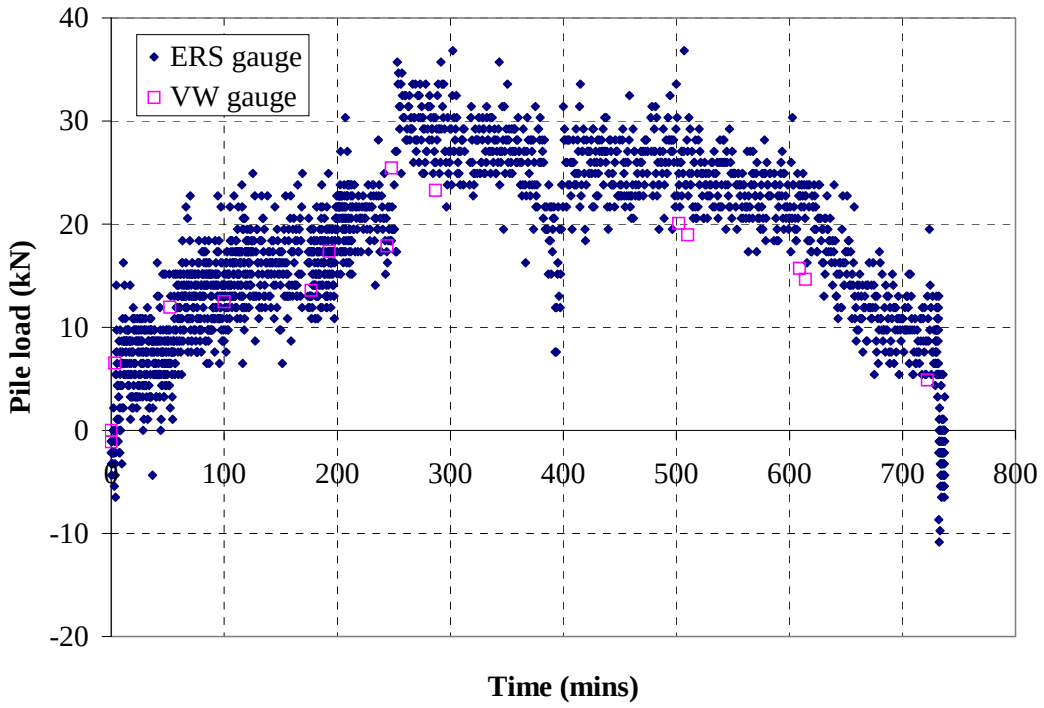

CG1[3]/s Loads at 2.0m (Bar B)

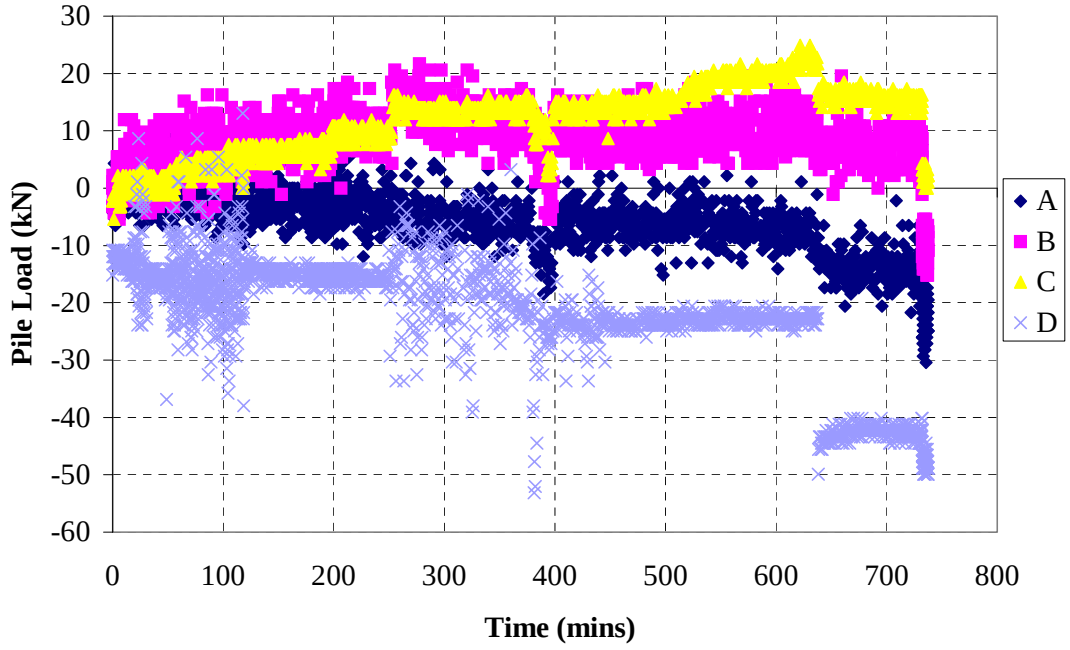

CG1[3]/s Loads at 4.5m (Bars A-D)

Appendix 6-1

Cyclic Load Test Data

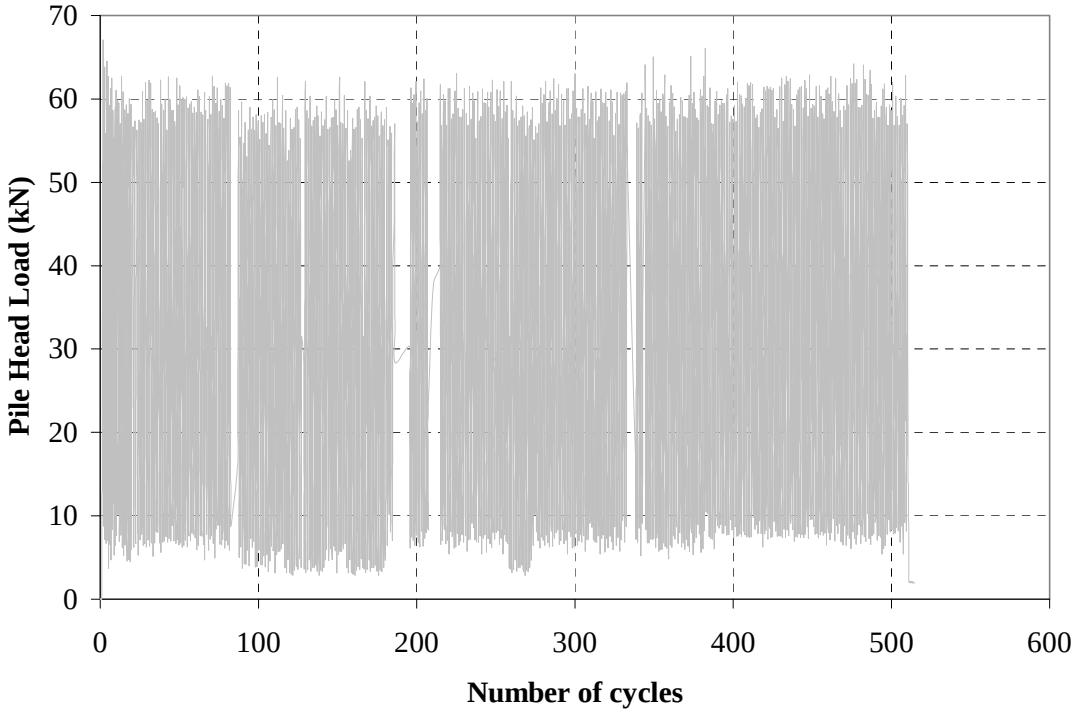
Pile Head Load (kN)
70
60
50
40
30
20
10
0
0
100
200
300
400
500
600
Number of cycles

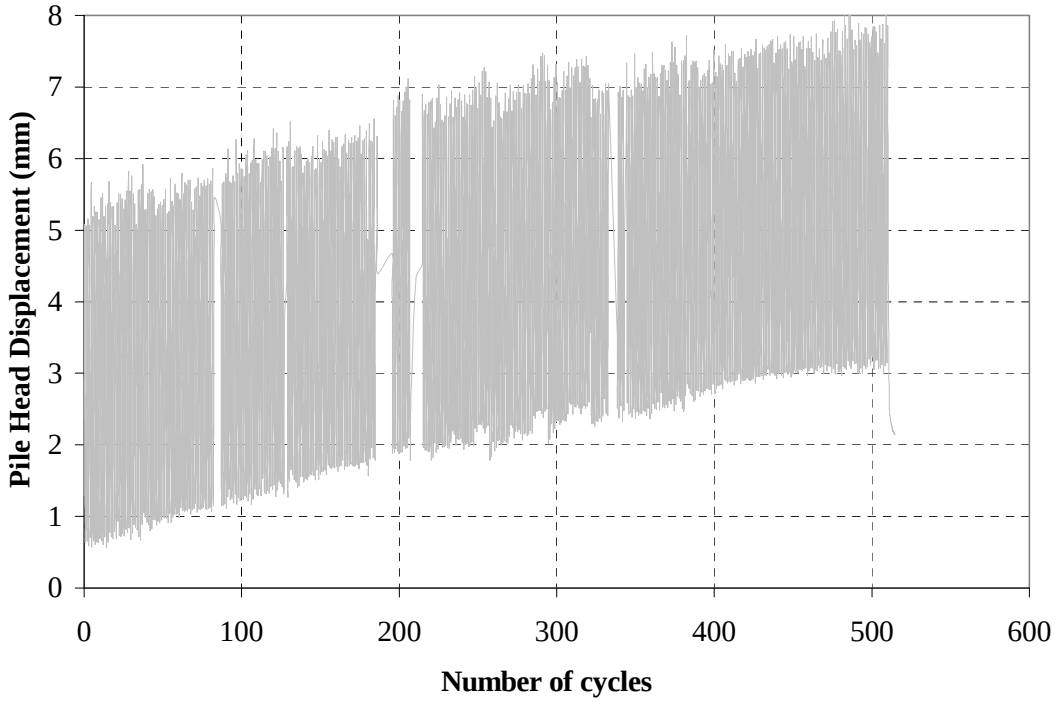
Pile Head Displacement (mm)
8
7
6
5
4
3
2
1
0
0
100
200
300
400
500
600
Number of cycles

TG1[1]/sc

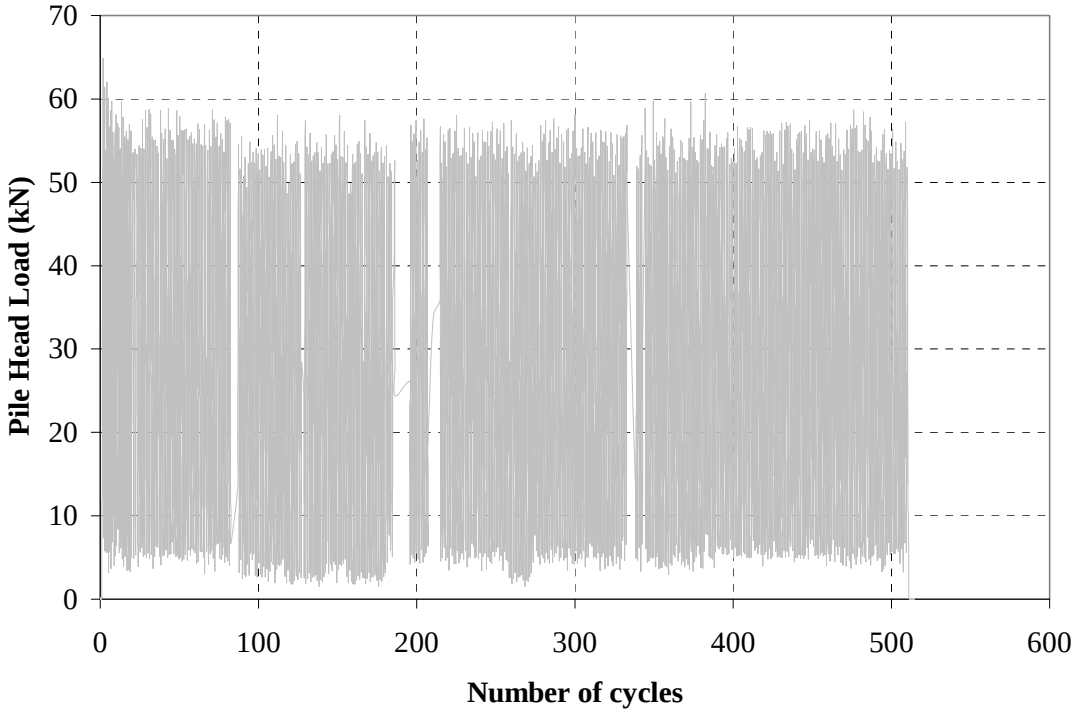
Pile Head Load (kN)
70
60
50
40
30
20
10
0
0
100
200
300
400
500
600
Number of cycles

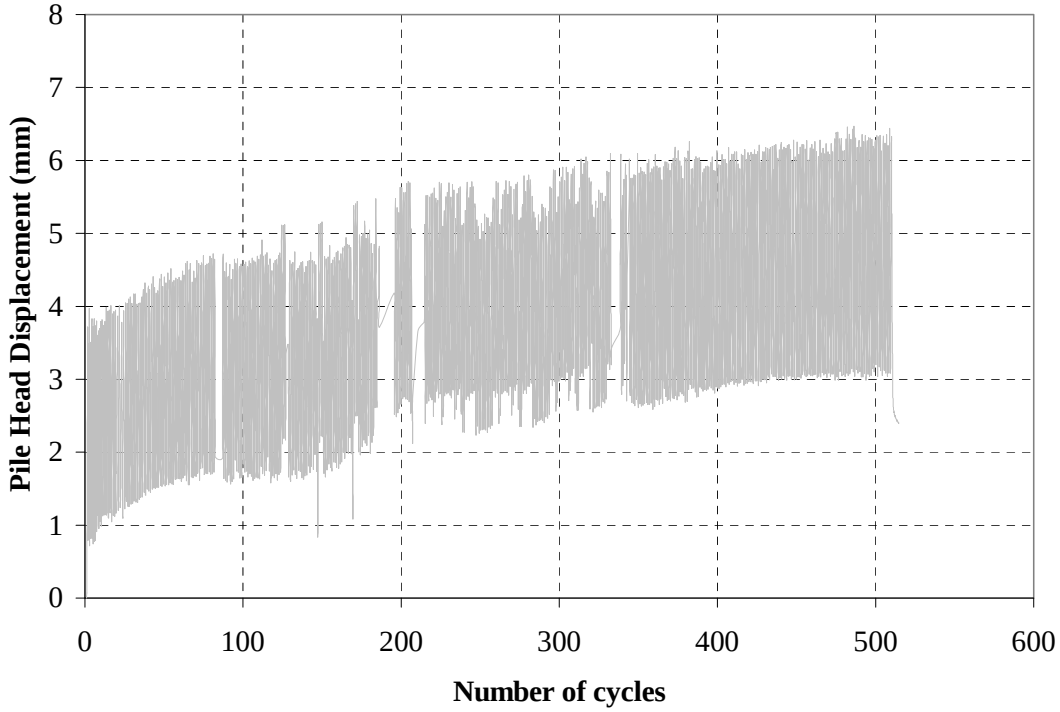
Pile Head Displacement (mm)
8
7
6
5
4
3
2
1
0
0
100
200
300
400
500
600
Number of cycles

TG1[2]/sc

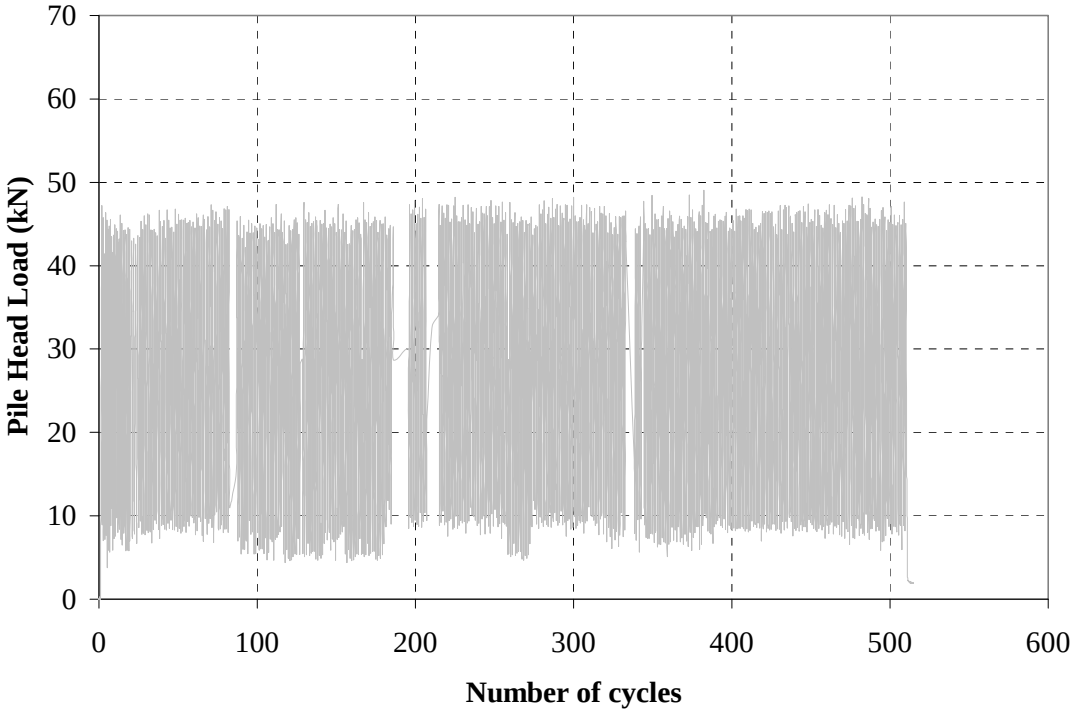
Pile Head Load (kN)
70
60
50
40
30
20
10
0
0
100
200
300
400
500
600
Number of cycles

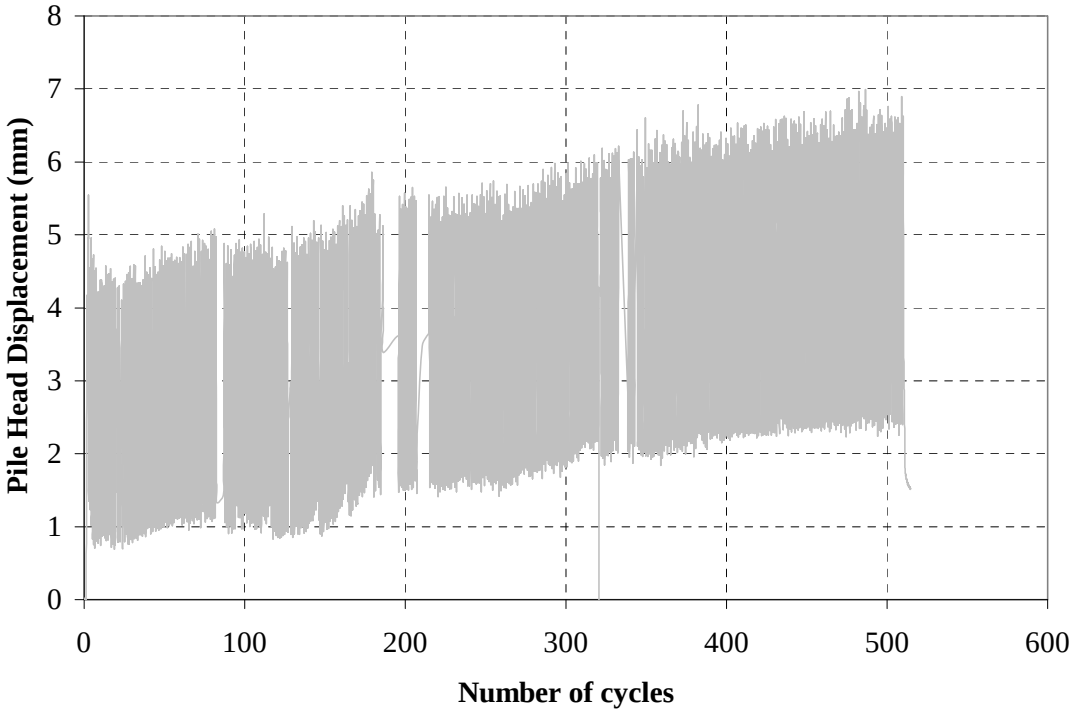
Pile Head Displacement (mm)
8
7
6
5
4
3
2
1
0
0
100
200
300
400
500
600
Number of cycles

TG1[3]/sc

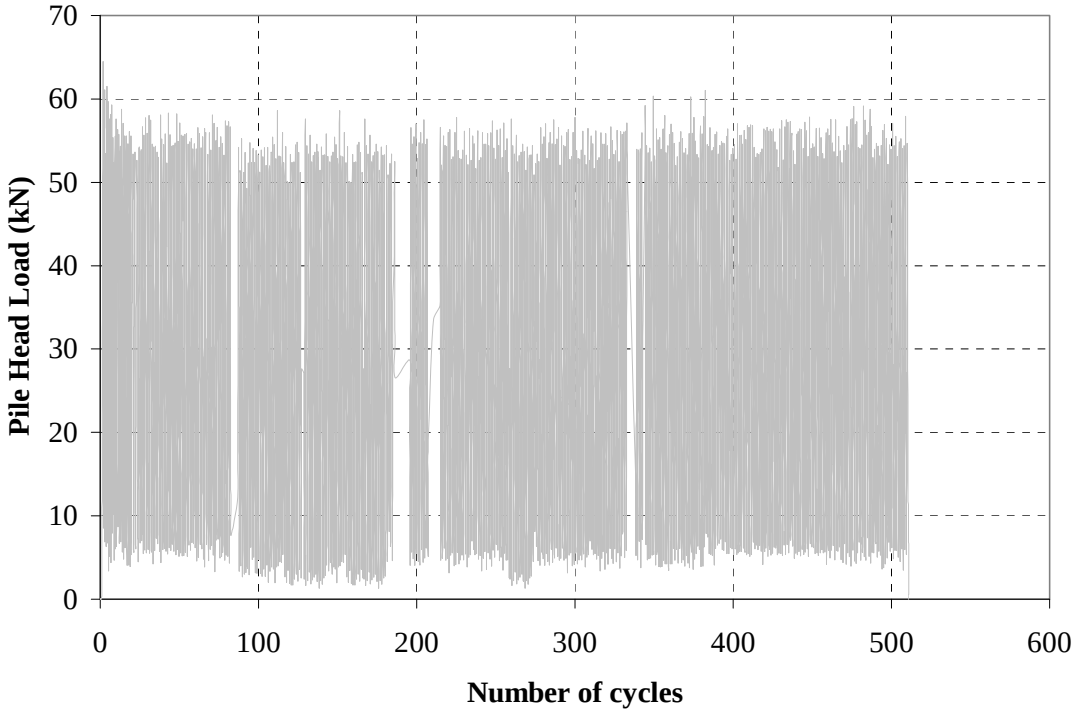
Pile Head Load (kN)
70
60
50
40
30
20
10
0
0
100
200
300
400
500
600
Number of cycles

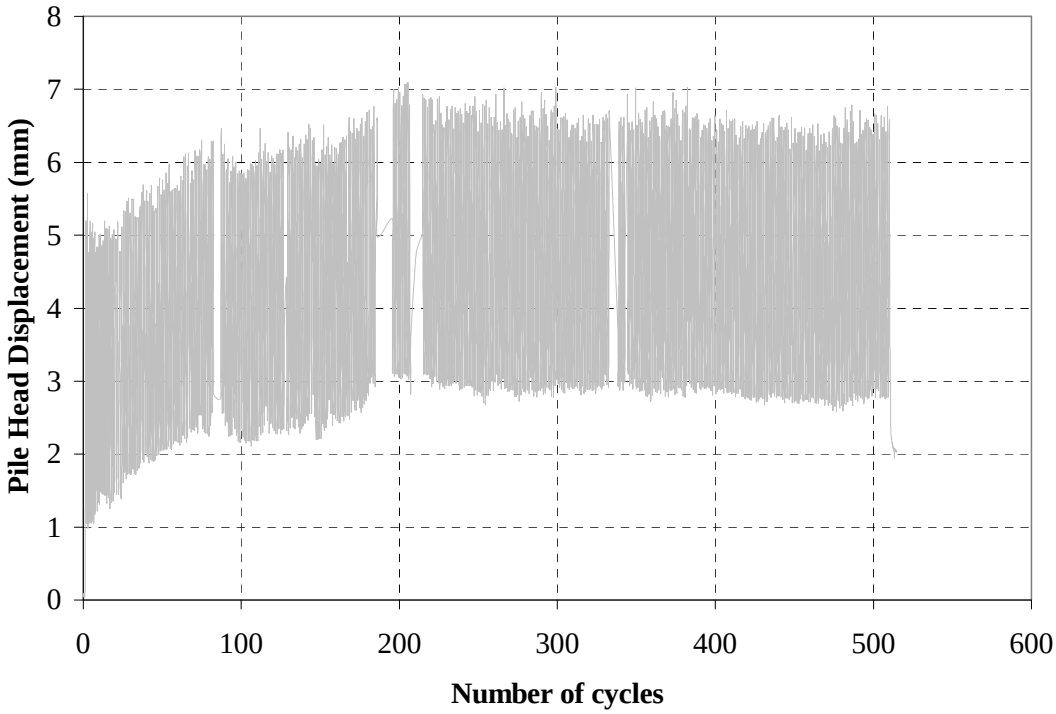
Pile Head Displacement (mm)
8
7
6
5
4
3
2
1
0
0
100
200
300
400
500
600
Number of cycles

TG1[4]/sc

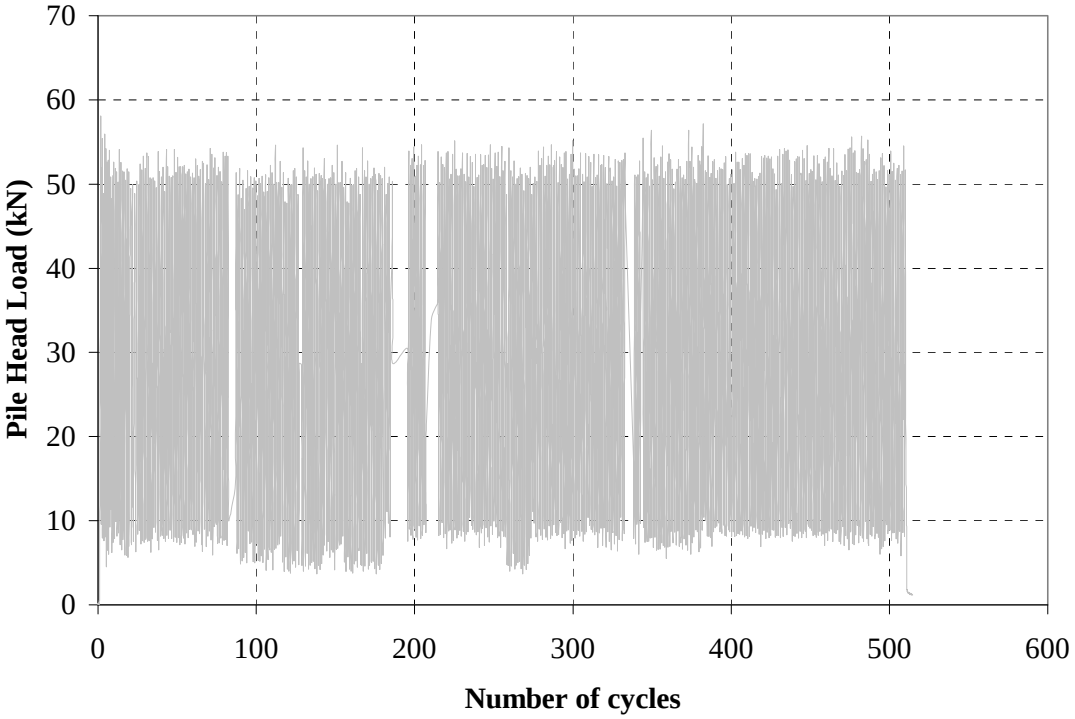
Pile Head Load (kN)
70
60
50
40
30
20
10
0
0
100
200
300
400
500
600
Number of cycles

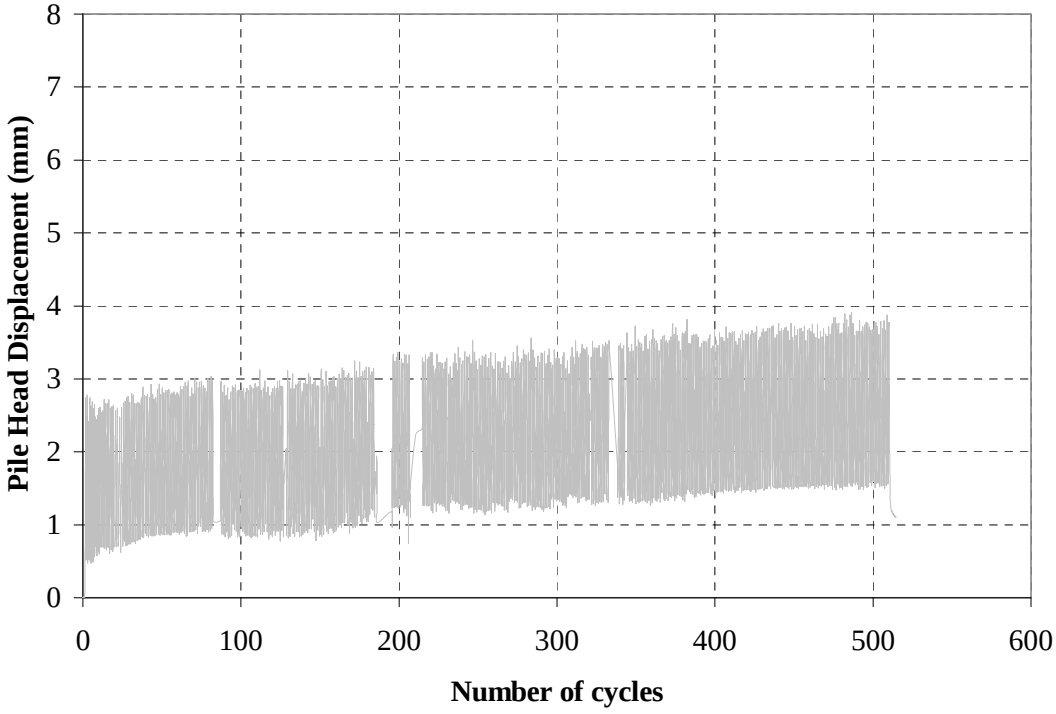
Pile Head Displacement (mm)
8
7
6
5
4
3
2
1
0
0
100
200
300
400
500
600
Number of cycles

TG1[5]/sc

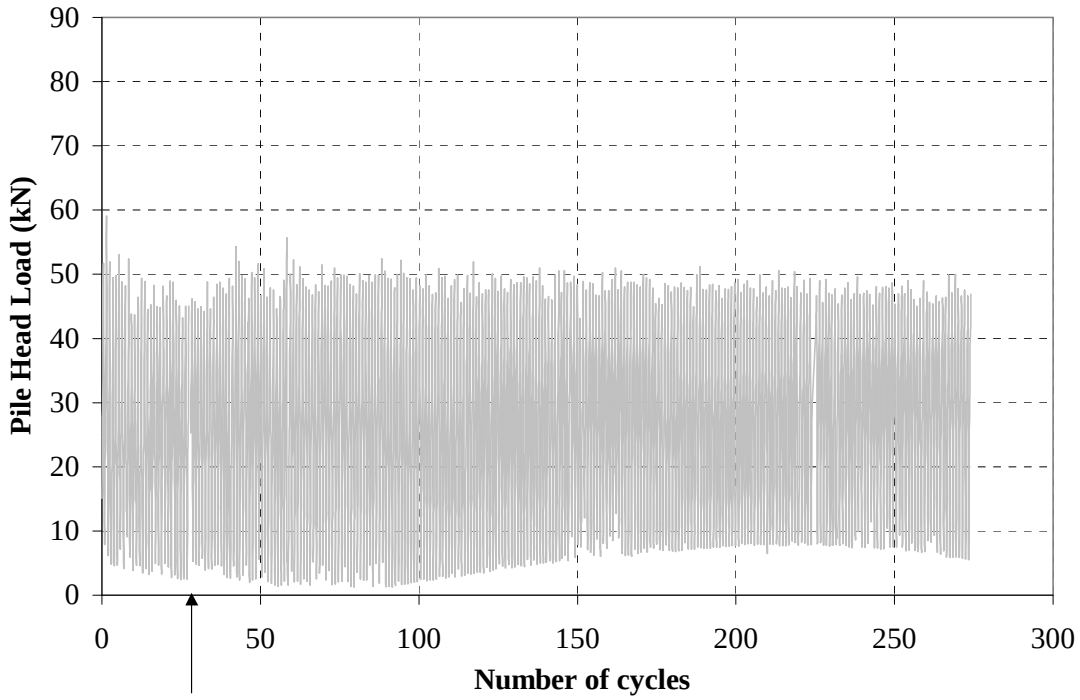
Pile Head Load (kN)
90
80
70
60
50
40
30
20
10
0
0
50
100
150
200
250
300
Number of cycles

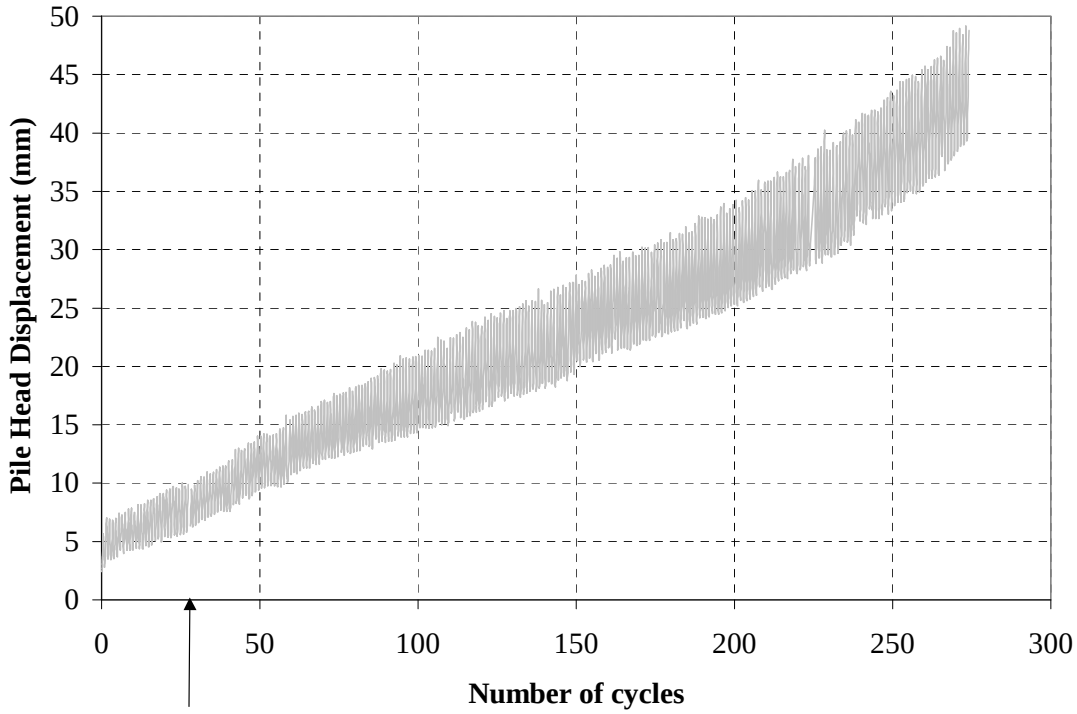
Pile Head Displacement (mm)
50
45
40
35
30
25
20
15
10
5
0
0
50
100
150
200
250
300
Number of cycles

CTG1[1]/sc

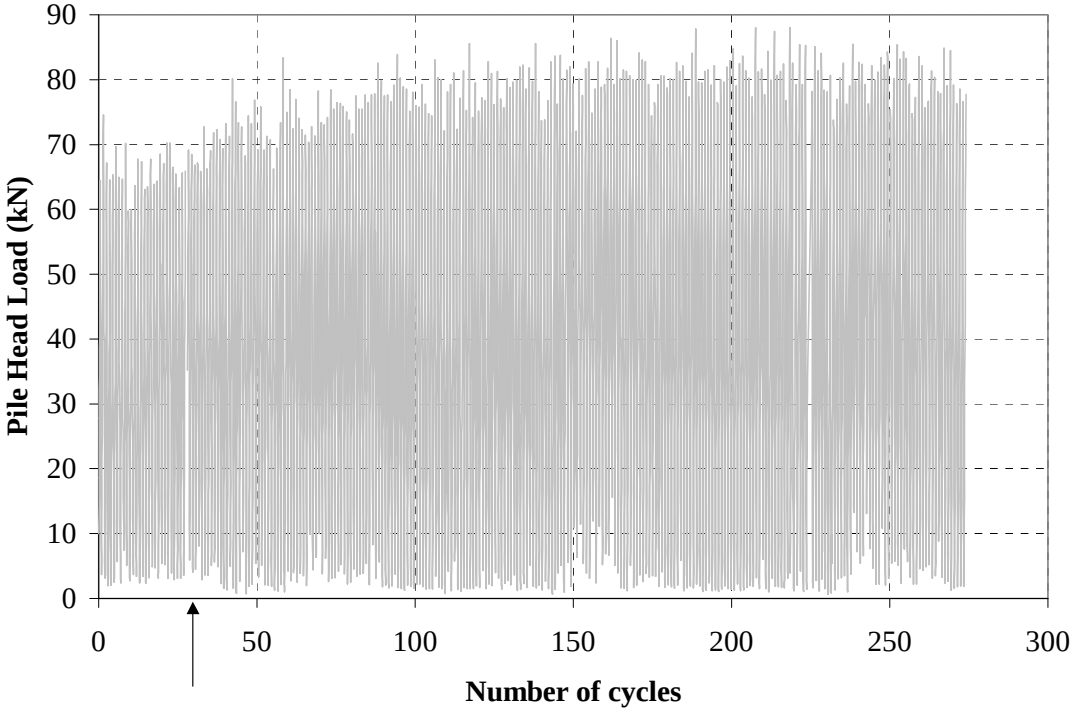
Pile Head Load (kN)
90
80
70
60
50
40
30
20
10
0
0
50
100
150
200
250
300
Number of cycles

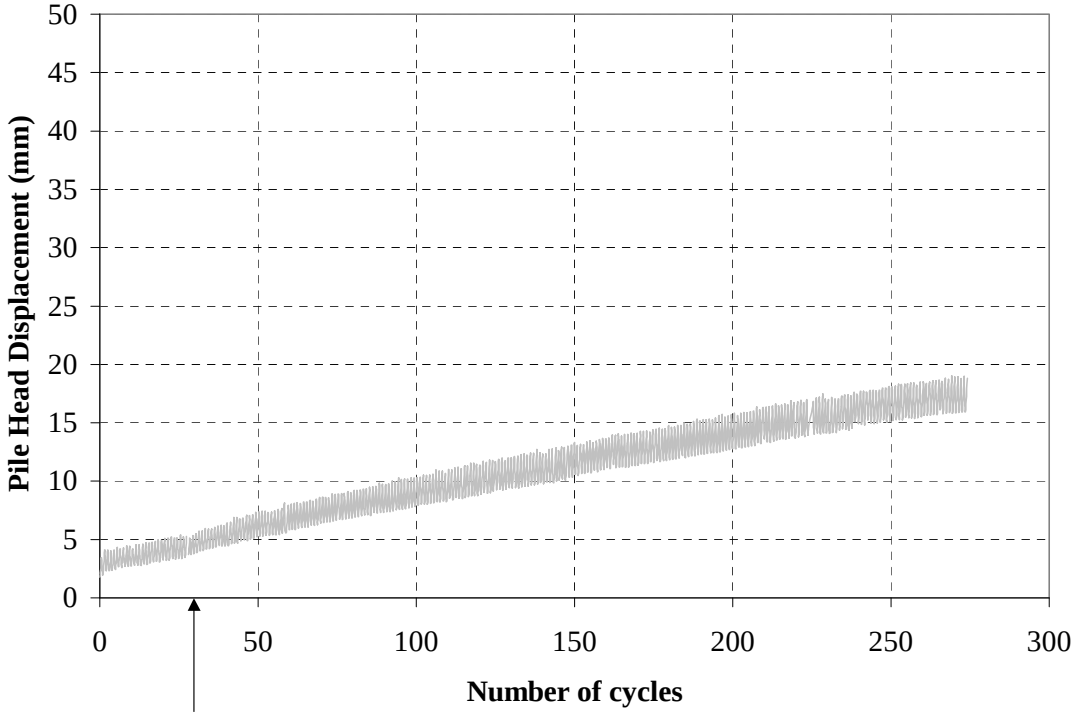
Pile Head Displacement (mm)
50
45
40
35
30
25
20
15
10
5
0
0
50
100
150
200
250
300
Number of cycles

CTG1[2]/sc

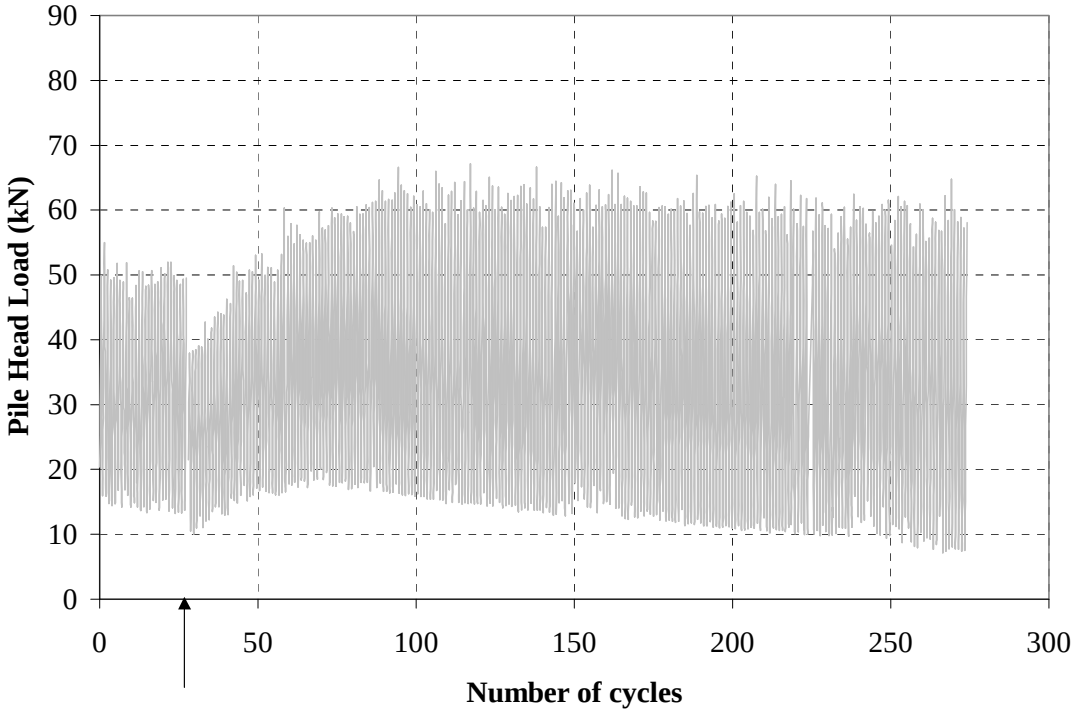
Pile Head Load (kN)
90
80
70
60
50
40
30
20
10
0
0
50
100
150
200
250
300
Number of cycles

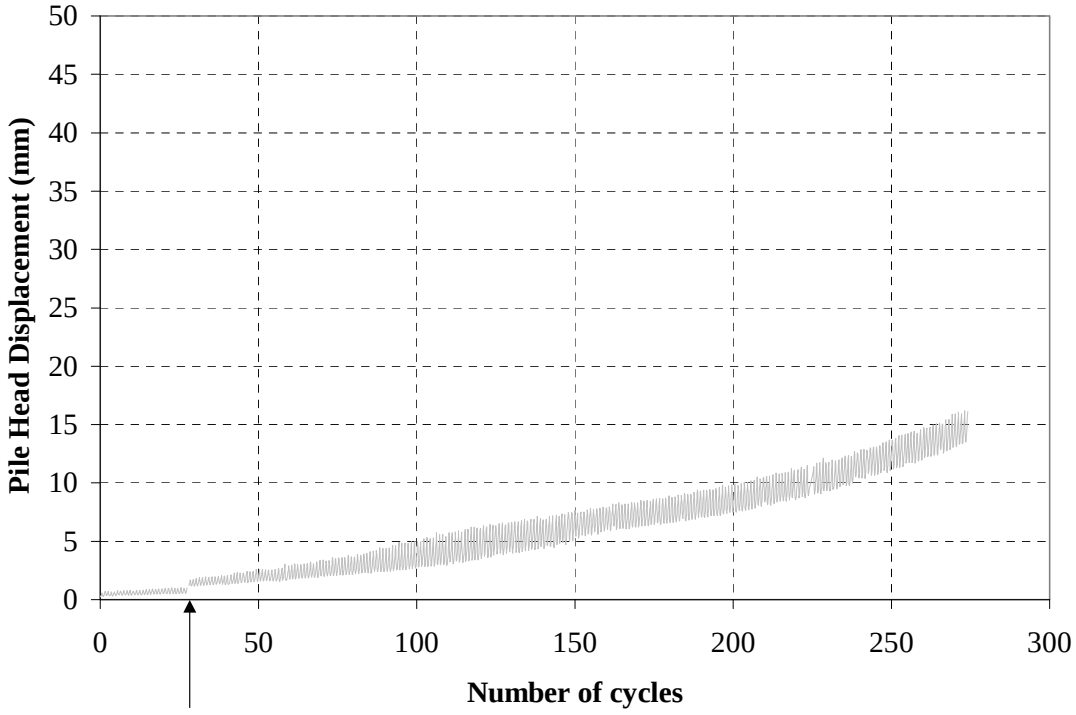
Pile Head Displacement (mm)
50
45
40
35
30
25
20
15
10
5
0
0
50
100
150
200
250
300
Number of cycles

CTG1[3]/sc

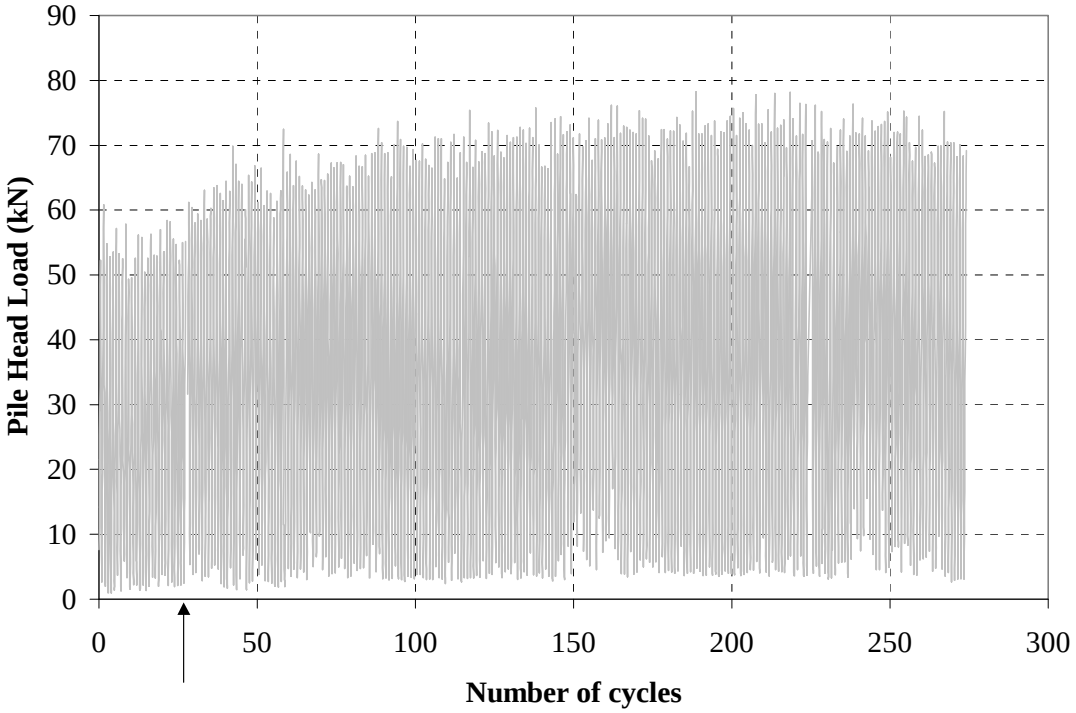
Pile Head Load (kN)
90
80
70
60
50
40
30
20
10
0
0
50
100
150
200
250
300
Number of cycles

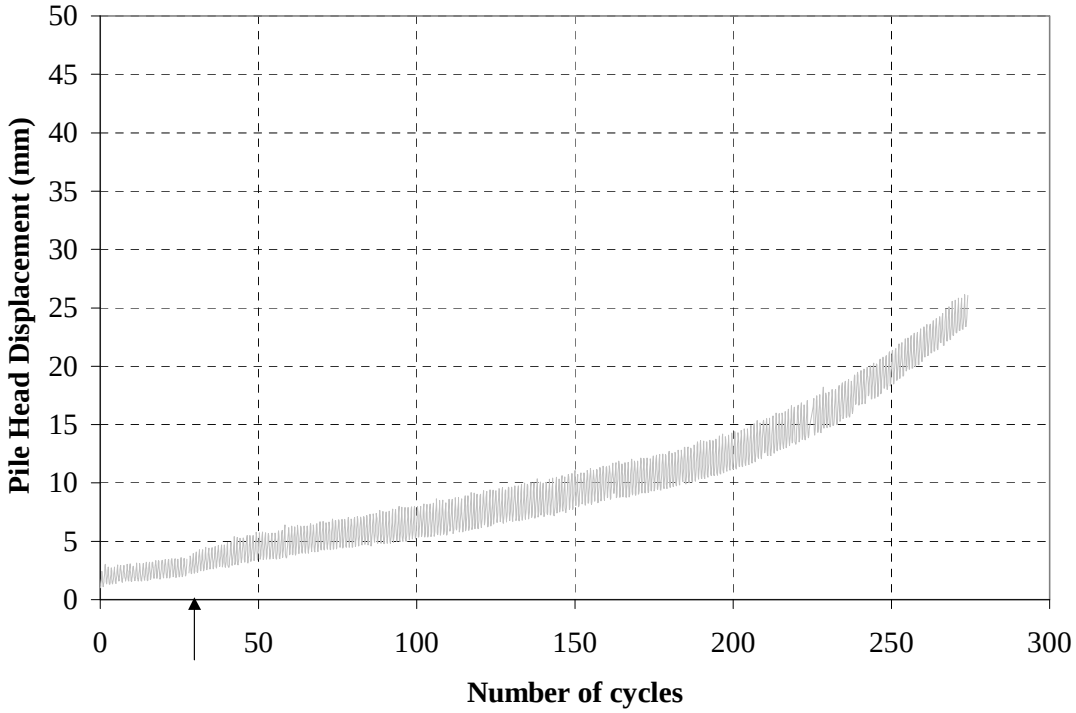
Pile Head Displacement (mm)
50
45
40
35
30
25
20
15
10
5
0
0
50
100
150
200
250
300
Number of cycles

CTG1[4]/sc

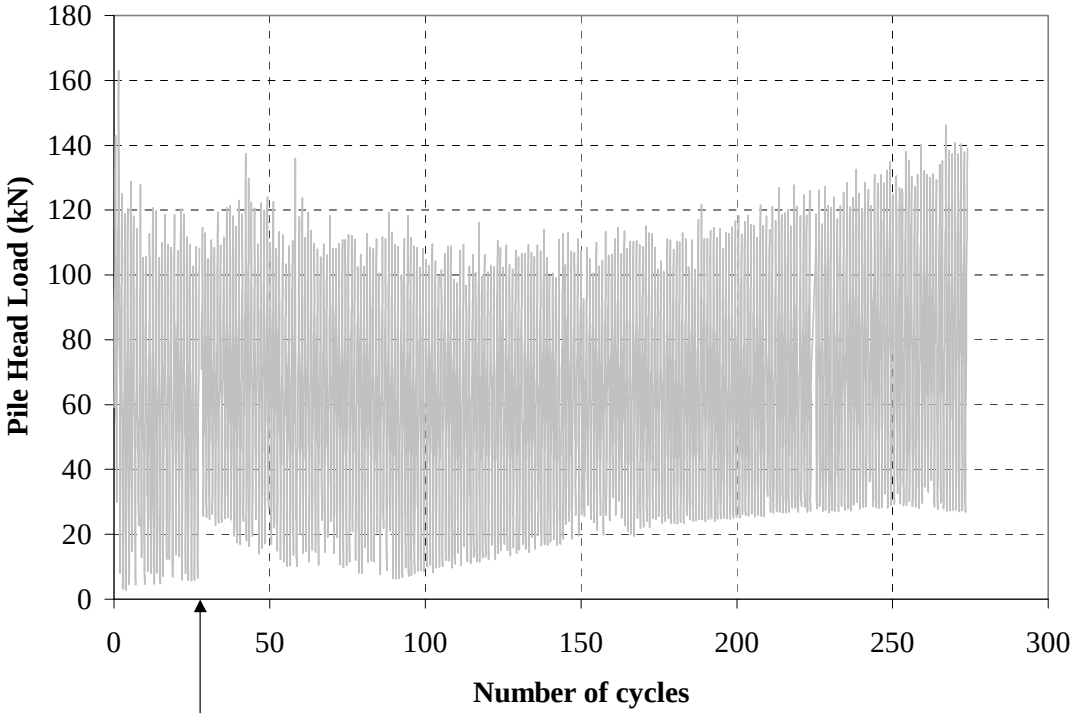
Pile Head Load (kN)
180
160
140
120
100
80
60
40
20
0
0
50
100
150
200
250
300
Number of cycles

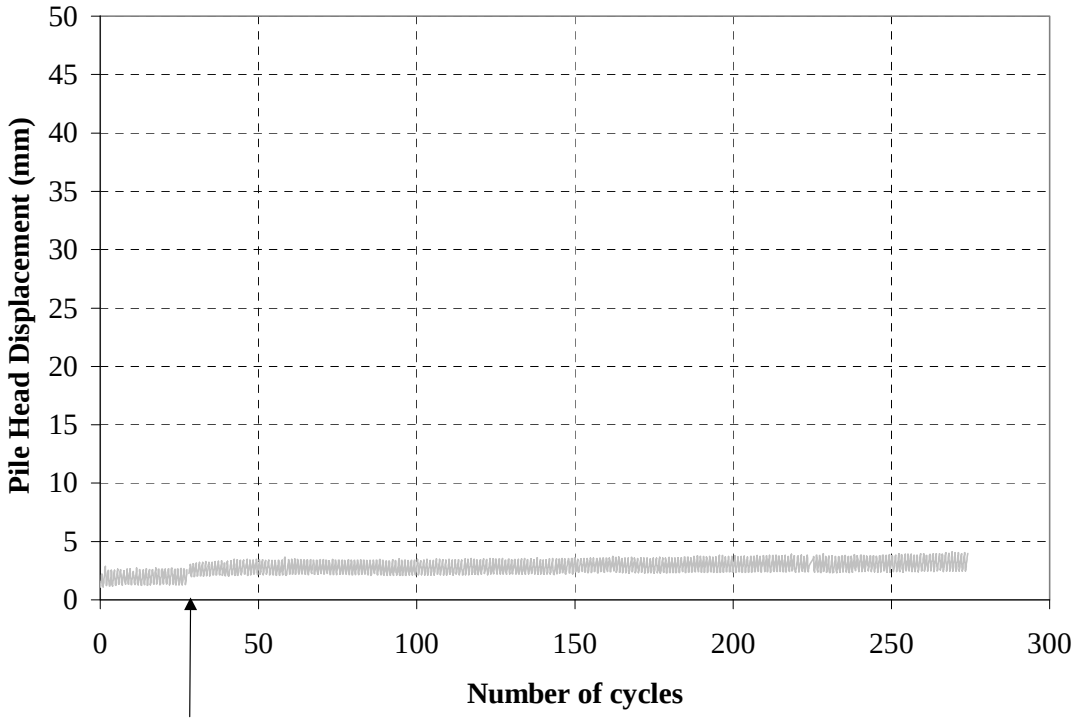
Pile Head Displacement (mm)
50
45
40
35
30
25
20
15
10
5
0
0
50
100
150
200
250
300
Number of cycles

CTG1[5]/sc

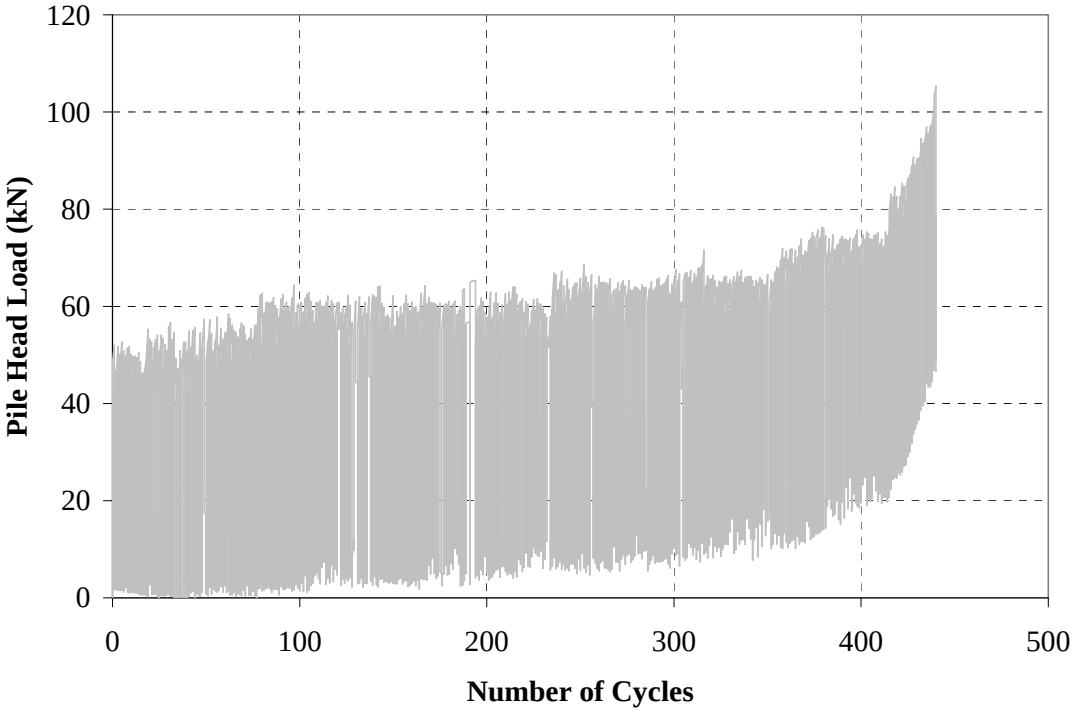
120
100
80
60
40
20
0
Pile Head Load (kN)
0
100
200
300
400
500
Number of Cycles

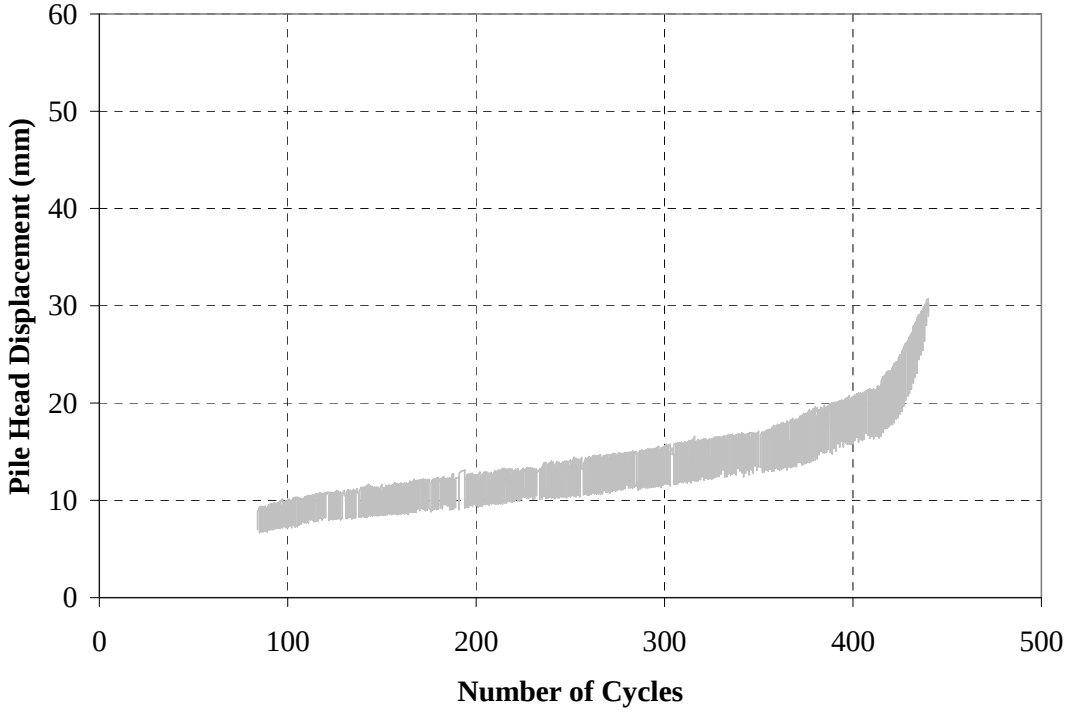
60
50
40
30
20
10
0
Pile Head Displacement (mm)
0
100
200
300
400
500
Number of Cycles

TG2[1]/c

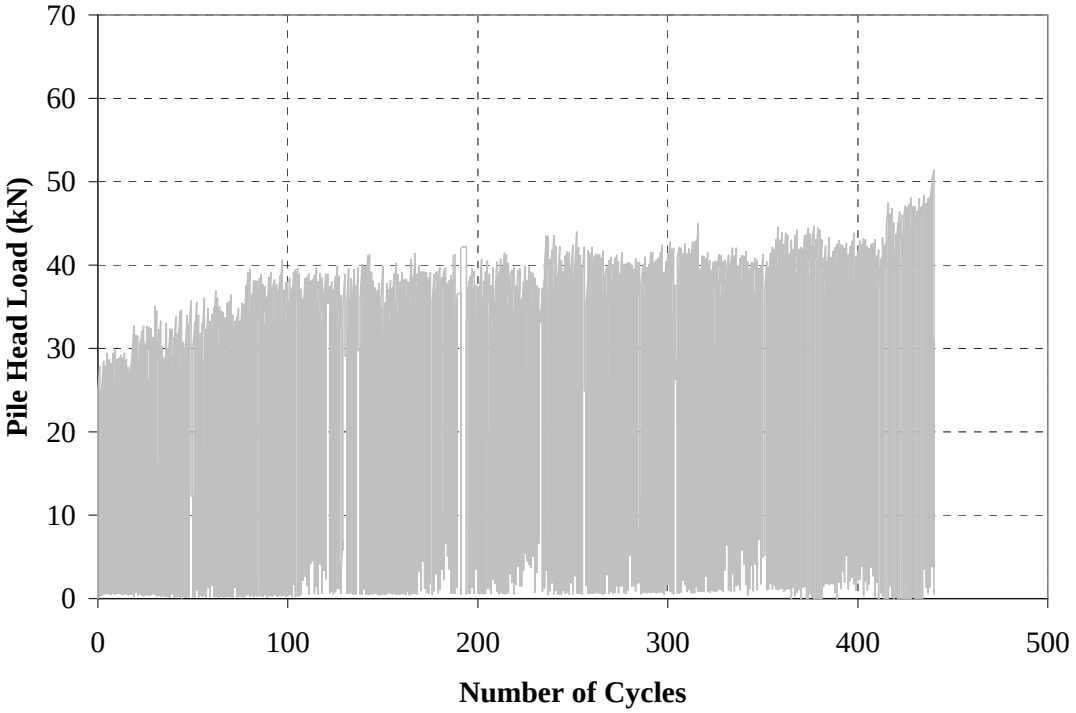
Pile Head Load (kN)
70
60
50
40
30
20
10
0
0
100
200
300
400
500
Number of Cycles

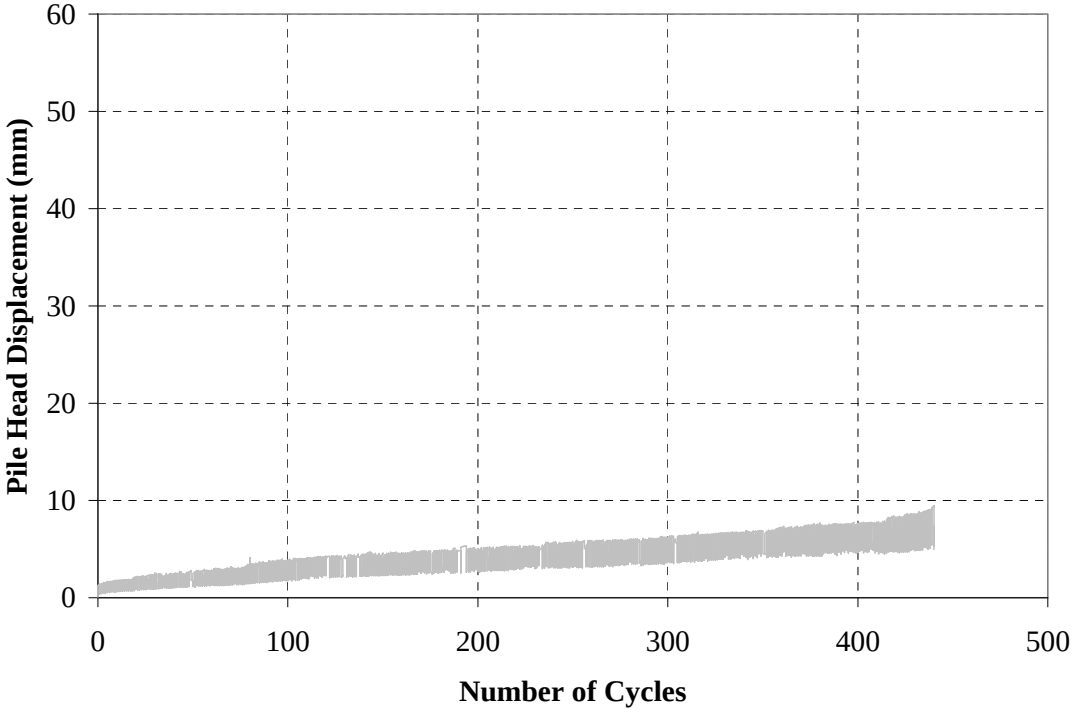
Pile Head Displacement (mm)
60
50
40
30
20
10
0
0
100
200
300
400
500
Number of Cycles

TG2[2]/c

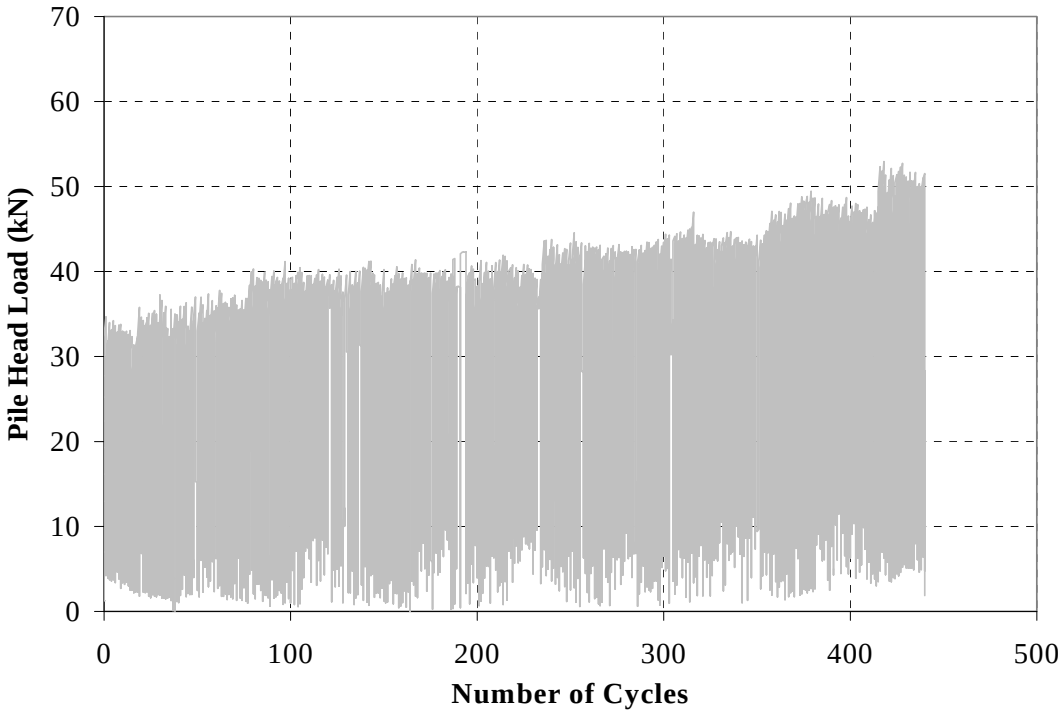
Pile Head Load (kN)
70
60
50
40
30
20
10
0
0
100
200
300
400
500
Number of Cycles

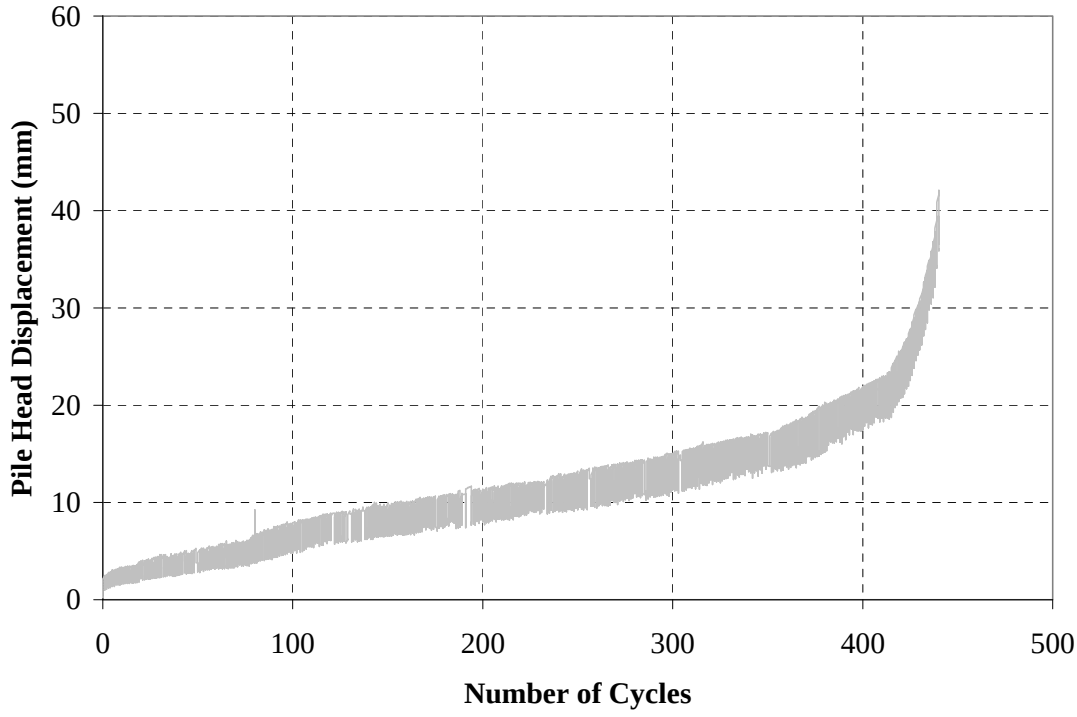
Pile Head Displacement (mm)
60
50
40
30
20
10
0
0
100
200
300
400
500
Number of Cycles

TG2[3]/c

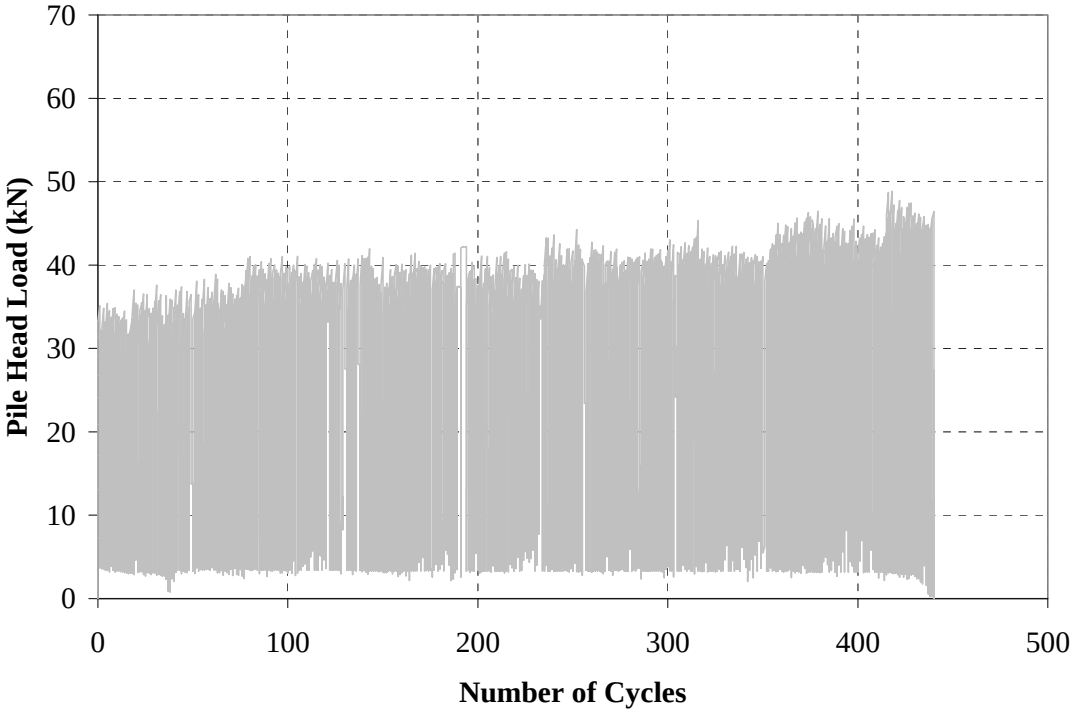
Pile Head Load (kN)
70
60
50
40
30
20
10
0
0
100
200
300
400
500
Number of Cycles

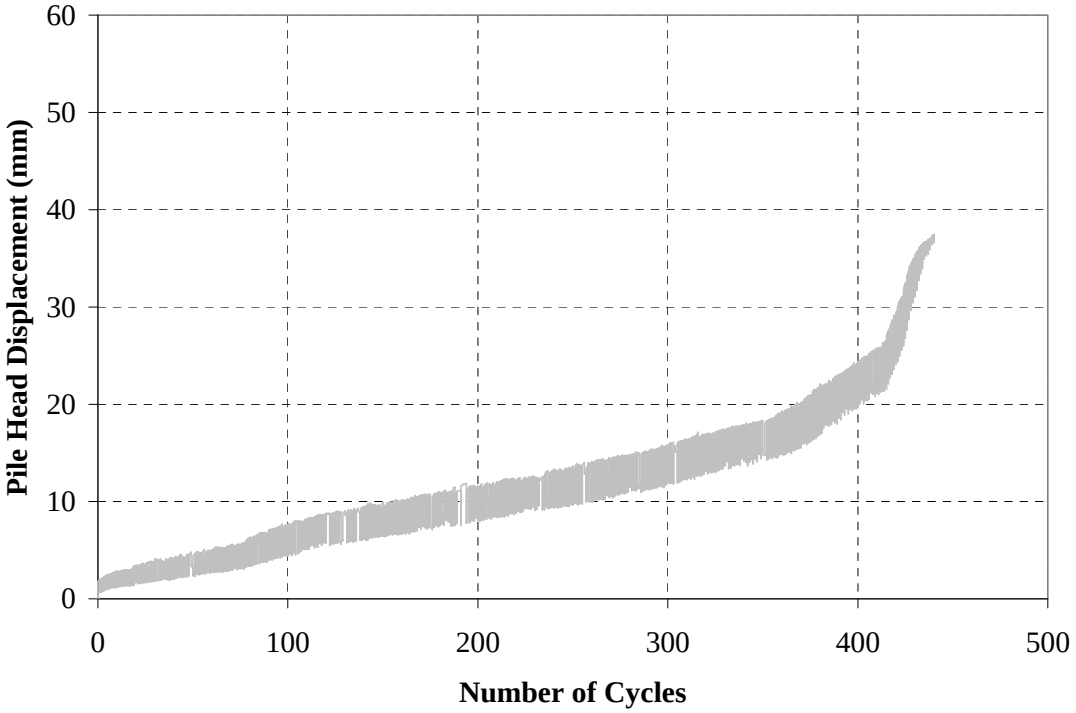
Pile Head Displacement (mm)
60
50
40
30
20
10
0
0
100
200
300
400
500
Number of Cycles

TG2[4]/c

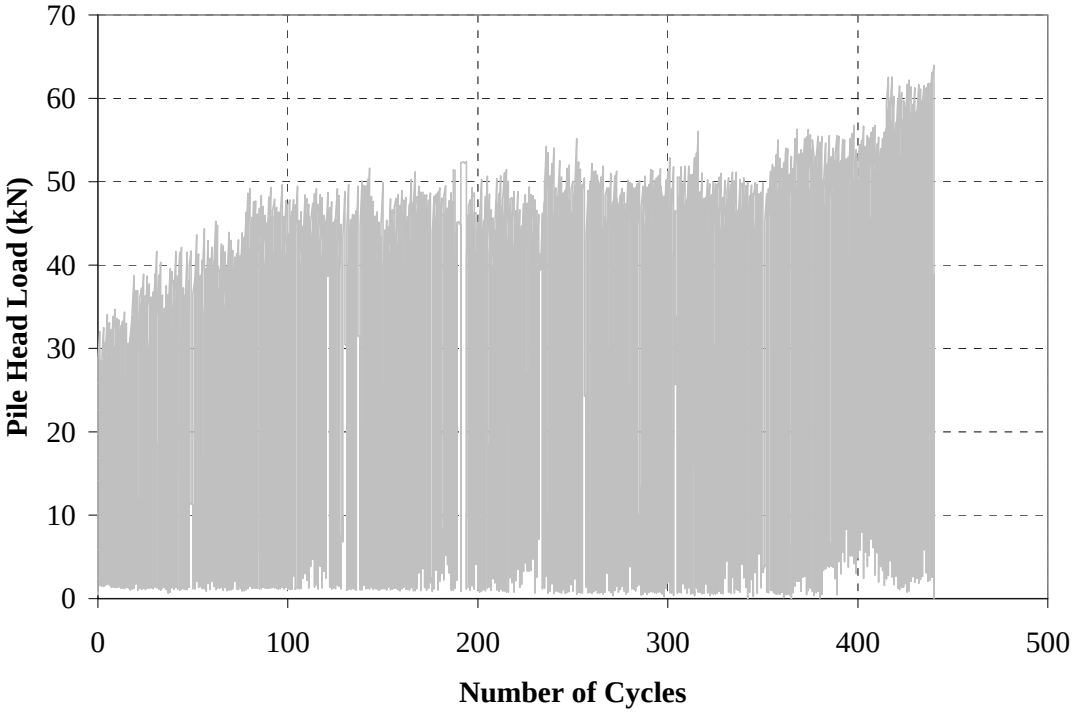
Pile Head Load (kN)
70
60
50
40
30
20
10
0
0
100
200
300
400
500
Number of Cycles

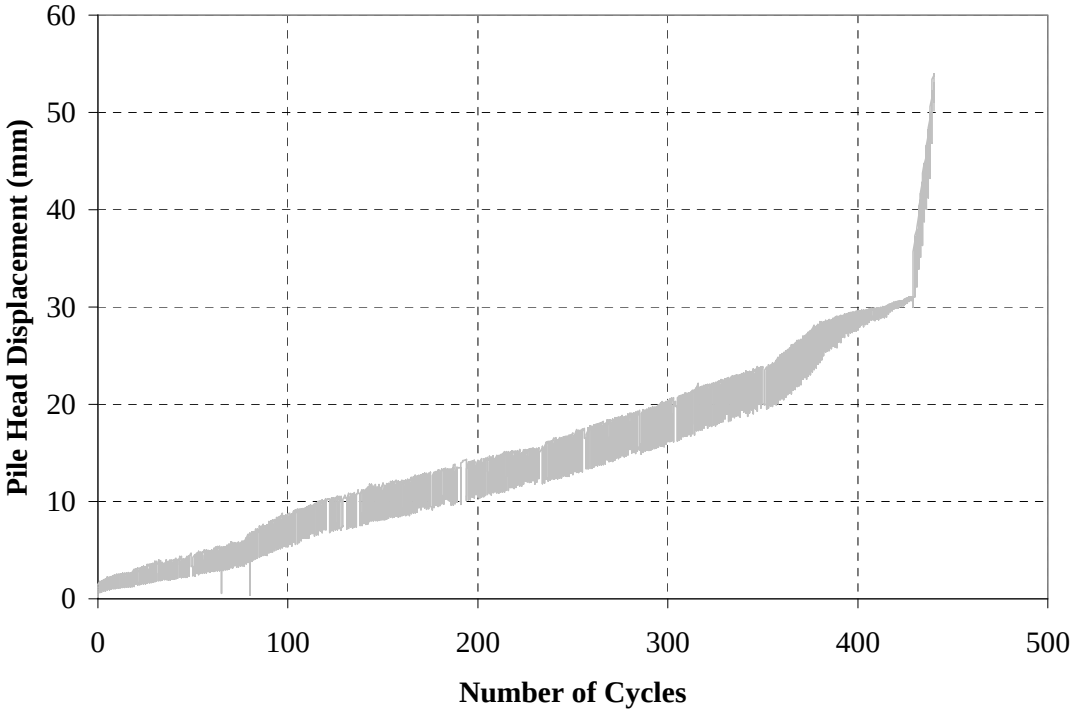
Pile Head Displacement (mm)
60
50
40
30
20
10
0
0
100
200
300
400
500
Number of Cycles

TG2[5]/c

Appendix 6-2

Static Re-test Data after Cycling

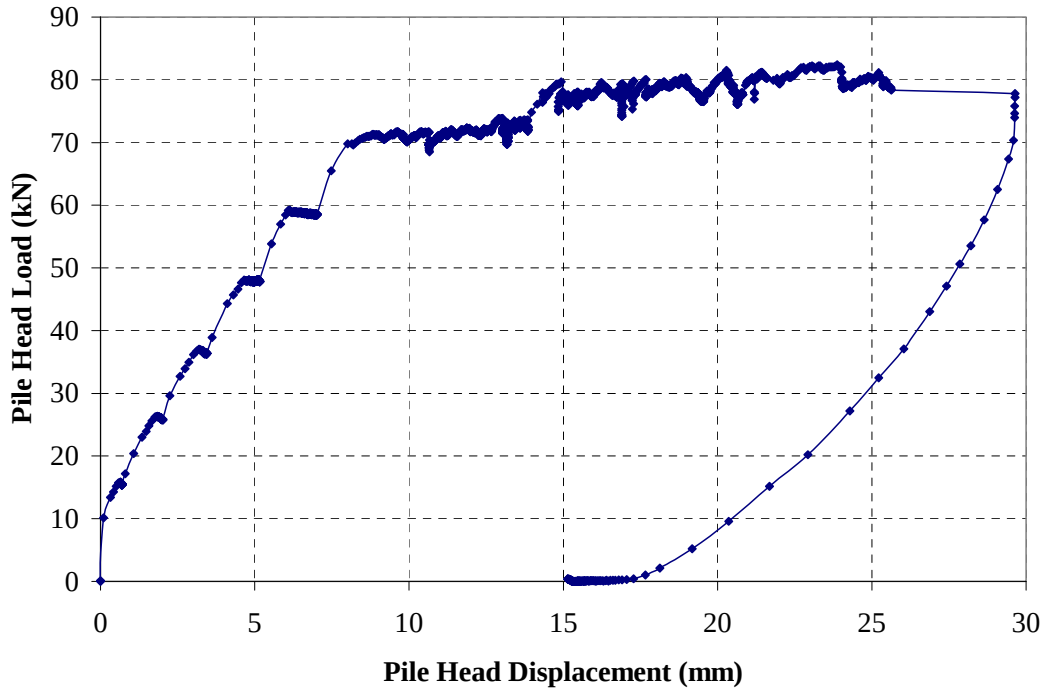

TG1[1]/scs

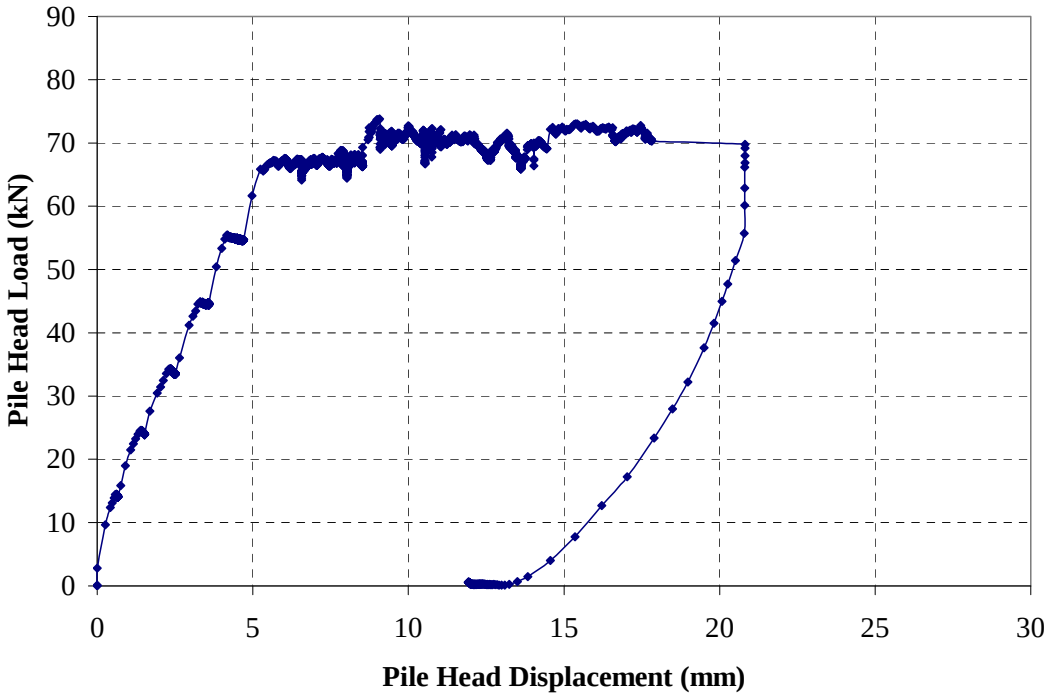

TG1[2]/scs

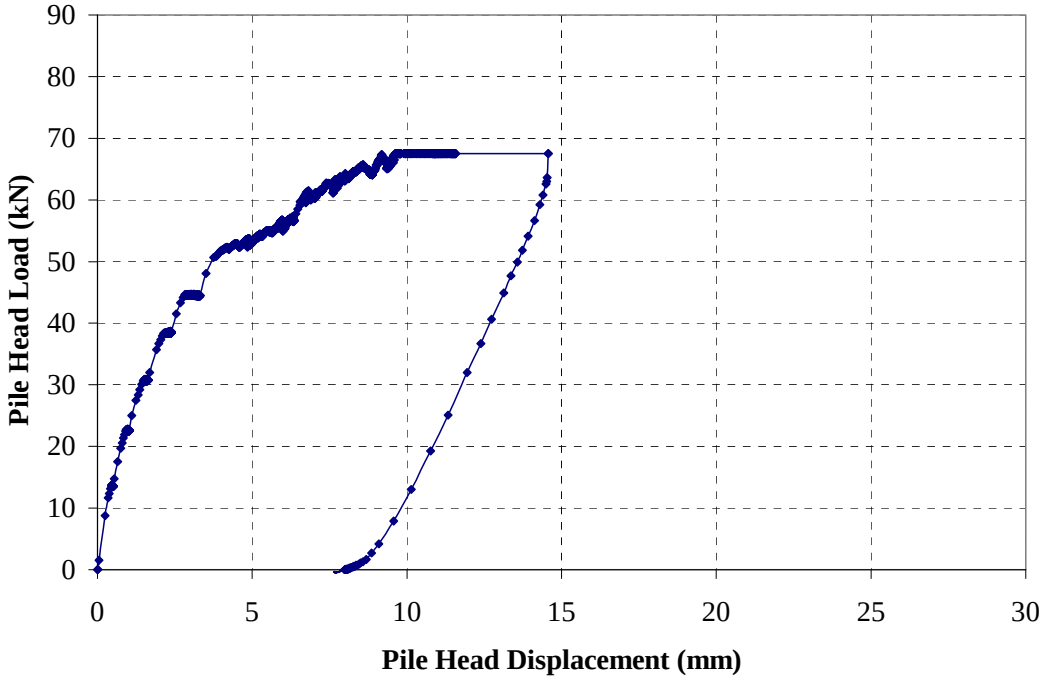

TG1[3]/scs

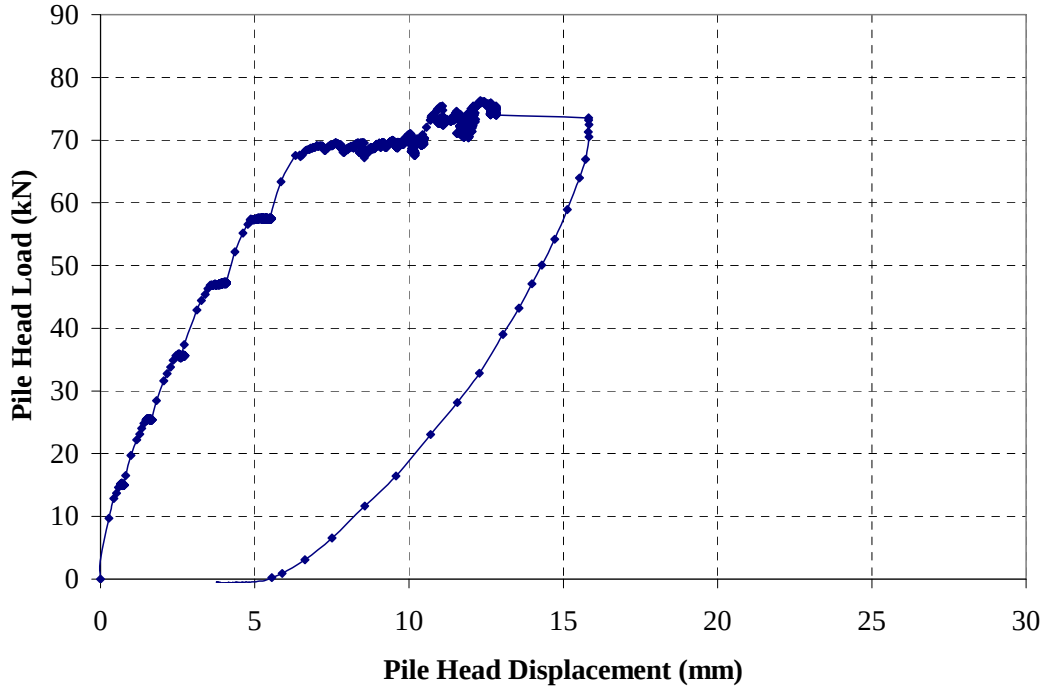

TG1[4]/scs

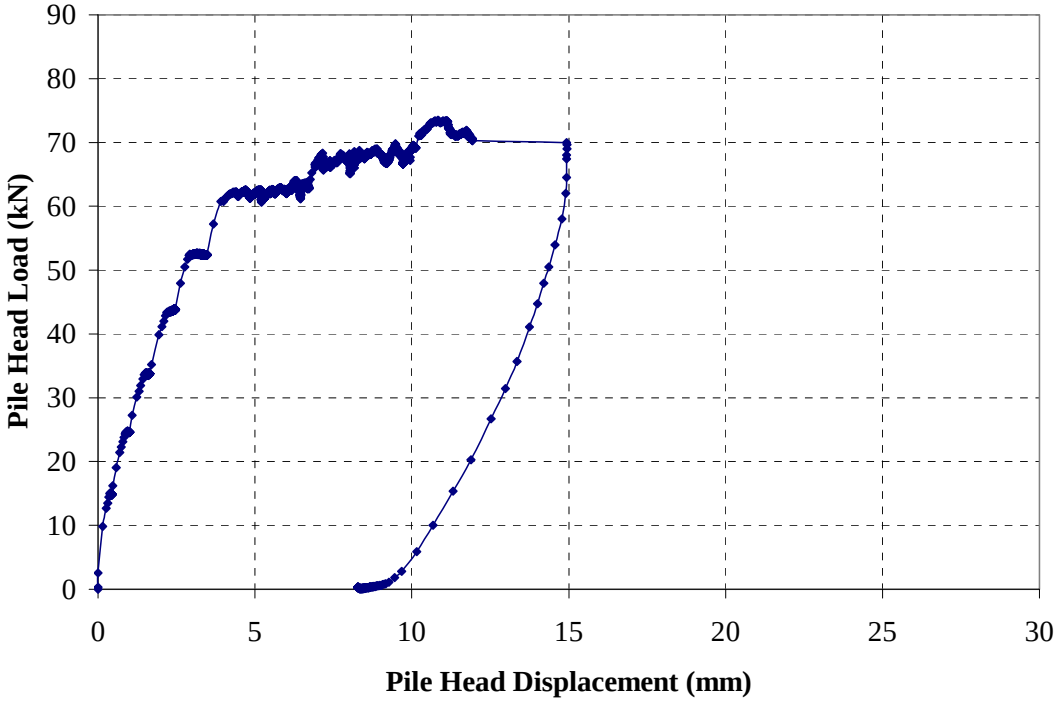

TG1[5]/scs

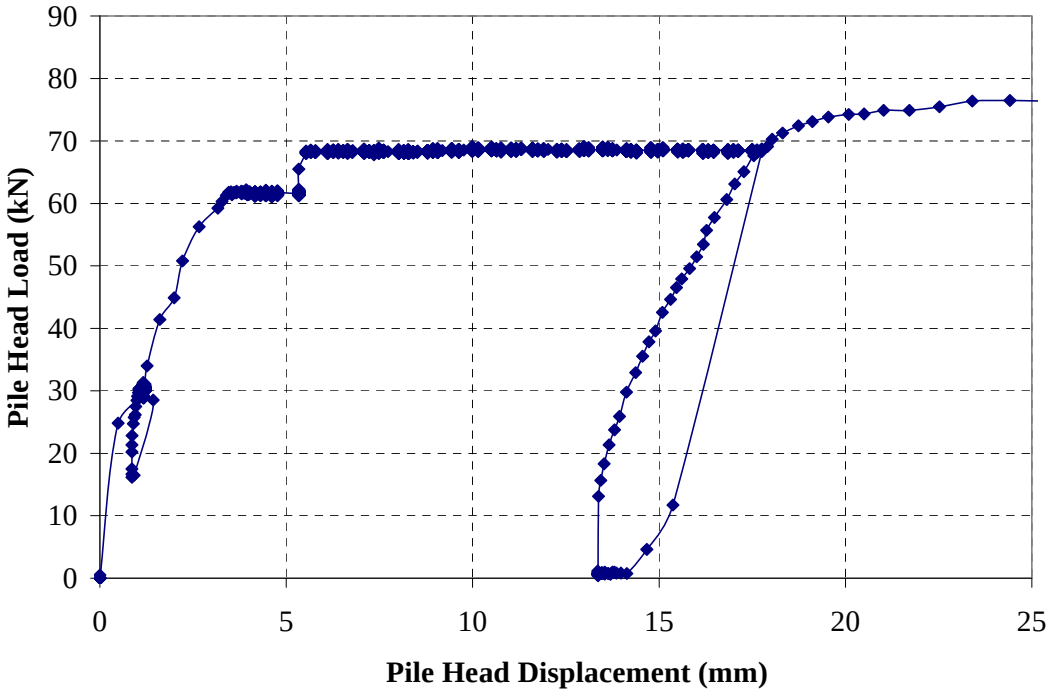

CTS1/scs

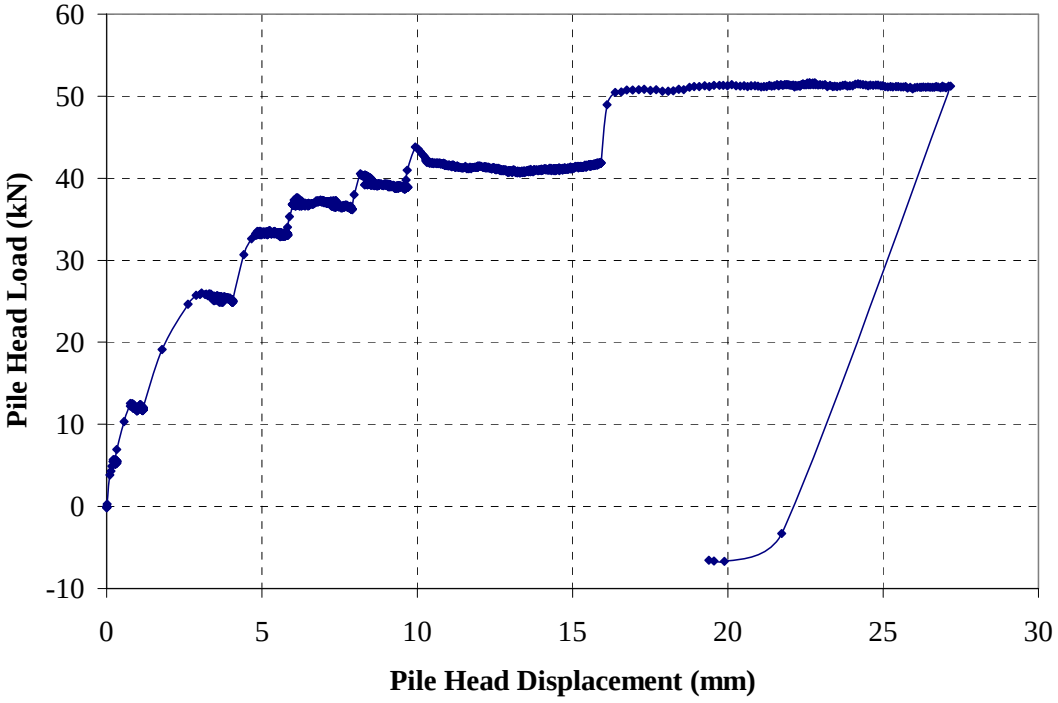

TG2[1]/cs

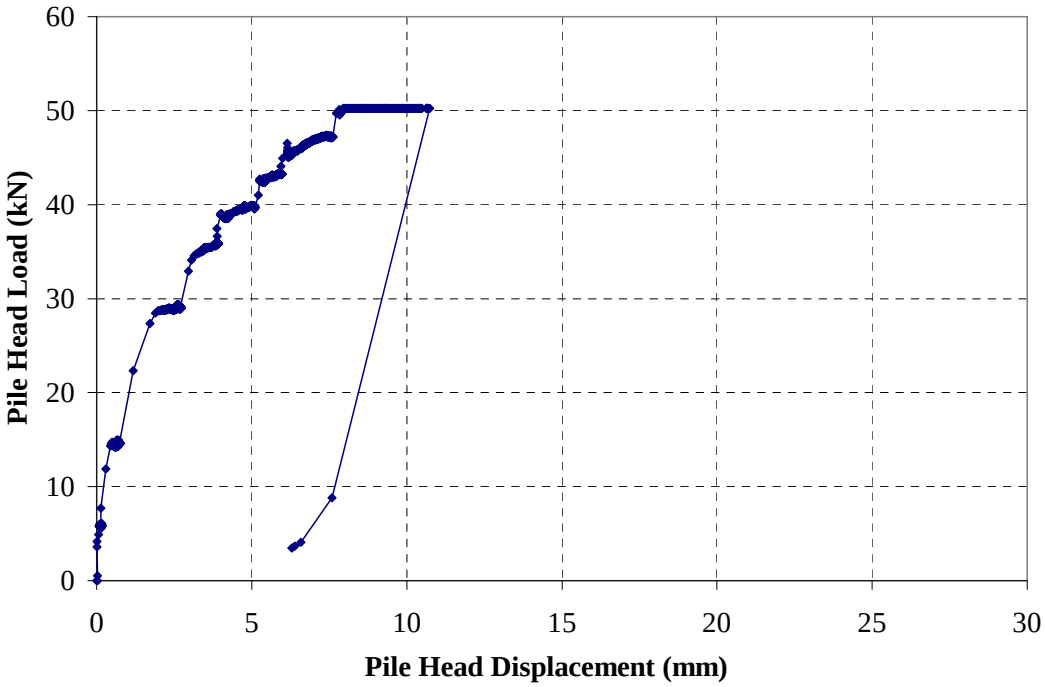

TG2[2]/cs

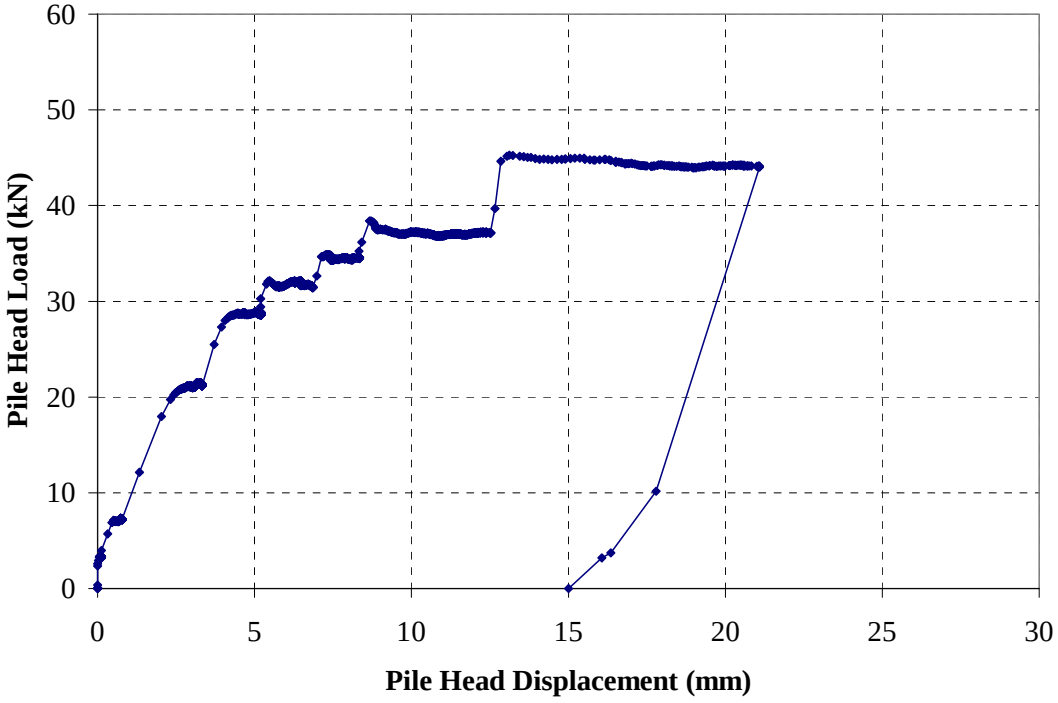

TG2[3]/cs

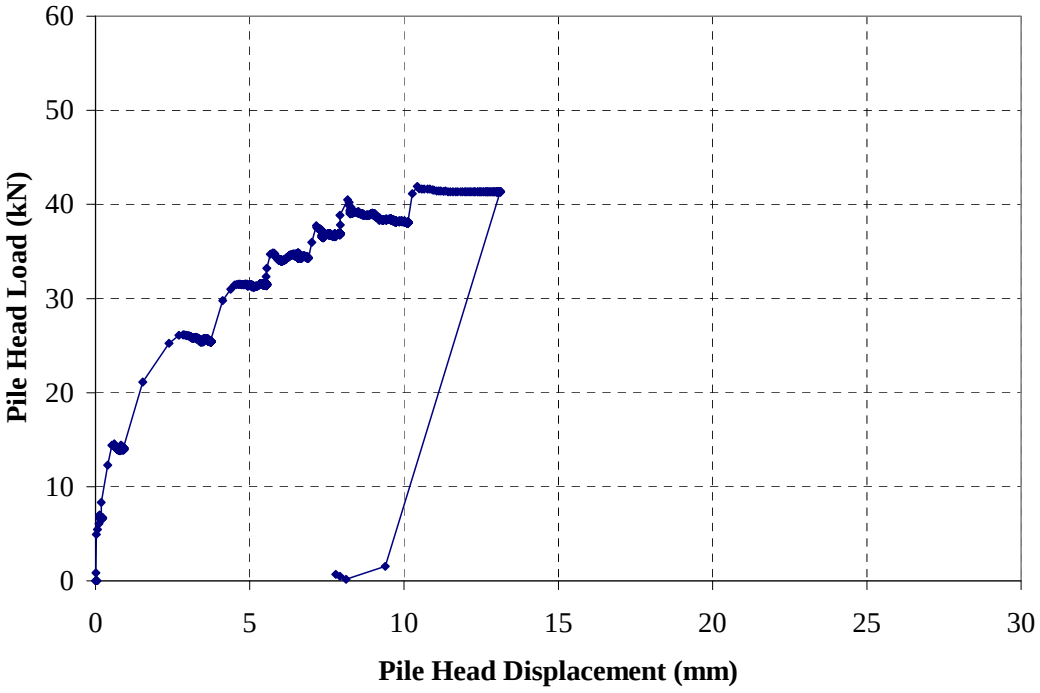

TG2[4]/cs

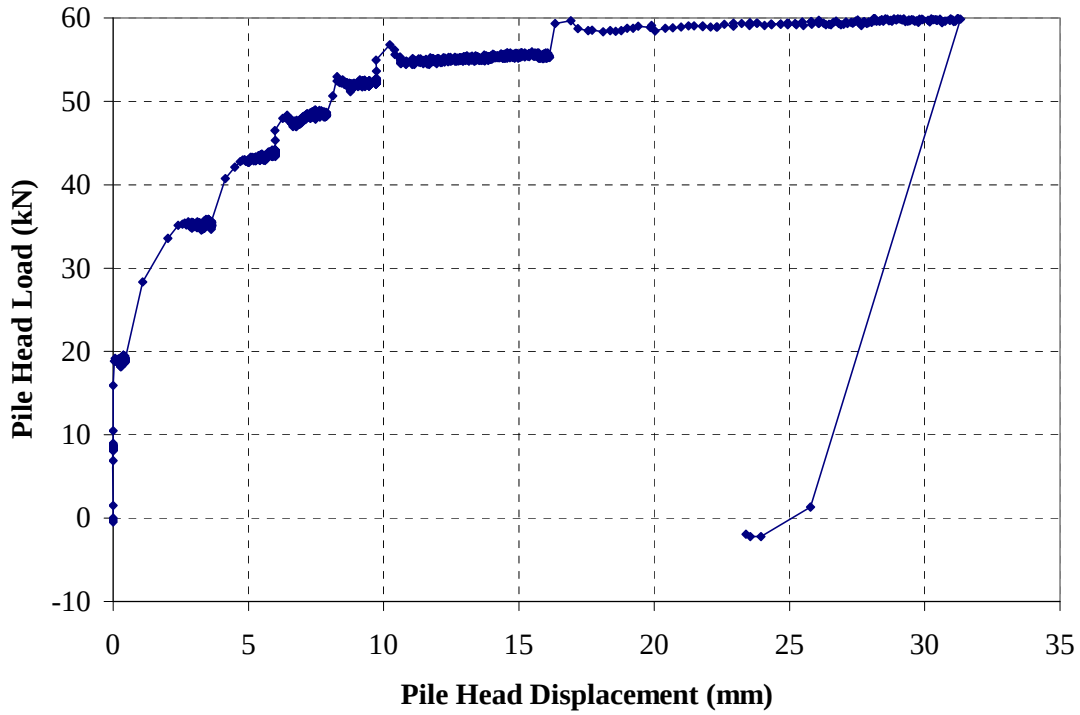

TG2[5]/cs

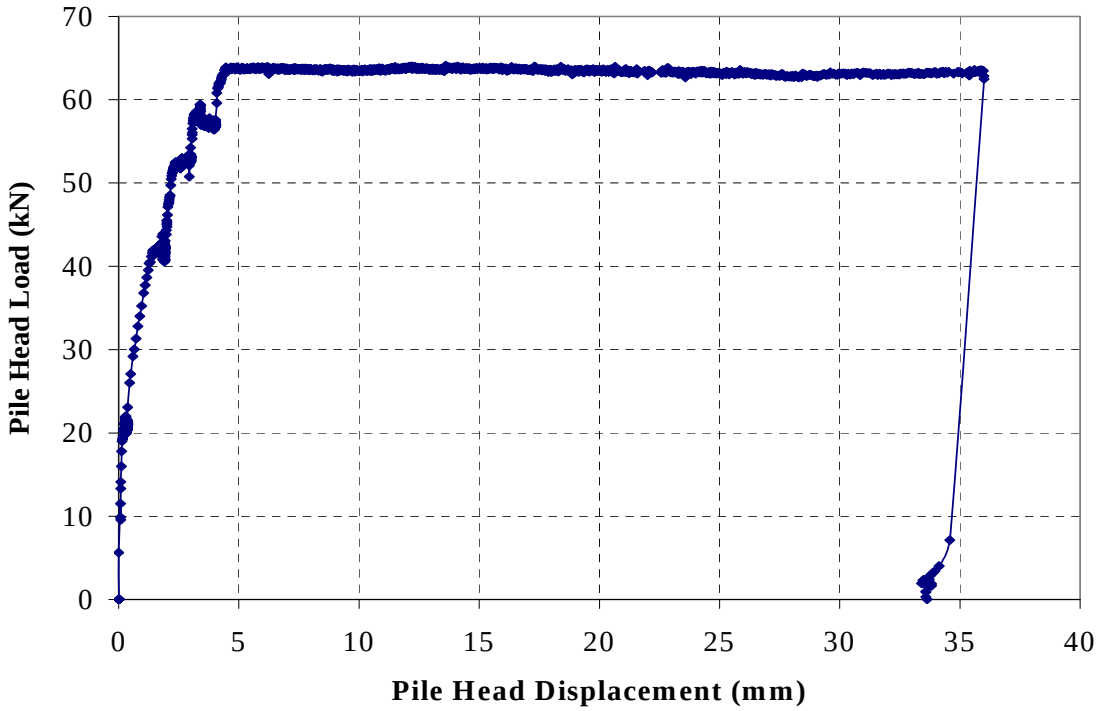

TS3/cs

Appendix 7-1

OASYS SAFE and BRICK programs

OASYS SAFE

OASYS SAFE is a finite element program specifically intended for geotechnical applications. The need to consider effective stress is the principal difference between geotechnical FE and other FE packages. OASYS SAFE offers the following features:

- Analysis of problems in 2D with plane strain, plane stress or axial symmetry options. Curvilinear quadratic elements with 4, 8 or 12 nodes may be used. Pressure and point loading may be applied and restraints may be fixed or modelled as spring stiffnesses.
- Initial K_o stress conditions may be defined in SAFE. Pore pressures and effective stresses in the ground are specified individually so that both drained and undrained analyses may be performed. Modelling drained behaviour requires that all stiffness and strength parameters are provided in terms of effective stress. Undrained stiffness parameters are given in terms of effective stress (including Poisson's ratio), whereas strength parameters may be defined in terms of either total or effective stress. Initial pore pressures must be specified.
- Available soil models (besides linear elastic) include:
  - (i) Elastic Mohr-Coulomb: stresses are calculated from linear elastic assumptions but are reduced if the standard Mohr-Coulomb criterion is violated. If dilation is specified, the mean normal stress is increased accordingly.
  - (ii) A version of the incremental elastic model of soil behaviour proposed by Duncan and Chang (1970), using elastic-type parameters which vary as straining proceeds. The SAFE version incorporates a number of modifications to the original version.
  - (iii) Modified Cam Clay (MCC): SAFE uses a 2-D version of MCC based upon the work of Simpson (1973), in which the main parameters are λ, κ (the slopes of the normal consolidation and unload-reload lines in e-(σ_1'+σ_2')/2 space respectively), and critical state parameters Γ (the voids ratio on the critical state line at 1kPa) and m (=sin ϕ' at critical state).
  - (iv) The BRICK soil model (Simpson 1992), described in more detail later.

- The construction process may be represented in discrete stages. Within each stage, loading may be applied incrementally. Material properties may be changed between stages (for example: to represent the transition over time from undrained to drained conditions or to replicate excavated material). These features are particularly useful in modelling embankments or excavations/basements.

OASYS BRICK

BRICK was originally developed to model the dependence of soil stiffness upon the previous stress path direction. The 2-D plane strain version developed by Simpson (1992) has been extended to a general 3-D version, which has been used in this Thesis. The model is elastic-plastic with multiple kinematic yield surfaces and is expressed in *strain* space. BRICK may be used as a stand-alone application, or implemented into the SAFE finite element software.

Simpson (1992) explains the BRICK concept by an analogy to a man walking around (in strain space) and dragging along a set of bricks on strings. The man represents the current strain state of a soil element, while the bricks represent the plastic current strains in proportions of the soil within the element. When the man moves without movement of the bricks, the strain is entirely elastic; when all of the bricks are moving by the same amount as the man, the strain is entirely plastic. As the strain level increases (i.e. as the man moves further), it is assumed that an increasing proportion of strain is plastic (i.e. more bricks move). This explains the S-shaped curve of normalized tangent shear stiffness (G_{tan}/G_o) against shear strain (γ). The S-shaped curve is simplified into a series of steps (on a G_{tan}/G_o-log(γ) plot), in which the step height represents a proportion of the material developing plastic straining and the string length indicates the total strain experienced.

G_{tan} is assumed to vary in direct proportion to the current mean effective stress *p'*, and the derivation of plastic strains follows the ideas of the Cam Clay model. BRICK uses a parameter β to distinguish between the strength and stiffness of normally consolidated and overconsolidated soils.

The 3-D BRICK model uses a volumetric strain (ε_v) component and five shear strain components (in orthogonal *x,y,z* axes) ε_z-$\varepsilon_{x,}$ $(2\varepsilon_y-\varepsilon_x-\varepsilon_z)/3^{0.5}$, γ_{xy}, γ_{yz} and $\gamma_{xz.}$ The string lengths (which govern the strain to failure and the derived angle of shearing resistance) are varied as a function of the relative proportions of the developing shear strains, giving a failure envelope of the type proposed by Drucker and Prager (1952).

At very low strains, soil behaviour is assumed to be elastic and the elastic shear modulus (G_{max}) may be determined from the initial stages of laboratory tests with high resolution local strain instrumentation or from shear wave velocity measurements. The small strain Poisson's ratio (ν) is used to relate G_{max} to the elastic bulk modulus (K_{max}). K_{max} is given as p'/ι, where ι is the small strain equivalent of λ and κ of the Cam Clay models.

Since BRICK assumes that stiffness varies directly with *p'* at all strain levels, separate BRICK parameters may be required for specific *p'* values when an alternative variation is to be modelled. It is therefore possible that the values of ι and β may need to be altered so that the area underneath the S-shaped curve is compatible with the peak friction angle of the material. Furthermore, although BRICK provides a model to cover a wide range of soil behaviour (including normally consolidated and heavily overconsolidated states), it is unlikely that it will fit the whole range equally well and specific parameters may have to be chosen for the range of greatest relevance to the user.

When used in SAFE, the principal difference between BRICK and other material models is its ability to model the entire geological history of the soil (from initial deposition as a slurry). In the case of simple consolidation histories, K_o is computed from the geological history and is stored along with associated brick positions (strains) as functions of OCR. More complicated histories (i.e. reloading after erosion, or groundwater lowering) must be represented as early stages of the finite element analysis. While BRICK material may be replaced by another material (i.e. soil replaced by concrete), it may not replace another material.

Appendix 8-1

Total and Effective Stress Ratios

A number of dimensionless horizontal stress coefficients may be employed to describe pile response, particularly over the installation and equalization periods. It is mainly *total* stress coefficients that are used in this Thesis, because the calculation of effective stresses would require that pore pressures and total stresses were measured simultaneously at the same location.

The value of the horizontal *total* stress (σ_h) at any stage of installation or equalization may be represented by the normalized *total* stress term (H) as:

$$H = \frac{\sigma_h - u_o}{\sigma_{vo}}$$

where u_o is the hydrostatic pore pressure and σ'_{vo} is the effective overburden pressure. A specific value of H may be defined to correspond with the maximum radial total stress (σ_{hi}) developed during installation, referred to as H_i. Once full equalization has been reached at a total radial stress of σ_{hc}, the term H_c may be used.

$$H_i = \frac{\sigma_{hi} - u_o}{\sigma'_{vo}} \qquad H_c = \frac{\sigma_{hc} - u_o}{\sigma'_{vo}}$$

Further useful ratios may be defined to relate the values of H at intermediate stages. H/H_i is a convenient unitless parameter, defining the variation in H relative to the installation H value. After equalization, this ratio takes on the value H_c/H_i and is termed the relaxation coefficient.

An equivalent normalized *effective* stress term is defined as K, where:

$$K = \frac{\sigma_h - u}{\sigma'_{vo}}$$

The value of u used is that existing concurrently with the value of σ_h used, rendering K an *effective* stress term. This term is not widely used in Chapter 8, since total and pore pressures were not measured simultaneously. However, once full equalisation is achieved

and pore pressures have reverted to hydrostatic values, the two terms become equivalent (i.e. $H_c=K_c$). Therefore, the terms H_c/H_i and K_c/H_i are interchangeable.

Maximum excess pore pressures surrounding a pile are often presented in terms of the excess pore pressure ratio, in which the maximum excess pore pressure is normalized by the vertical effective stress:

$$\frac{\Delta u_{\max}}{\sigma'_{vo}} = \frac{u_{\max} - u_o}{\sigma'_{vo}}$$

Research with the Imperial College Pile, summarized by Lehane et al (1994) has shown that the values of H, K and $\Delta u/\sigma'_{vo}$ at the pile-soil interface not only depend on the soil properties, but also depend on how far above the pile tip the sensor is located (h). This distance is normally quoted as a ratio of the distance above the pile tip h to the pile radius R. This *h/R effect* is also referred to in the analysis of Chapter 8.

Appendix 8-2

c_h backfigured from pneumatic piezometer measurements

Pore Pressure Measurements

Excess pore pressure dissipation records around TG1 provide an opportunity to estimate the coefficient of horizontal consolidation (c_h) of the soil surrounding a group of piles. The variation in pore pressure at each of the nine piezometer locations are shown in Figure A8-2.4 and the corresponding maximum excess pore pressures are shown in Figure 5-3. Piezometers 3, 8 and 9 did not provide any useful information for this analysis. Of the remaining piezometers, those which recorded pore pressure changes of at least 10kPa due to installation were most useful.

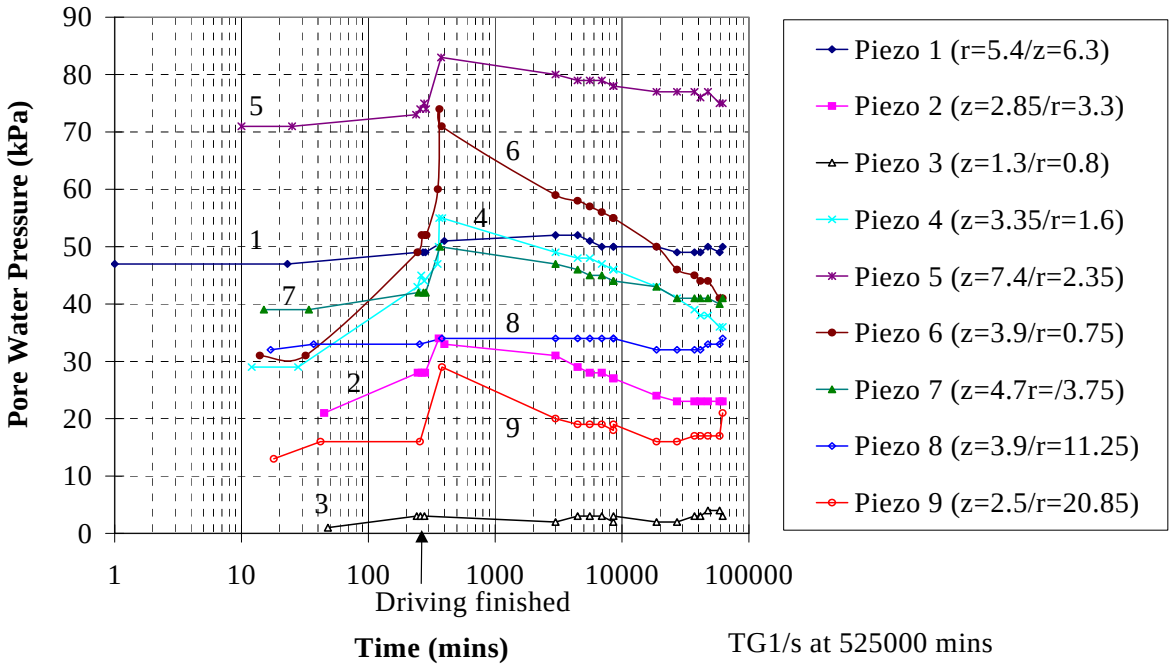

Figure A8-2.4 Pore pressures at the piezometer locations reflecting TG1 installation

3-D Linear Un-coupled Consolidation Theory

In situations where consolidation may be assumed to be radially symmetrical, the consolidation process may be described mathematically in polar coordinates as follows:

$$c_h\left(\frac{\partial^2 u}{\partial R^2}+\frac{1}{R}\frac{\partial u}{\partial R}\right)+c_v\frac{\partial^2 u}{\partial z^2}=\frac{\partial u}{\partial t}$$

where c_v is the coefficient of consolidation in the vertical plane, c_h is the coefficient of consolidation in the horizontal plane, z is the depth and R is the radial displacement.

The Central Difference approach provides a useful way of solving this equation; the derivatives in the above equation are assigned the following values:

$$\frac{\partial u}{\partial t} = \frac{u_{0,k+1} - u_{0,k}}{\Delta t};\quad \frac{\partial^2 u}{\partial z^2} = \frac{u_{2,k} + u_{4,k} - 2u_{0,k}}{\Delta z^2};\quad \frac{\partial^2 u}{\partial R^2} = \frac{u_{1,k} + u_{3,k} - 2u_{0,k}}{\Delta R^2};\quad \frac{\partial u}{\partial R} = \frac{u_{3,k} - u_{1,k}}{2\Delta R}$$

The relevance of the subscripts to the pore pressure terms are explained schematically in Figure A8-2.5; the first subscript represents position in r-z space while the second represents time stages in the consolidation process.

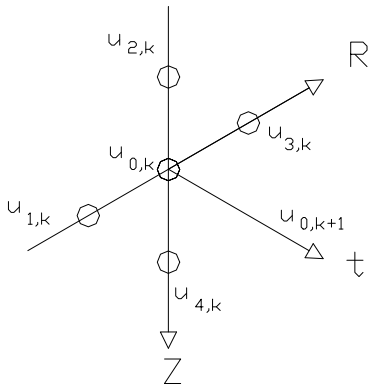

Figure A8-2.5 Central Difference Technique for consolidation analysis

Substituting these derivatives into the differential equation with common values for Δz, ΔR and h; $u_{0,k+1}$ may be expressed as:

$$u_{0,k+1} = u_{0,k}\left(1 - 2r_v(1+\Omega)\right) + \Omega r_v\left(u_{1,k}\left(1 - \frac{h}{2R}\right) + u_{3,k}\left(1 + \frac{h}{2R}\right)\right) + r_v\left(u_{2,k} + u_{4,k}\right)$$

$$r_v = \frac{c_v \Delta t}{h^2} \qquad r_h = \frac{c_h \Delta t}{h^2} \qquad \Omega = \frac{r_h}{r_v}$$

At the origin, where R = 0,

$$\frac{1}{R}\frac{\partial u}{\partial R} \rightarrow \frac{\partial^2 u}{\partial R^2}$$

and the following alternative expression applies:

$$u_{0,k+1} = u_{0,k}\left(1 - 2r_v(2\Omega + 1)\right) + r_v\left(u_{2,k} + u_{4,k} + 4\Omega u_{3,k}\right)$$

The above solutions are a mathematical representation of the fact that to calculate the excess pore pressure at some time increment k+1 (at some location in r-z space), the excess pore pressure at the previous time increment k at that same location is required, in addition those four which surround it (Figure A8-2.5). When R=0, there are only three surrounding values. However, to start this iterative process, an initial pore pressure distribution is required.

Initial distribution of excess pore pressures

An approximate contour map of $\Delta u_{max}/\sigma'_{vo}$ values in R-z space was developed based upon the six reliable piezometer readings (Figure A8-2.6). A grid of initial pore pressures at vertical and radial spacings of 0.2m (=Δz=ΔR=h) were estimated from this map. This grid extends from the pile group centre to a radial displacement of 30 pile diameters, and examines (predominantly) Stratum 3 between the bottom of the filled ground at 2.0m and the sand layer at 9.0m (a depth of 10 pile diameters below the pile base). Both top and bottom boundaries permit free drainage (Δu = 0). The same condition is imposed at the radial boundary, no excess pressures are assumed to exist. Estimates were sought of the $\Delta u_{max}/\sigma'_{vo}$ values close to the pile[1]; the following estimates proved useful:

[1] not provided by the piezometers, the closest being at 0.6m from the group centre

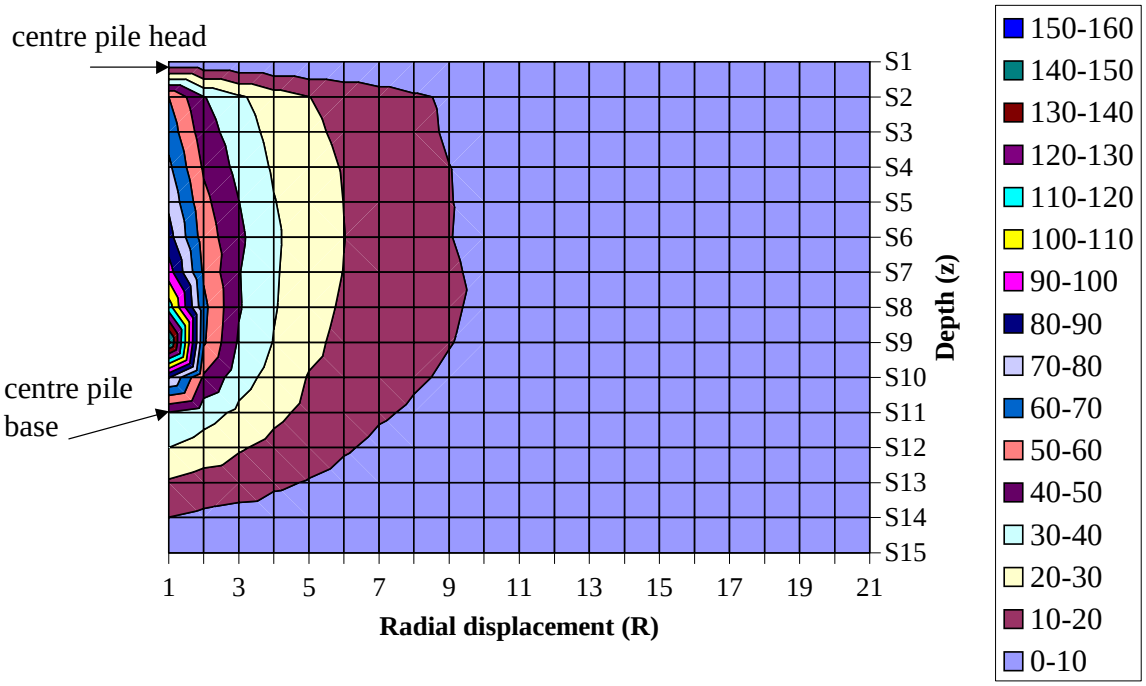

Figure A8.2-6 Map of initial pore pressure isochrones/contours (kPa)

- Estimates of $\Delta u_{max}/\sigma'_{vo}$ based upon σ_h measurements (Figure 8-2)
- Field tests performed in St. Alban's clay (Roy et al 1981) suggested that the variation in $\Delta u/\sigma'_p$ with radial distance from a single pile is approximately linear.

Spreadsheet solution to consolidation problem

The grid representing the pore pressure distribution was set up within an Excel spreadsheet. The initial distribution was entered from the contour plot, and the pressures at subsequent time intervals were calculated on different sheets using the formulae described.

To ensure convergence of the iterations involved in the central difference equation, values for r_v and r_h below 1/6 were necessary. The time interval was often as small as 3 hours, to accommodate this condition. Reducing the grid spacing would be a computationally more efficient method of ensuring convergence (since r depends on Δt and h^2). However the possibility of the solution being sensitive to the initial pressures close to the pile prompted

the reduction of the time period Δt (= $t_{k+1} - t_k$) as the better alternative. Sensitivity analyses suggested that pore pressure predictions beyond 1.0m from the pile group centre were relatively insensitive to the initial pore pressure distribution close to the pile group centre.

The following variables were incorporated in the spreadsheet:

- c_v; it was assumed that γ=2.
- c_v was assumed to remain constant with radial displacement from the pile group centre and with time (as consolidation proceeded); neither assumption is strictly speaking correct but useful in providing an approximation to the value of c_v.

Observations from the Consolidation Model

No single value of c_h produces a pore pressure decay trend to match all of the measured piezometer data satisfactorily and consistently. This is due in part to the simplifying assumptions made above. However, the following points are worth of note, in reference to Figures A8-2.7 to A8-2.10:

(i) c_h=50m^2/year was found to offer the best prediction of the *total* pore pressure drop over the two month period examined, although predictions were generally unsatisfactory at intermediate stages.

(ii) While c_h=10m^2/year strongly underpredicts the degree of dissipation over the first five days since group installation, the subsequent pore pressure decay (5 days to 2 months) is modelled quite well by this value.

(iii) Given that the state of soil overconsolidation may differ around the piezocone[2] and an installed pile group, and that c_h values are generally only estimable to within half an order of magnitude, the range of values suggested above are deemed reasonable approximations of the consolidation properties of the soil surrounding a group of piles.

[2] Piezocone dissipation tests at Belfast suggest that c_h=7-10m^2/year

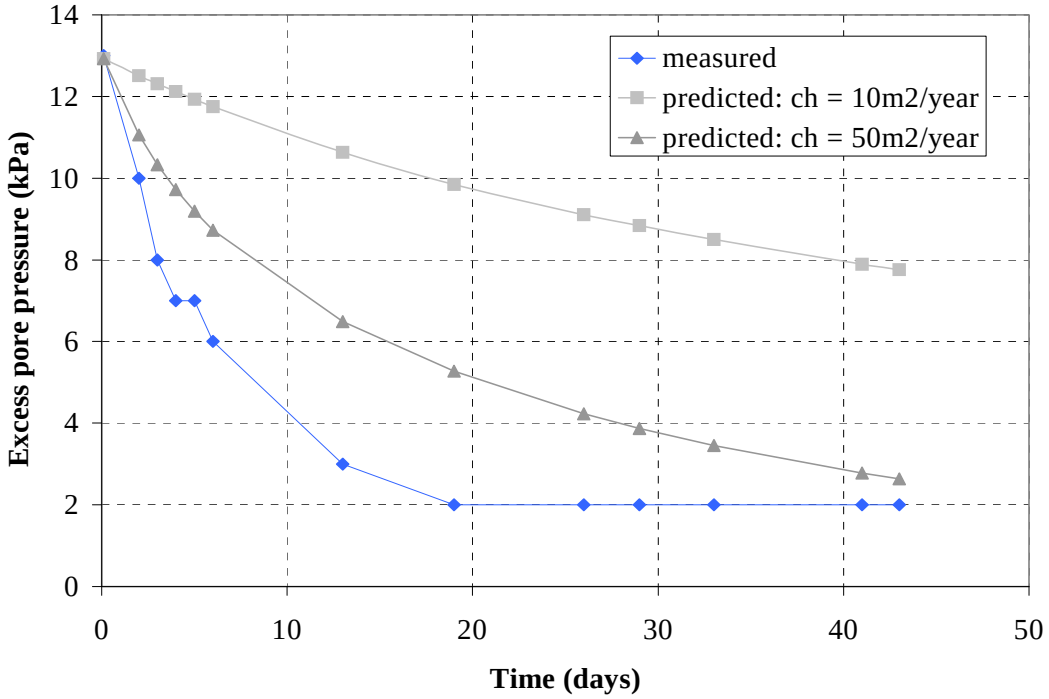

Figure A8-2.7 Pore pressure dissipation predictions at z=2.85m, r=3.3m

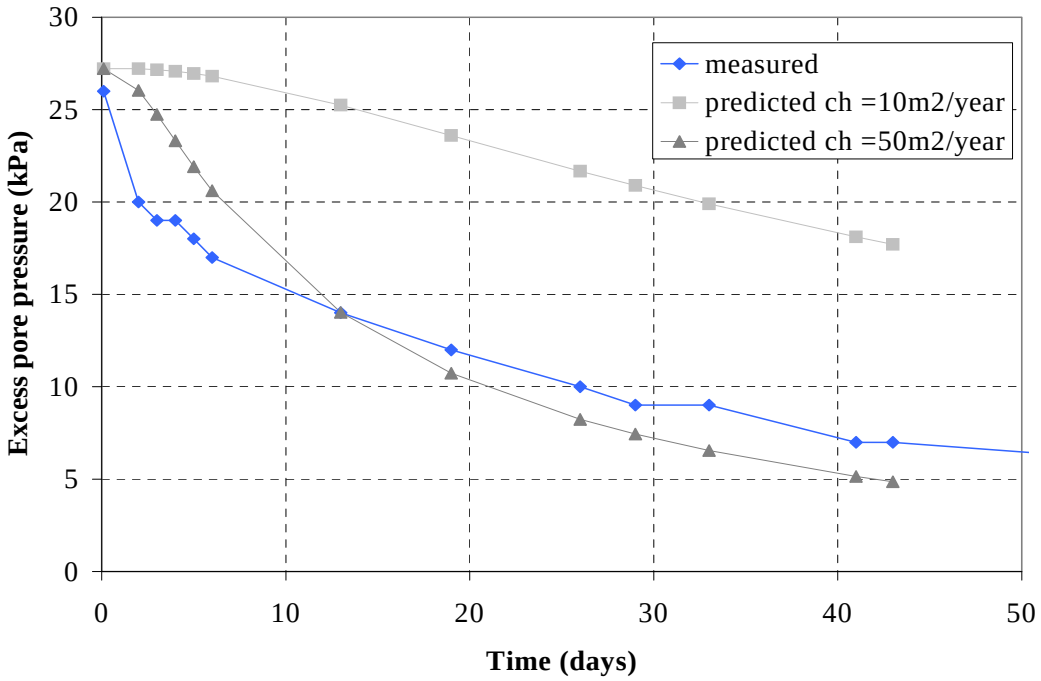

Figure A8-2.8 Pore pressure dissipation predictions at z=3.35m, r=1.6m

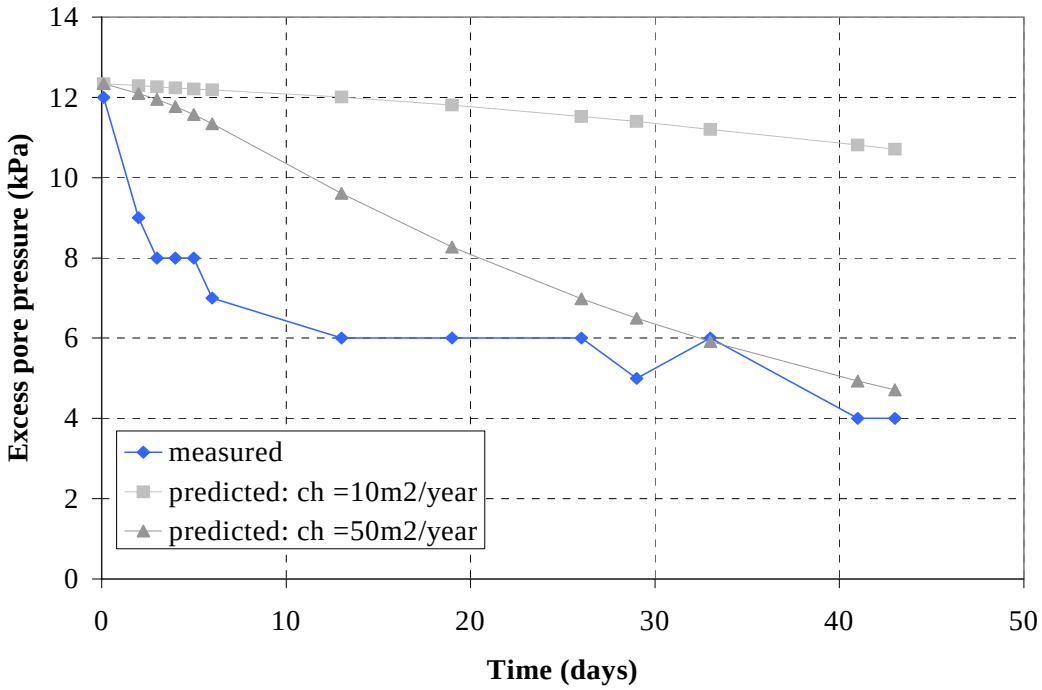

Figure A8-2.9 Pore pressure dissipation predictions at z=7.4m, r=2.35m

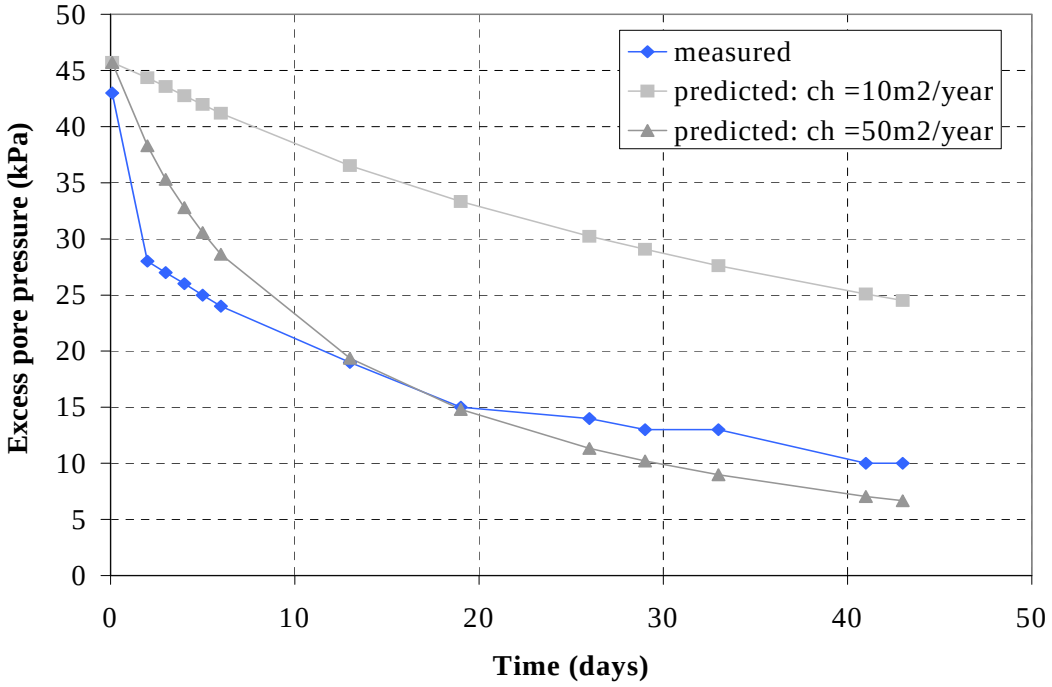

Figure A8-2.10 Pore pressure dissipation predictions at z=3.9m, r=0.75m

Appendix 8-3

Decay of σ_h around single pile

The basis of comparing the measured H/H_i decay for the centre group pile (CG1[3]) with a corresponding prediction for a single pile (based on Lehane 1992) lies in matching their decay curves (in terms of the time factor T) over the period that the centre pile behaves as a single pile. This amounts to a period of approximately 40 minutes which comes to an end once the first of the corner piles (CG1[1]) is installed. This is critical in ensuring that the single pile H/H_i prediction provides a realistic comparison with the group H/H_i measurements.

The decay in H while the centre pile (CG1[3]) is effectively a single pile is presented in Figure A8-3.1. It is clear that once σ_{hi} is reached, H drops as the excess pore pressure dissipates. However, the rate of decay of H/H_i at h/R=5.3 appears to be significantly quicker than at h/R=19.5.

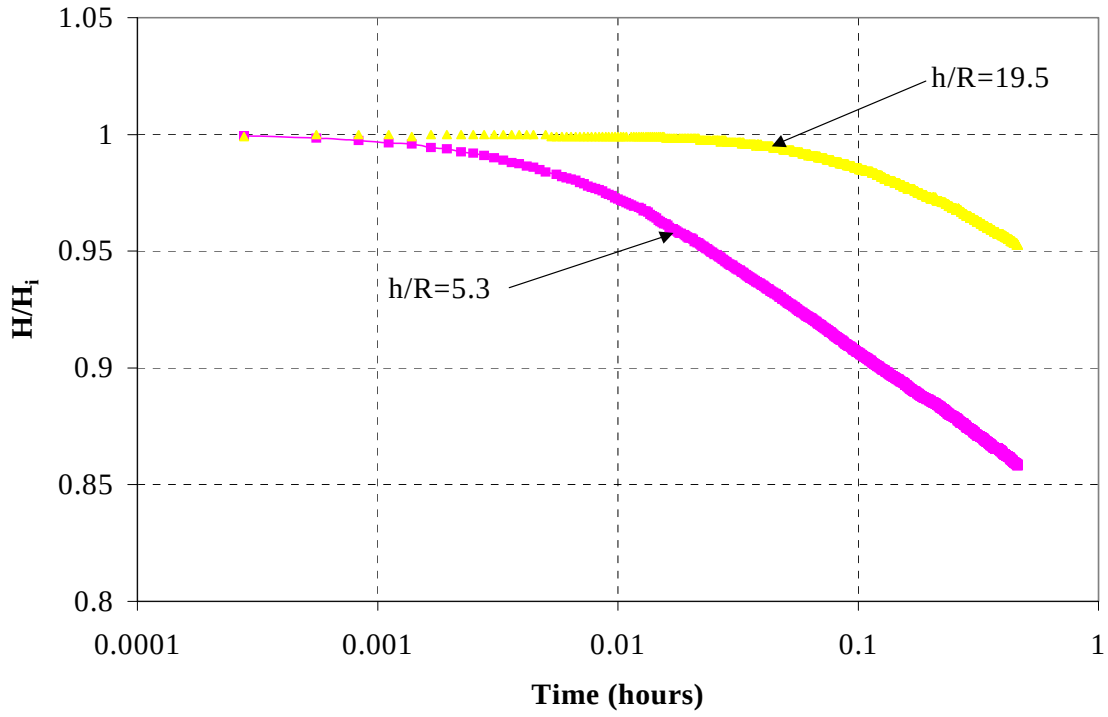

Figure A8-3.1: H/H_i decay after installation of centre pile CG1[3]

Houlsby and Teh (1988) conducted piezocone dissipation tests with porous stones at different distances from the pile tip. It was found that faster dissipation arose nearer the pile tip (low h/R values), where drainage was three-dimensional. Slower dissipation occurred

further up the cone shaft (larger h/R values) where the flow of pore water was predominantly radial. This is qualitatively consistent with the findings in Figure A8-3.1; however, the difference between the H/H_i dissipation rates (at h/R=5.3 and h/R=19.5) appears to be great enough to warrant closer examination. The significant difference is not consistent with measurements made by Lehane (1992), who showed that H/H_i during equalisation depends *relatively* little on h/R (at instrument positions h/R=8, 28 and 50).

The value of c_h applicable to the Belfast sleech was varied to seek a suitable match between the single pile H/H_i prediction and both centre pile H/H_i measurements at h/R=5.3 and 19.5. Satisfactory matches were provided by using c_h =25 m^2/year for h/R=19.5 (Figure A8-3.2) and c_h =500m^2/year for h/R=5.3 (see Figure A8-3.3). Based upon piezocone dissipation tests upon which c_h was found to be typically 7-10 m^2/year and c_h values backfigured from the piezometer data (Appendix 8-2), 25m^2/year appears to be a reasonably realistic figure[3]. On the other hand, c_h =500m^2/year cannot be reconciled with other available data, and the discrepancy may reflect an instrumentation or other unexplained problem.

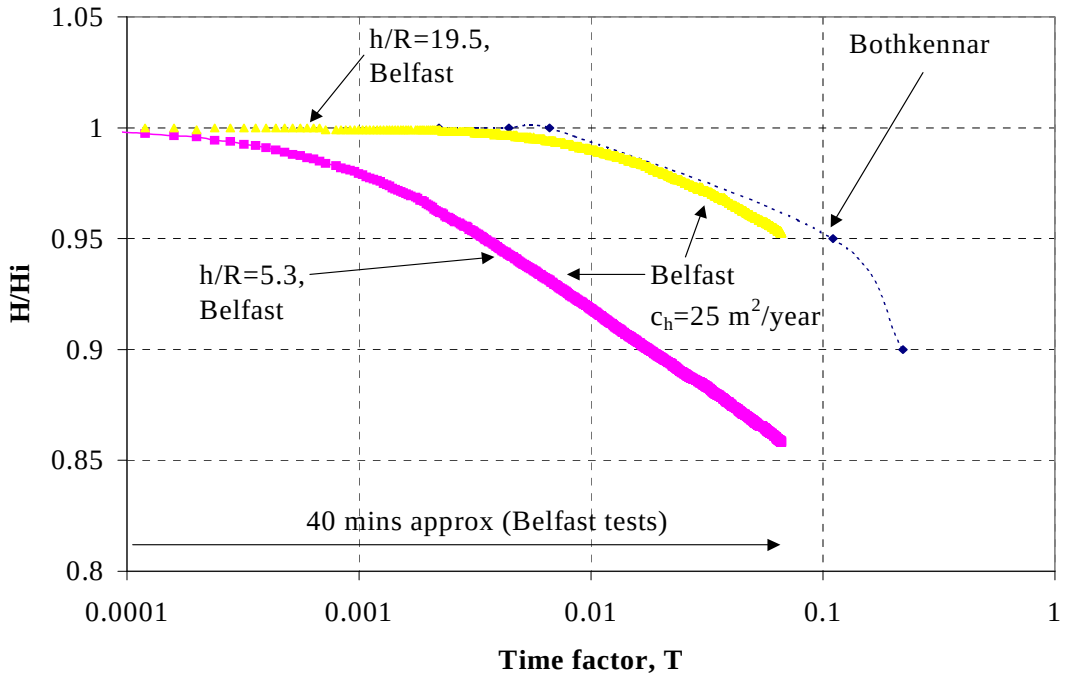

Figure A8-3.2 Variation of H/H_i with time factor T (Belfast c_h=25 m^2/year)

[3] Given that c_h is usually only estimable to within half an order of magnitude.

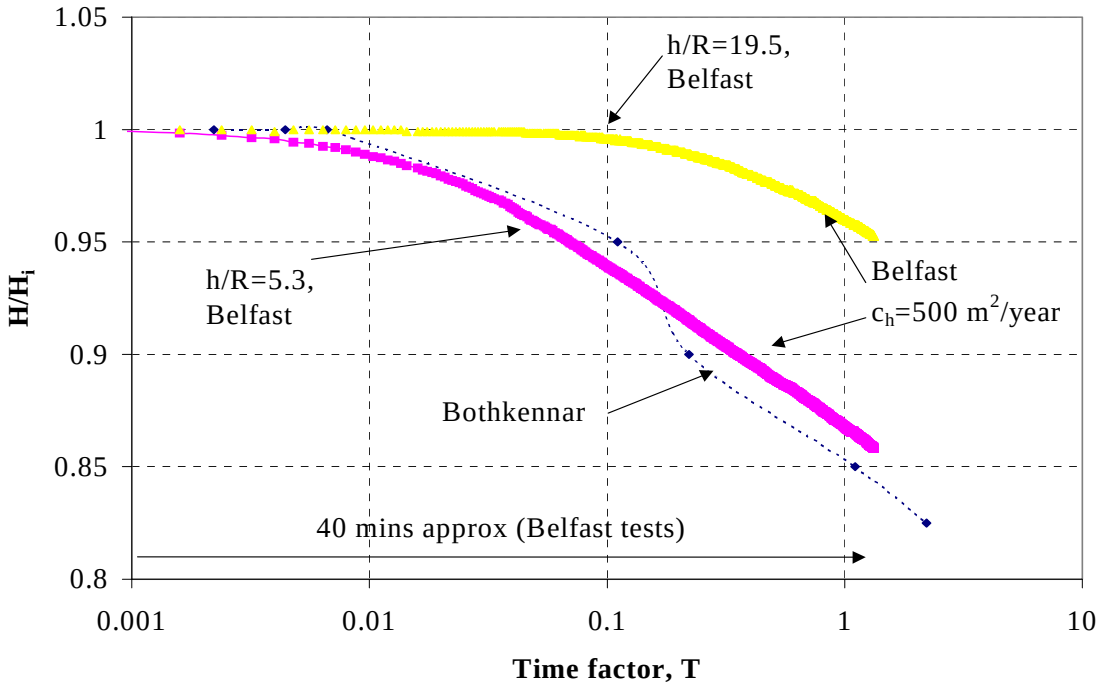

Figure A8-3.3 Variation of H/H_i with time factor T (Belfast c_h=500 m^2/year)

The value of H/H_i at h/R=5.3 just before installation of CG1[1] was adjusted to conform with H/H_i at h/R=19.5. This fixes both dissipation rates to be compatible with 25m^2/year over the period before CG1[1] is installed. All subsequent H/H_i values at h/R=5.3 were increased by the same amount. Figure 8-4 shows the data subject to this adjustment, but it should be noted that the conclusions formed in Section 8.3 are not particularly sensitive to this adjustment.

Appendix 8-4

Measured t-z curves

The load distributions measured in CS1, CG1[1] and CG1[3] have been used to develop curves tracking the development of shear stress (t) at the interface of pile and soil with the local pile displacement (z). The local displacement (z) is calculated as the pile head load less the elastic shortening of the pile between the pile head and the instrument level, assuming a composite modulus ($36MN/mm^2$) for the steel and concrete in the pile. In all cases the correction for the elastic shortening of the pile comprises a minor proportion of the imposed displacements. The t-z curves presented have not been corrected for the pile weight (since only compression piles are compared). It should be noted that subjective interpretation of the strain gauge output was required in deriving the values of t, with the result that the relative t/z ratios should be considered qualitatively at low values of z, rather than their absolute values.

Single pile load transfer curves

The t-z curves for CS1/s and normalized versions (t/t_{max}-z) are presented in Figure 1. The maximum shear stress t_{max} is mobilized by a local pile displacement z=15mm (no further gain in shaft load is expected at greater displacements). Features of these curves include:

(i) The value of t_{max} over much of the pile length is approximately 10kPa, which is consistent with the load carried at the head of CS1/s (63kN) at 15mm displacement. The shear stress development at 3.25m shows greater test stiffness at this level than at 5.25m, despite the same t_{max} values being reached in both instances.

(ii) The low stiffness and t_{max} values at 1.0m reflect how little load is transferred from the pile within the filled ground.

(iii) API RP2A's (1993) normalised load transfer curves for single piles in cohesive soils are superimposed upon Figure 1. They produce a moderate estimate of the *average* stiffness over the entire pile length at typical working loads ($0.3t_{max}<t<0.4t_{max}$), but do not allow for any variation in stiffness with h/R.

(iv) The measured t-z responses are more non-linear than the API curves.

(v) The API method predicts that 3mm displacement is sufficient to mobilize t_{max}, whereas the shear stress development is much slower in reality. Measured peak (t_{max}) and residual (t_{res}) shear stresses on the pile shaft are virtually the same,

showing consistency with findings from the ring shear interface tests on remoulded specimens (Figure 3-15).

Group pile load transfer curves

The t-z curves (and t/t_{max}-z curves) measured for corner pile (CG1[1]/s) and centre pile (CG1[3]/s) are shown in Figures 2 and 3 respectively. Further summary plots are provided in Figures 4 and in Figures 8-14 to 8-16. The salient features of the group load transfer curves may be summarized as:

(i) The response of a group pile is less stiff than a single pile at horizons along the pile shaft in the sleech (i.e. 3.25m and 5.25m). The centre pile responds more softly than a corner pile, but the extent is difficult to quantify. This trend is compatible with measured pile head load-displacement relationships. Therefore, the use of the API curves would grossly underpredict the settlement to which a group of piles would be subjected.

(ii) The t_{max} values recorded for the centre pile reflect (and are consistent with) its reduced pile head load capacity (over that of a single pile). Although t_{max} for the corner pile is similar to that of the single pile, which is slightly surprising, this has also been reflected in their similar ultimate pile head loads.

(iii) Comparison of t_{max} values at each level for the three *characteristic* piles suggests that the centre pile carries a greater proportion of load towards the lower shaft or base. The slight post peak reduction in t at the 1.0m level in the centre pile may indicate downward redistribution of load within this pile; however the values are too small to confirm this conclusively. All piles show that very little load is shed within the upper 2.0m, part of which is filled ground.

(iv) The t/t_{max}-z curves reflect the *rate* at which the maximum shear stress is developed. These curves are virtually coincident for centre and corner piles (at 3.25m and 5.25m), i.e the gradient $d(t/t_{max})/dz$ appears common to both. This also reflects the trend identified in Figure 5-17, where the centre pile assumed less than 20% of the group load from an early stage of the load test.

(v) The single pile requires less settlement than the group piles to mobilise its maximum shear stress.

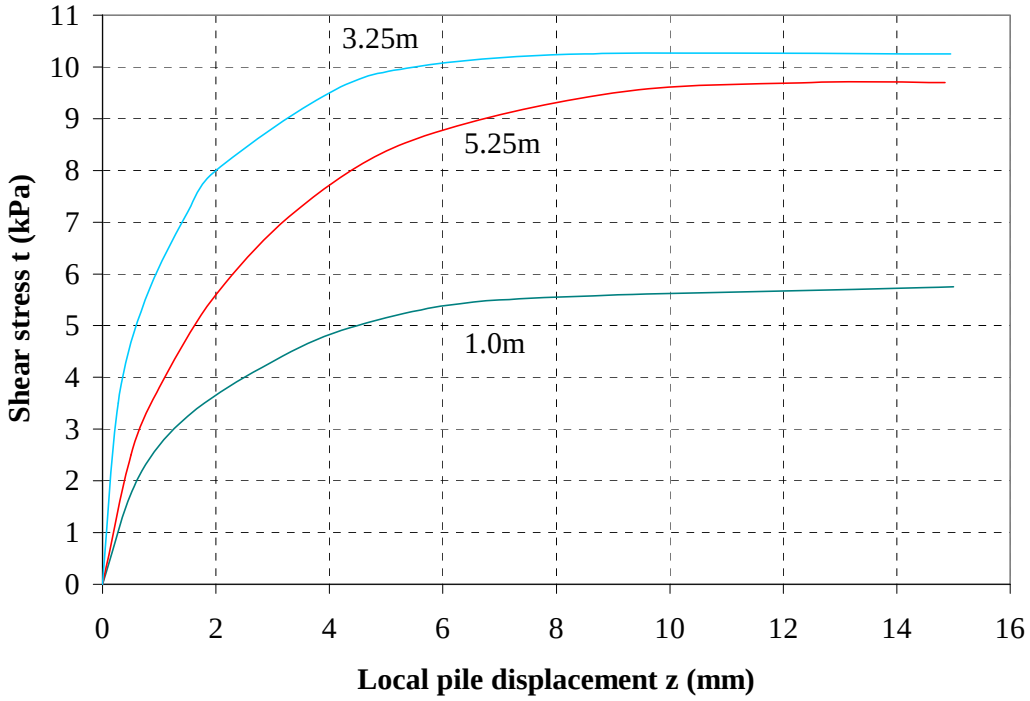

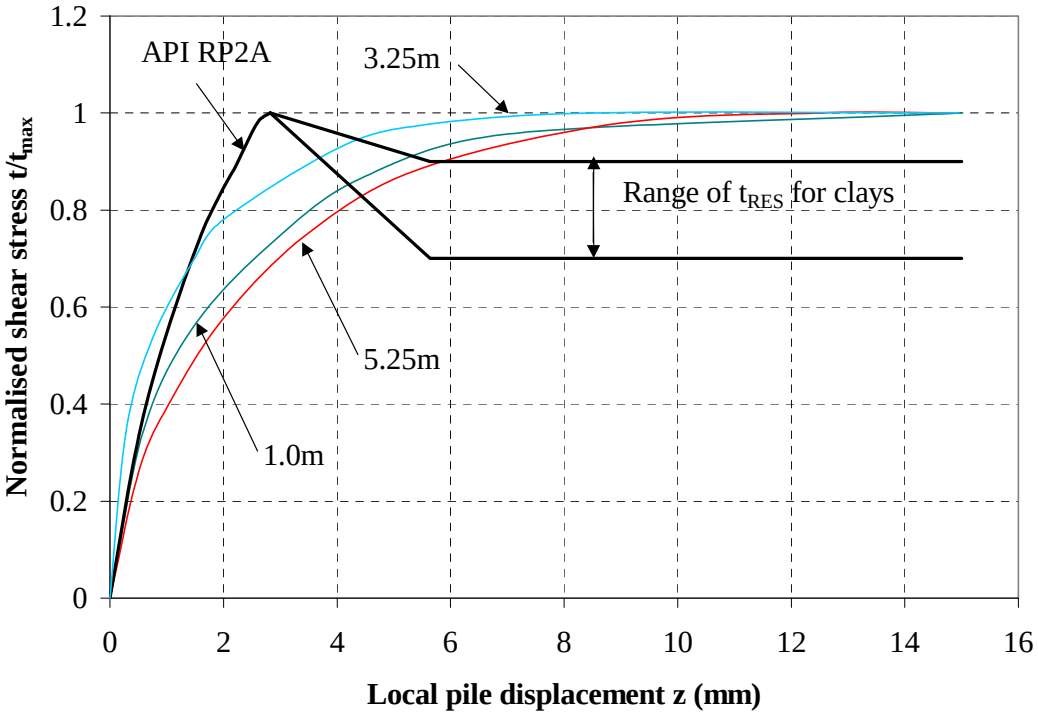

Figure 1: Single pile (CS1/s) load-transfer curves

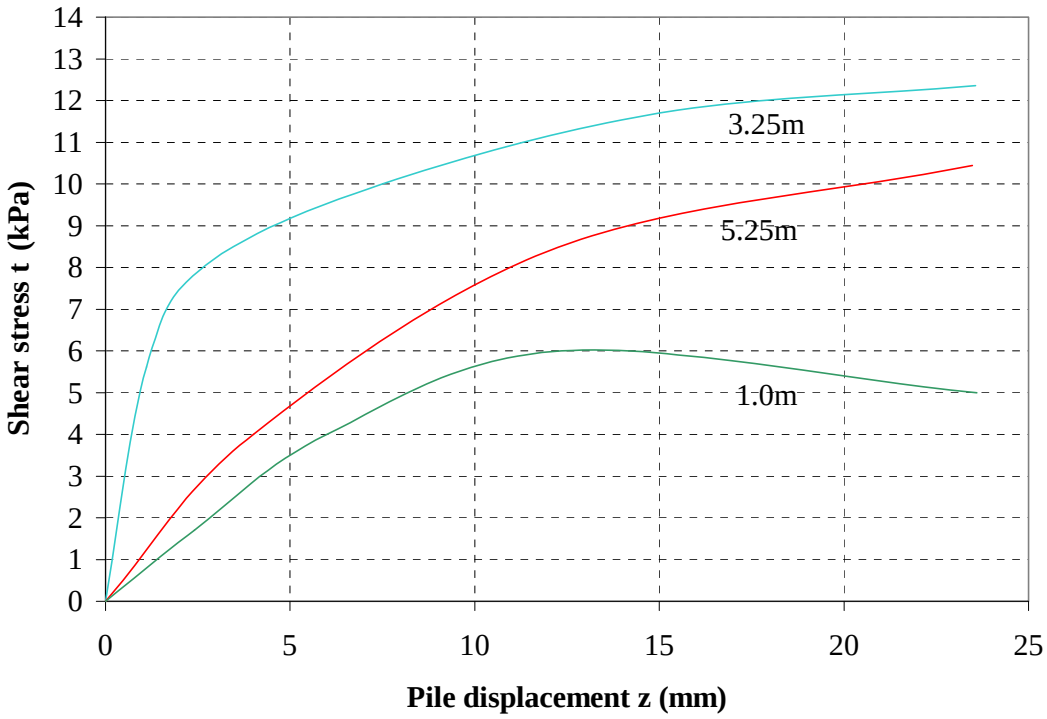

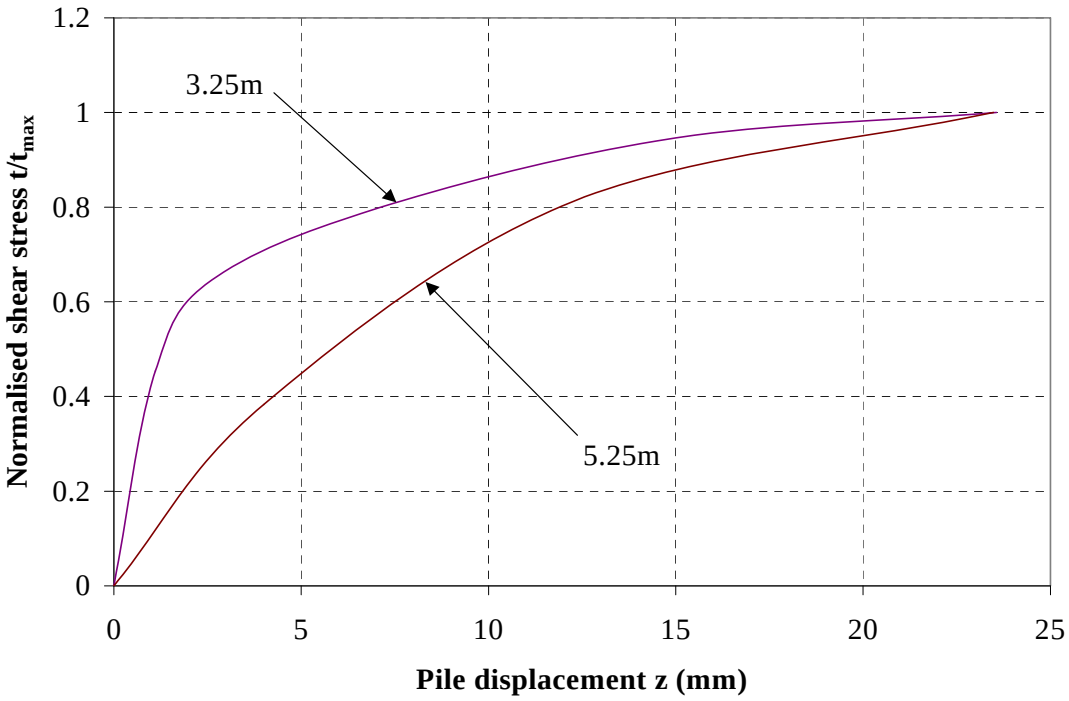

Figure 2: Corner pile (CG1[1]/s) load-transfer curves

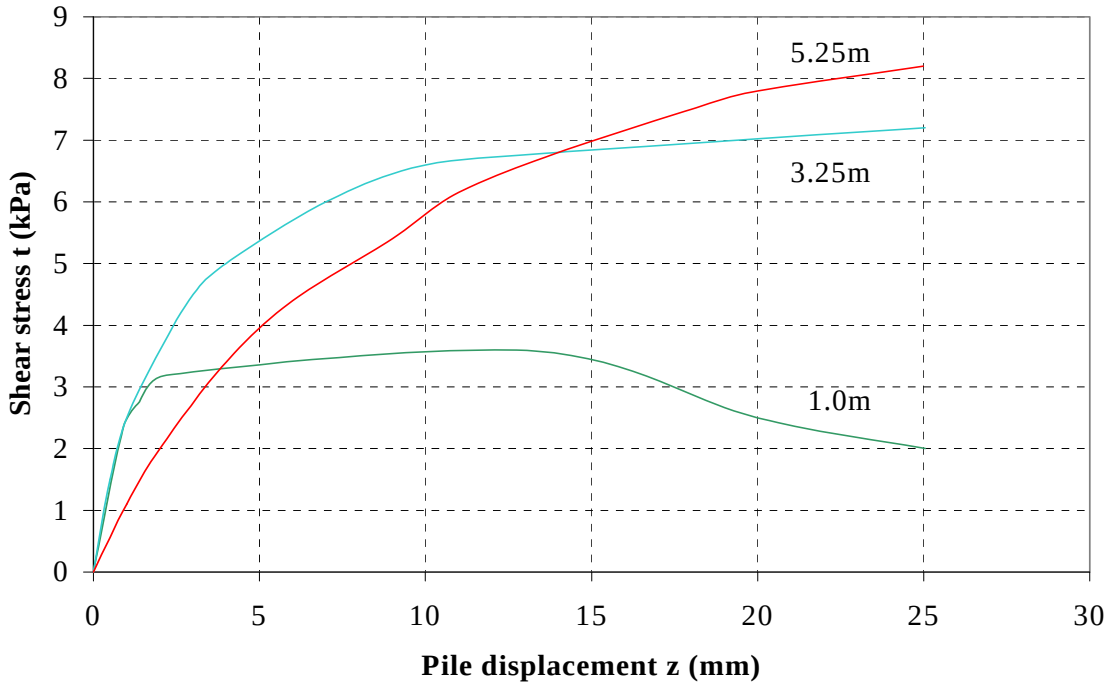

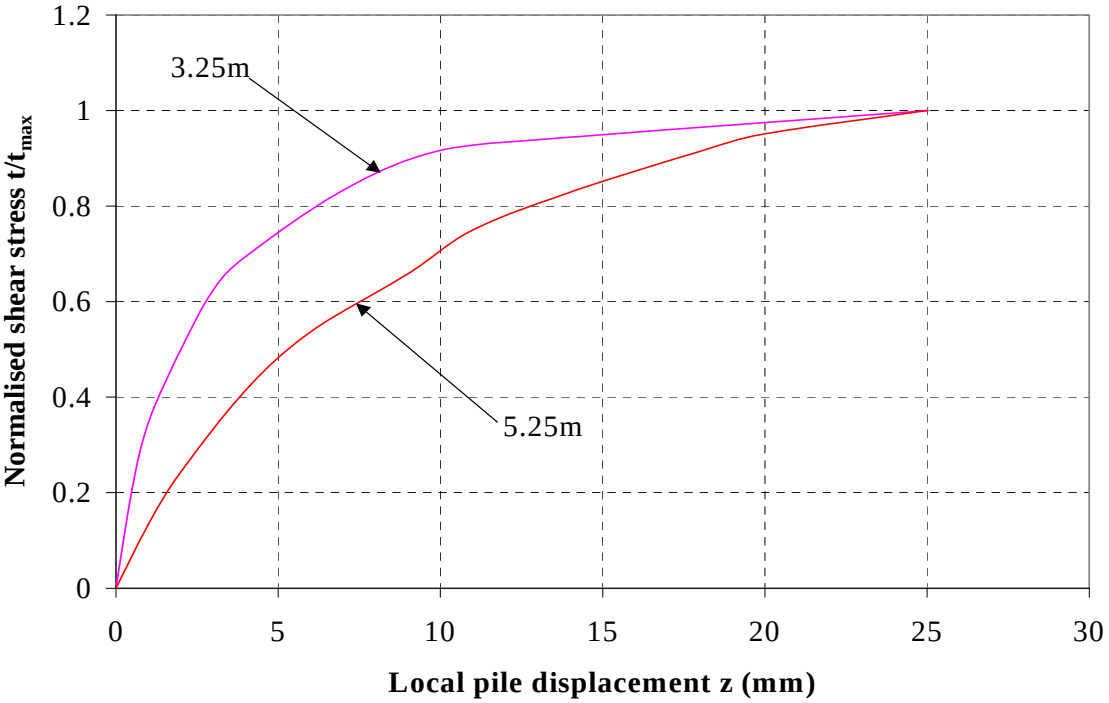

Figure 3: Centre pile (CG1[3]/s) load-transfer curves

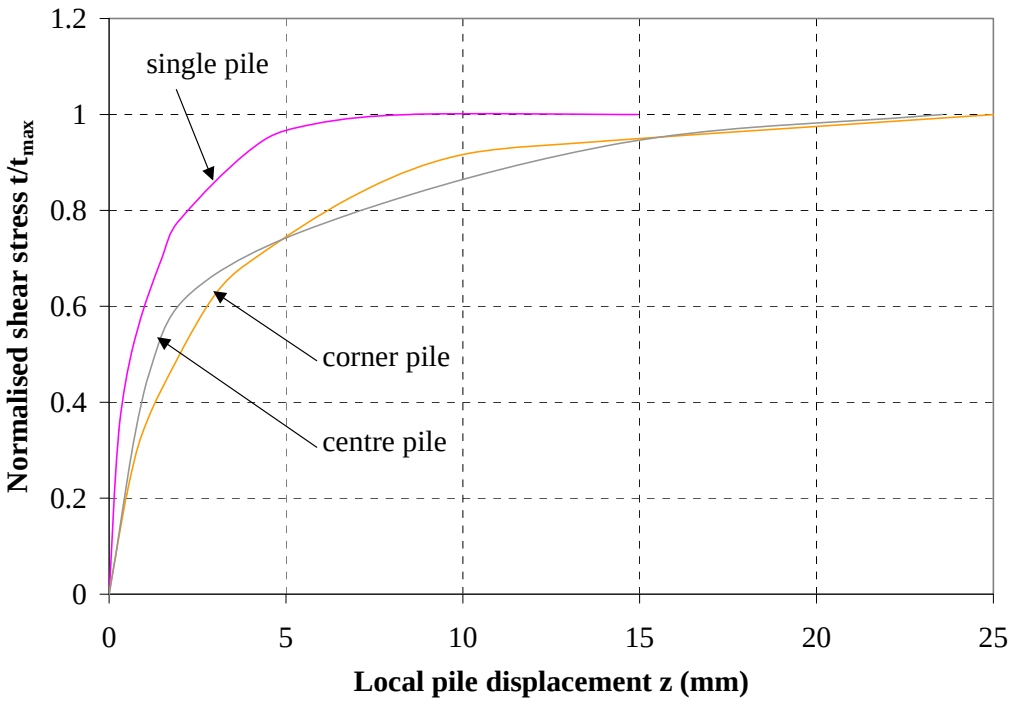

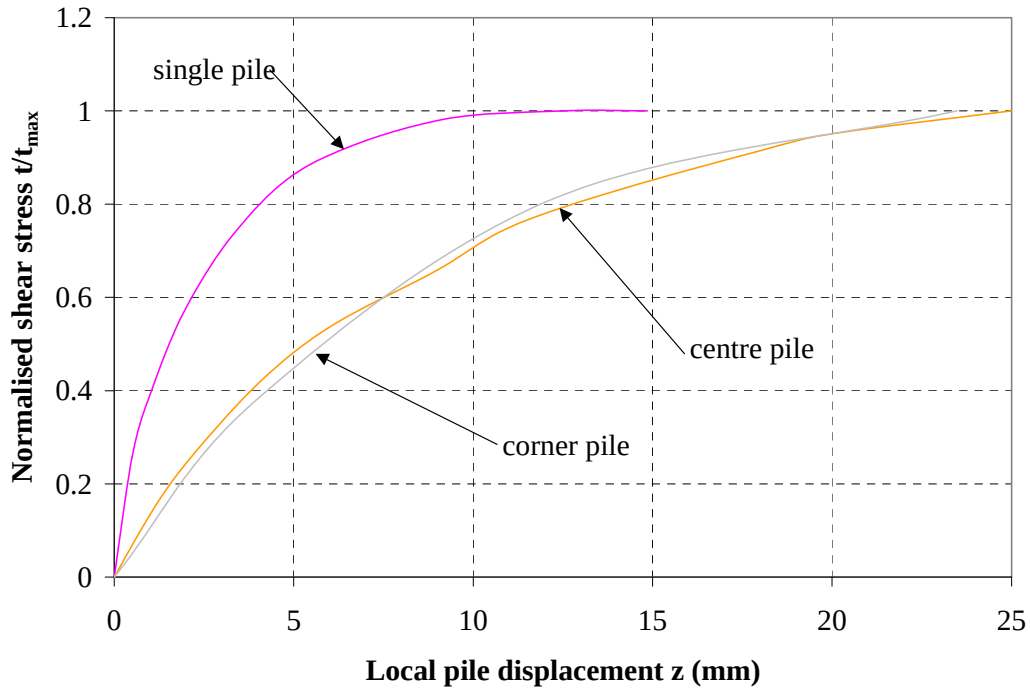

Figure 4: Load-transfer curves 3.25m (above), 5.25m (below)